


 Cite this: *RSC Adv.*, 2021, **11**, 35806

Journey of anthraquinones as anticancer agents – a systematic review of recent literature

 M. Shaheer Malik,^a Reem I. Alsantali,^b Rabab S. Jassas,^c Abdulrahman A. Alsimaree,^d Riyaz Syed,^e Meshari A. Alsharif,^a Kulkarni Kalpana,^f Moataz Morad,^a Ismail I. Althagafi^a and Saleh A. Ahmed^g

Anthraquinones are privileged chemical scaffolds that have been used for centuries in various therapeutic applications. The anthraquinone moiety forms the core of various anticancer agents. However, the emergence of drug-resistant cancers warrants the development of new anticancer agents. The research endeavours towards new anthraquinone-based compounds are increasing rapidly in recent years. They are used as a core chemical template to achieve structural modifications, resulting in the development of new anthraquinone-based compounds as promising anticancer agents. Mechanistically, most of the anthraquinone-based compounds inhibit cancer progression by targeting essential cellular proteins. Herein, we review new anthraquinone analogues that have been developed in recent years as anticancer agents. This includes a systematic review of the recent literature (2005–2021) on anthraquinone-based compounds in cell-based models and key target proteins such as kinases, topoisomerases, telomerases, matrix metalloproteinases and G-quadruplexes involved in the viability of cancer cells. In addition to this, the developments in PEG-based delivery of anthraquinones and the toxicity aspects of anthraquinone derivatives are also discussed. The review dispenses a compact background knowledge to understanding anthraquinones for future research on the expansion of anticancer therapeutics.

 Received 27th July 2021
 Accepted 6th October 2021

DOI: 10.1039/d1ra05686g

rsc.li/rsc-advances
^aDepartment of Chemistry, Faculty of Applied Sciences, Umm Al-Qura University, Makkah 21955, Saudi Arabia. E-mail: msmalik@uqu.edu.sa; saahmed@uqu.edu.sa

^bDepartment of Pharmaceutical Chemistry, College of Pharmacy, Taif University, P. O. Box 11099, Taif 21944, Saudi Arabia

^cDepartment of Chemistry, Jamoum University College, Umm Al-Qura University, 21955 Makkah, Saudi Arabia

^dDepartment of Basic Science (Chemistry), College of Science and Humanities, Shaqra University, Afif, Saudi Arabia

^eCentalla Discovery, JHUB, Jawaharlal Nehru Technological University Hyderabad, Kukatpally, Hyderabad 500085, India

^fDepartment of Humanities and Sciences (Chemistry), Gokaraju Rangaraju Institute of Engineering and Technology, Bachupally, Hyderabad 500090, India

^gDepartment of Chemistry, Faculty of Science, Assiut University, 71516 Assiut, Egypt


M. Shaheer Malik is currently Assistant Professor in chemistry at Umm Al-Qura University, Makkah (Saudi Arabia). He carried out his doctoral studies in organic chemistry at the Indian Institute of Chemical Technology, Hyderabad, and was awarded a PhD from Osmania University, India. Subsequently, he moved for a postdoctoral assignment to Yonsei University, Seoul (Korea),

working in biocatalysis. His research interest deals with the design and synthesis of novel chemical compounds as pharmaceutical agents and the application of enzymes in organic transformations. He regularly contributes and reviews research findings towards the advancement of science in his area of interest.



Prof. Dr Saleh A. Ahmed was born in Assiut, Egypt in 1968 where he undertook undergraduate and post-graduate studies. He received his Bachelor and MSc from Assiut University, Egypt and PhD in photochemistry (photochromism) under the supervision of Prof. Heinz Dürr at Saarland University, Saarbrücken, Germany. He worked as postdoctoral fellow, senior researcher and visiting professor in France (CNRS fellow), Japan (JSPS

fellow), Germany (AvH, DFG and DAAD fellows), Italy (TEMPUS fellow) and USA (Arab fund fellow). His current research interests include synthesis and photophysical properties of novel organic compounds, electronic devices and solar energy conversion, photocatalysis, nanomaterials and their applications, fluorophores and biologically active molecules.





TECHNICAL ARTICLE

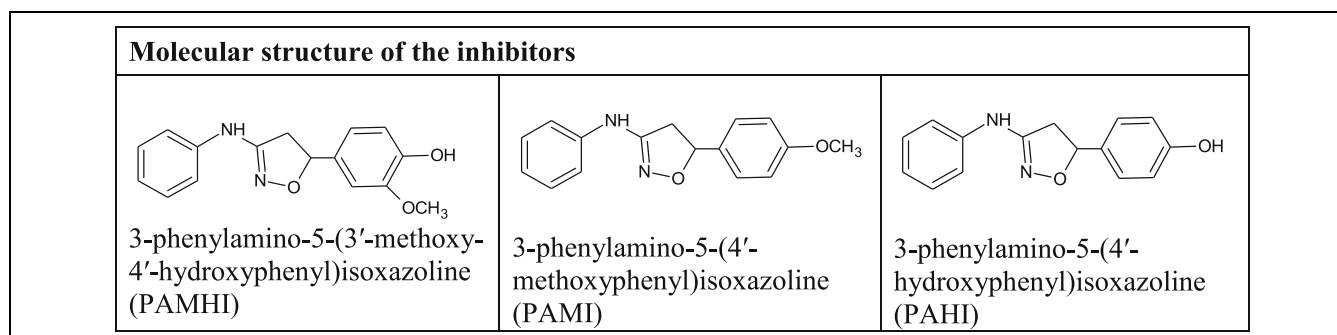
Isoxazoline Derivatives as Inhibitors for Mild Steel Corrosion in 1M H₂SO₄: Computational and Experimental Investigations

N. Anusuya, J. Saranya, F. Benhiba, I. Warad, A. Zarrouk, and S. Chitra

Submitted: 8 August 2021 / Revised: 4 December 2021 / Accepted: 29 January 2022

The isoxazoline derivatives namely 3-phenylamino-5-(3'-methoxy-4'-hydroxyphenyl) isoxazoline (PAMHI), 3-phenylamino-5-(4'-methoxyphenyl)isoxazoline (PAMI) and 3-phenylamino-5-(4'-hydroxyphenyl)isoxazoline (PAHI) were synthesized and tested for their inhibition capacity against the mild steel (MS) corrosion in 1 M H₂SO₄. Their inhibition performance toward MS has been studied through well-known methods namely weight loss (WL), electrochemical and surface analysis. The inhibition efficiency of PAMHI was 95.90% at 10mM concentration. The adsorption studies indicated that the isoxazoline derivatives obeyed Langmuir adsorption isotherm on the mild steel surface, and Gibbs free energy values were in the range of -32.05, -28.52 and -33.44 kJ mol⁻¹. These results suggested that the inhibitor molecules interacted with the mild steel surface through mixture adsorption. Also, mixed type behavior was observed for the studied inhibitors from polarization studies. The presence of a protective layer of organic matter was validated by scanning electron microscopy (SEM) and atomic force microscopy (AFM) techniques. Density-functional theory (DFT) method and molecular dynamics (MD) simulation have been studied and the results shown that the inhibitory efficiencies of the three molecules tested are almost the same.

Graphical Abstract



N. Anusuya and S. Chitra, Department of Chemistry, PSGR Krishnammal College for Women, Coimbatore, India; J. Saranya, Department of Humanities and Sciences (Chemistry), Gokaraju Rangaraju Institute of Engineering and Technology, Hyderabad, India; F. Benhiba, Laboratory of Separation Processes, Faculty of Sciences, Ibn Tofail University, PO Box 133, 14000 Kenitra, Morocco; and Laboratory of Materials, Nanotechnology and Environment, Faculty of Sciences, Mohammed V University in Rabat, Av. Ibn Battouta, P.O. Box. 1014, Agdal-Rabat, Morocco; I. Warad, Department of Chemistry, AN-Najah National University, P.O. Box 7, Nablus, Palestine; and A. Zarrouk, Laboratory of Materials, Nanotechnology and Environment, Faculty of Sciences, Mohammed V University in Rabat, Av. Ibn Battouta, P.O. Box. 1014, Agdal-Rabat, Morocco. Contact e-mails: jcsaranya.chem96@gmail.com azarrouk@gmail.com.

Keywords DFT, isoxazolines, mild steel corrosion, molecular dynamic simulation, SEM/AFM

1. Introduction

Corrosion is a natural process which results from physicochemical interactions between a metal and its environment that leads to a weakening of the metal surface, its surroundings and that could affect the technical systems of which they make a part of it. Generally, the resistance of the material depends upon the surrounding environment and of course is not an



Significance of Lorentz Force and Viscous Dissipation on the Dynamics of Propylene Glycol: Water Subject to Joule Heating Conveying Paraffin Wax and Sand Nanoparticles Over an Object with a Variable Thickness

Venkata Subrahmanyam Sajja¹ · Revathi Gadamssetty² · P. Muthu³ · M. Jayachandra Babu⁴ · I. L. Animasaun⁵

Received: 24 May 2021 / Accepted: 30 January 2022
© King Fahd University of Petroleum & Minerals 2022

Abstract

With emphasis on the motion of PG–Water + Paraffin Wax + Sand and PG–Water + Paraffin Wax on an object with a variable thickness experiencing Joule dissipation and n th order chemical reaction, nothing is known on the increasing Lorentz force, viscous dissipation, Prandtl number, and Schmidt number. The mathematical model that governs the transport phenomenon presented in this report was reduced to a coupled ordinary differential equations, non-dimensionalized, parameterized, and solved numerically using `bvp4c` solver (MATLAB built-in function). A statistical tool (correlation coefficient) was used to confirm the impact of pertinent parameters on heat and mass transfer rates, and surface drag force. It is worth concluding that magnetic field parameter and Eckert number have significant negative association with heat transfer rate. There is a significant positive association among chemical reaction parameter and mass transfer rate. Fluid temperature ameliorates with larger Eckert number, and surface drag force diminishes with larger magnetic field parameter. Prandtl number minimizes the temperature and escalates the heat transfer rate. Concentration minifies with larger Schmidt number and chemical reaction parameter. Furthermore, it is detected that the fluid concentration gets ameliorated with the raise in the order of chemical reaction.

Keywords Thin needle · Viscous dissipation · Hybrid nanofluid · Eckert number · Correlation coefficient · Magnetic field

✉ I. L. Animasaun
anizakph2007@gmail.com
Venkata Subrahmanyam Sajja
subrahmanyam@kluniversity.in
Revathi Gadamssetty
vsrglm@gmail.com
P. Muthu
muthuatbits@gmail.com
M. Jayachandra Babu
jayamacharla@gmail.com

- ¹ Department of Mathematics, Koneru Lakshmaiah Education Foundation, Vaddeswaram, Guntur, Andhra Pradesh 522502, India
- ² Department of Mathematics, Gokaraju Rangaraju Institute of Engineering and Technology, Bachupally, Hyderabad 500090, India
- ³ Department of Mathematics, National Institute of Technology, Warangal, Telangana 506004, India
- ⁴ Department of Mathematics, S.V.A. Government College, Srikalahasti, Andhra Pradesh 517644, India

1 Background Information

Axisymmetric boundary layer flow and heat transfer process has more importance because of its industrial and technological processes. It is attracted due to various industrial and technological applications like micro-scale cooling devices for heat elimination application, shielded thermocouple for determining the velocity of wind or hot wire anemometer, microstructure electronic devices, etc. One type of axisymmetric flow is thin needles. A thin needle is a slendering object with parabolic revolution and the flow caused by the thin needle is axisymmetric in nature, as the radius of the slendering needle is the same as that of the boundary layers established by the flow. By appropriately varying the radius of the needle, the partial differential boundary layer equations admit similarity solutions, which are more revealing than the direct numerical integration of the partial differential equa-

- ⁵ Department of Mathematical Sciences, Fluid Dynamics and Survey Research Group, Federal University of Technology, PMB 704, Akure, Nigeria

Review

Lavanya Kandikonda, Saranya Jagadeesan*, Ram Subbiah and Abdelkadar Zarrouk

Recent reviews on bio-waste materials for corrosion protection of metals

<https://doi.org/10.1515/correv-2021-0083>

Received October 1, 2021; accepted March 31, 2022;
published online May 23, 2022

Abstract: The present paper is aimed to review the efficiency of eco-friendly, natural and cheap bio-waste materials as corrosion inhibitors on metal surfaces in different corrosive media. Various bio-waste materials are the best substitutes for the synthetic organic, inorganic and polymeric inhibitors. Most of the bio-waste material adsorbed on the metal surface in aqueous medium followed the Langmuir adsorption isotherm. The presence of organic constituents in bio-waste materials is responsible for the protection of metals in aggressive medium. The effectiveness of these bio-waste materials to inhibit metal corrosion is well studied by non-electrochemical methods like weight loss and atomic absorption spectroscopy techniques as well as electrochemical methods like polarization and impedance measurements. Surface studies were studied through SEM, EDS, XRD, AFM and XPS techniques. Computational studies using DFT and MDS were also reported.

Keywords: adsorption; AFM; bio-waste; impedance; polarization; SEM.

1 Introduction

Corrosion is the structural damage of metals and their alloys through chemical or electrochemical interaction

*Corresponding author: **Saranya Jagadeesan**, Department of Humanities and Sciences (Chemistry), Gokaraju Rangaraju Institute of Engineering and Technology, Hyderabad, Telangana 500090, India, E-mail: jcsaranya.chem96@gmail.com

Lavanya Kandikonda, Department of Humanities and Sciences (Chemistry), Gokaraju Rangaraju Institute of Engineering and Technology, Hyderabad, Telangana 500090, India

Ram Subbiah, Department of Mechanical Engineering, Gokaraju Rangaraju Institute of Engineering and Technology, Hyderabad, Telangana 500090, India

Abdelkadar Zarrouk, Department of Chemistry, Laboratory of Materials, Nanotechnology and Environment, Faculty of Sciences, Mohammed V University, P.O. Box 1014, Rabat, Morocco

with the surrounding environment. Various factors like impurities on the metal surface, pressure, temperature, pH (Wang et al. 2018) and conductance of the medium can enhance the metal corrosion rate. Corrosion becomes a global problem due to rapid industrialization, leading to dangerous and expensive damage of various machinery, household materials and various constructions, impacting the environment too (Jacob and Parameswaran 2010), leading to a global economic loss of billions of dollars annually. It may affect the efficiency of machinery, infrastructure assets, the durability of machinery, etc. It sometimes leads to the shutdown of various industries, influencing the economic growth of all the countries. Many countries are spending 1–5% of their GDP (Rani and Basu 2012) on corrosion control/prevention.

Till now, several researchers used several ways to protect a metal from corrosion, such as modification of the design, change of the environment, metallic coatings, cathodic protection, anodic protection, inhibitors, etc. One of the prevalent ways to protect metals such as iron, steel and their alloys are corrosion inhibitors (Kadhim et al. 2021). Corrosion inhibitors can be organic (Jone Kirubavathy et al. 2017; Lavanya et al. 2018; Saranya et al. 2020)/polymers (Eswaramoorthi et al. 2016; Mohamed et al. 2020) out of which organic materials are comparatively efficient inhibitors for different metals in various aggressive media (Dai et al. 2021; Wang et al. 2018, 2021). Corrosion inhibitors (Hashim et al. 2020) can be used for several industrial systems like cooling towers, pipelines, boilers, oil and gas production units, water processing units, refineries, etc.

These compounds prevent metal corrosion by reducing the rate of anodic process or cathodic process, or mixed type (Hanoon et al. 2022). Chromate salts, zinc salts, phosphates, nitrite salts and silicate compounds are often used as corrosion inhibitors. These inorganic substances show a detrimental effect on the environment and impact human health (Wei et al. 2022). These inhibitors play a vital role (Wang et al. 2021) in textile, papermaking, pharmaceutical, electroplating, oil and gas, food, petrochemical and chemical industries

Research Article

Anita Rau Badami's Tamarind Mem – Unveiling of the Diverse Outlooks of Women in India through the Nostalgias of a Mother and a Daughter

Sailaja Eswara ¹, Dr. Joseph Ratna Jayakar T ²

Abstract

The present article explores the changing potentials of women in India through the characters in Tamarind Mem by Anita Rau Badami. Badami slots the novel into two fragments: the first part narrated by Kamini, the daughter of Saroja, and the second by Saroja herself. Through the main protagonists, Saroja and Kamini, Badami envisions the psychological gap between the two generations; and presents how the society subdues the inner conflicts they live in. Saroja camouflaged herself as a traditional wife and stood as the epitome of an ideal woman who encourages her children towards accomplishing their aspirations. After Dadda's death, Kamini and Roopa, her children immigrated to Canada. Kamini lives an independent life but is imprisoned in her memories, whereas Roopa marries and leads her own life. Saroja, who is always immersed in memories, plans to travel and visit places freely. The novel seeks to disclose the misunderstanding that generally occurs between the older and the younger generations.

Keywords: *changing possibilities, psychological gap, inner conflicts, misunderstanding*

¹ Sailaja Eswara, Assistant Professor, Department of Humanities and Sciences, Gokaraju Rangaraju Institute of Engineering and Technology, Hyderabad, India. sailu.eswara@gmail.com

² Dr. Joseph Ratna Jayakar T, Associate Professor, GITAM SCHOOL OF HUMANITIES AND SOCIAL SCIENCES, GITAM (Deemed to be University), Hyderabad, India. jayakar_ani@yahoo.com



Contents lists available at ScienceDirect

Materials Today: Proceedings

journal homepage: www.elsevier.com/locate/matpr

Slow evaporation technique to grow 3 – Amino benzene sulfonic acid single crystal for Non-Linear optical (NLO) transmission

B. Deepa^{a,*}, K. Gayathiridevi^b, M. Kalyan Chakravarthi^c, A. Shajahan^d, B Shanti Sree^e, Mohammed Imran Anees^f, Mohammad Habeeb^g

^a Department of Physics, A.V.V.M. Sripushpam College (Auto), Poondi, Thanjavur 613503, Tamilnadu, India

^b Department of Physics, Government Arts and Science College for Women (Constituent College of Bharathidasan University, Thiruchirappalli), Orathanadu 614625, Tamilnadu, India

^c School of Electronics Engineering, VIT-AP University, Amaravathi 522237, Andhra Pradesh, India

^d Department of Chemistry, Khadir Mohideen College, (Affiliated to Bharathidasan University, Thiruchirappalli), Adirampattinam 614701, Tamilnadu, India

^e Department of Physics, Gokaraju Rangaraju Institute of Engineering and Technology, Hyderabad 500090, Telangana, India

^f Pharmaceutical Chemistry Department, Y.B. Chavan College of Pharmacy, Aurangabad 431001, Maharashtra, India

^g Department of Pharmaceutics, Crescent School of Pharmacy, BS Abdur Rahman Crescent Institute of Science and Technology, Chennai 600048, Tamilnadu, India

ARTICLE INFO

Article history:

Available online xxxx

Keywords:

KDP crystal

Sulfonic crystal

Thermal analysis

Harmonic generation

ABSTRACT

Crystal 3 Amino benzene sulfonic acid single crystal was grown using a slow evaporation process. The functional groups contained in the substances are identified via FT-IR analysis. X-ray diffraction investigation gives type of crystal. The dielectric behaviour of generated crystal was investigated at various frequencies and temperatures. The Kurtz powder second harmonic generation exhibits material behaviour of second harmonic generation and has an efficiency of 0.55 times that of KDP, making it ideally suited for non-linear optical (NLO) transmission.

Copyright © 2022 Elsevier Ltd. All rights reserved.

Selection and peer-review under responsibility of the scientific committee of the International Conference on Design, Manufacturing and Materials Engineering.

1. Introduction

Nonlinear theories in optical studies are essential in materials science, and numerous research organizations have been researching their use in everyday life all around the world. The precise focusing of novel NLO materials and their important applications are a limit for frequency vibration in lasers, optical communication, optical frequency doubling, optical switching, optical data storage, and other fields [1,2]. Optical measuring, High-density optical recording, laser printing, and other applications, require optical materials with efficient second-harmonic generation (SHG) at short wavelengths [3,4].

Although several organic SHG materials have been explored in inorganic materials, only a few have been used in SHG devices [5,6]. The trade-off between transparency and efficiency, as well as underdeveloped crystal-processing technologies and limited expertise in high-quality crystal formation, remain practical drawbacks of organic materials [7,8,9]. Several transparent materials have recently been investigated for use in bulk and waveguide

SHG devices. Stable crystals enhanced in physical and chemical properties are required for the device processing, with notable properties such as high optical susceptibilities, higher damageable laser threshold resistance, constant thermal and mechanical behavior [10,11]. Typically, an organic crystal composed of highly polarizable molecules that are conjugated molecules in which highly delocalized electrons can easily flow between electron donor and acceptor groups on the molecule's opposite side, causing a molecular charge transfer [12,13]. Amino aromatic benzene derivatives are attractive materials in the field of optoelectronic applications. 3-Aminobenzenesulfonic acid (3ABSA), refer as m-sulfanilic acid, and metanilic acid (C₆H₇NO₃S), is a zwitterionic substance (1) that is often employed as a reagent in the production of azo colors and some sulfa medicines [14,15]. The zwitterion which may be produced strong hydrogen bond and close packing of [16]. Its ability to render normally water-insoluble chemicals soluble has led to a extensive variety of uses in dyes, detergents, and engine protection oil additives. It has lately been utilized in the production of copolymers. In addition, the 3- ABSA used in the field of optical communication, optical data storage and also fabrication of synthetic dyes, medicine and glucose biosensor [17]. The extensive literature survives reported only the X-ray

* Corresponding author.

E-mail address: bd14avvm@gmail.com (B. Deepa).



Analysis of Markovian queueing system with server failures, N-policy and second optional service

Roma Rani Das^{a,*}, V.N. Rama Devi^b, Abhishek Rathore^c, K. Chandan^d

^aDepartment of Statistics, Acharya Nagarjuna University, Guntur and Data Curator (SBDM), ICRISAT, Hyderabad, India

^bGRIET, Hyderabad, India

^cTheme Leader and Principal Scientist (SBDM), ICRISAT, Hyderabad, India

^dAcharya Nagarjuna University, Guntur, India

(Communicated by Madjid Eshaghi Gordji)

Abstract

The current work details the behaviour of a finite Markovian queueing system with a vacation in which the server may face problems of breakdowns while in service. The repair process does start immediately after a breakdown which immediately resumes the service. During this period any new customer is allowed to join the system. Whenever the server finds nobody, the server goes on vacation and resumes service after N customers are accumulated. Meanwhile, it triggers pre-service called start-up. Further, we considered two types of repair facilities for the broken-down server with an optional probability. The server first provides essential service to all customers and the second optional service will be provided with a probability of “p”. The customer may renege in the first phase of service. We adopted Runge-Kutta Method to find Transient state probabilities and computed various performance indices like the expected length of the system, the mean waiting time etc. We then performed the sensitivity analysis to explore the effect of different parameters.

Keywords: N-Policy, Second optional service, Start-up, Two types of repair facilities.

1. Introduction

Queuing theory is a tool of Operations Research to understand the dynamic pattern of the processes as well as for the performance evaluation of such systems. Recent eras have seen an increasing attention in queueing models due to their wide applications.

*Corresponding author

Email addresses: r.das@cgiar.org (Roma Rani Das), ramadevivr@gmail.com (V.N. Rama Devi), a.rathore@cgiar.org (Abhishek Rathore), kotagirichandan@gmail.com (K. Chandan)

Received: September 2021 Accepted: December 2021

“An analysis on the penetration of EV’s in Indian market”

Dr.D. Indira¹, Dr.M Chitra, Yerra SSV Pranay Kumar³, Narayani Alekhya Mantha⁴, and Shashidhar Reddy Narra⁵

¹Professor, Department of Humanities & Sciences, indiradendukuri@gmail.com, Gokaraju Rangaraju Institute of Engineering and Technology

²Associate Professor, School of Entrepreneurship, chitra.m@rishihood.edu.in, Rishihood University, Sonipat, Haryana

³Scholar, Department of Computer Science and Engineering, pranay.off09@gmail.com, Gokaraju Rangaraju Institute of Engineering and Technology

⁴Scholar, Department of Computer Science and Engineering, alekhyarevanth0416@gmail.com, Gokaraju Rangaraju Institute of Engineering and Technology

⁵Scholar, Department of Civil Engineering, nshashidharreddy44@gmail.com, Gokaraju Rangaraju Institute of Engineering and Technology

Abstract

The primary objective of this study has been to explore the requirement and future prospects of Electric Vehicles in the Indian market. It is to identify the developments that have been taking place in this field across the globe as well as in India. It is to assess the costs and benefits associated with electric vehicles as a transportation mode. It is a descriptive study based on the review of various articles researched in this field. It has been identified that in India the penetration of electric vehicles is considerably low and there is an immense potential for the growth of EV's in the coming years. The key factors that drive the growth have been identified in our study on electric vehicles. These results suggest that there is a need from the government side to develop an ecosystem that will fuel the growth of Electric vehicles as a whole.

Keywords:

Electric Vehicles, Renewable Energy, Costs and Benefits, Environment Friendly, Sustainable Energy.

Introduction:

Electric vehicles are playing a pivotal role in the midst of the world struggling with high carbon emissions and the threat of global warming. [2] Research also has validated this point that Ev's help in protecting the environment. A lot of Research and Development has been taking place in this field. The benefits of EVs are that they are far more effective when compared to combustion engines. They do not waste much energy when compared with traditional engines. The usage of Ev's will have a profound influence on the quality of air, with the

awareness of ecological balance and sustainability there is a significant increase in the worldwide registrations of Electric vehicles in the year 2020, and the same is estimated to grow in the coming decade as well. In fact, one of the interesting points to note is that during this pandemic, although there was a downfall in the sales of regular automobiles, in the case of Electric vehicles an increase in the registration was witnessed in 2020. It is also a positive sign that during this pandemic there was a phenomenal increase in the demand for electric vehicles. In this scenario, we put forth exploring the cost-benefits of electric vehicles as a sustainable energy source [10]

Literature Review

The present study has taken its roots from the various research carried over in this field Stephen Eaves in his

Research Article

Effect of Nano Ground Granulated Blast Furnace Slag (GGBS) Volume % on Mechanical Behaviour of High-Performance Sustainable Concrete

Seelam Srikanth ¹, Chunchu Bala Rama Krishna ¹, T. Srikanth,² K. J. N. Sai Nitesh,³ V. Swamy Nadh,⁴ Sanjeev Kumar,⁵ and Subash Thanappan ⁶

¹School of Civil Engineering, REVA University, Bangalore, India

²Department of Civil Engineering, Gokaraju Rangaraju Institute of Engineering and Technology, Hyderabad, India

³Department of Civil Engineering, Anurag University, Hyderabad, India

⁴Aditya College of Engineering, Affiliated to JNTUK, Surampalem, Andhra Pradesh, India

⁵Department of Civil Engineering, Graphic Era Deemed to be University, Bell Road, Clement Town, 248002 Dehradun, Uttarakhand, India

⁶Department of Civil Engineering, Ambo University, Ambo, Ethiopia

Correspondence should be addressed to Chunchu Bala Rama Krishna; chunchubalarama.krishna@reva.edu.in and Subash Thanappan; thanappansubash@gmail.com

Received 6 February 2022; Accepted 12 April 2022; Published 27 April 2022

Academic Editor: Lakshmiopathy R

Copyright © 2022 Seelam Srikanth et al. This is an open access article distributed under the Creative Commons Attribution License, which permits unrestricted use, distribution, and reproduction in any medium, provided the original work is properly cited.

Utilization of various mineral admixtures in producing mortar decreases the porosity and capillarity, hence improves the durability in opposition to water and competitive solutions. In this research work, Ground Granulated Blast Furnace Slag is used to replace 30 percent, 60 percent, and 70% of ordinary Portland cement (OPC) (GGBFS). Mechanical property (compressive strength) and durability properties (permeability, porosity, and sorptivity) of high-performance concrete (HPC) are tested. Water permeability of M85 is measured using three cell permeability apparatus. Compressive strength, porosity, and sorptivity of the same mixes are also found. According to the test results of HPC, 30% replacement level of GGBFS gives higher compressive strength than 60% and 70% replacement levels of GGBFS. An equation is developed for permeability of HPC based on mechanical strength and porosity. It is found that coefficient of permeability of water for HPC mixes ranges from 5.1×10^{-11} cm/sec to 7.8×10^{-11} cm/sec. It is concluded that 30% GGBFS used in HPC produces less porosity, less permeability, and less sorptivity than compared to other replacement levels.

1. Introduction

Excessive performance concrete (HPC) is a brand new magnificence of concrete that has evolved in latest decades. HPC has a low water content and can attain sufficient rheological properties by combining optimal granular packing with the addition of excessive-range water lowering admixtures. One primary high-quality best within the making of HPC is the virtual elimination of voids within the concrete matrix that generate deterioration. Therefore, HPC has a tendency to exhibit superior residences such as superior energy, dura-

bility, and lengthy-time period balance. In competitive contexts, the long-term durability of concrete systems is always a concern to consider. When it comes to structures that are continually in contact with water, such as offshore systems, parking decks, and dams, water penetration is the most important aspect that determines the structure's durability. As a result, the permeability of the concrete and its pore architecture are crucial to its long-term endurance. Supplementary cementitious materials in high-performance concrete showed excellent performance in durability [1]. Chakraborty et al. [2] reported concrete developed with

NANO GGBS produces a cohesive mix that reduces the permeability. Cheah and Chow [3] reported the replacement of cement by NANO GGBS improved the capillary penetration resistance of concrete significantly. Due to insufficient Ca (OH)₂ from cement hydration, NANO GGBS produces high amount of secondary C-S-H and C-A-S-H bonds that reduced both micro and macro pores in concrete. Therefore, an optimum performance was observed in tests of porosity, permeability, water absorption, and capillary absorption. It was reported concrete with NANO GGBS exhibited high resistance to ingress of chloride ions. Upon 80% or above replacement of NANO GGBS, compressive strength was greatly decreased [4]. Xie et al. [5] reported geo-polymer concrete developed with high amount of NANO GGBS exhibited decrease. Even after sulphate exposure during acid evaluations, there was less mass loss and a larger residual compressive electricity. As the amount of NANO GGBS in the diet grows, so does the sulphate resistance. Based on the findings of this literature review, it was discovered that there has been little research done on high-performance concrete made with large amounts of NANO GGBS. As a result, the primary goal of this project is to investigate the mechanical and durability properties of HPC for the desired concrete mixes developed with high volumes of NANO GGBS.

2. Experimental Studies

2.1. Ingredients of HPC. The cement used was Ordinary Portland Cement (OPC) 53 Grade having a specific gravity of 3.01. Effect of high volumes of NANO GGBS on strength and durability of high-performance concrete uses locally accessible river sand that conforms to grading zone II.

IS: 383–1970 [6] was used. The sand was screened at site to remove deleterious materials. Locally available coarse aggregate (12.5 mm) from quarry was used. Specific gravities of the coarse and fine aggregates have a density of 2.71 and 2.65, respectively. GGBFS (Ground Granulated Blast Furnace Slag) is a type of slag that comes from a blast furnace. Astrra chemicals, a local manufacturer company in India, was collected. Chemical properties were studied and compared to cement since being replaced as shown in Table 1. Super plasticizer GLENIUM B233, a modified polycarboxylic ether having pH ≥ 6 , was used.

2.2. Mix Design and Methodology. Methodology as shown in Figure 1 is followed in this research work. Concrete cubes of size 15 cm³ were kept in curing for 28 days to test permeability and sorption characteristics and also to determine strength as explained in methodology. Mix design procedure according to modified ACI method (Aitcin Method [7]) was followed and proportion is as shown in Table 2. In this mix, 30%, 60%, and 70% cement turned into changed by floor Granulated Blast Furnace Slag, retaining W/B ratio equal and the mix design named as GGBFS-30%, GGBFS-60%, and GGBFS-70% shown in Table 3. Formation of calcium silicate hydrate gel is the most important parameter in the concrete. The effect of maximum percentage of NANO GGBS may lead to less compressive strength in concrete.

TABLE 1: Chemical properties of mineral admixture.

Compound	Cement	GGBFS
SiO ₂	23.1	35.34
Al ₂ O ₃	4.51	11.59
Fe ₂ O ₃	2.5	0.35
CaO	63.3	41.99
MgO	1.0	8.04
Alkalies	0.88	0.94
SO ₃	1.3	1.3
Loss on ignition	2.41	0.45

2.3. Mixing and Specimen Testing Procedure. Mixing was performed in a concrete mixer gadget. Coarse aggregates, great aggregates, cement, and admixtures have been introduced to the mixer device and allowed to combine for 1 minute. Super-plasticizer was blended with the total water and then 50 percentage of water added to the mixture machine and allowed to mix for 2 minutes. Then, remaining 50 percentage of water poured in mixture machine and continued to mix for 2 minutes. Total mixing time was 5 minutes. Mixes were tried with varied mixing proportions and finally the proportion which gives the best results in terms of consistency and strength was selected. After demolding, the specimens had been saved for 28 days in curing water tank before testing. Dried specimens were examined for compressive electricity, porosity, permeability, and sorptivity. Compressive electricity takes a look at turned into carried out conforming to IS: 516 [8] on dice specimens of size one hundred mm \times a hundred mm \times a hundred mm. Permeability of 150 mm cube specimens and porosity of 100 mm cube specimens were calculated according to IS: 3085–1965 [9] and ASTM C642 [10], respectively. Sorptivity test of 100 mm cube specimens was carried out based on Taywood engineering (1993).

3. Results and Elobarations

3.1. Mechanical Strength. Compressive strength reduced with an addition of high volume of NANO GGBS as shown in Figure 2 and this reduction may be due to slower hydration rate and prolonged pozzolanic reaction [11]. Maximum compressive strength of 96.4 MPa at 28 days is found for the HPC specimens replaced with 30%. Table 4 shows the compressive strength of HPC concrete of GGBFS in Normal water curing. It is observed that performance of 30% replacement is almost similar to 0% replacement. This is due to the increase in the percentage of NANO GGBS in the mix design. Quantity of NANO GGBS decreases the quantity of gel formation.

3.2. Permeability. High volumes of NANO GGBS seriously affect durability. Permeability reduction is predominant at high NANO GGBS content [12]. As shown in Figure 3, permeability of HPC based on compressive power is expected. In comparison to GGBFS with a 30% substitution level, it has a low permeability value (3.2×10^{-11} cm/sec). It is

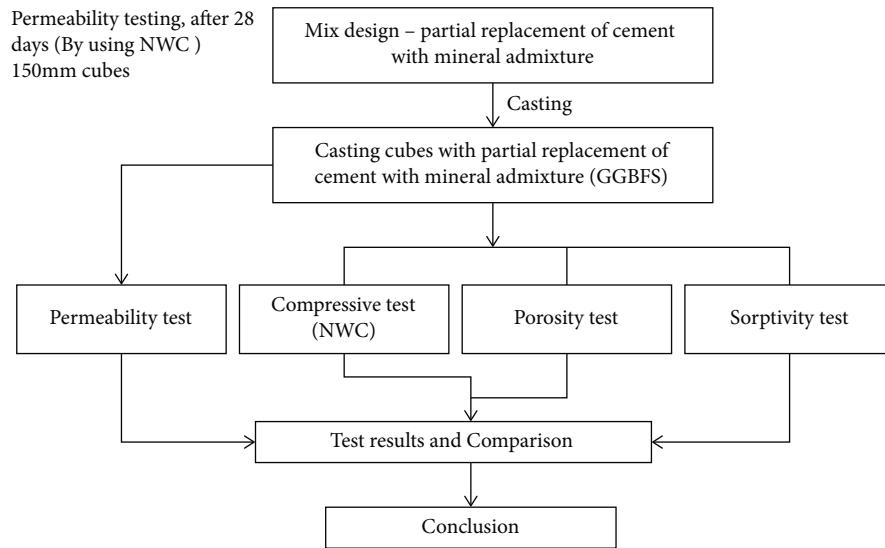


FIGURE 1: Methodology followed for testing HPC.

TABLE 2: Mix proportions for M80 grade concrete (Aitcin Method) were as mentioned.

W	C	FA	CA	SP
140	560	710.2	1075	5.7

TABLE 3: Mix design details of NANO GGBS.

Components	Replacement levels of NANO GGBS		
	GGBFS-30%	GGBFS-60%	GGBFS-70%
Water (lit.)	150.79	150.79	150.79
Cement (kg)	392	224	168
GGBFS (kg)	168	336	392
Coarse aggregate (kg)	1075	1075	1075
Fine aggregate (kg)	710.2	710.2	710.2
Super plasticizer (lit.)	5.503	5.503	5.503

TABLE 4: Compressive strength of HPC concrete at 28th day for various dosages of GGBFS.

Type of specimen	28th day compressive strength in N/mm ² (NWC)
0% GGBFS	97.375
30% GGBFS	96.4
60% GGBFS	82.34
70% GGBFS	73.5

observed 30% NANO GGBS exhibited promising performance amongst all concrete mixtures tested. NANO GGBS refines capillaries and hence dense structure of micro-pores is responsible for absorption.

$ok = A(fck)^2 + B(fck) + C$, where k and fck are the permeability (150 mm dice) and compressive energy (100 mm die) of concrete, respectively. The coefficients A , B , and C are obtained from the regression analysis [13].

The relationship between permeability and compressive power of concrete has been shown in parent four by way of employing NWC for GGBFS alternate levels [14]. From parent four, it was discovered that there was a significant association between permeability and concrete compressive strength, resulting in a regression coefficient (R^2) of zero. Permeability and compressive strength is shown in Figure 4.

3.3. *Porosity.* HPC was tested for porosity with various mineral admixtures (GGBFS). Table 5 shows the porosity results for the specimens that were tested [15]. GGBS gives more porous as this size is higher than the cement particles. That the reason we used NANO GGBS for better strength in the concrete. When compared to other replacements, GGBFS with 30% replacement level has a low porosity value (1.42 percent). To calculate the permeability of HPC using the porosity data provided in Figure 5 is sufficiently accurate [16].

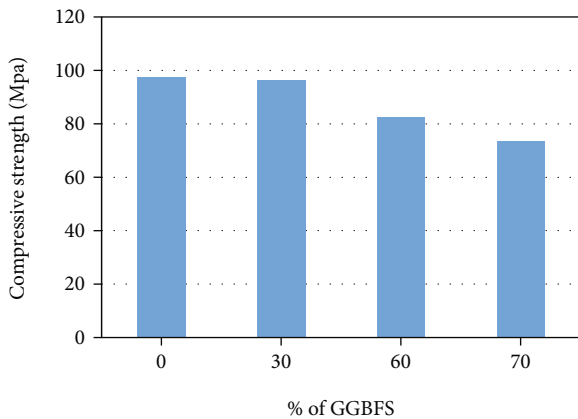


FIGURE 2: Variation of compressive strength at 28 days curing period.

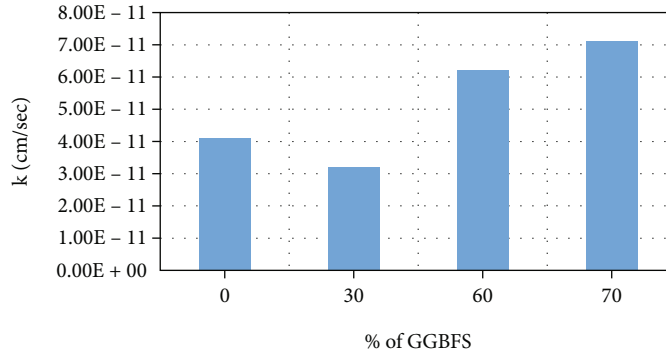


FIGURE 3: Variation of permeability at 28 days age.

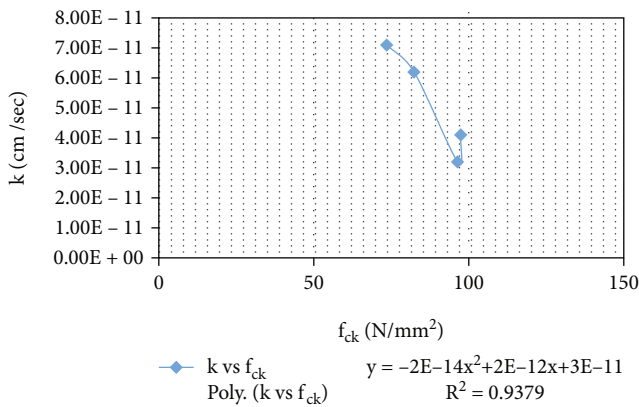


FIGURE 4: Permeability vs compressive strength.

TABLE 5: Porosity of HPC.

Mix	Porosity (%)
0% - GGBFS	1.65
30% - GGBFS	1.42
60% - GGBFS	2.08
70% - GGBFS	2.47

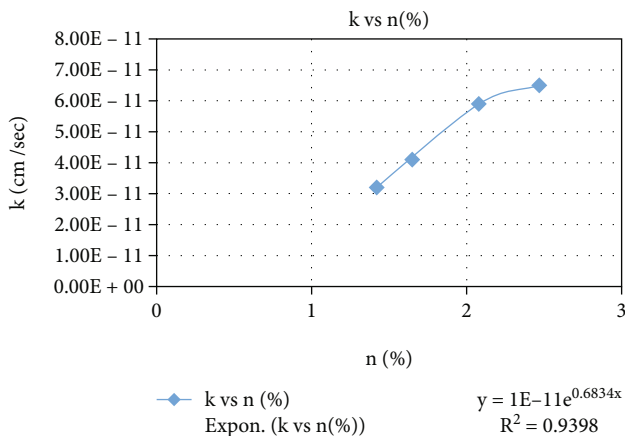


FIGURE 5: k vs n for GGBFS replacement levels.

TABLE 6: Sorptivity of HPC.

Mix	Sorptivity (m/√s) × 10 ⁻⁶	
	30 minutes	60 minutes
0% - GGBFS	1.68	1.95
30% - GGBFS	1.99	2.33
60% - GGBFS	2.13	2.6
70% - GGBFS	2.17	2.8

TABLE 7: Quality of concrete suggested by Taywood Engineering.

Concrete quality	Sorptivity (m/s ^{1/2}) × 10 ⁻⁴
Good	0.13
Acceptable	0.13 to 0.26
Poor	>0.26

Correlation between permeability and porosity

$k = A e^{Bn}$, where 'k' represents the concrete's permeability (150 mm cubes) and 'n' represents the concrete's porosity (100 mm cubes).

The coefficients A and B are the results of the regression analysis. For GGBFS replacements, a study of permeability vs porosity was conducted. Because of the significant association between permeability and porosity of the concrete shown in Figure 5, regression analysis yielded a correlation coefficient (R^2) of 0.939 [17].

3.4. Sorptivity. The test for sorptivity was conducted on 100 mm cubes [18]. Cubes were placed in a hot air oven at a temperature of 105°C up to which constant mass is obtained at an interval of time [19] and the weight was noted [20]. Then, the specimen is immersed in water for different interval of time (30 and 60 minutes), till the constant mass was obtained and it was noted. After 28 days of curing, all replacement levels of admixtures show less sorptivity as given in Table 6. 30-GGBFS replacement shows less value of sorptivity in 28 days curing. The obtained sorptivity values of HPC were in acceptable range according to Taywood engineering limits as given in Table 7.

4. Conclusions

NANO GGBS in high-performance concrete has exhibited promising performance in durability characteristics at 30% replacement compared to other concrete mixes. High volumes of NANO GGBS seriously affect durability. Permeability reduction is predominant at high NANO GGBS content. It is observed 0% NANO GGBS exhibited lower performance amongst all concrete mixtures tested. Compressive strength reduces with an increment in NANO GGBS content for cement replacement. However, 30% NANO GGBS concrete mix has mere performance to ordinary concrete. Both porosity and water absorption declined at 30% and increased at further replacements. Sorptivity values were in acceptable range and surface absorption increased due to NANO GGBS in concrete. It is necessary to evaluate the impact of twofold blending on HPC permeability and diffusivity.

Data Availability

The data used to support the findings of this study are included within the article. Should further data or information be required, these are available from the corresponding author upon request.

Conflicts of Interest

The authors declare that there are no conflicts of interest regarding the publication of this paper.

Acknowledgments

The authors thank REVA University and Aditya College of Engineering and Technology, Surampalem, for the technical assistance. The authors appreciate the support from Ambo University, Ethiopia.

References

- [1] S. Morino, "Recent developments on concrete-filled steel tube members in Japan," in *Composite Construction in Steel and Concrete*, vol. 4, pp. 644–655, Amsterdam, Netherlands, 2002.
- [2] S. Praburanganathan, N. Sudharsan, Y. B. S. Reddy, C. N. D. K. Reddy, L. Natrayan, and P. Paramasivam, "Force-deformation study on glass fiber reinforced concrete slab incorporating waste paper," *Advances in Civil Engineering*, vol. 2022, Article ID 5343128, 2022.
- [3] P. Sureshkumar, T. Jagadeesha, L. Natrayan, M. Ravichadran, D. Veeman, and S. M. Muthu, "Electrochemical corrosion and tribological behaviour of AA6063/Si₃N₄/Cu(NO₃)₂ composite processed using single-pass ECAP_A route with 120° die angle," *Journal of Materials Research and Technology*, vol. 16, pp. 715–733, 2022.
- [4] M. Udayakumar, S. Aravindan, and K. Rajkumar, "Experimental investigation of concrete-filled single-skin and double-skin steel oval hollow section stub columns," *Journal of Constructional Steel Research*, vol. 224, pp. 106–122, 2017.
- [5] K. Hemalatha, C. James, L. Natrayan, and V. Swamynadh, "Analysis of RCC T-beam and prestressed concrete box girder bridges super structure under different span conditions," *Materials Today: Proceedings*, vol. 37, no. 2, pp. 1507–1516, 2021.
- [6] F. X. Ding, D. R. Lu, Y. Bai et al., "Behaviour of CFRP-confined concrete-filled circular steel tube stub columns under axial loading," *Thin-Walled Structures*, vol. 125, pp. 107–118, 2018.
- [7] A. Merneedi, L. Natrayan, S. Kaliappan et al., "Experimental investigation on mechanical properties of carbon nanotube-reinforced epoxy composites for automobile application," *Journal of Nanomaterials*, vol. 2021, 7 pages, 2021.
- [8] J. Wang, Q. Shen, F. Wang, and W. Wang, "Experimental and analytical studies on CFRP strengthened circular thin-walled CFST stub columns under eccentric compression," *Thin-Walled Structures*, vol. 127, pp. 102–119, 2018.
- [9] S. Yogeshwaran, L. Natrayan, S. Rajaraman, S. Parthasarathi, and S. Nestro, "Experimental investigation on mechanical properties of epoxy/graphene/fish scale and fermented spinach hybrid bio composite by hand lay-up technique," *Materials Today: Proceedings*, vol. 37, no. 2, pp. 1578–1583, 2021.
- [10] R. S. Bhatia and K. Kudlipsingh, "The road to docker: a survey," *International Journal of Advanced Research in Computer Science*, vol. 8, no. 8, pp. 83–87, 2017.
- [11] F. Zhou and B. Young, "Tests of concrete-filled aluminum stub columns," *Thin-Walled Structures*, vol. 46, no. 6, pp. 573–583, 2008.
- [12] S. Yogeshwaran, L. Natrayan, G. Udhayakumar, G. Godwin, and L. Yuvaraj, "Effect of waste tyre particles reinforcement on mechanical properties of jute and abaca fiber-epoxy hybrid composites with pre-treatment," *Materials Today: Proceedings*, vol. 37, no. 2, pp. 1377–1380, 2021.
- [13] Q.-X. Ren, L.-H. Han, D. Lam, and C. Hou, "Experiments on special-shaped CFST stub columns under axial compression," *Journal of Constructional Steel Research*, vol. 98, pp. 123–133, 2014.
- [14] R. Suryanarayanan, V. G. Sridhar, L. Natrayan et al., "Improvement on mechanical properties of submerged friction stir joining of dissimilar tailor welded aluminum blanks," *Advances in Materials Science and Engineering*, vol. 2021, 6 pages, 2021.
- [15] Q. Wang, Q. Shi, E. M. Lui, and Z. Xu, "Axial compressive behavior of reactive powder concrete-filled circular steel tube stub columns," *Journal of Constructional Steel Research*, vol. 153, pp. 42–54, 2019.
- [16] L. Natrayan, A. Merneedi, G. Bharathiraja, S. Kaliappan, D. Veeman, and P. Murugan, "Processing and characterization of carbon nanofibre composites for automotive applications," *Journal of Nanomaterials*, vol. 2021, 7 pages, 2021.
- [17] Y. Geng, Y. Wang, and J. Chen, "Time-dependent behavior of recycled aggregate concrete-filled steel tubular columns," *Journal of Structural Engineering*, vol. 141, no. 10, article 04015011, 2015.
- [18] N. D. K. R. Chukka, L. Natrayan, and W. D. Mammo, "Seismic fragility and life cycle cost analysis of reinforced concrete structures with a hybrid damper," *Advances in Civil Engineering*, vol. 2021, 17 pages, 2021.
- [19] L. Natrayan and A. Merneedi, "Experimental investigation on wear behaviour of bio-waste reinforced fusion fiber composite laminate under various conditions," *Materials Today: Proceedings*, vol. 37, no. 2, pp. 1486–1490, 2021.
- [20] P. Manikandan, L. Natrayan, S. Duraimurugan, and V. Vasugi, "Influence of waste glass powder as an aluminosilicate precursor in synthesizing ternary blended alkali-activated binder," *Silicon*, vol. 15, pp. 1–10, 2022.

Cite this article

Lavanya C and Kumar ND (2022)
Effect of lime-stabilised copper slag cushion on swelling behaviour of highly plastic clay.
Geotechnical Research 9(1): 15–22,
<https://doi.org/10.1680/jgere.21.00006a>

Research Article

Paper 2100006a
Received 14/03/2021; Accepted 20/09/2021
Published online 29/10/2021
Published with permission by the ICE under the
CC-BY 4.0 license.
(<http://creativecommons.org/licenses/by/4.0/>)

Effect of lime-stabilised copper slag cushion on swelling behaviour of highly plastic clay

C. Lavanya PhD

Professor, Department of Civil Engineering, Gokaraju Rangaraju Institute of Engineering and Technology, Hyderabad, India

N. D. Kumar PhD

Assistant Professor and Head of the Department, Department of Civil Engineering, Jawaharlal Nehru Technological University Hyderabad College of Engineering Manthani, Peddapalli, India (corresponding author: ndkjntu@gmail.com)

Clay soil is prone to seasonal volume change due to variation in water content. The use of waste materials in civil engineering, especially in road construction, has been in vogue all over the world due to the development of road infrastructure. Copper slag is one such waste material available abundantly from the copper industry in India. This paper discusses the heave and swelling of copper slag-cushioned clayey subgrade prepared in a model test tank. The results revealed that the methodology adopted is effective in reducing the swelling of clay. The thickness ratios of the stabilised copper slag cushion and clayey subgrade bed adopted are 0.25, 0.5, 0.75 and 1.0. The copper slag cushion is stabilised with lime content varying from 2 to 10%. A reduction in heave of clayey soil subgrade bed is observed with an increase in the percentage of lime and the thickness of the copper slag cushion. For a cushion-clay soil subgrade thickness ratio $h_c/h_s = 1$, the reduction in the heave of a clayey subgrade bed is 84.4%. The swell potential observed from the present study follows well the trend obtained from the rectangular hyperbolic model.

Keywords: copper slag/cushion/expansive soil/heave/lime/stabilization/swelling potential

Notation

a, b	constants
h_c	thicknesses of lime-stabilised copper slag
h_s	thickness of expansive soil bed
S	amount of swell
T	time

1. Introduction

Swelling soils cause enormous damage to the buildings and pavements. Swelling soils are problematic because the clay mineral constituent which is present in them makes them exhibit shrink and swell behaviour. The shrink-swell behaviour makes the expansive soils unsuitable for construction directly in their natural form (Ikeagwuani and Nwonu, 2019). Expansive soils contain minerals such as clays that are capable of absorbing water. Since change in moisture content leads to swelling and shrinkage, it causes distress in structures; hence, it is mandatory to opt for suitable foundation/stabilisation techniques on these soils to avoid damages to buildings and road pavements due to distress.

Sharma *et al.* (2008) presented that the amounts of rice husk ash (RHA), lime and calcium chloride that were varied from 0 to 16%, 0 to 5%, and 0 to 2%, respectively, by the dry weight of soil, affected the unconfined compression strength (UCS) and California bearing ratio (CBR) of expansive clay. The stress-strain behaviour of expansive clay improved upon the addition of up to 5% lime or up to 1% calcium chloride. A maximum improvement in failure stress of 225 and 328% was observed at 4% lime and 1% calcium chloride, respectively. It was further concluded that the RHA content of 12% was found to be the optimum regarding both UCS and CBR in the presence of either lime or calcium chloride. The optimum dosages reported were 4% and 1% with respect to lime and calcium chloride even in clay-RHA mixes.

Kalkan (2011) studied the effects of wetting and drying cycles on the swelling behaviour of silica fume-modified expansive clayey soils and reported that the silica fume decreases the progressive deformation of modified expansive clayey soils.

The potential of copper slag as a replacement for fine aggregates in bituminous mixes can be a viable option. The mixture of copper slag, fly ash and soil has the potential for use in embankment, sub-base, base and wearing courses of road pavements (Havanagi *et al.*, 2007). The geotechnical properties of copper slag are like those obtained for medium sands; hence, copper slag can be used as a construction material in place of sand, as the backfill of retaining walls and as a fill material in embankment construction. Visser (2007) presented that sometimes, traditional laboratory tests are not able to predict the performance of these materials satisfactorily. Sometimes, conducting trial tests in the laboratory and field is important to identify a suitable stabiliser.

The favourable physico-mechanical characteristics of copper slag mean it can be utilised to make products like cement, fill, ballast, abrasive, aggregate, roofing granules, glass and tiles, apart from recovering the valuable metals by various extractive metallurgical routes (Bipra *et al.*, 2003). Copper slag is a non-plastic material, which has better compaction characteristics than sand, and its permeability is similar to that of sand. The material has a friction angle close to that of well-graded sand, and its use as backfill reduces the active lateral pressure on retaining walls (Dhir *et al.*, 2017). Deviator stress at failure and the elastic modulus of the slag/fly ash/dolime mixes are much greater than those of the wet mix macadam (WMM) (Patel and Shahu, 2017). A mix of 20% fly ash and 80% copper slag stabilised with 15% dolime gave optimum percentage for use in the base course of flexible pavements (Shahu *et al.*, 2013).

Copper slag specimens having 9% cement content and cured for a period of 28 days resulted in maximum compressive strength and tensile strength. Copper slag and fly ash when mixed in optimum proportions and stabilised with 6 and 9% cement can be effectively used as granular material in the sub-base and base layer of road pavement (Raj *et al.*, 2018). Copper slag can be used as a stabilising material for the improvement of problematic soils in embankments, pavement sub-grades and sub-bases. According to Katti (1979), an expansive soil, on saturation, helps arrest the heave below a depth of 1.0–1.2 m, due to the development of cementitious bonds in the soil. Copper slag when mixed with lime or cement can result in added advantage to stabilise expansive clay effectively (Lavanya *et al.*, 2014, 2017). Rao *et al.* (2008) reported that the fly ash cushion stabilised with 10% cement with thickness equal to that of the expansive soil bed had reduced heave by 75% in the first cycle, and with subsequent swell–shrink cycles, the performance further improved in arresting the heave. The experimental investigation and results are discussed in the following sections.

2. Experimental investigation

2.1 Tests conducted

The laboratory tests are conducted on the untreated and treated soil according to the standard test procedures presented in the Indian standard (IS) code of practices, and they are presented in Table 1.

2.2 Materials used

2.2.1 Expansive soil

Expansive clay soils are commonly found in the Telangana districts of India. Expansive clay used in the present study was collected from the Gundala Mandalam in the Telangana state of India. The soil collected was initially air-dried, and then the clay lumps were pulverised using a wooden mallet and sieved through a 20 mm sized sieve. Before using the clay soil sample for testing, it was kept in an oven for drying. Initially, the basic tests were conducted on a clay sample, and the basic properties of clay are presented in Table 2. The clay sample plasticity index is 40%, and its free swell index (FSI) value is 220%. The percentage of fine sand fraction present in the soil was 63.

Table 1. Tests conducted and their respective codes

Name of the test	IS code of practice
Grain size analysis	IS: 2720 (Part IV) (BIS, 1985a)
Liquid limit and plastic limit	IS: 2720 (Part V) (BIS, 1985b)
IS light compaction/standard compaction	IS: 2720 (Part VII) (BIS, 1980)
Free swell index	IS: 2720 (Part XXX) (BIS, 1977)
California bearing ratio	IS: 2720 (Part XVI) (BIS, 1987)
Coefficient of permeability	IS: 2720 (Part XVII) (BIS, 1986)

IS, Indian standard

Table 2. Basic properties of soil

Property	Value
Grain size analysis	
Gravel: %	4
Sand: %	33
Silt and clay: %	63
Consistency limits	
Liquid limit: %	75
Plastic limit: %	35
Plasticity index	40
IS classification	CH
Free swell index: %	220
Degree of expansiveness	Very high
Maximum dry density: kN/m ³	14
Optimum moisture content: %	21
California bearing ratio: %	1
Coefficient of permeability, <i>k</i> : cm/s	0.53×10^{-7}

2.2.2 Copper slag

The copper slag used in the present study was collected from the Sterilite Industries, Tuticorin, Tamil Nadu state, India. The physical properties and chemical composition of the copper slag are presented in Table 3 and Table 4, respectively. Copper slag

Table 3. Physical properties of copper slag

Property	Value
Grain size analysis	
Gravel size: %	1.00
Sand size: %	98.9
Silt and clay sizes: %	0.05
Hardness on Moh's scale	6.5–7.0
Specific gravity	3.6
Plasticity index	Non-plastic
Swelling index	Non-swelling
Granule shape	Angular with sharp edges
Maximum dry density: kN/m ³	23.5
Optimum moisture content: %	6
Direct shear test	
Cohesion: kN/m ²	0
Angle of internal friction: °	40
Coefficient of permeability, <i>k</i>	1.54×10^{-2} cm/s
CBR: %	3.5

CBR, California bearing ratio

(Courtesy: Sterilite Industries Ltd, Tuticorin, Tamil Nadu, India)

Table 4. Chemical composition of copper slag

Compound	% by weight
Iron oxide	55–60
Silica	28–30
Aluminium oxide	1–3
Calcium oxide	3–5
Magnesium oxide	1.0–1.5

(Courtesy: Sterilite Industries Ltd, Tuticorin, Tamil Nadu, India)

has a 99% fine sand fraction. The specific gravity of copper slag is 3.6, and its hardness found on Moh's scale is in the range of 6.5 to 7. The maximum dry unit weight of copper slag is 23.5 kN/m³. The iron oxide and silica mineral compositions are predominant in the copper slag.

2.2.3 Lime

Lime is used as an admixture in the study and was obtained from the local market. The hydrated lime obtained has 95% of calcium hydroxide (CaO).

2.3 Sample preparation in model test tank

In this test set-up, galvanised iron cylindrical tanks of size 280 mm dia. and 400 mm height are used. The cylindrical test tank is initially filled with a 15 mm thick sand layer at the bottom and levelled. A 250 mm dia. and 350 mm high thin casing pipe is placed in the cylindrical test tank. Expansive clay soil which was mixed thoroughly at its optimum moisture content is taken and compacted inside the casing in three layers. Each layer of 50 mm thickness, the overall thickness of the clay bed being 150 mm, is compacted to the maximum dry unit weight in the cylindrical test tank within the casing pipe. The expansive clay bed thickness is referred to as h_s throughout the paper. Fine-to-medium sand is poured in the gap between the casing and the cylindrical tank up to the height of the proposed cushion. The 15 mm thick sand layer poured around the cylindrical test tank served as a drain to allow water into the soil bed. After clay bed is compacted, the casing is withdrawn slowly until it reached the desired height of 150 mm. A hollow polyvinyl chloride pipe is placed on the top of the expansive soil bed, and a heave stake is placed on the top of the expansive soil bed through the hollow pipe. On top of the heave stake, a dial gauge of 0.01 mm sensitivity is arranged to measure the corresponding soil heave. Copper slag and the desired quantity of lime are thoroughly mixed in dry condition, and then the water corresponding to optimum moisture content is added to it. The percentages of lime added to the copper slag are 2, 4, 6, 8 and 10%. Copper slag, stabilised with lime, is placed over the expansive soil bed and compacted in three layers to its maximum dry density. The copper slag stabilised at different dosages of lime is called the lime-treated copper slag cushion, and its thickness is referred to as h_c throughout the paper.

Specimens in the test tanks are prepared for different ratios of thicknesses of lime-stabilised copper slag (h_c) and the expansive soil bed (h_s). In this study, the thickness of the expansive soil bed (h_s) is kept constant as 150 mm. The h_c is varied such that the ratio of h_c to h_s is maintained at 0, 0.25, 0.50, 0.75 and 1.00. Before allowing the water through the sand drain into the expansive clay bed for saturation, the initial dial gauge reading is noted through the heave stake arrangement made in the test tank. Then, water is allowed into the test tank through sand drain for the saturation of the expansive soil. The heave readings are taken corresponding to the attainment of equilibrium. The attainment of equilibrium is considered when there is no change in the dial gauge reading. Corresponding to this equilibrium stage, the undrained cohesion and water contents of the

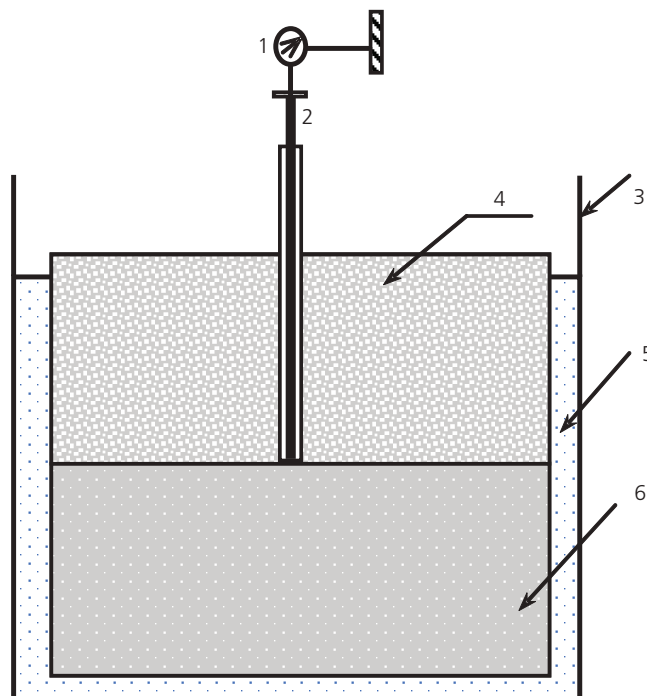


Figure 1. Schematic diagram of the experimental set-up: 1, dial gauge; 2, heave stake; 3, test tank (280 mm and 400 mm); 4, copper slag cushion with admixture thickness h_c ; 5, all around sand cushion 15 mm thick; 6, expansive clay bed thickness h_s

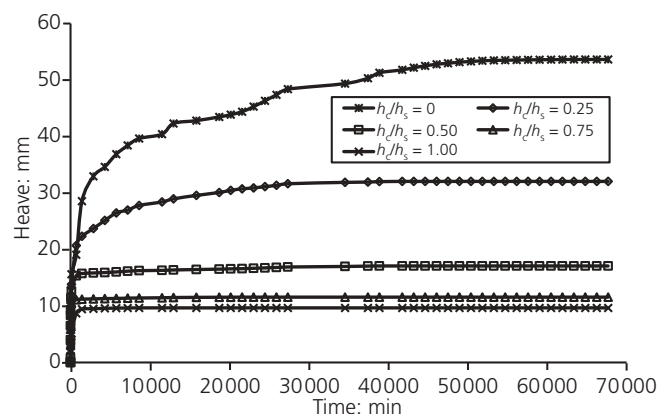


Figure 2. Time-heave plot of expansive soil bed with 6% lime added to the copper slag cushion

clay soil are measured, and these values are 26 kPa and 65%, respectively. A schematic diagram of the test tank set-up is shown in Figure 1.

2.4 Kondner's rectangular hyperbola

Some mathematical models are useful to simulate the non-linear swell-time curves of expansive soils to establish a relationship

between observed and predicted values. One such model, the Kondner's rectangular hyperbola (Kondner, 1963), is used to show the relationship between the time and heave for expansive soils and is presented in Equation 1:

$$1. \quad S = \frac{T}{(a + bT)}$$

where S = amount of swell corresponding to time T and 'a' and 'b' are constants.

The constants, a and b, can be obtained by linearising the non-linear curve. The maximum value of the swelling potential can be predicted by using the above equation.

3. Results and discussion

3.1 Influence of thickness ratio, h_c/h_s , on expansive clay bed

The heave of expansive clay bed laid under the lime-stabilised copper slag cushion of varied thicknesses is measured from the model test tank studies, and the respective results are discussed below. The clay bed of 150 mm thickness laid in the test tank without the lime-stabilised copper slag cushion – that is, $h_c/h_s = 0$ – showed a maximum heave of 53.64 mm. Figure 2 presents the variation of heave with passage of time for different cushion–soil thickness ratios, $h_c/h_s = 0, 0.25, 0.50, 0.75$ and 1.00, for the copper slag cushion stabilised with 6% lime. From these curves, it is noticed that as the thickness ratio, h_c/h_s , increases from 0 to 1.00, the heave of the expansive clay bed is decreasing. Especially for thickness ratios $h_c/h_s = 0.50, 0.75$ and 1.00, the increase in heave is

Table 5. Measured heave values in millimetres for various thickness ratios, h_c/h_s , and for lime proportions 2 and 4%

Time: min	Heave: mm for various thickness ratios, h_c/h_s , and 2% lime					Heave: mm for various thickness ratios, h_c/h_s , and 4% lime				
	0	0.25	0.50	0.75	1.00	0.25	0.50	0.75	1.00	
0	0.00	0.00	0.00	0.00	0.00	0.00	0.00	0.00	0.00	
1	0.09	0.22	0.59	0.78	0.27	0.50	0.20	0.31	0.06	
2	1.16	0.77	0.87	1.32	1.6	1.10	0.50	0.86	0.30	
5	2.93	2.08	3.3	3.31	2.51	3.00	4.12	2.91	1.19	
10	8.42	5.63	4.51	4.69	4.26	5.24	5.08	4.11	2.52	
20	9.99	7.99	6.52	5.43	4.26	7.40	6.85	5.05	3.43	
30	11.03	9.08	7.39	6.26	5.24	8.70	7.92	5.71	5.18	
60	12.68	12.29	8.67	7.87	7.92	11.72	9.76	6.74	5.18	
120	15.62	15.75	9.55	9.52	9.33	14.50	11.35	7.66	6.16	
720	19.08	20.44	10.09	11.29	10.72	17.50	12.55	9.85	7.65	
1440	28.56	22.92	12.2	11.62	11.31	21.55	14.15	11.49	8.88	
5760	36.87	27.05	13.9	12.16	12.13	25.47	15.23	11.72	10.09	
11 520	40.419	29.54	15.57	13.18	12.44	28.47	16.06	11.94	10.39	
37 440	50.32	33.39	19.08	13.85	—	31.99	17.55	12.14	—	
67 680	53.64	34.67	19.29	—	—	32.44	17.61	—	—	

Table 6. Measured heave values in millimetres for various thickness ratios, h_c/h_s , and for lime proportions 8 and 10%

Time: min	Heave: mm for various thickness ratios, h_c/h_s , and 8% lime					Heave: mm for various thickness ratios, h_c/h_s , and 10% lime				
	0	0.25	0.50	0.75	1.00	0.25	0.50	0.75	1.00	
0	0.00	0.00	0.00	0.00	0.00	0.00	0.00	0.00	0.00	
1	0.09	0.04	0.06	0.05	0.05	0.34	0.94	0.41	0.23	
2	1.16	0.31	0.63	0.13	0.15	0.96	1.54	0.82	0.32	
5	2.93	1.30	1.07	1.20	0.45	4.32	2.87	1.27	0.48	
10	8.42	2.23	2.00	2.26	0.94	6.92	3.85	1.73	0.61	
20	9.99	4.95	4.14	3.27	1.99	10.24	5.19	2.24	0.80	
30	11.03	9.11	5.70	4.52	2.87	11.58	6.37	2.61	0.94	
60	12.68	11.64	7.14	5.68	4.68	14.75	8.01	3.61	1.29	
120	15.62	14.43	10.29	8.48	7.14	17.86	9.69	4.91	1.81	
720	19.08	19.25	11.08	9.06	8.57	22.15	11.65	7.00	3.85	
1440	28.56	22.11	11.94	9.31	8.65	24.53	12.04	7.26	5.26	
5760	36.87	23.02	12.54	9.60	8.89	27.88	13.10	8.45	7.51	
11 520	40.419	24.77	13.28	10.33	9.15	29.46	13.69	8.91	8.37	
37 440	50.32	30.98	16.33	10.53	—	31.13	15.33	9.62	—	
67 680	53.64	31.49	16.36	—	—	31.24	15.35	—	—	

—, not applicable

Table 7. Percentage decrease in the heave of expansive soil bed with % lime added to the cushion

Thickness ratio (h_c/h_s)	% Lime				
	2	4	6	8	10
0.25	35.37	39.52	40.23	41.29	41.76
0.50	64.04	67.17	68.14	69.50	71.38
0.75	74.18	77.37	78.43	80.37	82.07
1.00	76.81	80.63	81.99	82.94	84.40

noticed within a short period of time, and thereafter, almost no change in heave is particularly noticed. The gradual increase in heave of expansive clay bed is noticed up to 28 days in the case of thickness ratio $h_c/h_s = 0.25$, and up to 40 days in the case of $h_c/h_s = 0$. The ultimate heave of the clay bed is achieved when the further passage of time does not cause any change or maintains a constant value. When compared to the ultimate heave of the clay bed for a thickness ratio of $h_c/h_s = 0$, the decrease in the ultimate heave for thickness ratios $h_c/h_s = 0.25, 0.50, 0.75$ and 1.00 is 40.2, 68.1, 78.4 and 82%, respectively. It means that at the

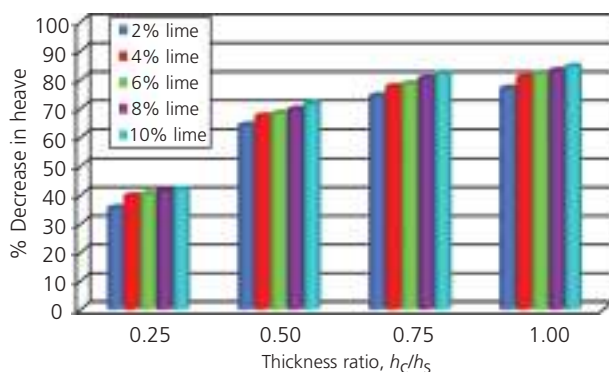


Figure 3. Percentage decrease in the heave of expansive soil with thickness ratio and % lime

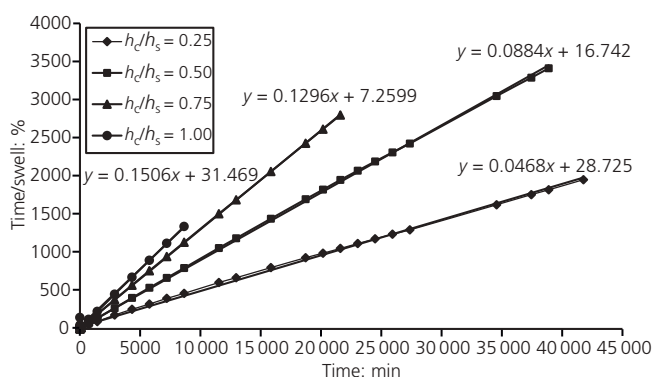


Figure 4. Time plotted against time/swell (%) of expansive soil bed with 6% lime added to the copper slag cushion

thickness ratios $h_c/h_s = 0.75$ and 1.00 , the copper slag cushion treated with 6% lime provides an optimal control of the heave of the expansive clay bed. It is further observed that it took very little time for almost the entire heave to occur when the expansive clay bed was overlain by the cushion. Such similar behaviour was noticed for the copper slag cushion treated with lime dosages of 2, 4, 8 and 10%. The heave-against-time data for copper slag cushions stabilised with lime dosages of 2, 4, 8 and 10% is presented in Tables 5 and 6.

It is further seen from Figure 2 that a large amount of the heave has occurred in the first two days following inundation, when the cushion was placed on the expansive soil bed. On the other hand, when a copper slag cushion was not provided over the expansive soil bed, the swelling was gradual, and it has taken a long time to attain equilibrium. This is one of the advantages of providing a cushion, as the time required to achieve equilibrium heave has significantly reduced. The percentage decrease in the heave of the expansive clay soil with various thicknesses of cushion when compared with no cushion placed on it is presented in Table 7. It is noticed that there is a significant reduction in the heave with the increase in the thickness of the cushion and with increase in the percentage of lime. The results presented in Table 7 are further depicted in the form of a histogram and presented in Figure 3. From this figure, it is clearly noticed that as the thickness ratio increases from 0.25 to 1.00, the reduction in heave is huge and it can be seen that it is almost the same level for the thickness ratios 0.75 and 1.00. It is also noticed that the influence of lime on the decrease in heave is nominal for any thickness ratio considered in the present study.

3.2 Swelling potential from rectangular hyperbola approach

Some mathematical models are useful to simulate the non-linear swell-time curves of expansive soils. Based on the rectangular hyperbola analysis, it is possible to establish a relationship between the observed values and the predicted values of the swelling potential of a lime-stabilised copper slag cushion-soil system. Kondner's rectangular hyperbola (1963) equation presented in Equation 1 is used to establish the relationship between the time and heave for expansive clay. A graph is plotted between time (as the abscissa) and time/swell (%) (as the ordinate). The legitimacy of the above equation can be demonstrated, if a transformed plot results in a straight line. The constants 'a' and 'b' are obtained from the slope of the straight line. The value 'b' gives the slope of the swelling path. The term 'b' is defined as the coefficient of the rate of swelling (Al-Rawas and Goosen, 2006; Hashim and Muntohar, 2006). A typical plot of time against time/swell (%) for different thickness ratios, $h_c/h_s = 0, 0.25, 0.50, 0.75$ and 1.00 , of expansive soil bed with 6% lime-stabilised copper slag cushion is shown in Figure 4.

Figures 5–9 show the typical graphs of the predicted and the observed swelling potential of the expansive clay for various thickness ratios and copper slag cushions which are stabilised with

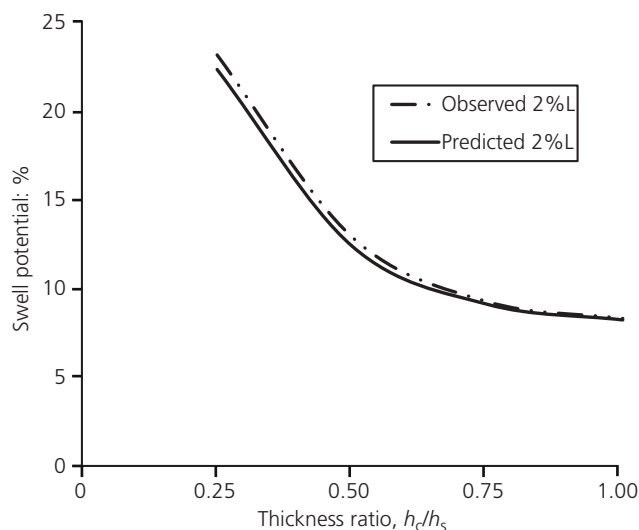


Figure 5. Predicted and observed values of swell potential of expansive soil bed with 2% lime added to the copper slag cushion for various thickness ratios

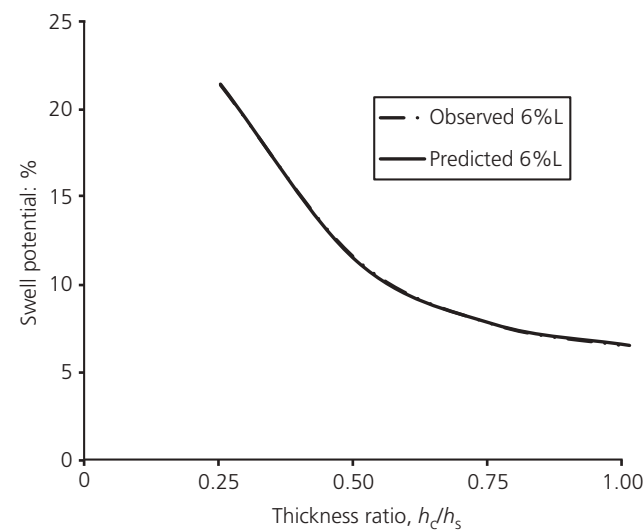


Figure 7. Predicted and observed values of swell potential of expansive soil bed with 6% lime added to the copper slag cushion for various thickness ratios

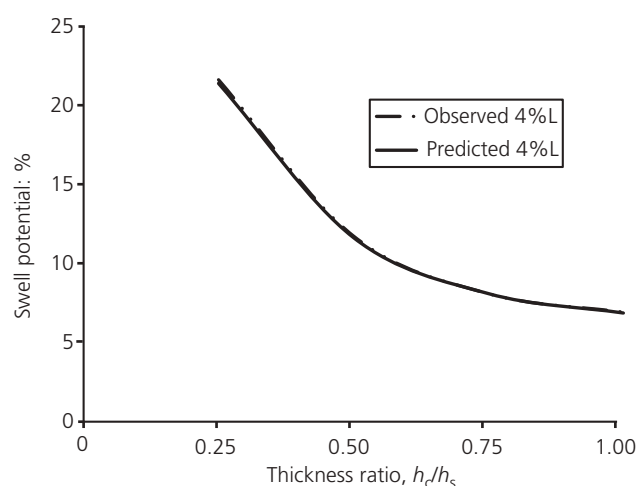


Figure 6. Predicted and observed values of swell potential of expansive soil bed with 4% lime added to the copper slag cushion for various thickness ratios

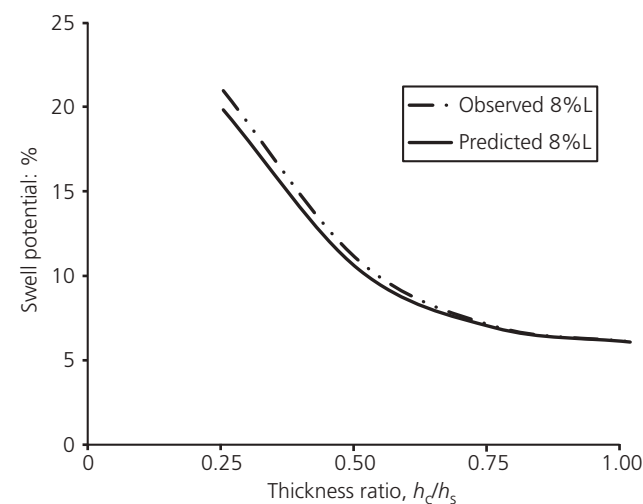


Figure 8. Predicted and observed values of swell potential of expansive soil bed with 8% lime added to the copper slag cushion for various thickness ratios

various percentages of lime. It can be seen that there is a close agreement between the predicted values of the swelling potential from the rectangular hyperbola and the observed values from the experimental work. The percentage decrease of observed and predicted values of the swelling potential of expansive clay soil with various thicknesses of the cushion when compared with no cushion placed on it is presented in Table 8. Earlier researchers have also observed that the hyperbolic relationship is accurate for predicting maximum swelling (Dakshnamurthy, 1978; Waddah *et al*, 1999). The percentage error is calculated for the predicted and observed values of the swelling potential. The percentage error of

the lime-stabilised cushions for various percentages of lime is 1.61, and the corresponding regression coefficient, R^2 , obtained is 0.998.

4. Conclusions

There is a considerable reduction in the heave of expansive soil subgrade bed when a lime-stabilised copper slag cushion is laid over it. With an increase in the percentage of lime, there is a reduction in heave, but it is marginal. However, the increased cushion thickness resulted in a significant reduction in heave. At all the thickness ratios, $h_c/h_s = 0.25, 0.50, 0.75$ and 1.00 , the decrease in the heave of the expansive soil subgrade overlain with

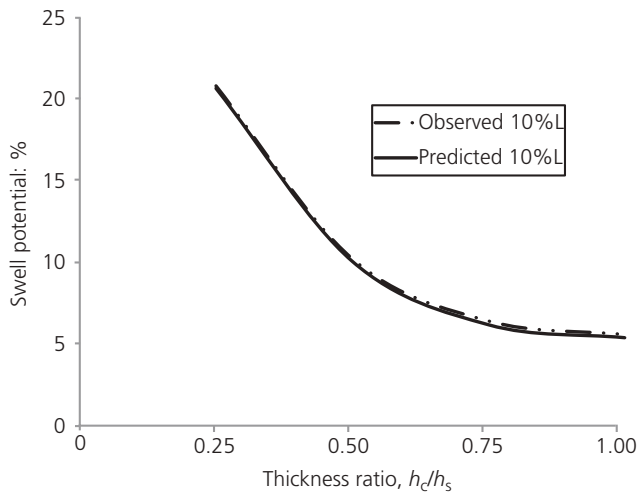


Figure 9. Predicted and observed values of swell potential of expansive soil bed with 10% lime added to the copper slag cushion for various thickness ratios

Table 8. Observed and predicted swell potential values (%) of expansive soil bed when lime is added to the cushion

% Lime	Values	Thickness ratio (h_c/h_s)			
		0.25	0.50	0.75	1.00
2	Observed value	23.11	12.86	9.23	8.29
	Predicted value	22.29	12.35	9.09	8.21
4	Observed value	21.63	11.74	8.09	6.93
	Predicted value	21.40	11.64	8.10	6.87
6	Observed value	21.37	11.39	7.71	6.44
	Predicted value	21.42	11.31	7.73	6.51
8	Observed value	20.99	10.91	7.02	6.10
	Predicted value	19.85	10.38	6.94	6.09
10	Observed value	20.83	10.23	6.41	5.58
	Predicted value	20.67	10.07	6.18	5.39

a lime-stabilised copper slag cushion when compared to the expansive soil subgrade bed without a cushion varies from 35.4 to 84.4%. The swelling potential of soil subgrade is predicted by using the rectangular hyperbola method of analysis. The predicted and observed values of swelling potential of expansive soil subgrade bed have been shown to vary by 1.61% for all the thickness ratios. It is concluded that the thickness ratio $h_c/h_s = 1$ is effective in controlling the heave.

REFERENCES

Al-Rawas AA and Goosen MFA (2006) *Expansive Soils – Recent Advances in Characterization and Treatment*. Taylor & Francis Group, London, UK.

Bipra Gorai B, Jana RK and Premchand (2003) Characteristics and utilisation of copper slag – a review. *Resources, Conservation and Recycling* **39**(4): 299–313, [https://doi.org/10.1016/S0921-3449\(02\)00171-4](https://doi.org/10.1016/S0921-3449(02)00171-4).

BIS (Bureau of Indian Standards) (1977) IS 2720, Part XXXX: Laboratory determination of free swell index. BIS, New Delhi, India.

BIS (1980) IS 2720, Part VII: Laboratory determination of standard proctor compaction (I.S. light compaction) (second revision). BIS, New Delhi, India.

BIS (1985a) IS 2720, Part IV: Laboratory determination of grain size analysis (second revision). BIS, New Delhi, India.

BIS (1985b) IS 2720, Part V: Laboratory determination of liquid limit and plastic limit (second revision). BIS, New Delhi, India.

BIS (1986) IS 2720, Part XVII: Laboratory determination of permeability (first revision). BIS, New Delhi, India.

BIS (1987) IS 2720, Part XVI: Laboratory determination of california bearing ratio (second revision). BIS, New Delhi, India.

Dakshanamuthy V (1978) A new method to predict swelling using a hyperbolic equation. *Geotechnical Engineering* **9**(1): 79–87.

Dhir RK, de Brito J, Mangabhai R and Lye CQ (2017) Use of copper slag in geotechnical applications. In *Sustainable Construction Materials: Copper Slag*. Woodhead, Duxford, UK, pp. 211–245.

Hashim R and Muntohar AS (2006) Swelling rate of expansive clay soils. In *Expansive Soils: Recent Advances in Characterization and Treatment* (Al-Rawas AA and Goosen MFA (eds)). Taylor & Francis Group, London, UK, pp. 139–148.

Havanagi VG, Mathur S, Prasad PS and Kamaraj C (2007) Feasibility of copper slag–fly ash–soil mix as a road construction material. *Transportation Research Record* **1989-2**: 13–20, <https://doi.org/10.3141/2F1989-43>.

Ikeagwuani CC and Nwonu DC (2019) Emerging trends in expansive soil stabilisation: a review. *Journal of Rock Mechanics and Geotechnical Engineering* **11**(2): 423–440, <https://doi.org/10.1016/j.jrmge.2018.08.013>.

Kalkan E (2011) Impact of wetting-drying cycles on swelling behavior of clayey soils modified by silica fume. *Journal of Applied Clay Science* **52**(4): 345–352, <http://doi.org/10.1016/j.clay.2011.03.014>.

Katti RK (1979) Search for solutions for problems in black cotton soils. *Indian Geotechnical Journal* **9**: 1–80.

Kondner RL (1963) Hyperbolic stress-strain response-cohesive soils. *Journal of Soil Mechanics and Foundation Division* **89**(1): 115–143, <https://doi.org/10.1016/0022-4898%2864%2990153-3>.

Lavanya C and Srirama Rao A (2017) Study of swelling potential of copper slag cushion laid over expansive soil bed. *Indian Geotechnical Journal* **47**(3): 280–285, <https://doi.org/10.1007/s40098-017-0227-9>.

Lavanya C, Srirama Rao A and Darga Kumar N (2014) Efficacy of copper slag cushion in arresting heave of an expansive soil. *International Conference on Recent Trends in Engineering & Technology, Pudukkottai, India*, pp. 658–662.

Patel S and Shahu JT (2017) Comparative study of slags stabilized with fly ash and dolime for utilization in base course. *Journal of Materials in Civil Engineering* **29**(10): 04017168, [http://doi.org/10.1061/\(ASCE\)MT.1943-5533.0002017](http://doi.org/10.1061/(ASCE)MT.1943-5533.0002017).

Raj S, Rai A and Havanagi V (2018) Suitability of stabilized copper slag and fly ash mix for road construction. *World Journal of Engineering* **15**(3): 336–344, <https://doi.org/10.1108/WJE-08-2017-0220>.

Rao MR, Rao AS and Babu RD (2008) Efficacy of cement-stabilized fly ash cushion in arresting heave of expansive soils. *Geotechnical and Geological Engineering* **26**(2): 189–197, <https://doi.org/10.1007/s10706-007-9156-1>.

Shahu JT, Patel S and Senapati A (2013) Engineering properties of copper slag-fly ash-dolime mix and its utilization in base course of flexible pavements. *Journal of Materials in Civil Engineering* **25**(12): 1871–1879, [https://doi.org/10.1061/\(ASCE\)MT.1943-5533.0000756](https://doi.org/10.1061/(ASCE)MT.1943-5533.0000756).

Sharma RS, Phani Kumar BR and Varaprasada Rao B (2008) Engineering behavior of a remolded expansive clay blended with lime, calcium chloride and rice husk ash. *Journal of Materials in Civil Engineering* **20**(8): 509–515, [https://doi.org/10.1061/\(ASCE\)0899-1561\(2008\)20:8\(509\)](https://doi.org/10.1061/(ASCE)0899-1561(2008)20:8(509)).

Visser AT (2007) Procedure for evaluating stabilization of road materials with non-traditional stabilizers. *Transportation Research Record* **1989-2**: 21–26, <https://doi.org/10.3141/1989-44>.





Waddah SA, Khalid AA and Al-Zou'bi SM (1999) Influence of pore water chemistry on the swelling behavior of compacted clays. *Applied Clay Science* **15(5-6)**: 447–462.

How can you contribute?

To discuss this paper, please submit up to 500 words to the editor at journals@ice.org.uk. Your contribution will be forwarded to the author(s) for a reply and, if considered appropriate by the editorial board, it will be published as a discussion in a future issue of the journal.

Review

Review on the Traditional and Integrated Passives: State-of-the-Art Design and Technologies

Muhammad Raza Khowja ^{1,*}, Robert Abebe ¹, Gaurang Vakil ¹, Adam Walker ¹, Chintan Patel ¹, Chris Gerada ^{1,2}, Phaneendra Babu Bobba ³ and Giuseppe Leonardo Cascella ⁴

- ¹ Power Electronics, Machines and Control (PEMC) Research Group, University of Nottingham, Nottingham NG7 2RD, UK; Robert.abebe@nottingham.ac.uk (R.A.); Gaurang.Vakil@nottingham.ac.uk (G.V.); Adam.Walker@nottingham.ac.uk (A.W.); crpatel19@gmail.com (C.P.); Chris.Gerada@nottingham.ac.uk (C.G.)
- ² Power Electronics, Machines and Control (PEMC) Research Group, University of Nottingham, Ningbo 315100, China
- ³ Department of Electrical Engineering, GRIET, Hyderabad 500090, India; bobbaphani@gmail.com
- ⁴ Department of Electrical Engineering and Information Technology, Politecnico di Bari, 70126 Bari, Italy; giuseppeleonardo.cascella@poliba.it
- * Correspondence: Raza.Khowja@nottingham.ac.uk

Abstract: With the increased necessity of a high power density and efficient system in aerospace and marine industries, integrated motor drives provide an excellent solution in the modern era. Therefore, a close structural and functional integration of passive components has become a prerequisite task to make a compact overall system. This article reviews the existing motor drives system with integrated passive technologies. To start, the design aspect of the traditional and integrated filter inductors, using the area product approach, is discussed. Subsequently, layouts of traditional and integrated inductors are presented. The available capacitor technologies, suitable for integration, are also discussed with pros and cons of each capacitor type.

Keywords: passive components; inductor; capacitor; integrated motor; filter branch windings; motor branch windings; aerospace applications



Citation: Khowja, M.R.; Abebe, R.; Vakil, G.; Walker, A.; Patel, C.; Gerada, C.; Bobba, P.B.; Cascella, G.L. Review on the Traditional and Integrated Passives: State-of-the-Art Design and Technologies. *Energies* **2022**, *15*, 88. <https://doi.org/10.3390/en15010088>

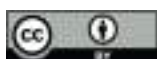
Academic Editors: Mauro Andriollo and Andrea Mariscotti

Received: 15 July 2021

Accepted: 7 December 2021

Published: 23 December 2021

Publisher's Note: MDPI stays neutral with regard to jurisdictional claims in published maps and institutional affiliations.



Copyright: © 2021 by the authors. Licensee MDPI, Basel, Switzerland. This article is an open access article distributed under the terms and conditions of the Creative Commons Attribution (CC BY) license (<https://creativecommons.org/licenses/by/4.0/>).

1. Introduction

Integrated motor drives with integrated passives are becoming more prevalent as the logical future in the industry of power electronics and motor drives, particularly in cases where weight and space are the major concern, such as aerospace, marine, and automotive application. These components contribute a significant portion of converter's weight and volume, which is larger than 50% [1,2]. Over a decade, there has been a shift from traditional separated passive components to integrated ones packed within the motor drive system. The use of passive integration over traditionally designed passive components in motor drive systems offers many benefits [3–10]:

- Space and mass reduction over traditional drive components (discrete ones).
- Fewer manufacturing process.
- Possible reduction of EMI problems at high frequency due to the elimination of cables transferring power.
- Ability to replace direct online machines with variable frequency machines without significantly adjusting the associated plant.
- Single package installation which further reduces installation time and cost.
- Drive topologies from greater design synergy greater flexibility in the machine.

Therefore, for applications where aforementioned benefits are needed, the use of the integrated technologies seems to be the best solution [8–10]. The passive components (discretely placed in the system) associated with the motor drive systems, such as capacitors, inductors, or transformers, occupy a significant amount of space and have added fines and

Article

A High-Gain Multiphase Interleaved Differential Capacitor Clamped Boost Converter

Dogga Raveendhra ^{1,*}, Poojitha Rajana ², Kalamchety Srinivasa Ravi Kumar ³ , Praveen Jugge ¹, Ramesh Devarapalli ⁴ , Eugen Rusu ^{5,*}  and Hady H. Fayek ⁶ 

¹ EEE Department, Gokaraju Rangaraju Institute of Engineering and Technology, Hyderabad 500090, India; drjpraveen@griet.ac.in

² Zunik Energies Pvt. Ltd., I-2, TIDES Business Incubator, IIT Roorkee, Roorkee 247667, India; ceo@zunikenergies.com

³ EEE Department, MVGR College of Engineering, Vizainagaram 535005, India; raviks1999@mvgrce.edu.in

⁴ Department of Electrical Engineering, B. I. T. Sindri, Dhanbad 828123, India; ramesh.ee@bitsindri.ac.in

⁵ Department of Mechanical Engineering, Faculty of Engineering, 'Dunarea de Jos' University of Galati, Domneasca Street, 800008 Galati, Romania

⁶ Electromechanics Engineering Department, Faculty of Engineering, Heliopolis University, Cairo 11785, Egypt; hady.habib@hu.edu.eg

* Correspondence: doggaravi19@gmail.com (D.R.); eugen.rusu@ugal.ro (E.R.)

Abstract: A step-up for a non-isolated interleaved differential capacitor clamped boost (IDCCB) DC–DC converter is proposed in this manuscript. Because of its ability to produce high voltage gains, it is used in high-power applications. This converter's modelling and control design are applicable to any number of phases. A six-phase interleaved differential capacitor clamped boost prototype is tested in this work, with an input voltage of 60 V, an output voltage of 360 V, and a nominal output power of 2.2 kW. The components of the converter are placed and controlled in such a way that the output voltage is the sum of the two capacitor voltages and the input voltage, which is two times higher than the supply voltage when compared to a conventional interleaved differential dual-boost converter. This converter reduces the stress on the capacitor with reference to the conventional interleaved differential boost converter for the same conversion gain. This prototype is considered and the developed approach is applied, after which the experimental results are obtained. This converter has potential for application in areas such as renewable energy conversion and electric vehicles.

Keywords: capacitor clamped converter; high-gain converter; DC–DC power converter



Citation: Raveendhra, D.; Rajana, P.; Kumar, K.S.R.; Jugge, P.; Devarapalli, R.; Rusu, E.; Fayek, H.H. A High-Gain Multiphase Interleaved Differential Capacitor Clamped Boost Converter. *Electronics* **2022**, *11*, 264. <https://doi.org/10.3390/electronics11020264>

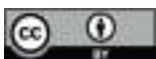
Academic Editors: Juan Rodríguez Méndez and Aitor Vázquez Ardura

Received: 18 November 2021

Accepted: 10 January 2022

Published: 14 January 2022

Publisher's Note: MDPI stays neutral with regard to jurisdictional claims in published maps and institutional affiliations.



Copyright: © 2022 by the authors. Licensee MDPI, Basel, Switzerland. This article is an open access article distributed under the terms and conditions of the Creative Commons Attribution (CC BY) license (<https://creativecommons.org/licenses/by/4.0/>).



1. Introduction

New challenges in energy conversion technology are being faced due to the increased use of renewable energy sources. One such challenge is that several types of devices that store or produce electrical energy, such as ultra-capacitors, solar panels, batteries, and fuel cells, are manufactured using low-voltage cells, which must be series-connected to attain reasonable voltages [1–3]. In such cases, the complexity of the system is increased due to the series connection of a large number of cells, which reduces the performance due to the differences among the cells, such as fabrication variations and other various working conditions. Moreover, the notable variations in the output voltages of this kind of electrical energy source depend on factors such as the state of charge, the output current, and the solar radiation [4].

Using comparatively high and stable voltages in typical applications such as in electrical motor drives, power infusion into the grid is essential at times. For this, a step-up converter is used to increase the voltage of the source based on the requirements of the application and to produce a stable output voltage, even if variations exist in the voltages of the source [5–8]. For instance, let us contemplate the electronic circuits in a Toyota Prius.

Article

Capacitor Clamped Coupled Inductor Bi-Directional DC-DC Converter with Smooth Starting

Kalamchety Srinivasa Ravi Kumar ¹, Alagappan Pandian ^{1,*}, Vedula Venkata Sastry ²
and Dogga Raveendhra ^{3,*}

¹ Department of Electrical and Electronics Engineering, Koneru Lakshmaiah Education Foundation, Guntur 520002, Andhra Pradesh, India; raviks1999@mvgrce.edu.in

² Department of Electrical and Electronics Engineering, Gayatri Vidya Parishad College of Engineering, Vizag 530048, Andhra Pradesh, India; sastryvv@gvpce.ac.in

³ Department of Electrical and Electronics Engineering, Gokaraju Rangaraju Institute of Engineering and Technology, Hyderabad 500090, Telangana, India

* Correspondence: pands07@kluniversity.in (A.P.); doggaravi19@gmail.com (D.R.)

Abstract: In this paper, a new type of capacitor clamped coupled inductor bidirectional DC–DC converter is proposed, which offers high voltage gain with smooth starting current transients, as well as reduced stresses on the capacitor. Steady state operation, mathematical modelling, and state space modelling for the proposed converter are presented in detail. A simplified single voltage clamped circuit is developed to mitigate the voltage spikes caused due to the coupled inductor by recovering the leakage energy effectively. Moreover, the clamping capacitor helps in reducing the ripples in output voltage, which in effect significantly reduces the stress on the switch and offers less ripple content at the load terminals. Simulation of the proposed converter is carried out using Simulink/MATLAB for the conversion of 24V DC to 200V DC. For this conversion, simulation results have proven that there is reduction of 13.64% of capacitor voltage stresses. Further, under line varying conditions, converter responses have proven that there is a 119% and 25.25% reduction in input current and output voltage transients, respectively. Similarly, 25.25% and 76.5% transient reductions of input current are observed for line and control parameter variations. The hardware investigation of the converter was carried out with a 100 W, 24 V/200 V setup. The converter achieved efficiency of 93.8%. The observations supplement the simulation results.

Keywords: bi-directional converter; DC-DC power converter; coupled inductor bi-directional converter; bi-directional power flow



Citation: Kumar, K.S.R.; Pandian, A.; Sastry, V.V.; Raveendhra, D. Capacitor Clamped Coupled Inductor Bi-Directional DC-DC Converter with Smooth Starting. *Machines* **2022**, *10*, 47. <https://doi.org/10.3390/machines10010047>

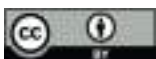
Academic Editor: Antonio J. Marques Cardoso

Received: 25 October 2021

Accepted: 17 December 2021

Published: 8 January 2022

Publisher's Note: MDPI stays neutral with regard to jurisdictional claims in published maps and institutional affiliations.



Copyright: © 2022 by the authors. Licensee MDPI, Basel, Switzerland. This article is an open access article distributed under the terms and conditions of the Creative Commons Attribution (CC BY) license (<https://creativecommons.org/licenses/by/4.0/>).

1. Introduction

In the modern era, the environment is prone to pollution caused due to various aspects, especially vehicles powered by fossil fuels. As the pollution prone system is becoming of greater concern, replacing these vehicles with plug-in electric vehicles (PEV) is becoming an attractive proposition. To take this technology forward to next level of sophistication, one needs to provide not only an optimal charging system, but also the most effective power conditioning unit to drive the motor more effectively. This results in more flexibility for PHEV customers [1–4]. Usually, a bi-directional DC-DC converter (BDC) is associated with the design of charger as well as the power conditioning unit of an EV or PHEV, as shown in Figure 1, as it allows bidirectional power flow (charging and discharging and similarly during motoring and braking periods respectively).

The broad categorization of these BDCs refers to isolated (transformer based) converters and non-isolated (transformer less) converters. Conventional isolated converters are used to meet the high gain requirements of EVs, which provides the flexibility of reduced operating voltages at the battery side in the design of EVs. For this purpose, step-up natured isolated converters, e.g., flyback, push-pull, current-fed half bridge, and current-fed



Study on machinability of Ti6Al4V with coated inserts–cutting force, surface finish and material removal rate prediction using ANN

Satyanarayana Kosaraju¹ · Devaraju Aruri² · Murahari Kolli³ · G. Sai Kumar⁴ · Phaneendra Babu Bobba⁵

Received: 14 January 2022 / Accepted: 15 March 2022

© The Author(s), under exclusive licence to Springer-Verlag France SAS, part of Springer Nature 2022

Abstract

Titanium alloys are known for their potentiality to withstand extreme environmental conditions. However, due to its higher fabrication and machinability cost of these alloys are limited their applications to defense, aerospace and marine sectors. To enhance their domestic applicability, either their fabrication or machining costs must be controlled. With an intention to reduce machinability cost; Cutting force, surface roughness and material removal rate of Titanium alloy Ti6Al4V are predicted through artificial neural network computational technique was applied in this investigation. A full factorial design set of experiments are conducted on precision lathe machine to predict the influence of input parameters like cutting speed, feed, depth of cut and rake angle. The output responses emphasized are the cutting forces, surface roughness and material removal rate during machining with carbide tool inserts with coated TiAlN layer. Neural network models were developed using back propagation algorithms by training on this data to prediction output responses. The models are further validated by addition 8 different experimental data sets. Sufficient level of fitness was observed for the trained model. A comparison was made between experimental response values and the predicted values. The prediction accuracies were found to be sufficiently high which indicates the effectiveness of the model.

Keywords Machining · Ti6Al4V · Coated insert · Artificial neural network

1 1. Introduction

Usage of Titanium alloy has increased in the recent times in aerospace, marine, automobile industries and chemical processing industries because of their light weight, good fatigue strength and corrosion-resistance properties. The specific weight of titanium is about two thirds that of steel and

about 60 percent higher than that of aluminum. Whereas titanium's strength is far greater than that of many alloy steels, giving it the highest strength-to-weight ratio when compared to any of today's structural metals. Titanium alloys also have high melting points, which is usually a sign of excellent thermal stability [1]. Presently, Ti6Al4V is one of the most widely used titanium alloys, accounting for more than half of all titanium tonnage in the world, and no other titanium alloys threaten its dominant position [2, 3] because of its unique characteristics and applications. Ti-6Al-4V, a $\alpha + \beta$ alloy constitutes nearly 50% of the wrought alloys produced. It features good machinability and excellent mechanical properties. The Ti6Al4V alloy offers the best all-round performance for a variety of weight reduction applications in aerospace, automotive and marine equipment. Despite increase of the usage and production of titanium alloys, they are expensive when compared to other metals because of the complexities of the extrusion process, difficulties during melting, fabrication and machining [4–6]. In order to meet the demands, manufacturing process parameters have to be chosen in the best possible way. Different

✉ Satyanarayana Kosaraju
satyanarayana.kosaraju@gmail.com

¹ Mechanical Engineering Department, Gokaraju Rangaraju Institute of Engineering and Technology, Hyderabad, Telangana, India

² Mechanical Engineering Department, Kakatiya Institute of Technology and Science, Warangal, Telangana, India

³ Department of Mechanical Engineering, Lakireddy Bali Reddy College of Engineering, Mylavaram, Andhra Pradesh, India

⁴ Mechanical Engineering Department, Kakatiya Institute of Technology and Science, Warangal, Telangana, India

⁵ Electrical and Electronics Engineering Department, Gokaraju Rangaraju Institute of Engineering and Technology, Hyderabad, Telangana, India

INTERVAL TYPE-2 FUZZY SPACE VECTOR MODULATION FOR MATRIX CONVERTER

¹G. Durgasukumar, ²M. Nagaraju and ³B. Pakkiraiah

¹Professor & Principal, Department of EEE, Vignan Institute of Technology and Science, Deshmukhi, Telangana, India,

¹Email: durgasukumar@gmail.com

²Assistant Professor, Department of EEE, Vignan's Lara Institute of Technology & Science, Vadlamudi, Guntur, A.P,

²India, ²Email: nmurikipudi@gmail.com

³Associate Professor, Department of EEE, Gokaraju Rangaraju Institute of Engineering and Technology-Autonomous,

³Bachupally-500090, Telangana, India, ³Email: pakki1988@gmail.com

Abstract – A Matrix converter which does conversion from AC to AC in a single stage. Among the various existed control techniques space vector modulation technique is mainly used to control Matrix converter. But the disadvantage of the SVM method in Matrix Converter is the switching frequency is limited at the converter and inverter side due to non-linearity complex on-line computation that's why output cannot be obtained properly. By using soft computing based techniques this problem can be overcome. This article presents Type-2 Fuzzy controlled space vector pulse width modulation technique to reduce distortions in the output due to the conventional space vector pulse width modulation. The Type-2 Fuzzy logic can handle uncertainty of rule measurement unlike Type-1 Fuzzy Logic Systems. In this controller, the type-2 fuzzy logic sets (FLS) are characterized by a three-dimensional fuzzy membership functions (MFs) with including a footprint of uncertainty (FOU). The FOU and the third dimension of MFs are utilized properly to provide an additional degree of freedom in the controller to design the model and to handle parameter uncertainties. Here, the intersection point of a membership function is smaller in order to have a better centroid value for more preciseness in the obtained outcomes compared to that of T1NFC. The operation of Matrix converter under fed Induction motor under dynamic operation conditions is investigated. The training data for Type-2 fuzzy-based system is generated from the conventional space vector pulse width modulation technique. The obtained simulation results are experimentally verified using the Micro lab box. The matrix converter output in terms of the total harmonic distortion of line-line voltages of the Type-2 fuzzy system is compared with Type-1 and conventional space vector pulse width modulation methods. Under different operating conditions the motor performance parameters such as Torque ripple, phase Currents and speed are also compared through simulation and experiment.

Index Terms- Space vector pulse width modulation (SVPWM), Type-2 Fuzzy (TY2FS), Type-1 Fuzzy (TY1FS), Total Harmonic Distortion (THD), Matrix Converter (MC).

I. INTRODUCTION

Matrix converter is converts A.C to A.C without any energy storage elements as compared to voltage source inverter. The voltage source inverter is used to converts AC-DC-AC; in this process required additional capacitor in DC link [1, 2].The conversion of AC-AC in matrix converter by using PWM method produces harmonics. In order to decrease line voltage harmonics proposed by simple two PWM patterns [3]. If any input voltage

changes it produces non-sinusoidal out voltage .It produces the more harmonics, losses are increased and efficiency is decreased. To avoid above drawback introduces direct matrix converter with space vector modulation (SVM) to improve dynamic performance of the induction motor [4].The matrix converter is employed with Propositional and integral (PI) and Fuzzy controller to estimate the speed, torque & current of induction motor. The PI controller is not recommended for complex networks but in fuzzy controller settling time is more compared with PI controller [5]. The comparison of fuzzy PI controller with conventional PI controller of IM drives. The fuzzy PI gives efficient speed control and good performance as compared with conventional PI controllers [6].

Matrix converter is a technique divides direct and indirect matrix converter topology .Here indirect matrix converter is technique is employed with space vector modulation with better implementation and safe operation compared with direct matrix converter topology [7-8].The indirect matrix converter is a topology is replace with space vector modulation to get three to five phase with simple configuration and commutation process [9].The space vector modulation is a technique employed to three to five phase matrix converter topology with improved THD compared with conventional PWM. The algorithm reduced for space vector modulation and number of space vector also reduced [10]. The space vector modulation of multilevel matrix converter is applied to improve duty cycle calculation .In this method amplitude co-efficient of capacitor clamped voltage balancing and more advantages are discussed [11]. An interval type-2 fuzzy-based direct torque control of the induction motor drive instead of PI controllers is used along with a five-level diode-clamped inverter [12].The speed control of induction motor is investigate with fuzzy based closed loop control from matrix converter presented .The main drawback of closed loop of fuzzy control implementation time is more as compared with other control algorithms [13-14].

Indirect space vector based technique is employed to multi modulation matrix converter .In this method duty ratios calculation applied both in the rectification and inversion stage to produce final gating signals [15-16].The fuzzy based algorithm developed for induction



Real-time monitoring of battery state of charge using artificial neural networks

Sai Vasudeva Bhagavatula^a, Venkata Rupesh Bharadwaj Yellamraju^a, Karthik Chandra Eltem^a, P. N. Shashank^a, Phaneendra Babu Bobba^a, Satyanarayana Kosaraju^b and Naveen Kumar Marati^c

^aDepartment of Electrical & Electronics Engineering, GRIET, Hyderabad, India; ^bDepartment of Mechanical Engineering, GRIET, Hyderabad, India; ^cArchitect, Electric Vehicle CoE, Wipro Limited, Bangalore, India

ABSTRACT

The main highlight of this paper is to present the implementation of a battery health augury system using artificial neural networks (ANNs). We were able to predict the amount of charge in the battery only by taking preliminary parameters like voltage, current and ambient temperature of the battery, in the growing field of portable energy storage (ES) technology. An optimal solution was demanded to increase the age of the battery. We were able to predict the state of the battery in terms of charge for its performance. A feed forward neural network (FFNN) and long short-term memory (LSTM) neural nets were used for the implementation whose prediction accuracy is acceptable for this application. An optimal data-driven model for FFNN and LSTM for the prediction which made sure that our neural network (NN) models can be used for the estimation of charge in the battery for any charging cycle based on the preliminary parameters. These results can also help us to extend the implementation by estimating the health condition of the battery and also to be used for real-time monitoring and prediction of the performance characteristics and to improvise various NN methods in these fields for perfect accuracy in predicting the performance.

ARTICLE HISTORY

Received 12 October 2021
Accepted 24 February 2022

KEYWORDS

BMS – battery management system; ESU – energy storage unit; SoC – state of charge; SoH – state of health; ML – machine learning; ANN – artificial neural networks

1. Introduction

The recent growth in latest technologies like portable electronics, futuristic transportation, healthcare and areas of power & energy gave rise to the need of prodigious batteries or energy storage units (ESUs). The need for portability, durability, robustness and longevity in battery technology has become a challenge for battery engineers and researchers; different parameters for enhancement of these ESUs like supercapacitors, hybrid (battery supercapacitors) or batteries alone were observed. Figure 1 shows the block diagram architecture of BMS.

A battery management system (BMS) in short BMS (He et al. 2012) is a device that manages, computes, protects, monitors and communicates with the battery (Lee, Kuo, and Wang 2004). A BMS is like a brain for a battery and can be used for any ESU as the parameters affecting the performance are the same. The SoC and SoH (Tsang and Chan 2013) are the terms that give us an understanding on the performance of any ESU. SoC is the amount of charge in the ESU, and SoH (Yang et al. 2017) is the condition of ESU. Some factors that affect the SoC and SoH are as shown in Figure 2.

Estimating the performance using these parameters can be achieved in many ways also involving data-driven methods like machine learning (ML) and artificial neural network (ANN) being a branch of ML. Figure 3 is the graphical representation of various estimation techniques.

Neural network (NN) is a data-driven method (Zou et al. 2014) similar to ML that took its place in one of the fastest growing

technologies due to its ability to learn and model the relationships between inputs and outputs that are nonlinear and complex for any data. NN is widely used in many latest areas, inspired from multi-variable regression, and is being used for both regression and classification problems. Some of the mostly used NN architectures are mentioned in Figure 4.

Earlier, other methods like direct methods, battery-based models (Remmlinger et al. 2011), filtering estimations involving methods like Coulomb counting, open circuit voltage (OCV), ECM - equivalent circuit model (ECM) and Kalman filtering methods (Charkhgard and Farrokhi 2010; Wang and Chen 2020) and later due to increase in computational power of computer and many open-source frameworks, implementing NN has become easily available for all. The model-based methods discussed by Wei et al. (2021) and Bian et al. (2021b) clearly explain how the state of charge for lower order models can be clearly estimated and give comparatively better results than higher order models and estimating the state of charge in lithium-ion battery even in the absence of current sensor. Multiple parameters were taken into consideration for the performance estimation of the battery; these included vital attributes like voltage, current and temperature but battery researchers had to know the capacity of the battery which is also another vital parameter in order to understand the performance of the battery better. Capacity-based estimation came out to be the best estimating techniques for battery performance as it elucidates how battery deteriorate over a period and how the instantaneous capacity of the battery and its maximum



Optimized power generation in solar using carbon substrate for reduced greenhouse gas effect

Suresh Kumar Tummala¹ · Satyanarayana Kosaraju² · Phaneendra Babu Bobba¹

Received: 18 September 2021 / Accepted: 22 December 2021
© King Abdulaziz City for Science and Technology 2022

Abstract

Traditionally, power is produced through non-renewable energy sources which has a major drawback of greenhouse gas emission effecting the climatic conditions and ozone layer. In this paper, carbon substrate-deposited solar cell for improved power generation in reducing greenhouse gas effects are discussed with various analysis. Poly-crystalline solar cells are etched with carbon substrate for analysis. The same are compared with silicon carbide-etched solar cells. Scanning electron microscopy (SEM) analysis is carried out to show the variations in the cell structure. Electrical analysis is also carried out to show the performance difference in voltage and overall efficiency of the cell.

Keywords Carbon · Silicon carbide · Greenhouse gas · Solar cell · Etching

Introduction

Power generation through renewable energy sources has gained attention which reduces Greenhouse gases (GHG) as years pass on. In such renewable energy sources, solar energy is in front for producing electricity through sun radiation. Existing solar panel have been designed for power generation without any optimization (Saïdi et al. 2020). Solar Module Glass does not absorb maximum radiation but acts a protective element for the panel from climatic conditions and there is no scope for storage of energy resulting in lower efficiency (app. 20%) (Tummala and Kosaraju 2020). Making solar or photovoltaic cells requires potentially toxic heavy metals such as lead, mercury, and cadmium (Basher et al. 2019). It even produces GHG, such as carbon dioxide, that contribute to global warming. Still, the researchers found that if people switched from conventional fossil fuel-burning power plants to solar cells, air pollution would be cut by roughly 90%.

A solar cell is an electronic gadget which straightforwardly changes over daylight into power. Light sparkling

on the solar powered cell produces (Verayiah and Iyadurai 2017; Taşçıoğlu and Vardar 2016) both a flow and a voltage to create electric force. This procedure requires right off the bat, a material wherein the retention of light raises an electron to a higher energy state, and furthermore, the development of this higher energy electron from the solar cell into an outside circuit. The electron at that point disperses its energy in the outer circuit and comes back to the solar cell. An assortment of materials (Kaule et al. 2014) and procedures can conceivably fulfill the prerequisites for photovoltaic energy change; however, practically speaking about all photovoltaic energy transformation utilizes semiconductor materials as a p–n intersection.

The fundamental strides in the activity of a solar powered cell are:

- a) the age of light-produced bearers,
- b) the assortment of the light-produced conveys to create a current,
- c) the age of an enormous voltage over the solar powered cell, and (Dobrzański et al. 2013)
- d) the dispersal of intensity in the heap and in parasitic protections.

Natural photovoltaic or solar cells are made of thin films (under 100 nm) of natural (Dobrzański et al. 2013) semiconductor materials to change over sun-based energy into electrical energy. This innovation is increasingly (Hannebauer

✉ Suresh Kumar Tummala
sureshkumar255@gmail.com

¹ Electrical Engineering, Gokaraju Rangaraju Institute of Engineering and Technology, Hyderabad, India

² Mechanical Engineering, Gokaraju Rangaraju Institute of Engineering and Technology, Hyderabad, India



Stability improvement in microgrids using hybridization of RSFCL along with fuzzy based SAPF

M Uma Maheswara Rao¹ · C Subba Rami Reddy² · P Lakshmi Narayana¹ · D. S. N. M RAO³ · Idamakanti kasireddy⁴

Received: 27 January 2022 / Accepted: 5 May 2022

© The Author(s), under exclusive licence to Springer-Verlag France SAS, part of Springer Nature 2022

Abstract

Present-day, microgrids play a major role in human life as usage of energy increases day by day. In this work, the number of Distributed Generations (DGs) are three such as fuel cell, wind energy, and solar energy. These three DGs are interconnected with the utility grid. Using phase-locked loop circuits synchronization process is done in between DGs and main grid. In this proposed work LLL-G fault is formed closer to the wind DG, then abnormal currents are increased, and voltage levels are reduced hence, the system does not have stability. Till now, circuit breakers have been used for safety but it suffers from drawbacks. To avoid such type of drawbacks, Resistive type Superconducting Fault Current Limiter (RSFCL) is connected in the microgrid. Under healthy conditions, RSFCL performs as a superconductor, and in abnormal circumstances, it turns into a high impedance path then fault currents are limited and continuity of supply is possible. RSFCL have some drawbacks such as it does not compensate for the reactive power hence voltage magnitudes are not recompensed due to that reason, fuzzy controller-based Series Active Power Filter (SAPF) is hybridized with RSFCL.

Keywords Circuit Breaker (CB) · Distributed Generation (DG) · Phase-Locked Loop circuits (PLL) · Resistive type Superconducting Fault Current Limiter (RSFCL) · Series Active Power Filter (SAPF)

1 1. Introduction

Now a day's microgrid safety is a main inspiring task because the number of DGs are synchronized with the main grid. Here synchronization process is very tough, in this work PLL circuits are used for synchronization [15]. This proposed work having three DGs such as fuel cell, solar, and wind. Compare to primary energy sources these DGs having so many advantages such as no need to input fuel, no transportation of fuel cost, it's free from pollution and free from environment [11]

[12]. Whenever DGs are interconnected fault currents are raised such currents are called short circuit currents. Till now, CBs are used for safety, but CB has some drawbacks such as under fault conditions breaker terminals are opened then continuity of supply is not possible, and it allows 3-cycles of fault current into the system. Here RSFCL is used to overcome that drawback, in RSFCL conductor material is finished with YBCO (Yttrium Barium Copper Oxide) [1]. YBCO is a superconductor material and its internal resistance is low under healthy conditions but under faulty circumstances it turns as a high impedance path and due to that impedance fault currents are limited hence continuity of supply is possible [13]. RSFCL can break the fault currents within the first cycle [2]. In general, RSFCL having some difficulties such as it's not recompensed the reactive power hence voltage magnitudes are not remunerated which means the system does not come into the complete stability state [3]. Due to that reason SAPFs are used along with RSFCL.

Fuzzy controller-based SAPF is used for the compensation of voltage sag and swell. Here SAPF having a three-phase inverter, electrolytic capacitors, injection transformer, and fuzzy logic controller [7]. The fuzzy logic controller can compare the operating value of the voltage with the pre-setting

✉ M Uma Maheswara Rao
umamaheswar9999@gmail.com

¹ Department of Electrical & Electronics Engineering, Vignana's Foundation for Science, Technology and Research Deemed to Be University, Guntur, Andhra Pradesh 522213, India

² Department of Electrical & Electronics Engineering, B V Raju Institute of Technology, Vishnupur, Narsapur, Medak, Telangana 502313, India

³ Department of Electrical & Electronics Engineering, Gokaraju Rangaraju Institute of Engineering & Technology, Hyderabad 500090, India

⁴ Department of Electrical & Electronics Engineering, Vishnu Institute of Technology, Bhimavaram, India



Modelling and performance evaluation of 18w PEM Fuel Cell considering H₂ pressure variations

Neerudi Bhoopal¹, Dokku Sivanaga Malleswara Rao², Nagineni Venkata Sireesha³, Idamakanti Kasireddy⁴, Ranjith Kumar Gatla⁵, Devineni Gireesh Kumar^{1*}

¹Department of Electrical & Electronics Engineering, B V Raju Institute of Technology, Narsapur, Telangana, 502313, India

²Department of EEE, Gokaraju Rangaraju Institute of Engineering & Technology, Hyderabad, Telangana, 500090, India

³Department of Information Technology, Institute of Aeronautical Engineering, Dundigal, Telangana, 500043, India

⁴Department of Electrical and Electronics Engineering, Vishnu Institute of Technology, Bhimavaram, AP, 533428, India

⁵Department of Electrical and Electronics Engineering, Institute of Aeronautical Engineering, Telangana, 500043, India

Corresponding Author Email: gireesh218@gmail.com

ABSTRACT

The chemical energy of a hydrogen-oxygen reaction is converted directly into dc electrical energy by fuel cells (FC). PEMFCs (Proton Exchange Membrane Fuel Cells) are a feasible alternative for electrical transportation and stationary applications. This paper presented a PEMFC modelling approach using Artificial Intelligence. The main objective of this research is to build a model of an 18w Polymer Electrolyte Membrane (PEM) fuel cell and test its performance under different hydrogen pressure conditions. The physical model of the 18W hydrogen fueled PEM fuel cell is designed and tested at BHEL R&D. Additionally, a method for predicting a PEMFC's operating temperature using the voltage and current measures is suggested and successfully tested. However, the proposed technique is validated using experimental data from an 18W fuel cell. The analytical data and testing procedures required for determining the parameter values used in the proposed model are specified.

Received: April 21-2021 Accepted: September 30-2021 <https://doi.org/10.14447/jnmes.v25i1.a01>

1. INTRODUCTION

Due to high efficiency, zero-emissions when running on pure hydrogen, and low operating temperature, proton exchange membrane fuel cells (PEMFC) are considered a potential green power source for electrical transportation and stationary applications. Designing a power converter capable of conditioning the output power with high efficiency and reliability is the major challenge of PEMFC systems. The power converters are responsible for about 80% of the damage in the PEMFC system. The power converter must be tested and altered with a valid PEMFC during the design phase, and it must therefore be validated. However, the design and implementation of a PEMFC, including auxiliaries such as air compressor control testing, power and energy management, and performance optimization, will readily destroy a PEMFC. Furthermore, the cost of testing (hydrogen utilization and secured facility requirements) is also high for experiments with a realistic PEMFC.

These drawbacks highlight the critical importance of developing a real-time PEMFC emulator based on a model material for HIL applications (Hardware In the Loop). Power converters and auxiliaries can be validated and augmented in real-time with a PEMFC emulator during the design process of the PEMFC power system, with no risk to the stack and low system running cost. PEMFC modelling has sparked a lot of interest in the literature, where it's generally done with sophisticated models based on the understanding of the physicochemical phenomena [1-3]. These models require a

strong knowledge of the parameters and how it works [4-7]. These parameters for PEMFC systems are generally not easy to determine. A PEMFC stack's transient behavior pattern is presented in [8]. However, the intrinsic parameters of the membrane and electrode overflowing and drying should be identified as the ohms resistance. These internal parameters are meaningful if the cell voltage is considered, although the necessary Parameters were not considered in this mathematical model. Hybrid models could meet these challenges. A PEMFC model has been built in [9], distinguishing the cell either in a constant or transient state. The suggested model, combined with the electric circuit and the empirical models, is consistent with experimental findings. However, only a small range of this model is accurate.

However, behavioral modelling can be achieved without all these parameters being identified employing a model known as the "black box." These models are based on factors that can be easily measured, such as temperature, pressure or cell current, and the output voltage of the PEMFC is estimated. Currently, the literature does not include dynamic models of PEMFC systems based on Artificial Networks (ANN). However, several models with significantly stable results [10-13] have been developed. A static and dynamic ANN-based PEMFC model was suggested in [13], with experimental findings. The proposed model uses the temperature measurements, the fuel cell current, the two gases' stoichiometry, and moisture. This modelling approach produces good results, but it suffers from an adverse temperature change. In [14], the high-power PEMFC neuronal modelling is shown in which temperature



SEM & EDAX analysis of super capacitor

Suresh Kumar Tummala ^a, Phaneendra Babu Bobba^a and Kosaraju Satyanarayana ^b

^aElectrical Engineering, Gokaraju Rangaraju Institute of Engineering & Technology, Hyderabad, INDIA;

^bMechanical Engineering, Gokaraju Rangaraju Institute of Engineering & Technology, Hyderabad, INDIA

ABSTRACT

Super capacitors have the ability of high power densities for longer charging (or) discharging cycles. Material used in the super capacitors effects the performance of the device. It is obvious that the material used in super capacitors shall increase the energy density for smaller volumes while maintain the cycle stability. The right structure of super capacitors should exhibit best mechanical and electrical properties. The analysis of the above properties can be discussed by looking into the microstructure, elemental structure, etc. of the materials used. In this paper, scanning electron microscopy and energy dispersive X-ray analysis are performed on a super capacitor to study the microstructure and elemental parameters. This analysis will help in determining the electrical and mechanical properties of the super capacitors.

ARTICLE HISTORY

Accepted 6 February 2022

KEYWORDS

Super capacitors; microstructure; elemental analysis; SEM; EDAX

1. Introduction

Super capacitors possess the ability of storing energy (charge) in large amounts. Super capacitors are also referred as ultra capacitors or sometimes called as double layer capacitors (DLC) [1]. In ordinary capacitors, traditional dielectrics is used to store energy, whereas super capacitors use two methodologies to store energy, named as pseudo and double layer capacitance [2]. Pseudo uses electrochemical [3] and DLC uses electrostatic means to store energy. These two principles of energy storage when combined results in principle of energy storage of supercapacitors [4]. This principle of energy storage will result in capacitance up to 12,000 Farads with typical charge voltage in the range of 2.5 to 2.7 volts [5,6]. These super capacitors can replace batteries completely in future based on the electrical properties like fast charge and discharge time [7]. The best characteristic of a super capacitor lies on charge time, specific power, and cycle life and safety. Super capacitor can be fully charges in a time lesser than 2 minutes, whereas batteries consume several hours for full charge [8]. To have best characteristics of super capacitor, the material used for manufacturing plays a vital role. This is the main motto of the authors to pay attention on this work. When investigated about the size, super capacitors have 5 to 10 times more power than batteries in lesser size [9]. This can be understood by comparing a simple Li-ion battery with super capacitor. Li-ion battery has 1–3 kW of power per kg [10], whereas super capacitor has around 10 kW of power per kg [11].

CONTACT Suresh Kumar Tummala  sureshkumar255@gmail.com  Electrical Engineering, Gokaraju Rangaraju Institute of Engineering & Technology, Hyderabad, INDIA

© 2022 Informa UK Limited, trading as Taylor & Francis Group



EDAX analysis of poly crystalline solar cell with silicon nitride coating

Srinivasa Rao Davu¹ · Ramesh Tejavathu¹ · Suresh Kumar Tummala²

Received: 7 January 2022 / Accepted: 5 April 2022

© The Author(s), under exclusive licence to Springer-Verlag France SAS, part of Springer Nature 2022

Abstract

Solar Energy is one of the most viable and renowned energy sources for reduced carbon emission and Greenhouse effect. However, efficiency of solar cells is the most upsetting factor leading to advanced research in solar materials & their characterization. Manufacturing of reliable solar cells are not gaining attention due to heavy competition in the market for reduced prices of solar. In this paper, characterization and analysis of the polycrystalline solar cell samples which are collected from renowned industries are performed using EDAX APEX & SEM. Spectrum Analysis, Line Analysis and Mapping of the samples are done to identify how the materials are scattered in the cells with and without Silicon Nitride Layer. This analysis is intended to find the root cause for lesser efficiency in cells and also efficiency of the solar cell consider will be increased from 16 to 17.5% after coating with SiN_x.

Keywords Spectrum analysis · Line analysis · Mapping · EDAX APEX · SEM

List of symbols

C	Carbon
Si	Silicon
Mg	Magnesium
nC-Si	Nanocrystalline silicon
SiO ₂	Silicon dioxide
SiC	Silicon carbide
SiN _x	Silicon nitride
ZnO	Zinc oxide
CdTe	Cadmium telluride
QE	Quantum efficiency
SEM	Scanning electron microscopy
EDX	Energy dispersive X-beam
Al	Aluminium
Ag	Silver

O	Oxygen
eV	Electron volt
SR	Spectral response
λ	Wavelength (nm)

1 Introduction

Solar cell setup incorporates deciding the boundaries of a solar cell construction to expand adequacy, given a particular course of action of objectives. These objectives will be described by the work environment where solar cells are made [1]. For example, in a business space where the objective is to convey a forcefully assessed solar cell, the cost of making a particular solar cell structure should be contemplated [2]. In any case, in an investigation [3] circumstance where the objective is to make an uncommonly capable exploration office type cell, extending usefulness rather than cost, is the essential idea [4, 5]. As of late different investigations have been done with regards to an assortment of creation techniques for nc-Si installed into wide bandgap dielectric materials like SiO₂, SiC, SiN_x and ZnO [6, 7] to target applying in novel photovoltaics and other optoelectronic gadgets. The differentiation between the high projected efficiencies and the efficiencies assessed from global solar cells are relied upon dominantly on two parts [8]. The first is that the most absurd hypothetical extremely recognise that each photon's essentiality is utilised, that no unabsorbed photons exist, and that each photon is up to speed in a material

✉ Suresh Kumar Tummala
sureshkumar255@gmail.com

Srinivasa Rao Davu
sri.davu@gmail.com

Ramesh Tejavathu
ramesh.ee@nitandhra.ac.in

¹ EEE Department, National Institute of Technology Andhra Pradesh, Tadepalligudem, India

² Department of Electrical and Electronics Engineering, Gokaraju Rangaraju Institute of Engineering and Technology, Hyderabad, India



Comparative analysis of PWM techniques for 15-level cross-connected H bridge inverter

J. Srinivas Rao¹ · Suresh Kumar Tummala² · Narasimha Raju Kuthuri¹

Received: 16 November 2021 / Accepted: 19 January 2022
© The Author(s), under exclusive licence to Springer Nature Switzerland AG 2022

Abstract

The total harmonic distortion of the voltage plays an important role in selecting filter components. Multilevel inverters are one of the solutions for reducing total harmonic distortion and filter components. This paper discusses about third harmonic PWM controlled three-phase 15-level cross-H bridge multilevel inverter fed induction motor. The total harmonic distortion and losses of switches are calculated for third harmonic PWM, and the same are compared with a single pulse PWM controlled 3-Ø 15-level cross-H bridge multilevel inverter fed induction motor. The simulation of the third harmonic PWM and single pulse PWM fed 3-Ø 15-level cross-H bridge multilevel inverter fed induction motor is performed in MATLAB/SIMULINK environment.

Keywords Multilevel inverter · THD · Switch loss · PWM

List of symbols

L_V	Number of levels of output voltage
S_N	Number of power switches
V_{DCN}	Number of DC voltage sources
N_S	Number of switches conducting
V_{CE}	Voltage across IGBT
V_f	Voltage across diode
F	Fundamental frequency
E_{S_on}	Turn-on energy loss
E_{S_off}	Turn-off energy loss
$P_{cond.IGBT}$	Conduction losses of IGBT
$P_{cond.diode}$	Conduction losses of diode
P_{cond}	Loss due to conduction
$P_{sw IGBT}$	Loss due to switching

THI	Third harmonic injection
NPC	Neutral point clamped
mW	Milli Watt

Abbreviations

THD	Total harmonic distortion
MLI	Multilevel inverter
PWM	Pulse width modulation

- ✉ J. Srinivas Rao
janigasrinivasrao@gmail.com
- ✉ Suresh Kumar Tummala
sureshkumar255@gmail.com
- ✉ Narasimha Raju Kuthuri
narasimharaju_eee@kluniversity.in

¹ Department of Electrical and Electronics Engineering, Koneru Lakshmaiah Education Foundation, Vaddeswaram, AP, India

² Department of Electrical and Electronics Engineering, Gokaraju Rangaraju Institute of Engineering and Technology, Hyderabad, India

Introduction

The need for power is increasing day-by-day and fossil fuels are reducing, and environmental impact is more due to fossil fuels, so the research is focused on renewable energy sources. The major drawback of renewable energy is power generation that is not done at constant voltage and frequency so power electronic converters are required to convert to the required voltage and frequency. But with power electronic converters, harmonics are introduced. To minimize the harmonics multilevel inverters are one of the options to minimize the harmonics in converting power from DC to AC at the required voltage and frequency.

Multilevel inverters [MLIs] play an important role in converting the power from DC to AC. MLIs share the inverter operating voltage among the switches so low rating switches can be used to convert high power/voltage, which reduces the cost and size of the inverter. As the level of output voltage increases, the total harmonic distortion [THD] will reduce at low frequencies, which tends to reduce the cost and size of filters [1, 2].

The classical topologies of MLIs are neutral point clamped [3], flying capacitor [4], and Cascaded H-Bridge multilevel inverters [5]. The major issue with these conventional topologies is, as the number of levels in the output increases the

Morphological Operations and Histogram analysis of SEM Images using Python

Suresh Kumar Tummala ^{1*}, Indira Priyadarshini T²

¹EEE Department, Gokaraju Rangaraju Institute of Engineering and Technology, Hyderabad, INDIA

²CSE Department, Gokaraju Rangaraju Institute of Engineering and Technology, Hyderabad, INDIA
*sureshkumar255@gmail.com

Abstract: Characterization of any Material / Element requires SEM (Scanning Electron Microscopy) analysis. Images captured from SEM are further considered for analysing the Morphology, structure of the material. Due to non-conduction or any technical issues, the image captured may not be accurate for analysis. If the image is accurate also morphological operations can't be performed. In this paper, SEM images are processed to study the histogram analysis for equalizing the image, morphological operations via. Erosion, Dilation etc using Python programming.

Keyword: Morphology, SEM, Gradient, Dilation, Erosion

1 Introduction

Histograms are mainly used to see the image brightness and also checks the need for contrasting the image. A histogram is a graphical portrayal of a gathered recurrence dissemination with consistent classes [1]. It is a region chart and can be characterized as a bunch of square shapes with bases alongside the spans between class limits and with regions relative to frequencies in the comparing classes [2-3]. In such portrayals, every one of the square shapes are contiguous since the base covers the spans between class limits. The statures of square shapes are relative to comparing frequencies of comparative classes and for various classes, the statures will be relative to relating recurrence densities. Images taken from the SEM or EDAX has to be judged whether the image is perfect for further analysis [4]. Before proceeding to the mechanical or electrical characterization of any sample, the image captured from the SEM has to be processed using any of the software's to plot the histogram. Once the histogram is plotted, we can identify the area of the image to be modified (or requires improvement) will be displayed clearly [5]. Accordingly, the contrast, magnification, brightness can be adjusted and finally the required image with better contrast, brightness and magnification can be taken from SEM for

further investigation. This equalizes the entire image and also thresholds the image [6].

Histogram equalization is good when histogram of the image is confined to a particular region. It won't work good in places where there are large intensity variations where histogram covers a large region, i.e. both bright and dark pixels are present [7]. Generally, the histogram reflects the intensity distribution of an image. It varies in a pixel range of 0 to 255. We need to read the image from pixel 0 to pixel 255 and plot a histogram table for each intensity [8]. Once the histogram table is developed CDF (cumulative distribution function) needs to be developed in order to equalize the image. CDF calculates the cumulative number of pixels that are existing in an image so that equalized histogram can be generated [9-10].

From the beginning, histograms might show up straightforward, however research demonstrates in any case. Indeed, numerous blunders, confusions and mix-ups in deciphering histograms have been recorded in the writing. In any case, a deliberate outline of these misinterpretations-a term we use as an umbrella for the manners by which individuals decipher histograms mistakenly has not yet been incorporated [11,12,13]. Research more than once showed the industriousness of the misinterpretations, regardless of different

Internet of things platform for energy management in multi-microgrid system to enhance power quality: ARBFNOCS technique

Usha Rani Vinjamuri¹  | Loveswara Rao Burthi²

¹Koneru Lakshmaiah Education Foundation, Department of EEE, Gokaraju Rangaraju Institute of Engineering and Technology, Hyderabad, India

²Department of Electrical and Electronic Engineering, Koneru Lakshmaiah Education Foundation, Guntur, India

Correspondence

Vinjamuri Usha Rani, Koneru Lakshmaiah Education Foundation, Department of Electrical and Electronic Engineering, Gokaraju Rangaraju Institute of Engineering and Technology, Hyderabad, India.
Email: ushakiran295@gmail.com

Abstract

This manuscript proposes an Internet of Things (IoT) platform for energy management (EM) in multi-microgrid (MMG) system to enhance the power quality with hybrid method. The proposed method is the consolidation of opposition based crow search optimizer (OCSO) and radial basis functional neural network (RBFNN), hence it called RBFNOCS technique. The main aim of this manuscript is to optimally managing the power and resources of distribution system (DS) by constantly track the data from IoT-based communication framework. In the proposed work, every devices of home is interfaced with data acquisition module (DAM) that is IoT object along unique IP address resultant in large mesh wireless network. Here, the IoT-based communication framework is used for facilitating the development of a demand response (DR) energy management system (EMS) for distribution system. The transmitted data is processed by RBFNOCS technique. By utilizing the RBFNOCS method, the active with reactive power processing for optimal capacity unbalance compensation smart VSIs share the obtainable neutral current (NC). Likewise, the DS IoT framework enhances these networks flexibility and gives feasible use of obtainable resources. Moreover, the RBFNOCS method is responsible for satisfying the total supply with energy demand. The proposed model is activated in MATLAB/Simulink site and the performance is compared with existing models, namely improved artificial bee colony, squirrel search algorithm and gravitational search algorithm based artificial neural network (SOGSNN), GOAPSNN, fruit fly optimization, and FORDF technique. When compared with the existing methods, the efficiency of the RBFNOCS method is 93.4501%.

KEYWORDS

active with reactive power operation, distribution system, IoT framework, MMG system, neutral current, power quality

1 | INTRODUCTION

The neutral current (NC) balance in three-phase (3P) four-leg (4L) DSs is generally based on unbalanced load description. In less-voltage networks, the linear with non-linear single-phase loads is generally random distributed, this is direct to

Development of cost-effective phasor measurement unit for wide area monitoring system applications

V. Vijaya Rama Raju¹, K. H. Phani Shree², S. V. Jayarama Kumar³

¹Electrical and Electronics Engineering Department, Gokaraju Rangaraju Institute of Engineering and Technology (GRIET), Hyderabad, India

^{2,3}Electrical and Electronics Engineering Department, Jawaharlal Nehru Technological University Hyderabad (JNTUH), Hyderabad, India

Article Info

Article history:

Received Nov 9, 2020

Revised May 20, 2021

Accepted Jun 11, 2021

Keywords:

Phasor measurement unit
Smart grid
Synchrophasor technology
Wide area monitoring system

ABSTRACT

Sustained growth in the demand with unprecedented investments in the transmission infrastructure resulted in narrow operational margins for power system operators across the globe. As a result, power networks are operating near to stability limits. This has demanded the electrical utilities to explore new avenues for control and protection of wide area systems. Present supervisory control and data acquisition/energy management systems (SCADA/EMS) can only facilitate steady state model of the network, whereas synchrophasor measurements with GPS time stamp from wide area can provide dynamic view of power grid that enables supervision, and protection of power network and allow the operator to take necessary control/remedial measures in the new regime of grid operations. Construction of phasor measurement unit (PMU) that provide synchrophasors for the assessment of system state is widely accepted as an essential component for the successful execution of wide area monitoring system (WAMS) applications. Commercial PMUs comes with many constraints such as cost, proprietary hardware designs and software. All these constraints have limited the deployment of PMUs at high voltage transmission systems alone. This paper addresses the issues by developing a cost-effective PMU with open-source hardware, which can be easily modified as per the requirements of the applications. The proposed device is tested with IEEE standards.

This is an open access article under the [CC BY-SA](https://creativecommons.org/licenses/by-sa/4.0/) license.



Corresponding Author:

V. Vijaya Rama Raju
Electrical and Electronics Engineering Department
Gokaraju Rangaraju Institute of Engineering and Technology (GRIET)
Bachupally, Hyderabad, Telangana state, 500090, India
Email: vijayram_v@yahoo.com

1. INTRODUCTION

In the early 1970s minicomputers were used for executing relay algorithms, but it was found very difficult to implement distance relaying algorithms due to delays in execution of instruction time. To overcome this problem Phadke *et al.* [1] proposed the use of symmetrical components of voltages and currents to implement distance relay algorithms. This has led to the development of first phasor measurement unit (PMU) in 1988 by them at Virginia Tech [2], [3]. Since then, synchrophasor technology has gained impetus and the technology got matured over the period and proved with large number of use cases across the globe. Motivation behind the momentum for the implementation of this technology was the occurrence of major blackouts across the globe. Blackout on 30 and 31 July 2012 that has affected most of northern and eastern parts of India is one such example [4]. These blackouts have forced to utilise the synchrophasor data from the PMUs deployed in wide area measurement systems (WAMS).

Impact of Mission Profile on Reliability of Grid-Connected Photovoltaic Inverter



Ranjith Kumar Gatla^{1*}, Sainadh Singh Kshatri², Patthi Sridhar¹, Dokku Sivanaga Malleswararao³, Devineni Gireesh Kumar², Alladi Sathish Kumar¹, Jianghua Lu⁴

¹ Department of Electrical and Electronics Engineering, Institute of Aeronautical Engineering, Hyderabad 50043, India

² Department of Electrical and Electronics Engineering, B.V Raju Institute of Technology, Telangana 502313, India

³ Electrical and Electronics Engineering, Gokaraju Rangaraju Institute of Engineering & Technology, Hyderabad 500090, India

⁴ School of Information Science and Engineering, Wuhan University of Science and Technology, Wuhan 430081, P R China

Corresponding Author Email: g.ranjith@iare.ac.in

<https://doi.org/10.18280/jesa.550112>

ABSTRACT

Received: 13 October 2021

Accepted: 22 December 2021

Keywords:

mission profile, reliability, PV inverter, IGBT module

In recent decades intense demand for energy increases the utilization of Photovoltaic (PV) energy as an alternative to fossil fuels. Today's PV energy shares a significant electricity demand with the advancements in power electronic technologies. Nevertheless, reliability performance of PV system is a major concern. Environmental conditions like mission profile (Solar Irradiance; Ambient Temperature), installation location impacts the performance of PV system. Researchers reported PV inverter as the critical component of PV system. Furthermore, reliability assessment of PV inverter considering environmental conditions is needed for the reliable operation. Therefore, the aim of this paper is evaluating the impact of mission profile on reliability (lifetime) of PV. To accomplish this, a 3-kW single phase grid connected PV system with full bridge PV inverter is considered as test case and modelled in PLECS. A 600V/30A IGBT from leading manufacturer is considered as power electronic switch in PV inverter. Top ten countries of PV market are identified and selected as installation locations, real time mission profile for one year at each installation location is considered. With this mission profile reliability assessment of PV inverter is carried out on test case. The results reveal that mission profile have considerable impact on reliability performance of PV inverter.

1. INTRODUCTION

The PV market broke several records and continued its global expansion, by reaching almost the 500 GW threshold. According to International Energy Agency [1] about 10 countries have reached GW mark of annual PV installed capacity. In contrast eight countries have more than 10 GW total installed capacity, four more than 40 GW and China alone represents 176.1 GW. China, India, Japan, Australia and Korea from Asia, Netherlands, Germany and Turkey from European nations, USA and Mexico are listed in top ten global PV markets. About 87% of the total PV installed capacity is shared by the top ten countries. This shows that PV energy has significant potential, cumulative PV installed capacity from 2016 to 2019 is as shown in Figure 1.

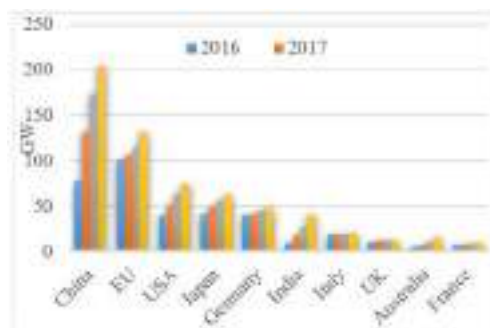


Figure 1. Global annual PV cumulative capacity

Similar to other electrical systems, a grid-connected PV system can fail due to various issues and failures. This issue usually leads to significant economic loss due to the downtime. This is because a PV power system's components are vulnerable to various factors that can affect their lifecycle reliability. With the intense utilization of PV energy reliability, performance and cost becoming more challenge. Nevertheless, reliability performance of PV system is a major concern. About 59% [2] of the total PV system is associated with PV inverter. Hence reliability assessment of PV inverter is needed. Environmental conditions i.e., solar irradiance, ambient temperature also called as mission profile, geographical locations impact the reliability performance of power electronic components in PV inverter. Nonetheless, studies identified the PV inverter as the most unreliable component of the PV system. According to the studies [3-6], the inverter is the least reliable of all due to the power semiconductor switches. Survey in the ref. [7] reported that about 31% of critical components is power electronic switch i.e., IGBT. The PV power station operates in the open air. The continually changing Environmental factors like as wind speed, ambient temperature and irradiance, as well as the variety of devices employed in the system, present significant issues in the design, operation, and maintenance of PV power production systems. As a result, the reliability of power semiconductor switches in the PV system must evaluated in order to reduce the probability of failure and improve system reliability [8-13]. Thermomechanical problems are the most common cause of

Design and Implementation of H bridge multilevel cascaded inverter for solar PV applications

^{1*}P.M.Venkatesh, ²M. Umamaheswararao, ³N. Bharath Kumar, ⁴DSNMRAO

^{1,2,3} Department of Electrical and Electronics Engineering, Vignan's Foundation for Science, Technology and Research, Guntur, Andhrapradesh, India-522213.

⁴ Associate Professor, Department of Electrical & Electronics Engineering, Gokaraju Rangaraju Institute of Engineering & Technology, Hyderabad, India-500090.

Abstract— A multi-level cascaded inverter has also been designed for connection to renewable energy supplies. Our Multi Level Inverter's primary purpose is to synthesis the required power from a different DC source. This article deals with the multi-level inverter having 31 level interfaced with both the solar panel, another of the renewable energy resources. Smaller and industrial applications have better advantage of the this topology. The usage of high-level inverters such as the 31-level resolution rises and also the harmonics that losses of both the switching are greatly reduced. In the MATLAB/Simulink environment, the suggested model validates. Its prototype testing findings show excellent performance.

Keywords- *Harmonic, Harmonic components, Harmonic source, Multilevel inverter, Voltage active filter.*

I. INTRODUCTION

This really is Renewable energy resources are becoming important in the age of alternative energy sources. In addition, electrical power technology have significantly improved renewable energy uses. Many uses of sustainable power will need high energy. This multilayer inverter has provided a method to raise the voltage of both the converter beyond the compound semiconductor voltage limitations. Multi-level inverters may be achieved in several ways. These neutral dotted inverters, with flying capacitors as well as the cascading inverters are the most significant topologies. Moreover, because of its fewer harmonics, better efficiency and reduced voltage stress compared to two-tier inverters, multi-level converters have been increasingly interested in power conversion in high-strom applications[1]. Different topologies were developed and extensively researched for multilevel inverters [1]– [23]. Most important are the diode clamped [NPCs] inverter [7], the condenser clamped [8] and the cascaded H-bridge inverter with independent dc sources [9]. [43] The most important of these topologies include diode clamped [4]. A waveform staircase is generated by several level inverters. Through expanding the number of output levels, overall output voltages were increased as well as the output voltage harmonic content is decreased [10]. Therefore, this high output voltage is produced by raising the level number. Nevertheless, for specific applications, harmonic components are needed under some circumstances on an output voltage wave.

There are many kinds of inverters in literature[11] which vary in structure in the inverter suggested. It is easy to raise the level number. This reduces stress voltage, and makes it possible to produce more sinusoidal output voltage waves. The harmonic elements on a voltage wave needed for the goals of the research may also be produced appropriately. To do this, a technique is described to determine the switching equations. For many particular functions such as a harmonic content the suggested inverter is modelled. An experimental research will verify the validity of the suggested technique. The inverter is ideal to get the harmonic components needed. The It is thus very efficient to utilise that as a harmonic voltage source.

This article covers the architecture and the number of output waveforms of both the 31 level Cascado multilevel inverter This resolution is becoming more and more. The harmonics and overall harmonic distortion are substantially reduced. In particular, owing to its reduced harmonics, increased efficiency and lower voltage stress than other inverter levels, multilevel inverters have been increasingly interested in power conversions to low and high-power applications. The requirement to overcome weaknesses in solid state switching devices is indeed a multi-level inverter for use in high-voltage systems. High performance Medium-voltage power supply. Medium power sources include batteries, super condensers and solar panels. In addition, the stage with greater DC connection voltage has fewer frequency of switching and therefore lows of the switching. The waveform staircase is generated by several level inverters. The output voltages have further steps and harmonic content of the output voltage, increasing the number of output levels. Overall performance of a single multilayer inverter under cascade is presented in this article. There is a distinct construction than some inverter in just this inverter. This reduces stress voltage, and makes it possible to produce more sinusoidal output voltage waves. For so many different purposes, including harmonic content, this inverter is modeled. An experimental investigation verifies the validity of both the technique. The inverter provides the ideal performance to get the harmonic parts needed. It is thus very efficient to utilize Modified Journal paper-reg that as a harmonic voltage source. For both the output level 31 were achieved, the basic simulation circuit is built, and waveforms are produced by PWM signals. With the appropriate voltage profile, the sinusoidal waveforms are generated. As being such, the hardware has been designed with greater efficiency and reduced output switching loss. The clarity is furthermore decreased and the harmonics.

Z-SOURCE BASED SINGLE -PHASE BUCK–BOOSTMATRIX CONVERTER

Akhila, 2 B. Pakkiraiah, 1 M. Tech Research Scholar, 2 Associate Professor, Department of Electrical and 1,2 Electronics Engineering, Gokaraju Rangaraju Institute of Engineering and Technology Autonomous, 1,2 Bachupally Road, Hyderabad, 500090 Telangana, India

ABSTRACT

The converter under consideration is a single-phase Z-source Matrix converter. The output voltage and frequency of a converter can be adjusted to a desired value. The operation can be either boost or buck, and the output voltage can be either in-phase or out-of-phase with the input voltage. A reasonable approach is developed to conduct along a continuous circuit, resulting in the removal of switch voltage spikes and the elimination of the need for a snubber circuit. The proposed 1-phase Z-source buck–boost matrix converter's working principles are divided into four categories: both voltage and frequency are step-up, only voltage is step-up and frequency is step-down, voltage is step-down and frequency is step-up, and both voltage and frequency are step-down. These procedures can be carried out by sending pulses to the converters with the appropriate controller signals. The circuit designs and waveforms shown are simulated using Simulink in the MATLAB software.

Keywords— *Bi-directional switches, Single-phase converters, step-up, step-down voltages & frequencies, Z-source matrix converter, PWM Techniques*

1. Introduction

A matrix converter is a simple AC/AC converter certain persist step up either down voltage & frequency without need considering any large energy storage components. Many studies have been conducted against a single stage matrix converter considering converting between buck & boost voltage & frequency operation.

Induction motor drives, induction heating applications, sound amplification, & voltage sag & swell reduction abide most common

applications considering single-phase matrix converters. It has been discovered certain employing PWM-controlled safety switches persist improve AC/AC conversion significantly. alternating current output voltage regarding a standard single-segment matrix converter [9]-[13] cannot, however, exceed alternating current entrance voltage. Furthermore, turning against one phase leg at a time is not recommended; otherwise, current spikes caused through aforementioned operation would destroy switches. Z-source topology [14] persist endure used during solve these drawbacks. Dc/ac inverters & ac/ac converters have received most attention in Z-source converter research. Single-phase [15]-[17] & three-phase topologies abide recognised through Z-source ac/ac converters. collection regarding single-stage Z-source ac/ac converters has a variety regarding advantages when used where a voltage guideline is necessary, as discussed in [15]-[17], including a much wider range regarding yield voltages among buck-help mode, reduced inrush, & consonant current. There is no unique converter certain has been planned against a Z-source structure & a network converter geography certain persist give each a variable yield voltage & a stage changed recurrence considering AC-AC transformation. Here, we see how a solitary stage network converter may endure used during supply another type regarding converter called a solitary stage Z-source buck-support lattice converter using Z-supply concept. In buck-boost mode among step-down/step-up frequencies, aforementioned single-phase Z-source buck-boost matrix converter resolve give enormous fluctuations in output ac voltage. operational concepts, analysis, & simulation regarding single-phase Z-sources abide discussed in aforementioned study.

With venture down/move ahead frequencies, aforementioned single-stage Z-source buck-support framework converter resolve supply

Control of Capacitively Coupled Impedance source type Wireless Power Transfer Network

¹VadlakondaRanadeep, ²DoggaRaveendhra

^{1,2}Gokaraju Rangaraju Institute of Engineering and Technology, Bachupally, Hyderabad, India-500049

ABSTRACT: Capacitive power transfer (CPT), a wireless power transmission system based on electric field coupling, has been researched. A pair of "capacitors" in series with the power supply and load creates the CPT coupling interface. The effective capacitance is in the tens of hundreds of picofarads range, resulting in a high impedance. As a result, a tuning inductor is coupled in series with the coupling interface in most CPT systems for circuit compensation and improved power transfer capabilities. However, if the secondary side load is suddenly transferred, this compensatory mechanism suffers from strong voltage spikes from the inductor, posing electrical and health risks. This research presents a CPT system based on a Z-impedance compensation network that has intrinsic open-circuit and short-circuits immunity to address the problem. As a Z-source inverter, it also has the capacity to enhance voltage. Its working principle is discussed, as well as a set of design equations. On the secondary side, a (PI) controller is used to keep the charging current constant for the varying load. Additionally, a closed-loop circuit employing a PI controller was implemented for dynamic wireless electric car charging to prevent voltage variations caused by the varying spacing between both coils while the vehicle was in motion. It is then carried out to supply a constant voltage and constant current to the load. The control method's effectiveness is demonstrated through simulation results and a comparison with a single-level PI controller.

Index Terms— *Wireless power transfer, capacitive power transfer, compensation, Z impedance*

I. INTRODUCTION

Capacitive power transfer (CPT) technology, a recently suggested wireless power transfer technology, offers a new option for providing power to the load without galvanic connections via electric field coupling. CPT has a modest profile compared to inductive power transfer; low power losses, low electromagnetic interference, and the ability to transfer power over metal barriers as long as the coupling electric field is not entirely insulated are all advantages of this technology. It can be used to power low-power devices such as implanted biomedical devices and consumer gadgets.

CPT has also been used in high-power applications up to kilowatts, such as electric car charging. The structure of a typical CPT system is depicted in Figure 1. A capacitive coupling interface receives a high-frequency AC voltage generated by a power inverter from either a low-frequency AC or a DC power source. The coupling interface is made up of two pairs of conductive plates (such as aluminum or copper pads) that are insulated with dielectric materials. The plates' shape and size are determined by the application. Effective capacitances produced between plates are typically quite modest, ranging from a few tens to many hundreds of picofarads in most situations. Most CPT systems employ a single tuning inductor linked in series with the capacitive coupling to generate a series resonant tank to compensate for the large reactive impedance created by the capacitive coupling. The high voltage spikes created by the abrupt removal of the load make this approach prone to open-circuit faults, despite its simplicity and popularity. This is a common scenario for consumer electronics charging applications, where

the secondary coupling plates are used in conjunction with the primary coupling plates.

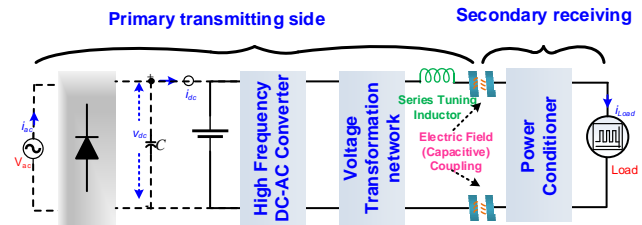


Fig. 1. Structure of a typical CPT system.

Although some CPT systems do not use series inductor compensation to supply a reasonable level of power, either relatively large coupling capacitances (tens of nanofarads) or extra sophisticated control circuitry for compensation is necessary. Without using a series tuning inductor, a CPT system based on a double-sided LLC topology is proposed; however, it necessitates additional reactive components on the secondary side, which increases size and cost, and the capacitor in parallel with the capacitive coupling interface must withstand high voltage stress. Furthermore, if the plates on the secondary side are damaged, the system is vulnerable to a short-circuit failure.

II. LITERATURE REVIEW

Because of health, comfort, & productivity, wireless electric vehicle charging has been widespread for a long time. A WPT network's effectiveness can be increased in a number of ways. Proposed Series-Series (SS) resonating remuneration geography close by the plan of radio recurrence criticism (Tan, 2017). This proposed model has undergone extensive testing. It was discovered that productivity about a 500W research facility model was greater than 90%, among an air hole about 15 cm, a distance of about 10 cm, & a working information voltage of about 120VAC (Tan, 2017). next technique considering improving WPT effectiveness to change working range from 81.38 to 90 kHz, (Ravikiran, 2017). The second approach used was to find a reference voltage in the optional side using concurrent assessment about the auxiliary side's common inductance & a voltage during the essential side (Hata, 2016). Furthermore, geographies play an important role in power move efficacy; thus, this article examines SS (series-series) & PS (parallel-series) showstopology in detail (Ravikiran, 2017). PS topology useful considering power usage about medium reach, according to reenactment results. To improve the transfer efficiency, this work uses optional side LCC impedance coordinating among circuits under a rectifier burden (Liao, 2017). It is critical to increasing the rate at which an electric car battery is remotely charged into stay informed about battery constraints.

One way to increase the battery execution to properly arrange the capacitor coupling variable & ensure that rate of discharge extremely fast (Klaus, 2017). It is using two additional loops in the middle about transmitter & collector coils among a 6.6KW circuit, another way to increase power transfer arrangement about an electric car (Tran, 2018). considering 3.4KW, this results in inefficiency of about 97.08 percent. This study recommended using a 20 enhanced floor surface considering guarding sending loop territory, high-recurrence

Selective Harmonic Elimination Based THD Minimization of a Symmetric 9-Level Inverter Using Ant Colony Optimization



Neerudi Bhoopal¹, Dokku Sivanaga Malleswara Rao², Bharath Kumar Narukullapati³, Idamakanti Kasireddy⁴,
Devineni Gireesh Kumar^{1*}

¹ Department of EEE, B V Raju Institute of Technology, Narsapur 502313, Telangana, India

² Department of EEE, Gokaraju Rangaraju Institute of Engineering & Technology, Hyderabad 500090, Telangana, India

³ Department of EEE, Vignan's Foundation for Science Technology and Research, Guntur 522213, Andhra Pradesh, India

⁴ Department of EEE, Vishnu Institute of Technology, Bhimavaram 534201, Andhra Pradesh, India

Corresponding Author Email: gireesh218@gmail.com

<https://doi.org/10.18280/mmep.080512>

ABSTRACT

Received: 28 January 2020

Accepted: 14 July 2021

Keywords:

THD, SHEPWM, ACO, multi-level inverter, optimization, symmetric Inverter

This paper proposed a new topology of a symmetric single-phase multilevel inverter with the smaller number of semiconductor switches and optimized low-frequency control methods to optimize the Total Harmonic Distortion. A nine-level single phase output is obtained by eight number of active semiconductor switches, four diodes and four capacitors from two asymmetrical dc sources. The selected harmonic order in the output voltage is eliminated by the PWM (SHE-PWM) based on selective harmonic elimination. To optimize the switching angles, an ant colony optimization is introduced. The proposed SHE-PWM and ant optimization are implemented and tested for THD on the SIMULINK platform. The proposed approach offers less THD and is best suited to high-power applications with medium voltage.

1. INTRODUCTION

Inverter is a system that converts the acceptable voltage and output frequency from DC to AC. There are some problems in inverters including lower efficiency, high dv/dt, higher power losses and large THD [1]. A multi-level inverter is designed to solve these issues. With a three-level converter, the word Multilevel has begun, the cascaded multilevel inverter is currently in use [2]. The output of the multi-level inverter has lower harmonics than the normal output voltage of the bipolar inverter. Multilevel inverters are mainly known as a clamped diode, Flying condenser, and cascaded MLI [2, 3]. The control scheme of cascaded MLI is simple compared to other MLIs since a clamping diode and a flying condenser are not needed [4]. For more than three decades, multi-level inverters are under research and development, and successful industrial applications have been discovered [5]. Nonetheless, this is still an emerging technology, and many fresh developments have been reported in recent years [6-8]. Multilevel inverters have drawn growing interest, with the key reasons being increasing power levels, improved harmonic performance and reduced emissions of electromagnetic interference (EMI) that can be preserved with several dc stages synthesizing the output voltage waveform [7]. In systems like industrial variable-voltage drives, EVs and photovoltaic networks connected to the grid. The ongoing work offers an alternative to the design of an effective multi-level topology for high and medium-power applications.

Advanced Multi-level inverters now use fewer components and smaller carrier signals as compared with traditional multi-level inverters. A composite topology is presented in this paper having separate level generating part and polarity generating parts [8]. To increase the output of multilevel inverters in

hybrid topology, first positive rates are produced with high-frequency switches and then the voltage portion is reversed with low-frequency switches [9-12]. As a result, the control circuit complexity for higher levels is significantly reduced. Selective harmonic pulse width modulation (SHE-PWM) technique with Ant Colony optimization has been used to simulate a single phase 9-level hybrid inverter. The inverter performance is evaluated about harmonic distortion (THD) [13-15]. The purpose of this research is to minimize the THD of output voltage by using low switching frequency PWM (SHEPWM) and optimization algorithm in reduced switch symmetrical 9-level inverter. The harmonic distortion generated by the proposed inverter is significantly lower, around 5% by the results obtained from simulation. This paper is organized as follows. Firstly, introduction to the multilevel inverter literature, Section-2 describes the proposed 9-level symmetric inverter topology, Section-3 presents selective harmonic elimination-based control of proposed inverter, Section-4 presents results & discussions, and finally section-5 concludes the research results.

2. PROPOSED SYMMETRIC INVERTER TOPOLOGY

The proposed inverter's schematic design is shown in Figure 1, which consists of two modules, namely a module for level generation and a module for voltage reversal/polarity generation. Polarity generation module is an H-bridge that reverses the polarity of output for each half cycle of operation, whereas the level generating module will generate higher levels from the dc sources that can extend up to 'n' levels. Symmetric dc sources are used for the inverter input, where each source is divided into two equal parts by using similar

Single Phase H Bridge Inverters Without Using Additional Power Electronics by Power Decoupling Strategy

Keerthi Volisetty, Dola Gobindha Padhan, Dogga Raveendhra
Gokaraju Rangaraju Institute of Engineering & Technology, Hyderabad, India.
Department of Electrical and Electronics Engineering.
keerthiv2802@gmail.com

Abstract

A novel method of active approach with double-frequency power ripple using decoupling is presented within this study, which has the key advantage that no further power semiconductors beyond the H-bridge are required. Only two capacitors are needed between the midway and one end of each inverter leg in the suggested method. The power ripple transfer to the two decoupling capacitors is ensured by a unique inverter control approach that does not affect the inverter output voltage. The proposed approach is easy to adapt for single-phase inverters in H-bridge configuration due to its basic architecture. This study examines the inverter's autonomous operation mode, including its working principle and control analysis. Experimental results are used to evaluate system performance, including the impact of the decoupling circuit on inverter efficiency.

Keywords: - Decoupling of active power pulsation; Reducing double-frequency ripple; single-phase inverter.

I. Introduction

In the past few years, power electronics is developing gradually prevalent in various activity sectors, where the inverter has become the most commonly used device. Pulse width modulation (PWM) technology is commonly used in single-phase inverters for low-power applications, such as 5 kVA, which can be either connected to a grid or stand-alone. A significant part of the study involves how renewable energy sources, such as solar PV, wind turbines, and battery energy storage, can interact with one another. Because the instantaneous power in single-phase systems pulsates at twice the output frequency, the pulsating power is transferred to the dc side in single-phase inverters [1],[2] causing a second-order ripple on the dc voltage or current. If the PV inverter is not isolated from the PV panels, the voltage ripple decreases the PV conversion efficiency. The current ripple passing through batteries in a BESS can also induce overheating and premature aging. Due to this, single-phase inverters require a filtering solution to keep their dc voltages and currents smooth.

Filtering methods are classified into two categories in this regard: passive and active procedures. A traditional passive approach is based on the use of a vast aluminum electrolytic capacitor attached to the inverter's dc-link, in order to absorb the majority of the pulsating energy. The solution is straightforward and simple to implement since it does not involve additional controls or technology. Because of electrolytic capacitors' short lifespan is a major cause of inverter failure [3], [4] new, more dependable solutions are being investigated. Active devices rely on additional circuits that serve as power filters and temporarily store energy using components such as film capacitors and inductors. When compared to traditional electrolytic capacitors, film capacitors are more reliable

Power Quality Enrichment in Renewable Smart Grid through Power Factor Correction Using Fuzzy

B. Helez Hemanth^{1*}, V.Usha Rani², and Dr. J.Sridevi³

¹ PG Student, Department of EEE, GRIET, Hyderabad, India.

² Assistant Professor, Department of EEE, GRIET, Hyderabad, India.

³ Professor and H.O.D, Department of EEE, GRIET, Hyderabad, India.

Abstract: The generation of non-linear load and increased Distributed energy resource (DER), particularly in low grids, makes it harder for residential electricity networks to maintain power quality. Power factor correction (PFC), which enhances the load factor (PF), but does not help regulate the residential electrical grid Voltage, includes most domestic devices Total Harmonic Distortion (THDV). Analysis and implementation of the power factor converter in real time utilizing the fuzzy logic controller. Thus, the PFCs operate either in the THDI or regular resistance emulator mode and contribute to THDV and PF control of distribution feeders. They are consequently used for the distribution system. Fuzzy logic control methods are used to increase the performance of the boost inverter. MATLAB/Simulink controls the stability of the controller; the results show that fuzzy controller gives an optimal results.

1. Introduction

Harmonic limits are specified by international standards and grid rules on AC electrical networks to ensure efficient and accurate operation of the subsystems and equipment connected to the grid, e.g. power generators, and storage systems loads. The suggested harmonic standards in Electro Power Systems[1] were applied and monitored to establish limitations for particular harmonics as well as for current THD. In electric distribution systems, the current voltage and harmonic distortions are strongly connected and, if very nonlinear charges are coupled, the tap-screw THDV-boundary may be exceeded[2].

THDV increase with residential charges, particularly in 3rd, 5th, 7th, 9th, 11th, 13th harmonics[9]. This voltage is mostly due to a harmonic backdrop. In residential settings, the impact of harmonics is reduced by local or large-scale mitigation methods. Local load-side energy sources[11] or the active power filter features[12] are utilized. This requires the distributed generation and active forward storage as adjustable harmonic impedances[12]. In particular through the allocation of compensatory priorities to DERs, the coordination of local solutions provides a framework for the broad strategy of mitigation[13]. By altering the DER intake,[15] or by employing low-voltage distributed equipment for current harmonic filters,[16] the THDV can be optimized by means of a droop approach[13]. Increased P-F and voltage disturbance mitigating effects [17]-[19] is also supported by a distributional power feed system, i.e. active hybrid power filters, which incorporates a mitigation device. DER compensation capability and availability is limited by its nominal rating i.e. the LCL

Voltage instability identification with modified L-index using synchrophasor data

V. Vijaya Rama Raju¹, K. H. Phani Shree², S.V.Jayarama Kumar³

¹Electrical and Electronics Engineering Department, GRIET, Hyderabad, Kukatpally, Hyderabad, Telangana state, India

^{2,3}Electrical and Electronics Engineering Department, JNTUHCE, Kukatpally, Hyderabad, Telangana state, India

Article Info

Article history:

Received May 20, 2021

Revised Jul 28, 2021

Accepted Aug 4, 2021

Keywords:

L-index

Phasor measurement unit

Synchrophasor data

Voltage stability

Wide area monitoring system

ABSTRACT

In the prevailing open-access environment, one of the limitations for power exchanges has been voltage stability. The study of voltage stability necessitates a complete network representation. In this paper, the advantage of the dynamic behavior of generators is considered by incorporating dynamic models for generators. It has been shown dynamic models resulted in more accurate results compared to the conventional PV buses or ideal voltage source models that are used in most of the voltage stability studies. Moreover, the traditional L-index is augmented by incorporating real-time and synchronized phasor data collected from the optimally located phasor measurement units (PMU) in a wide-area measurement system (WAMS) to estimate more accurate voltage stability margins. Simulation studies carried out on IEEE 9-bus and IEEE 14-bus systems under various system conditions. It has been demonstrated that the inclusion of dynamic models and synchrophasor data from WAMS significantly improves the precision with which voltage stability analysis results are obtained.

This is an open access article under the [CC BY-SA](https://creativecommons.org/licenses/by-sa/4.0/) license.



Corresponding Author:

V. Vijaya Rama Raju

Electrical and Electronics Engineering Department

GRIET, Kukatpally, Hyderabad, Telangana state, India

Email: vijayram_v@yahoo.com

1. INTRODUCTION

In the beginning, stability problems encountered in power system were mainly related to generator rotor angle stability and frequency stability problems, which are mainly generator driven [1]. Voltage instability was later established as a major threat to the operation of power systems, which is mainly load driven. Growing demand for power with constrained transmission capabilities, voltage stability and voltage collapse problems has gained the importance. In its most simplistic form, this can be explained as the system's inability to provide necessary reactive power or the system's excessive absorption of reactive power. Earlier it was associated with weak systems and long transmission lines, but now the load behaviour has a big effect on it. Voltage instability has been a significant concern to the activity of many power networks around the world in the last three decades. This has caused havoc on the economy and had important social implications. It has been one of the key causes of several worldwide blackouts like 1987's Tokyo blackout and 2003's United States, United Kingdom, Canada, Sweden, Italy and Denmark blackouts [2], [3]. In order to estimate the voltage instability, researchers have suggested many voltage stability indices, and a few have been used for voltage stability analysis in real time. They include traditional indices defined using minimum eigenvalue, P-V and P-Q curves [4], [5], continues power flow [6], singular value decomposition [7], sensitivity analysis methods [8], bifurcations theory [9], and L-index [10].

THD Mitigation for Critical Loads by Using Current-Source Inverter with ANN Based Electrical Spring

¹Mr. N. Saiteja,²V. Vijaya Rama Raju

P.G. Scholar in Electrical power system at Gokaraju Rangaraju Institute of Engineering and Technology, Hyderabad, Telangana, India.

²Associate Professor in the Department of Electrical and Electronics Engineering, GRIET, Hyderabad, India.

Abstract—A new management technique for direct current monitoring and harmonic elimination features akin to control of an activated electricity filter is proposed for the usage of a new type of electricity spring (ES) with a current source inverter (CSI) to enhance ES' performance. By changing the voltage-source converter (VSI) into CSIs and replacing the voltage control with direct-current management, the total harmonic distort (THD) can be significantly reduced compared to existing control methods. An additional harmonic function of suppression akin to APF, in which the input current through the one phase dq0 transformation is divided into a fundamental part and others. can also further increase the system performance. The proposed direct current control can also interpret the concept of ESs more effectively. It is well illustrated that the ES and control proposed are operating concepts. Simulation results have confirmed the effectiveness of the control strategy.

Keywords: Spring Electric, CSI, direct monitoring current, harmonic reduction, microgrid, renewable power supply.

I. INTRODUCTION

Traditional fossil energy sources such as wind and solar [1] should replace renewable energy (RES) for low-carbon living. However, as the stability difficulties are sporadic, the penetration of such sources becomes more difficult. In order to ensure critical loads (CL) operated within defined ranges and passed from the fluctuations to the non-critical loads (NCLs), a new control paradigm was proposed for electrical springs (ESs). The initial design and the first version, which only works with a pure reactive power compensation function. Another version has eight compensating functions detailed in [3]. Included in two-way grid converters, the third version [4] of the active suspension concept is without the NCL's. A great deal of effort was done on the ESs. Implementation of control and hardware is provided in [5]. In [6]–[9], the uses of these systems are described. The ESs [6] and [7] can be used to achieve unity-power factor (PF). In [10] and [11] the dynamic modeling is shown. However, all the above-mentioned ESs are manufactured using inverters from voltage sources, neither of which is made up of inverters from the current source (CSIs). CSI benefits are thoroughly explained in comparison with VSIs in [11]. Direct current controls for CSIs, for example, can be adopted. Another important aspect of CSI is that CSI works as an Inverter Boost type for power

Article

MoSe₂-WS₂ Nanostructure for an Efficient Hydrogen Generation under White Light LED Irradiation

Tatiparti Padma ^{1,†}, Dheeraj Kumar Gara ², Amara Nadha Reddy ², Surya Veerendra Prabhakar Vattikuti ^{3,†} and Christian M. Julien ^{4,*}

¹ Department of Electronics & Communications Engineering, Gokaraju Rangaraju Institute of Engineering and Technology, Kukatpally, Hyderabad 500090, Telangana, India; propadmat@gmail.com

² Malla Reddy College of Engineering and Technology, Doolapally, Hyderabad 500100, Telangana, India; dheeru498@gmail.com (D.K.G.); amarnadha@gmail.com (A.N.R.)

³ School of Mechanical Engineering, Yeungnam University, Gyeongsan 38541, Korea; vsvprabu@gmail.com

⁴ Institut de Minéralogie, de Physique des Matériaux et de Cosmochimie (IMPMC), Sorbonne Université, CNRS-UMR 7590, 4 Place Jussieu, 75252 Paris, France

* Correspondence: christian.julien@sorbonne-universite.fr

† These authors contributed equally to this work.

Abstract: In this work, MoSe₂-WS₂ nanocomposites consisting of WS₂ nanoparticles covered with few MoSe₂ nanosheets were successfully developed via an easy hydrothermal synthesis method. Their nanostructure and photocatalytic hydrogen evolution (PHE) performance are investigated by a series of characterization techniques. The PHE rate of MoSe₂-WS₂ is evaluated under the white light LED irradiation. Under LED illumination, the highest PHE of MoSe₂-WS₂ nanocomposite is 1600.2 μmol g⁻¹ h⁻¹. When compared with pristine WS₂, the MoSe₂-WS₂ nanostructures demonstrated improved PHE rate, which is 10-fold higher than that of the pristine one. This work suggests that MoSe₂-WS₂ could be a promising photocatalyst candidate and might stimulate the further studies of other layered materials for energy conversion and storage.

Keywords: hydrogen production; layered materials; photocatalysts; WS₂; MoSe₂



Citation: Padma, T.; Gara, D.K.; Reddy, A.N.; Vattikuti, S.V.P.; Julien, C.M. MoSe₂-WS₂ Nanostructure for an Efficient Hydrogen Generation under White Light LED Irradiation. *Nanomaterials* **2022**, *12*, 1160. <https://doi.org/10.3390/nano12071160>

Received: 22 February 2022

Accepted: 30 March 2022

Published: 31 March 2022

Publisher's Note: MDPI stays neutral with regard to jurisdictional claims in published maps and institutional affiliations.



Copyright: © 2022 by the authors. Licensee MDPI, Basel, Switzerland. This article is an open access article distributed under the terms and conditions of the Creative Commons Attribution (CC BY) license (<https://creativecommons.org/licenses/by/4.0/>).

1. Introduction

Presently, energy shortage and environmental pollution are the major problems [1–3]. Intuitively, the current photocatalytic hydrogen (H₂) generation from water through semiconductor nanostructures is an ideal approach, and this technique is considered as a potential, economical way to overcome the issue of energy shortage [4–7]. Over the years, there has been substantial experimental data calibrated on transition-metal (TM) oxide-based photocatalysts for energy-storage applications [6–8] with minimal environmental pollution. Though these materials display excellent photocatalytic activity just beneath the UV illumination, they exhibit poor activity in visible light due to their wide bandgap. In order to stimulate photocatalytic activity in visible light, recent attempts on anion-doped TM oxides-, sulfides-, and selenides-based nanostructures have been reported [9,10]. However, these TMs are unstable, making them inert towards commercial applications. Henceforth, there is a challenge for the researchers to identify and develop potential, stable and economically novel photocatalysts for H₂ evolution.

In lieu of this, the two-dimensional (2D) MoSe₂ semiconductor is a compelling potential catalyst for next-generation hydrogen evolution due to its narrow bandgap (1.2 eV), specific surface area and more metallic nature, which prompts higher electrical conductivity that is more favorable to hydrogen evolution reactions. However, there are few reports on the preparation of MoSe₂-based composites through diverse approaches, which display an enhanced photocatalytic activity (PCA) when compared with the bare MoSe₂ [11]. In spite of this enhanced photocatalyst, there is provision to promote further the PCA in the



An energy-efficient reconfigurable accelerators in multi-core systems using PULP-NN

Siva Sankara Phani Tammireddy¹ · Mamatha Samson² · P. Rahul Reddy³ · A. Kishore Reddy⁴ · Asisa Kumar Panigrahy² · Sudharsan Jayabalan² · M. Durga Prakash⁵

Received: 16 July 2021 / Accepted: 28 August 2021
© King Abdulaziz City for Science and Technology 2021

Abstract

Emerging developments in embedded computer systems and applications demand low energy consumption and high performance. Owing to increased demand for low-voltage computing and lowered technology returns, academia and industry are interested primarily in energy-efficient accelerators. Hardware accelerators have the greatest disadvantage that they are not programmable. It can also be misused for a particular task. The number of accelerators in a device can cause scalability problems. Flexibility and scalability issues are present in programmable accelerators. Coarse-grained reconfigurable architecture (CGRA) design, implementation, computer systems integration and compilation for CGRA are the key contributions in this proposed design. First of all in parallel ultra-low-power processing system (PULP), the CGRA-based integrated programmable array (IPA) is implemented. Second, PULP-NN is a coding library that has been developed for the RISC-V cluster with parallel, high–low storage. The key development in PULP-NN is that the latest move towards aggressive quantization of deep neural network inferences which is a collection of kernels which use bytes and sub-byte information types up to INT-1. The library in the proposed procedure utilizes advanced sign handling expansions in the RISC-V PULP processors and in bunch matches, to accomplish ideal energy effectiveness of estimation execution.

Keywords PULP-NN · CGRA · Reconfigurable accelerators · Embedded computer systems

Introduction

The transistor density increases very slightly with each generation of Moore law. The portion of transistors which can be operated at high frequencies, therefore, decreases exponentially with a set chip level power budget. Empirical

studies in Hesham et al. (2020) show that it is impossible that the strategy of raising the output of core components would fail because of or near stopping the lower voltage, and that energy consumption of single core components is not reduced enough to increase the number of computer operating units. Therefore, a deteriorating portion of the silicon should be indistinct, i.e., technically shut down or clocked. More than 50% of the chip is dark at 8 nm for this investigation. A multiplex contains a range of different custom hardware accelerators (HWACs), all designed for particular purposes, including graphic handling, signal processing and calculation of cryptography, etc.

The trend was to speed up the use of ASIC-HWACC and general-purpose graphics processing units (GPGPU's) with few highly custom-made hardware accelerators, depending on the particular field of operation. Even if ASIC-HWACCs have the highest efficiency, the lack of flexibility restricts its applicability to just a few fields (i.e. large volumes or silicone costs can be applied). High-performance computing (HPC) graphics processing units are very common. For such

✉ M. Durga Prakash
mdprakash@vrsiddhartha.ac.in; mdprakash82@gmail.com

- ¹ Department of ECE, Koneru Lakshmaiah Education Foundation, Green Fields, Vaddeswaram, Andhra Pradesh 522502, India
- ² Department of ECE, Gokaraju Rangaraju Institute of Engineering and Technology, Hyderabad, Telangana 500090, India
- ³ Department of ECE, Geethanjali Institute of Science and Technology, Nellore, India
- ⁴ Department of ECE, Andhra Engineering College, Nellore, India
- ⁵ Department of ECE, Velagapudi Ramakrishna Siddhartha Engineering College, Kanuru, Andhra Pradesh 520007, India



Design and Development of Graphene FET Biosensor for the Detection of SARS-CoV-2

B. Vamsi Krsihna¹ · Shaik Ahmadsaidulu² · Surapaneni Sai Tarun Teja² · D. Jayanthi³ · Alluri Navaneetha⁴ · P. Rahul Reddy⁵ · M. Durga Prakash²

Received: 19 August 2021 / Accepted: 1 September 2021
© Springer Nature B.V. 2021

Abstract

The most affected disease in recent years is Severe Acute Respiratory Syndrome Coronavirus 2 (SARS-COV-2) that is notable as COVID-19. It has been started as a disease in one place and arisen as a pandemic throughout the world. A serious health problem is developed in the lungs due to the effect of this coronavirus. Sometimes it may result in death as a consequence of extensive alveolar damage and progressive respiratory failure. Hence, early detection and appropriate diagnosis of corona virus in patient's body is very essential to save the lives of affected patients. This work evolves a Silicon (Si) based label-free electrical device i.e. the reduced graphene oxide field-effect transistor (rGO FET) for SARS-CoV-2 detection. Firstly rGO FET functionalized with SARS-CoV-2 monoclonal antibodies (mAbs). Then the rGO FET characteristic response is observed to detect the antibody-antigen reaction of SARS-CoV-2 with different molar ranges. The developed GFET shows better performance towards the drain current and limit-of-detection (LoD) up to 2E-18 M. Therefore, we believe that an intense response was observed than the earlier developed devices and signifies impressive capability for subsequent implementation in point-of-care (PoC) diagnostic tests.

Keywords FET · SARS-CoV-2 · rGO · Biosensor · Limit of detection

1 Introduction

Emerging contagious diseases, such as severe acute respiratory syndrome (SARS), Flu, and Ebola infection illness, pose a major risk to human health. In December 2019, a series of patients were admitted to the hospital with symptoms of pneumonia and severe acute respiratory syndrome (SARS) in a place named Wuhan, China. The causes for this disease were unknown initially. From there on, 2019 novel Covid (2019-

nCov) was perceived inside the patient's nasal liquid. Subsequently, it was named again as Severe Acute Respiratory Syndrome Coronavirus 2 (SARS-CoV-2) [1, 2]. World Health Organization (WHO) alluded to this infection as Corona Virus Disease (Covid-19). It declared that the virus causes this disease as a 2019 novel coronavirus (2019-nCoV). On March eleventh, 2020 WHO recognized this Covid-19 as pandemic as it is transmitting among the people of different countries with rapid speed [3]. The basic symptoms of this disease may include fever, loss of taste or smell, dry cough, and fatigue. The severe symptoms of this disease may contain chest pain or pressure, shortness of breath or difficulty in breathing, and loss of speech or movement. This novel coronavirus is transmitted by droplets and aerosols of human saliva. The severity of this pandemic can be observed by the statistics provided by WHO.

The total number of cases globally is approximately 18.5 crores and the total deaths are 40 Lakhs up to July 1st week. Due to this pandemic entire world faced different socio-economic problems. To avoid these difficulties, the patients need to be properly diagnosed and treated with utmost care. Even though there are some measures to prevent or control this coronavirus, like WHO-recommended medicines or

✉ M. Durga Prakash
mdprakash82@gmail.com

¹ Department of ECE, Koneru Lakshmaiah Education Foundation, Guntur 522502, Andhra Pradesh, India

² Department of ECE, Velagapudi Ramakrishna Siddhartha Engineering College, 520007 Kanuru, Andhra Pradesh, India

³ Department of ECE, Gokaraju Rangaraju Institute of Engineering & Technology, 500090 Hyderabad, Telangana, India

⁴ Department of ECE, Mahatma Gandhi Institute of Technology, 500075 Hyderabad, Telangana, India

⁵ Department of ECE, Geethanjali Institute of Science and Technology, 524137 Nellore, Andhra Pradesh, India

Lifetime maximization energy-aware routing protocol for route optimization to improve quality of service in wireless sensor networks

Vinod Kumar R¹ | Kavithaa G² | Jayanthi D³

¹Department of Electronics and Communication Engineering, Saveetha Engineering College (Autonomous), Chennai, India

²Department of Electronics and Communication Engineering, Government College of Engineering, Salem, India

³Department of Electronics and Communication Engineering, Gokaraju Rangaraju Institute of Engineering and Technology, Hyderabad, India

Correspondence

Vinod Kumar R, Department of Electronics and Communication Engineering, Saveetha Engineering College (Autonomous), Saveetha Nagar, Chennai, India.
Email: vinodrangarajan@yahoo.co.in

Abstract

Wireless sensor networks (WSNs) are part of the short-term networks, including sensitivity, computation, and Wi-Fi connectivity capability. Many routing, range management, and log transfer protocols are specifically designed for WSN. The previous method showed less efficiency in routing management. The proposed lifetime maximization energy-aware routing protocol (LTMEARP) protocol is known for its high routing efficiency, giving a higher lifetime and throughput performance. The requirement for a routing system approach is advanced with Internet service provider's protocols by recalculating the routing table after the link stage's substitution worldwide, leading to responses and connection failures by sharing important data after traffic. LTMEARP routing protocol has assured high availability routing performances during traffic conditions. LTMEARP support sends homogeneous and expanded nodes. Analyze a new approach to routing-based selection algorithms for homogeneous node WSNs. The number of connections is limited and must be adjusted using separate paths and header packets to meet the user's network access location. The results show that the LTMEARP has achieved quality without introducing excessive network access program overhead, which

Visit Nature news for the latest coverage and read Springer Nature's statement on the Ukraine conflict

Application of soft computing | [Published: 05 March 2022](#)

Cardiac arrhythmia detection using dual-tree wavelet transform and convolutional neural network

[K. Reddy Madhavi](#), [Padmavathi Kora](#), [L. Venkateswara Reddy](#), [J. Avanija](#), [K. L. S. Soujanya](#) & [Prabhakar Telagarapu](#)

[Soft Computing](#) **26**, 3561–3571 (2022)

123 Accesses | [Metrics](#)

Abstract

The non-stationary ECG signals are used as key tools in screening coronary diseases. ECG recording is collected from millions of cardiac cells and depolarization and re-polarization conducted in a synchronized manner as: the P wave occurs first, followed by the QRS-complex and the T wave, which will repeat in each beat. The signal is altered in a cardiac beat period for different heart conditions. This change can be observed in order to diagnose the patient's heart status. Simple naked eye diagnosis can mislead the detection. At that point, computer-assisted diagnosis (CAD) is therefore required. In this paper dual-tree wavelet transform is used as a feature extraction technique along with deep learning (DL)-based convolution



Segmentation and detection of brain tumor through optimal selection of integrated features using transfer learning

K Swaraja¹ · K Meenakshi¹ · Hima Bindu Valiveti¹ · G Karuna¹

Received: 26 October 2020 / Revised: 22 April 2021 / Accepted: 25 January 2022

© The Author(s), under exclusive licence to Springer Science+Business Media, LLC, part of Springer Nature 2022

Abstract

Understanding and analyzing of Magnetic resonance imaging (MRI) used in detecting the brain anomaly by specialists manually is a time-consuming, cumbersome and susceptible to intra-subject variations. Hence the proposed non-invasive Computer Aided Diagnosis (CAD) based on brain MRI is aimed to aid the radiologists and physicians to detect the presence of Glioma tumors and its variants on pulse sequences of T1, T1C, T2 and Flair. After preprocessing, using segmentation best features that differentiate one class of objects from another are selected by integrating deep learning features with handcrafted features. Later in the Classification phase, the integrated features of deep learning and handcrafted features are optimized by implementing Particle Swarm Optimization (PSO) algorithm. Finally, these integrated features are classified by Classifiers such as MSVM, KNN, ESDN and Softmax. The GoogLeNet is a pre-trained Convolution Neural Network (CNN) model employed for deep features extraction. Two popular datasets BRATS and Figshare is used for Classification of variants of Glioma tumors using a ten-fold cross-validation. The proposed system achieves high classification accuracy with MSVM Classifier when compared with Softmax, KNN and ESDA Classifiers, thus outperforming all state-of-the-art methods. The performance metrics used in this work are the Area Under Curve - Region of Operating Characteristic curve (AUC-ROC), Precision, Recall, and Specificity. Overall outcome clearly reveals that the proposed framework outperforms both the Segmentation and Classification algorithms of Brain tumors mainly in terms of computation time in contrast to the state-of-the-art methods.

Keywords Brain tumor · Transfer learning · GoogLeNet · Features extraction · Handcrafted features · Softmax

✉ K Swaraja
kswaraja@gmail.com

¹ GRIET, Hyderabad, India

Brain Tumor Classification of MRI Images Using Deep Convolutional Neural Network



Swaraja Kuraparathi^{1*}, Madhavi K. Reddy², C.N. Sujatha³, Himabindu Valiveti¹, Chaitanya Duggineni⁴, Meenakshi Kollati¹, Padmavathi Kora¹, Sravan V¹

¹Gokaraju Rangaraju Institute of Engineering and Technology, Hyderabad 500090, India

²Sree Vidyanikethan Engineering College, Tirupati 517102, India

³Sreenidhi Institute of Science and Technology, Hyderabad 501301, India

⁴G.Pulla Reddy Engineering College, Kurnool 518218, India

Corresponding Author Email: k.swaraja@griet.ac.in

<https://doi.org/10.18280/ts.380428>

ABSTRACT

Received: 23 January 2021

Accepted: 19 July 2021

Keywords:

brain tumor, data augmentation, deep convolutional neural networks, magnetic resonance images, transfer learning, support vector machine

Manual tumor diagnosis from magnetic resonance images (MRIs) is a time-consuming procedure that may lead to human errors and may lead to false detection and classification of the tumor type. Therefore, to automatize the complex medical processes, a deep learning framework is proposed for brain tumor classification to ease the task of doctors for medical diagnosis. Publicly available datasets such as Kaggle and Brats are used for the analysis of brain images. The proposed model is implemented on three pre-trained Deep Convolution Neural Network architectures (DCNN) such as AlexNet, VGG16, and ResNet50. These architectures are the transfer learning methods used to extract the features from the pre-trained DCNN architecture, and the extracted features are classified by using the Support Vector Machine (SVM) classifier. Data augmentation methods are applied on Magnetic Resonance images (MRI) to avoid the network from overfitting. The proposed methodology achieves an overall accuracy of 98.28% and 97.87% without data augmentation and 99.0% and 98.86% with data augmentation for Kaggle and Brat's datasets, respectively. The Area Under Curve (AUC) for Receiver Operator Characteristic (ROC) is 0.9978 and 0.9850 for the same datasets. The result shows that ResNet50 performs best in the classification of brain tumors when compared with the other two networks.

1. INTRODUCTION

The development of unusual cells in the human brain is called a brain tumor. Researchers don't completely comprehend the reasons for the brain tumor, however some risk factors help in tracing the brain tumor stage. The Brain tumor is categorized into two types, primary and secondary brain tumor. The Primary brain tumor mainly originates from the brain or any part of the brain without infecting the other parts of the body. Malignant and benign are the most common types of tumors. The Secondary brain tumor does not directly originate in the brain, but the tumor gets spread from different parts of the body. Malignant tumors are mostly considered secondary type tumors. A benign tumor can be further classified into meningiomas and gliomas; these are regarded as low-grade tumors. A malignant tumor is a high-grade tumor, classified into glioblastoma and astrocytoma.

The imaging practices like Magnetic Resonance Imaging (MRI), Computed Tomography (CT), Positron Emission Tomography (PET) and Single Photon Emission Computer Tomography (SPECT) are essentially utilized in investigating the brain images. MRI and CT imaging techniques are the most widely used among these techniques due to their high-resolution image quality and widespread availability. Brain tumor detection commonly uses MRI imaging technique rather than CT imaging technique because it can examine pathological or other physiological alternations of living tissues. The standard type of brain tumor resulting in adults is

Gliomas, which can be identified with the help of magnetic resonance (MR) images of different categories, such as T1-weighted (T1), T2-weighted contrast-enhanced (T1c), T2-weighted and fluid-attenuated inversion recovery (Flair). Early detection of tumor plays an essential role in the treatment process. The radiologist uses classification methods to categorize the MR image as normal or abnormal. If the resultant outcome is odd, then the type of tumor is detected for the other treatment process. Manual classification is an expensive and time-taking assignment. In addition, they can get different conclusions from various observers or dissimilar findings from the similar observer in distinguishing tumor. Therefore, automatic classification techniques are obligatory.

Instead of developing a new model, deep transfer learning adapts an existing deep model that has already proven its effectiveness. As a result, the costs of complex layer parameters as well as prolonged validation processes are reduced.

The significant contributions of the proposed framework are listed as below.

- Pertaining to the performance, a significant progression is achieved with deep CNN features of transfer learned models when they are classified with multi SVM classifier instead of stand-alone Softmax classifier.
- The proposed framework recorded the highest classification accuracy in comparison to the earlier relevant research works, since data augmentation with SVM Classifier is trained to classify brain MR images.



Entropy based single image dehazing with refined transmission using holistic edges

T.R.Vijaya Lakshmi¹ · Ch.Venkata Krishna Reddy² · K. Padmavathi³ · K. Swaraja³ · K. Meenakshi³

Received: 10 June 2021 / Revised: 26 October 2021 / Accepted: 25 January 2022

© The Author(s), under exclusive licence to Springer Science+Business Media, LLC, part of Springer Nature 2022

Abstract

The natural occurrences of haze, mist and fog obscures the optically captured outdoor scenes. The essential parameters of the atmospheric scattering model for dehazing are air-light (which depends on atmospheric light) and transmission map. Inaccurate estimation of these parameters leads to halo-artifacts, color distortions, etc. The performance of the available single-image dehazing models is limited by the color shifts caused due to the offset of light sources. The proposed work estimates the atmospheric light component by considering the lowest entropy from the quad-decomposed image as the haze opaque regions in the scene considered has low entropy. The transmission map is estimated by computing the scattering parameter, further refined with the holistic edges to calculate haze at different densities. A regression model is trained with the haze relevant features such as hue disparity, contrast, and darkness to compute the scattering coefficient rigorously. This improves the color shifts and visibility of the degraded outdoor scenes and mitigates the imbalances in the haze density concentrations in the scenes. The current model is evaluated using reference-based and non-reference based metrics to emphasize its perceptibility on hazy images when blended with pure light and non-achromatic light. The evaluations on real-hazy images signify that the true colors are well preserved, and the degree of visibility is improved compared to the state-of-the-art models.

Keywords Haze removal · Scattering coefficient · Depth and Transmission maps · Hue disparity · Non-achromatic atmospheric light

✉ T.R.Vijaya Lakshmi
trvijayalakshmi.ece@mgit.ac.in

Ch.Venkata Krishna Reddy
chvkrishnareddy_eee@cbit.ac.in

¹ Department of ECE, Mahatma Gandhi Institute of Technology, Hyderabad, India

² Department of EEE, Chaitanya Bharathi Institute of Technology, Hyderabad, India

³ Department of ECE, GRIET, Hyderabad, India

EfficientNet-B0 Based Monocular Dense-Depth Map Estimation

Yasasvy Tadepalli, Meenakshi Kollati, Swaraja Kuraparthi*, Padmavathi Kora

Gokaraju Rangaraju Institute of Engineering and Technology, Hyderabad 500090, India

Corresponding Author Email: k.swaraja@griet.ac.in



<https://doi.org/10.18280/ts.380524>

ABSTRACT

Received: 9 September 2020

Accepted: 12 August 2021

Keywords:

depth maps, monocular images, efficient net, up-sampling, Jaccard score, validation loss, mean actual error

Monocular depth estimation is a hot research topic in autonomous car driving. Deep convolution neural networks (DCNN) comprising encoder and decoder with transfer learning are exploited in the proposed work for monocular depth map estimation of two-dimensional images. Extracted CNN features from initial stages are later upsampled using a sequence of Bilinear UpSampling and convolution layers to reconstruct the depth map. The encoder forms the feature extraction part, and the decoder forms the image reconstruction part. EfficientNetB0, a new architecture is used with pretrained weights as encoder. It is a revolutionary architecture with smaller model parameters yet achieving higher efficiencies than the architectures of state-of-the-art, pretrained networks. EfficientNet-B0 is compared with two other pretrained networks, the DenseNet-121 and ResNet50 models. Each of these three models are used in encoding stage for features extraction followed by bilinear method of UpSampling in the decoder. The Monocular image is an ill-posed problem and is thus considered as a regression problem. So the metrics used in the proposed work are F1-score, Jaccard score and Mean Actual Error (MAE) etc., between the original and the reconstructed image. The results convey that EfficientNet-B0 outperforms in validation loss, F1-score and Jaccard score compared to DenseNet-121 and ResNet-50 models.

1. INTRODUCTION

Object detection and subsequent maneuvering have been the primary motto of any autonomous vehicle project. In terms of conventional single-lens cameras, the world is perceived in 2D, the two dimensions being the Width and the Height, but the real world and its objects have a 3D structure. The third dimension is perceived as Depth in Computer Vision. This factor is highly significant in self-driving cars for controlling the vehicle's speed and its movement. Ultrasonic sensors have a meager distance range so for high-end self-driving cars, sophisticated sensors like LIDAR, RADAR, Stereo camera setup, or a combination of some of the above technologies, including various sensors and cameras, are used for 3D mapping of the surroundings. These 3D point clouds are generated by the on-board computer depending on the incoming light signals/radio signals. LIDAR has a great future in autonomous vehicles. Though LIDAR technology is highly efficient and reliable, it is not cost-effective. LIDAR equipment installed on the car costs almost double when compared to the cost of the vehicle itself. High cost was the main driving motto to shift the research from LIDAR technology to stereoscopic and monocular depth estimation. Stereo cameras contain more than one lens, each with their own image sensors and they mimic human binocular Vision, such phenomenon is termed as Stereo Disparity. However, to find correlations, the two images need to have sufficient details and texture or non-uniformity.

Moreover, Depth can be perceived accurately only at short distances. Still, stereo-vision based research is the most trending one in the field of depth map estimation. The other research field is looking into estimating the Depth from

monocular images, i.e., images/videos taken using a single-lens camera. Many revolutionary methods are proposed to estimate the Depth from monocular estimation like Markov Random Fields, Continuous Random Fields, Deep learning, adversarial learning, etc., Datasets like NYU2-Depth dataset and KITTI datasets were also created to aid the supervised deep learning approach. It was observed that the modern deep learning models are efficient at extracting Depth than traditional handcrafted features. Many deep learning models have been utilized for supervised deep learning-based depth map estimation like ResNet, DenseNet, VGG, etc. This project is one such effort that uses the supervised transfer learning approach to estimate the Depth.

The architecture employed in this is based on the Encoder-Decoder concept. The encoder is used for feature extraction, and the decoder is used to improve the depth map's resolution. The deep learning model used for the encoder is EfficientNet-B0, a new model developed using a compound scaling approach. A decoder consisting of consecutive UpSampling blocks and convolutional and ReLU activation layers are added to upscale the image to the desired resolution. The name 'EfficientNet' emphasizes that this model is minimal in terms of the number of training parameters requirement and computational power. Yet, it delivers efficiencies more excellent than the previous state of the art deep learning models. In this project, the depth information is extracted in the form of a depth map. A depth map is an image that consists of RGBD parameters in which the D indicates the Depth. Many universities worldwide are working on this depth map estimation model and have brought out many databases. In this project, the NYU2 dataset (New York University) is used. It contains all images from various indoor scenes. The depth map

Robust Methods for Wideband Compressive Spectrum Sensing Under Non-Gaussian Noise

Bandaru Bhavana¹, Graduate Student Member, IEEE, Swetha Namburu², Member, IEEE, Trilochan Panigrahi³, Member, IEEE, and Samrat L. Sabat⁴

Abstract—In a cognitive radio network, non-reconstruction-based wideband compressive spectrum sensing poses challenges under the non-Gaussian noise environment. The maximum correntropy criterion (MCC) is robust to impulsive noise whereas, the Parzen window Renyi entropy is a good choice for spectrum sensing in the presence of Gaussian noise at a low signal-to-noise ratio (SNR). However, the detection performance of these algorithms depends on the accuracy of measured noise variance, which is sensitive to impulsive noise. In this letter, we improve the sensing performance of both the aforementioned algorithms in a non-Gaussian noise environment by modifying the kernel and threshold using robust statistics. The robust technique minimizes the influence of impulsive noise in the received signal. Finally, we carry out the simulation results to illustrate the superior performance of robust sensing algorithms under both Bernoulli's distribution and symmetric α stable ($S\alpha S$) distribution channel noise. The performance is compared with the non-robust counterpart for sensing multi-carrier Universal-Filtered Multi-Carrier (UFMC) signal.

Index Terms—Compressive sensing, impulsive noise, symmetric α stable ($S\alpha S$) noise, robust statistics, Parzen window Renyi entropy.

I. INTRODUCTION

COGNITIVE Radio (CR) is a leading paradigm for meeting the current requirements of wireless communications. It exploits the opportunistic spectrum usage by automatically detecting the surrounding RF stimuli and adapting its parameters to the network infrastructure without interfering with legacy primary users (PU). Many existing sensing algorithms exploit the spectral opportunities in the narrow spectral range [1]. However, communication systems such as electronic warfare, radar detection/jammer require monitoring a wideband signal of bandwidth, $W = f_{max} - f_{min}$ exceeding the coherent bandwidth, B of the channel. A typical wideband channel has a spectrum ranging from few hundreds of MHz to a few GHz for achieving higher opportunistic throughput.

Manuscript received June 26, 2021; accepted July 12, 2021. Date of publication July 19, 2021; date of current version October 11, 2021. This work was partly supported by the University Grant Commission, Govt of India, grant number 190520285492. The associate editor coordinating the review of this letter and approving it for publication was Y. Wu. (Corresponding author: Swetha Namburu.)

Bandaru Bhavana and Samrat L. Sabat are with the Centre for Advanced Studies in Electronics Science and Technology, School of Physics, University of Hyderabad, Hyderabad 500046, India (e-mail: 18pnp03@uohyd.ac.in; slssp@uohyd.ac.in).

Swetha Namburu is with the Department of Electronics and Communication Engineering (ECE), GRIET, Hyderabad 500090, India (e-mail: swethakarima@gmail.com).

Trilochan Panigrahi is with the Department of Electronics and Communication Engineering (ECE), National Institute of Technology Goa, Ponda 403401, India (e-mail: tpanigrahi@nitgoa.ac.in).

Digital Object Identifier 10.1109/LCOMM.2021.3098235

Hence, wideband spectrum sensing is used in practice. In the wideband sensing receiver, the ADC sampling frequency is defined by the Nyquist rate, i.e., $2W$, which is beyond the capacity of the conventional ADC. Hence, compressive sensing wideband receiver architecture that uses sub-Nyquist rate ADC is reported and demonstrated [2].

In conventional compressive spectrum sensing, the acquired compressed measurements are reconstructed before sensing [3]. Spectrum sensing does not require the complete information of the signal; hence direct sensing technique is reported [2]. It has less computational complexity due to the absence of reconstruction steps in the algorithm with marginal compromise on detection performance.

Numerous sensing algorithms such as energy detector, entropy detector, covariance detector, eigen detector assume additive white Gaussian noise (AWGN) in the channel due to the simplicity of algorithm analysis. However, the practical wireless channel will have non-Gaussian noise either due to environmental effect or malfunctioning of electronics, resulting in the performance degradation of sensing algorithms [4].

In a non-Gaussian noise channel, robust detectors are proposed for spectrum sensing. The robust spectral estimation using modified ridge regressor and Huber cost function outperforms periodogram-based detection [5]. It estimates the spectrum of a parametric signal using regression method. A convolutional neural network (CNN) based detection technique using likelihood ratio test (LRT), and Rao tests are formulated to counter the different behaviors of impulsive noise [6]. However, it is a data-driven technique that works for $SNR > 0$ dB and requires high complex neural networks. The least-squares spectral estimation technique is used in compressive wideband sensing under Gaussian noise model [7]. However, the compressive sensing algorithm's performance under non-Gaussian noise models is not explored so far. In Gaussian noise environment, Parzen window entropy-based sensing is used to enhance the detection performance in a low signal-to-noise ratio (SNR) environment [8]. The disadvantage with the Parzen window entropy-based detector (PWED) is that it is sensitive to the kernel bandwidth, which is sensitive to the estimation accuracy of noise standard deviation. In a non-Gaussian noise environment, the classical noise variance estimator fails to estimate the standard deviation of noise accurately; hence its performance will degrade under a non-Gaussian environment. The maximum correntropy criterion (MCC) can sense PU signals under a non-Gaussian environment, however, it is not robust at a low SNR regime [9].

In the current work, we considered the advantages of Parzen window entropy and MCC technique and devised its



Adaptive Compressed Spectrum Sensing Using Neural Networks in Cognitive Radio Networks

Kashavoina Kalyan, K. V. D. S. N. K. Sai Pratheek, Palumari Raju, Yadavalli Vivek & Swetha Namburu

To cite this article: Kashavoina Kalyan, K. V. D. S. N. K. Sai Pratheek, Palumari Raju, Yadavalli Vivek & Swetha Namburu (2021): Adaptive Compressed Spectrum Sensing Using Neural Networks in Cognitive Radio Networks, IETE Journal of Research, DOI: [10.1080/03772063.2021.1929516](https://doi.org/10.1080/03772063.2021.1929516)

To link to this article: <https://doi.org/10.1080/03772063.2021.1929516>



Published online: 25 May 2021.



[Submit your article to this journal](#)



Article views: 55



[View related articles](#)



[View Crossmark data](#)



Adaptive Compressed Spectrum Sensing Using Neural Networks in Cognitive Radio Networks

Kashavoina Kalyan, K. V. D. S. N. K. Sai Pratheek, Palumari Raju, Yadavalli Vivek and Swetha Namburu

Department of ECE, GRIET, Hyderabad 500090, India

ABSTRACT

In today's era of Internet of Things (IoT) applications, Cognitive Radio (CR) is recognized as the most promising technology to access the unused spectrum. Such CR networks can be easily built using Wide-band spectrum sensing. However, the processing of wide-band signals involves a high sampling rate. In such scenario, Compressed Spectrum Sensing (CSS) overcomes the challenges of real-time signal recovery and sampling. CSS uses Sparse signals which are widely used in many applications as they aid in processing large data. Beyond sparsity, all the real-world signals will have special structures (like Restricted Isometric property, Null space property). Moreover, it is very hard to determine the domain in which the signal is sparse. To find this we need a random measurement matrix which plays an important role in extracting the sparse coefficients of the signal. In this paper, a customized neural network is employed to identify the peculiar structures of sparse signals for efficient recovery in real time. The neural network learns and trains an adaptive measurement matrix from the sparse signals to reduce the sensing overhead. The transmitter and receiver systems are configured using Universal Software Radio Peripheral (USRP) boards with LabVIEW[®] and MATLAB[®] extensions for peer to peer communications. The implementation results depict the superior performance of neural network based recovery in assimilating the additional structures of real-time signals.

KEYWORDS

Compressed spectrum sensing (CSS); l_1 -minimization; recovery; sparsity; universal filtered multi-carrier (UFMC)

1. INTRODUCTION

In Compressive sensing (CS), the signal processing complexity is reduced by considering only important features of the signal. The signal is recovered from very few measurements sampled at less than Nyquist rate [1]. If the sub-samples are properly chosen, the length of the measurement vector can be much smaller than the actual signal length [2]. However, the signal should satisfy the properties like restricted isometry property (RIP), and incoherence [3]. Also, many signal processing techniques do not require complete recovery of signals. CS has been incorporated in radar systems, medical imaging and signal processing applications [4]

There are many recovery algorithms in the literature, out of which the l_1 -minimization algorithm provides exact reconstruction of signal [1]. It is an NP-hard problem. Hence, the reconstruction algorithm uses l_1 norm minimization techniques to improve the accuracy. In [5] a data-assisted non-iteratively re-weighted least squares (DNRLS) based compressive sensing algorithm with a geo-location database is developed.

In addition, an iterative re-weighted l_1 minimization technique is proposed in [6] in order to reconstruct wide-band signals. In [7], the authors have proposed a linear encoder and l_1 -decoder pair to learn adaptive measurement vectors. In addition, Bayesian model strengths and the Toeplitz matrix structure are incorporated to address the uncertainty in random measurements [8].

In the real world, we encounter either noisy measurements or incorrect sparsity or both. The incorrect sparsity refers to low significant features but not zero. Such approximate sparse signals can also be compressed and recovered using adaptive measurements in neural networks. The selection of measurement matrix in CS play a crucial role on accuracy and sparse reconstruction of signals. In literature, a number of measurement matrices are proposed. These matrices are generated using either random Gaussian and Bernoulli distributions or deterministic circulant and Toeplitz representations. Moreover, not all the matrices can be adopted directly for CS acquisition. Hence, there is a need to develop an alternative that learns the measurements adaptively and trains the

Hardware efficient circuit for low error logarithmic converter

Bhaskara Rao Jammu^{a,*}, L. Guna Sekhar Sai Harsha^a, Nalini Bodasingi^b,
Sreehari Veeramachaneni^c and Noor Mohammad SK^d

^a*Department of ECE, GVP College of Engineering (A), Visakhapatnam, India*

^b*Department of ECE, JNTUK UCEV, Vizianagaram, India*

^c*Department of ECE, GRIET, Hyderabad, India*

^d*Department of CSE, IIITDM Kancheepuram, Tamilnadu, India*

Abstract. The need to implement high-speed Signal processing applications in which multiplication and division play a vital role made logarithmic arithmetic a prominent contender over the traditional arithmetic operations in recent years. But the logarithm and antilogarithm converters are the bottlenecks. In order to reduce the logarithmic conversion complexity, several works have been introduced from time to time for correcting the error in Mitchell's algorithm but at the cost of hardware. In this work, we propose a 32-bit binary to the binary logarithmic converter with a simple correction circuit compared with existing techniques. Unlike the current methods that use the linear piece-wise approximation in the mantissa, we propose a weighted average method to correct the error in Mitchell's approximation. The maximum error percentage from the proposed work is 0.91%, which is 16.9% of Mitchell's error percentage.

Keywords: Logarithmic arithmetic, logarithmic number system, logarithmic conversion, Mitchells algorithm, error correction, DSP systems

1. Introduction

In many applications like radio communications, audio, video, aircraft, and in a large number of compact mobile consumer goods, digital signal processing (DSP) thus becomes pervasive. With the growing demand for DSP, there has been a rising need for hardware distribution of binary multipliers and binary dividers that are quicker and more productive in the area. The use of logarithms simplifies the arithmetic computations in both binary and decimal, as in [1]. Logarithms were used to simplify multiplication, division, and powering operations to the stage of addition and subtraction, where powering operations are simplified to multiplication [2].

The exact method for calculating the logarithm involves storing the logarithmic tables in memory, and such approaches are highly-priced for speed and hardware. For a few applications like image processing and DSP applications, a trade-off can be rendered by raising the conversion's precision to reduce the system's delay and power consumption. To simplify the logarithm computations, [3] proposed an algorithm for calculating the estimated \log_2 of a binary word. Here, the author used a straight-line

*Corresponding author: Bhaskara Rao Jammu, Department of ECE, GVP College of Engineering (A), Visakhapatnam, India.
E-mail: jbhaskararao@gvpce.ac.in.



A Low Error, Hardware Efficient Logarithmic Multiplier

L. Guna Sekhar Sai Harsha¹ · Bhaskara Rao Jammu¹  · Nalini Bodasingi² · Sreehari Veeramachaneni³ · Noor Mohammad SK⁴

Received: 5 October 2020 / Revised: 6 July 2021 / Accepted: 6 July 2021

© The Author(s), under exclusive licence to Springer Science+Business Media, LLC, part of Springer Nature 2021

Abstract

The ever-increasing requirement for high-performance signal processing blocks in artificial intelligence, IoT, and neural networks has rendered the Logarithmic arithmetic as front runner of advanced processors. As they require complex mathematical operations such as multiplication and division but they can be quickly done in the logarithmic domain as they are reduced to addition and subtraction operations, respectively. The task, though, is to move from binary to logarithmic and vice versa. Several algorithms have been suggested for the logarithmic and antilogarithmic conversion, but there is a compromise between hardware difficulty and accuracy. Within this work, we are introducing the correction circuit for both logarithmic and antilogarithmic conversion that is based on Mitchell's algorithm. Here the correction terms are generated using a weighted average approach and are stored using 16 X 8 ROM. The terms for correction are selected using the characteristic of the logarithmic value. Then, these converters are used to design a logarithmic multiplier. To further simplify the multiplier, an optimized multiplier is proposed. It involves only the addition of a single term to the result before performing an antilogarithm operation, which also streamlined the application of the multiplier. The proposed multiplier and optimized multiplier involves only a memory unit and an adder apart from Mitchell's logarithmic multiplier, so the hardware metrics are closely similar to Mitchell's logarithmic multiplier while having a peak error rate of 9.4 % and 7.5 % which is 11.1 % for Mitchell's multiplier and has nearly 95% of input combinations have less than 5% error when multiplication is performed using proposed multipliers.

✉ Bhaskara Rao Jammu
j.bhaskararao@gmail.com

L. Guna Sekhar Sai Harsha
saiharsha196@gmail.com


¹ Department of ECE, GVP College of Engineering (A), Visakhapatnam, India

² Department of ECE, JNTUK UCEV, Vizianagaram, India

³ Department of ECE, GRIET, Hyderabad, India

⁴ Department of CSE, IITDM Kancheerapuram, Chennai, India

Efficient design of 15:4 counter using a novel 5:3 counter for high-speed multiplication

Hemanth Krishna L.¹ | Neeharika M.² | Vishvanath Janjirala³ |
Sreehari Veeramachaneni³ | Noor Mohammad S² 

¹Department of Electronics and Communication Engineering, Gayatri College of Engineering, Andhra Pradesh, India

²Department of CSE., Indian Institute of Information Technology Design and Manufacturing (IIITDM) Kancheepuram, Chennai, Tamil Nadu, India

³Department of Electronics and Communication Engineering, Gokaraju Rangaraju Institute of Engineering and Technology, Hyderabad, Telangana, India

Correspondence

Noor Mohammad S, Department of CSE., Indian Institute of Information Technology Design and Manufacturing (IIITDM) Kancheepuram, Chennai 600127, Tamil Nadu, India.
Email: noor@iitdm.ac.in

Abstract

This paper proposes an efficient approach to design high-speed, accurate multipliers. The proposed multiplier design uses the proposed efficient 15:4 counter for the partial product reduction stage. This proposed 15:4 counter is designed using a novel 5:3 counter. The proposed 5:3 counter uses input re-ordering circuitry at the input side. As a result, the number of output combinations can be reduced to 18 from 32. As a result, the circuit complexity reduces. The proposed 5:3 counter and 15:4 counter are on an average 28% and 19% improvement in the power delay product compared with the existing designs. The 16-bit multiplier designed using 5:3 and 15:4 counters is an average 22.5% improvement in power delay product compared with the existing designs.

1 | INTRODUCTION

Multiplier circuit is a data-path element of the processor and specialised hardware circuits that are used for signal/image processing applications. The high-speed multiplier design is still a need of the hour. One can design a high-speed multiplier by reducing the delay of the partial product reduction stage. Many techniques are available in the literature for the reduction of partial products. Among all, the compressor and counter-based reduction techniques are popular ones [1,2]. The basic difference between compressor and counter depends on the carry and Cout weights [1,2]. For example, a 4:2 compressor will be designed using two full adders, as shown in Figure 1, with the following equations.

$$X_0 + X_1 + X_2 + X_3 + Cin = (Cout + Carry) \cdot 2^1 + Sum \cdot 2^0 \quad (1)$$

The 5:3 counter is designed using two full adders and one half adder, as shown in Figure 2. The 5:3 counter will have the equation as follows:

$$X_0 + X_1 + X_2 + X_3 + X_4 = Cout \cdot 2^2 + Carry \cdot 2^1 + Sum \cdot 2^0 \quad (2)$$

From the compressor Equation (1), the Cout and Carry will have the same weights (2^1), but from the counter Equation (2), the Cout and Carry will have different weights, that is, 2^1 and 2^0 , respectively. The compressor and counter functionality is the same (both counts the number of 1's present in the input). It produces the results as binary in different weights. For example, consider $X_0 = 1$, $X_1 = 1$, $X_2 = 1$, $X_3 = 1$, and $Cin = 1$ then the 4:2 compressor produces the result as (Cout, Carry and Sum) = 111 (value is five based on Equation (1)) and the 5:3 counter will produce the result as (Cout, Carry and Sum) = 101 (value is five based on the Equation (2)). The rest of the input combinations and their corresponding outputs for the compressor and counter is shown in truth Tables 1 and 2.

This paper proposes a novel 5:3 counter and the proposed design is efficient in terms of area, power and delay. The proposed 5:3 counter is used in designing the 15:4 counter. The 15:4 counter block diagram is shown in the Figure 3. The 15:4 counter will have 15 inputs and 4 outputs and the equations for the 15:4 counter is as follows.



Authentication of symmetric cryptosystem using anti-aging controller-based true random number generator

Yalamanchili Sangeetha¹ · Sankararao Majji² · Ayyagari Srinagesh³ · Tulasi Radhika Patnala⁴ · Sunanda Nalajala⁵ · Boppuru Rudra Prathap⁶

Received: 3 June 2021 / Accepted: 6 July 2021
© King Abdulaziz City for Science and Technology 2021

Abstract

In today's digital world, data protection is extremely important. Every company's data is a valuable asset, so it's important to ensure that it's secured from outside threats. Information security is not only an effective but also a necessary element to protect data from unauthorized access. The confidentiality of any communication system is strengthening with the help of random number generators along with some analog circuitry. This type of analog models demands more power and area. So analog circuit-based hardware Random Number Generators (RNG) are least preferred over digital RNGs. To improve the security every industry depends on the one-time password (OTP). Which gives the security but generation of the OTP is very easy. Random number generator is used for the generation of OTP. Similarly, hacking such OTP is easier than creating them. This paper introduces the Anti-Aging controller TRNG, a highly stable high-performance random number generator Anti-Aging Cryptographically Secured True Random Number Generator (AACTRNG). Implementation of this work can be done by using TANNER EDA Tools and ModelSim-Altera 6.4a (Quartus-II 9.0) used for the simulation to retrieve random numbers.

Keywords Random number generator · Cryptography · TRNG · AES

Introduction

Security is the more important in digital life. Data transfer through electronic gadgets is faster compared to conventional data transfer methods. In present days data security is concerned along with data transfer rate. Key generation is the crucial factor in data security (Garcia-Bosque et al. 2019). In earlier days key is transmitted along with data over a transmission medium which is more vulnerable to data

hackers. So key generation is a primary concern in secure data transfer.

Data are a powerful tool for every company and is therefore very important to protect it from external attacks. Protection of information is not only an interesting but necessary feature to safeguard data from unauthorized access. The key factors for data security are data encryption, decryption and key management. One such option of data securement is random sequence generation (Abdullah et al. 2018b). Random numbers can be generated using the LFSR pseudorandom property with different cryptographic applications.

The Random Number (RNG) Generators (RRNG) produce random numbers (PRNGs). While in most applications, random numbers are required, output is often ignored. Key generation of cryptosystems is important. Various primary application-dependent generation processes are used (Patnala et al. 2020a). Because of their deterministic existence, many digital systems use PRNGs. In the seed selection number pool, all variations of the input devices are stored. This seed produces the PRNG keys. During key generation, attackers can predict data. Due to deterministic PRNG. One such method must not be to generate the key via the

✉ Yalamanchili Sangeetha
sangeetha18.yalamanchili@gmail.com

¹ Department of IT, Velagapudi Rama Krishna Siddardha Engineering College, Vijayawada, India

² Department of ECE, GRIET, Hyderabad, India

³ Department of CSE, RVR & JC College of Engineering, Chowdavaram, Guntur, India

⁴ Shanax Technologies, Hyderabad, India

⁵ Department of CSE, Koneru Lakshmaiah Education Foundation, Greenfields, Vaddeswaram, Guntur, India

⁶ CHRIST University, Bangalore, India



Diagnosis of fault node in wireless sensor networks using adaptive neuro-fuzzy inference system

M. Sundar Rajan¹ · Golda Dilip² · Nithiyananthan Kannan³ · M. Namratha⁴ · Sankararao Majji⁵ · Srikanta Kumar Mohapatra⁶ · Tulasi Radhika Patnala⁵ · Santoshachandra Rao Karanam⁷

Received: 18 March 2021 / Accepted: 7 June 2021
© King Abdulaziz City for Science and Technology 2021

Abstract

Wireless networks (WSN) are sometimes inaccessible to humans and can be found in deep forests, diverse risky fields, high-mountainous areas and even underwater environments at least. Owing to continuous or instant changes in environmental parameters, failures in sensor networks are unavoidable. A fault can lead to a misread, which can harm the environment economically and physically. In several primary applications, wireless sensor networks (WSNs), including battlefield control, environmental monitoring and forestry fire monitoring are widely used. Research is being conducted to reduce energy usage, improve the longevity and life of the WSN network. This paper provides an ANFIS method for the summation, based on the neuro-fuzzy optimization model estimator of defect-tolerant WSNs. For WSNs, the scheme proposes the use of an intra-cluster and inter-cluster failure detection estimator adaptive neuro-fuzzy inference system (ANFIS). Traditional detection strategies for malfunction include a centralized mechanism for avoiding failure detection when the principal defect detector fails. In typical methods, the fault nodes are discarded. To solve these problems, we propose the identification and classification of distributed fault nodes by means of adaptive neuro-fuzzy inference method.

Keywords Wireless sensor networks · Distributed fault node · Adaptive neuro-fuzzy inference system

Introduction

The wide range of lightweight, cost-efficient, low-energy sensor nodes in wireless sensor networks (WSNs) is spread randomly across many areas of interests. In case of energy

conservation, these sensor nodes are arranged normally in groups and extend life in the network (Ding et al. 2005). The world sensor nodes of the non-cluster head-sensor, collect and send data to its cluster heads (CHs), to achieve those phenomena of concern. In-line data aggregation is performed by the CH node and the collected data are then transmitted to the base station with a hop or more, according to network topology. The WSN is widely used for many purposes including search and rescue, frontline tracking, protection of the environment, forest fire management, household and weather supervision (Akyildiz et al. 2002). WSNs are typically configured to work with minimal human interference in harsh environments. Since WSNs have limited resources, a sensor node will depend on its limited battery power. The failure of a WSN can be caused by several factors.

As a consequence, a WSN can fail due to failure, hardware or software for some components, communication layer faults or application layers or battery losses. The defect tolerance refers to the device's ability to work even though the necessary level has defects. Several research papers were released on the topic of failure detection and restoration (Crossbow 2003; Di

✉ M. Sundar Rajan
sundararbaminch@gmail.com

¹ Faculty of Electrical and Computer Engineering, Institute of Technology, Arbaminch University, Arba Minch, Ethiopia

² Department of Computer Science and Engineering, SRM Institute of Science and Technology, Vadapalani Campus, Chennai, India

³ Department of Electrical Engineering, Faculty of Engineering, King Abdulaziz University, Rabigh, Saudi Arabia

⁴ B.M.S. College of Engineering, Bangalore, India

⁵ GRIET, Hyderabad, India

⁶ Chitkara University Institute of Engineering and Technology, Chitkara University, Chandigarh, Punjab, India

⁷ Anurag University, Hyderabad, India



A novel Internet of Things (IoT)-enabled platform for patients with type 1 diabetes

Mannava Srinivasa Rao¹ · N. C. Santosh Kumar² · Narasimha Reddy Soora³ · Kama Ramudu⁴ · Sudharsan Jayabalan⁵ · Vikas Rao Vadi⁶

Received: 24 August 2021 / Accepted: 24 September 2021
© King Abdulaziz City for Science and Technology 2021

Abstract

Diabetic patients with type 1 diabetes (T1D) are constantly confronted with the decision of how much insulin to inject prior to each meal in order to maintain a healthy blood glucose level. As a result of recent research, it has been discovered that it is possible to construct an artificial pancreas (AP). The use of a closed-loop system, which combines an insulin pump with a continuous glucose monitor, can be beneficial for people with diabetes because it can help them manage their condition more effectively (CGM). The chronic disease diabetes with transient insulin resistance (T1D) necessitated daily insulin injections and close monitoring of blood glucose levels. T1D is characterised by insulin resistance that develops over time. Technologies for the management of type 1 diabetes, such as insulin pumps and Continuous Glucose Monitoring (CGM), have advanced significantly in the past decade, making them more effective in the management of type 1 diabetes patients. These systems may help to reduce treatment anxiety while also improving glycaemic control, according to the evidence. We describe how an attacker can cause physical harm to a victim by using their insulin pump, which is connected to the Internet, and how this can be done.

Keywords Type 1 diabetes · Celiac disease · Continuous glucose monitoring · Blood glucose

Introduction

Autoimmune diabetes (Type 1 diabetes, or T1D), also known as type 1 diabetes (T1D), is characterised by insulin deficiency, which results in hyperglycaemia and other complications. Type 1 diabetes (T1D) is a chronic endocrine disease characterised by the loss of pancreatic beta cells,

which results in insulin deficiency and hyperglycaemia complications (Aiello et al. 2020). Type 1 diabetes is a chronic endocrine disease characterised by the loss of pancreatic beta cells. It is the most common type of diabetes. Insulin-dependent diabetes is the most common type of diabetes. It affects approximately 5% of the population. It is the most common type of diabetes. A chronic immune-mediated enteropathy caused by the ingestion of dietary gluten, which is found in grains such as wheat, rye, and barley, celiac disease (CD) is a condition in which the immune system attacks the small intestine. It is characterised by the body attacking its own tissues, and it is the most common autoimmune disease in the world (Sun et al. 1906). As evidenced by disease concordance in monozygotic twin pairs and concordance in monozygotic twin pairs, both T1D and CD, which are characterised by a significant role for the immune system, have a strong genetic basis, as well as concordance in monozygotic twin pairs T1D patients' siblings have a 6% chance of developing the disease, compared to a 0.4% chance of developing the disease in the general population, and their concordance rates are 50% in monozygotic twins, according to the study. A study conducted on first degree relatives

✉ Mannava Srinivasa Rao
srinivasaomannava849@gmail.com

¹ Department of ECE, PVP Siddhartha Institute of Technology, Vijayawada, India

² Department of CSE, Kakatiya Institute of Technology and Science, Warangal, Telangana, India

³ Department of CSE, Kakatiya Institute of Technology and Science, Warangal, Telangana, India

⁴ Department of ECE, Kakatiya Institute of Technology and Science, Warangal, Telangana, India

⁵ Department of ECE, Gokaraju Rangaraju Institute of Engineering and Technology, Hyderabad, India

⁶ Department of Computer Science/IT, Don Bosco Technical School, Bosco Technical Training Society, Delhi, India



Implementation and Performance Evaluation of Ferroelectric Negative Capacitance FET

R. Deepa¹ · M. Parimala Devi² · N. Arun Vignesh³ · S. Kanithan⁴

Received: 11 January 2022 / Accepted: 26 January 2022
© The Author(s), under exclusive licence to Springer Nature B.V. 2022

Abstract

With the constant increase in power dissipation of nanoscale transistors, the almost four-decade-old cycle of performance advancement in complementary metal–oxide–semiconductor (CMOS) technology is in danger of being disrupted. As revealed in the first study, negative capacitance states in an isolated ferroelectric capacitor can be identified almost instantly when the capacitor is switched on. Increasing ferroelectric volume fraction depolarization, as demonstrated by phase-field modelling, results in rapid expansion of domain walls, which results in a negative capacitance signature. One must understand how the ferroelectric material is connected to the interfacial oxide and semiconductor, as well as how negative capacitance values can be achieved, in order to obtain amplification and margin of error. If one can adhere to these guidelines, your design will be optimized and free of hysteresis issues. The negative capacitance effect of ferroelectric oxides, according to our research, can be leveraged to drastically minimize power dissipation in nanoscale semiconductor transistors. The SS can be reduced to less than 60 mV/dec by using FETs with negative capacitance, such as FE-FETs and other comparable devices. These FETs' gate dielectric is comprised of an unstable substance, making them unstable.

Keywords Ferroelectric Negative Capacitance · Semiconductors · FE FET · Baseline MOSFET and Polarization · Ferroelectric material

1 Introduction

Computing, in addition to all other forms of electrical power conversion, accounts for a large share of total electricity use. Moore's law, which states that the number of transistors on an integrated circuit doubles approximately every two years, has made this possible in the past [1]. Using Moore's law as an incentive and a guideline when defining goals for the next generation of transistors, the semiconductor industry set the bar high for itself. As an illustration of Fig. 1. Therefore, transistors became smaller, allowing for greater performance while also lowering the cost of manufacturing. Feature size and other physical and electrical attributes are targeted by the ITRS for each of the technological nodes, which has

accurately forecasted the rise in transistor quality over the last few decades.

These figures are based on the ITRS Executive Reports, 2015 [2], which forecasts LG, SS and ION for each technology node up to 2030 in Fig. 1 (a) and Fig. 1 (b) for each technology node. Short-channel effects and greater leakage currents are projected to be eliminated by LG by the year 2021. Vertical gate all-around devices are expected to reduce physical dimensions even more [3].

The pictures show two-figure schematics for a bulk Si MOSFET (a) and a negative capacitance FET (b). As shown in Fig. 2(a), an example of a "baseline MOSFET," which has a high-K gate oxide, is depicted in this figure. Ferroelectric oxide is created by depositing it onto a metallic template constructed on the oxide of a baseline MOSFET, as shown in

✉ R. Deepa
rangarajdeepa@gmail.com

¹ Department of EIE, Bannari Amman Institute of Technology, Sathyamangalam, Erode, Tamil Nadu 638401, India

² Department of ECE, Velalar College of Engineering and Technology, Erode, Tamil Nadu 638012, India

³ Department of ECE, Gokaraju Rangaraju Institute of Engineering and Technology, Hyderabad 500090, Telangana, India

⁴ Department of ECE, MVJ College of Engineering, Bengaluru, India



Temperature Influence on Dielectric Tunnel FET Characterization and Subthreshold Characterization

S. Kanithan¹ · S. Anthoniraj² · P. Manikandan³ · T. Ramaswamy⁴ · Ravi Kumar⁵ · N. Arun Vignesh⁶ · Asisa Kumar Panigrahy⁶

Received: 2 February 2022 / Accepted: 15 February 2022
© The Author(s), under exclusive licence to Springer Nature B.V. 2022

Abstract

VLSI technology is being developed to lower the size of semiconductor devices due to the increasing importance of integrated circuits (ICs). Short channel effects, for example, make it difficult to operate these devices as technology continues to advance. Thus, the device's downsizing is made possible by designing new structures and leveraging new methods of current transfer. Many researchers believe that for low-power applications, TFETs, which rely on band-to-band tunnelling for current transfer, are a viable alternative to MOSFETs. For the purposes of mixed signal applications, this study examines the TFET from the perspective of both device and circuit-level simulations. It has been suggested that the negative capacitance (NC) of ferroelectrics could be used to overcome the basic limit of MOSFETs by utilising the differential amplification of the gate voltage under certain circumstances. It's a negative capacitance heterostructure based on these two ideas. As a result, the surrounding gate structure concept has improved the output characteristics of TFETs. By reducing channel resistance and tunnelling width, the suggested device size can be optimised. The TFET topologies discussed above are ideal for low-power switching and analogue RF applications. The proposed analytical models were tested using MATLAB and confirmed using the nanoscale device simulator Technology Computer-Aided Design (TCAD). The stacked surrounding gate TFET device, according to the data, is an interesting device contender to replace VLSI technology.

Keywords NCFET · TFET · Short channel effect · MOSFET · Transfer characteristics

✉ N. Arun Vignesh
arunvignesh44@gmail.com

- ¹ Department of ECE, MVJ College of Engineering, Bangalore, Karnataka 560067, India
- ² Department of Information Science and Engineering, MVJ College of Engineering, Bangalore, Karnataka 560067, India
- ³ Department of Robotics and Automation Engineering, Muthayammal College of Engineering, Kakkaveri, Rasipuram, Tamil Nadu 637408, India
- ⁴ Department of ECE, Sreenidhi Institute of Science and Technology, Hyderabad, Telangana 501301, India
- ⁵ Department of ECE, Jaypee University of Engineering and Technology, Guna 473226, India
- ⁶ Department of ECE, Gokaraju Rangaraju Institute of Engineering and Technology, Hyderabad, Telangana 500090, India


1 Introduction

An interfacial layer and a ferroelectric oxide layer form the gate dielectric stack in a FET with a negative capacitance. Electrostatic amplification of the gate voltage at the oxide-semiconductor interface results to a less than 60 mV/decade sub-threshold slope and considerable on-current increase due to the ferroelectric negative capacitance layer [1].

An interfacial layer and ferroelectric layer are added to the gate oxide in this work to form an NCFET, which has a 14 nm FinFET as its baseline transistor [2, 3]. The equivalent capacitance-based circuit model of an NCFET is shown in the inset of Fig. 1. In order to calculate the NCFET effective gate capacitance, the equivalent capacitance of all positive capacitors is modelled as CMOS.



Analysis and Design of Novel Doping Free Silicon Nanotube TFET with High-density Meshing Using ML for Sub Nanometre Technology Nodes

Ravi Kumar¹ · B. Aruna Devi² · V. Sireesha³ · A. Kishore Reddy⁴ · I. Hariharan⁵ · E. Konguvel⁶ · N. A Vignesh⁷ 

Received: 3 March 2022 / Accepted: 28 March 2022
© The Author(s), under exclusive licence to Springer Nature B.V. 2022

Abstract

Beyond the 25 nm technological node, MOSFETs (metal oxide semiconductor FETs) have worse channel electrostatic control than FinFETs (Fin field-effect transistors). It is necessary to use novel gate and channel engineering architecture in MOSFET devices at low technology nodes to decrease short-channel effects (SCEs). Future nano devices will replace present MOSFET with graded channel double gate MOSFETs and FinFETs for increased I_{ON} current and reduced leakage currents. Double gate MOSFETs have been identified by researchers in the last few years to considerably reduce short channel effects (SCE). Graded channel double gate MOSFETs provide superior switching characteristics and higher transconductance than single gate MOSFETs in ULSI/VLSI applications with many nodes. Transistors with hot carrier effects and subthreshold properties degrade at lower technological nodes than 25 nm. To increase on-state drive current and off-state leakage current separately in the gate-to-channel direction, super-halo and retrograde channel doping are used. As a result, semiconductor businesses must place a premium on precise doping levels, which drives up fabrication costs enormously. A revolutionary doping-free Silicon nanotube FET (DF-Si-NT-FET) with sub-nm technology nodes is presented in this paper. They are extremely resistant to SCE due to the strong charge control offered by both the inner and outside channels. Also, machine learning (ML) algorithm used with high-density meshing during simulation. TCAD was used to create all the simulations for this work.

Keywords FinFET · Doping free · Silicon-nanotube · DF-Si-NT-FET · TCAD · Short channel effects · Sub-nm technology nodes · GAA FET

1 Introduction

ICs have relied on planar transistors for decades, and transistor size has been steadily dropping since the 1990s, thanks to Moore's law and other experts. After every 18 months, Moore's law says, the number of transistors on a chip will have doubled. Gordon Moore, Intel's co-founder, stated this law in 1965. However, everything has come to a grinding halt recently. To keep up with Moore's law, researchers have

created a new type of transistor called a multiple gate field effect transistor (MuGFET). A MuGFET appears to be a promising alternative to CMOS because of its use in this application. Nanotechnology has been transformed by FinFET technology.

Comparing FinFET to CMOS transistors, the channel controllability and sub-threshold slope are significantly improved. There are many gates surrounding the channel in a Fin Field Effect Transistor (FinFET), which improves electrical control

✉ N. A Vignesh
arunvignesh44@gmail.com

¹ Department of ECE, Jaypee University of Engineering and Technology, Guna 473226, India

² Department of ECE, Dr. N.G.P Institute of Technology, Dr. N.G.P. Nagar, Kalapatti Road, Coimbatore, Tamil Nadu 641048, India

³ Department of CSE, Geethanjali Institute of Science and Technology, Nellore 524137, Andhra Pradesh, India

⁴ Department of ECE, Andhra Engineering College, Nellore 524322, Andhra Pradesh, India

⁵ Department of Micro and Nano Electronics Engineering, School of Electronics Engineering, Vellore Institute of Technology, 632014 Vellore, India

⁶ Department of Embedded Technology, School of Electronics Engineering, Vellore Institute of Technology, Vellore 632014, India

⁷ Department of ECE, GRIET, 500090 Hyderabad, Telangana, India

Silicon

Optimal Design and performance analysis of Vertically Stacked nanosheet Tunnel Field Effect Transistor --Manuscript Draft--

Manuscript Number:	SCON-D-22-00345R1
Full Title:	Optimal Design and performance analysis of Vertically Stacked nanosheet Tunnel Field Effect Transistor
Article Type:	Original Research
Keywords:	TFET; TCAD; Vertical Field; Strained Channel; Vertically stacked TFET; BTBT; Strain layer.
Corresponding Author:	Anthoni Raj MVJ College of Engineering INDIA
Corresponding Author Secondary Information:	
Corresponding Author's Institution:	MVJ College of Engineering
Corresponding Author's Secondary Institution:	
First Author:	S Anthoni Raj
First Author Secondary Information:	
Order of Authors:	S Anthoni Raj K. Saravanan Vinay Raj A.S N. A Vignesh
Order of Authors Secondary Information:	
Funding Information:	
Abstract:	<p>Tunneling field effect transistors (TFETs) have been proposed as switches for low-power integrated circuits. A negative-capacitance vertical-tunnel FET that improves vertical tunnelling over corner tunnelling. This is due to the fact that when there is negative capacitance, a stronger vertical electric field is formed. The device can be altered to operate in the TFET or MOSFET modes and tweaked to act as an n-type or p-type FET by changing the electrostatic doping utilising multiple gates. Tunnel FET is a device that has a lot of potential for replacing MOSFETs and their shortcomings (TFET). Applying the appropriate gate bias turns ON this simple gated P I N diode. Because of the Band To Band Tunneling (BTBT) concept underpinning these Tunneling FETs, a current can flow from the p-valence region's band to the intrinsic area's conduction band. Low-power applications can benefit from this design because of the reduced OFF-state leakage current (IOFF). As a result, the proposed study makes use of a novel vertically stacked TFET structure that combines the benefits of uniformly doped junctionless transistors with the tunnelling effect. A 2D TCAD simulation programme is used to simulate and confirm the analytical model findings. As a result of the findings, the device's surface potential, electric field, and threshold voltage have all been greatly improved.</p>
Response to Reviewers:	<p>Response to the reviewer comments</p> <p>Reviewer #1:</p> <p>"Optimal Design and performance analysis of Vertically Stacked nanosheet Tunnel Field Effect Transistor" is really an interesting work. I have some questions prior to</p>



Negative Capacitance Ferroelectric FET Based on Short Channel Effect for Low Power Applications

S. Kanithan¹ · N. Arun Vignesh² · S. Jana³ · C. Gokul Prasad⁴ · E. Konguvel⁵ · S. Vimalnath⁶

Received: 9 November 2021 / Accepted: 16 December 2021
© Springer Nature B.V. 2022

Abstract

The electrical properties of ferroelectric (Fe) FETs with Negative Capacitance (NC) have been explored theoretically at temperatures ranging from -280 to +360 degrees Celsius. Temperature influences ferroelectric thin film surface potential amplification with a fixed thickness, according to the findings. As the temperature of the ferroelectric NC effect rises, the device's transfer and output qualities deteriorate. The findings of this work could be used in the future to help improve FeFET design and performance for applications that require low power dissipation. The NC effect in symmetric long channel double-gate Junctionless transistors with two gates is predicted using an analytical model based on the charge principle. We explored the effect of ferroelectric thickness on I-V characteristics to better understand ferroelectric materials. In our model, positive capacitance lowers short channel effects while enhancing current overdrive, resulting in lower power consumption and more efficient transistor size scaling. Based on our calculations for a long channel Junctionless with NC, the device's ON current will be six times higher than that of a Junctionless FET. We use oxygen ion mobility to explain sub-60 mV/dec results in thin-film Ta₂O₅/ZnO transistors with dynamic gate bias sweep. The oxygen ions in Ta₂O₅ direct the model in dynamic gate bias sweep, resulting in NC. When achieving a sub 60 mV/decade subthreshold slope, the study finishes by revealing design tradeoffs that give an engineer or physicist insight into the current status of ferroelectric nanowires and ferroelectric FETs' uses and limitations.

Keywords Double gate Junction less Transistor · Ferroelectric FET · JLFET · Negative Capacitance · Short Channel Effect

1 Introduction

Advanced aggressive scaling with ordinary metal-oxide semiconductor field-effect transistors necessitates a variety of extra technological boosters in modern MOSFET processing. Even more advanced methods of local strain control have been presented in various studies [1]. When it comes to the latest MOSFETs, extensive junction and contact engineering is required. Slope transistors have been studied recently [2], although the nanoelectronics industry has not yet used them. The notion of junctionless field-effect transistors (JLFETs) has been developed to circumvent the limits of nanoscale junction engineering [3–5]. Activation of S/D dopants for nanoscale scaling and cost reduction does not need the processes necessary to build ultra-steep junctions or high thermal annealing [6, 7].

However, scaling MOS devices increases power consumption and worsens off-state current when the power supply is decreased [8]. The most important limiting factor is the intrinsic subthreshold swing limit of MOS devices at 300

✉ S. Kanithan
kani.rex@gmail.com

✉ N. Arun Vignesh
arunvignesh44@gmail.com

¹ Department of ECE, MVJ College of Engineering, Bangalore, India

² Department of ECE, Gokaraju Rangaraju Institute of Engineering and Technology, Hyderabad, Telangana 500090, India

³ Department of ECE, Veltech Rangarajan Dr. Sagunthala R&D Institute of Science and Technology, Chennai 600062, India

⁴ Department of ECE, SNS College of Engineering, Coimbatore 641107, India

⁵ Department of Embedded Technology, School of Electronics Engineering, Vellore Institute of Technology, Vellore 632014, India

⁶ Department of ECE, Erode Sengunthar Engineering College, Erode, Tamilnadu 638057, India

Design and experimental investigation on VL-MLI intended for half height (H-H) method to improve power quality using modified particle swarm optimization (MPSO) algorithm

Satish Kumar Ramaraju^a, Thenmalar Kaliannan^b, Sheela Androse Joseph^c, Umadevi Kumaravel^d, Johny Renoald Albert^{b,*}, Arun Vignesh Natarajan^e and Gokul Prasad Chellakutty^f

^a*Department of Medical Electronics Engineering, Sengunthar College of Engineering, Namakkal, Tamilnadu, India*

^b*Department of EEE, Vivekanandha College of Engineering for Women, Namakkal, Tamilnadu, India*

^c*Department of EEE, Kongu Engineering College, Perundurai, Tamilnadu, India*

^d*Department of EEE, Sengunthar Engineering College, Namakkal, Tamilnadu, India*

^e*Department of ECE, Gokaraju Rangaraju Institute of Engineering and Technology, Hyderabad, Telangana, India.*

^f*Department of ECE, SNS College of Engineering, Coimbatore, Tamilnadu, India*

Abstract. A Voltage lift performance is an excellent role to DC/DC conversion topology. The Voltage Lift Multilevel Inverter (VL-MLI) topology is suggested with minimal number of components compared to the conventional multilevel inverter (MLI). In this method, the Modified Particle Swarm Optimization (MPSO) conveys a primary task for the VL-MLI using Half Height (H-H) method, it determine the required optimum switching angles to eliminate desired value of harmonics. The simulation circuit for fifteen level output uses single switch voltage-lift inverter fed with resistive and inductive loads (R & L load). The power quality is developed by voltage-lift multilevel inverter with minimized harmonics under the various Modulation Index (MI) while varied from 0.1 up to 1. The circuit is designed in a Field Programmable Gate Array (FPGA), which includes the MPSO rules for fast convergence to reduce the lower order harmonics and finds the best optimum switching angle values. To report this problem the H-H has implemented with MPSO to reduce minimum Total Harmonic Distortion (THD) for simulation circuit using Proteus 7.7 simulink tool. Due to the absence of multiple switches, filter and inductor element exposes for novelty of the proposed system. The comparative analysis has been carried-out with existing optimization and modulation methods.

Keywords: Solar-Photovoltaic, voltage lift-multilevel inverter, particle swarm optimization algorithm, half height, field program gate array

1. Introduction

The electrical system has major problems due to the presence of harmonic contents in the power quality features. The harmonics may be classified into

*Corresponding author. Johny Renoald Albert, Department of EEE, Vivekanandha College of Engineering for women, Namakkal, Tamilnadu, India. E-mail: jorenoeee@gmail.com.



Anisotropy Enhancing Vertically Aligned Silicon-Germanium Nanowire

A. Mohamedyaseen¹ · P. Suresh Kumar² · K. R. Kavitha³ · N. A. Vignesh⁴

Received: 19 March 2022 / Accepted: 11 April 2022
© The Author(s), under exclusive licence to Springer Nature B.V. 2022

Abstract

For the past four decades, the microelectronics industry has relied on silicon complementary MOS (metal oxide semiconductors). Because of their excellent characteristics, MOSFETs have become key components in VLSI. A new method for fabricating nano bridge arrays of various materials makes use of a sacrificial template structure: a suspended silicon nanowire array. This method produces nano bridge arrays of diverse materials. Energy harvesters such as thermoelectric micro/nano generators could be used to power Internet of Things sensors. According to the findings of this work, a planar micro/nano generator was constructed using silicon micromachining technologies and a thermoelectric material composed of silicon-germanium (SiGe) nanowire arrays. A top-down nanofabrication approach and electro-chemical lithography are utilised to produce silicon nanowires from SOI wafers using direct-write electron beam lithography (EBL). VLS (Vapor Liquid Solid Growth) was utilised to demonstrate monolithic integration of bottom-up nano wire arrays on pre-made micro platforms (CVD-VLS). It is demonstrated in this study that MacEtch may be used to manufacture Si NW arrays on vertically aligned Si wafers. Template-assisted manufacturing techniques have also been used to construct vertically aligned Si NW arrays with regulated diameter and number density.

Keywords Silicon-germanium · Silicon · VLSI · Nano wire · SiNW-based FETs · Etching · Electron beam lithography

1 Introduction

The development of silicon nanowire technology over the last few decades has showed promise in future electrical, optoelectronic, and chemical/biological sensing applications. Silicon nanowires have been employed in a wide range of applications, including memory, transistors, sensors, quantum information processing, solar cells, thermoelectric energy harvesting, and electrometers [1]. As a result of its low cost and widespread use in semiconductor manufacturing, silicon has become an ideal material for various applications.

Nanowire MOSFETs are viewed as excellent solutions for scaling semiconductor devices rapidly. In addition to a number of variables, nanowire transistor research has grown in popularity. Ultra Large Scale Integration (ULSI) applications benefit from their high yield and consistent electrical characteristics. Second, “bottom-up” generated nanowire materials offer well-controlled size that is at or beyond the limitations of lithography in comparison to “top-down” nanofabricated device designs [2]. Furthermore, the crystalline structure, flat surfaces, and ability to produce radial and axial hetero structures help reduce dispersion. When compared to other similar-sized nanodevices, this one has a higher carrier mobility. To conclude, nanowire diameters can be controlled to less than 10 nanometres [3]. Nanowire-based electronics can therefore keep their electric quality even while their gate length increases rapidly. Planar MOSFETs are unable to easily obtain this characteristic. Silicon Nanowire FETs have metal source and drain connections unlike planar MOSFETs. That is, instead of using degenerately doped semiconductors, metals are used for the source and drain connections [4]. As a result of the metal work function and Fermi level pinning at the metal/semiconductor contact, Schottky barriers are created. The quality of a device’s physical interface with its users has a

✉ A. Mohamedyaseen
mohamedyaseenece@gmail.com

¹ Department of ECE, Excel Engineering College, Namakkal, India
² Department of EEE, Mahendra Engineering College (Autonomous), Namakkal, India
³ Department of ECE, Sona College of Technology, Salem, Tamilnadu 636005, India
⁴ Department of ECE, GRIET Hyderabad, 500090 Telangana, India



Design and Analysis of Junctionless FinFET with Gaussian Doped for Non-polar Structure

E. Sathish Kumar¹ · Suresh Kumar P² · N. Arun Vignesh³ · S. Kanithan⁴

Received: 23 November 2021 / Accepted: 16 December 2021
© The Author(s), under exclusive licence to Springer Nature B.V. 2022

Abstract

Modern transistors have two metallurgical junctions, one at the source/channel region and the other at the drain/channel region. A strong doping profile at these junctions is required to scale semiconductor devices below 10 nm. Considering all possible attempts to improve gadget attributes. Junctionless MOSFETs, FinFETs, and Tunnel FETs are all examples of non-classical semiconductor devices that use this principle. Junctionless FinFETs reduce short channel effects and improve I_{ON}/I_{OFF} . However, in Junctionless FinFETs, ON current and ION/IOFF ratio are trade-offs. To overcome this problem, Gaussian doping was added into Junctionless FinFETs. Thus, combining Gaussian doping and junctionless FinFETs improves electrical properties and alleviates MOSFET problems. Thus, physics-based analytical modelling is essential to comprehend device behavior. This work focuses on Gaussian Doped Junctionless FinFETs for CMOS. This section compares the features of various doping configurations in Junctionless FinFETs. Bulk substrate Junctionless FinFETs can be doped uniformly, Gaussian uniformly, or graded uniformly (GRJL- FinFETs). To compare device Id-Vs, the first segment examined device Fin width, Fin height, channel length, oxide thickness, dielectric constant, and temperature.

Keywords Junctionless FinFET · MOSFET · Gaussian doping · SRAM · Non-polar structure · GRJL- FinFETs · FeFET

1 Introduction

MOSFETs with conventional characteristics that have been shrunk down to the nanoscale region. During the device construction process, it is challenging to create exceedingly thin connections in this regime. The thermal budget and annealing are increased as a result of this. Lee and colleagues created junctionless transistors in order to eliminate shallow junctions and improve the performance of the device. The source-to-drain connector on this device is not present, as seen in Fig. 1. The junctionless transistor is disabled when

a fermi level is reached at the gate terminal [1]. As a result, accumulation mode transistors are used. The device performance, electrostatic control, and resistance to short channel effects are all improved with the use of junctionless transistors. At 65 Mv/v, they have a subthreshold swing that is comparable to that of MOSFETs. When designing SRAM, Oscillator, and amplifier circuits, it is recommended that you use junctionless transistors. When compared to other devices, the OFF-state current of junctionless transistors is quite substantial [2]. Junctionless transistors with three gates (Trigate, Surrounding gate, and Rectangular gate) being investigated for their ability to reduce subthreshold leakage current. Trigate allows for more gate control, better charge transit between the source and drain, and fabrication practicality due to the increased gate control.

The junctionless FinFET structure outperforms the junctioned FinFET structure in terms of high ON current, low subthreshold current, good switching properties, and immunity to short channel effects. [2]. Several studies on junctionless FinFETs have been conducted in order to better understand their properties and reliability concerns. Engineers can now use more advanced techniques like channel engineering, gate engineering, and multi-gate

✉ E. Sathish Kumar
sathishelangobe@gmail.com

¹ Department of ECE, Gnanamani College of Technology, Namakkal, Tamil Nadu 637018, India

² Department of EEE, Mahendra Engineering College, Namakkal, Tamil Nadu 637503, India

³ Department of ECE, Gokaraju Rangaraju Institute of Engineering and Technology, Hyderabad, Telangana 500090, India

⁴ Department of ECE, MVJ College of Engineering, Bengaluru, Karnataka 560067, India



Time Dependent Behaviour of Amino Silane-treated Aramid Fibre and Waste Latex Rubber Powder Toughened Epoxy Composite

K. K. Arun¹ · M. Bala Theja² · L. Girisha³ · N. Arun Vignesh⁴ · N. S. Sivakumar⁵ · Ram Subbiah⁶ · S. Kaliappan⁷

Received: 2 August 2021 / Accepted: 9 October 2021

© Springer Nature B.V. 2021

Abstract

The purpose of this research was to investigate the time-dependent behaviour of an epoxy composite prepared from silane-treated aramid fibre and waste latex rubber powder (LRP). To increase the adhesive behaviour of reinforcement with matrix, the aramid fibre and latex rubber powder were surface treated using amino silane. The composites were made using hand layup method and cured at room temperature. The fatigue strength of LRP in fibre-epoxy composite was improved up to 82.1 % when compared to fibre-epoxy composite. Similarly, incorporating LRP into the resin increased the energy storage up to 4.7GPa, which was equal to 34.04 % with neat epoxy. The addition of latex rubber powder to the resin enhanced the energy dissipation factor in dynamic mechanical analysis (DMA). These mechanically toughened epoxy composites made from industrial crop waste could be used in engineering applications that demand great toughness and stiffness.

Keywords PMC · Aramid fibre · Latex · Fatigue · Fracture toughness · DMA

1 Introduction

Epoxy resins are a flexible class of polymers with two or more oxirane rings or epoxy groups in their molecular structure that can be hardened into thermosetting plastics with an appropriate curing agent [1]. Because of its superior adhesiveness, chemical resistance, and mechanical and physical qualities,

epoxy resins have a wide range of uses as coatings, adhesives, electrical insulators, electronic encapsulation materials, and matrices for fibre components [2]. Due to their highly cross-linked three-dimensional network structure, cured epoxy resins have greater stiffness, strength, heat resistance, solvent barrier characteristics, and creep resistance than thermoplastic polymers [3]. The pressure required to fabricate epoxy resins is lower than that required to fabricate other thermosetting resins. The cured materials have substantially lower shrinkage and residual stress than the unsaturated polyester resins treated via vinyl polymerization. Epoxy resin comes in a variety of viscosities, from a low viscosity liquid to a tack-free solid, and cured epoxy polymers can be used at a wide range of temperatures by using the right hardener and keeping the cross-linking degree under control. Epoxy, on the other hand, is primarily a hard and brittle polymeric substance due to its extensively cross-linked structure, and it has low impact and crack initiation resistance in the cured condition [4]. In the past years significant amount of research studies were conducted in natural fibre toughening in polymer composites. Since natural fibre contains potential reinforcement capability without affecting the environment thus they are highly demand in composite manufacturing [5]. However when making high performance industrial composites the natural fibres have limitations. They can't affordable to high temperature environment and high moisture prone zones. Moreover the

✉ S. Kaliappan
kaliappan261975@gmail.com

¹ Department of Mechanical Engineering, Kumaraguru College of Technology, Coimbatore, Tamilnadu, India

² Department of Mechanical Engineering, SVR Engineering College, Nandyal, India

³ Department of Mechanical Engineering, PES Institute of Technology and Management, Karnataka, India

⁴ Department of Electronics and Communication Engineering, Gokaraju Rangaraju Institute of Engineering & Technology, Telangana, India

⁵ Department of Mechatronics Engineering, TISHK International University, Erbil, Iraq

⁶ Department of Mechanical Engineering, Gokaraju Rangaraju Institute of Engineering & Technology, Telangana, India

⁷ Department of Mechanical Engineering, Velammal Institute of Technology, panchetti, Tamilnadu, India



A Study of an Ultrasensitive Label Free Silicon Nanowire FET Biosensor for Cardiac Troponin I Detection

M. Durga Prakash¹ · B. Vamsi Krsihna² · B. V. V. Satyanarayana³ · N. Arun Vignesh⁴ · Asisa Kumar Panigrahy⁴ · Shaik Ahmadsaidulu¹

Received: 9 August 2021 / Accepted: 24 August 2021

© Springer Nature B.V. 2021

Abstract

This study evolves an ultrasensitive label free electrical device, the silicon nanowire field effect transistor (SiNW FET) for cardiac troponin I (cTnI) in acute myocardial infarction (AMI). In this work, SiNW FET is designed, simulated using COMSOL semiconductor module to identify the presence of different concentrations of cTnI present in human blood. The surface of the SiNW is functionalized with the cTnI monoclonal antibody (mAb-cTnI) on attached to detect cTnI antigen. The response of the device is also studied using cTnI at different concentrations with the lowest limit of detection of 0.002 ng/mL. The presented SiNW FET in this study shows considerable response than the earlier developed devices and signify impressive capability for subsequent implementation in point-of-care (PoC) detection.

Keywords SiNW FET · Biosensor · Ultrasensitive · cTnI · Limit of detection

1 Introduction

Nanotechnology turns out to be one of the vital things in our day-to-day life which includes bio-medical applications too. Major bio medical applications comprise bio-sensors. These bio-sensors are greatly desirable for the early detection of the lethal diseases. These sensors are the analytical devices integrated with molecular recognition and sensing materials. The detection principle in sensors is subjected to the interaction between its target and the recognition molecule. Sensitivity of the sensors is the foremost criterion for sensor designing. SiNWs can be used as one of the prominent devices for the

implementation of bio-sensors due to their high surface to volume ratio and high chemical reactivity [1, 2]. SiNW provides higher sensitivity than bulk FETs, because SiNWs acts as gate in a nanowire FET. SiNW FETs are also used for the detection of ultra-low concentrations of biomolecules [3, 4].

Nanowires are similar in size when compared to cells, proteins which allow them to associate with those materials which will further brings some characteristic change in the Nanowire devices. Sensing devices comprised of nanowires with reduced lengths exhibited higher sensitivity than nanowires with greater lengths, so the device sensitivity depends on the channel dimensions and doping concentration [5–7]. The brilliant feature of nanowire FETs is the binding of a charged element on their surface brings computable variations in their conductivity. This variation in the conductivity over the nanowires carries further a change in the current through them as these nanowires offer a high surface to volume ratio (S/V). The sensitivity of these biosensors is certainly high while they function at room temperature. The sensitivity of nanowire-based sensors can spot the level to micromoles and show quicker response time [8]. The raise in drain current enhances the sensitivity value. The resistance of nanowires has a key influence on the sensitivity of the nanowire. Nanowires with more lengths and narrower diameters provide higher sensitivity towards bio marker detection. The sensitivity of these sensors also affected by the variation of the surface

✉ M. Durga Prakash
mdprakash82@gmail.com

✉ Shaik Ahmadsaidulu
ahmed0474@gmail.com

¹ Department of ECE, Velagapudi Ramakrishna Siddhartha Engineering College, Kanuru 520007, Andhra Pradesh, India

² Department of ECE, Koneru Lakshmaiah Education Foundation, 522502 Guntur, Andhra Pradesh, India

³ Department of ECE, Vishnu Institute of Technology, Vishnupur, Bhimavaram 534202, Andhra Pradesh, India

⁴ Department of ECE, Gokaraju Rangaraju Institute of Engineering & Technology, 500090 Hyderabad, Telangana, India



Tunnel Field Effect Transistor Design and Analysis for Biosensing Applications

B. Vamsi Krsihna¹ · G. Anith Chowdary² · S. Ravi³ · Kunduru Venkat Reddy⁴ · K. R. Kavitha⁵ · Asisa Kumar Panigrahy⁶ · M. Durga Prakash^{1,2}

Received: 19 February 2022 / Accepted: 11 March 2022
© The Author(s), under exclusive licence to Springer Nature B.V. 2022

Abstract

The physical modelling of the tunnel field effect transistor (TFET) is done in this study. The Silvaco TCAD tool is used to design and simulate the TFET structure. The FET device has attracted a lot of attention as the ideal tool in creating biosensors because of its appealing properties such as ultra-sensitivity, selectivity, low cost, and real-time detection capabilities in sensing point of view. These devices have a lot of potential as a platform for detecting biomolecules. Short channel effects, specificity, and nano-cavity filling have all been improved in FET-based biosensors. FET-based biosensors are appropriate for label-free applications. Random dopant variations and a thermal budget are seen during the construction of a JLFET. To overcome this problem, the charge-plasma-based concept was established in FETs in this study. Different metallurgical functions for electrodes were employed in this biosensor to behave as a p-type source and n-type drain. To alleviate the short channel effects, a dual material gate work function for the gate electrode was devised, as well as a double gate architecture. Biomolecules can be neutral or charge-based, and both types of biomolecules can be identified using a proof-of-concept FET-based biosensor. Changes in the drain current (I_d) of the device were achieved by varying dielectric values and charges in the cavity region with variable cavity lengths.

Keywords TFET · JLFET · Biosensor · Short-channel effect · Sensitivity · p-type · n-type · DIBL · FET-based biosensor

1 Introduction

The consistently developing VLSI industry is investigating ultralow power consuming gadgets that fulfill nanoscale creation, high bundle thickness, high awareness and simultaneously, are additionally innovatively feasible [1, 2]. As we follow Moore's regulation past the 20 nm system, a creating exceptionally

doped intersection present major issues like random dopant fluctuations (RDF) and requires expensive strategies of particle implantation furthermore diffusion. The size of the devices is reducing drastically [3]. This led to prominent short channel effects primarily due to this device performance is degrading. As the device size commences to 20 nm, fabricating the high concentration junctions is complex. As a result, a junction less transistor fabricated with heavily doped silicon nanowires are proposed, because these transistors do not need any formation of junctions. Although a junction less field-effect transistor (JLFET) is smoother, random dopant fluctuation (RDF) causes high variability, which is a critical issue when the device is dimensions are reduced [4]. So, we are using charge-plasma-based concept is introduced [5].

The basic structure of tunnel field effect transistors (TFET) with performance characteristics of biomolecules shown in Fig. 1(a) and (b) is emerged as a possible replacement for several engineered gated MOSFETs due to their outstanding improvement in having low subthreshold swing, speed, power consumption and other factors [5]. Tunnel Field Effect Transistor works on the principle of inter band tunneling [6]. The tunnel is formed between the source and the channel electrode, where the tunnel width is modulated by applying

✉ M. Durga Prakash
mdprakash82@gmail.com; durgaprakash.m@srmmap.edu.in

¹ Department of ECE, Koneru Lakshmaiah Education Foundation, Guntur 522502, Andhra Pradesh, India

² Department of ECE, SRM University-AP, 522240 Mangalagiri, Andhra Pradesh, India

³ Department of ECE, Seshadri Rao Gudlavalluru Engineering College, Gudlavalluru, Vijayawada 521356, Andhra Pradesh, India

⁴ Department of ECE, Sreenidhi Institute of Science and Technology, 501301 Hyderabad, Telangana, India

⁵ Department of ECE, Sona College of Technology, 636005 Salem, Tamilnadu, India

⁶ Department of ECE, Gokaraju Rangaraju Institute of Engineering & Technology, 500090 Hyderabad, Telangana, India



Design and Modelling of Highly Sensitive Glucose Biosensor for Lab-on-chip Applications

M. Durga Prakash¹ · Shaik Lathifa Nihal¹ · Shaik Ahmadsaidulu¹ · Raghunandan Swain² · Asisa Kumar Panigrahy³

Received: 3 September 2021 / Accepted: 10 November 2021
© The Author(s), under exclusive licence to Springer Nature B.V. 2021

Abstract

Medical diagnosis has been developed with new techniques which are capable of performing very sensitive detection and quantifying certain parameters. Microfluidic based sensors are taking very essential part in the diagnosis of several parameters. These parameters can be correlated with the presence of specific molecules and their quantities. A lab-on-chip biosensor is a miniaturized device integrated in a single chip which can perform one or several analyses including human diagnostics done in the laboratory. This work presents, design and model of a lab on chip biosensor with molecule parameters using COMSOL multi-physics. In this paper, designed a glucose sensor, which can be used to track the glucose levels in body which helps diabetic patients maintain their glucose levels. The aim of this work is to design of a glucose sensor which is highly sensitive. The sensor is designed with an electrode and reaction surface in a micro channel. The designed sensor harvests a decent sensitivity in terms of average current density and with a limit-of-detection value 0.01 μ M.

Keywords Biosensor · COMSOL Multi Physics · Electrode · Micro fluids · Lab-on- chip · Reaction surface

1 Introduction

LoC (Lab-on-Chip) technology is a combination of fluidics, transducers (biosensors), and electronics on a single chip. When compared to traditional laboratory operations, LoC conducts a single or several laboratory functions on a single chip configuration, which can save money and time. Chips range in size from a few millimeters to a few square centimeters. It can handle fluids with a volume of less than a Pico liter. The primary benefit of LoC technology is directly related to microfluidics, which is basically a mix of physics and small-scale fluid manipulation to achieve multiplexing, automation, and high throughput screening. LoC for point of care applications is a multifunctional device which holds entire set of biochemical process on a single chip [1]. It has a

biological sample manipulation, fundamental fluidic operations, detection, automation, advanced operations, packaging and portability of microfluidic devices including device fabrication [2].

Now-a-days research started worldwide on this technology because of its immense advantages including fast response, less expensive and good sensitivity. LoC is part of Micro Total Analysis Systems (μ TAS) and Micro-Electromechanical Systems (MEMS). These are subset of Micro-Electromechanical Systems (MEMS), with μ TAS referring to the integration of a total sequence of lab processes in order to perform chemical analysis, and LoC referring to the integration of one or more lab processes onto a single chip. Micro-electromechanical systems (MEMS) are grown from micro-electronics with different technical approaches. The handling process of complex liquids automatically leads to the microfluidic integration to begin with lab-on-chip. For handling these liquids several devices known as micro valves, micro pumps, sensing elements, electronics circuits and techniques which are pressure driven, electro kinetic driven, centrifugal driven, capillary driven, droplet based and electro wetting- based can be taken into consideration. The electro-kinetic technique is a simple process for lab-on-chip applications because of microfluidic channels and electrodes without moving parts. Based on the type of sample or/

✉ M. Durga Prakash
mdprakash82@gmail.com

¹ Department of ECE, SRM University AP, 522502 Amravati, India

² Department of ETC, Parala Maharaja Engineering College, 761003 Berhampur, Odisha, India

³ Department of ECE, Gokaraju Rangaraju Institute of Engineering & Technology, 500090 Hyderabad, Telangana, India



Performance Analysis of Ion-Sensitive Field Effect Transistor with Various Oxide Materials for Biomedical Applications

M. Durga Prakash¹ · Beulah Grace Nelam¹ · Shaik Ahmadsaidulu¹ · Alluri Navaneetha² · Asisa Kumar Panigrahy³

Received: 30 August 2021 / Accepted: 20 September 2021

© Springer Nature B.V. 2021

Abstract

Ion Sensitive Field Effect Transistors (ISFET) are most widely used in medical applications due to simple integration process, measurement of sensitivity and its dual properties. These ISFETs are originated from Metal Oxide Semiconductor Field Effect Transistors (MOSFET) with improvements in structure. ISFETs are used as bio-sensors for the detection of biomarkers in blood, DNA replication and several other medical applications. In this article, we design the ISFET pH sensor in two dimensions with integration of two models namely, semiconductor model and electrolyte model are represented using manageable global equations. The sensitivity of ISFET with different oxide layers is measured and compared. We also measure the sensitivity of the designed 2D-ISFET in two different solutions and compare it with different oxides to know the best oxide material to be used to design the device.

Keywords Ion Sensitive Field Effect Transistor (ISFET) · Oxides · Sensitivity · pH sensor · Bio-sensors

1 Introduction

The origin of Ion Sensitive Field Effect Transistor (ISFET) has been emerged from the structure of Metal Oxide Semiconductor Field Effect Transistor (MOSFET) having additional improvements making these devices to be widely used in medical field as biosensors [1, 2] (http://www.idc-online.com/technical_references/pdfs/mechanical_engineering/ISFET-Bergveld.pdf). In the initial stages, experiments are done on the structure of MOSFET, and the characteristics can be studied from and improvements are made for ISFET [3, 4]. The drawbacks of the conventional FET such as less sensitivity, delayed response time and high leakage currents make ISFETs popular in the field of sensor designing. The main difference between the structure of

Conventional FET or a MOSFET and Ion Sensitive Field Effect Transistor (ISFET) is the position of gate. We know that any of the transistor structure consists of Source, Drain and Gate on the surface of the substrate. In the same manner, the conventional FET structure consists of Gate deposited on the surface of substrate along with source and drain. But when we observe the gate is separated from the surface of the substrate. The gate separated from the structure of the substrate as the “Reference electrode”. The gate voltage is applied along the reference electrode. Association between the gate dielectric and the ions is regulated by varying the gate voltage which results in determining the ion concentration.

The process of surface interactions takes place from “Site-Binding model”, hydroxyl ions are present on the surface of metal oxide that interacts with the insulator material. In this article, four different oxides namely Silicon Dioxide (SiO_2), Aluminium Oxide (Al_2O_3), Tantalum Oxide (Ta_2O_3) and Hafnium Oxide (HfO_2) are deposited on the surface of the substrate with two different electrolyte solutions filled in the electrolyte tank are implemented. In the existing literature, the temperature characteristics and the improvement in the sensing of pH parameter are obtained, where the values of temperature and pH are limited [5]. The sensitivity of ISFET through the process of chemical surface modification can be studied through and the function of ISFET to measure the buffer capacity is surveyed in [6–8]. The primary application of ISFET

✉ M. Durga Prakash
mdprakash82@gmail.com

¹ Department of ECE, Velagapudi Ramakrishna Siddhartha Engineering College, Kanuru 520007, Andhra Pradesh, India

² Department of ECE, Mahatma Gandhi Institute of Technology, 500075 Hyderabad, Telangana, India

³ Department of ECE, Gokaraju Rangaraju Institute of Engineering & Technology, Hyderabad, Telangana 500090, India



Enhancement in performance of DHTprecoding over WHT for EC companded OFDM in wireless networks

A. Lakshmi Narayana¹ · B. Prasad² · Prabhakara Rao Kapula³ · Dumpa Prasad⁴ · Asisa Kumar Panigrahy⁵ · D. N. V. S. L. S. Indira⁶

Received: 23 June 2021 / Accepted: 8 August 2021
© King Abdulaziz City for Science and Technology 2021

Abstract

In this paper, a new hybrid methodology that combines precoding transform and companding transforms is being proposed for next-generation heterogeneous wireless networks. This method will improve the performance of the orthogonal frequency division multiplexing (OFDM) system by reducing the Peak to average power ratio (PAPR). A hybrid methodology that combines exponential companding (EC), which is a non-linear companding technique with Discrete Hartley Transform (DHT), as well as Walsh Hadamard Transform (WHT), is proposed and investigated. When the three simulated results are compared with original OFDM signal, piecewise linear companding shows an improvement factor of 28.8% over the original OFDM signal. Exponential companding is having an improvement factor of 33.49% over the original OFDM signal. Walsh Hadamard transform combined with exponential companding shows an improvement factor of 34.99% over OFDM. Discrete Hartley Transform combined with Exponential Companding is having an improvement factor of 38.09% over OFDM. The two proposed methods do not introduce any In-band distortion as well as Out-of-band Radiation when compared to the existing technique PLC (Meixia et al. in IEEE Trans Broadcast 60(3):532-539, 2014) which can be observed from the PSD analysis. Among the two proposed methods, the DHT precoded OFDM with the EC system shows significant BER improvement over the remaining methods. In addition to AWGN Channel, this proposed method shows significant BER performance improvement under the SUI-1 to 6 (WiMAX Channels) channels making use of 256-QAM as the modulation technique. As we move to a higher-order constellation, it is possible to transmit more bits per symbol; in such cases, the proposed technique will achieve better improvement in the performance of BER over all the existing techniques.

Keywords Peak-to-average power ratio · Companding distortion · Exponential Companding · Walsh Hadamard transform · Discrete Hartley transform

Introduction to OFDM

Orthogonal Frequency Division Multiplexing, a widely used multi-carrier modulation methodology, for broadband applications, has problems, despite its merits, like peak power limitation in pragmatic conditions. High peak power is due to the peak amplitude of the signal, which has a more significant value, and such high magnitude signals will cause massive overhead for the corresponding analog circuitry. Also, the average value will be less because of the interference between the many sub-carriers used for modulating the different sub-channels. So, it is imperative to reduce peak power, i.e., Peak to Average Power Ratio (PAPR) (Fidele et al. 2016), for better performance (Wang et al. 1999). A High Power Amplifier (HPA) is inevitable at the transmission end, and when it works to maintain linearity,

✉ A. Lakshmi Narayana
aln2hanumu@gmail.com

¹ Department of ECE, ANITS, Visakhapatnam, India

² Department of IT, Vignan Institute of Information Technology (A), Visakhapatnam, India

³ B V Raju Institute of Technology, Narsapur, India

⁴ Sasi Institute of Technology and Engineering, Tadepalligudam, India

⁵ Department of ECE, Gokaraju Rangaraju Institute of Engineering and Technology, Hyderabad, India

⁶ Department of IT, Gudlavalleru Engineering College, Gudlavalleru, AP, India

ORIGINAL ARTICLE

Optimal multiple key-based homomorphic encryption with deep neural networks to secure medical data transmission and diagnosis

Jafar A. Alzubi  Omar A. Alzubi, Majdi Beseiso, Anil Kumar Budati, K. Shankar

First published: 11 November 2021 | <https://doi.org/10.1111/exsy.12879>

[Read the full text >](#)

 PDF  TOOLS  SHARE

Abstract

Medical database classification problems can be considered as complex optimization problems to assure the diagnosis support precisely. In healthcare, several computer researchers have employed different deep learning (DL) approaches to enhance the classification performance. Besides, encryption is an effective way to offer secure transmission of medical data over public network. With this motivation, this paper presents new privacy-preserving encryption with DL based medical data transmission and classification (PPEDL-MDTC) model. The presented model derives multiple key-based homomorphic encryption (MHE) technique with sailfish optimization (SFO), called MHE-SFO algorithm-based encryption process. In addition, the cross-entropy based artificial butterfly optimization based feature selection technique and optimal deep neural



[International Journal of Intelligent Systems and Applications](#)
for health and medical supply chain systems/IWINAC 2019
May 2022
e12879


Related


Information

Recommended

[Many-to-one homomorphic encryption scheme](#)

Hong Zhong, Jie Cui, Ruihua Shi, Chao Xia

[Security and Communication Networks](#)

[A fully homomorphic encryption based on magic number fragmentation and El-Gamal encryption: Smart healthcare use case](#)

Mosafa Kara, Abdelkader Laoud, Mohammed Amine Yagoub, Renhard Euler, Sadi Medleh, Mohammad Hammoudeh, Amna Elayar, Aheane Bounceur

Reduction of satellite images size in 5G networks using machine learning algorithms

Talari Venkata Krishna Moorthy¹ | Anil Kumar Budati²  | Sandeep Kautish³  | S.B. Goyal⁴  | Kolalapudi Lakshmi Prasad⁵

¹ Sasi Institute of Technology and Engineering, Tadepalligudem, Andhra Pradesh, India

² Department of Electronics & Communication Engineering, Gokaraju Rangaraju Institute of Engineering & Technology, Hyderabad, Telangana, India

³ Lord Buddha Education Foundation Campus, Kathmandu, Nepal

⁴ City University, Malaysia, Petaling Jaya, Malaysia

⁵ BV Raju Institute of Technology, Narasapur, Telangana, India

Correspondence

Sandeep Kautish, Dean-Academics, Lord Buddha Education Foundation Campus, Kathmandu Nepal.
Email: dr.skautish@gmail.com

Abstract

The high data volume of multispectral satellite images is compressed for better visual perception without loss of image and statistical properties of the local or global image to provide superior information for obtaining effective results using 5G networks. This compression is a technique applied to remote sensing applications to analyse the data for prediction or forecasting the real-time applications by remote sensing applications like IoT and data transmission over 5G wireless networks. The extensive data images have multiple bands, which contain earth surface/object information with various frequencies. It is difficult to handle this extensive data for processing data. The compression is mandatory to avoid this complexity by removing redundancy data, unnecessary pixel information and non-visual redundancy data between bands. There are various standard compression techniques are available like JPEG 2000, Wavelet and DCT methods. The proposed method is implemented with a combination of intra coding and machine learning algorithm. The standard compression technique does not give better results due to degradation of pixels, lack of spatial and spectral information. This paper enriches progressive results by reduced satellite images for transmission of data in IoT and 5G wireless networks, in which qualitative results are compared by standard compression technique with suitable parameters.

1 | INTRODUCTION

The satellite images are handling a wealth of information, and problems arise in managing massive data at each stage of the image acquisition process. To reduce the data volume for communication and storage, we need to apply compression algorithms to extensive data. The multispectral satellite images are obtained from a suitable satellite receiver, which is a burden from data transmission and storage. The compression of these images is mandatory to avoid the complexity of preceding the data. The extensive data processing and operation is costly and complex to do further analysis for classification and detection of the objects. In recent days, remote sensing is shown a significant role in analysing and studying the earth's surface for various applications such as urban development, utilization of resources, surveying etc. [1]. This imagery contains spatial, spec-

tral and temporal resolution based on many applications. The corresponding satellite images and resolutions are shown in Table 1.

Low-resolution remote sensing images have not given clear information of the particular object because these images are not interpreted and are more evident [2]. To preserve the quality of the image after compression operation. Including this difficulty to transmit and store images with extensive data, the compressed image store into the server for forecasting applications with time series analysis of the data. Two compression techniques are mostly preferred in digital image processing applications, such as the lossy and lossless compression techniques [3]. In lossless compression technique is critical for a multispectral image due to more number repeated data. The images contain earth surface information with high spatial and spectral information in multiple bands. So, difficult to handle in preprocessing

This is an open access article under the terms of the [Creative Commons Attribution](https://creativecommons.org/licenses/by/4.0/) License, which permits use, distribution and reproduction in any medium, provided the original work is properly cited.

© 2022 The Authors. *IET Communications* published by John Wiley & Sons Ltd on behalf of The Institution of Engineering and Technology

International Journal of Communication Systems / Volume 35, Issue 2 / e4142

SPECIAL ISSUE ARTICLE

Identify the user presence by GLRT and NP detection criteria in cognitive radio spectrum sensing

Anil Kumar Budati , HimaBindu Valiveti

First published: 16 August 2019

<https://doi.org/10.1002/dac.4142>

Citations: 11

Summary

Spectrum sensing in cognitive radio networks is vital and is used for identifying the user presence or absence in the available spectrum. Energy detection and matched filter detection are the few methods to identify the user presence in the spectrum. There are various authors that proposed their research on spectrum sensing using matched filter detection with fixed threshold and predefined dynamic threshold. In this paper, authors proposed the novel matched filter detection method with dynamic threshold by using generalized likelihood ratio test (GLRT) and Neyman Pearson (NP) observer detection criteria. Due to which the probability of detection (P_D) is increased, probability of false alarm (P_{fa}) and probability of missed detection (P_{md}) has been reduced when compare with the existing methods. The results are simulated using MATLAB Software and also plotted the receiver operating characteristic (ROC) curve for estimation of the receiver sensitivity.

Citing Literature



[Download PDF](#)

A Novel Resource Oriented DMA Framework for Internet of Medical Things Devices in 5G Network

Publisher: IEEE

[Cite This](#)

[PDF](#)

Mohammad Kamrul Hasan ; Shayla Islam ; Imran Memon ; Ahmad Fadzil Ismail ; Salwani Abdu... [All Authors](#)

54

Full

Text Views



Abstract

Abstract:

The Internet of Medical Things (IoMT) mobile devices such as ambulance, medical done, and emergency mobile medical equipment face severe signal distortions due to interference, end-to-end packet loss, handoff delays, and lower throughputs during mobility. Network Mobility Basic Support Protocol (NBSP) has been proposed using the IP-based wifi solution to solve these issues. However, the weak signal, extra signaling overhead, and higher delays were identified during handover due to patients' excessive requisites, resulting in radio link failure. Therefore, this paper proposes a novel

Authors

Keywords

Metrics



Guest editorial: Cognitive models for peer to peer networking in 5G and beyond networks and systems

Anil Kumar Budati¹ · George Ghinea² · Dileep Kumar Yadav³ · Hafeez Basha Ranipet⁴

Accepted: 18 June 2021

© The Author(s), under exclusive licence to Springer Science+Business Media, LLC, part of Springer Nature 2021

The problem of integrated cognition devices belongs to a multi-disciplinary area of advanced 5G and beyond networks. The multi-disciplinary focusing on cognitive models at Base Transceiver Stations (BTS) and Mobile Switching Networks (MSN), such as system architectures, Device Sensors, computing techniques, computation intelligence algorithms, mobile devices, Multiplexing devices, helps to reveal a broader and deeper understanding of system architecture and signal processing are part of everyday life and society. Over the past decades many cognitive architectures have been proposed and steadily developed, based on different approaches and computational intelligence methodologies for the network up-gradations, but still current cognitive architectures are far from the goal of covering the requirements for general intelligence in the area of Advanced networks like 5G and beyond wire/wireless Networks. Recent research in the area of evolutionary computational algorithms and genetic programming is used in this study as an inspiration for developing the new version of integrated cognitive architecture devices for advanced communication networks are the knowledge applied to the architecture as well for Industry 4.0 requirements.

A cognitive architecture models and computing algorithms specifies the underlying infrastructure for an intelligent

communication networks. Briefly, architecture includes those aspects of developments in Latest BTS, MSN, computing algorithms and Computational intelligent techniques that are constant over time and across different application domains like Cognitive Radio Networks, Software Defined Networks and all wireless Ad hoc Networks. The cognitive devices must have the capacity typically include, the short-term and long-term memories that store content about the user's information, nodes information, computational evolutionary algorithms, and knowledge about data transmission along with the speed of the Network transmissions. The advanced on chip boards, Artificial Intelligence, Deep Learning and Machine Learning models are expecting to give the solutions for the problems involved in the advanced wireless networks.

This special issue aims to address the various issues on cognitive architectures, computational intelligence algorithms like Hardware Description Languages, Signal processing, Communication devices, Artificial Intelligence (AI) algorithms, Machine Learning, Deep Learning on 5G and beyond Networks and the papers contributed high quality theoretical and practical works. The proposed submissions and presentations should be original and unpublished works.

This article is part of the Topical Collection: *Special Issue on Cognitive Models for Peer-to-Peer Networking in 5G and Beyond Networks and Systems*

Guest Editors: Anil Kumar Budati, George Ghinea, Dileep Kumar Yadav and R. Hafeez Basha

✉ Anil Kumar Budati
anilkumar@griet.ac.in; anilbudati@gmail.com

George Ghinea
George.Ghinea@brunel.ac.uk

Dileep Kumar Yadav
dileep.yadav@galgotiasuniversity.edu.in

Hafeez Basha Ranipet
drhafeez@basharesearch.com

¹ Department of ECE, GRIET (Autonomous), Hyderabad 500090, India

² Department of Computer Science, Brunel University London, Uxbridge, UK

³ Department of CSE, Galgotias University, Greater Noida, Uttar Pradesh, India

⁴ Basha Research Corporation, Station-H Corporation (Non-Profit), Block 690 B, # 05 - 170, Woodlands Drive:75, Woodlands 732690, Singapore

Published: 12 October 2021

An automated brain tumor detection and classification from MRI images using machine learning techniques with IoT

Arij Kumar Budati & Rajesh Babu Katta 

Environment, Development and Sustainability (2021) | [Cite this article](#)

102 Accesses | 2 Citations | [Metrics](#)

Abstract

In medical imaging applications, the accurate diagnosis of brain tumors from magnetic resonance imaging (MRI) at an early stage is a challenging task to researchers nowadays. The early detection of the tumor reduces the mortality rate from brain cancer-related deaths. Among various medical imaging techniques, the MRI is utilized due to less ionization and

Part of a collection:

[Industrial internet of things for intelligent transportation system to decrease the environmental pollution](#)

[Industrial Internet of Things for Intelligent Transportation System to Decrease the Environmental Pollution](#)

Access options

[Buy article PDF](#)

34,95 €

Price includes VAT (India)

High speed data encryption technique with optimized memory based RSA algorithm for communications

Anil Kumar Budati

Department of ECE, Gokaraju Rangaraju Institute of Engineering and Technology, Hyderabad, India

Ganesh Srv

Department of EEE, Avanthi Institute of Engineering and Technology, Narsipatnam, India

Kumar Cherukupalli

Department of EEE, PVP Siddhartha Institute of Technology, Vijayawada, India

Anil Kumar P.

Department of ECE, CVR College of Engineering, Hyderabad, India, and

Venkata Krishna Moorthy T.

Department of ECE, Audisankara College of Engineering and Technology, Gudur, India

Abstract

Purpose – The privacy of the information is a major challenge in the communication process. In the present modern generation, the cryptography plays a vital role in providing security for data, such as text, images and video while transmitting from source to destination through internet or intranet. The Rivest-Shamir-Adleman (RSA) is an asymmetric key cryptographic system, where the security of the method works on the strength of the key.

Design/methodology/approach – In an asymmetric key crypto system, a pair of keys is generated one public key for encryption and one private key for decryption. The major challenge of implementing the RSA is the power function which becomes tedious and time consuming as the exponential value increases. The Chinese remainder theorem proves to be the best for data encryption when it comes to execution time of the algorithm. The proposed novel RSA algorithm with lookup table (LUT) is an extension to the Chinese remainder algorithm, which works better for image and video in terms of time complexity.

Findings – This paper presents a LUT approach for implementing the RSA with a minimal processing time. The proposed algorithm was compared with the standard algorithms like, Chinese remainder theorem, binary approach and squared multiplication approach. As the size of the exponent value increases, the proposed method shows better performance compared to other standard methods.

Originality/value – This paper presents a LUT approach for implementing the RSA with a minimal processing time. The proposed algorithm was compared with the standard algorithms like, Chinese remainder theorem, binary approach and squared multiplication approach. As the size of the exponent value increases, the proposed method shows better performance compared to other standard methods.

Keywords Cryptography, Binary approach, RSA, Image encryption, Lookup table

Paper type Research paper

1. Introduction

In the present digital world, sharing of security information such as text, image and video over the wireless channel has become a part of our real-time process. The protection of the information from the hackers has become quite essential for effective communication (Apau *et al.*, 2016). The data needs to be encrypted from source end and the recipient should have the proper key to read the data. These encryption and decryption forms a part of the cryptosystem. The cryptography provides the confidentiality, authentication,

integrity and non-repudiation to the sender's data (Rughani and Pandya, 2012). Cryptography is a process of converting the original data to unidentifiable data such as cipher data with the public key. The cipher data were converted to plain data with private key at the receiving end. Based on the nature of the keys, cryptography is categorized into symmetric and asymmetric key cryptography system. If the same key is used in symmetric cryptography otherwise it is asymmetric cryptography. The symmetric cryptography does not provide any security to the data and hence it is not widely used. In a public key cryptography, a pair of key used one at the sender and the other key is at the receiver. The key at the sender is called public key, whereas the key on the receiver is called the private key (Stallings, 2003).

The current issue and full text archive of this journal is available on Emerald Insight at: <https://www.emerald.com/insight/0305-6120.htm>



Circuit World
47/3 (2021) 269–273
© Emerald Publishing Limited [ISSN 0305-6120]
[DOI 10.1108/CW-10-2020-0282]

Received 16 October 2020

Revised 8 December 2020

Accepted 25 January 2021



Design of approximate reverse carry select adder using RCPA

Rajasekhar Turaka, Koteswara Rao Bonagiri, Talla Srinivasa Rao, Gundugonti Kishore Kumar, Sudharsan Jayabalan, V. Bharath Sreenivasulu, Asisa Kumar Panigrahy & M. Durga Prakash

To cite this article: Rajasekhar Turaka, Koteswara Rao Bonagiri, Talla Srinivasa Rao, Gundugonti Kishore Kumar, Sudharsan Jayabalan, V. Bharath Sreenivasulu, Asisa Kumar Panigrahy & M. Durga Prakash (2022): Design of approximate reverse carry select adder using RCPA, International Journal of Electronics Letters, DOI: [10.1080/21681724.2022.2062791](https://doi.org/10.1080/21681724.2022.2062791)

To link to this article: <https://doi.org/10.1080/21681724.2022.2062791>



Published online: 29 Apr 2022.



Submit your article to this journal



View related articles



View Crossmark data



Metamaterial Loaded Endfire Circularly Polarized High-Gain Microstrip Patch Antenna for L Band Frequency Applications

A. Ushasree^{1,2} · Vipul Agarwal¹

Received: 30 October 2021 / Accepted: 1 April 2022
© The Author(s), under exclusive licence to Shiraz University 2022

Abstract

In this paper, a circularly polarized wideband and high-gain microstrip patch antenna is presented. A coplanar-waveguide-feed square patch microstrip antenna is chosen as a reference design. The bandwidth of the antenna is improved by truncating the ground plane, and circular polarization is obtained by making two diagonally placed plus-shaped slots in the radiator. These slots are orthogonally distributing the current resulting in circular polarization. The truncation of the ground plane yields a wideband response but an omnidirectional pattern thus lowering the directivity and gain. The measured realized gain of the proposed antenna is improved by 7.3 dBi using a novel wideband metamaterial electronic bandgap structure (EBG) placed beneath the antenna. The integration of this metamaterial is also transforming the omnidirectional pattern to the endfire radiation. The simulation and characterization of the proposed wideband circularly polarized antenna and metamaterial are done using a full-wave electromagnetic simulator. The prototype of the antenna is built and tested. The measured -10 dB impedance bandwidth is 67%, -3 dB axial ratio bandwidth of the antenna is 57%, and peak realized gain is 10.5 dBi. The antenna has stable performance over the operating frequency range.

Keywords Circular-polarization · Directivity · Endfire antenna · High-gain antenna · Metamaterial · Wideband antenna

1 Introduction

The microstrip antenna is most preferred for wireless applications due to its low-profile structure and flexible design process. It can be designed to meet the requirements of different characteristics as radiation pattern, bandwidth, polarization, multiband and reconfigurable operation. However, a specific design procedure needs to be followed to achieve the desired characteristics. A vast literature is available to overcome the limitations of narrow bandwidth ($\approx 2\%$), low-gain ($\approx 3-4$ dBi), and impure polarization.

In the initial stage, the bandwidth of the microstrip antenna was slightly improved using a gap or aperture-coupled feeding technique (Aanandan et al. 1990; Targonski and Pozar 1993; Song and Zhang 1995). Later, the bandwidth of more than 50% is achieved by introducing the new shape radiator. Some of the most popular shapes are fractal (Singh and Verma 2021), bowtie (Singh and Verma 2021), Vivaldi (Shi et al. 2021), E-shaped (Noguchi et al. 2016), and log-periodic (Amini et al. 2015). In the recent era, slots in patch or ground (Lu et al. 2018), combining multi-modes (Hao et al. 2020), metamaterial (Iliyasu 2018) are being used to achieve a much wider bandwidth. These techniques have effectively enhanced the bandwidth of the microstrip antennas but also affects the other antenna parameters as radiation pattern and efficiency, and gain. To maintain the main lobe in broadside or endfire direction with reasonable antenna gain, some additional efforts are required. Naturally, a microstrip antenna is elliptically polarized. Whereas circular polarization is preferred due to the low polarization loss. Like bandwidth enhancement, researchers have reported many techniques in the literature to obtain circular polarization. The fundamental theory to excite the circular polarization

A. Ushasree and Vipul Agarwal have contributed equally to this work.

✉ A. Ushasree
ushasreemishra@gmail.com
Vipul Agarwal
agarvipul@gmail.com

- ¹ Department of ECE, Koneru Lakshmaiah Education Foundation, Guntur, Andhra Pradesh, India
- ² Department of ECE, Gokaraju Rangaraju Institute of Engineering and Technology, Hyderabad, Telangana, India

Contents lists available at [ScienceDirect](https://www.sciencedirect.com)

Computers and Electrical Engineering

journal homepage: www.elsevier.com/locate/compeleceng

Deep learning based optimised data transmission over 5G networks with Lagrangian encoder

B. Shilpa^{a,*}, Anil Kumar Budati^b, L. Koteswara Rao^c, S.B. Goyal^d^a Department of ECE, KLEF, Hyderabad, India^b Department of ECE, GRIET, Hyderabad, India^c Department of ECE, KLEF, Hyderabad, India^d Faculty of Information technology, City University, Malaysia

ARTICLE INFO

Keywords:

Coding tools and techniques
 Compression technologies
 Video coding
 Wireless communication
 Deep neural networks
 Learning-based
 Lagrangian encoder
 Video transmission
 High-efficiency video coding (HEVC)
 Low latency
 High resolution

ABSTRACT

Video data transmission without buffering is ubiquitous for all contemporary appliances. The increased consumption of video content has created the demand for more efficient video compression algorithms for high-resolution videos. In this study, a video compression technique is presented that uses a Lagrangian encoder (LE) with H.265 protocol. This architecture provides compression with less bandwidth compared to contemporary encoders, and it is compatible with 5 G network transmission speed and latency. Adding LE in the H.265 protocol architecture reduced the buffering delay and increased the efficiency. Along with these parameters, this study focused on the quality of video streaming, which was measured by metrics such as peak signal to noise ratio (PSNR), structural similarity index (SSIM), and video multi-method assessment fusion (VMAF). A comparison of the values of compression ratio and latency with and without H.264 architecture showed improved performance in the architecture. Thus, deep learning-based optimised data transmission can improve accuracy and reduce computational complexity.

1. Introduction

Increasing video data transmission and the need for video data applications has led to increased demand for compression technologies. Transmission of uncompressed video signals leads to large data sizes. At the same time quality, higher resolution and fidelity are essential to access the video content. Exclusive use of videos—with high resolutions such as HD, UHD, and 4K—such as remote home surveillance, video chats, wearable cameras increase video traffic and put a big load on communication networks and data storage [1,2]. 5 G technology plays a crucial role in meeting the demands for such applications. 5 G technology can be used to connect numerous IoT devices as well as people [3,4]. The high speed of 5 G (100 times faster than 4 G) and low latency make it more attractive. Thus, there is the need for compression techniques. In a previous study, compression was carried out using several lossless algorithms, and different metrics were compared [5]. However, these algorithms could not achieve sufficient data shrinkage.

Artificial intelligence and mature machine learning techniques have revolutionised compression technologies. The diverse applications enabled by machine learning models have also led to considerable changes in networking and communication in addition to video compression. The advent of deep learning-based convolutional neural networks has enabled achievement of increasing accuracy.

This paper is for special section VSI-pscs. Reviews were processed by Guest Editor Dr. Rohit Sharma and recommended for publication.

* Corresponding author

E-mail addresses: shilpagriet2020@gmail.com (B. Shilpa), anilkumar@griet.ac.in (A.K. Budati).

<https://doi.org/10.1016/j.compeleceng.2022.108164>

Received 9 December 2021; Received in revised form 2 June 2022; Accepted 3 June 2022

0045-7906/© 2022 Elsevier Ltd. All rights reserved.



Performance Analysis of Doping Less Nanotube Tunnel Field Effect Transistor for High Speed Applications

S. Arun jayakar¹ · T. Rajesh¹ · N. A. Vignesh² · S. Kanithan³

Received: 27 February 2022 / Accepted: 15 March 2022
© The Author(s), under exclusive licence to Springer Nature B.V. 2022

Abstract

The DL-Si-NT-TFET (doping-free tunnelling Silicon Nanotube TFET) structure is described in this article. In metals with adequate work functions, the Si-NT-TFET semiconductor can be found in both the source and drain regions. To create the source and drain zones, two metals with different work functions are positioned close to each other. By boosting the ON-current while preserving a subthreshold slope of 31.38 mV/dec, the new architecture improves the device's performance. Transconductance, transfer properties, and output conductance of two nanotube structures can all be measured. It has been demonstrated that Si-NT-FETs with a tubular channel and an outside and inner gate can perform well. They are particularly resistant to short channel effects due to the strong charge management provided by both the inner and outer gates. TCAD was used to create all of the simulations for this study.

Keywords Doping Less Nanotube TFET · Silicon nanotube · Tunnel FET · Transconductance · Silicon nanotube · Si-NT-FET · TCAD · GAA

1 Introduction

For short-channel regulation, SiNT's tubular channel topology is the most ideal topology. Charge carriers can be physically and electrically confined by the inner and outer gates of a short channel control. It is possible to achieve FD or PD transistor performance by modifying the tubular silicon thickness. To make transistors with numerous voltage thresholds (V_t), the same manufacturing method can be utilised to operate each gate individually. This means that transistors can be used in both high- and low-performance circuits because the inner and outside gate controllers are separate [1]. Additionally, because of the device's unique construction, stress can be applied to improve carrier movement. eSiGe and eSiC can be used to apply stress to the

source and drain regions of pTFETs and nTFETs, respectively. CMOS manufacturing processes can also be used to apply stress in the opposite direction of the carrier transport.

Even when the tube diameter is increased, SiNT still provides good SCE compared to other 3D device topologies, as long as the channel thickness is maintained. As an example, the SCE in GAA 3D FETs decreases as the channel thickness increases [2]. The study of silicon's atomic layer transport properties can be aided by continually shrinking the channel in SiNT. The transition point between silicon's bulk transport properties and atomic layer transport properties may be detected using SiNT, which has far-reaching implications. In 2012, Daniel Tekleab et al. introduced the Silicon Nanotube Tunnelling Field Effect Transistor and patented the fabrication process for this new multi-gate device [3]. Figure 1 depicts the SiNT FET's construction. Dynamic non-local charge tunnel models were used to simulate both devices in order to determine the advantages of a nanotube architecture for tunnel FETs.

✉ S. Arun jayakar
arunjayakars@gmail.com

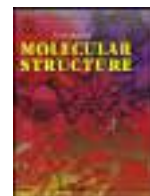
¹ Department of Electronics and Instrumentation Engineering, Bannari Amman Institute of Technology, Sathyamangalam, Erode 638401, India

² Department of ECE, GRIET, Hyderabad 500090, Telangana, India

³ Department of ECE, MVJ College of Engineering, Bangalore 560067, Karnataka, India

2 Dopingless Nanotube TFET

3D TCAD simulator is used to generate the JL-SiNT-FET in this study [4]. Because the device is devoid of a junction, the doping



Enhanced optical, magnetic, and photocatalytic activity of Mg²⁺ substituted NiFe₂O₄ spinel nanoparticles



S. Kanithan^a, N. Arun Vignesh^b, Khadijah Mohammedsahleh Katubi^{c,*}, Partha Sarathi Subudhi^{d,j,*}, Ekrem Yanmaz^d, Joshuva Arockia Dhanraj^e, Norah Salem Alsaieri^c, Khamael M. Abualnaja^f, M. Sukumar^g, M. Sundararajan^{h,*}, S. Baskar^h, Srikanta Sahuⁱ, Chandra Sekhar Dash^{i,*}

^a Department of Electronics and Communication Engineering, MVJ College of Engineering, Channasandra Main Rd, Near ITPB Whitefield, Bengaluru, Karnataka 560067, India

^b Department of ECE, Gokaraju Rangaraju Institute of Engineering and Technology (GRIET), Hyderabad 500090, India

^c Department of Chemistry, College of Science, Princess Nourah bint Abdulrahman University, P. O. Box 84428, Riyadh 11671, Saudi Arabia

^d Department of Electrical and Electronics Engineering, Faculty of Engineering and Architecture, Nisantasi University, Istanbul, Turkey

^e Department of Mechatronics Engineering, Hindustan Institute of Technology and Science, Rajiv Gandhi Salai (OMR), Padur, Kelambakam, Chennai, Tamil Nadu 603103, India

^f Department of Chemistry, College of Science, Taif University, Taif 21944, Saudi Arabia

^g Department of Physics, Anand Institute of Higher Technology, Kazhipattur, Chennai, 603103, India

^h PG and Research Department of Physics, Paavendhar College of Arts & Science, M.V South, Thalavasal, Salem, Tamil Nadu 636 121, India

ⁱ Department of Electronics and Communication Engineering, Centurion University of Technology and Management, Odisha, Bhubaneswar 752 050, India

^j Department of Electrical Engineering, Bajaj Institute of Technology, Pipri, Wardha, Maharashtra, 442001, India

ARTICLE INFO

Article history:

Received 16 November 2021

Revised 4 May 2022

Accepted 11 May 2022

Available online 13 May 2022

Keywords:

Microwave combustion method

Nickel ferrites

Ferromagnetic behavior

Photocatalysis

Fenton reaction

ABSTRACT

Magnesium doped nickel ferrite spinel nanostructured were prepared using a microwave combustion method. The structural characterization by XRD analyses confirmed that undoped NiFe₂O₄ showed a single phase cubic spinel structure. However, with increasing Mg²⁺ concentration in the range 0.1 to 0.5 induced the crystallization of secondary α -Fe₂O₃ phase. The cubic nanostructured exhibited an average crystallite size between 20 and 35 nm. The presence of tensile/compressive strain in Mg²⁺ doped NiFe₂O₄ was determined from Williamson–Hall (W–H) method. The appearance of FT-IR bands at around 435, 459, and 581 cm⁻¹, characteristics of spinel cubic and rhombohedral stretching modes. The optical band gap as determined by diffuse reflectance spectroscopy (DRS) decreases with increasing Mg²⁺ content due to the quantum confinement effect. Surface morphology showed nanosized crystalline grains agglomerated with spherical shapes and energy dispersive X-ray analyses was used to examine the elemental composition of the Mg²⁺ doped NiFe₂O₄ spinel nanoparticles and confirmed the presence of nickel, magnesium, iron and oxygen elements. Magnetization–Field (*M* – *H*) hysteresis curves revealed the appearance of ferromagnetic behavior at room temperature. The as-fabricated Mg²⁺ doped NiFe₂O₄ spinel nanostructures were evaluated for the photocatalytic degradation of rhodamine B under visible light irradiation for atmospheric conditions. When a small amount of H₂O₂ was added during photocatalysis, indicating the samples possessed photo-Fenton like catalytic activity. This type of spinel nanoparticles behaves as an efficient catalyst with high efficiency around above 99%.

© 2022 Elsevier B.V. All rights reserved.

1. Introduction

Rhodamine B (RhB) is dye solvent in water and is utilized as a color in food, materials, calfskin, paints, paper, beautifiers, and labs, and so on [1]. RhB released of wastewater, if inappropriately

treated, prompts genuine natural and other medical issues that influence the human body and its frameworks [2]. It is, thusly, important to treat the RhB wastewater before it is delivered to ensure the climate and individuals. Ozonation, electrochemical cycles, Fenton measures, progressed oxidation cycles, adsorption, and hydrodynamic cavitation are utilized to eliminate harmful mixtures [3–8]. Set of electrons opening are made that are utilized for the decrease and oxidation process. Noticeable light is more significant on the grounds that apparent light records for around half

* Corresponding authors.

E-mail addresses: Kmkatubi@pnu.edu.sa (K.M. Katubi), parthasarathi.subudhi@nisantasi.edu.tr (P.S. Subudhi).

Research Article

Silicon Wearable Body Area Antenna for Speech-Enhanced IoT and Nanomedical Applications

N. Arun Vignesh,¹ Ravi Kumar,² R. Rajarajan,³ S. Kanithan,⁴ E. Sathish Kumar,⁵ Asisa Kumar Panigrahy,¹ and Selvakumar Periyasamy⁶

¹Department of Electronics and Communication Engineering, Gokaraju Rangaraju Institute of Engineering and Technology, Hyderabad 500090, India

²Department of Electronics and Communication Engineering, Jaypee University of Engineering and Technology, Guna 473226, India

³Department of Electrical and Electronics Engineering, MVJ College of Engineering, Bangalore 560067, India

⁴Department of Electronics and Communication Engineering, MVJ College of Engineering, Bangalore 560067, India

⁵Department of Electronics and Communication Engineering, Gnanamani College of Technology, Namakkal, India

⁶Department of Chemical Engineering, School of Mechanical, Chemical and Materials Engineering, Adama Science and Technology University, Adama 1888, Ethiopia

Correspondence should be addressed to Selvakumar Periyasamy; selvakumar.periyasamy@astu.edu.et

Received 31 March 2022; Revised 20 April 2022; Accepted 7 May 2022; Published 23 May 2022

Academic Editor: Samson Jerold Samuel Chelladurai

Copyright © 2022 N. Arun Vignesh et al. This is an open access article distributed under the Creative Commons Attribution License, which permits unrestricted use, distribution, and reproduction in any medium, provided the original work is properly cited.

We propose in this paper a reduction in the size of wearable antennas on silicon (Si) for medicinal frameworks and Internet of things (IoT) in various nanoapplications. This research also introduces one more type of dynamic patch antenna designed in favor of speech-enhanced healthcare applications. The most significant impediment to the adoption of smart correspondence and medical services frameworks is voice-enabled IoT. The primary objective of a body area network (BAN) is to give ceaselessly clinical information to the doctors. Actually, wireless body area network is flexible, dense, trivial, and less expensive. On the other hand, the main disadvantage is low efficiency for small printed antenna. Microstrip silicon antenna recurrence is changed because of ecological conditions, distinctive reception apparatus areas, and diverse framework activity modes. By using tunable antenna, the efficiency of bandwidth usage can be increased. Amplifiers are associated with the feed line of antenna in order to build its dynamic range. In this study, a dynamic polarized antenna is constructed, analysed, and attempted for fabrication. The gain of the antenna is 13 ± 2 dB for the frequency range of 390 to 610 MHz. The output of the polarized antenna is roughly 19 dBm. At different environmental conditions, the performance and ability to control the antenna could vary. To achieve stable performance, we have used varactor diode and voltage-controlled diode. This silicon wearable antenna can be fabricated and tested for many medical applications like health monitoring system and pacemakers. Furthermore, micromachining techniques can be used to lower the practical dielectric constant of silicon and hence improve radiation efficiency.

1. Introduction

Wearable frameworks have a few applications in close to home specialized device and clinical device as introduced in [1–6]. A preprint has previously been published [7]. WBAN and healthcare systems frequently use printed antennas in wearable applications [8, 9]. Printed antennas are also cost-effective, flexible, and can be utilized in many medical and IoT applications.

These antennas are analysed and studied in [10–14]. Examination of radio transmission that occurs when a wearable antenna is working near a human system has been analysed in [15–20]. Notwithstanding, little printed antennas experience the ill effects of low productivity [21–24]. Dynamic reception apparatuses for correspondence frameworks are introduced in [25–31]. This research introduces a unique dynamic and tunable wireless antenna for WBAN applications. Acquiring and



Analysis and Design of Novel Doping Free Silicon Nanotube TFET with High-density Meshing Using ML for Sub Nanometre Technology Nodes

Ravi Kumar¹ · B. Aruna Devi² · V. Sireesha³ · A. Kishore Reddy⁴ · I. Hariharan⁵ · E. Konguvel⁶ · N. A Vignesh⁷

Received: 3 March 2022 / Accepted: 28 March 2022
© The Author(s), under exclusive licence to Springer Nature B.V. 2022

Abstract

Beyond the 25 nm technological node, MOSFETs (metal oxide semiconductor FETs) have worse channel electrostatic control than FinFETs (Fin field-effect transistors). It is necessary to use novel gate and channel engineering architecture in MOSFET devices at low technology nodes to decrease short-channel effects (SCEs). Future nano devices will replace present MOSFET with graded channel double gate MOSFETs and FinFETs for increased I_{ON} current and reduced leakage currents. Double gate MOSFETs have been identified by researchers in the last few years to considerably reduce short channel effects (SCE). Graded channel double gate MOSFETs provide superior switching characteristics and higher transconductance than single gate MOSFETs in ULSI/VLSI applications with many nodes. Transistors with hot carrier effects and subthreshold properties degrade at lower technological nodes than 25 nm. To increase on-state drive current and off-state leakage current separately in the gate-to-channel direction, super-halo and retrograde channel doping are used. As a result, semiconductor businesses must place a premium on precise doping levels, which drives up fabrication costs enormously. A revolutionary doping-free Silicon nanotube FET (DF-Si-NT-FET) with sub-nm technology nodes is presented in this paper. They are extremely resistant to SCE due to the strong charge control offered by both the inner and outside channels. Also, machine learning (ML) algorithm used with high-density meshing during simulation. TCAD was used to create all the simulations for this work.

Keywords FinFET · Doping free · Silicon-nanotube · DF-Si-NT-FET · TCAD · Short channel effects · Sub-nm technology nodes · GAA FET

1 Introduction

ICs have relied on planar transistors for decades, and transistor size has been steadily dropping since the 1990s, thanks to Moore's law and other experts. After every 18 months, Moore's law says, the number of transistors on a chip will have doubled. Gordon Moore, Intel's co-founder, stated this law in 1965. However, everything has come to a grinding halt recently. To keep up with Moore's law, researchers have

created a new type of transistor called a multiple gate field effect transistor (MuGFET). A MuGFET appears to be a promising alternative to CMOS because of its use in this application. Nanotechnology has been transformed by FinFET technology.

Comparing FinFET to CMOS transistors, the channel controllability and sub-threshold slope are significantly improved. There are many gates surrounding the channel in a Fin Field Effect Transistor (FinFET), which improves electrical control

✉ N. A Vignesh
arunvignesh44@gmail.com

¹ Department of ECE, Jaypee University of Engineering and Technology, Guna 473226, India

² Department of ECE, Dr. N.G.P Institute of Technology, Dr. N.G.P. Nagar, Kalapatti Road, Coimbatore, Tamil Nadu 641048, India

³ Department of CSE, Geethanjali Institute of Science and Technology, Nellore 524137, Andhra Pradesh, India

⁴ Department of ECE, Andhra Engineering College, Nellore 524322, Andhra Pradesh, India

⁵ Department of Micro and Nano Electronics Engineering, School of Electronics Engineering, Vellore Institute of Technology, 632014 Vellore, India

⁶ Department of Embedded Technology, School of Electronics Engineering, Vellore Institute of Technology, Vellore 632014, India

⁷ Department of ECE, GRIET, 500090 Hyderabad, Telangana, India

Design and experimental investigation on VL-MLI intended for half height (H-H) method to improve power quality using modified particle swarm optimization (MPSO) algorithm

Satish Kumar Ramaraju^a, Thenmalar Kaliannan^b, Sheela Androse Joseph^c, Umadevi Kumaravel^d, Johny Renoald Albert^{b,*}, Arun Vignesh Natarajan^e and Gokul Prasad Chellakutty^f

^a*Department of Medical Electronics Engineering, Sengunthar College of Engineering, Namakkal, Tamilnadu, India*

^b*Department of EEE, Vivekanandha College of Engineering for Women, Namakkal, Tamilnadu, India*

^c*Department of EEE, Kongu Engineering College, Perundurai, Tamilnadu, India*

^d*Department of EEE, Sengunthar Engineering College, Namakkal, Tamilnadu, India*

^e*Department of ECE, Gokaraju Rangaraju Institute of Engineering and Technology, Hyderabad, Telangana, India.*

^f*Department of ECE, SNS College of Engineering, Coimbatore, Tamilnadu, India*

Abstract. A Voltage lift performance is an excellent role to DC/DC conversion topology. The Voltage Lift Multilevel Inverter (VL-MLI) topology is suggested with minimal number of components compared to the conventional multilevel inverter (MLI). In this method, the Modified Particle Swarm Optimization (MPSO) conveys a primary task for the VL-MLI using Half Height (H-H) method, it determine the required optimum switching angles to eliminate desired value of harmonics. The simulation circuit for fifteen level output uses single switch voltage-lift inverter fed with resistive and inductive loads (R & L load). The power quality is developed by voltage-lift multilevel inverter with minimized harmonics under the various Modulation Index (MI) while varied from 0.1 up to 1. The circuit is designed in a Field Programmable Gate Array (FPGA), which includes the MPSO rules for fast convergence to reduce the lower order harmonics and finds the best optimum switching angle values. To report this problem the H-H has implemented with MPSO to reduce minimum Total Harmonic Distortion (THD) for simulation circuit using Proteus 7.7 simulink tool. Due to the absence of multiple switches, filter and inductor element exposes for novelty of the proposed system. The comparative analysis has been carried-out with existing optimization and modulation methods.

Keywords: Solar-Photovoltaic, voltage lift-multilevel inverter, particle swarm optimization algorithm, half height, field program gate array

1. Introduction

The electrical system has major problems due to the presence of harmonic contents in the power quality features. The harmonics may be classified into

*Corresponding author. Johny Renoald Albert, Department of EEE, Vivekanandha College of Engineering for women, Namakkal, Tamilnadu, India. E-mail: jorenoeee@gmail.com.



Available at www.sciencedirect.com

ScienceDirect

journal homepage: www.elsevier.com/locate/bbe



Review Article

Transfer learning techniques for medical image analysis: A review



Padmavathi Kora^a, Chui Ping Ooi^b, Oliver Faust^c, U. Raghavendra^d, Anjan Gudigar^d, Wai Yee Chan^e, K. Meenakshi^a, K. Swaraja^a, Pawel Plawiak^{f,j}, U. Rajendra Acharya^{g,b,h,i,*}

^aGokaraju Rangaraju Institute of Engineering & Technology, Hyderabad 500090, India

^bSchool of Science and Technology, Singapore University of Social Sciences, 599494, Singapore

^cEngineering and Mathematics, Sheffield Hallam University, Sheffield S1 1WB, UK

^dDepartment of Instrumentation and Control Engineering, Manipal Institute of Technology, Manipal Academy of Higher Education, Manipal 576104, India

^eDepartment of Biomedical Imaging, Universiti Malaya Research Imaging Centre, Faculty of Medicine, Universiti Malaya, 50603, Malaysia

^fDepartment of Computer Science, Faculty of Computer Science and Telecommunications, Cracow University of Technology, Warszawska 24, 31-155 Krakow, Poland

^gSchool of Engineering, Ngee Ann Polytechnic, Clementi 599489, Singapore

^hDepartment of Biomedical Informatics and Medical Engineering, Asia University, Taichung, Taiwan

ⁱInternational Research Organization for Advanced Science and Technology (IROAST), Kumamoto University, Kumamoto, Japan

^jInstitute of Theoretical and Applied Informatics, Polish Academy of Sciences, Baltycka 5, 44-100 Gliwice, Poland

ARTICLE INFO

Article history:

Received 18 August 2021

Received in revised form

27 November 2021

Accepted 28 November 2021

Available online 13 December 2021

Keywords:

Medical image

Machine learning

Convolutional neural networks

Transfer learning

ABSTRACT

Medical imaging is a useful tool for disease detection and diagnostic imaging technology has enabled early diagnosis of medical conditions. Manual image analysis methods are labor-intensive and they are susceptible to intra as well as inter-observer variability. Automated medical image analysis techniques can overcome these limitations. In this review, we investigated Transfer Learning (TL) architectures for automated medical image analysis. We discovered that TL has been applied to a wide range of medical imaging tasks, such as segmentation, object identification, disease categorization, severity grading, to name a few. We could establish that TL provides high quality decision support and requires less training data when compared to traditional deep learning methods. These advantageous properties arise from the fact that TL models have already been trained on large generic datasets and a task specific dataset is only used to customize the model. This eliminates the need to train the models from scratch. Our review shows that AlexNet, ResNet, VGGNet, and GoogleNet are the most widely used TL models for medical image analysis. We found that these

* Corresponding author at: Department of Instrumentation and Control Engineering, Manipal Institute of Technology, Manipal Academy of Higher Education, Manipal 576104, India.

E-mail address: raghavendra.u@manipal.edu (U. Rajendra Acharya).

<https://doi.org/10.1016/j.bbe.2021.11.004>

0168-8227/© 2021 Nalecz Institute of Biocybernetics and Biomedical Engineering of the Polish Academy of Sciences. Published by Elsevier B.V. All rights reserved.



Design of approximate reverse carry select adder using RCPA

Rajasekhar Turaka, Koteswara Rao Bonagiri, Talla Srinivasa Rao, Gundugonti Kishore Kumar, Sudharsan Jayabalan, V. Bharath Sreenivasulu, Asisa Kumar Panigrahy & M. Durga Prakash

To cite this article: Rajasekhar Turaka, Koteswara Rao Bonagiri, Talla Srinivasa Rao, Gundugonti Kishore Kumar, Sudharsan Jayabalan, V. Bharath Sreenivasulu, Asisa Kumar Panigrahy & M. Durga Prakash (2022): Design of approximate reverse carry select adder using RCPA, International Journal of Electronics Letters, DOI: [10.1080/21681724.2022.2062791](https://doi.org/10.1080/21681724.2022.2062791)

To link to this article: <https://doi.org/10.1080/21681724.2022.2062791>



Published online: 29 Apr 2022.



Submit your article to this journal



View related articles



View Crossmark data

Hybrid filter detection network model for secondary user transmission in cognitive radio networks

HFDNM for
secondary user
transmission

D. Vijaya Saradhi and Swetha Katragadda

Malineni Perumallu Educational Society's Group of Institutions, Guntur, India, and

Hima Bindu Valiveti

Gokaraju Rangaraju Institute of Engineering and Technology, Hyderabad, India

Received 17 August 2021
Revised 23 September 2021
Accepted 2 October 2021

Abstract

Purpose – A huge variety of devices accumulates as well distributes a large quantity of data either with the help of wired networks or wireless networks to implement a wide variety of application scenarios. The spectrum resources on the other hand become extremely unavailable with the development of communication devices and thereby making it difficult to transmit data on time.

Design/methodology/approach – The spectrum resources on the other hand become extremely unavailable with the development of communication devices and thereby making it difficult to transmit data on time. Therefore, the technology of cognitive radio (CR) is considered as one of the efficient solutions for addressing the drawbacks of spectrum distribution whereas the secondary user (SU) performance is significantly influenced by the spatiotemporal instability of spectrum.

Findings – As a result, the technique of the hybrid filter detection network model (HFDNM) is suggested in this research work under various SU relationships in the networks of CR. Furthermore, a technique of hybrid filter detection was recommended in this work to enhance the performance of idle spectrum applications. When compared to other existing techniques, the suggested research work achieves enhanced efficiency with respect to both throughputs as well as delay.

Originality/value – The proposed HFDNM improved the transmission delay at 3 SUs with 0.004 s/message and 0.008 s/message when compared with existing NCNC and NNC methods in case of number of SUs and also improved 0.02 s/message and 0.08 s/message when compared with the existing methods of NCNC and NNC in case of channel loss probability at 0.3.

Keywords Hybrid filter detection, Cognitive radio, Throughput, Primary user, Secondary user

Paper type Research paper

1. Introduction

Many smart spaces that include various smart cities, smart buildings, as well as smart transportation, might evolve during the next few years. With the help of a wireless or wired network, the above-mentioned smart space would necessitate significantly large devices which are associated with the Internet. However, the efficient communication applications of such devices mainly depend on spectrum resources and thus entailing necessary resources of the spectrum to transmit a huge volume of information (Zhu *et al.*, 2017). Currently, the existing frequency spectrum of radio is been distributed significantly and many of them are licensed bands. On the other hand, most of the licensed bands are unused in the space domain as well as in the time domain also the useful spectrum resources are not efficiently used (Hassan *et al.*, 2017; Zhu *et al.*, 2012; Poncha *et al.*, 2018). However, in the present technique of spectrum distribution, only a small portion of unlicensed spectrum is available. Meanwhile, the utilization of spectrum gets saturated because only a few unlicensed spectrums are utilized by new applications as well as new consumers.

The technology of cognitive radio (CR) was established to enhance the application of low-spectrum licensed frequency bands so that it can fulfill the emerging marketing



Diagnosis of COVID-19 using 3D CT scans and vaccination for COVID-19

Gangadhar Ch

Department of Electronics and Communication Engineering, Prasad V Potluri Siddhartha Institute of Technology, Vijayawada, India

S. Jana

Vel Tech Rangarajan Dr Sagunthala R&D Institute of Science and Technology, Chennai, India

Sankararao Majji

Department of Electronics and Communication Engineering, GRIET, Hyderabad, India

Prathyusha Kuncha

NRI Institute of Technology, Krishna, India

Fantin Irudaya Raj E.

Dr Sivanthi Aditanar College of Engineering, Tiruchendur, India, and

Arun Tigadi

KLE Dr. M.S. Sheshagiri College of Engineering and Technology, Belagavi, India

Abstract

Purpose – For the first time in a decade, a new form of pneumonia virus, coronavirus, COVID-19, appeared in Wuhan, China. To date, it has affected millions of people, killed thousands and resulted in thousands of deaths around the world. To stop the spread of this virus, isolate the infected people. Computed tomography (CT) imaging is very accurate in revealing the details of the lungs and allows oncologists to detect COVID. However, the analysis of CT scans, which can include hundreds of images, may cause delays in hospitals. The use of artificial intelligence (AI) in radiology could help to COVID-19-positive cancer in this manner is the main purpose of the work.

Design/methodology/approach – CT scans are a medical imaging procedure that gives a three-dimensional (3D) representation of the lungs for clinical purposes. The volumetric 3D data sets can be regarded as axial, coronal and transverse data sets. By using AI, we can diagnose the virus presence.

Findings – The paper discusses the use of an AI for COVID-19, and CT classification issue and vaccination details of COVID-19 have been detailed in this paper.

Originality/value – Originality of the work is, all the data can be collected genuinely and did research work done own methodology.

Keywords AI, COVID-19, CT scan, 3D data set

Paper type Research paper

1. Introduction

Wuhan, China was the birthplace of Coronaviruses, which were first discovered in 2019. Coronavirus is known as viral pneumonia, which include the CO19, MERS and corona virus, and this is referred to as both SARS and MERS.

Until recently, coronaviruses were being transmitted from human-to-human beings, and no existing vaccines were available. It is rumoured that the most effective ways to reduce the transmission of coronaviruses are rapid diagnosis of large populations and confinement of the infected in isolation to avoid the virus spreading (Chen and Guestrin, 2016). Thus, the standard COVID test is required for human identification.

The primary use of the real-time reverse-transcriptase polymerase chain reaction (RT-PCR) test is to enable the classification of individuals who have been diagnosed with the CO19 antibody at hospitals.

It takes a long time and causes risks to apply imaging. Because of these findings, the researchers advise use of a RT-PCR and chest imaging in the examination of suspicious patients (Eisenhofer and Weyrich, 2019). Diagnostic tool selection is varied in three clinical situations. Our deep learning approach will concentrate on diagnoses of CO19 on three-dimensional (3D) CT scans to ensure quick and reliable findings. In the event of an epidemic, it might be impossible to read more than a person's CT scan.

Cabin angiography is a special form of angiography which uses the imaging technology of computed tomography (CT) to make 3D images of the heart and lungs. A chest X-ray is more accurate in detecting coeliac disease than a chest CT scan. Up

The current issue and full text archive of this journal is available on Emerald Insight at: <https://www.emerald.com/insight/1708-5284.htm>



Role of digital technologies to combat COVID-19 pandemic

Ratchana Rajendran

Christ University, Bangalore, India

Biswas Piali

Jamshedpur Women's College, Ranchi, India

Panguluri Chandrakala

Aurora's Post Graduate College, Ramanthapur, India

veerraju Gampala

Koneru Lakshmaiah Education Foundation, Guntur, India, and

Sankararao Majji

GRIET, Hyderabad, India

Abstract

Purpose – The unexpected epidemic of the latest coronavirus in 2019, known as COVID-19 by the Globe, a number of governments worldwide have been put in a vulnerable situation by the World Health Organization. The effect of the COVID-19 outbreak, previously experienced by China's citizens alone, has now become more pronounced. For practically every nation in the world, this is a matter of grave concern. The lack of assets to withstand the infection of COVID-19, mixed with the perception of overwhelmed medical mechanisms, pressured a number of places in a state of partial or absolute lockdown.

Design/methodology/approach – The medical photos such as computed tomography (CT) and X-ray play a key role in the worldwide battle against COVID-19, while artificial intelligence (AI) has recently appeared. The power of imaging is further increased by technology tools and support for medical specialists. In comparison to the related direct health effects because of the COVID-19 disaster, this research identifies its impacts on the overall society.

Findings – This paper hereby examines the rapid answers in the medical imaging community toward COVID-19 (empowered by AI). For example, the acquisition of AI-empowered images will significantly assist automate the scanning process and reshape the procedure as well. AI, too, may improve the quality of the job by correctly delineating X-ray and CT image infections, promoting subsequent infections, quantification. In addition, computer-aided platforms support radiologists make medical choices, i.e. for illness tracking, diagnosis and prognosis.

Originality/value – This research encompasses the whole medical imaging pipeline and methods for research related to COVID-19, include a collection of images, segmentation, diagnosis and monitoring. In drawing stuff to minimize the effects of the COVID-19 epidemic, this paper is investigating the use of technologies such as the internet of things, unmanned aerial vehicles, blockchain, AI, big data and 5G.

Keywords IoT, Artificial intelligence, Diagnosis, COVID-19, Coronavirus, BigData

Paper type Research paper

1. Introduction

As the world is now facing an epidemic of an infectious disease, the understanding and leadership of COVID-19 is beneficial to us. For many, particularly in emerging countries, where the large proportion face poverty and focus on non-sustainable sources of energy, the threat of COVID-19 is enormous. The coronavirus is an infection that is transmitted by a subsequently detected coronavirus (COVID-19). Most individuals diagnosed with the COVID-19 virus will suffer mild to moderate respiratory disease and heal without older adults

needing special care, including those with existing health problems are most probable to suffer serious illnesses, such as heart disorder, diabetes, respiratory diseases and cancer. The World Health Organization (WHO) assesses that most of the reports up to now are virus has been confirmed and many people have died, for the most part, in the age group over 60 years and in persons with pre-existing medical conditions (Dhinam and Kumar, 2017). Dyspepsia, respiratory symptoms, cough and fever are among the outstanding individual. In difficult circumstances, multi-organ failure, pneumonia, septic shock, severe respiratory syndrome and even death can result from the disease. Death also occurs from 0–9 years of age (Dhinam and Chahar, 2018b). Cases of respiratory syndromes with COVID-19 have been found to be quicker compared to those with COVID-19 safe individuals.

The current issue and full text archive of this journal is available on Emerald Insight at: <https://www.emerald.com/insight/1708-5284.htm>



World Journal of Engineering
© Emerald Publishing Limited [ISSN 1708-5284]
[DOI 10.1108/WJE-01-2021-0043]

Received 20 January 2021

Revised 8 February 2021

Accepted 9 February 2021

Design of inset fed circular dual band patch antenna for WLAN frequencies

Bagade Shilpa*

Department of ECE,
KLH, GRIET,
Hyderabad, India
Email: shilpa.me1437@gmail.com
*Corresponding author

L. Koteswara Rao

Department of ECE,
KLEF, HYD,
Hyderabad, India
Email: koteswararao@klh.edu.in

N. Arun Vignesh and Vadladi Vijaya Kumar

Department of ECE,
GRIET,
Hyderabad, India
Email: arunvignesh44@gmail.com
Email: vijay20052009@gmail.com

Abstract: A circular patch with internal feed and oblong slot on the radiation part for the dual-frequency operation is proposed. The antenna resonates at two frequencies i.e., 2.45 GHz and 5 GHz (ISM bands). These bands support WLAN with no extra cost of licensed band. The objective in using WLAN is that we can expect higher gain and ease of transmission. The advantage is it provides increased bandwidth about eight and less side lobe power than the rectangular type. The antenna can find its application in CR which efficiently uses bandwidth. The mode buoyed considering the ground plane, the dielectric material acts as a cavity which is of the circular type. The modes can be controlled by the means of radius. VSWR ratio is 2 for both bands. The design can be made to resonate in TM₁₀ and TM₁₁ and radiation characteristics with the plane unaffected. Good radiation characteristics can be achieved without affecting VSWR with impedance matching.

Keywords: circular antenna; inset feed; return loss; dual band; wireless local area network; WLAN.

Reference to this paper should be made as follows: Shilpa, B., Rao, L.K., Vignesh, N.A. and Kumar, V.V. (2022) 'Design of inset fed circular dual band patch antenna for WLAN frequencies', *Int. J. Systems, Control and Communications*, Vol. 13, No. 1, pp.56–66.

Performance analysis for user identification in CR networks by various modulation transmission techniques

Budati Anil Kumar

Department of ECE,
KL Deemed to be University,
Vijayawada, India
Email: anilbudati@gmail.com

Mohammed Saleem Pasha*

Department of ECE,
Vignana Bharathi Institute of Technology,
Hyderabad, India
Email: saleempasha436@gmail.com
*Corresponding author

Abstract: The rapid development of newly invented wireless devices and its applications tends to spectrum scarcity. Cognitive radio (CR) is a technology, which gives solution for the spectrum scarcity problem with dynamic spectrum access. The user presence or absence is identified by a spectrum sensing technique in CR networks. There are various methods like energy detection (ED), matched filter detector (MFD), etc. are used for identification of user presence or absence in the spectrum. The performance of the user identification is estimated by the parameters of probability of detection (PD) and the probability of false alarm (Pfa). The performance of the spectrum sensing method with Bayesian detection (BD) criteria by using static threshold is estimated by existing author for the above said parameters. In this paper, the authors estimated the performance of the above parameters with Neyman Pearson (NP) detection criteria is applying to MFD sensing method by using dynamic threshold. The performance is analysed by comparing the existing BD with the proposed NP by using the modulation transmission techniques 8-PSK, 8-QAM and identified the better detection criteria.

Keywords: cognitive radio; spectrum sensing; Neyman Pearson approach; probability of false alarm; Pfa; probability of detection; phase shift keying; PSK; quadrature amplitude modulation; QAM.

Reference to this paper should be made as follows: Kumar, B.A. and Pasha, M.S. (xxxx) 'Performance analysis for user identification in CR networks by various modulation transmission techniques', *Int. J. Computer Aided Engineering and Technology*, Vol. X, No. Y, pp.xxx-xxx.

Biographical notes: Budati Anil Kumar received his BTech in ECE from the V.R.S. and Y.R.N. College of Engineering and Technology, Andhra Pradesh, India in 2007 and MTech in Systems and Signal Processing from the Lakireddy Bali Reddy College of Engineering, Andhra Pradesh, India in 2010. He is currently pursuing his PhD with Wireless Communications from the GITAM

AN EFFECTIVE PARKINSON'S DISEASE PREDICTION USING LOGISTIC DECISION REGRESSION AND MACHINE LEARNING WITH BIG DATA

Kranthi Kumar Singamaneni¹, Dr.G.Puthilibai², D.Saravanan³, Dr.P,Sagaya Aurelia⁴,
P Gopala Krishna⁵, Dr.D.StalinDavid⁶

¹Associate Professor, Department of CSE, Gokaraju Rangaraju Institute of Engineering & Technology,
Kukatpally, Hyderabad,

²Professor, Department of Chemistry, Sri Sairam Engineering College, Chennai,

³Associate Professor, Department of CSE, IFET College of Engineering, Villupuram,

⁴Assistant Professor, Department of CSE, CHRIST (Deemed to be University), Bangalore,

⁵Associate Professor, Department of IT, Gokaraju Rangaraju Institute of Engineering & Technology,
Kukatpally, Hyderabad,

⁶Assistant Professor, Department of CSE, IFET College of Engineering, Villupuram,

kkranthicse@gmail.com, vgputhili@gmail.com, saranmds@gmail.com,
sagaya.aurelia@christuniversity.in, gopalakrishna@griet.ac.in, sdstalindavid707@gmail.com

ABSTRACT

Background: Medical data is conducive to early identification of diseases, patient treatment, and community service. Parkinson's disease prediction by Machine Learning (ML) in large data and reliable study of biomedical and healthcare community develop big data; medical data is conducive to early detection of diseases, patient care, and community service. The machine learning algorithm is being used to successfully forecast the prevalence of chronic illness populations.

Proposed Methodology: Parkinson's disease is a serious neurodegenerative disease that affects people when they become older (mostly past the age of 50). It is the most serious and harmful of the non-curable neurodegenerative diseases. Parkinson's disease is challenging to diagnose at an early level and the origin of subtle early signs is difficult to identify. Due to the heavy responsibility of the condition on the Parkinson disease patient, a clinical care scheme has been developed. To classify Parkinson's disease and overcome this complicated challenge, the suggested Machine Learning (ML) induced Logistic Decision Regression (LDR) algorithm is used. Early diagnosis of Parkinson's disease will contribute to improved care and disease control, thereby enhancing the quality of life of patients. To create such successful decision support, an automatic prediction system focused on machine learning was developed and presented.

Result and Findings: This data collection would be used to classify possible biomarkers of Parkinson's disease using Machine Learning (ML) and Big Data (BD) technologies. The organization's disease prediction technology, which is focused on machine learning and large data, enhances human wellbeing while further promoting the big data industry of disease prediction. In comparison to other current approaches, the simulation findings indicate a strong reliability.

Keywords: Parkinson's disease, Machine Learning (ML), Big Data (BD), Logistic Decision Regression (LDR), Prediction, Classify.

I. INTRODUCTION

Parkinson's disease is a neurodegenerative disorder that affects millions of people around the globe. Muscle fatigue, tremor (upper and lower arms, as well as jaw vibration), voice disturbances, deadpan, slow motion, apathy, postural dysfunction (depression and mood changes), repetitive gestures, dementia (loss of memory), what not to do, sleep disorders, and thinking are also typical symptoms of Parkinson's disease. The batch size, all the properties of velocity, veracity, length, meaning, and variety are all present in Parkinson's disease data, which

is referred to as Big Data (BD). These five have been identified in greater depth in the context of Parkinson's data in the following manner. Velocity is provided by the pace of the data contained within, as well as the processing speed of the storage indication, which aids in real-time decision making and modern real-time prediction processing. Veracity is a software company that specialises in data and precision analysis. A key aspect of consistency is issues and knowledge concerning the reliability of data quality. The information on Parkinson's disease is heterogeneous, multi-source, unreliable, contradictory, and scarce. In disorders like Parkinson's disease, medical and biological predictions are extremely significant. Stable people with Parkinson's disease treatment judgments boundary evidence from their alienation and Parkinson's disease for the diagnosis efficacy and computational performance class boundaries mechanisms

Parkinson's disease is a chronic brain condition marked by non-motor symptoms as well as two motor symptoms (motor). The personal introduction shown in the conditions, in addition to all of the typical symptoms, is something that everyone will witness. Stiffness or rigidity may occur in people with Parkinson's disease. People with Parkinson's disease may also become frozen or unable to shift for a brief amount of time. Parkinson's disease is a neurodegenerative disease characterised by the destruction of dopamine-producing cells. Parkinson's syndrome may be isolated from other disorders that have identical clinical manifestations, but accurate testing is difficult to come by. The scientific practise of patient background and analysis is used to make a diagnosis. Movement conditions, commonly involving neurological illnesses such as depression and schizophrenia, are the most common causes, although they may often lead to the progression of other diseases. It's possible that you'll lose your autonomy and be in agony as a result. People with a deteriorating standard of life and major obstacles and challenges were impacted as the disease advanced. There is a chance that family members and caregivers may have an indirect impact.

The physical activity data obtained on the wearable smart terminal is also pre-processed on the computer, after which it is fixed and stored by the wireless relay base station to the online tracking management network, and all data is summarised as decided on the cloud online management platform for web pages and smartphone apps, called visual. Both physical activity details, on the other hand, must be in a particular data format based on Hadoop-bigdata, which implements the format of data files from the online monitoring portal, utilising high data analysis and corresponding data analysis technologies, with high data integration advantages, and highly effective data analysis.

To maintain the integrity of the data files, all of them will be copied at the same time. After that, I'll run the abbreviated research software for the particular diagram in order to do the parallel analysis efficiently and in accordance with the calculation's analysis specifications. Following the completion of the calculation, different analyses are performed, and the calculation's result is output, with many of the resulting files being generated and extracted. Big Data (BD) and Machine Learning (ML). Following that, the company will notify the online administration in compliance with the agreed-upon procedure and apply the site's sports data processing results. Finally, partner members can access related analytics data using the online management tool for spoken smartphone apps.

II. RELATED WORK

An organisation, which is generally described in depth as a structured collection of processes, protocols, and the concept of designing procedures to carry out specific activities or solve specific problems, successfully applies to public health from a variety of mechanisms, including mechanical systems. The data representation framework relevant to continuous surveillance, review, and device control, management, and strategic preparation is referred to as System Health Monitoring and Management (SHMM) [1]. A dynamic engineering system's requirement for brain health and quality pre-sales testing has become critical. The integration of big data, intelligent flight coding, and the introduction of popular classification algorithms, the secret mining of historical data knowledge, and the capacity to achieve quality forecasts of brain health are all dependent on intelligent decision-making [2]. Stuff for measuring brain health content are developed on an internet-based architecture, and classification approaches are used to accomplish real-time data collection and analysis. Obstructive Sleep Apnoea (OSA) is a serious sleep condition that has a strong detrimental effect on one's quality of life. Reduced mood changes are a symptom of depression, and certain OSAs are caused by behavioural and attitude problems [3]. As a result, there is a pressing need for treatment solutions for this disease to be monitored in real time. There are many OSA detection systems available. The pervasive usage of medical / health-related data is the at an exponential pace, thanks to the growth of maturity and the Internet, cloud infrastructure, and technology across the Internet, medical / health information technology. Simultaneously, the usage of mainstream and genomic technologies, as well as the exponential

function error feature identification and operational error clever detection action feature to obtain a system instability error prediction approach and function error feature detection and operational error clever detection action feature to obtain a hierarchical correlation between big data and function error [14]. Diabetes has become more common in the world. To meet this aim, diabetics must be monitored on a regular basis and must be actively engaged with their health care. Mobile Health (MH) is a growing trend in information and telecommunications technology that can help chronic patients in a smart world. It will review the existing status of MH technology in order to overcome its shortcomings [15]. Current study papers are evaluated in terms of validity and degree of applicability by patients and medical care professionals in the MH literature. The Patient will remotely track patients using Internet of Things (IoT) big data processing sensors. The literature, on the other hand, supports experiments that acknowledge the relatively large number of virtual instruments and the common use of a sleep predictor. A simulation-based smart bed load sensor is provided by the Design sluggish motion agent-based simulation platform [16]. The arrangement specifies the sleep predictor identification indicators and enables the outcomes of the dull taken indicator to be compared. The effects of the graph star map, chart evolution, and the final visual output of the bed sensor state are presented in this novel befit dummy, which helps users to discover the results of the graph star chart, chart evolution, and the final visual performance of the bed sensor state. While health networks for Parkinson's disease (PD) exist and have been discussed in the literature, the majority of them lack the capacity to analyse vast volumes of data generated and gathered from medical exams and organised in a pre-defined manner. Centered on the study of massive numbers, proposes a modern model of health network [17]. The planned architecture's key goal is to assist physicians in conducting purposeful assessments of common Parkinson's disease motor issues and improvements. Machine health control devices are commonly used in the modern sector to accomplish proactive maintenance, with applications such as fault monitoring, unemployment reduction, and property safety. Since predicting the appearance of certain faults (up to and including forecasting potential operating conditions and remaining service life [18], data-based health management has produced significant results in the big machine data age. The data source sensor is comprised of numerous effective trapezoids of digital data expression. The conventional approach is labor-intensive since it typically necessitates specialised knowledge and relies on manual labour. Wearable Health Monitoring Systems (WHMS) that are disabled will allow for continuous monitoring of possible patient physiological parameters from either place. Furthermore, utilising multiple biosensors, such a device will be unable to achieve a comprehensive measure of the user's wellbeing. Java-based simulation platform [19] that is multi-sensor supported or equivalent to the petri net model. This work has been extended to accommodate for synchronisation issues as well as time-dependent variables.

III. MATERIALS AND METHODS

Parkinson's disease is caused by the death of dopamine-producing neurons in the brain. Early signs of infections may be tough to detect since they are mild at first. Owing to the high pressure placed on patients, there is a health-care system that delays detection. The diagnosis of Parkinson's disease using Machine Learning (ML) and Big Data (BD) methods leads to a greater explanation of the disease decade.

Figure 1 shows the pre-processing of a Parkinson's disease dataset, which eliminates noise and unnecessary data while using feature selection to find the right attributes and eventually classifying the Parkinson's disease prediction result.

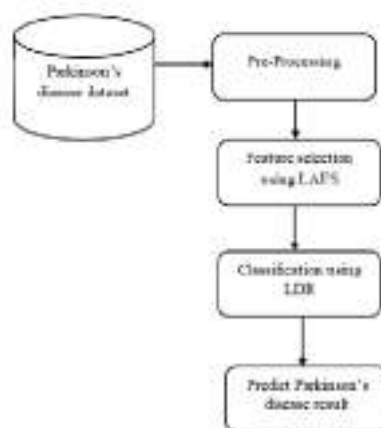


Figure 1: Block diagram

3.1 Pre-processing

It is a typical data pre-processing approach that is defined by the use of a data processor. Filtering, normalisation, and target recognition are also part of the pre-processing procedure. The performance at this stage is a set of important parts and components. Light varies often, and there is less comparison, according to the data. As a result, the platform must process the data immediately. To protect random lighting and noise medical records, improvements are needed. It's a technique for filtering out unnecessary information from the background noise. Clinical evidence were often altered prior to improvement. This is a phase in the data pre-processing method that will increase performance.

3.2 Feature selection using Least Absolute Shrinkage and Feature Selection (LAFS) algorithm

In machine learning, feature selection refers to the process of choosing the most appropriate features for the model disease results. There is a propensity to increase the tempo, precision, or both training by limiting the number of features you want to use (not only the data that hasn't modified the model supplied), but there is also a tendency to improve the speed, accuracy, or both training by limiting the number of features you want to use (not just the data that hasn't changed the model supplied). Using the LAFS algorithm, it picks shivering, voice problems, postural instability, and movement problems.

Algorithm Steps

Input: Parkinson's disease dataset

Output: Feature selection disease Dataset

Start

Step 1: Initialize the disease dataset

Step 2. Read the dataset

Step 3. Split the Dataset

Step 4. For (Calculate each intensity data)

Feature selection disease dataset

End of

Step 5. Select best features (shivering, speech problem, Movements)

Exit

Any Parkinson's disease data is gathered during the phases of this algorithm, making the data a very delicate operation. The LAFS algorithm is used to select the Parkinson's disease functions.

3.3 Classification using Logistic Decision Regression

The large-scale estimation issue of Parkinson's disease is found in the general public health. Machine learning-based approaches were used to differentiate between stable individuals and those with Parkinson's disease. Via a network of space exploration lectures, LDR is able to achieve its goals. It is reliant on a number of inputs, which are usually used to estimate the estimated function.

Algorithm steps

Input: Feature selection disease dataset

Output: Classification of Parkinson's disease

Start

Step 1: Import the feature selection disease dataset

Step 2: Read the feature selection disease dataset

Step 3: Remove unnecessary data

Step 3: Calculate the classification using LDR

Stop

IV. RESULT AND DISCUSSION

The outcomes and consequences of the new development process would be evaluated using the Anaconda tool and a medical dataset for Parkinson's disease. The results evaluation During the re-run process of test data,

sensitivity, accuracy, and classification efficiency are determined. Support Vector Machine (SVM) and Convolutional Neural Network (CNN) are two known approaches that are compared to the proposed Logistic Decision Regression (LDR) algorithm (CNN).

Table 1: Simulation parameters

Parameters	Values used
Tool	Anaconda
Language	Python
Input data	Parkinson's disease data set
Training dataset	120
Testing dataset	30

Table 1 shows the simulation parameters for proposed implementation process using python language.

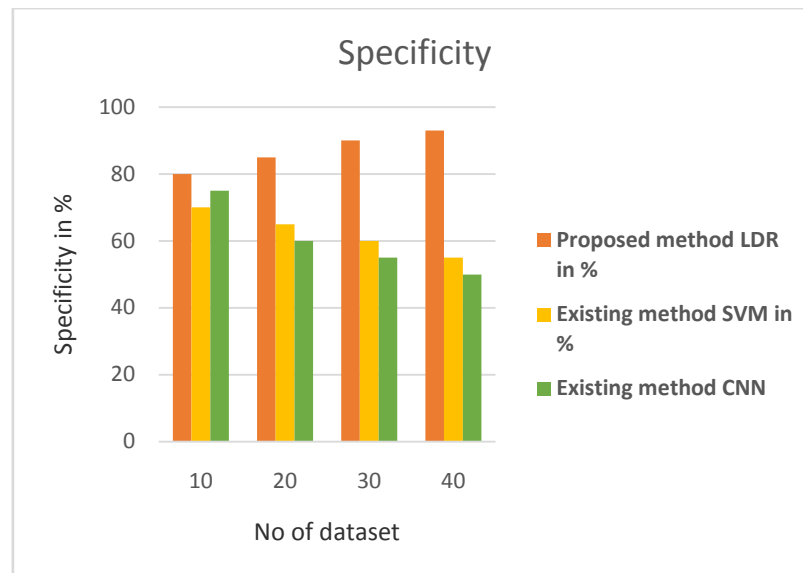


Figure 2: Analysis of specificity

The study of accuracy in percentages is depicted in Figure 2. The sensitivity to Parkinson's disease tests refers to the number of times they are correctly identified. The suggested sensitivity result from Logistic Decision Regression (LDR) is 93 percent. The results of the current approaches are 55 percent for the Support Vector Machine (SVM) and 50 percent for the Convolutional Neural Network (CNN).

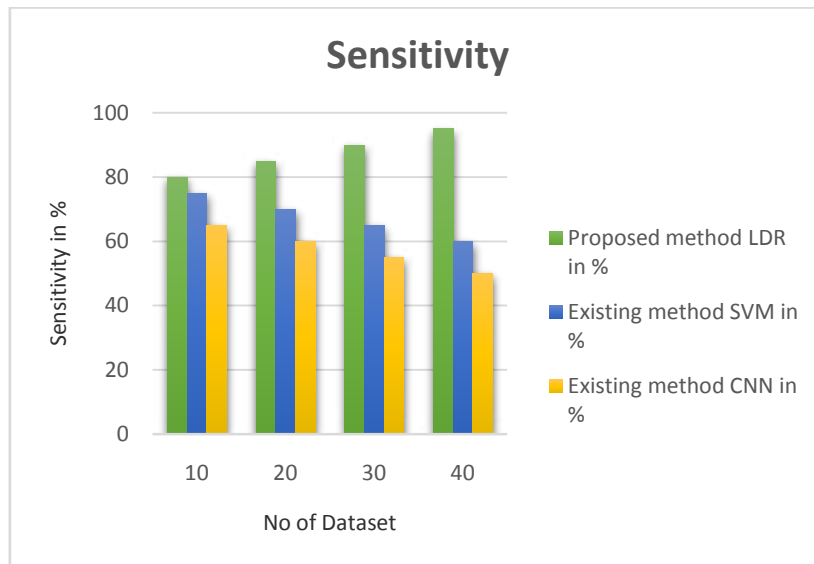


Figure 3: Analysis of sensitivity

The sensitivity study in percentage as seen in Figure 3. As a proportion of correctly negative for Parkinson's disease, specificity tests have been established. The specificity result of the suggested Logistic Decision Regression (LDR) is 95%. Support Vector Machine (SVM) results are 60% and Convolutional Neural Network (CNN) results are 50%, respectively, with the latest processes.

Table 2: Analysis of classification performance

No of dataset	LDR in %	SVM in %	CNN in %
14	81	76	72
25	87	61	66
33	92	66	64
42	98	58	49

Table 2 shows the analysis of classification performance the proposed algorithm classify the Parkinson disease and it provide high performance compared to other methods.

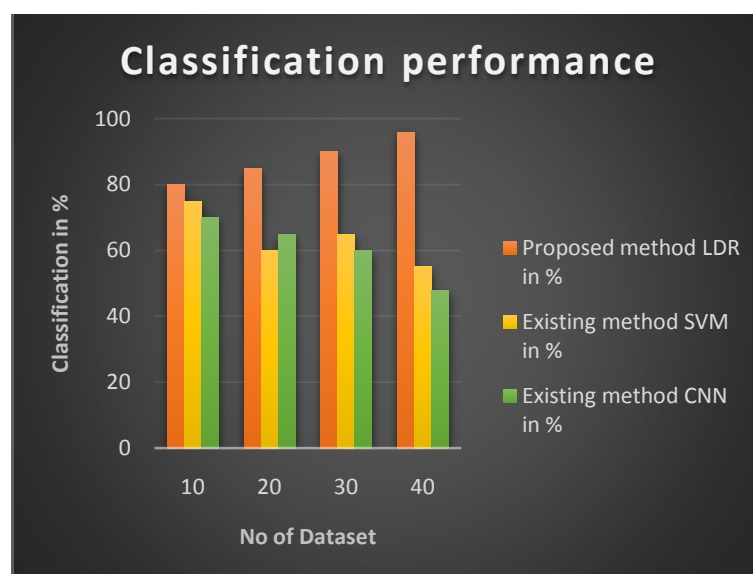


Figure 4: Classification performance

Figure 4 depicts the classification success rate as a percentage. The suggested specificity result for Logistic Decision Regression (LDR) is 96 percent. The results of the latest approaches are 55 percent for Support Vector Machines (SVM) and 48 percent for Convolutional Neural Networks (CNN).

V. CONCLUSION

People may not have a clear way of determining whether or not they are suffering from Parkinson's disease through a particular examination, such as a blood test or an ECG. Diagnosis of Parkinson's disease requires a specific test, such as a blood test or an ECG. To classify Parkinson's disease and overcome this complicated challenge, the suggested Machine Learning (ML) induced Logistic Decision Regression (LDR) algorithm is used. Early diagnosis of Parkinson's disease will contribute to improved care and disease control, thereby enhancing the quality of life of patients. The organization's disease prediction technology, which is focused on machine learning and large data, enhances human wellbeing while further promoting the big data industry of disease prediction. The proposed LDR algorithm has a sensitivity of 95 percent, a precision of 93 percent, and a classification efficiency of 97 percent.

REFERENCE

1. Kwok Leung Tsui ; Yang Zhao, "Big Data Opportunities: System Health Monitoring and Management", IEEE Access (Volume: 7) 2019.
2. Yuan Huang ; Qiang Zhao, "Air Quality Forecast Monitoring and Its Impact on Brain Health Based on Big Data and the Internet of Things", IEEE Access (Volume: 6)2018.
3. Diana C. Yacchirema ; David Sarabia-JáCome, "A Smart System for Sleep Monitoring by Integrating IoT With Big Data Analytics", IEEE Access (Volume: 6)2018.
4. Jingyi Zhang ;Tong Zhao, "Analysis Method of Motion Information Driven by Medical Big Data", IEEE Access (Volume: 7), 2019.
5. Deepak Puthal ; Xindong Wu, "SEEN: A Selective Encryption Method to Ensure Confidentiality for Big Sensing Data Streams", IEEE Transactions on Big Data (Volume: 5 , Issue: 3 , Sept. 1 2019).
6. Yin Zhang ; Meikang Qiu, "Health-CPS: Healthcare Cyber-Physical System Assisted by Cloud and Big Data", IEEE Systems Journal (Volume: 11 , Issue: 1 , March 2017).
7. Abdulsalam Yassine ; Shailendra Singh, "Mining Human Activity Patterns From Smart Home Big Data for Health Care Applications", IEEE Access (Volume: 5), 2017.
8. Antonino Galletta ; Lorenzo Carnevale, "An Innovative Methodology for Big Data Visualization for Telemedicine", IEEE Transactions on Industrial Informatics (Volume: 15 , Issue: 1 , Jan. 2019).
9. Abdur Rahim Mohammad Forkan ; Ibrahim Khalil, "BDCaM: Big Data for Context-Aware Monitoring—A Personalized Knowledge Discovery Framework for Assisted Healthcare", IEEE Transactions on Cloud Computing (Volume: 5 , Issue: 4 , Oct.-Dec. 1 2017).
10. Jong Wook Kim ; Jong Hyun Lim, "Collecting Health Lifelog Data From Smartwatch Users in a Privacy-Preserving Manner", IEEE Transactions on Consumer Electronics (Volume: 65 , Issue: 3 , Aug. 2019).
11. Ying Yang, "Medical Multimedia Big Data Analysis Modeling Based on DBN Algorithm", IEEE Access (Volume: 8)2020.
12. Tianshu Wu ; Shuyi Chen, "Intelligent fault diagnosis system based on big data", The Journal of Engineering (Volume: 2019 , Issue: 23 , 12 2019).
13. Shaker El-Sappagh ; Farman Ali, "Mobile Health Technologies for Diabetes Mellitus: Current State and Future Challenges", IEEE Access (Volume: 7), 2018.
14. Iván García-Magariño ; Raquel Lacuesta , "Agent-Based Simulation of Smart Beds With Internet-of-Things for Exploring Big Data Analytics", IEEE Access (Volume: 6),2017.
15. Abdulsalam Yassine ; Shailendra Singh "Mining Human Activity Patterns From Smart Home Big Data for Health Care Applications", IEEE Access (Volume: 5),2017.
16. Leonarda Carnimeo ; Gianpaolo Francesco Trotta, "Proposal of a health care network based on big data analytics for PDs", The Journal of Engineering (Volume: 2019 , Issue: 6 , 6 2019).
17. Rui Zhao ; Dongzhe Wang, "Machine Health Monitoring Using Local Feature-Based Gated Recurrent Unit Networks", IEEE Transactions on Industrial Electronics (Volume: 65 , Issue: 2 , Feb. 2018).
18. Alexandros Pantelopoulous, "SPN-model based simulation of a wearable health monitoring system" IEEE Access, 2017.
19. Mary M. Rodgers ; Vinay M. Pai, "Recent Advances in Wearable Sensors for Health Monitoring", IEEE Sensors Journal (Volume: 15 , Issue: 6 , June 2017).
20. In cheol Jeong ; David Bychkov, "Wearable Devices for Precision Medicine and Health State Monitoring", IEEE Transactions on Biomedical Engineering (Volume: 66 , Issue: 5 , May 2019).
21. Stalin David D, Saravanan D, "Enhanced Glaucoma Detection Using Ensemble based CNN and Spatially Based Ellipse Fitting Curve Model", Solid State Technology, Volume 63, Issue 6, PP.3581-3598.
22. Stalin David D, Saravanan M, Jayachandran A, "Deep Convolutional Neural Network based Early Diagnosis of multi class brain tumour classification", Solid State Technology, Volume 63, Issue 6, PP.3599-3623.
23. R.Parthiban, Dr.K.Santhosh Kumar, Dr.R.Sathya, D.Saravanan, "A Secure Data Transmission And Effective Heart Disease Monitoring Scheme Using Mecc And Dlmnn In The Cloud With The Help Of Iot", International Journal of Grid and Distributed Computing, ISSN: 2005 – 4262, Vol. 13, No. 2, (2020), pp. 834 – 856.
24. R.Bhavya, G.I.Archanaa, D.Karthika, D.Saravanan, " Reflex Recognition of Tb Via Shade Duplicate Separation, Built on Geometric Routine", International Journal of Pure and Applied Mathematics 119 (14), 831-836.
25. D Saravanan, R Bhavya, GI Archanaa, D Karthika, R Subban, " Research on Detection of Mycobacterium Tuberculosis from Microscopic Sputum Smear Images Using Image Segmentation", 2017 IEEE International Conference on Computational Intelligence and Computing Research (ICIC).
26. D Saravanan, R Parthiban, " Automatic Detection of Tuberculosis Using Color Image Segmentation and Statistical Methods", International Journal of Advance Research in Science and Engineering, Volume 6, Issue 10.
27. D. Stalin David, 2019, "Parasagittal Meningioma Brain Tumor Classification System based on MRI Images and Multi Phase level set Formulation", Biomedical and Pharmacology Journal, Vol.12, issue 2, pp.939-946.
28. D. S. David and A. Jeyachandran, "A comprehensive survey of security mechanisms in healthcare applications," 2016 International Conference on Communication and Electronics Systems (ICCES), Coimbatore, 2016, pp. 1-6, doi: 10.1109/CESYS.2016.7889823.

29. D Stalin David, A Jayachandran, 2018, Robust Classification of Brain Tumor in MRI Images using Salient Structure Descriptor and RBF Kernel-SVM, TAGA Journal of Graphic Technology, Volume 14, Issue 64, pp.718-737.
30. D Stalin David, 2016, Robust Middleware based Framework for the Classification of Cardiac Arrhythmia Diseases by Analyzing Big Data, International Journal on Recent Researches In Science, Engineering & Technology, 2018, Volume 4, Issue 9, pp.118-127.
31. Stalin David D, Saravanan D, 2020, 'Multi-perspective DOS Attack Detection Framework for Reliable Data Transmission in Wireless Sensor Networks based on Trust', International Journal of Future Generation Communication and Networking , Volume 13, Issue 4, PP.1522–1539.
32. Dr. D. Stalin David, Mr. D. Saravanan, "Certain Investigation On Iot Therapeutic Image Recognition And Rivaroxabanpreclude Thrombosis In Patients", 2021, pg.no:51-66, ISBN: 978-81-948555-1-4.
33. D Saravanan, R Parthiban," Automatic Detection of Tuberculosis Using Color Image Segmentation and Statistical Methods", International Journal of Advance Research in Science and Engineering, Volume 6, Issue 10.
34. D.Saravanan, S.Rajasekaran, Dr. D.Stalin David, P.Hemalatha, Dr.U.Palani. (2021). Detection of Sickle Cell Anemia from Microscopic Blood Images Using Different Local Adaptive Thresholding Techniques. Annals of the Romanian Society for Cell Biology, 6549 –. Retrieved from <http://annalsofrcsb.ro/index.php/journal/article/view/3254>.
35. Dr.BrahmadesamViswanathan Krishna, Dr.G.Amuthavalli, Dr.D.StalinDavid, E. FantinIrudaya Raj, D.Saravanan. (2021). Certain Investigation of SARS-COVID-2-Induced Kawasaki-Like Disease in Indian Youngsters. Annals of the Romanian Society for Cell Biology, 1167–1182. Retrieved from <http://annalsofrcsb.ro/index.php/journal/article/view/4469>.

RESEARCH ARTICLE

Driver's Drowsiness Detection Using Dlib and IoT

Prasanna Lakshmi Kompalli¹, Padma Vallakati¹, Ganapathi Raju Nadimpalli¹, Vinod Mahesh Jain¹ and Samuel Annepogu¹

¹Department of Information Technology, Gokaraju Rangaraju Institute of Engineering and Technology, Hyderabad, India

Abstract: Background: Road accidents are a major cause of deaths worldwide. This is enormously due to fatigue, drowsiness, and microsleep of the drivers. This does not just risk the life of the driver and co-passengers but also a great threat to the vehicles and humans moving around that vehicle.

Methods: Research, online content, and previously published papers related to drowsiness are reviewed. Using the facial landmarks in DAT file, the prototype locates and identifies the eye coordinates, and then calculates Eye Aspect Ratio (EAR). The EAR indicates whether the driver is drowsy or not based on the result of various sensors that get activated, such as an alarm generator, LED indicators, LCD message scroll, message sent to the owner, and the engine that gets locked.

Results: The prototype is able to locate eyes in the frame and detect whether the person is sleepy or not. Whenever the person is feeling drowsy, an alarm is generated in the cabinet, and afterward, LED indicators will start glowing, messaging will be scrolling at the rear part of the vehicle so that other vehicles and humans get cautioned. After this, the vehicle slows down, and the engine gets locked.

Conclusion: This prototype will help in the reduction of road accidents due to human intervention. It is not only helpful to the person who installs it in their vehicle but also for the other vehicles and humans moving around it.

ARTICLE HISTORY

Received: May 12, 2020
Revised: June 20, 2020
Accepted: July 17, 2020

DOI:
10.2174/2210327910666201218162536

Keywords: IoT, face detection, drowsiness detection, fatigue identification, sensors, raspberry pi, alert system, eye aspect ratio.

1. INTRODUCTION

The Internet of Things is a system of interrelated processing gadgets, mechanical and advanced machines provided with identifiers of one of a kind and the capacity to move information over a network without needing human-to-human or human-to-computer interaction. The mechanism is to change the physical world into a huge data framework comprising empowered objects called things associated with each other and communicate with one another with the accessible infra-structure [1-22]. IoT gadgets are a part of the broader idea of home automation, which can incorporate lighting, heating and air conditioning, media, and security frameworks. IoT paves the way for everything around us to work cooperatively in order to achieve outcomes efficiently.

Machine learning is the study of computer algorithms that improve consequently through understanding. It is large

ly based on mathematical optimization, which provides strategies, hypotheses, and application domains to the field [21]. To be precise, machine learning is an area that is heavily reliant on inputs to yield outputs. The set of inputs is often referred to as the dataset in machine learning. Unlike deep learning methods, which require a lot of inputs, machine learning algorithms tend to perform better even if there is less input data [21]. Machine learning can be categorized into three types, which include supervised, unsupervised, and semi-supervised learning. Machine learning essentially complexes around classification and regression based on known features previously learned from the training data [21].

It is inevitable that most of the drivers who drive for long periods are susceptible to sleepiness. The drowsiness of drivers has been one of the major concerns in the modern-day world. Drowsiness is a state of an individual wherein the individual continuously feels asleep [19]. Drowsiness is a consequence of a lack of proper sleep. Sound sleep is very important for human beings especially for drivers who drive for long distances in order to ensure active functioning of the

*Address correspondence to this author at the Department of Information Technology, GRIET, Hyderabad, India; Tel: 9849547910; E-mail: prasanakompalli@gmail.com

brain. Fatigue is often misunderstood as drowsiness, but it varies from drowsiness.

Fatigue refers to the absence of an ability to keep performing a similar task over and over again. According to numerous studies, drowsiness has been one of the prominent parameters in road accidents. Around 90% of all accidents occur due to human errors [13], and a considerable part of them occur due to drowsiness. Long hours of driving causes driver fatigue and, consequently, reduces his/her response time [15]. Road accidents have a huge chance of occurrence, especially in the case of drivers who deal with heavy vehicles and travel great distances because the drivers who often handle heavy vehicles are prone to drowsiness.

The driver who has been feeling lethargic enters a state wherein his concentration levels become minimal, and ultimately the driver will not be able to brake or deviate the vehicle in order to minimize the effect or rather avoid the accident [13]. To eliminate or reduce the number of road accidents, intellects have come up with quite a few solutions in order to tackle the issue of drowsiness. Driver's Drowsiness Detection Systems have been developed to counter road accidents [2]. These systems basically use image processing to determine the behaviour of the driver by focusing on facial expressions, especially by capturing the eyes of the driver and, in turn, by calculating the eye aspect ratio. Numerous physical phenomena can be monitored and analysed in order to detect the drowsiness of a driver [16].

The methods that are taken into consideration in order to identify drowsiness are based upon vehicles, physiology, and behaviour of the driver [1]. Some of the methods which are taken into account on the basis of a vehicle include steering movements and accelerator pattern. On the other hand, the methods of drowsiness detection on the basis of behaviour of the driver include eye closure, yawning, and eye blinking [7, 10]. The methods based on physiology include pulse rate and heartbeat. All of the existing systems are machine learning-centric. In reality, some transport operators report beginning of their daily work already with a sleep debt (as, of course, some non-commercial drivers before they get behind the wheel) [17].

2. LITERATURE SURVEY

Mehta [1] developed an application that runs on Android devices in order to detect drowsiness of the driver by capturing live images and sending them to a local server. Subsequently, the Dlib library is utilized to detect facial landmarks and calculate eye aspect ratio, which ultimately detects whether the driver is drowsy or not using Naïve Bayes, SVM, and Random Forest with a maximum accuracy of 84%.

Lee and Chung [2] proposed a technique to monitor driver's wellbeing levels utilizing a data fusion approach such as eye characteristics, variation of biological signals, temperature within the vehicle, and vehicle speed.

In a work "Detection of fatigue using Smartphone aims to use a smartphone (with Android operating system or IOS) to

detect fatigue in the driver" [3], Roberson and others used the front camera of the smartphone to capture images of the driver and then used propelled algorithms of computer vision to identify his face and eyes.

Galarza [4] presented a surveillance system to detect drowsiness and alert the driver using artificial vision techniques by implementing the system for an Android smartphone in the form of a mobile application.

Subbarao [5] designed a prototype for drowsiness detection by making use of an eye blink sensor, alcohol sensor, and a tilt sensor, and by warning the driver with the help of a buzzer.

Alioua [6] proposed a strong and nonintrusive system for driver's fatigue and drowsiness detection by yielding the face from the video frame using the Support Vector Machine face detector. Circular Hough Transform has also been applied for eye and face state analysis.

Marimuthu and Suresh [7] proposed a method for detecting the eyes on the face of the driver and calculating the sleepiness of the driver by observing the movement of eyelids.

Cehovin and Mandeljc [8] designed a system that estimates landmark positions and extracts eye aspect ratio. Later, the SVM classifier detects eye blinks.

Zhu and Ji [9] proposed a prototype that uses remotely located cameras equipped with active IR illuminators to capture video images of the driver.

3. METHODOLOGY

3.1. Existing System

The following section outlines the methodologies of the existing systems. The existing systems to detect driver's drowsiness use IR/Night Vision cameras in order to check for drowsiness of the driver. Some of the existing systems use methods based on the behavior of the driver, such as eye blink or closure to predict drowsiness, while some of the other existing systems make use of methods on the basis of the physiological state of the driver, which include heartbeat and pulse rate and also some methods are based on the vehicle such as steering movements [1]. In 2018, an android application was developed to predict drowsiness of the driver by implementing deep neural networks. The system was designed based on multilayer perceptron classifiers [18]. One of the existing systems has been equipped with an eye blink sensor to detect drowsiness of the driver. This system makes use of a spectacle with an eye blink sensor, which is IR based. It has also been equipped with an alcohol sensor and a tilt sensor [12]. Another existing system extracts movements of the eye and mouth on the basis of Circular Hough Transform (CHT) [6]. A system that determines the percentage of eye closure was also developed. This system mainly aims at detecting micro-sleep periods by capturing the iris [16]. The systems make use of either active systems or passive systems. Active systems have been assessed to be reliable. Active systems are of higher configuration, such as infrared

cameras, whereas passive systems are reliant on standard cameras [1]. Therefore, we have proposed a system with higher standards of safety for the drivers in order to eradicate or curtail the number of road accidents in the future.

3.2. Proposed System

This section provides a detailed approach of the proposed system of Driver's Drowsiness Detection. Block Diagram for Driver's Drowsiness Detection is shown below (Fig. 1):

The prominent hardware components of the system are mentioned below:

1. Raspberry Pi 4
2. IR / Night Vision Camera
3. LCD Display
4. Motors

3.2.1. Raspberry Pi 4

Raspberry Pi 4 is a microcomputer that is equipped with a Broadcom BCM2711 SoC (System on Chip). It can process tasks with a maximum clock frequency of up to 1.5GHz. It has been implemented on a 64-bit architecture. It is a brand new version of the Raspberry Pi series. It comprises two USB 3.0 ports, two USB 2.0 ports, a 2-lane MIPI CSI

camera port, and a 2-lane MIPI DSI display port. It also consists of a micro-SD card slot for loading the operating system and storing data.

There are three variants of Raspberry Pi 4 on the basis of RAM. It does not come with accessories like a keyboard, mouse, and case built with it. Instead, they have to be externally attached. As Raspberry Pi is a computer, it requires an operating system to function. The operating system that has been installed in the Raspberry Pi 4 is Raspbian. Raspberry Pi is responsible for performing all the significant operations in our system like processing the frames, running the motor, displaying the message, and sending the message (Fig. 2).

3.2.2. IR / Night Vision Camera

It is a camera that utilizes infrared rays to capture images and videos, even in darkness or low light conditions (Fig. 3). The digital signal processor of the night vision camera is often altered, which makes up for the difference in illumination between day and night. HDR technology is also used in some night vision cameras to enhance the performance of the camera. The night vision camera in our prototype helps in continuously monitoring the driver and capturing the features of the eyes of the driver. Unlike standard cameras, the night vision camera can perform at its best even though the surroundings are not bright enough [23-25].

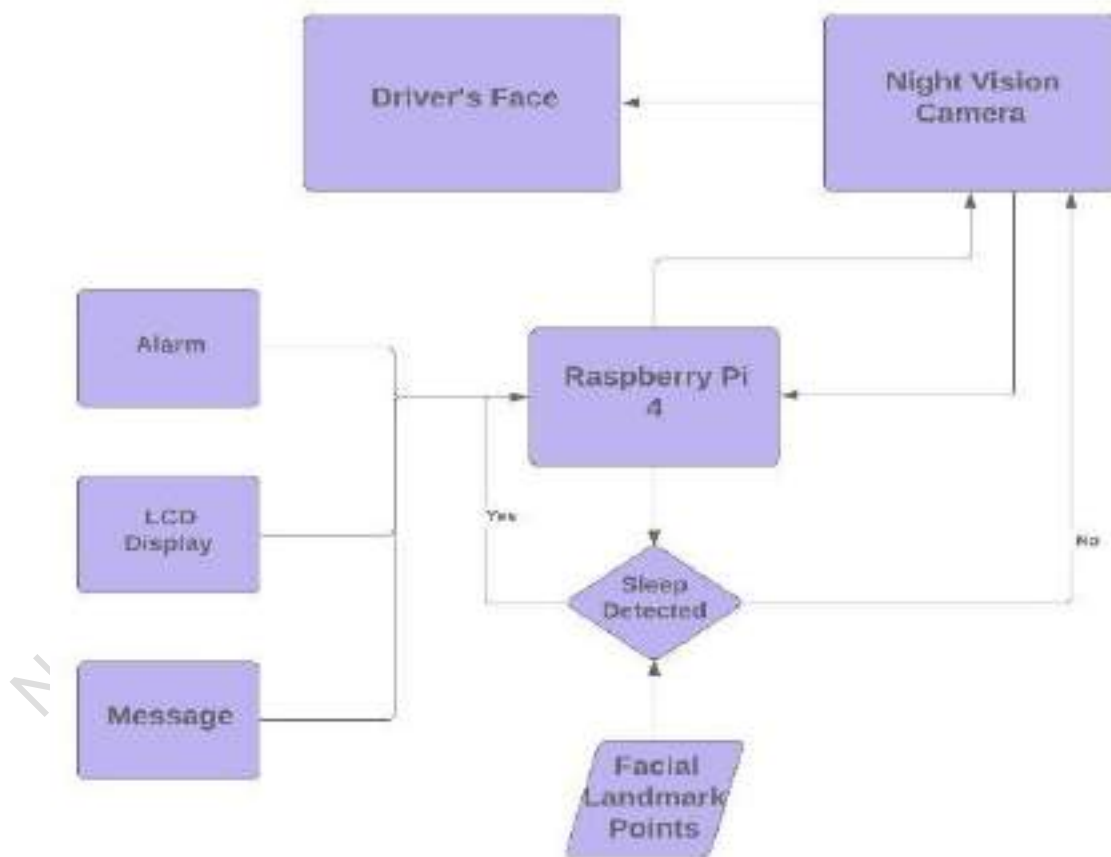


Fig. (1). Block diagram of driver's drowsiness detection system. (A higher resolution / colour version of this figure is available in the electronic copy of the article).



Fig. (2). Raspberry pi 4 model. (A higher resolution / colour version of this figure is available in the electronic copy of the article).



Fig. (3). Night vision camera. (A higher resolution / colour version of this figure is available in the electronic copy of the article).

3.3. LCD Display

Liquid Crystal Display (LCD) is a flat display that is used in order to display contents. It has the ability to point characters, numbers, and graphics. Liquid crystals emit light indirectly by using an improvised reflective surface. It suffers from discoloration problems since it does not contain phosphor. It is liable to be influenced by image persistence. LCDs are used in a large variety of applications like calculators, watches, mobile phones, televisions, and computer monitors (Fig. 4).

3.4. Motors

Motors are utilized to change electrical vitality into mechanical vitality. The simultaneous involvement of the magnetic field and electric current in a winding pave the way for the generation of force in the form of torque. A motor consists of a rotor, bearings, stator, windings, and a commutator. Magnetism, static electricity, and piezoelectricity are the three principles on which a motor operates. Motors in our prototype are used to run the vehicle of the car model (Fig. 5).

3.5. Implementation

This section covers the in-depth real-time work performed by our system. The most important purpose of creating the prototype is to detect the drowsiness of the driver by continuously monitoring the eyes of the driver with the assis-

tance of a night vision camera. The below image represents our system's architecture and its components (Fig. 6):



Fig. (4). LCD display screen. (A higher resolution / colour version of this figure is available in the electronic copy of the article).



Fig. (5). Electric motor. (A higher resolution / colour version of this figure is available in the electronic copy of the article).

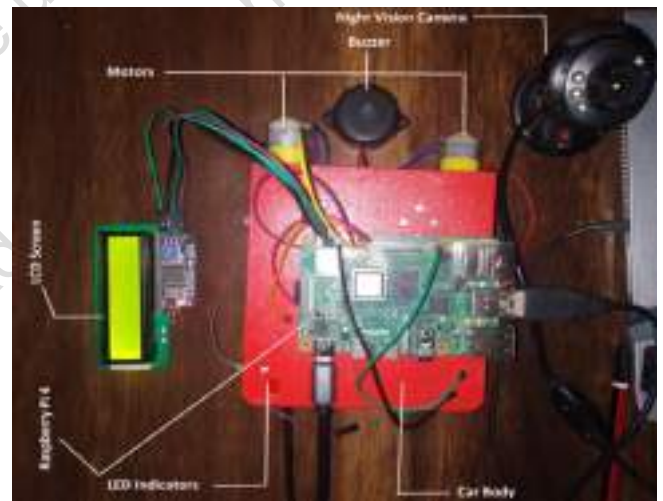


Fig. (6). System architecture of driver's drowsiness detection system. (A higher resolution / colour version of this figure is available in the electronic copy of the article).

The camera starts taking the images of the person while driving, and the microprocessor uses the below given (Fig. 7) facial landmarks points in-order to locate the eye of the person from the entire frame. Facial landmarks detector consists of 68- facial points towards eyes, nose, mouth, and jawline.

Once the eyes are located in the frame, the microprocessor-calculates the eye aspect ratio of the driver. Eye aspect ratio is outlined as the ratio of height and breadth of the attention. The eye aspect ratio determines the field of view of the driver. If the eye aspect ratio is smaller, then the field of view of the driver decreases, and if the eye aspect ratio is larger, then it increases the field of view of the driver. The dividend denotes the peak of the eye, and the divisor denotes the breadth of the attention. The Eye Aspect Ratio (EAR) equation,

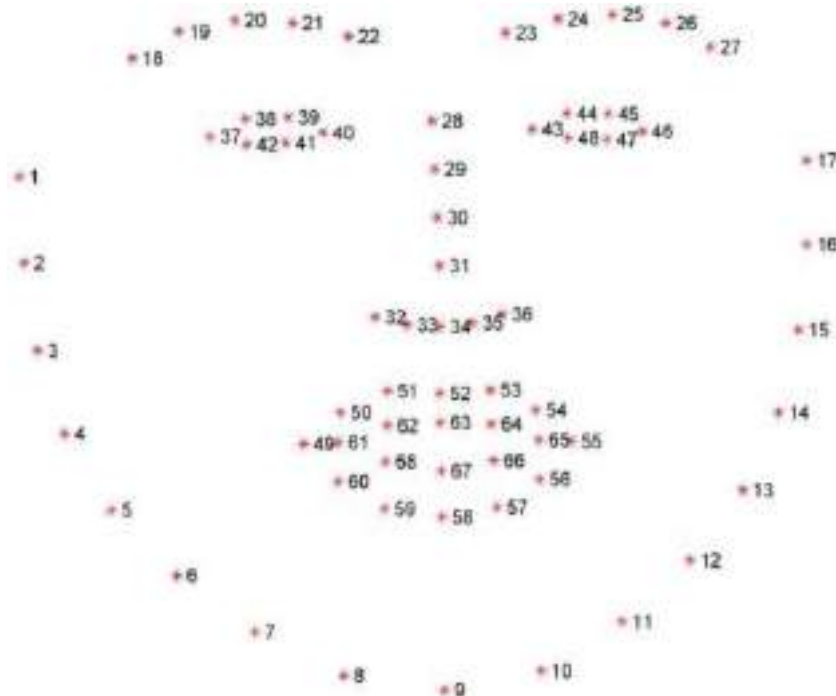


Fig. (7). Facial landmarks points, according to the Dlib library.

which was proposed in a previous study [8], can identify the eye squint using the scalar value. For example, if the driver squints eyes more frequently, it implies that the driver is in the condition of languor. The equation accustomed to calculating the attention ratio is as follows:

$$(\| P2 - P6 \| + \| P3 - P5 \|)$$

$$\text{Eye Aspect Ratio} = 2 * (P1 - P4)$$

Where P1, P2, P3, P4, P5, and P6 are 2D landmark locations, as depicted in Fig. (8).



Fig. (8). Calculate the eye aspect ratio. (A higher resolution / colour version of this figure is available in the electronic copy of the article).

Table 1 shows the obtained EAR values in different situations with six subjects, and the average EAR values when the eyes opened and closed are 0.2907 and 0.1187, respectively. If the driver is found to be drowsy in fifteen consecutive frames, then it is considered as one sleep. If the individual is detected to be sleepy for the first time, then the system warns the driver by generating an alarm. Later if the drowsiness keeps recurring and the individual is detected to be sleepy for the fourth time, then a notification starts to scroll on the LCD display, which is placed at the rear part of the

vehicle stating “Caution Driver Sleeping! Be Careful” in order to alert the nearby vehicles. Even after these warnings, if the driver is found to be sleepy for the fifth time, then the owner of the vehicle will be informed through an SMS mentioning that the driver is sleepy and he can rest for a while and continue to drive later on. If the camera detects the driver to be sleepy for the sixth time, then the vehicle gradually begins to retard and finally reaches a halt.

Table 1. The average range of EAR during eyes opened and closed from six different subjects.

Subjects	EAR During Open Eyes	EAR During Closed Eyes
1	0.2813	0.099
2	0.3014	0.1017
3	0.2946	0.1621
4	0.3179	0.1038
5	0.2791	0.1131
6	0.2699	0.1329
Average	0.2907	0.1187

3.6. The Below Code Snippet Guides the System in Calculating the Eye Aspect Ratio

Def of Eye Aspect Ratio (eye):

$$X = \text{dist.euclidean}(\text{eye}[1], \text{eye}[5])$$

$$Y = \text{dist.euclidean}(\text{eye}[2], \text{eye}[4])$$

$$Z = \text{dist.euclidean}(\text{eye}[0], \text{eye}[3]) \text{ ear} = (X+Y) / (2.0 * Z)$$

return ear

where Euclidean distance from A to B is ($\|A - B\|$)

A buzzer is a device that sends signals through audio. A buzzer is used in a large variety of applications like alarm devices, timers, mouse clicks, and keystroke. The electric buzzer was first created by Joseph Henry in 1831. The buzzer in our prototype helps in alerting that the individual is sleepy by generating an audio or buzz sound.

LCD plays a crucial role in our system as it displays a message regarding the status of the driver's drowsiness. It is placed at the rear part of the vehicle to warn the nearby vehicles. When the driver is found to be sleepy, a notification will scroll on the LCD display, stating, "Caution Driver Sleeping! Be Careful." LCD makes our system unique from the existing systems.

The message is generated in our system using the Twilio account, which is an open-source software available on the Internet. The owner of the vehicle will be informed that the driver is sleepy through an SMS. Later, if the driver keeps falling sleepy, then the vehicle starts to retard gradually, and parallelly the engine gets locked, and the vehicle comes to a halt.

4. EXPERIMENTAL RESULTS

The below two figures showcase the detection of drowsiness of an individual in real-time. Fig. (9) shows that the individual is awake, and the eye aspect ratio of the individual has been measured, and the system finally displays the resultant value. In Fig. (10), the individual is detected to be sleepy, and the eye aspect ratio of the individual is displayed after calculation by the system.

```

Begin
1: i <- 1;
2: while i <= 10 do
3:   Generate an Alarm
4:   call sleep(0.5) wait for 0.5 seconds
5:   Turn off the Alarm
6:   call sleep(0.5) wait for 0.5 seconds
7:   i = i + 1
8: end while
end

```

Algorithm (1). Algorithm for generating the alarm

```

Begin
1: LCD <- lcd();
2: P <- 0;
3: while P <= 3 do
4:   call LCD lcd_screen_string("CAUTION",1);
5:   call LCD lcd_screen_string("Driver is Sleepy",2);
6:   call time.sleep(2);
7:   call LCD lcd_clear();
8:   call LCD lcd_screen_string("Be Careful",1);
9:   call time.sleep(2);
10:  call LCD lcd_clear();
11:  P = P + 1
12: end while
end;

```

Algorithm (2). Algorithm for scrolling the message on the LCD Screen

```

Begin
1: client <- call Client(private_account_sid,
                        private_auth_token);
2: msg <- "Hey Mahesh Jain, Your Vehicle Driver of
         TS88FK4068, is found to be sleepy many
         times! kindly Inform him to take rest
         of some time, Lateron he can Drive!!!"
3: call client.api.account.messages.create
   (To,from,msg);
end

```

Algorithm (3). Algorithm for sending a message to the vehicle owner using Twilio.

```

Begin
1: T <- 100
2: Flag <- 1
3: call sleep(3);
4: pwn_left <- call GPIO.PWN(16,100);
5: pwn_right <- call GPIO.PWN(15,100);
6: call pwn_left.start(100);
7: call pwn_right.start(100);
8: while True do
9:   call pwn_left.ChangeDutyCycle(T);
10:  call pwn_right.ChangeDutyCycle(T);
11:  call sleep(2);
12:  T = T - 10;
13:  if T == 0 then
14:    Flag = 0;
15:    break;
16:  end if
17: end while
18: if Flag == 0 then
19:  call exit();
20: end if
End

```

Algorithm (4). Algorithm for slowing down the speed of the motor.



Fig. (9). Driver before feeling sleepy while driving a vehicle. (A higher resolution / colour version of this figure is available in the electronic copy of the article).

If the system detects sleep for the fourth time, then a notification will begin to scroll on the LCD display placed at the rear part of the vehicle. The notification that is displayed on the LCD in order to alert the nearby vehicles is shown in Figs. (11 and 12).

If the driver is detected to be sleepy for the fifth time, then an SMS is sent to the owner of the vehicle using the

Twilio account. The SMS which is to be sent to the owner of the vehicle is mentioned below in the figure:



Fig. (10). Driver feeling sleepy while driving a vehicle. (A higher resolution / colour version of this figure is available in the electronic copy of the article).

hicle gradually begins to retard, and parallelly the engine of the vehicle gets automatically locked.

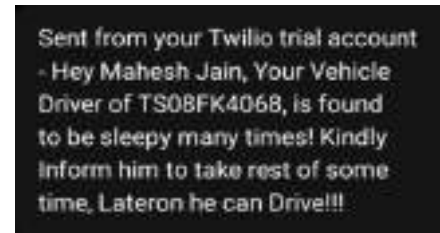


Fig. (13). Message sent to the owner of the vehicle. (A higher resolution / colour version of this figure is available in the electronic copy of the article).



Figs. (11, 12). LCD displaying a caution message. (A higher resolution / colour version of this figure is available in the electronic copy of the article). (A higher resolution / colour version of this figure is available in the electronic copy of the article).

Table 2 represents the various scenarios taken into consideration in-order to the accuracy of the system in special situations as well.

Table 2. Accuracy levels for different parameters under various scenarios.

Test	Number of Observations	Number of Hits	Percentage of Hits
Eye Blink Counter	200	198	99%
Sleep Detection with Glasses	200	179	89.5%
Sleep Detection without Glasses	200	184	92%
Driver with Cap on head	20	18	90%
Driver without Cap	20	20	100%
Driver with hair on the face	20	15	75%

In Fig. (13), as we can see that the SMS which is sent to the owner of the vehicle is shown. Later, even after all these warnings, if the driver is detected to fall asleep, then the ve-

The below graph, Fig. (14), represents the levels of accuracy of the previously designed prototype in a study[1] and this proposed system using different algorithms. This system predicted 179 accurate observations out of 200 observations of drowsiness.



Fig. (14). Accuracy (in %) when compared to pre-existing models mentioned in a study [1] with this proposed system.

The accuracy of the existing system mentioned in one of the studies[1], using Naïve Bayes is 80%, support vector machine gives 80% accuracy, and random forest gives 84% accuracy. Our model best performs in various conditions with an accuracy of 89.5%.

CONCLUSION

The aim of this work is to instill a sense of quality in driver's drowsiness detection systems. The prototype analyses the drowsiness of the driver with an infrared camera, which can deliver great results even in darkness or low light conditions. The prototype has shown promising results in real-life scenarios in order to reduce the number of accidents with respect to the drowsiness of the person who drives the vehicle. This is useful in situations when the drivers are used to the strenuous workload and drive continuously for a longer duration of time without having a proper sleep. In this paper, drowsiness of the driver has been detected using the Eye Aspect Ratio of the driver and besides the driver is cautioned using an alarm system, and the other vehicles which move around him are also notified using the LCD screen at the rear end of the vehicle as well as the owner of the vehicle is informed using SMS. The modern-day drivers must be

provided with additional safety features. The road accidents due to the drowsiness of the drivers not only affect the lives of drivers but also the drivers of the vehicles nearby the vehicle of the drowsy driver. The drowsiness of the driver is detected utilizing various parameters. It is exceedingly difficult to detect drowsiness with the help of image processing alone. The field of machine learning has gained a lot of prominence in the modern-day world due to the challenges faced by it.

CONSENT FOR PUBLICATION

Not applicable.

AVAILABILITY OF DATA AND MATERIALS

Not applicable.

FUNDING

None.

CONFLICT OF INTEREST

The authors declare no conflict of interest, financial or otherwise.

ACKNOWLEDGEMENTS

Declared none..

REFERENCES

- [1] Mehta S, Dadhich S, Gumber S, Jadhav Bhatt A. Real-time driver drowsiness detection system using eye aspect ratio and eye closure ratio. SSRN Electron J [Internet]. 2019; Available from: <http://dx.doi.org/10.2139/ssrn.3356401>.
- [2] Lee BG, Chung WY. A smartphone-based driver safety monitoring system using data fusion. *Sensors (Basel)* 2012; 12(12): 17536-52. <http://dx.doi.org/10.3390/s121217536> PMID: 23247416
- [3] He J, Roberson S, Fields B, Peng J, Cielocha S, Coltea J. Fatigue detection using smartphones. *J Econ* 2013; 3(03): 1-7.
- [4] Galarza EE, Egas FD, Silva FM, Velasco PM, Galarza ED. Real time driver drowsiness detection based on driver's face image behavior using a system of human computer interaction implemented in a smartphone. In: *Proceedings of the International Conference on Information Technology & Systems (ICITS 2018)*. Cham: Springer International Publishing; 2018; 563-72. http://dx.doi.org/10.1007/978-3-319-73450-7_53
- [5] Driver drowsiness detection system for vehicle safety. *Special Issue*. 2019;8(6S4):815-9.
- [6] Alioua. Amine, Rziza M, Aboutajdine D. Driver's fatigue and drowsiness detection to reduce traffic accidents on road In: Real P, Diaz-Pernil D, Alioua, Amine, Molina-Abril H, Berciano A, Kropatsch W, Eds. *Computer Analysis of Images and Patterns CAIP 2011 Lect Note Comput Sci* 2011; 6855.
- [7] Marimuthu R, Suresh A, Alamelu M, Kanagaraj S. Driver fatigue detection using image processing and accident prevention. *Int J Pure Appl Math*. 2017; 116(11):91-9.
- [8] Soukupova T, Cech J. Eye blink detection using facial landmarks. 21st computer vision winter workshop. Rimske Toplice, Slovenia. 2016.
- [9] Zhu and Ji. Real time and non-intrusive driver fatigue monitoring *Proceedings the 7th International IEEE Conference on Intelligent Transportation Systems (IEEE Cat No04TH8749)*. Washington, WA, USA. 2004; 657-62.
- [10] Xu L, Li S, Bian K, Zhao T, Yan W. Sober-Drive: A smartphone-assisted drowsy driving detection system. 2014 International Conference. 398-402.
- [11] Singh H, Bhatia JS, Kaur J. Eye tracking based driver fatigue monitoring and warning system. 2010 India International Conference. 1-6. <http://dx.doi.org/10.1109/IICPE.2011.5728062>
- [12] Kurt MB, Sezgin N, Akin M, Kirbas G, Bayram M. The ANN-based computing of drowsy level *Expert Syst Appl* 2009; 36: 2534-42. <http://dx.doi.org/10.1016/j.eswa.2008.01.085>
- [13] Transportation.gov. [cited 2021 Jul 7]. Available from: <https://www.transportation.gov/sites/dot.gov/files/2021-03/Privacy%20-%20NHTSA%20-%20CDAN%20-%20PIA%20-%20Approved%20-%2003021.pdf>
- [14] Ueno H, Kaneda M, Tsukino M. Development of drowsiness detection system *Proceedings of 1994 Vehicle Navigation and Information Systems Conference*. Yokohama, Japan. 1994;15-20. <http://dx.doi.org/10.1109/VNIS.1994.396873>
- [15] Zhou G. Application of deep learning in object detection 2017 *IEEE/ACIS 16th International Conference on Computer and Information Science (ICIS)*. Wuhan. 2017; 631-4.
- [16] Saito H, Ishiwaka T, Sakata M, Okabayashi S. Applications of driver's line of sight to automobiles: What can driver's eye tell. *Proceedings of 1994 Vehicle Navigation and Information Systems Conference*. Yokohama, Japan. 1994; 1994Z: 21-6. <http://dx.doi.org/10.1109/VNIS.1994.396872>
- [17] Du X, Cai Y, Wang S, Zhang L. Overview of deep learning 2016 31st Youth Academic Annual Conference of Chinese Association of Automation (YAC). Wuhan. 2016; 159-64. <http://dx.doi.org/10.1109/YAC.2016.7804882>
- [18] Fukuda J, Adachi K, Nishida M, Akutsu E. Development of driver's drowsiness detection technology. *Toyota Tech Rev* 1995; 45: 34-40.
- [19] Richardson JH. *The development of a driver alertness monitoring system. Fatigue and driving: Driver impairment, driver fatigue and driver simulation*. London: Taylor & Francis 1995.
- [20] Shrestha A, Mahmood A. Review of deep learning algorithms and architectures. *IEEE Access* 2019; 7: 53040-65. <http://dx.doi.org/10.1109/ACCESS.2019.2912200>
- [21] Xin Y. Machine learning and deep learning methods for cybersecurity. *IEEE Access* 2018; 6: 35365-81. <http://dx.doi.org/10.1109/ACCESS.2018.2836950>
- [22] Somayya MR, Ramaswamy ST. Internet of Things (IoT): A literature review. *Journal of Computer and Communications* 2015; 3: 164-73. <http://dx.doi.org/10.4236/jcc.2015.35021>
- [23] Kompalli PL. Knowledge discovery using data stream mining: an analytical approach social network analytics for contemporary business organizations 2018; 231-58. <http://dx.doi.org/10.4018/978-1-5225-5097-6.ch012>
- [24] Prasanna Lakshmi K. Video genre classification using convolutional recurrent neural networks *Int j. adv comput sci applications* 2020; 11: 170-6.
- [25] Prasanna Lakshmi K. A study on internet of things with block chain technology *IEEE 3rd International conference on trends in electronics and informatics*. Tirunelveli, India. 2019; 502-6.



Intrusion detection in big data using hybrid feature fusion and optimization enabled deep learning based on spark architecture

Ramkumar M.P.^{a,*}, P.V. Bhaskar Reddy^b, J.T. Thirukrishna^c, Ch. Vidyadhari^d

^a Assistant Professor, Department of Computer Science and Engineering, Thiagarajar College of Engineering, Madurai, 625015, India

^b Professor, School of Computer Science and Engineering, REVA University, Bangalore, Karnataka, India

^c Associate Professor, Department of Information Science and Engineering, Dayananda Sagar Academy of Technology and Management, Bangalore, 560082, Karnataka, India

^d Assistant Professor, Department of Information Technology, Gokaraju Rangaraju Institute of Engineering and Technology, Bachupally, Hyderabad, India

ARTICLE INFO

Article history:

Received 7 October 2021

Revised 27 January 2022

Accepted 22 February 2022

Available online 24 February 2022

Keywords:

Big data

Deep learning

Intrusion detection

Deep residual network

and Spark model

ABSTRACT

With the rapid expansion of Internet services and increasing intrusion issues, conventional intrusion detection techniques cannot work well with several difficult intrusions. Though several intrusion detection methods have been introduced in the past years, developing an Intrusion Detection Systems (IDS) with prevailing intrusion detection strategy is still very much desirable. Hence, a robust and effective intrusion detection approach, named RV coefficient+Exponential Sea Lion Optimization-enabled Deep Residual Network (ExpSLO-enabled DRN) using spark is devised for the intrusion detection. Here, the unique features are selected using proposed RV coefficient-based hybrid feature fusion, which is designed by the incorporation of wrapper, class-wise information gain (CIG), and Canberra distance in slave node. With the distinctive features selected, the process of data augmentation is done using oversampling for making the data more appropriate to perform the further process in the slave node. Moreover, DRN classifier is utilized for detecting the intrusions in the master node where the DRN training is done using devised ExpSLO algorithm, which is the hybridization of Exponentially Weighted Moving average (EWMA) and Sea Lion Optimization (SLnO). Furthermore, the devised method obtained better performance by considering the evaluation metrics, such as precision, recall, and F-measure with the higher values of 0.8800, 0.8845, and 0.8822 based on without attacks using dataset-2.

© 2022 Elsevier Ltd. All rights reserved.

1. Introduction

Big data is more complex to accumulate, handle or operate using various conventional approaches. The features of big data include velocity, volume, and variety (Zikopoulos and Eaton, 2011) and these features signify a main confront for the IDS (Suthaharan, 2014). Volume defines the amount of data and the generation of data from a variety of sources has emerged drastically over the present years. Hence, it is important to observe and control the traffic in the network to incorporate with processing and management of big data (Jadhav and N, 2019). Besides, the massive quantity of big data is related with an additional confront, which is variety and thus various types of semi-structured, structured, and unstructured data sources (Faker and Dogdu, 2019) need to be included. In addition, the various prospective challenges for handling big data include testing, handling, adaptation, storage,

visualization, searching, sharing, and security. Furthermore, the scientific improvements in internet, communications, and the networking facilitate massive data to be formed each day from numerous sources as different as social media, business, healthcare (Sinjari et al., 2020), and transportation. Besides, Spark is a type of distributed computing framework introduced by UC Berkeley AMP Lab. Moreover, IDS remains as an important research topic because of the varying big data structure, constant growth, growing speed of networking systems, and the varying techniques of intruders (Hassan et al., 2020). Spark supports numerous ways to integrate with various platforms of big data, which facilitates it to efficiently progress the massive-scale data. Meanwhile, its memory-driven Resilient Distributed Dataset (RDD) strategy permits the intermediary cached data in memory, thereby storing a set of input/output computation overheads, and is trained for ensemble and iterative algorithms. Hence, this spark model has distinctive benefits in big data processing (Liu et al., 2020).

Intrusion detection is one of the significant techniques to protect the system from various types of malicious attacks (Veeraiah and Krishna, 2018). IDS are the fundamental system

* Corresponding author.

E-mail address: ramkumar@tce.edu (R. M.P.).

utilized in cyber security applications (Sadanand Savyanavar and Ghorpade, 2019). IDS are the software or hardware that evaluates the flow of data through computers and networks for recognizing the security issues which threaten the integrity, privacy (Prasanalakshmi et al., 2011), or accessibility of the resources in the system (Di Pietro et al., 2008). IDS employ two fundamental techniques, such as anomaly detection, and misuse detection method to analyze various events in order to detect the attacks. Signature-driven detection or Misuse detection is the assessment of different actions performed in the system to search and detect attack patterns same as previously recognized attack patterns, which are stored in the IDS database. In addition, anomaly detection detects the unusual characteristics present in the network traffic. It depends on the building models which represent the usual actions of hosts, networks, and users. Moreover, the patterns that diverge from these methods are recognized and signified as anomalous actions. The anomaly identification approaches on the basis of deep learning, artificial neural networks, and machine learning approaches have been extensively utilized in the expansion of IDS to mine and extract knowledge through testing and training process of datasets (Chandola et al., 2009).

In recent times, numerous deep learning approaches have been developed for handling big data in different applications. Among them, the most commonly used techniques are Long Short-Term Memory (LSTM) networks, Convolutional Neural Networks (CNN), and Deep Belief Networks (DBN) (Hochreiter and Schmidhuber, 1997 Hassan et al., 2020;). DBN is mainly utilized for analyzing the patterns, and they train faster than several deep learning mechanisms. In (Faker and Dogdu, 2019 Hassan et al., 2020;), three different classifiers like random forest, Deep Neural Networks (DNN), and Gradient Boosted Tree are utilized in big data environments for categorizing the attacks in multiclass modes for improving the detection performance. In (Khan et al., 2019 Hassan et al., 2020;), a two-stage deep learning framework was developed for finding the intrusions in the network using an auto-encoder compiled with soft-max classifier. In addition, various traditional machine learning techniques utilized for IDS (Khan and Gumaei, 2019 Hassan et al., 2020;), have shallow models and are not suitable for detecting intrusions in a big data framework. They detect anonymous attacks with complexity, cannot recommend real time solutions, and cannot manipulate the widespread noises present in large data sets (Hassan et al., 2020). Furthermore, various intrusion detection methods are utilized in big data (Mishra et al., 2017). Signature-driven IDS recognizes the known attacks, but it failed to identify the unknown attacks. Furthermore, the anomaly-driven IDS train on abnormal traffic and regular traffic dataset for identifying malicious attacks (Haggag et al., 2020).

1.1. Research questions

1. How the feature selection is done with the developed RV coefficient-based hybrid feature fusion?
2. How the oversampling process is helpful in the data augmentation process?
3. How the hybrid feature fusion helps to improve the performance of the model?
4. How the intrusions are detected effectively using the developed ExpSLO-based DRN?

The key objective of this work is described as follows,

- **Developed RV coefficient-enabled hybrid feature fusion:** In the spark architecture, RV coefficient based hybrid feature fusion is employed for the feature selection process, which is designed by the combination of wrapper, CIG and Canberra distance.

- **Proposed ExpSLO-based DRN:** An effective approach is developed to detect intrusions in big data using developed ExpSLO-based DRN classifier. Here, the DRN classifier is employed for the intrusion detection so that the fitness measure is considered for generating the finest intrusion detection result. Moreover, the training procedure of DRN is done using the devised ExpSLO, which is the combination of EWMA and SInO.

The structure of the research paper is configured as follows: the existing intrusion detection techniques are portrayed in Section 2, the devised intrusion detection approaches using spark are portrayed in Section 3, Section 4 portrays the implementation outcomes, and lastly the conclusion is described in Section 5.

2. Motivations

IDS act as a primary role in finding network security threats. It secures the network from viruses, worms, vulnerable source code, and unauthorised intruders for several internet applications. Despite many advanced techniques developed for detecting intrusions, there exist many network-based security problems. Hence, this section reviews different existing intrusion detection approaches with its benefits and challenges that encourage the research experts to propose a novel method for intrusion detection.

2.1. Literature review

The eight different approaches based on intrusion detection in big data are elucidated in this section with its merits and demerits Karatas et al. (2018). designed a deep learning enabled IDS technique for detecting intrusions. This approach effectively improved the flexibility of the model, whereas this approach failed to reduce the computational complexity problems Haggag et al. (2020). devised a deep learning framework with Apache spark platform for intrusion detection. In this model, spark cluster configuration was used for minimizing the training procedure while devising the IDS with several hyperparameters. This method improved the attack detection accuracy. However, this approach failed to utilize more datasets for handling various types of attacks Hassan et al. (2020). introduced a hybrid deep learning approach for detecting intrusions in big data framework. Here, deep CNN was employed for extracting significant features from IDS big data, whereas weight-dropped LSTM (WDLSTM) was utilized for retaining the long-term dependencies between the extracted features in order to reduce the over fitting problems on the recurrent connections. This approach effectively avoided the gradient vanishing problems, but the computational time of this approach was very high Faker and Dogdu (2019). devised a deep learning technique with Apache Spark and the Keras deep learning library for intrusion detection. In this model, gradient boosted tree, random forest classifiers, and a deep neural network was utilized to perform the classification, while the k-means clustering method was utilized for selecting the significant features by computing the degree of homogeneity. This approach enhanced the multiclass classification performance. Meanwhile, this approach failed to reduce the cost of computation.

Zhong et al. (2020) modeled a big data-enabled hierarchical deep learning system (BDHDLs) for detecting intrusions. This model substantially reduced the construction time while deploying multiple machines, while this model failed to reduce the utilization of the resources for improving training speed Gurung et al. (2019). developed a Deep learning technique for detecting intrusions in network. In this approach, a deep network was employed to categorize the network traffic among the intrusions and the normal connections. This technique had the flexibility to adjust to new intrusion patterns, but was not utilized in the real time applications

Gao et al. (2020). developed a deep learning-based Omni supervisory control and data acquisition (SCADA) for detecting the correlated and uncorrelated attacks. This approach enhanced the detection potential of IDS, whereas the performance of the system was affected as the memory consumption of this method was high Elmasry et al. (2020). designed a Double Particle Swarm Optimization (PSO) approach for detecting the network intrusions. In this algorithm, an finest feature subset was chosen for the specified dataset, whereas the vector of finest hyper parameters was evaluated for maximizing the accuracy. This algorithm effectively minimized the class imbalance problems. However, the energy consumption was very high in this method Mighan and Kahan (2021). implemented a hybrid method on the basis of machine learning and deep learning approaches. Apache Spark was used for large data processing and identifying the network traffic. This approach attained good accuracy with less amount of time. However, some important features were not considered for the performance evaluation. Noor Mohd, et al. [31] developed a technique named hierarchical classification for the detection of intrusions. This method attained good detection rate than the other comparative methods. However, this method used a small dataset for experimentation.

2.2. Challenges

The different challenges faced by various existing intrusion detection approaches in big data are illustrated as follows,

- The deep learning method with Apache Spark Platform (Haggag et al., 2020) was developed for detecting intrusions. However, this approach failed to utilize various tools for evaluating the performance of the developed technique in real-time configurations.
- In Hassan et al. (2020), a hybrid deep learning approach was presented for detecting the intrusions in big data surroundings, but this method does not analyze larger and difficult datasets to perform real-time intrusion detection.
- Deep block-chain Framework was modelled in Faker and Dogdu (2019) for detecting intrusions using big data, but the main challenge lies in enhancing the intrusion detection procedure by applying feature selection based on homogeneity metrics.
- The simple decision fusion strategy developed in Zhong et al. (2020) failed to achieve optimal solution at all times. Thus, the challenge lies in developing advanced decision fusion algorithms for reducing computational complexities.
- Deep learning method was devised for the intrusion detection systems. Meanwhile, this approach does not consider latest datasets with different deep learning techniques for analyzing the developed technique for minimizing the computational complexities (Karatas et al., 2018).

3. Proposed RV coefficient+ExpSLO-based DRN for the intrusion detection in big data

Big data represents a massive set of distinctive structured data obtained from diverse heterogeneous sources assembled on storage devices. It is very crucial to accomplish security in big data because of its exponential increase in data sizes. Hence, IDS is employed for detecting the intrusions on computers, networks, or workstations. The main role of the research is to devise an intrusion detection approach in big data using an optimization enabled-deep learning approach with spark architecture considering slave and master nodes. The developed intrusion detection approach mainly includes three stages, namely feature selection, data augmentation, and intrusion detection. At first, the big data input acquired from the dataset is partitioned, which is then fed into

spark model wherein the feature selection process and data augmentation is performed at the slave set-1. The feature selection is done for selecting unique features using proposed RV coefficient-based hybrid feature fusion which is devised by the combination of wrapper (Kohavi and John, 1997), CIG (Zhang and Tan, 2013) and Canberra distance. After selecting the unique features, then the data augmentation process is performed using oversampling method in slave set-2. Finally, the intrusion detection process is carried out in master node using DRN classifier (Chen et al., 2019) which is trained by the devised ExpSLO algorithm. Moreover, the devised ExpSLO is newly devised by the combination of EWMA (Machaka et al., 2016) and SLnO (Masadeh et al., 2019) Fig. 1. depicts the diagram of the devised RV coefficient+ExpSLO-enabled DRN for detecting the intrusions.

3.1. Acquisition of input data

Let us assume a dataset D with different attributes, and it is given as,

$$D = \{X_{u,v}\}; \quad (1 \leq u \leq U), (1 \leq v \leq V) \quad (1)$$

where, $X_{u,v}$ signifies data with v^{th} attribute of u^{th} data, V specifies the overall data and U signifies the total attributes. The big data input is partitioned into various subsets for performing the further process. However, the partitioned big data input is given as,

$$X_{u,v} = B_a; \quad (1 \leq a \leq d) \quad (2)$$

where, B_d signifies the partitioned data, which is fed to the spark architecture that comprises of slave nodes and master nodes.

3.2. Spark architecture

In the spark architecture, the feature selection and the data augmentation is carried out in the slave nodes, whereas the intrusion detection process is performed in the master node.

3.2.1. Slave set-1: Feature selection

The feature selection is done at slave set-1 using the proposed RV coefficient-based hybrid feature fusion. The feature selection phase is a significant process as it makes the intrusion detection process more effective. Once the partitioned data is subjected to slave nodes, the feature selection process is performed at each slave node to obtain the unique features for further processing. The proposed RV coefficient-based hybrid feature fusion is designed by incorporating the unique features obtained from wrapper method, CIG, and Canberra distance and the process is illustrated below as follows,

3.2.1.1. Wrapper method. The wrapper method (Kohavi and John, 1997) is one of the techniques used for selecting the significant features for enhancing the detection performance by minimizing the size space of data. The wrapper method is wrapped around the classifier for computing all the feature subsets. This method performs the searching practice with the possible parameters in the search space. Here, the searching space needs a search engine, initial state, state space, and a termination form. In this method, the operators define the association between different states. The major objective of wrapper method is to recognize states with highest evaluation using heuristic function. Here, the accuracy is predicted by heuristic function and evaluation function. Besides, the heuristic function enables the predicted accuracy for executing cross validation several times on smaller datasets than the larger datasets. Furthermore, this approach effectively reduces the classification error and it also enhances the detection performance. Hence, the size of features selected from partitioned data using wrapper is denoted as $m \times f_1$.



Fig. 1. Schematic representation of the developed RV coefficient+ExpSLO-based DRN for the intrusion detection.

3.2.1.2. *CIG*. Here, the more appropriate and powerful features needed for the intrusion detection process is effectively selected based on CIG (Zhang and Tan, 2013) considering the class information. It measures the distinctiveness of the feature for finding a precise class, and it selects the features with maximum contents for a definite class. These features are utilized for recognizing their equivalent classes. However, the selected features based on CIG is formulated as,

$$f = H(v_l = 1, K_q) \cdot \log \frac{H(v_l = 1, K_q)}{H(v_l = 1)H(K_q)} + H(v_l = 0, K_q) \cdot \log \frac{H(v_l = 0, K_q)}{H(v_l = 0)H(K_q)} \quad (3)$$

where, f specifies the selected features, K_q implies the gathered information, $H(v_l, K_q)$ signifies the probability that feature v_l in K_q . As a result, the size of features selected from partitioned data using CIG is denoted as $m \times f_2$.

3.2.1.3. *Canberra distance*. The Canberra distance is a measure of distance between the pair of vector points in the vector space. Here, the Canberra measure is used for computing the distance score of every feature in such a way that the significant features needed for the further process are effectively selected, which is expressed as,

$$C(A, B) = \sum_{i=1}^p \frac{|A_i - B_i|}{|A_i| + |B_i|} \quad (4)$$

where, A and B are denoted as vectors, and the size of features selected from partitioned data using Canberra distance is denoted as $m \times f_3$.

3.2.1.4. Hybrid feature fusion. The feature selection is done using proposed RV coefficient-based hybrid feature fusion, which is designed by hybridizing the output of wrapper, CIG, and Canberra distance. The RV coefficient is defined as the multivariate simplification of the squared Pearson correlation coefficient as the RV coefficient considers the values within the range 0 and 1. In addition, it determines the closeness of two different set of points that is specified in a matrix. Moreover, the size of the unique features selected using wrapper, CIG, and Canberra distance is specified as $m \times f_n$, respectively.

$$F = RV(f_u, f_t) \quad (5)$$

Furthermore, the equation for RV coefficient is formulated as,

$$RV(P, Q) = \frac{Cov(P, Q)}{\sqrt{Var(P)Var(Q)}} \quad (6)$$

where, RV represents RV coefficient among unique features and the target, f_u denotes the unique features, f_t signifies the target features, (P, Q) signifies the matrices of centered random vectors, cov and var implies the covariance and variance of (P, Q) . For $F > Threshold$, the effective features are selected.

3.2.2. Slave set-2: Data augmentation

The data augmentation process is done to reduce the over fitting issues, and is very effective in improving the dimensionality of the data. Once the unique features F are selected, data augmentation is performed in slave set-2. Here, the data augmentation is performed based on oversampling method where the data is split based on class labels and then the new samples are generated by performing oversampling. The augmented data output D is presented to master nodes for performing intrusion detection in big data.

3.2.3. Master node: IDS using proposed ExpSLO-based DRN

The process of intrusion detection is performed using DRN (Chen et al., 2019) which is trained by the devised ExpSLO. Meanwhile, the devised ExpSLO is designed by the integration of EWMA (Machaka et al., 2016) and SLnO (Masadeh et al., 2019). DRN classifier is very effective in detecting the intrusions in such a way that the detection process takes the augmented data D as an input and generates the detected outcome as normal or attack.

a) Structure of DRN

The DRN classifier (Chen et al., 2019) consists of several layers, namely convolutional (conv) layer, pooling layer, activation function, batch normalization, residual blocks, and linear classifier. The input image considered is in the dimension of $32 \times 32 \times 3$ with 'zerocenter' normalization. In addition, 20 convolution layers are considered with 5×5 convolutions using stride (Karatas et al., 2018; Karatas et al., 2018) and padding $[0, 0, 0, 0]$. The ReLU layer is used by 2×2 max pooling through stride (Haggag et al., 2020; Haggag et al., 2020) and padding $[0, 0, 0, 0]$. Moreover, 3 fully connected layers and softmax are considered, whereas the cross entropy ex is measured as a detection output.

(i) Convolutional (conv) layer:

The two-dimensional conv layer is very efficient in decreasing free parameters during the process of training. This layer enhances the performance of the system by utilizing weight sharing and receptive fields. The input image is processed in the conv layer using a sequence of filters called as kernels. The mathematical function of conv layer specifies the dot product of kernels with the inputs.

However, the equation for conv layer is represented as,

$$C2d(M) = \sum_{i=0}^{W-1} \sum_{j=0}^{W-1} E_{i,j} \cdot M_{(u+i),(v+j)} \quad (7)$$

$$C1d(M) = \sum_{Y=0}^{N_n-1} G_Y * M \quad (8)$$

where, M signifies the input image with CNN features, u and v records the coordinates, G signifies the kernel with $W \times W$ matrix, and i and j specifies the index of kernel matrix. Hence, G_Y denotes the dimension of kernel for Y^{th} input neuron, and $*$ implies the cross correlation operator.

(ii) Pooling layer:

This layer is usually connected among conv layers, and is utilized for minimizing the spatial size of feature maps. Thus, average pooling is considered to work on every slice and feature map depth.

$$r_{out} = \frac{r_{in} - k_r}{\theta} + 1 \quad (9)$$

$$s_{out} = \frac{s_{in} - k_s}{\theta} + 1 \quad (10)$$

where, r_{in} signifies the input matrix width, s_{in} signifies the input matrix height, r_{out} and s_{out} implies the output value. Moreover, k_r defines the width of kernel size, and k_s specifies the height of kernel size.

(iii) Activation function:

The Rectified Linear Unit (ReLU) is considered as a non-linear activation function to learn non-linear and intricate features so that the non-linearity of extracted features is enhanced. However, the ReLU function is given as,

$$ReLU(M) = \begin{cases} 0 & ; T < 0 \\ T & ; T \geq 0 \end{cases} \quad (11)$$

Here, T denotes the feature.

(iv) Batch normalization:

Batch normalization layer partitions the training data into several small sets known as mini batches for the purpose of training. It attains an effective tradeoff among convergence rate and computational complexity. Accordingly, the normalization of input layers is done by scaling and varying activations for enhancing training speed and reliability.

(v) Residual blocks:

It defines the shortcut association among conv layers. Here, the input is connected to output by a short line only if the input and output are of the same dimension. For varying dimension, the dimension matching factor is accomplished for input and output matching.

$$J = \Re(H_i) + H_i \quad (12)$$

$$J = \Re(H_i) + \eta H_i \quad (13)$$

where, H_i and J indicates residual blocks input and output, \Re implies mapping ink , and η is the matching factor dimension.

(vi) Linear classifier:

It is designed by the incorporation of softmax function and fully connected layer where the fully connected layer links each neuron between the layers and the normalization of input vector to probability vector is done using softmax function.

$$J = \lambda J + \gamma \quad (14)$$

Here, λ signifies the matrix weight, and γ represents the bias. The architecture of DRN is presented in Fig. 2. The output of DRN

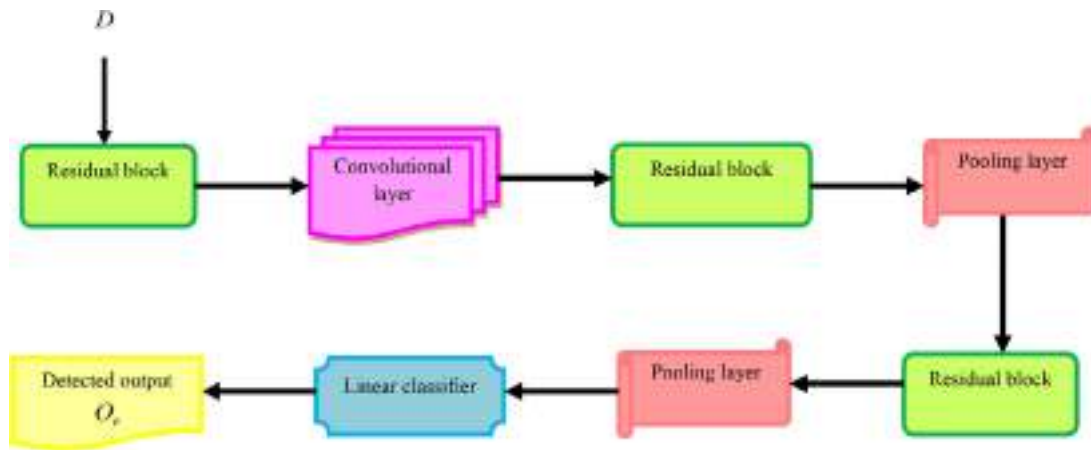


Fig. 2. Architecture of DRN.

is signified as O_t that assists in detecting the intrusions as normal and attack.

b) Training procedure of DRN using devised ExpSLO

The training practice of DRN (Chen et al., 2019) is done using devised ExpSLO for performing intrusion detection. However, the developed ExpSLO is designed by the incorporation of EWMA (Machaka et al., 2016) and SlnO (Masadeh et al., 2019). EWMA (Machaka et al., 2016) is used to determine the small shifts in processing the target values. Meanwhile, SlnO (Masadeh et al., 2019) algorithm is encouraged by the hunting character of sea lions. In addition, it is also motivated by sea lions' whiskers to identify the prey. This algorithm achieves better exploration potential and also improves the convergence speed. Moreover, the integration of EWMA and SlnO minimized the computational problems and attains global optimal solution by improving the overall detection performance. The algorithmic phases of devised ExpSLO are represented below as:

Step 1: Initialization

The solution initialization is represented as S which is formulated as,

$$S = \{S_1, S_2, \dots, S_i, \dots, Q_j; 1 \leq i \leq j\} \quad (15)$$

where, j denotes overall solutions and S_i signifies i^{th} solution.

Step 2: Fitness computation

It assists to determine the most excellent solution by calculating the optimal value of fitness, and the function utilized for computing the fitness value is formulated as,

$$\delta = \frac{1}{\vartheta} \sum_{\ell=1}^{\vartheta} |J_{\ell} - O_t|^2 \quad (16)$$

where, δ implies fitness measure, O_t denotes output of the DRN classifier, and J_{ℓ} specifies the target output.

Step 3: Detecting and tracking phase

Based on SlnO (Masadeh et al., 2019), the sea lions make use of its whiskers for measuring the dimension, shape, and location of prey. The SlnO considers that the target prey is the current finest solution or nearer to optimal solution. The sea lions progress in the path of target prey and are expressed as,

$$\vec{S}(g+1) = \vec{Q}(g) - \vec{L}\vec{R} \quad (17)$$

$$\vec{S}(g+1) = \vec{Q}(g) - |2\vec{H}\vec{Q}(g) - \vec{S}(g)|\vec{R} \quad (18)$$

Assume $\vec{Q}(g) > \vec{S}(g)$,

$$\vec{S}(g+1) = \vec{Q}(g) - (2\vec{H}\vec{Q}(g) - \vec{S}(g))\vec{R} \quad (19)$$

$$\vec{S}(g+1) = \vec{Q}(g)(1 - 2\vec{H}\vec{R}) + \vec{S}(g)\vec{R} \quad (20)$$

By combining SlnO with EWMA, the overall algorithmic performance is improved by attaining global best solution. According to (Machaka et al., 2016), the standard equation of EWMA is expressed as,

$$\vec{S}(g)^E = \beta \vec{S}(g) + (1 - \beta) \vec{S}(g-1)^E \quad (21)$$

$$\vec{S}(g) = \frac{\vec{S}(g)^E - (1 - \beta) \vec{S}(g-1)^E}{\beta} \quad (22)$$

By substituting Eq. (22) in Eq. (20), the following equation becomes,

$$\vec{S}(g+1) = \vec{Q}(g)(1 - 2\vec{H}\vec{R}) + \frac{\vec{S}(g)^E - (1 - \beta) \vec{S}(g-1)^E}{\beta} \vec{R} \quad (23)$$

$$\vec{S}(g+1) = \vec{Q}(g)(1 - 2\vec{H}\vec{R}) + \frac{\vec{R}}{\beta} \vec{S}(g)^E - \frac{(1 - \beta)}{\beta} \vec{S}(g-1)\vec{R} \quad (24)$$

where, $(g+1)$ signifies the next iteration, \vec{H} denotes the random vector between the range [0,1], $\vec{Q}(g)$ implies position vector of target prey, $\vec{S}(g)$ signifies position vector of sea lion, \vec{L} specifies the distance between sea lion and target prey, \vec{R} indicates the parameter that linearly reduces from 2 to 0 for all the iterations, β signifies the random vector between the range [0,1], $\vec{S}(g)^E$ indicates the position vector of sea lion from exponential at current iteration, the position vector of sea lion from exponential at iteration $(g-1)$ is represented as $\vec{S}(g-1)^E$, respectively.

Step 4: Vocalization phase

The sea lions cooperate with the remaining sea lions by vocalizations mainly when they chase and hunt as subgroups. Once the prey gets identified by the sea lion, then it calls the remaining members to encircle and attack the prey, which is given as,

$$S_{leader} = |(\vec{I}_1 + (1 + \vec{I}_2)) / \vec{I}_2| \quad (25)$$

where, I_1 signifies speed of sounds in water, I_2 implies speed of sounds in air, and S_{leader} specifies speed of sound of sea lion leader. Consequently, the speed of sound in water is formulated as,

$$\vec{I}_1 = \text{Sin } \theta \quad (26)$$

The speed of sounds in air is formulated as,

$$\vec{I}_2 = \text{Sin } \varphi \quad (27)$$

Step 5: Attacking phase (Exploitation phase)

The two various phases, such as dwindling encircling method and circle updating method are introduced for modeling the hunting characteristics of sea lions.

a) Dwindling encircling strategy

This type of characteristics relies on \vec{R} , that helps the leader of sea lion to travel in the track of prey in order to encircle.

b) Circle updating position strategy

The sea lions hunt bait ball of fishes starting from edges which is given as,

$$\vec{S}(g+1) = |\vec{Q}(g) - \vec{S}(g)| \cdot \text{Cos}(2\pi m) + \vec{Q}(g) \quad (28)$$

Assume $\vec{Q}(g) - \vec{S}(g)$

$$\vec{S}(g+1) = \vec{Q}(g) \cdot \text{Cos}(2\pi m) - \vec{S}(g) \cdot \text{Cos}(2\pi m) + \vec{Q}(g) \quad (29)$$

$$\vec{S}(g+1) = \vec{Q}(g)(1 + \text{Cos}(2\pi m)) - \vec{S}(g) \cdot \text{Cos}(2\pi m) \quad (30)$$

Based on EWMA (Machaka et al., 2016), the update equation is expressed as,

$$\vec{S}(g) = \frac{\vec{S}(g)^E - (1 - \beta)\vec{S}(g-1)^E}{\beta} \quad (31)$$

By substituting Eq. (31) in (30), the equation becomes,

$$\vec{S}(g+1) = \vec{Q}(g)(1 + \text{Cos}(2\pi m)) - \frac{\vec{S}(g)^E - (1 - \beta)\vec{S}(g-1)^E}{\beta} \cdot \text{Cos}(2\pi m) \quad (32)$$

where, the distance among the optimal solution and search agent is denoted as $|\vec{Q}(g) - \vec{S}(g)|$, the absolute value is specified as $||$, m implies the random number within the value $[-1, 1]$, and $\text{Cos}(2\pi m)$ signifies the actions of the sea lions swimming around prey besides the circle shaped part to start hunting.

Step 6: Searching for prey (Exploration phase)

The finest search agent updates the position of sea lions in exploitation stage, whereas the location of search agents is updated with respect to the randomly chosen sea lion which is formulated as,

$$\vec{L} = |2\vec{H} \cdot \vec{S}_{rand}(g) - \vec{S}(g)| \quad (33)$$

where, $\vec{S}_{rand}(g)$ specifies the random sea lion selected from population.

$$\vec{S}(g+1) = \vec{S}_{rand}(g) - \vec{L} \cdot \vec{R} \quad (34)$$

Step 7: Evaluation of solution feasibility

The finest solution is obtained using fitness function such that the best value of fitness is considered as finest solution.

Step 8: Termination

The above illustrated phases are repeated until the finest solution is achieved. Table 1 portrays the pseudo code of devised ExpSLO.

4. Results and discussion

This section illustrates the experimental assessment of the designed RV coefficient+ExpSLO-based DRN approach based on the evaluation measures, namely precision, recall, and F-measure.

4.1. Experimental setup

The execution of the devised RV coefficient+ExpSLO-enabled DRN technique is done in Matlab tool with PC having Intel i3 core processor, Windows 10 OS, and 2GB RAM.

Table 1
Pseudo code of devised ExpSLO.

1	Input: Solution set S , maximal iterations g_{max}
2	Output: Optimal solution $\vec{S}(g+1)$
3	Begin
4	Initialize the solution
5	Choose $\vec{S}_{rand}(g)$
6	Calculate fitness for all search agent by Eq. (16)
7	\vec{S}^* defines candidate search agent with best fitness
8	If $g < g_{max}$
9	Calculate \vec{S}_{leader} by Eq. (25)
10	If ($\vec{S}_{leader} < 0.25$)
11	If ($ \vec{R} < 1$)
12	Update the location of present search agent using Eq. (32)
13	else
14	Choose random search agents $\vec{S}_{rand}(g)$
15	Update the location of current search agent using Eq. (17)
16	End if
17	Update the location of current search agent using Eq. (34)
18	End if
19	If search agent does not belong to any of the \vec{S}_{leader}
20	Go to step 9
21	Else
22	Calculate fitness function for each search agent using Eq. (16)
23	Update \vec{S}^* , if best solution exists
24	Return \vec{S}^*
25	End if
26	End if
27	End

4.2. Dataset description

The developed RV coefficient+ExpSLO-based DRN approach for the intrusion detection is performed using Message Queuing Telemetry Transport-Internet of Things-Intrusion Detection System (MQTT-IoT-IDS2020) (dataset-1) (MQTT 2021), and Apache Web Server dataset (dataset-2) (Apache web server 2021).

4.2.1. Dataset-1

This dataset (MQTT 2021) is created by the simulation of MQTT network model. The network consists of a simulated camera, a broker, twelve sensors, and an attacker. Each file contains five different recorded scenarios of network, namely ordinary process, aggressive scan, User Datagram Protocol (UDP) scan, MQTT brute-force attack, and Sparta secure shell (SSH) brute-force. In addition, extraction of various significant features is done once raw pcap files are saved. Moreover, three feature abstraction levels such as packet features, unidirectional and bidirectional flow features are extracted from raw pcap files. Besides, the csv files are more suitable for machine learning (ML) practice, whereas the raw pcap files are suitable for the assessment of MQTT IoT communication and attacks associated with it.

4.2.2. Dataset-2

This dataset (Apache web server 2021) is collected from apache access log server. It comprise of date time, request, IP address, gmt, user agent, size, country, status, and label. This dataset shows the malicious activities present in request, IP address, request, and so on.

4.3. Performance metrics

The assessment of the devised technique is done using the performance measures given below:

Precision: It is a metric which defines the proportion of true positives to all positives, and the equation is expressed as,

$$\kappa = \frac{L}{L+M} \quad (35)$$

where, κ denotes the precision, L signifies true positives, and M denotes the false positives.

Recall: It specifies the proportion of true positives to the overall true positives and false negatives and the equation is formulated as,

$$\alpha = \frac{L}{L + N} \quad (36)$$

where, α signifies precision measure, and N represents the false negatives.

F-measure: It is used for determining mean difference among precision and recall measure, which is expressed as,

$$\xi = 2 * \left(\frac{\kappa * \alpha}{\kappa + \alpha} \right) \quad (37)$$

where, ξ denotes F-measure.

4.4. Comparative methods

The various methods taken for the assessment are Deep Learning (Haggag et al., 2020), CNN+LSTM (Hassan et al., 2020), CNN+RNN (Zhong et al., 2020), LSTM (Gao et al., 2020), Self-taught Learning (STL) (Gurung et al., 2019), Double PSO (Elmasry et al., 2020), and proposed RV coefficient+ExpSLO-based DRN approach.

4.5. Comparative assessment

The comparative assessment of the devised method is done with respect to dataset-1 and dataset-2 using the metrics, like precision, recall, and F-measure using training data percentage.

a) Assessment based on with attacks using dataset-1

Fig. 3 represents the assessment with respect to with attacks using dataset-1. The assessment using precision is portrayed in Fig. 3a). For the 50% of training data, the devised ExpSLO attained a precision value of 0.807, while the precision achieved by the existing techniques, like Deep learning is 0.677, CNN+LSTM is 0.717, CNN+RNN is 0.729, LSTM is 0.691, STL is 0.752, and Double PSO is 0.769. The performance enhancement computed by the devised ExpSLO technique in comparison with the existing approaches is 16.131%, 11.179%, 9.631%, 14.410%, 6.88%, and 4.67%. The analysis using recall measure is shown in Fig. 3b). The recall value measured by the Deep learning is 0.691, CNN+LSTM is 0.717, CNN+RNN is 0.730, LSTM is 0.705, STL is 0.732, Double PSO is 0.750, and developed ExpSLO is 0.787 for 60% of training data. The performance enhancement achieved by the devised technique in comparison with the existing approaches is 12.218%, 8.909%, 7.284%, 10.459%, 7.056%, and 4.797%. The assessment using F-measure is portrayed in Fig. 3c). For the 70% of training data, the value of F-measure obtained by the Deep learning, CNN+LSTM, CNN+RNN, LSTM, STL, Double PSO, and developed ExpSLO is 0.717, 0.731, 0.760, 0.731, 0.778, 0.796, and 0.834. The performance improvement computed by the devised approach when compared with the existing methods is 13.953%, 12.269%, 8.812%, 12.381%, 6.66%, and 4.53%.

b) Assessment based on without attacks using dataset-1

The assessment based on without attacks using dataset-1 is illustrated in Fig. 4. The assessment in terms of precision is shown in Fig. 4a). The developed ExpSLO measured a precision of 0.847, while the precision value achieved by the existing techniques like Deep learning is 0.756, CNN+LSTM is 0.791, CNN+RNN is 0.812, LSTM is 0.778, STL is 0.783, and Double PSO is 0.800, for 50% of training data. The performance achievement measured by the devised technique in comparison with the existing techniques is 10.805%, 6.688%, 4.137%, 8.222%, 6.629%, and 4.507% Fig. 4.b) presents the assessment with respect to recall measure. When the training data is 60%, the value of recall measured by the Deep learning is 0.766, CNN+LSTM is 0.806, CNN+RNN is 0.826, LSTM is 0.772, STL is 0.793, Double PSO is 0.810, and developed ExpSLO is

0.847. The performance gain computed by the devised technique in comparison with the existing approaches is 9.625%, 4.907%, 2.536%, 8.823%, 6.551%, and 4.454%. The F-measure analysis is portrayed in Fig. 4c). For the 70% of training data, the F-measure value attained by the existing techniques, like Deep learning is 0.768, CNN+LSTM is 0.812, CNN+RNN is 0.831, LSTM is 0.791, STL is 0.794, and Double PSO is 0.812, while the developed ExpSLO computed an F-measure of 0.857. The performance gain computed by the devised technique in comparison with the existing techniques is 10.363%, 5.259%, 3.021%, 7.779%, 6.652%, and 4.448%.

c) Assessment in terms of with attacks using dataset-2

The assessment based on with attacks using dataset-2 is illustrated in Fig. 5. The precision analysis is depicted in Fig. 5a). The designed ExpSLO measured a precision value of 0.838, whereas the precision computed by the existing techniques like Deep learning is 0.732, CNN+LSTM is 0.771, CNN+RNN is 0.791, LSTM is 0.746, STL is 0.792, and Double PSO is 0.809 for training data value 50%. The performance improvement measured by devised approach in comparison with the existing approaches is 12.699%, 8.046%, 5.675%, 10.958%, 6.558%, and 4.459%. The analysis in terms of recall measure is portrayed in Fig. 5b). For the 60% of training data, the value of recall obtained by the Deep learning is 0.732, CNN+LSTM is 0.778, CNN+RNN is 0.798, LSTM is 0.756, STL is 0.792, Double PSO is 0.809 and developed ExpSLO is 0.848. The performance gain calculated by the designed technique in comparison with the existing techniques is 13.728%, 8.234%, 5.891%, 10.864%, 6.558%, and 4.459%. The F-measure analysis is shown in Fig. 5c). For the training data 70%, the F-measure computed by the existing methods, namely Deep learning is 0.734, CNN+LSTM is 0.787, CNN+RNN is 0.807, LSTM is 0.761, STL is 0.802, and Double PSO is 0.820 while the developed ExpSLO obtained an F-measure value of 0.849. The performance gain computed by the designed method in comparison with the existing methods is 13.542%, 7.291%, 4.952%, 10.447%, 6.481%, and 4.406%.

d) Assessment based on without attacks using dataset-2

Fig. 6 presents assessment considering without attacks using dataset-2. The analysis using precision is presented in Fig. 6a). When the training data is 50%, the value of precision obtained by the devised ExpSLO is 0.841, whereas the value of precision achieved by the existing approaches, like Deep learning is 0.723, CNN+LSTM is 0.748, CNN+RNN is 0.775, LSTM is 0.756, STL is 0.785, Double PSO is 0.803. The performance gain attained by the proposed technique in comparison with the existing approaches is 13.935%, 10.974%, 7.776%, 10.023%, 6.61%, and 4.494% Fig. 6.b) presents the analysis using recall measure. When considering 60% of training data, the value of recall achieved by the Deep learning is 0.753, CNN+LSTM is 0.784, CNN+RNN is 0.796, LSTM is 0.774, STL is 0.802, Double PSO is 0.819 and developed ExpSLO is 0.857. The performance increase computed by the devised technique by the comparison with the existing techniques is 12.173%, 8.535%, 7.112%, 9.712%, 6.482%, and 4.407%. The assessment using F-measure is presented in Fig. 6c). When considering training data 70%, the value of F-measure achieved by the Deep learning, CNN+LSTM, CNN+RNN, LSTM, STL, Double PSO and developed ExpSLO is 0.782, 0.802, 0.809, 0.802, 0.800, 0.818, and 0.856. The performance increase attained by the devised technique in comparison with the existing methods is 12.173%, 8.535%, 7.112%, 9.712%, 6.491%, and 4.413%.

4.6. Comparative discussion

Table 2 explains the comparative assessment of the proposed technique in comparison with the various existing approaches, namely Deep learning, CNN+LSTM, CNN+RNN, LSTM, and RV coefficient+ExpSLO-based DRN approach for the training data 90% using dataset-1 and dataset-2.

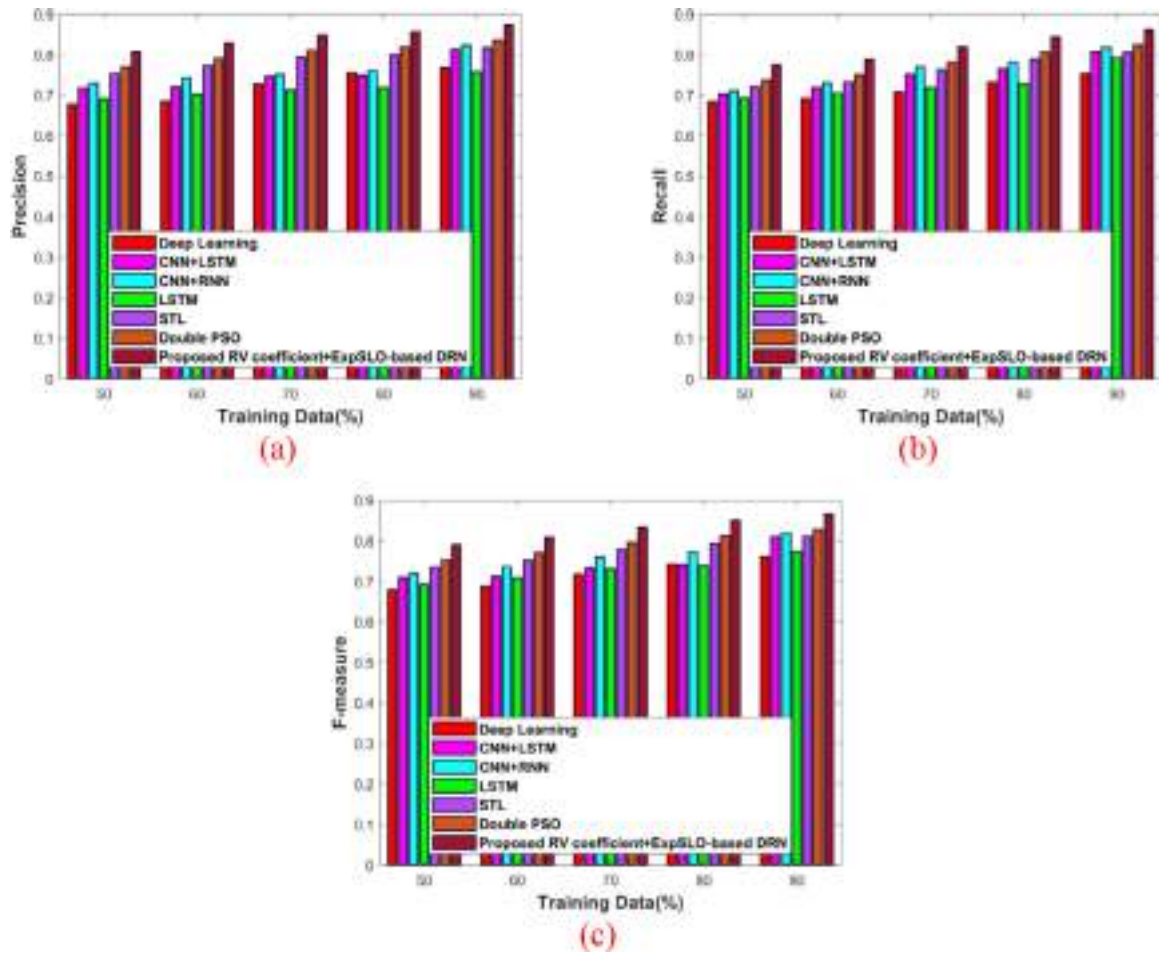


Fig. 3. Assessment based on with attacks using dataset-1 a) Precision, b) Recall, and c) F-measure.

Table 2
Comparative discussion of the developed technique.

	Metrics	Deep Learning	CNN+LSTM	CNN+RNN	LSTM	STL	Double PSO	Proposed RV coefficient+ExpSLO-based DRN
Dataset-1								
With attacks	Precision	0.7680	0.8133	0.8233	0.7574	0.8169	0.8347	0.8725
	Recall	0.7530	0.8083	0.8177	0.7919	0.8062	0.8240	0.8618
	F-measure	0.7605	0.8108	0.8205	0.7742	0.8115	0.8293	0.8671
Without attacks	Precision	0.7821	0.8258	0.8521	0.8065	0.8078	0.8256	0.8690
	Recall	0.7961	0.8310	0.8561	0.8086	0.8063	0.8241	0.8721
	F-measure	0.7890	0.8284	0.8541	0.8075	0.8070	0.8248	0.8705
Dataset-2								
With attacks	Precision	0.7461	0.8064	0.8263	0.7721	0.8134	0.8312	0.8634
	Recall	0.7507	0.8078	0.8277	0.7763	0.8165	0.8343	0.8619
	F-measure	0.7484	0.8071	0.8270	0.7742	0.8149	0.8327	0.8626
Without attacks	Precision	0.8087	0.8298	0.8596	0.8211	0.8244	0.8422	0.8800
	Recall	0.8132	0.8343	0.8618	0.8256	0.8289	0.8467	0.8845
	F-measure	0.8109	0.8320	0.8607	0.8233	0.8266	0.8444	0.8822

The precision value achieved by the Deep learning approach is 0.7680, CNN+LSTM is 0.8133, CNN+RNN is 0.8233, LSTM is 0.7574, STL is 0.8169, Double PSO is 0.8347 and proposed RV coefficient+ExpSLO-enabled DRN is 0.8725. The recall computed by the devised RV coefficient+ExpSLO-based DRN approach is 0.8619, whereas the recall achieved by the various existing methods, like Deep learning is 0.7507, CNN+LSTM is 0.8078, CNN+RNN is 0.8277,

LSTM is 0.7763, STL is 0.8062, and Double PSO is 0.8240. The developed RV coefficient+ExpSLO-enabled DRN achieved a F-measure of 0.8671, while the various existing methods, like Deep learning, CNN+LSTM, CNN+RNN, LSTM, STL, and Double PSO obtained an F-measure of 0.7605, 0.8108, 0.8205, 0.7742, 0.8115, and 0.8293.

The precision value attained by the developed RV coefficient+ExpSLO-enabled DRN approach is 0.8800, whereas

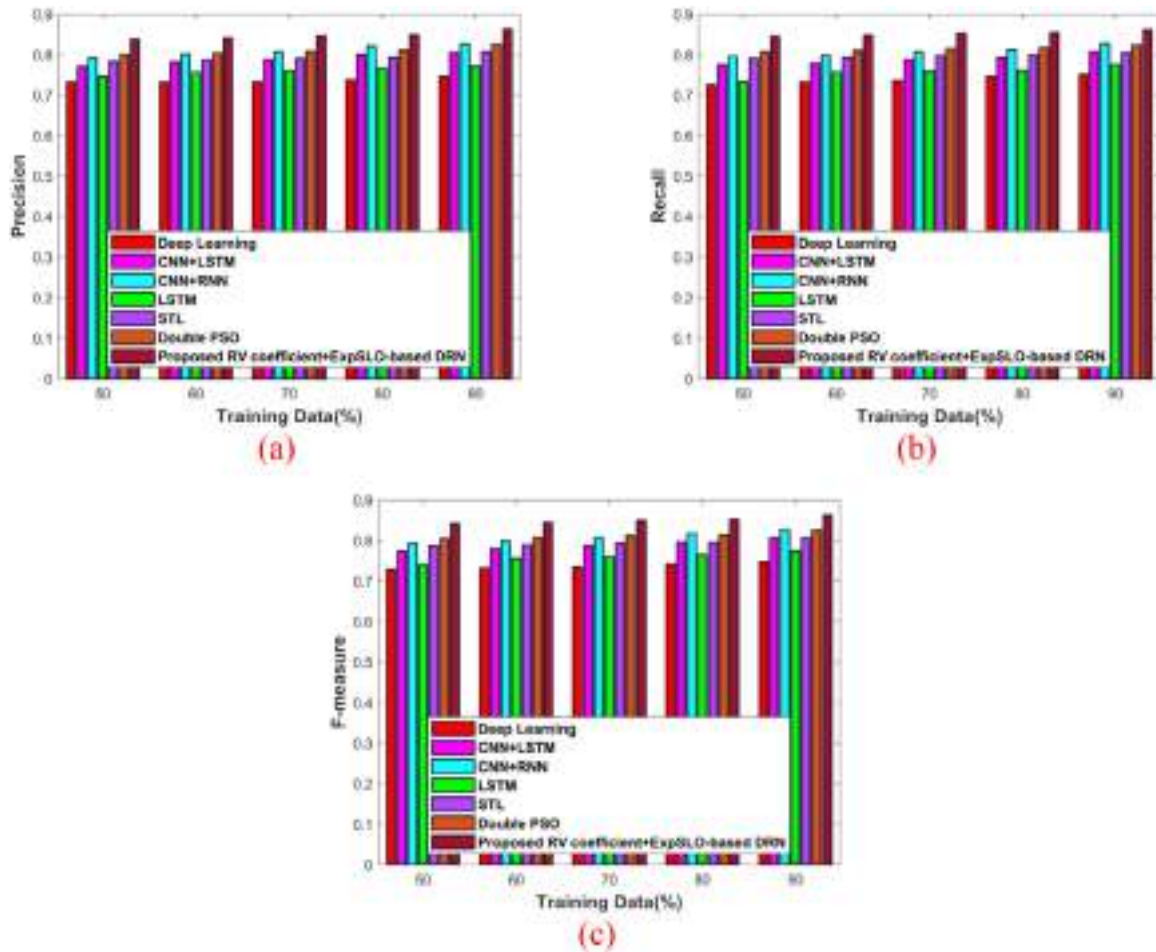


Fig. 4. Assessment based on without attacks considering dataset-1 a) Precision, b) Recall, and c) F-measure.

Table 3 Security analysis of the developed technique.

Security Issues	Deep Learning	CNN+LSTM	CNN+RNN	LSTM	STL	Double PSO	Proposed method
Provides mutual authentication	Yes	Yes	Yes	Yes	Yes	Yes	Yes
Provides multi-level authentication	Yes	Yes	Yes	Yes	Yes	Yes	Yes
Requires identity-verification table	Yes	Yes	Yes	Yes	Yes	Yes	Yes
Server spoofing attack resistance	Yes	Yes	Yes	Yes	Yes	Yes	Yes
Stolen verifier attack resistance	No	Yes	Yes	Yes	Yes	Yes	Yes
Privileged insider attack resistance	Yes	Yes	Yes	Yes	Yes	Yes	Yes
Password guessing attack resistance	Yes	Yes	Yes	Yes	Yes	Yes	Yes
Provides strong user anonymity	Yes	Yes	Yes	Yes	Yes	Yes	Yes
Known session-specific temporary information attack resistance	No	Yes	Yes	Yes	Yes	Yes	Yes
Impersonation attack resistance	Yes	Yes	No	No	Yes	No	Yes
Reply attack resistance	Yes	Yes	Yes	Yes	Yes	Yes	Yes
Man-in-the-middle attack resistance	Yes	Yes	Yes	Yes	Yes	Yes	Yes
Provision for revocation and re-registration	Yes	Yes	Yes	Yes	Yes	Yes	Yes
Free from denial of service attack	No	Yes	Yes	Yes	Yes	Yes	Yes
Profile table-stolen resistance	No	No	Yes	Yes	No	Yes	Yes
Free from Zero-Day Attacks	No	Yes	No	Yes	Yes	No	Yes
Key resilience	No	No	No	No	No	No	Yes
Reconnaissance attack resistance	No	No	No	No	No	No	Yes
Free from theft attack	No	No	No	No	No	No	Yes

the value of precision achieved by the various existing approaches, namely Deep learning is 0.8087, CNN+LSTM is 0.8298, CNN+RNN is 0.8596, LSTM is 0.8211, STL is 0.8244, and Double PSO is 0.8422. The value of recall computed by the Deep learning approach is 0.8132, CNN+LSTM is 0.8343, CNN+RNN is 0.8618, LSTM is

0.8256, STL is 0.8289, and Double PSO is 0.8467 and proposed RV coefficient+ExpSLO-enabled DRN is 0.8845. The devised RV coefficient+ExpSLO-enabled DRN measured an F-measure of 0.8822, while the different existing techniques, like Deep learning,

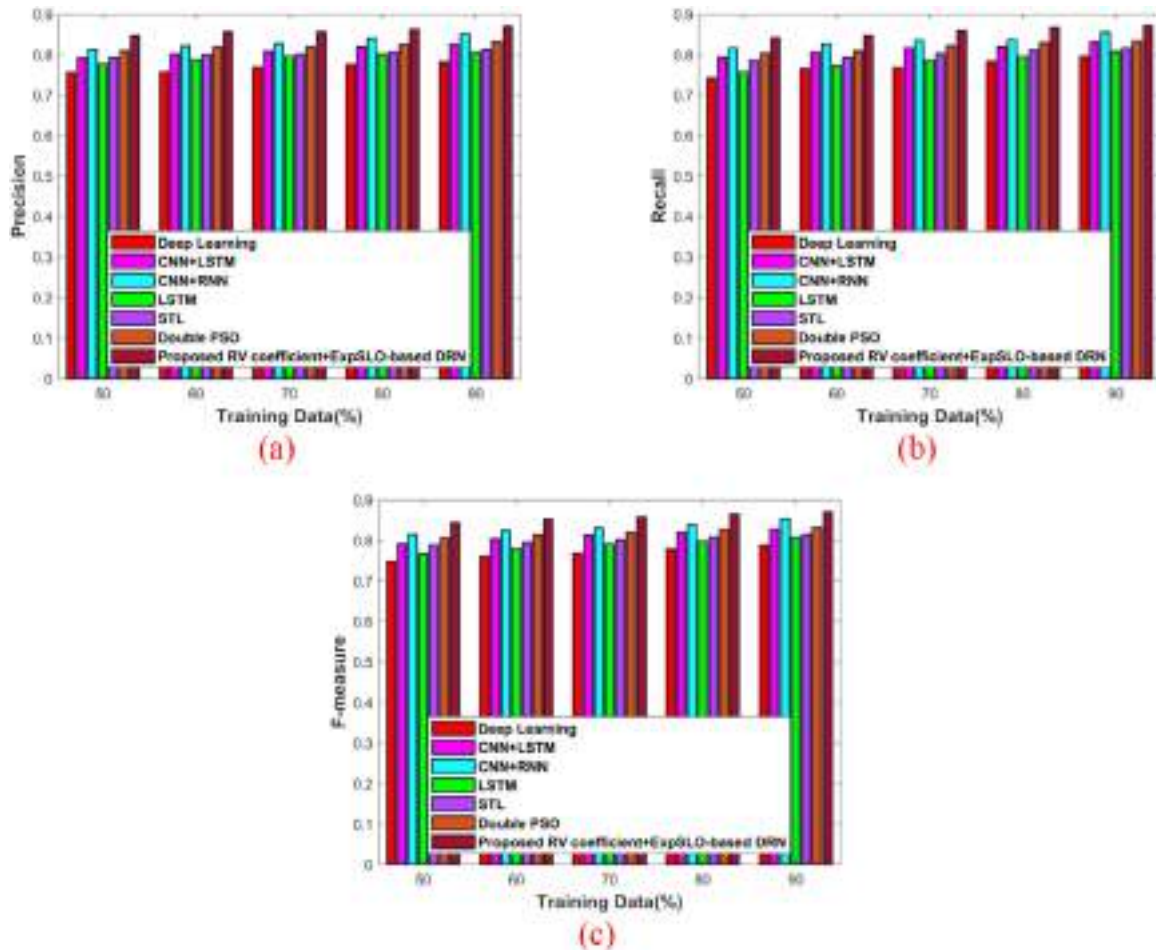


Fig. 5. Assessment with respect to with attacks considering dataset-2 a) Precision, b) Recall, and c) F-measure.

CNN+LSTM, CNN+RNN, LSTM, STL, and Double PSO computed an F-measure of 0.8109, 0.8320, 0.8607, 0.8233, 0.8266, and 0.8444.

Thus from the above table, it is clearly shown that the developed technique attained a maximum precision of 0.8725, maximum recall of 0.8619, and maximum F-measure of 0.8671 using with attacks, whereas the developed approach computed a highest precision of 0.8800, highest recall of 0.8845, and highest F-measure of 0.8822, using without attacks respectively.

4.8. Security analysis

Table 3 shows the security analysis of the developed technique with the existing methods, such as Deep Learning, CNN+LSTM, CNN+RNN, LSTM, STL, and Double PSO. The analysis is achieved with respect to the numerous attacks and the implemented method is able to provide resistance to numerous network attacks.

5. Conclusion

This research presents a robust approach for detecting the intrusions using RV coefficient+ExpSLO-based DRN approach with spark architecture. Here, the feature selection and the data augmentation process are performed in slave nodes, while the intrusion detection process is performed at the master nodes. The proposed RV coefficient based hybrid feature fusion is accomplished for selecting the unique features, and then the data augmentation process is carried out for enhancing the data dimensions. In addition, the data augmented result is fed to the master node where the intrusion detection process is performed using DRN classifier.

However, the proposed ExpSLO designed by the combination of EWMA and SLnO is used for training the DRN classifier. The performance of the devised technique is analyzed using the evaluation measures, namely precision, recall, and F-measure. The developed RV coefficient+ExpSLO-based DRN technique outperformed different existing intrusion detection approaches in big data with the maximum precision of 0.8800, maximum recall of 0.8845, and maximum F-measure of 0.8822. However, the implemented approach is not applied for the network traffic identification in the big data environments and we will consider this in our future work. Also, the performance will be enhanced by combining different deep learning networks and presented using the case study.

Declaration of competing interest

The authors declare that they have no known competing financial interests or personal relationships that could have appeared to influence the work reported in this paper.

CRediT authorship contribution statement

Ramkumar M.P.: Conceptualization, Methodology, Software, Data curation, Writing – original draft, Writing – review & editing, Visualization, Investigation, Software, Validation. **P.V. Bhaskar Reddy:** Visualization, Investigation, Software, Validation. **J.T. Thirukrishna:** Visualization, Investigation, Software, Validation, Supervision. **Ch. Vidyadhari:** Supervision.

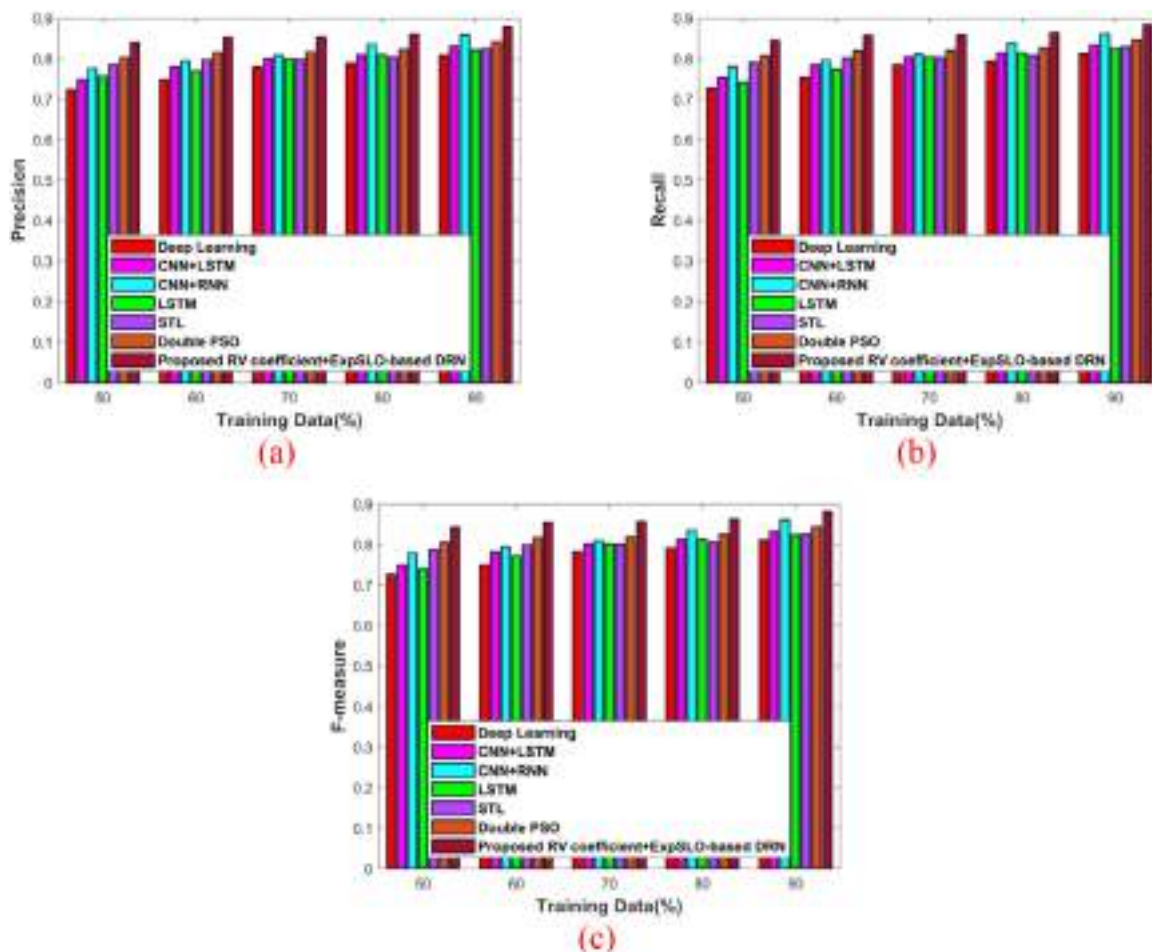


Fig. 6. Assessment based on without attacks using dataset-2 a) Precision, b) Recall, and c) F-measure.

References

Apache web server - access log pre-processing for web intrusion detection dataset will be taken from, "https://iee-dataport.org/open-access/apache-web-server-access-log-pre-processing-web-intrusion-detection", accessed on July 2021.

Chen, Z., Chen, Y., Wu, L., Cheng, S., Lin, P., 2019. Deep residual network based fault detection and diagnosis of photovoltaic arrays using current-voltage curves and ambient conditions. *Energy Convers. Manage.* 198, 111793.

Chandola, V., Banerjee, A., Kumar, V., 2009. Anomaly detection: a survey. *ACM Comput. Surv. (CSUR)* 41 (3), 1–58.

Di Pietro, R., Mancini, L.V., 2008. "Intrusion Detection Systems", 38. Springer Science & Business Media.

Elmasry, W., Akbulut, A., Zaim, A.H., 2020. Evolving deep learning architectures for network intrusion detection using a double PSO metaheuristic. *Comput. Netw.* 168, 107042.

Faker, O., Dogdu, E., 2019. Intrusion detection using big data and deep learning techniques. In: *InProceedings of the 2019 ACM Southeast Conference*, pp. 86–93 April.

Gurung, S., Ghose, M.K., Subedi, A., 2019. Deep learning approach on network intrusion detection system using NSL-KDD dataset. *Int. J. Comput. Netw. Inf. Secur.* 11 (3), 8–14.

Gao, J., Gan, L., Buschendorf, F., Zhang, L., Liu, H., Li, P., Dong, X., Lu, T., 2020. Omni SCADA intrusion detection using deep learning algorithms. *IEEE Internet Things J.* 8 (2), 951–961.

Haggag, M., Tantawy, M.M., El-Soudani, M.M., 2020. Implementing a deep learning model for intrusion detection on apache spark platform. *IEEE Access* 8, 163660–163672 August.

Hassan, M.M., Gumaei, A., Alsanad, A., Alrubaiyan, M., Fortino, G., 2020. A hybrid deep learning model for efficient intrusion detection in big data environment. *Inf. Sci. (Ny)* 513, 386–396 March.

Hochreiter, S., Schmidhuber, J., 1997. Long short-term memory. *Neural. Comput.* 9 (8), 1735–1780 November.

Jadhav, Amolkumar Narayan, N, Gomathi, 2019. DIGWO: hybridization of dragonfly algorithm with improved grey wolf optimization algorithm for data clustering. *Multimedia Res.* 2 (3).

Karatas, G., Demir, O., Sahingoz, O.K., 2018. Deep learning in intrusion detection systems. In: *proceedings of 2018 International Congress on Big Data, Deep Learning and Fighting Cyber Terrorism (IBIGDELFT)*, pp. 113–116.

Kohavi, R., John, G.H., 1997. Wrappers for feature subset selection. *Artif. Intell.* 97 (1–2), 273–324.

Khan, F.A., Gumaei, A., Derhab, A., Hussain, A., 2019. A novel two-stage deep learning model for efficient network intrusion detection. *IEEE Access* 7, 30373–30385 February.

Khan, F.A., Gumaei, A., 2019. A comparative study of machine learning classifiers for network intrusion detection. In: *Proceedings of International Conference on Artificial Intelligence and Security*, pp. 75–86 July.

Liu, Z., Su, N., Qin, Y., Lu, J. and Li, X., "A deep random forest model on spark for network intrusion detection", *Mobile Inf. Syst.*, 2020.

Mishra, P., Pilli, E.S., Varadharajan, V., Tupakula, U., 2017. Intrusion detection techniques in cloud environment: a survey. *J. Netw. Comput. Appl.* 77, 18–47 January.

Mighan, Soosan Naderi, Kahan, Mohsen, 2021. A novel scalable intrusion detection system based on deep learning. *Int. J. Inf. Secur.* 20 (387–403) .

MQTT Internet of things intrusion detection dataset taken from, "https://iee-dataport.org/open-access/mqtt-iot-ids2020-mqtt-internet-things-intrusion-detection-dataset", accessed on July 2021.

Masadeh, R., Mahafzah, B.A., Shariieh, A., 2019. Sea lion optimization algorithm. *Sea* 10 (5).

Machaka, P., Bagula, A., Nelwamondo, F., 2016. Using exponentially weighted moving average algorithm to defend against DDoS attacks. In: *proceedings of 2016 Pattern recognition association of South Africa and robotics and mechatronics international conference (PRASA-RobMech)*, pp. 1–6 November.

Prasanalakshmi, B., Kannammal, A., Sridevi, R., 2011. Frequency domain combination for preserving data in space specified token with high security. In: *the proceeding of International Conference on Informatics Engineering and Information Science*. Springer, Berlin, Heidelberg, pp. 319–330.

Suthaharan, S., 2014. Big data classification: problems and challenges in network intrusion prediction with machine learning. *ACM SIGMETRICS Perform. Evaluat. Rev.* 41 (4), 70–73.

Sadanand Sayyanavar, Amit, Ghorpade, Vijay Ram, 2019. Application Checkpointing technique for self-healing from failures in mobile grid computing. *Int. J. Grid High Perform. Comput. (IJGHPC)* 11 (2), 50–62.

Sinjari, Bruna, Feragalli, Beatrice, Cornelli, Umberto, Belcaro, Giovanni, Vita-colonna, Ester, Santilli, Manlio, Rexhepi, Imena, D'Addazio, Gianmaria, Zuc-

cari, Francesca, Caputi, Sergio, 2020. Artificial saliva in diabetic Xerostomia (AS-DIX): double blind trial of Aldiamed® versus placebo. *J. Clin. Med.* 9 (7), 1–12.

Veeraiah, Neenavath, Krishna, Dr.B.T., 2018. Intrusion detection based on piecewise Fuzzy C-Means clustering and fuzzy naive bayes rule. *Multimedia Res.* 1 (1), 27–32.

Zhong, W., Yu, N., Ai, C., 2020. Applying big data based deep learning system to intrusion detection. *Big Data Min. Anal.* 3 (3), 181–195.

Zikopoulos, P., Eaton, C., 2011. Understanding Big data: Analytics for Enterprise Class Hadoop and Streaming Data. McGraw-Hill Osborne Media.

Zhang, P., Tan, Y., 2013. Class-wise information gain. In: proceedings of third International Conference on Information Science and Technology (ICIST), pp. 972–978 March.



Ramkumar, M.P. received his B.E. degree in Computer Science and Engineering from Manonmaniam Sundaranar University, Tirunelveli in 2000, M.E. degree in Computer Science and Engineering from Anna University, Chennai during 2004 and completed Ph.D. degree in Information and Communication Engineering, Anna University. Currently working as an Asst. Professor in Thiagarajar College of Engineering, Madurai. His research areas of interest are Data Management and Computer Networks.



P.V. Bhaskar Reddy working as a Professor in School of Computer Science and Engineering at REVA UNIVERSITY, Bangalore. He obtained his Doctorate (Ph. D) degree in Computer Science & Engineering department at Sri Venkateshwara University, Tirupati, Andhra Pradesh India in 2016. He has 15 years of experience in teaching under various colleges and Universities. He has published more than 25 papers in international level Journals and Conferences. He has published 5 patents in various domains. He is thereviewer for various National and International Journals. He is a Life member of Computer Society of India (CSI), Fellow of the Institution of Engineers (FIE) and Member of IEEE and ACM. His major fields of

interests are in image retrieval, Computer networks, Sentiment Analysis and Data mining.



J.T. Thirukrishna received the M.E. degree in Computer Science and Engineering (First Class with Distinction) from Sona College of Technology, Salem, Tamil Nadu, India in 2010 and the Ph.D. degree in Information Communication and Engineering (CSE) at Anna University, Chennai, Tamil Nadu, India. Since 2020, he has been an Associate Professor with the Information Science and Engineering Department, Dayananda Sagar Institutions, Bangalore, India. He is the author of more than 15 articles, patent and book. His research interests include Wireless Sensor Networks, Data Science and Artificial Intelligence. He is a Journal Reviewer of SCI/SCIE/Web of Science/Scopus indexed Journals. He has applied many funding proposals to DST, CSIR, VGST and AICTE etc. Dr. J.T. Thirukrishna was a recipient of “Award of Excellence in Research Award 2020-2021 from Novel Research Academy and Global Teacher Award 2019 for Excellence, and the Senior member of IEEE, Life Member of ISTE and Cryptology Research Society of India. Completed global certification in Palo Alto Cyber Security Certified Trainer (PCCET).



Ch. Vidyadhari currently working as an Assistant Professor at Gokaraju Rangaraju Institute of Engineering and Technology, Hyderabad. I have completed B.Tech from BPUT in 2004. She has completed M.Tech (Software Engineering) from Aurora's Engineering college, Hyderabad in the year 2008 and pursuing Ph.D in Computer Science and Engineering from JNTU college of Engineering, Kakinada. I have an experience of 14 years in teaching. Her research area is Data Mining, Web Mining, Big Data Analysts, Social Networking. Dedicated, resourceful and goal-driven professional educator with a solid commitment to the social and academic growth and development of every Student. She has published papers in international conferences and journals and certified as an Oracle Certified Java Standard Edition 6 Programmer (OCJP) and Oracle Certified Associate. She had actively engaged in Create strong network with the Alumni and ensure that all stake holders are benefited, enhance endowment fund of GRIET through donations from alumni and well-wishers and assist management in its effective utilization and guided P.G and U.G. student projects.

Rice Plant Disease Detection Using Sensing Recognition Strategy Based on Artificial Intelligence

T. Daniya^{1,*}, Ch. Vidyadhari² and Srilakshmi Aluri²

¹*Department of Information Technology, GMR Institute of Technology, Rajam, Andhra Pradesh, India*

²*Department of Information Technology, Gokaraju Rangaraju Institute of Engineering and Technology, Hyderabad, Telangana, India*
E-mail: daniya.t@gmrit.edu.in; chalasanividyardhari@gmail.com; alurisrilaxmi@gmail.com

**Corresponding Author*

Received 14 July 2021; Accepted 11 September 2021;
Publication XX XXXXXX XXXX

Abstract

In current history rice infections have often appeared, causing severe destruction of rice cultivation. As one of the top ten countries that creates and destroys the world, India relies heavily on rice for its economy and to meet its food needs. To ensure the sound and legal growth of rice crops it is important to identify any diseases in the schedule and to pre-apply the expected treatment to the affected plants. Since the detection of disease is time-consuming and labor-intensive, it is certainly wise to have a system with robots. Infection of rice crops is considered to be a growing factor behind the horticultural, financial and general situation in the future development of the rural field. However, leaf scald and eyespot are the pivotal trouble in paddy fields. Hence, to conquer these issues a novel Sensing Recognition Strategy has been proposed. In Proposed method, optical sensors identify identification of disease and Enhanced Grasshopper Detection Algorithm utilizing the grasshoppers' forces, path and position carries out detection.

Journal of Mobile Multimedia, Vol. 18.3, 1–18.

doi: 10.13052/jmm1550-4646.18311

© 2022 River Publishers

The accuracy of the suggested framework is to attain 97.94% with healthy rice crops.

Keywords: Rice plant disease, grasshopper, sensing recognition strategy, artificial intelligence.

1 Introduction

Rice, (*Oryza sativa*), an eatable oat and grass plant (Poaceae family) is created. About a large portion of the total populace, including practically the entirety of East and Southeast Asia, depend altogether on rice as a staple food; About 95% of the world's rice crop is devoured by people. Rice is bubbled, or it tends to be ground into flour. It is eaten alone and has a wide assortment of soups, side dishes, and primary dishes in Asia, the Middle East, and numerous different plans. Different items incorporate rice for breakfast grains, noodles, and cocktails like Japan. Rice is the staple food of a great many people on the planet today. Without rice is the most significant of the numerous illnesses that plague rice. It is found any place rice is developed, it is consistently significant, and it is consistently hazardous.

The disappointment of the entire rice crop is straightforwardly brought about by illnesses brought about by rice. The test for research keeps on being to deliver great food, with consistently expanding costs and minimal expense, which is all an indefensible and constant microorganism. All examination strategies and procedures for the treatment of plant illnesses created by research have been brought into the blast of rice, however they have normally had restricted achievement. The rice blast has never been killed from the rice-developing area, and a solitary change in rice development or hereditary obstruction can prompt huge infection misfortunes even following quite a while of effective administration.

This infection is an illustration of the reality, nonattendance, and life span of other plant sicknesses. The rice blast has been broadly concentrated all throughout the planet. Numerous specialists have accepted it to act as an illustration of examining hereditary qualities, the study of disease transmission, parasitic cell pathology and science. Ongoing advances in understanding the qualities that control the mix of avirulence (obstruction) and harmfulness (vulnerability) have been made through the blast of rice, and each progression has assisted us with seeing how other plant illnesses work. Note that all genome of rice impact growth and rice are followed and that *M. oryzae* is the

main pathogenic organism to develop its genome and be delivered to people in general.

Rice is a key foodstuff that devoured huge numbers of people. The rice fields are harmed every year by several parasites and illnesses, which are of considerable importance to the farming if they are not properly monitored and handled [1]. In order to properly mitigate illnesses, on-going surveillance and diagnosis are therefore needed. Illnesses can have a serious impact the growth without prompt action. The computerized diagnosis of plant illness is thus an important issue for Agro-informatics [2]. Plant health during the past several years has therefore been an interesting research topic concentrating on the management of illness and the manipulate of the proportion of pesticide to be addressed [3].

Many diseases are frequently tracked during crop development, including rice blasting, sheathing, spotting in the leaf, rice curling, bacterial leaf blight, and bacterial strain infections. Numerous diseases occur in all rice components, including leaves, neck and ears [4]. During the previous two centuries there have been a lot of attempts to diagnosis diseases with leaf pictures of various crops. Some researchers are striving to establish a high categorization of healthy and unhealthy plant image processing algorithms in this domain [5]. Hence, the critical challenges in rice plant disease are leaf scald and eyespot provoke considerable sterility, flower deformation and discoloration. Therefore, to vanquish these illnesses an innovative methodology has to developed. The IoT [21] is the major application for plant monitoring system for identification of diseases in the plants.

The configuration of the article is Ordered as Section 2 decipher the literature survey of Previous methods Section 3 portrays the Proposed Methodology to detect the disease Section 4 designates the results and Section 5 narrates the conclusion.

2 Literature Survey

Chen et al. [6] proposed the Bacterial Leaf Streak (BLS) Net method to detect the BLS leaf lesion recognition and segmentation for rice plant leaves. The accuracy of the proposed method achieved 98.2%. Senan et al. [7] introduced the Convolutional Neural Network (CNN) technique to classify and detect the paddy disease as well as accuracy attained 93.60%. Chen et al. [8] proposed that Rice talk project with innovative spore germination mechanism based on IoT devices to recognize the rice blast disease. The Rice talk prediction achieved the accuracy 89.4%. Sethy et al. [9] proposed

Fuzzy Logic with K Means Segmentation technique to estimate the severity in leaves as well as to detect the disease in rice crops then accuracy reached upto 86.35%. Matin et al. [10] proposed that Alexnet framework to discern the bacterial blight, brown spot and leaf smut. This framework was unique classification mechanism based on deep learning and achieved high accuracy as 99%.

In [6] cannot determine the leaf scald disease in rice plant also [7] not utilized the entropy and gain parameters for studying high order features from paddy photographs. Similarly [8] barometric pressure of multiple location in paddy fields are not investigated. In [9] more diseases and large dataset in rice plant cannot be studied and [10] has context of accuracy and processing time is still not having an opportunity to use K means clustering. Hence to tackle these difficulties a novel framework has to be proposed.

This paper audits practically all papers somewhere in the range of 2007 and 2018. This exploration helps the specialist in social occasion data on paddy shortcoming according to their development. Likewise, this paper gives a concise outline of pre-handling, grouping, include evacuation, determination of characterization methods and strategies. Different issues identified with the conclusion of foot-and-mouth illness are examined and a worthy structure has been raised. Here is likewise a synopsis of other reasoning methods, for example, hyperspectral and warm imaging. These imaging frameworks rely straightforwardly upon the picture quality, number of preparing pictures and test highlights. In case there is a deformity in the filtering framework, it meddles with its immediate activity. Additionally, becoming accustomed to CNN needs earlier development with PC and memory assets [11]. One answer for this is a shrewd blend of master programming ideas in PC vision and AI procedures. Endeavors to foster such a framework would be of extraordinary premium to examiners in this field.

Recognizing sicknesses in photos of this plant is quite possibly the most intriguing regions for research in the PC and farming fields [12]. This paper gives research on the different imaging modalities and mechanical techniques used to analyze rice plant illnesses dependent on pictures of tainted rice plants. This paper presents a multidisciplinary examination as well as sums up the critical ideas of picture handling and AI utilized for diagnostics and arrangement. We did a definite 19-page study, consolidating crafted by illnesses of rice plants with different plants and different leafy foods, and introduced the investigation of these papers as indicated by the key conditions. These strategies incorporate picture data set size, no.

of classes (infections), handling, characterization strategies, sorts of order, exactness of classifiers and so on. We utilize our examination and study to propose and plan our work in the location and arrangement of rice plant sicknesses.

This paper traces how to adapt precisely to recognize three infections of the rice leaves: leaf filth, bacterial scourge curse and neighborhood earthy colored illness [13]. The work has a huge financial meeting 2019 International on Sustainable Technologies for Industry 4.0 (STI), 24–25 December, Dhaka the significance of Bangladesh. Examinations between four AI calculations (counting those of KNN, Decision Tree, Logistic retreat and Naive Bayes) in the space of rice leaf discovery have been made. Calculations foresee rice leaf illness with differing levels of precision. It was tracked down that the choice tree performed very well with 97.9167% exactness in the test information. Since we have recognized the nearest calculation, we desire to grow this examination further as excellent informational collections will be accessible later on.

Illnesses of rice harvests can cause genuine agrarian misfortunes if not enough tended to. Utilizing PC and correspondence innovation, a robotized framework can be fostered that can recognize the illness early. Simultaneously, we attempted to give our commitments to the utilization of pictures and AI for that program [14]. We have discovered that there are a wide range of approaches to work distinctively in the utilization of pictures and AI. This paper has looked into and summed up the procedures for picture handling and AI used to analyze illnesses. We tracked down that the expulsion of the illness area from the leaf picture is a main impetus, which we have contemplated and thought about various grouping methods. We have utilized our examination and study, introduced in this paper, to propose our work similarly. This paper introduced an unmistakable sketch of the proposed project and examined the key advances. Right now, we are attempting to finish the execution of the proposed project. The blend of picture preparing and AI procedures can offer specialists the chance to manage issues in an assortment of areas that straightforwardly or by implication influence society.

This paper tells the best way to identify rice leaf illnesses from the knowledgeable AlexNet convolutional neural organization to accomplish analytic information arrangement dependent on preparing information. An information base of this work was gathered from <https://www.kaggle.com> called the analysis of rice leaf curse [15]. The information base contained three picture records of rice leaf scourge named after bacterial curse, earthy colored spot and leaf filth. Each document contained 40 pictures. From this information

base, we have 120 pictures altogether relating to three rice leaf infections. These 120 pictures were too little to even consider working with our proposed interaction. Thus, we have expanded the size of our data set by utilizing picture improvement. After picture broadening, our information base size was expanded to 900 pictures. In our work, we have stacked our custom data set as a picture information store that isolates rice leaf sicknesses from envelope names and stores information as a picture information store thing. The plan measures for our proposed project are displayed in Figure 2. We separated our data set into two sections, for example, preparing information and test information. 70% and 30% of our information base is utilized as preparing and testing information separately. In this way, our data set contained 630 preparing photographs and 270 test pictures.

Sicknesses that influence the leaves of plants, particularly rice leaves, are one of the serious issues confronting ranchers. Along these lines, it is truly challenging to bring the measure of food required for more seasoned individuals. Infection illnesses have made usefulness and financial misfortunes in the rural area. It can similarly affect the pay of ranchers who rely upon agribusiness and nowadays ranchers are ending it all because of the awful circumstance they face in horticulture. The recognition of irresistible infections in plants will assist with arranging different infectious prevention measures. The proposed strategy portrays the different strategies utilized with the end goal of the rice leaf illness. Harm to the leaves of the microorganisms, Leaf muck and Brown tainted region pictures were partitioned utilizing the Otsu strategy [16].

In the current setting, the Indian economy is vigorously reliant upon agrarian creation and horticulture. Thusly, recognizing and distinguishing illnesses in plants or plants is vital, as it is normal for plants in the fields to be contaminated with specific infections brought about by microorganisms or growths. If not dealt with from the start, this could appear to be a calamity for the quality and amount of the item, or it might be said that the creation all in all. To be viable in such manner, AI ideas can be extremely valuable, as opposed to simply visual and visual. The accompanying investigation gives an outline of the finding and arrangement of sicknesses in rice crops, one of the biggest Indian food crops, utilizing pictures of polluted rice crops. The three illnesses were chiefly gathered in Bacterial leaf curse, Brown region, and Leaf filth. The Rice Leaf Disease Dataset, from the UCI Machine Learning Repository, was utilized. To characterize pictures into the ideal sickness classifications, the Residual Neural Network was discovered to be a quicker, more productive and more successful way than plain

Convolutional Neural Network and different classifiers like Support Vector Machines, by not permitting the model to arrive at full information levels or more profound organizations. We found about 95.83% exactness in the data set [17].

Populace development requires an expansion in agrarian creation. By and large, the main factor in farming is influencing the amount and nature of plants for infection illnesses. Normally, the rancher realizes that his yield is helpless to infection in a positive manner. Notwithstanding, this interaction is at times mistaken. With the improvement of AI innovation, the recognition of plant sicknesses can be computerized utilizing inside and out learning. In this examination, we report on a thorough rice-based learning program that we have created, which comprises of an AI program on a cloud worker and a program on a cell phone. The elements of the cell phone application are to take photos of the leaves of the rice plant, send them to the application on the cloud worker, and get the consequences of the precise data on the sorts of plant illnesses. The outcomes showed that the cell phone based rice sickness identification framework functioned admirably, which had the option to identify diseases in rice plants. The viability of the VGG16 rice sickness recognition framework has a substantial train worth of 100% and a test precision of 60%. The worth of test precision can be improved by expanding the quantity of data sets and expanding the nature of the information base. It is trusted that through this program, the control of rice illnesses should be possible successfully to build yields [18]. Daniya et al. [19, 20] Reviewed and proposed a deep neural network, which effectively detects the diseases on plants.

3 Sensing Recognition Strategy Based on Artificial Intelligence

In several places around the globe, rice is the predominant foodstuff. The rice harvests in the agricultural business today take a leading role since the quality and quantity of the cereals are influenced by pathogens. Multiple fungal illnesses affect the growth of rice crops. One of the most fungal diseases are Leaf scald and eyespot. Therefore, a novel Sensing Recognition Strategy has been proposed to overcome these challenges.

At first the images are captured using latest CMOS sensors then the images of disease are identified by new sensor named as optical sensors. This optical sensor sensed the illness of rice leaf diseases as leaf scald and identified infections are detected using Grasshopper Detection Algorithm

based on Artificial intelligence. Figure 1 depicts the overall architecture of Sensing Recognition Strategy is given below



Figure 1 Overall architecture of Sensing Recognition Strategy.

The detection algorithm of the proposed method based on Artificial Intelligence can be discuss in the below section.

3.1 Enhanced Grasshopper Detection Algorithm

Grasshoppers are pests that ruin cultivation, reducing the effectiveness to consume. Consequently, insects are also called pests. Grasshoppers are forming enormous swarms that cause producers the overwhelm fears. There are 2 kinds of grasshoppers in the environment, such as the juvenile shape and the maturity, i.e., the completely developed shape.

The mathematical theorem called the GDA is used to imitate grasshoppers' swarming characteristics, as demonstrated below. The position of every grasshopper in the swarm is a viable way to address the issue of recognition. Equation (1) represents the position of i th grasshopper as Y_i

$$Y_i = E_i + G_i + B_i \quad (1)$$

Where

E_i = Environment connection

G_i = Gravitational force

B_i = Wind boundary layer

Grasshoppers' swarming strength is defined by their attracting forces, repulsive forces and grasshoppers' path. Equation (2) depicts the current location of the grasshopper

$$Y_{id} = a_j = 1, \quad j i M_{cubd} - lbd2s(|yjd - yid|)y_j - yjdi_j + Td \quad (2)$$

The improved Grasshoppers Algorithm is given below,

- 1: Initialize c_{max} , c_{min} and $Maxit$
- 2: Initialize the occupants of swarms $Y_i = \{i = 1, 2, \dots, n\}$ arbitrary
- 3: Calculate every solution in the occupants
- 4: Place B as the best solution
- 5: **while** ($k < Maxit$)
- 6: Amend C using $C = c_{max} - l_{c_{max}} - c_{min} * Maxit$
- 7: **for** every solution
- 8: Normalize the separation of grasshopper
- 9: Amend the position of the present solution utilizing Equation (2)
- 10: Replace the present solution (if it breaches the margins of search space)
- 11: **end for**
- 12: Amend B if there is a better solution in the occupants
- 13: $k = k + 1$
- 14: **end while**
- 15: return B that's depicts the total recognition solution
- 16: End

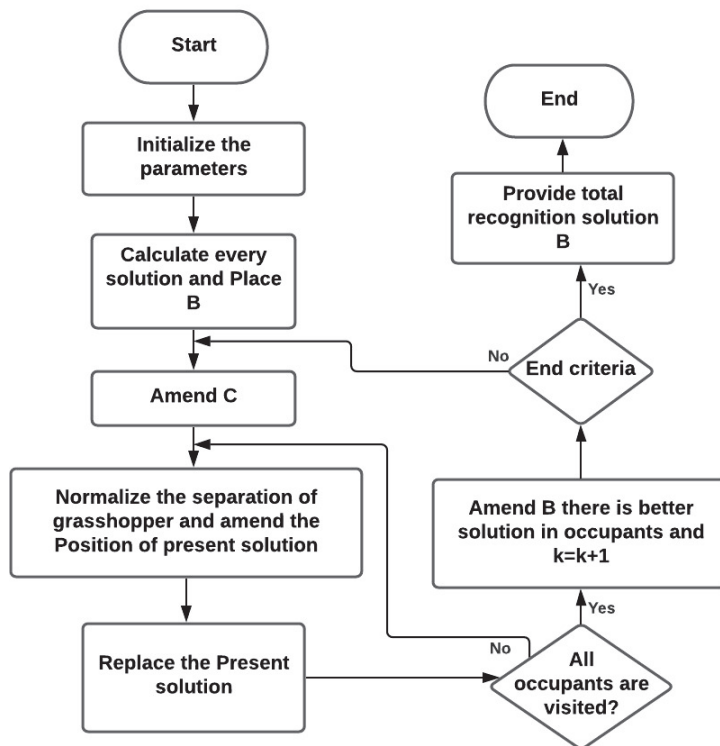


Figure 2 Flow chart of the Enhanced Grasshopper Detection Algorithm.

At last, the Sensing Recognition Strategy has been identified by optical sensors and detected the diseases by Grasshopper Detection Algorithm with high accuracy. The result section will be discuss in the below section.

4 Results

The proposed algorithm is developed using python tool and the sample image of the affected disease images collected from internet source are depicted in Figure 2. The data set collected from github [22] and work carried out using Core i3 machine with 8GB RAM and Windows 10 Operating system. The following Figure 3 shows the sample various type of plant diseases [23].

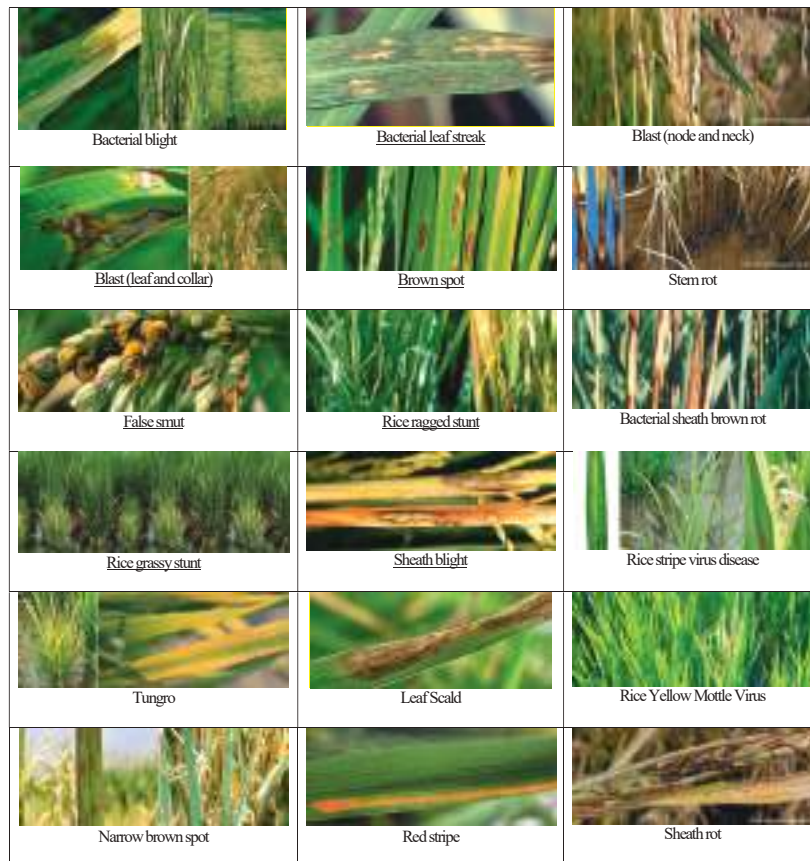


Figure 3 Sample various type of Rice Plant Diseases.

The outcomes of the proposed method are discussed by performance metrics and comparison results are given below.

4.1 Performance Metrics

Accuracy: It is directly Proportional to the summation of true positive and true negative and inversely proportional to the summation of true positive, true negative, false positive and false negative.

$$Accuracy = \frac{TP + TN}{TP + FN + FP + TN}$$

Precision: It is measured as the correlation of true positives to the aggregate of true positives and false positives.

$$Precision = \frac{TP}{TP + FP}$$

Sensitivity: It proclaimed as the proportion of positives accurately recognized via test out of the entire quantity of positive substantially evaluated.

$$Sensitivity = \frac{True\ positive}{true\ positive + false\ positive}$$

Specificity: It is denoted as the proportion of negatives adequately distinguished via test out of the whole amount of negative literally assessed.

$$Specificity = \frac{True\ negative}{true\ negative + false\ positive}$$

F1-Score: It is calculated as the Harmonic mean of precision and recall

$$F1-Score = 2 * \frac{precision * recall}{precision + recall}$$

4.2 Comparison Results

The comparison results of Proposed method are compared with existing methodologies including BLS Net Method (BLS Net), Convolutional Neural Network Technique (CNNT), Rice Talk Project (RTP), Fuzzy logic with K means Segmentation Technique (FL-K-means ST) and Alexnet.

The performance metrics such as accuracy, precision, sensitivity, specificity and F1-score of the Sensing Recognition Strategy are achieved highly efficient for detected the diseases when compared with prior techniques in rice plant. The Table 1 shows the performance comparison of proposed work with existing algorithms.

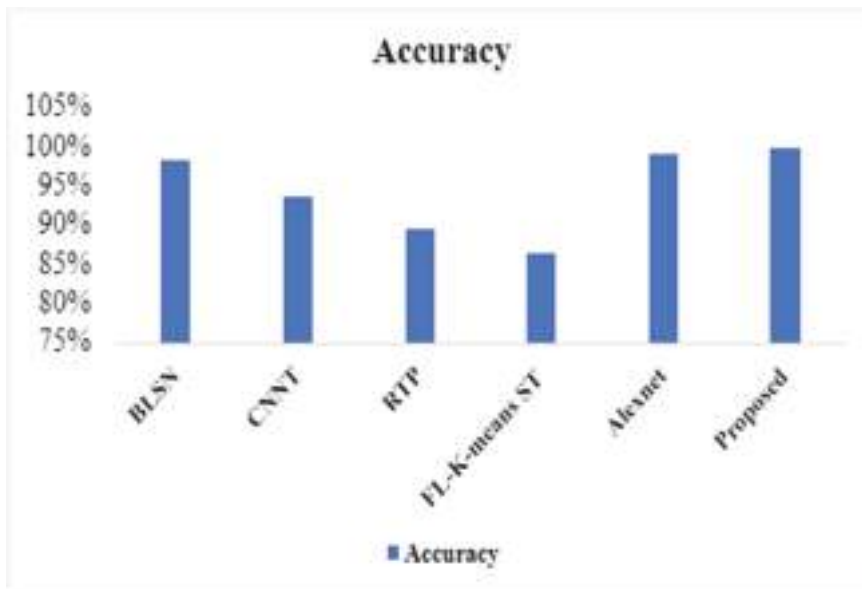


Figure 4 Accuracy of the SR Strategy.

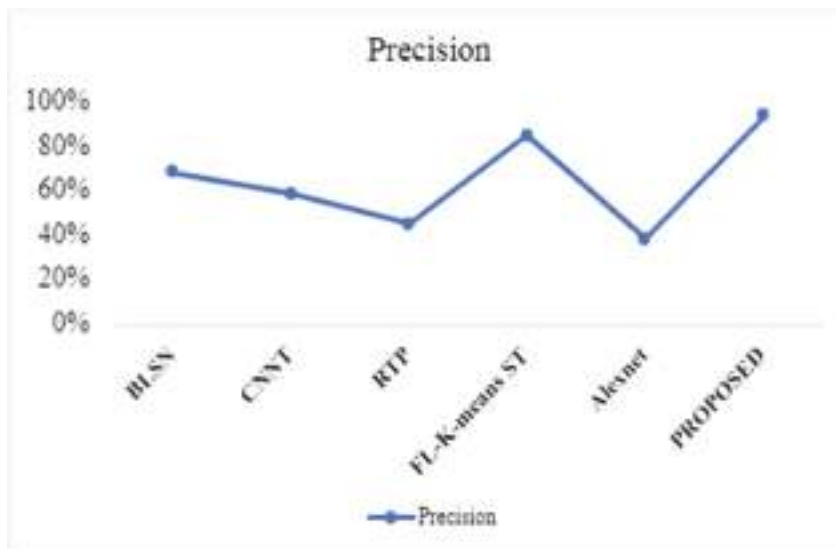


Figure 5 Precision of the SR Strategy.

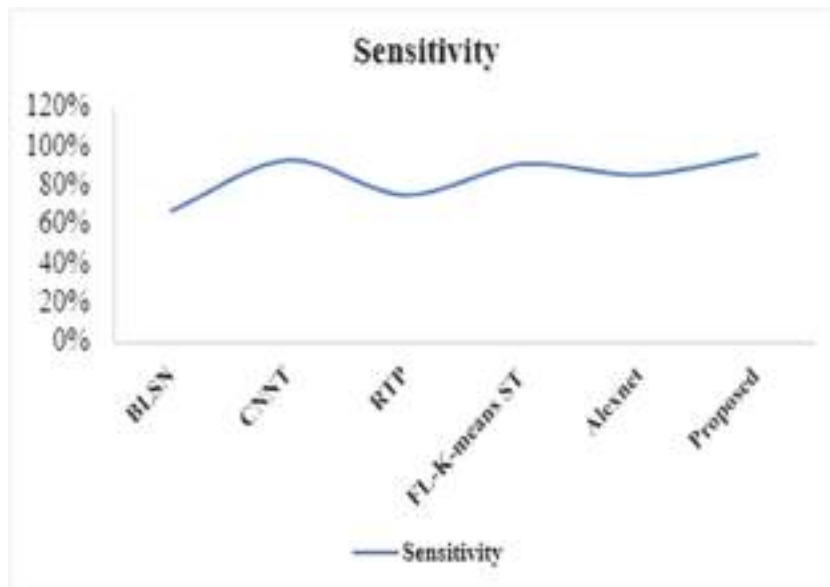


Figure 6 Sensitivity of the SR Strategy.

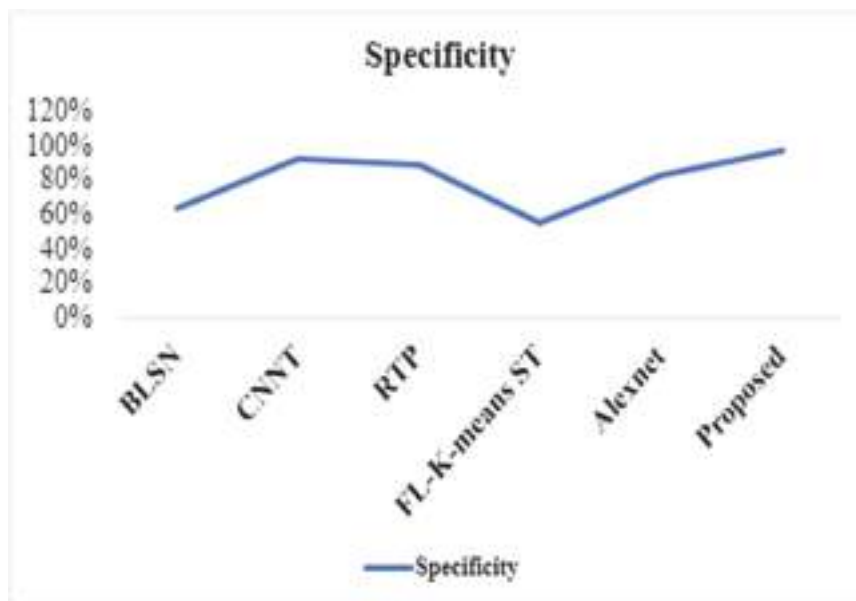


Figure 7 Specificity of the SR Strategy.

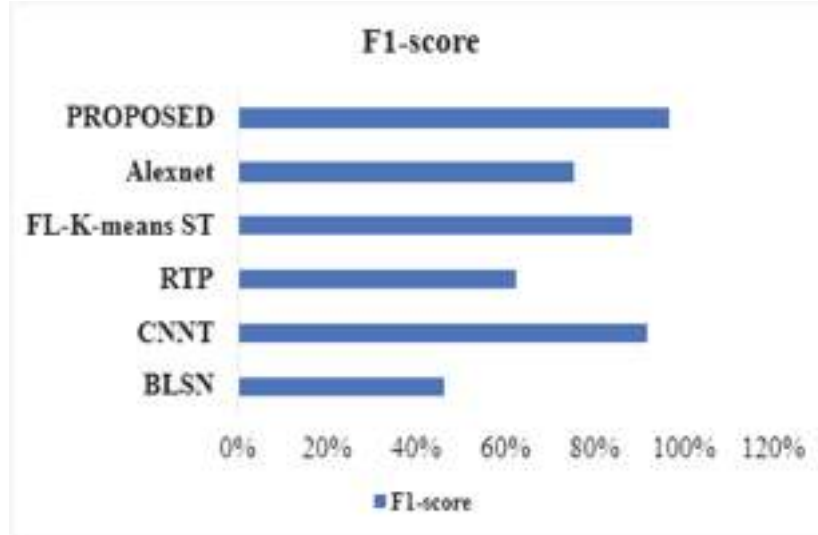


Figure 8 F1-score of the SR Strategy.

Metrics	Accuracy	Precision	Sensitivity	Specificity	F1-Score
Alexnet	0.965	0.728	0.657	0.602	0.865
FL-K-means ST	0.925	0.624	0.854	0.867	0.955
RTP	0.890	0.576	0.756	0.889	0.780
CNNT	0.805	0.827	0.831	0.652	0.815
BLSN	0.950	0.625	0.886	0.724	0.590
SR Strategy	0.979	0.934	0.896	0.971	0.969

5 Conclusion

In Rice plant diseases, leaf scald and eyespot are crucial challenges in rice plant leaf illness can be identified using sensors and detected the illness by Enhanced Grasshopper detection Algorithm. From the end of the fifteenth year on plant infection in the form of coping techniques that remain sharp is an income among professionals. In any plant, diseases are brought on by micro-organisms, growth, and infection. In rice plants, the most common ailments are the Bacterial leaf curse, Brown spot, Leaf barrel, Leaf impact, and Sheath. The Algorithm is recognized based on position, forces and path of the grasshopper. The Proposed method are compared with prior technologies and obtained the Accuracy of 99.94% with highly effective recognition. Further

development is carried out to detect the rice crop disease based on IoT with Artificial Intelligence.

References

- [1] Krishnamoorthy, D. and Parameswari, V.L., Rice Leaf Disease Detection Via Deep Neural Networks with Transfer Learning for Early Identification. *Turkish Journal of Physiotherapy and Rehabilitation*, 32, p. 2.
- [2] Azim, M.A., Islam, M.K., Rahman, M.M. and Jahan, F., 2021. An effective feature extraction method for rice leaf disease classification. *Telkomnika*, 19(2), pp. 463–470.
- [3] Nguyen, T.T., Ospina, R., Noguchi, N., Okamoto, H. and Ngo, Q.H., 2021. Real-time Disease Detection in Rice Fields in the Vietnamese Mekong Delta. *Environmental Control in Biology*, 59(2), pp. 77–85.
- [4] Jiang, F., Lu, Y., Chen, Y., Cai, D. and Li, G., 2020. Image recognition of four rice leaf diseases based on deep learning and support vector machine. *Computers and Electronics in Agriculture*, 179, p. 105824.
- [5] Basit, A. and Ali, Z., 2021. Detection of Disease Onset in Rice Plant Leaves in Monochrome Light. *The Nucleus*, 57(3), pp. 100–105.
- [6] Chen, S., Zhang, K., Zhao, Y., Sun, Y., Ban, W., Chen, Y., Zhuang, H., Zhang, X., Liu, J. and Yang, T., 2021. An Approach for Rice Bacterial Leaf Streak Disease Segmentation and Disease Severity Estimation. *Agriculture*, 11(5), p. 420.
- [7] Senan, N., Aamir, M., Ibrahim, R., Taujuddin, N.S.A.M. and Muda, W.H.N.W., 2020. An efficient convolutional neural network for paddy leaf disease and pest classification. *Int. J. Adv. Comput. Sci. Appl*, 11(7), pp. 116–122.
- [8] Chen, W.L., Lin, Y.B., Ng, F.L., Liu, C.Y. and Lin, Y.W., 2019. RiceTalk: Rice blast detection using internet of things and artificial intelligence technologies. *IEEE Internet of Things Journal*, 7(2), pp. 1001–1010.
- [9] Sethy, P.K., Negi, B., Barpanda, N.K., Behera, S.K. and Rath, A.K., 2018. Measurement of disease severity of rice crop using machine learning and computational intelligence. In *Cognitive science and artificial intelligence* (pp. 1–11). Springer, Singapore.
- [10] Matin, M.M.H., Khatun, A., Moazzam, M.G. and Uddin, M.S., 2020. An Efficient Disease Detection Technique of Rice Leaf Using AlexNet. *Journal of Computer and Communications*, 8(12), p. 49.

- [11] Prabira Kumar Sethy, Nalini Kanta Barpanda, Amiya Kumar Rath, Santi Kumari Behera, 2020. "Image Processing Techniques for Diagnosing Rice Plant Disease: A Survey". *Procedia Computer Science*, Vol. 167, pp. 516–530,
- [12] J. P. Shah, H. B. Prajapati and V. K. Dabhi, "A survey on detection and classification of rice plant diseases," 2016 IEEE International Conference on Current Trends in Advanced Computing (ICCTAC), 2016, pp. 1–8.
- [13] Ahmed, Kawcher, Shahidi, Tasmia, Irfanul Alam, Syed and Momen, Sifat, 2019. "Rice Leaf Disease Detection Using Machine Learning Techniques". 2019 International Conference on Sustainable Technologies for Industry 4.0 (STI), pp. 1–5.
- [14] Shah, Jitesh, Prajapati, Harshadkumar and Dabhi, Vipul, 2016. "A survey on detection and classification of rice plant diseases." pp. 1–8.
- [15] Matin, M., Khatun, A., Moazzam, M. and Uddin, M. (2020) An Efficient Disease Detection Technique of Rice Leaf Using AlexNet. *Journal of Computer and Communications*, Vol. pp. 49–57.
- [16] M. E. Pothen and M. L. Pai, "Detection of Rice Leaf Diseases Using Image Processing," 2020 Fourth International Conference on Computing Methodologies and Communication (ICCMC), 2020, pp. 424–430.
- [17] Patidar S., Pandey A., Shirish B.A., Sriram A. (2020) Rice Plant Disease Detection and Classification Using Deep Residual Learning, International Conference on Machine Learning, Image Processing, CCIS, vol. 1240, pp. 278–293.
- [18] H. Andrianto, Suhardi, A. Faizal and F. Armandika, 2020. "Smartphone Application for Deep Learning-Based Rice Plant Disease Detection," 2020 International Conference on Information Technology Systems and Innovation (ICITSI), pp. 387–392.
- [19] T. Daniya and S. Vigneshwari, 2021. Deep Neural Network for Disease Detection in Rice Plant Using the Texture and Deep Features, *The Computer Journal*.
- [20] T. Daniya and S. Vigneshwari, 2020. "A Review on Machine Learning Techniques for Rice Plant Disease Detection in Agricultural Research", *International Journal of Advanced Science and Technology*, vol. 8, no. 13.
- [21] S. Velliangiri, R. Sekar, and P. Anbazzhagan "Using MLPA for smart mushroom farm monitoring system based on IoT". *International Journal of Networking and Virtual Organisations* 2020, Vol. 22 Issue 4, pp. 334–346.

- [22] Rice disease dataset. <https://github.com/aldrin233/RiceDiseases-DataSet/tree/master> (accessed August 2021).
- [23] <http://www.knowledgebank.irri.org/step-by-step-production/growth/pets-and-diseases/diseases>

Biographies



T. Daniya received her B.Tech degree in Information Technology from Anna University, Chennai, India and M.Tech degree from MS University, India, in 2009 and 2011 respectively. She is currently doing Ph.D degree in Computer Science and Engineering at Sathyabama Institute of Science and Technology Chennai, India. She is currently working as an Assistant Professor with the Department of Information Technology, GMRIT, Rajam, India. Her research interest is AI, Machine Learning and Deep Learning. She Published 15 research articles in various journals and conferences.



Ch. Vidyadhari currently working as an Assistant professor in the Department of Information Technology at Gokaraju Rangaraju Institute of Engineering and Technology, Bachupally, Kukatpally, Hyderabad. Her research area is Data Mining and Machine Learning. She has published around 10 papers in reputed international journals and has an experience of 12 years in teaching.



Srilakshmi Aluri working as an Assistant Professor, Department of Information Technology, in Gokaraju Rangaraju Institute of Engineering and Technology, Hyderabad, Telangana, India. She completed M.Tech in Computer Science and Engineering from JNTU Kakinada in the year 2013. Her area of research interest includes Artificial Intelligence, Machine Learning, and Data Science. She has 8 years of teaching experience.

Squirrel Search Deer Hunting-Based Deep Recurrent Neural Network for Survival Prediction Using PAN-Cancer Gene Expression Data

RAMACHANDRO MAJJI^{1,*}, R. RAJESWARI², CH. VIDYADHARI³ AND R. CRISTIN¹

¹*Department of Computer Science and Engineering, GMR Institute of Technology, GMR Nagar, Rajam, Andhra Pradesh 532127, India*

²*Department of Electronics and Communication Engineering, Rajalakshmi Institute of Technology, Kuthambakkam, Chennai, Tamil Nadu 600124, India*

³*Department of Information Technology, Gokaraju Rangaraju Institute of Engineering and Technology, Bachupally, Hyderabad, Telangana 500090, India*

*Corresponding author: rama00565@gmail.com

This paper devises a novel technique, namely Squirrel Search Deer Hunting-based deep recurrent neural network (SSDH-based DRNN) for cancer-survival rate prediction using gene expression (GE) data. Initially, the input GE data are transformed using the polynomial kernel data transformation. Then entropy-based Bayesian fuzzy clustering is employed for gene selection. Then, the selected features are strengthened through survival indicators based on time series data features, like simple moving average (SMA) and rate of change. Finally, the survival rate prediction is performed using a deep recurrent neural network (DRNN), in which the training is carried out with squirrel search deer hunting (SSDH). The proposed SSDH algorithm is devised by combining Squirrel Search Algorithm (SSA) and deer hunting optimization algorithm (DHOA). The performance of the proposed methodology is analyzed using Pan-Cancer (PANCAN) dataset with a prediction error of 4.05%, RMSE of 7.58, the accuracy of 90.98%, precision of 90.80%, recall of 92.03% and F1-score of 91.41%. The devised method with higher prediction accuracy and the lower prediction error is employed for the cancer survival prediction of the patients for the cancer prognosis. Besides, it will be helpful for the clinical management of cancer patients.

Keywords: survival rate; cancer prediction; deep recurrent neural network; polynomial kernel; gene expression data

Received 21 October 2020; Revised 28 June 2021; Editorial Decision 3 July 2021

Handling editor: Domenico Rosaci

1. INTRODUCTION

Nowadays, the assessment of gene expression (GE) data has become a promising domain and has gained immense interest in precision medicine. The gene-expression data are adapted in a model for advanced research in the clinical process and aims at building the medicine more participatory, tailored, pre-emptive and prognostic [1]. These days, DNA microarray technologies are an imperative method for diagnosing different cancer types with GE data. Genes represent regions of encoding which

construct imperative block in cell and shows means to proteins that acquired huge functions. The microarray dataset is arranged in a matrix of value expression wherein each row indicates a specific gene and each column indicate various samples [2–4]. A variety of instantaneous gene expression profiles are traced with microarray technologies. Here, the count of genes contained in the microarray data is huge compared to the count of samples with different types of cancer classes contained in the microarray data are unclear, imperceptible, indefinite and

overlapping [5]. Generally, the gene expression data pose the following features. Firstly, the size of gene expression data is large and consists of thousands of genes. The size of the dataset is generally very small or very high as noisy data. The majority of genes are inappropriate for cancer detection. There is a huge demand to devise computational methods for diagnosing cancer. In addition, prognosis and therapeutics help discover complicated patterns and assist in the classification of cancer [6, 7]. GE is featured with the huge size of the sample and enormous noise while few genes investigated play a crucial function in predicting cancer [1, 8, 9].

Cancer is a risky disease, and many deaths have occurred because of cancer [9]. Thus, there is a requirement to devise a precise computation technique for predicting cancer survival rate that could devise management and diagnosis. Thus, it is essential to lower the death rate and improve the quality of living of cancer patients [7]. Cancer is considered an accumulation of related diseases that include abnormal growth of cells having the ability to split without stopping and increasing to adjoining tissues [10]. Cancer is the main cause of mortality and morbidity, and the determination of cancer in the earlier phases is of great significance for its cure [11]. In addition, cancer is assorted wherein the results may change for patient's behavior [12, 13] with same treatment who receive similar action routine [11]. The prediction of cancer at initial phases has been termed as an imperative area to scientists across the globe [5]. Due to the huge alertness of precision medicine and earlier detection methods, the desire for adapting new machine learning techniques for discovering novel biomarkers and has been termed as one of the major driving aspects in several translational requests [5, 14, 15]. The cancer is prevented by motivating the students [16–18] for the avoidance of tobacco like recommendation of studies. The survival prediction techniques should provide most accurate result because it plays the main role in treatment progress and health services. The existing methods have drawbacks like expensive, time-consuming and low efficiency leads to risky diagnosis.

2. MOTIVATION

The survival prediction helps to evaluate the data from time to event in medical research. The cancer survival prediction is necessary because the survival rate of these patients is very low. It helps the physicians in decision-making regarding the treatment. The predictive tools play a very important role in the prediction of cancer survival rate. GE data prevent errors caused by fatigue. Hence, better accuracy can be obtained. Machine learning technologies can efficiently predict the cancer survival rate. The major challenges faced by the existing system are low accuracy, failure to predict the survival rate on large datasets, and multilayer networks. The proposed SSDH-based DRNN overcame these factors to predict cancer survival rate using GE data as the DRNN is trained using the proposed SSDH

algorithm. Hence, better accuracy with low error prediction is possible.

The paper aims to devise a novel method, namely SSDH-based DRNN, for predicting cancer survival rate using GE data. In this method, the GE data undergo a polynomial kernel for data transformation. The transformed data are employed for gene selection in which the Bayesian clustering with entropy is adapted for similar grouping genes. After grouping, the best genes are selected from the groups. Then, the survival rate prediction is made with the survival indicator, which is based on time series data features, like SMA and rate of change. The survival prediction is carried out using DRNN, in which the training of DRNN is carried out using the proposed SSDH. The proposed SSDH is devised by combining SSA and DHOA.

The key contribution of the paper is:

- **Proposed SSDH-based DRNN for cancer-survival rate prediction:** The proposed SSDH-based DRNN is devised for predicting the rate of cancer survival using GE data. Here, the training of DRNN is done by the proposed SSDH, which is devised by combining DHOA and SSA.

The paper is arranged in the following manner: Section 1 portrays the introductory part of cancer survival prediction with GE data. Section 2 displays classical methods for cancer survival prediction using GE data. Section 3 presents the proposed model for predicting the cancer survival rate associated with GE data. Section 4 illustrates the outcomes of the proposed model in cancer survival prediction. At last, section 5 presents conclusions.

3. LITERATURE SURVEY

The review of eight classical methods using cancer-survival rate prediction with GE data is illustrated. López *et al.* [10] devised a pre-train convolutional neural network model for predicting the survival rate using the gene-expression data. The model was fine-tuned for predicting the progression of lung cancer. Here, the convolutional network was applied to gene-expression data to extract the imperative features. However, the method failed with other types of cancers. Wang *et al.* [7] devised a similar network fusion algorithm for predicting the cancer survival rate using gene expression data. Here, different genomic data, DNA methylation and exon expression were applied for generating a similarity matrix. Here, min-redundancy and max-relevance (mRMR) algorithm were utilized for selecting features of different genomic data. Ayyad *et al.* [4] present a classification method, namely modified k-nearest neighbor (MKNN), to predict cancer using GE data. Here, MKNN was adapted on two cases, namely the largest modified KNN (LMKNN) and the smallest modified KNN (SMKNN). Both executions were taken to improve the KNN

performance. The goal is to adapt vigorous neighbors with training data considering the weighting method. However, the method failed to speed up and enhance competence. Auslander *et al.* [19] devised a metabolic classifier and feature generator (MCF) that incorporated GE data for discovering cancer. The method inferred the composition of cancer trail that improves cancer versus adjoining noncancerous tissue with five types of cancer. The method provided improved predictions in distinguishing cancer versus noncancerous samples. Kumar and Greiner [11] devised a method based on topic modeling for deriving the expressive features with GE data. Here, a document was modeled as a mixture considering small topics wherein each topic was linked with certain words for accommodating the heterogeneity. Xiao *et al.* [1] devised a method that adapted deep learning as an ensemble, incorporating different machine learning for analyzing the cancer-survival rate prediction. Here, informative gene data chosen from differential GE analysis was given to classification. Halder and Kumar [5] devised an active learning method using a rough-fuzzy classifier (ALRFC) considering gene expression data to predict cancer. Here, the method can manage the overlappings, uncertainty and indiscernibility of GE data classes. However, the method failed to analyze the performance using other gene expression datasets like microRNA. Arnab *et al.* [20] developed Bayesian data integration and variable selection for pan-cancer survival prediction using protein expression data. It achieved the high dimensional shrinkage and integration of data. They did not find the feature strengthening using multiple factors. Arwinder *et al.* [21] developed eBreCaP breast cancer survival prediction using an extreme learning machine (ELM) with gradient boosting. However, the accuracy of prediction is low.

3.1. Challenges

The issues faced by classical cancer-survival rate prediction methodologies are illustrated below:

- In [10], transfer learning using CNN was devised for predicting the cancer survival rate using gene expression data. However, the devised method failed to provide improved classification accuracy, and the efficiency of this method is low.
- Semi-supervised training with GCN [7] was presented for predicting the rate of cancer survival considering gene expression data. However, this method was unsuitable for multitask learning considering different cancer-related researches.
- In [5], an active learning technique based on a rough-fuzzy classifier was devised for predicting the cancer survival rate using gene data. However, the method failed to manage large numerical attributes for training.
- The eBreCaP methodology is developed for breast cancer survival prediction [21], but the accuracy is low.

4. METHOD

4.1. Dataset description

The dataset, namely Pan-Cancer (PANCAN) dataset [22], contains 18 469 samples with gene expression phenotype. The input taken from the PANCAN dataset is the gene expression data, in which every gene has numerical values.

4.2. Experimental set-up

The implementation of the proposed strategy is performed in MATLAB, with the desktop having Windows 10 OS, Intel i3 core processor and 4GB RAM.

4.3. Evaluation measures

The analysis of the proposed SSDH-based DRNN method is computed using two measures that involve prediction error, RMSE, accuracy, precision, recall and F1-score.

4.3.1. Prediction error

The prediction error refers to stoppage of some expected event to occur, and it is formulated as,

$$PE = \frac{M_v - P_v}{M_v} \times 100 \quad (1)$$

where M_v represent measured value and P_v signifies predicted value.

4.3.2. RMSE

The square root of the differences between estimated values and observed values is termed as RMSE.

$$RMSE = \sqrt{o_n^L - o_n^P} \quad (2)$$

where o_n^P represents the expected outcome and o_n^L is the predicted result.

4.3.3. Accuracy

The degree of closeness of the measured value and the actual value is termed as accuracy. It is given as,

$$\gamma = \frac{w_p + w_n}{w_p + w_n + s_p + s_n} \quad (3)$$

where w_p refers to the true positive, w_n refers to the true negative, s_p refers to the false positive and s_n refers to the false negative.

4.3.4. Precision

Precision refers to the highest level of exactness, which is given as,

$$P = \frac{w_p}{w_p + s_p} \quad (4)$$

4.3.5. Recall

It is defined as the proportion of positive results detected and is represented as,

$$R = \frac{w_p}{w_p + s_n} \quad (5)$$

4.3.6. F1-score

It is defined as the harmonic mean of precision and recall and is expressed as,

$$F_1 = 2 * \frac{P * R}{P + R} \quad (6)$$

4.4. Proposed squirrel search deer hunting-based deep recurrent neural network for cancer survival prediction

Cancer is a deadly disease that has become a major threat to human disease. The higher mortality rate is due to the complication of cancer and the crucial differences in clinical results. Several computation methods for predicting cancer survival rates have been devised, but most of them produce prediction techniques by utilizing gene data. The classification of gene expression microarray is a major area in cancer survival prediction and diagnosis system. However, a precise and effective classification of these samples is a major issue. The prediction of cancer using classical methods is devised using clinical diagnosis and tumor morphologies. These methods are expensive and sometimes imprecise, and time-consuming [5, 7]. For addressing these problems and to offer less costly, first diagnosis and cancer prediction, modern computational methods like microarray data is utilized [5]. Several machine-learning methods are employed for dealing with a cancer diagnosis and prediction using gene-expression data [1, 23].

Meanwhile, previous knowledge is utilized to choose particular genes that confirm gene signatures, namely biomarkers that can be utilized to predict clinical results like benefits of diagnosis, recurrence, metastasis and so on [1, 8]. Various automatic feature extraction and selection methods are utilized to minimize input dimensionality and have become an initial step to adapt various machine-learning techniques [1, 24]. The techniques like elastic net are employed to regularize the Cox methods that aim to minimize the count of input features for solving the tasks of survival prediction [1, 25]. Survival prediction techniques are utilized that involve decision-tree method that has devised to be resistant towards over-fitting problems in huge dimensional cases. At last, neural network methods are mostly used in the tasks of survival prediction with fewer dimension data. Still, the efficiency of the techniques for right-censored data outperformed other models based on data structure [1, 26]. Several machine learning methods exist with unsupervised, semi-supervised classification [5, 14], supervised [5, 27] and semi-supervised clustering [5, 28] for analyzing microarray data.

In order to overcome the problems faced by the existing techniques, the proposed SSDH-based DRNN is introduced. The aim is to devise a novel method, namely the proposed SSDH-based DRNN, to predict cancer survival with GE data. At first, the input gene expression data are subjected to the data transformation phase, which is performed using the polynomial kernel method. The obtained polynomial kernel is fed to gene selection that utilizes entropy-based Bayesian fuzzy clustering to select the genes. The selected genes undergo feature strengthening using SMA and rate of change factors. The obtained features are finally fed to DRNN for survival prediction, wherein proposed SSDH is employed for training DRNN [29]. The training of DRNN is done to obtain weights and is performed using the proposed SSDH, which is devised by combining SSA [30] and DHOA [31]. The block diagram of the cancer survival prediction using the proposed SSDH-based DRNN is depicted in Fig. 1.

4.5. Procedure

4.5.1. Acquisition of input data

The gene expression data are modeled as a real-valued matrix wherein row objects gene expression measurements with a certain number of experiments and columns present a pattern of expression of all genes considering each patient. Assume a gene expression dataset $D \in G^{g \times h}$, which is composed of g samples of different patients and h gene records. A gene profile is a single data item (row) constituting g measurements like $p = (p_1, p_2, \dots, p_g)$. Each patient contains genes linked to the column of gene expression matrix so that $m = (m_1, m_2, \dots, m_h)$ where h is total genes present in the patient's data.

4.5.2. Data transformation using polynomial kernel method

Data transformation is the procedure performed by a mathematical function, and it is executed on the data. In this method, an extensive transformation employed for transforming data is the polynomial kernel method. This process is utilized for compressing massive data. For example, if the processing of huge data is done, then the small values get overwhelmed by bigger values. Thus, consideration of the polynomial kernel guarantees visualization to be clearer. Here, the input gene expression data m_k are chosen and is fed to the pre-processing stage, wherein GE data m_k are pre-processed with the polynomial kernel method. Pre-processing of data helps to transform raw data into an understandable format. The goal of pre-processing is to minimize redundant values for improving data quality.

Kernel methods are the classical method that helps to address the issues of machine learning. The kernel-based techniques utilize the information encoded in the inner-product amongst all data items that compute the feature vector for a given input. The kernel method solves the issues by mapping data into a huge feature. Each coordinate is associated with one feature of

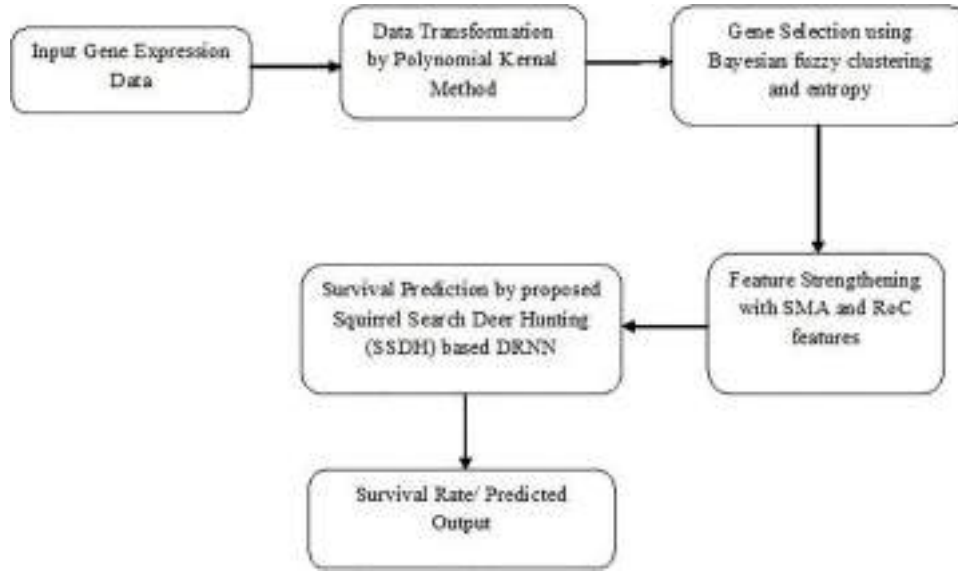


FIGURE 1. Schematic view of the cancer survival prediction using the proposed SSDH-based DRNN.

the data item that transforms data using Euclidean space. Here, different methods are utilized to determine the data relation.

For degree b polynomials, the polynomial kernel is expressed as,

$$k(q, r) = (q^T r + s)^b \quad (7)$$

where q and r signifies vector in input space, which indicates vector of features obtained from training and test samples and $s \geq 0$ represents a free parameter trading in the polynomial.

A kernel k is linked to the inner product of feature space based on some mapping ϕ and is expressed as,

$$k(u, v) = \{\phi(q), \phi(s)\} \quad (8)$$

The nature of ϕ can be expressed as,

$$k(q, r) = \left(\sum_{\ell=1}^h q_{\ell} r_{\ell} + s \right)^d \quad (9)$$

4.5.3. Gene selection using Bayesian fuzzy clustering and entropy

BFC [32, 33] is devised to realize fuzzy clustering considering the principle of MAP. The specific feature of BFC is contained with three factors. The fuzzy clustering is executed in a probabilistic way using fuzziness and probability, efficiently combined in clustering fuzzy. The count of clusters using fuzzy clustering can be evaluated using Bayesian inference. The fuzzifier constraint $m > 1$ in FCM may be relaxed so that m acquires a value less than one or negative. The BFC comprises

data likelihood distribution, namely fuzzy data likelihood.

$$P(D|E, F) = \prod_{a=1}^A FDL(d_a|e_a, F) \quad (10)$$

$$P(D|E, F) = \prod_{a=1}^A \frac{1}{B(e_a, c, F)} \prod_{f=1}^F \aleph(d_a|\mu = o_f \Lambda = e_{a,f}^c I) \quad (11)$$

$$\tilde{P}(E|F) = \prod_{a=1}^A FCP(e_a, F) \quad (12)$$

$$\tilde{P}(E|F) = \prod_{a=1}^A B(e_a, c, F) \left(\prod_{f=1}^F e_{a,f}^{cH/2} \right) Dirchlet(e_a|\alpha) \quad (13)$$

where A signifies count of data points, F symbolize number of clusters, C signifies data dimensionality, $e_{a,f}$ symbolizes data point membership, d_a signifies cluster a , c represents fuzzifier, o_f is cluster prototype, and I signifies D dimensional identity matrix and $B(e_a, c, F)$ represent normalization constant, α denote shape parameter.

And distribution of Gaussian prior using cluster prototypes is expressed as,

$$P(F) = \prod_{f=1}^F \aleph(o_f|\mu_o, \sum o) \quad (14)$$

The Dirichlet likelihood using vector α is given as,

$$\text{Dirichlet}(d|\alpha) = \frac{\Gamma\left(\sum_{x=1}^X \alpha_x\right)}{\prod_{x=1}^X \Gamma(\alpha_x)} \prod_{x=1}^X d_x^{\alpha_x-1} \quad (15)$$

Thus, the objective function from the joint likelihood is expressed as,

$$\begin{aligned} M(D, E, F) = & \sum_{a=1}^A \sum_{f=1}^F e_{a,f}^C \|d_a - o_f\|^2 - 2 \sum_{a=1}^A \sum_{f=1}^F (\alpha_f - 1) \\ & \times \log(e_{a,f}) + \sum_{f=1}^F (o_f - \mu_o)^T \sum_o^{-1} (o_f - \mu_o) \end{aligned} \quad (16)$$

Thus, the clusters obtained from the BFC is expressed as,

$$N = \{c_1, c_2, \dots, c_t\} \quad (17)$$

where t signifies total clusters.

The entropy [34] is a benchmark factor utilized to discover the uncertainty of any data and is utilized to maximize mutual information by performing various operations. Thus, the entropy of two gene expression data targets the difference to spot the best gene. Moreover, the entropy helps to define states of different levels of intensity that each pixel can acquire. Thus, the entropy of the selected genes is computed as,

$$F = -P \log(P) \quad (18)$$

where P signifies probability distribution of data.

4.5.4. Strengthening the gene features with time-series features

The rapid evolution of evidence on genetic data is important for combining human genomics in the practice of medicine. The genetic factors mostly affect the existence of different common diseases, and thus the identification and characterization of the associated risk are imperative to improve the understanding of etiology. In this method, the simple moving average (SMA) and rate of change (RoC) features are adapted for strengthening the gene expression data.

4.5.4.1. SMA Moving averages are the indicator in technical analysis, and there exist different versions. The SMA is the simplest moving average to construct. It represents the average genes over a specific period. The average is termed as moving as plotted on the chart bar by a bar that forms the line, which moves over the chart as the average value changes. The SMA computes the average of a selected range of genes concerning the time, and it is formulated as,

$$\text{SMA} = \frac{A_1 + A_2 + \dots + A_n}{n} \quad (19)$$

where n signifies number of total periods and A_n represent genes of a patient at period n .

4.5.4.2. RoC The RoC refers to the change in rate, which defines how the quantity changes concerning other quantities. If x is the independent variable and y is the dependent variable, then the RoC is given as,

$$\text{RoC} = \frac{\text{change in } y}{\text{change in } x} \quad (20)$$

4.5.5. Survival prediction using proposed squirrel search deer hunting-based deep recurrent neural network

Here, the prediction of survival rate is made with the proposed SBDH-based deep recurrent neural network, and prediction is carried out using the survival indicator that considers time series data features, like SMA and RoC. The survival indicator is fed to survival rate prediction module, which is performed using DRNN, and training is performed with proposed SBDH, which integrates the SSA and DHOA. The internal model parameters of the classifier are optimally tuned using the proposed SBDH for increasing the efficiency of survival prediction. The purpose of the proposed SBDH is to discover the survival rate from the input data based on obtained feature vector. DHOA [31] is motivated by the human's behavior towards hunting the deer. The DHOA can acquire global optimum more easily due to the combined method of exploration. DHOA is effective in addressing test issues and is reasonable in contrast to other techniques. Hence, it ensures that the DHOA can acquire a tradeoff between exploitation and exploration. The ability to search in DHOA can attain favorable regions, and it is noted to be high. The method can effectively address the behavior of convergence in a better manner and can solve engineering issues. On the other hand, the SSA [30] is motivated by the dynamic foraging behavior of squirrels, and it is an effective way for locomotion, also known as gliding. The behavior of squirrels is mathematically formulated considering the features of food search. The SSA acquires global optimal solutions with improved convergence behavior. The efficiency of SSA is more accurate, consistent and offers the best solutions for real-time issues. Thus, the combination of SSA and DHOA is performed to improve overall algorithmic performance. The architecture of DRNN and its algorithmic steps are given below.

4.5.5.1. Architecture of DRNN The features H that are extracted using input gene expression data are fed as an input to DRNN. DRNN [29] is a model that comprises different recurrent hidden layers in layers of network hierarchies. In DRNN, the recurrent connection contains a hidden layer. The DRNN effectively functions alternating length of input feature using information sequence. It utilizes knowledge of preceding input states in current prediction and process iteration with information of hidden states. The structural design of DRNN is expressed in Fig. 2.

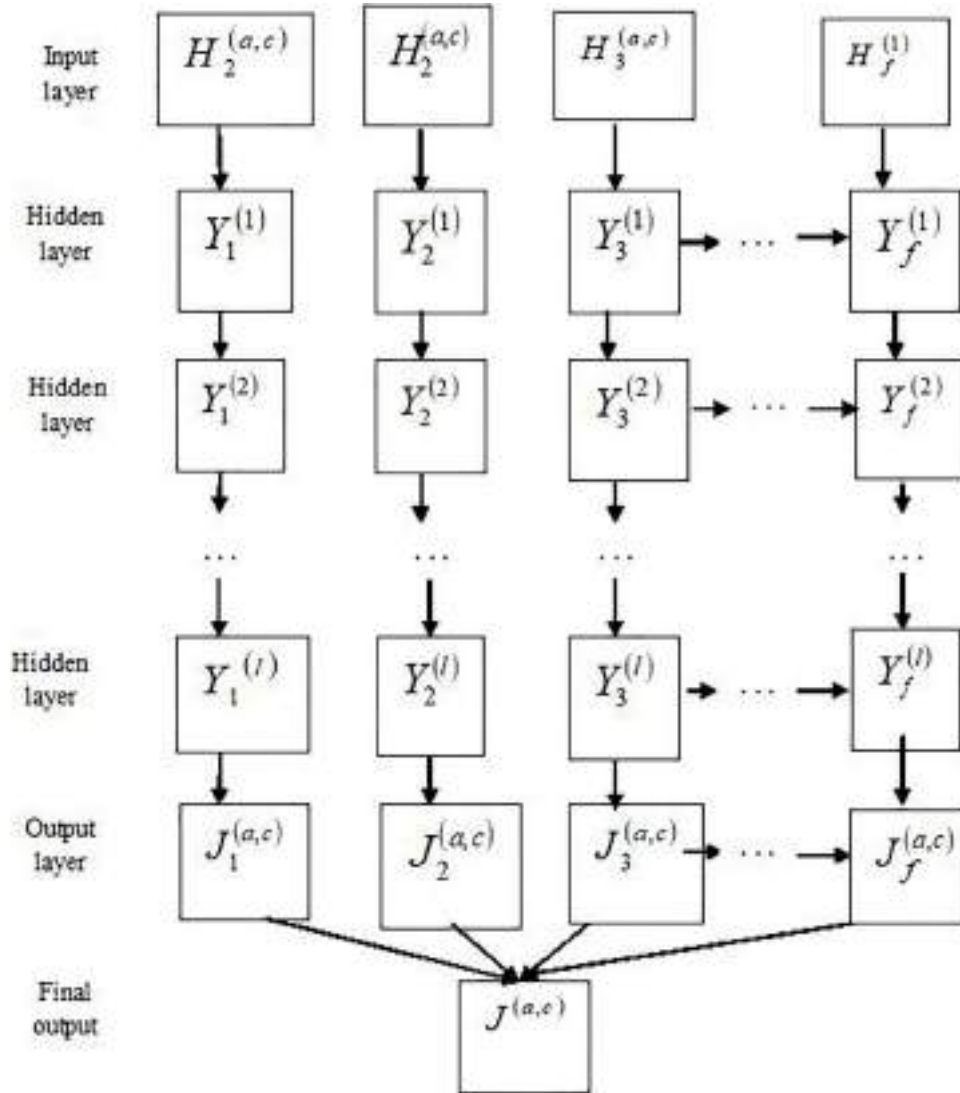


FIGURE 2. Structural design of DRNN.

The DRNN structure is employed by adapting the input of a^{th} layer at c^{th} time as $H^{(a,c)} = \{H_1^{(a,c)}, H_2^{(a,c)}, \dots, H_e^{(a,c)}, \dots, H_f^{(a,c)}\}$ an output vector of a^{th} layer at c^{th} time as, $J^{(a,c)} = \{J_1^{(a,c)}, J_2^{(a,c)}, \dots, J_e^{(a,c)}, \dots, J_f^{(a,c)}\}$. The pair of input and output vectors are modeled as a unit. This method e signifies the random number of a^{th} layers, and f represents the total units of a^{th} layer. Furthermore, the random and total units of $(a-1)^{\text{th}}$ layer are expressed as g and E . The input weight from $(a-1)^{\text{th}}$ layer to a^{th} layer is expressed as, $W^{(a)} \in T^{f \times E}$, and recurrent weight of a^{th} layer is expressed as $w^{(a)} \in T^{f \times f}$. Here, T denotes a set of weights. However, input vector components is expressed as,

$$H_e^{(a,c)} = \sum_{h=1}^E d_{eh}^{(a)} J_h^{(a-1,c)} + \sum_{e'}^f f_{ee'}^{(a)} J_{e'}^{(a,c-1)} \quad (21)$$

where $d_{eh}^{(a)}$ and $f_{ee'}^{(a)}$ signifies elements of $W^{(a)}$ and $w^{(a)}$, e' signifies a random unit of a^{th} layer. The output vector of a^{th} layer is expressed as,

$$J_e^{(a,c)} = \beta^{(a)} \left(F_e^{(a,c)} \right) \quad (22)$$

where, $\beta^{(a)}$ signifies activation function. Thus, the activation functions, such as sigmoid function as $\beta(H) = \tanh(H)$, rectified linear unit function (ReLU) as $\beta(H) = \max(H, 0)$, and logistic sigmoid function as $\beta(H) = \frac{1}{1+e^{-H}}$ are commonly utilized activation function.

To shorten process, 0^{th} weight as $d_{a0}^{(a)}$ and 0^{th} unit as $J_0^{(a-1,c)}$ are devised, and thus bias is represented

as,

$$J^{(a,c)} = \beta^{(a)} \cdot \left(W^{(a)} J^{(a-1,c)} + w^{(a)} J^{(a,c-1)} \right) \quad (23)$$

Here, $J^{(a,c)}$ denotes the output of classifier.

4.5.5.2. Training of DRNN The training procedure of DRNN is done with the SBDH algorithm. Here, the weight of the classifier is trained using the proposed SBDH for obtaining an optimal solution. SBDH modifies the DRNN by integrating the SSA [30] with the DHOA [31] to select optimal weights by following an update process. For survival rate prediction, the optimization, namely SBDH, is proposed in this research. By integrating the SSA with DHOA, the parametric features from both the optimization are inherited, which boosts survival rate prediction performance. The algorithmic procedure for survival rate prediction is given below.

Step 1: Initialization

The first step is solution initialization, which is expressed as,

$$Q = \{Q_1, Q_2, \dots, Q_j, \dots, Q_k\} \quad (24)$$

where D_j indicate j^{th} solution, and k signifies total solutions.

Step 2: Determination of error

The optimum solution is detected using fitness and is considered a minimization issue. Hence, the solution with the least mean square error (MSE) is chosen as the optimal solution and is formulated as,

$$MS_{err} = \frac{1}{R} \sum_{r=1}^R [F_r - F_r^*]^2 \quad (25)$$

where F_r refers expected output and F_r^* denotes predicted output, R denote total data in the dataset, where $1 < r \leq R$.

Step 3: Determination of update solution

The technique considers candidate solutions closer to the optimum considering fitness function. Here, three solutions are considered near-optimal. The first solution is propagation through position angle, the second solution is propagation through successor, and the third solution is propagation through the leader's position. According to DHOA [31], the propagation with position angle is given as,

$$Q_{t,y}^{i+1} = Q^{lead} - P | \text{Cos}(\varepsilon) \times Q^{lead} - Q_{t,y}^i | \quad (26)$$

where Q^{lead} represent first best solution, P signifies coefficient vector, $Q_{t,y}^i$ represent the position at current iteration and $Q_{t,y}^{i+1}$ represent the position at next iteration and $\text{Cos}(\varepsilon)$ represent the angle of visualization.

The propagation with successor is given as,

$$Q_{t,y}^{i+1} = Q^{successor} - Z_{t,y}^i \cdot P \cdot | R \times Q^{lead} - Q_{t,y}^i | \quad (27)$$

where $Q^{successor}$ signifies successor position R and $Z_{t,y}^i$ represents a coefficient vector.

The update is performed on SSA considering the propagation with leader's position and is given as,

$$Q_{t,y}^{i+1} = Q^{lead} - Z_{t,y}^i \cdot P \cdot | R \times Q^{lead} - Q_{t,y}^i | \quad (28)$$

SSA begins with the arbitrary location of flying squirrels. Here, the flying squirrels are on acorn nut trees and can move to hickory nut trees. According to SSA [30], the update equation is expressed as,

$$Q_{t,y}^{i+1} = Q_{t,y}^i + S_I N_J (Q_{r,y}^i - Q_{t,y}^i) \quad (29)$$

$$Q_{t,y}^{i+1} = Q_{t,y}^i [1 - S_I N_J] + S_I N_J Q_{t,y}^i \quad (30)$$

where S_I represent random gliding distance, i signifies current iteration, $Q_{t,y}^i$ symbolize flying squirrel on acorn nut tree, $Y_{r,y}^i$ represent flying squirrel on a normal tree, N_J represent gliding constant.

$$Q_{t,y}^i = \frac{Q_{t,y}^{i+1} - S_I N_J Q_{t,y}^i}{1 - S_I N_J} \quad (31)$$

Substitute equation (25) in equation (22),

$$Q_{t,y}^{i+1} = Q^{lead} - Z_{t,y}^i \cdot P \cdot | R \times Q^{lead} - \frac{Q_{t,y}^{i+1} - S_I N_J Q_{t,y}^i}{1 - S_I N_J} | \quad (32)$$

$$Q_{t,y}^{i+1} - \frac{Z_{t,y}^i \cdot P Q_{t,y}^{i+1}}{1 - S_I N_J} = Q^{lead} - Z_{t,y}^i \cdot P \cdot | R Q^{lead} - \frac{S_I N_J Q_{t,y}^i}{1 - S_I N_J} | \quad (33)$$

$$Q_{t,y}^{i+1} = \frac{1 - S_I N_J}{1 - S_I N_J - Z_{t,y}^i \cdot P} \left\{ Q^{lead} - Z_{t,y}^i \cdot P \cdot | R Q^{lead} - \frac{S_I N_J Q_{t,y}^i}{1 - S_I N_J} | \right\} \quad (34)$$

The update of solution is done to perform weight update for training DRNN. Hence, the weights linked to minimal error are adapted for DRNN training.

Step 4: Determination of best solution

The ranking of solutions is done using error and poses a solution that ranked the maximal as an optimal solution.

Step 5: Terminate

The best solutions are obtained repeatedly till maximal iteration is attained. Algorithm 1 represents the pseudo-code of the proposed SSDH.

5. RESULTS AND DISCUSSION

This section defines the efficiency of the proposed SSDH-based DRNN using prediction error, RMSE, accuracy, precision, recall and F1-Score. Varying training data percentages carry

A. Algorithm 1. Pseudo-code of proposed SSDH.

Input: Initialized population Q .
Output: First best solution Q^{lead} , Second best solution $Q^{successor}$.
Begin
 While ($i < i_{max}$)
 For each solution in Q .
 Evaluate fitness using equation (19).
 Update algorithmic parameters Z, p, R
 If ($p < 1$)
 If ($|R| \geq 1$)
 Update position of each agent with equation (34).
 Else.
 Update position of each agent with equation (21).
 End if.
 Else.
 Update position of each agent with equation (20).
 End if.
 End for.
 Re-evaluate the fitness.
 Update Q^{lead} and $Q^{successor}$; $i = i + 1$
 End while
Return Y^{lead}
End

TABLE 1. Simulation parameters.

Parameter	Value
No. of input vectors in the input layer	200×1
No. of layers	3
Number of neurons in the hidden layer and output layers	20
Gliding distance-random numbers belong to the range	[0, 1]
Maximum iteration for algorithm convergence	100
Number of classes in cancer survival prediction	2

out the analysis. Furthermore, the performance is evaluated using certain classes.

5.1. Performance analysis

The assessment of the proposed SSDH-based DRNN is done using prediction error, RMSE, accuracy, precision, recall and F1-score by varying percentages of training data. The simulation parameter is shown in Table 1.

5.1.1. Analysis of methods using $c = 2$

Figure 3 describes the analysis of the proposed SSDH-based DRNN with $c = 2$ considering prediction error, RMSE, accuracy, precision, recall and F1-score. The analysis of the proposed SSDH-based DRNN with prediction error is depicted in Fig. 3a). For 40% training data, the corresponding prediction error measured by proposed SSDH-based DRNN with

layer = 5 is 19.685%, layer = 10 is 19.577%, layer = 15 is 19.498%, layer = 20 is 19.39% and layer 25 is 19.29%. Likewise, for 80% training data, the corresponding prediction error measured by proposed SSDH-based DRNN with layer = 5 is 6.5%, layer = 10 is 6.28%, layer = 15 is 6.20%, layer = 20 is 6.1% and layer 25 is 5.99%. Similarly, for all the other matrices like RMSE, accuracy, precision, recall and F1-score, the proposed SSDH-based DRNN has better results with increased training percentage.

5.1.2. Analysis of methods using $c = 3$

Figure 4 describes the analysis of the proposed SSDH-based DRNN with $c = 3$ considering prediction error, RMSE, accuracy, precision, recall and F1-score. The analysis of the proposed SSDH-based DRNN with RMSE is described in Fig. 4b). For 40% training data, the corresponding RMSE measured by proposed SSDH-based DRNN with layer = 5 is 8.21, layer = 10 is 8.09, layer = 15 is 8.09, layer = 20 is 8.08 and layer 25 is 8.06. Likewise, for 80% training data, the corresponding RMSE measured by proposed SSDH-based DRNN with layer = 5 is 7.81, layer = 10 is 7.71, layer = 15 is 7.70, layer = 20 is 7.69 and layer 25 is 7.67. Similarly, for all the other matrices like prediction error, accuracy, precision, recall and F1-score, the proposed SSDH-based DRNN has better results with increased training percentage.

5.1.3. Analysis of methods using $c = 4$

Figure 5 describes the analysis of the proposed SSDH-based DRNN with $c = 4$ considering prediction error, RMSE, accuracy, precision, recall and F1-score. The analysis of the proposed SSDH-based DRNN with RMSE is described in Fig. 5b). For 40% training data, the corresponding RMSE measured by proposed SSDH-based DRNN with layer = 5 is 7.21, layer = 10 is 7.18, layer = 15 is 7.06, layer = 20 is 7.05 and layer 25 is 7.03. Likewise, for 80% training data, the corresponding RMSE measured by proposed SSDH-based DRNN with layer = 5 is 6.82, layer = 10 is 6.81, layer = 15 is 6.79, layer = 20 is 6.74 and layer 25 is 6.65. Similarly, for all the other matrices like prediction error, accuracy, precision, recall and F1-score, the proposed SSDH-based DRNN has better results with increased training percentage.

5.2. Comparative analysis

The methods, like transfer learning-based CNN [10], GCGCN [7], DRNN [29] and proposed SSDH-based DRNN are taken for the analysis. The analysis of methods is done using prediction error and RMSE by varying the percentage of training data and K-fold validation.

5.2.1. Analysis by varying the training percentage

5.2.1.1. Analysis of methods using $c = 2$ Figure 6 describes the analysis of methods with $c = 2$ considering prediction error, RMSE, accuracy, precision, recall and F1-score. The evalua-

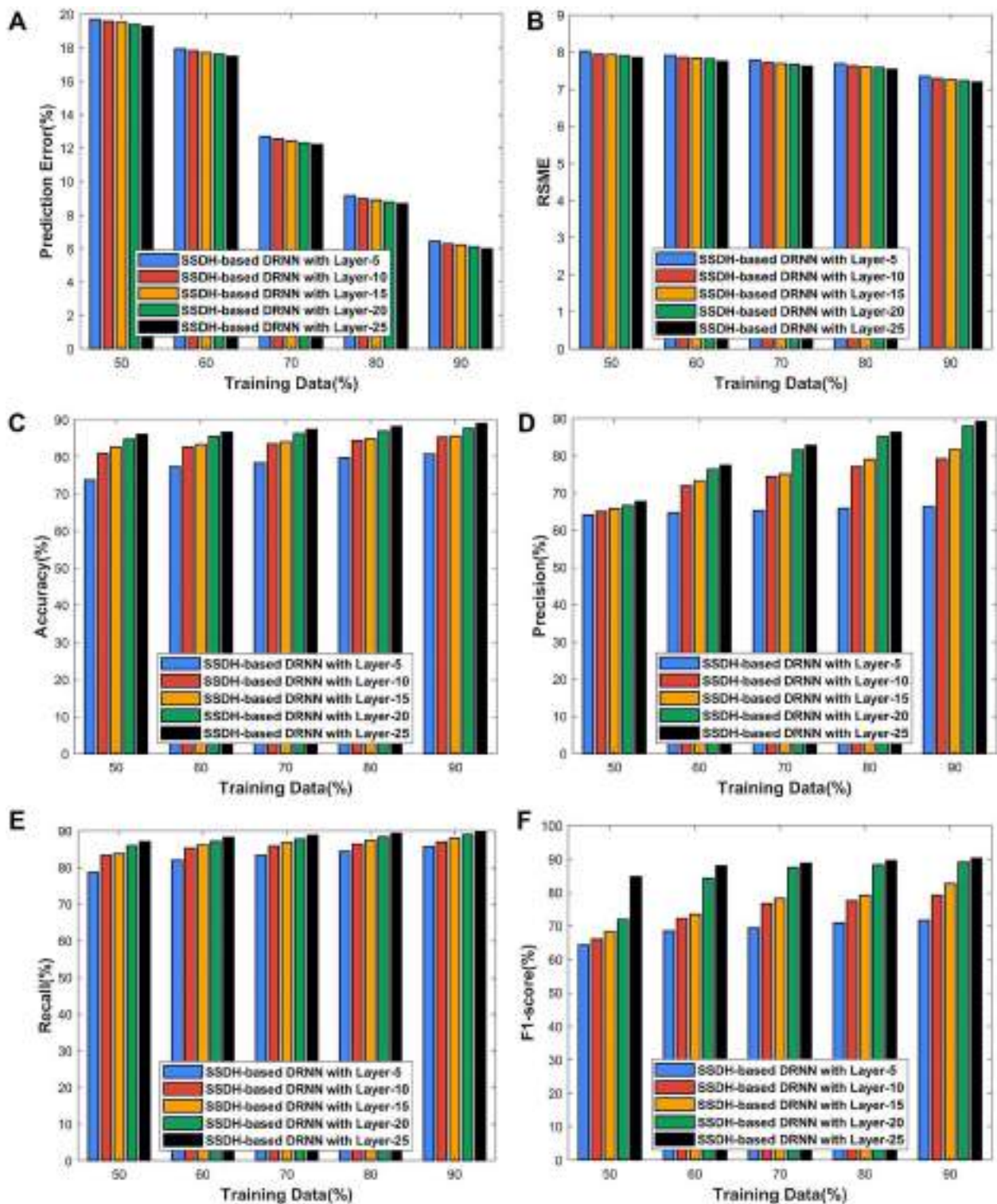


FIGURE 3. Analysis of proposed SSDH-based DRNN using $c = 2$ considering a) Prediction error b), RMSE, c) accuracy, d) precision, e) recall and f) F1-score.

tion of methods with prediction error is described in Fig. 6a). For 40% of training data, the corresponding prediction error

measured by transfer learning-based CNN, GCGCN, DRNN and proposed SSDH-based DRNN are 24.71, 23.65, 22.86 and

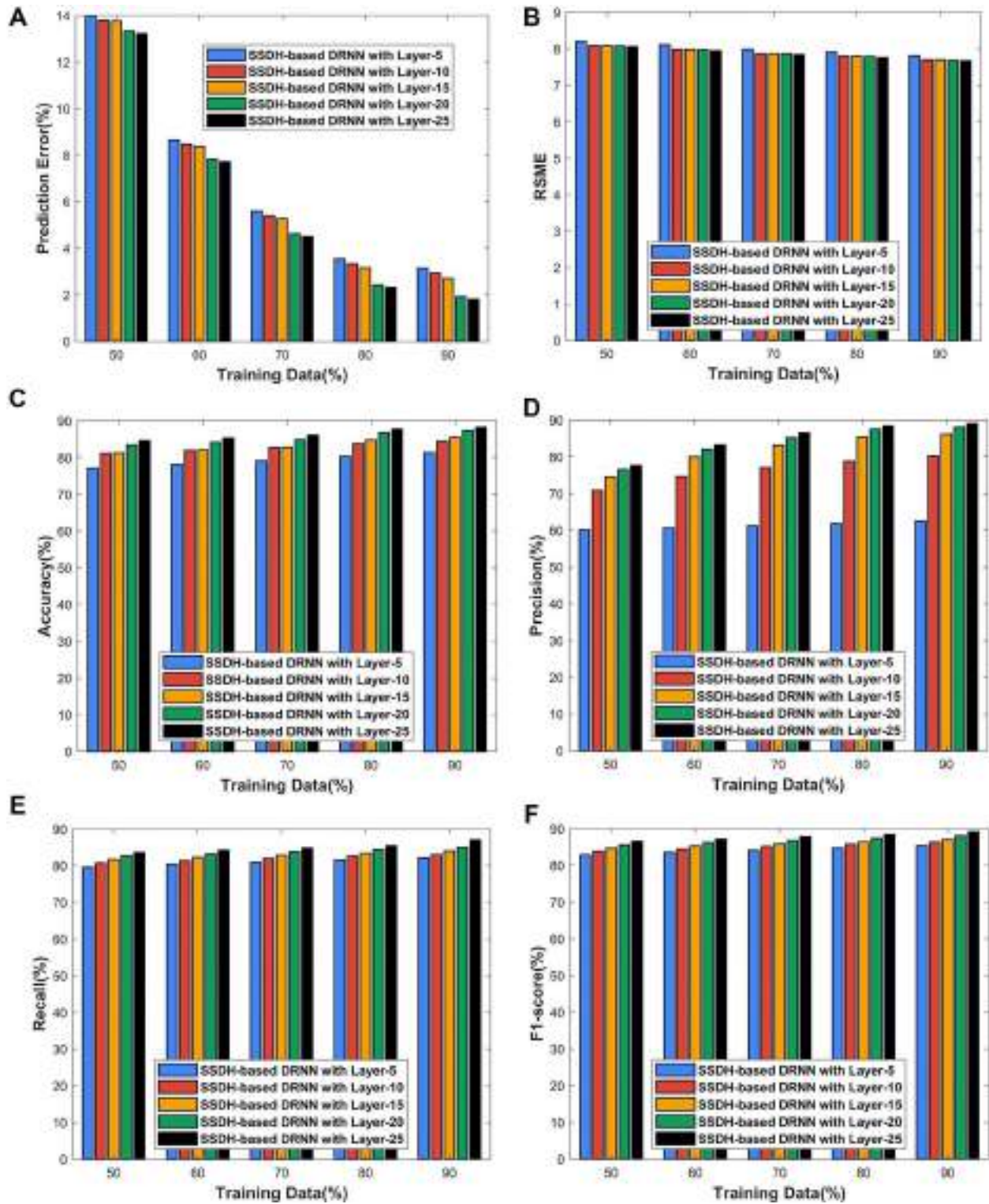


FIGURE 4. Analysis of proposed SSDH-based DRNN using $c = 3$ considering a) prediction error b) RMSE c) accuracy, d) precision, e) recall and f) F1-score.

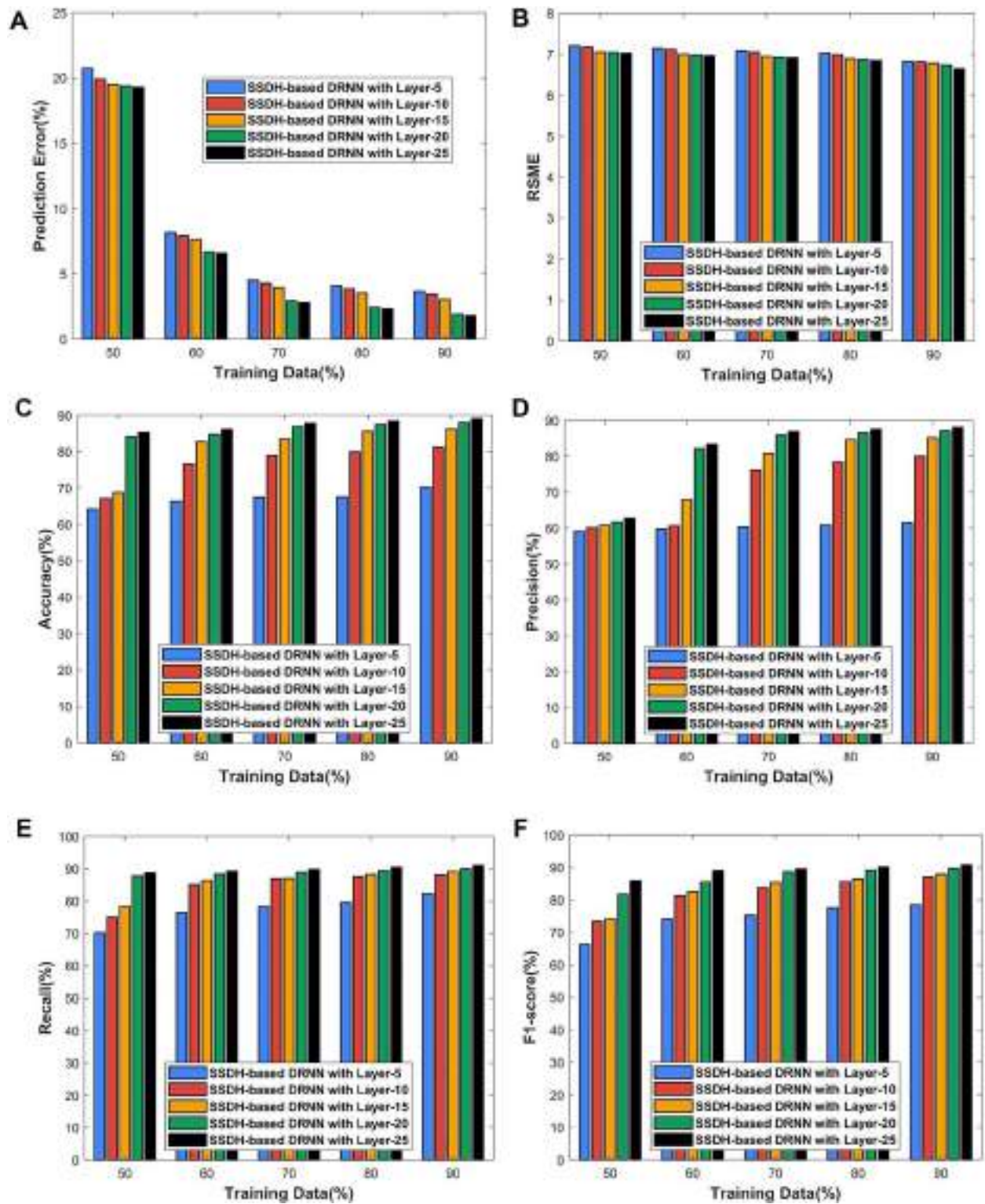


FIGURE 5. Analysis of proposed SSDH-based DRNN using $c = 4$ considering a) prediction error b) RMSE c) accuracy, d) precision, e) recall and f) F1-score.

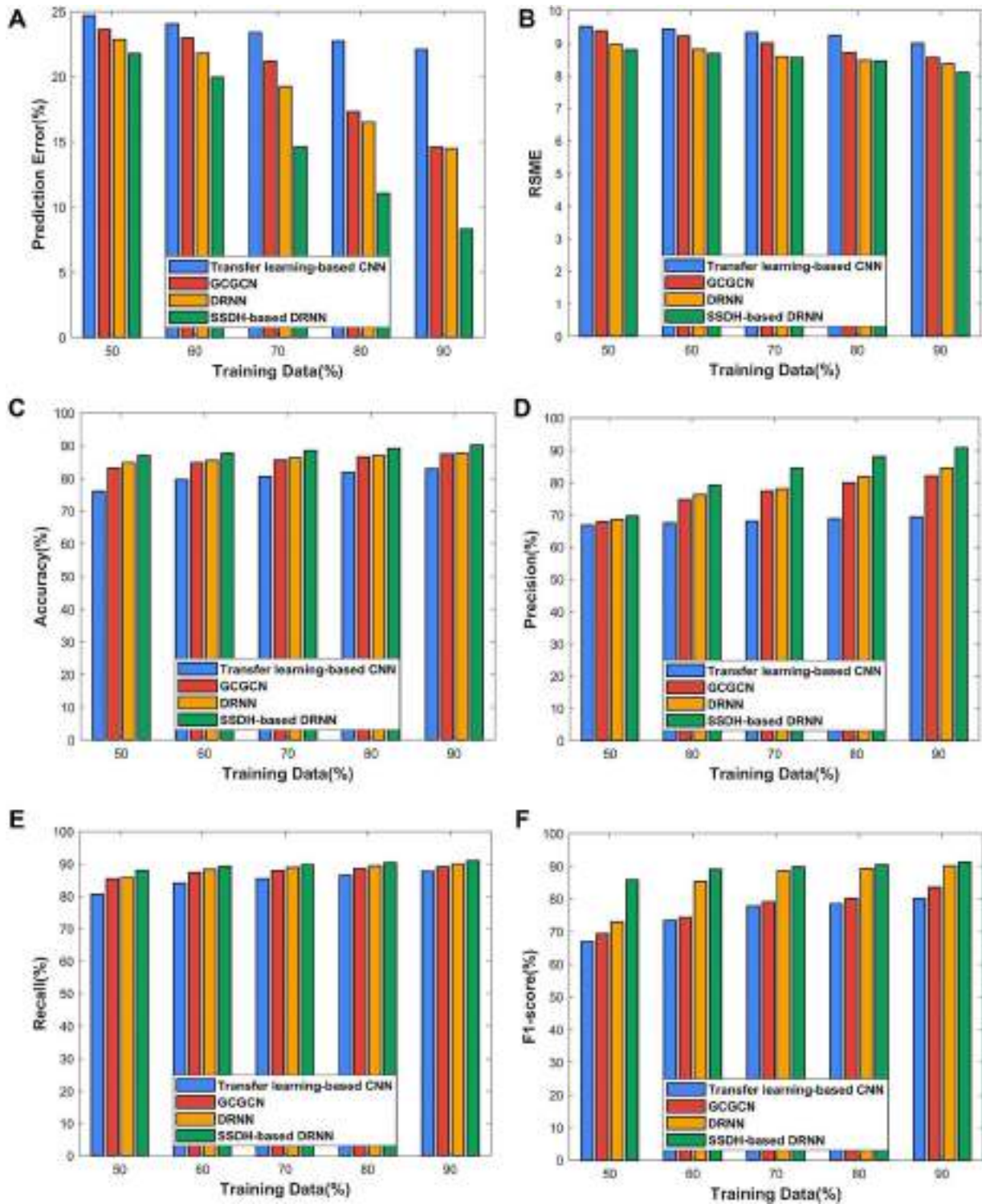


FIGURE 6. Analysis of methods using $c = 2$ considering a) prediction error b) RMSE c) accuracy, d) precision, e) recall and f) F1-score.

21.78%. Likewise, for 80% of training data, the corresponding prediction error measured by transfer learning-based CNN, GCGCN, DRNN and proposed SSDH-based DRNN are 22.09, 14.62, 14.49 and 8.29%. Similarly, while considering all the other matrices, the proposed method outperformed all the other existing techniques.

5.2.1.2. Analysis of methods using $c = 3$ Figure 7 describes the analysis of methods with $c = 3$ considering prediction error, RMSE, accuracy, precision, recall and F1-score. The analysis of methods with RMSE is described in Fig. 7b). For 40% of training data, the corresponding RMSE measured by transfer learning-based CNN, GCGCN, DRNN and proposed SSDH-based DRNN are 9.598, 9.586, 9.407 and 8.1%. Likewise, for 80% training data, the corresponding RMSE measured by transfer learning-based CNN, GCGCN, DRNN and proposed SSDH-based DRNN are 9.23, 8.90, 8.70 and 8.57%. Similarly, while considering all the other matrices, the proposed method outperformed all the other existing techniques.

5.2.1.3. Analysis of methods using $c = 4$ Figure 8 describes the assessment of methods with $c = 3$ considering prediction error, RMSE, accuracy, precision, recall and F1-score. The analysis of methods with accuracy is described in Fig. 8c. For 50% of training data, the corresponding prediction error measured by transfer learning-based CNN, GCGCN, DRNN and proposed SSDH-based DRNN are 67.16, 70.08, 71.66 and 87.03%. Likewise, for 90% of training data, the corresponding prediction error measured by transfer learning-based CNN, GCGCN, DRNN and proposed SSDH-based DRNN are 73.22, 84.22, 89.08 and 90.98%. Similarly, while considering all the other matrices, the proposed method outperformed all the other existing techniques.

5.2.2. Analysis using K-fold validation

5.2.2.1. K-fold analysis of methods using $c = 2$ Figure 9 describes the assessment of methods with $c = 2$ considering prediction error, RMSE, accuracy, precision, recall and F1-score. The k-fold analysis of methods with precision is described in Fig. 9d). For $k = 6$, the corresponding precision measured by transfer learning-based CNN, GCGCN, DRNN and proposed SSDH-based DRNN is 66.55, 73.81, 75.24 and 78.24%. Likewise, for $k = 9$, the corresponding prediction error measured by transfer learning-based CNN, GCGCN, DRNN and proposed SSDH-based DRNN are 68.37, 81.03, 83.53 and 89.81%. Similarly, while considering all the other matrices, the proposed method outperformed all the other existing techniques.

5.2.2.2. K-fold analysis of methods using $c = 3$ Figure 10 describes the assessment of methods with $c = 2$ considering prediction error, RMSE, accuracy, precision, recall and F1-score. The k-fold analysis of methods with recall is described in Fig. 10e). For $k = 7$, the corresponding recall measured by

transfer learning-based CNN, GCGCN, DRNN and proposed SSDH-based DRNN are 81.93, 82.89, 83.85 and 84.81%. Likewise, for $k = 9$, the corresponding prediction error measured by transfer learning-based CNN, GCGCN, DRNN and proposed SSDH-based DRNN are 83.08, 84.04, 85.00 and 88.00%. Similarly, while considering all the other matrices, the proposed method outperformed all the other existing techniques.

5.2.2.3. K-fold analysis of methods using $c = 4$ Figure 11 describes the assessment of methods with $c = 3$ considering prediction error, RMSE, accuracy, precision, recall and F1-score. The k-fold analysis of methods with an F1-score is described in Fig. 11e). For $k = 7$, the corresponding recall measured by transfer learning-based CNN, GCGCN, DRNN and proposed SSDH-based DRNN are 83.41, 85.08, 88.32 and 89.27%. Likewise, for $k = 9$, the corresponding prediction error measured by transfer learning-based CNN, GCGCN, DRNN and proposed SSDH-based DRNN are 86.71, 87.5435, 89.46 and 90.42%. Similarly, while considering all the other matrices, the proposed method outperformed all the other existing techniques.

5.3. Comparative discussion

Table 2 depicts the comparative analysis of techniques with prediction error, RMSE using $c = 2, 3$ and 4. Using $c = 2$, the minimal prediction error of 8.29% is computed by proposed SSDH-based DRNN, while the prediction error measured by classical transfer learning-based CNN, GCGCN and DRNN are 22.09, 14.62 and 14.49%, respectively. The minimal RMSE of 8.102% is computed by proposed SSDH-based DRNN, whereas the RMSE measured by classical transfer learning-based CNN, GCGCN and DRNN are 9.01, 8.57 and 8.37%. The accuracy of 90.26% is computed by proposed SSDH-based DRNN, whereas the accuracy measured by classical transfer learning-based CNN, GCGCN and DRNN are 83.00, 87.49 and 87.75%, respectively. The precision of 90.80% is computed by proposed SSDH-based DRNN, whereas the precision measured by classical transfer learning-based CNN, GCGCN and DRNN are 69.35, 82.02 and 84.52%, respectively. The recall of 90.97% is computed by proposed SSDH-based DRNN, whereas the recall measured by classical transfer learning-based CNN, GCGCN and DRNN are 87.69, 89.05 and 90.01%, respectively. The F1-score of 91.27% is computed by the proposed SSDH-based DRNN, whereas the F1-score measured by classical transfer learning-based CNN, GCGCN and DRNN are 80.11, 83.58 and 90.05%, respectively. Similarly, for all the class values, the proposed system outperformed all the other existing techniques. From the table, it is inferred that the proposed SSDH-based DRNN is effective in cancer-survival rate prediction with minimal error.

The proposed SSDH algorithm is devised by combining SSA and DHOA. Although the search behavior of DHOA is not

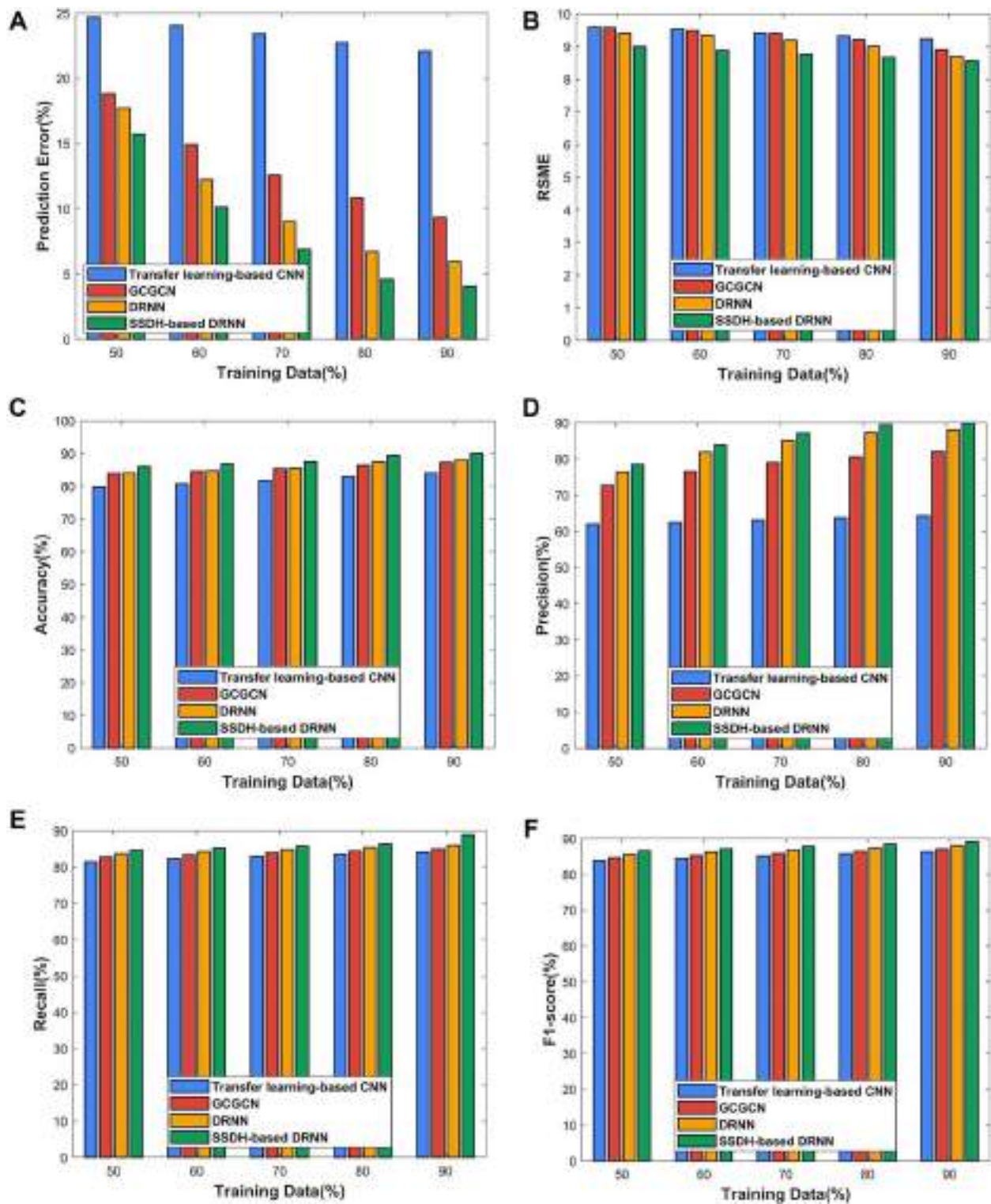


FIGURE 7. Analysis of methods using $c = 3$ considering a) prediction error b) RMSE c) accuracy, d) precision, e) recall and f) F1-score.

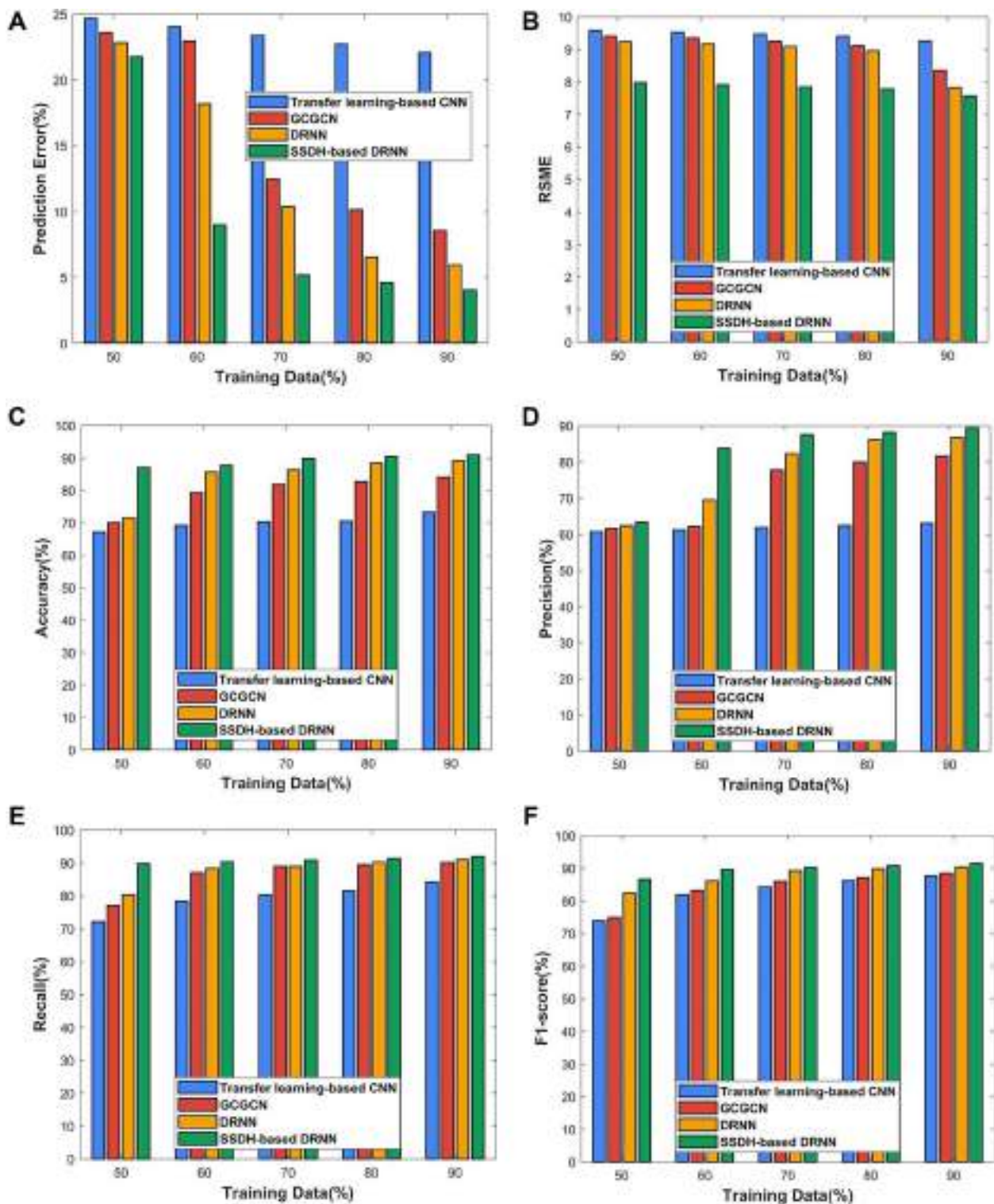


FIGURE 8. Assessment of methods using $c = 4$ considering a) prediction error b) RMSE c) accuracy, d) precision, e) recall and f) F1-score.

consistent, its convergence rate is good, and hence it improves the classification accuracy. SSA has a fast convergence rate. Hence, by combining both the algorithms, a better convergence

rate with high accuracy can be obtained. The DRNN is the best predictor for time series. Moreover, it processes the input of any length.

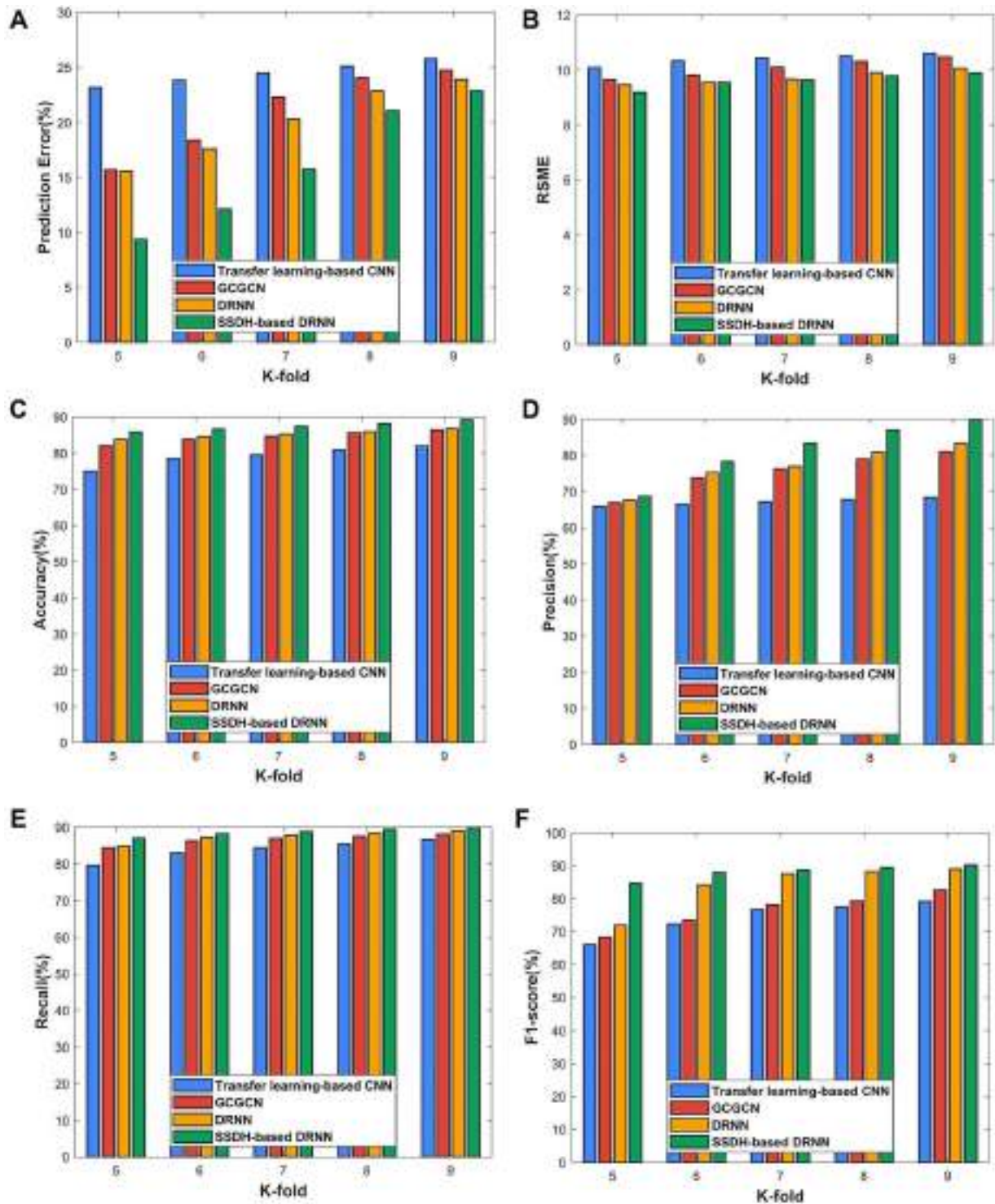


FIGURE 9. K-fold analysis using $k = 6$ considering a) prediction error b) RMSE c) accuracy, d) precision, e) recall and f) F1-score.

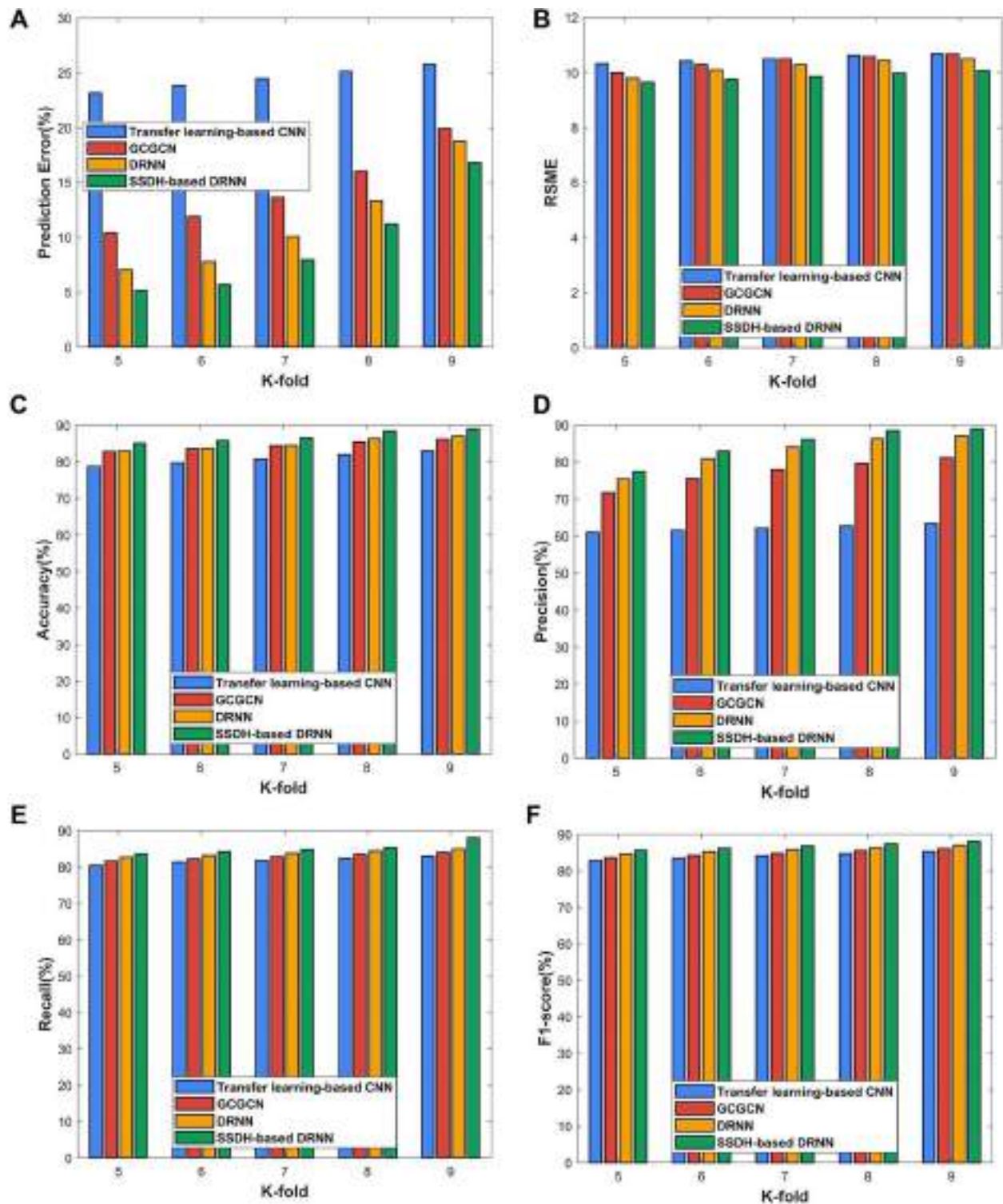


FIGURE 10. K-fold analysis using $c = 3$ considering a) prediction error b) RMSE c) accuracy, d) precision, e) recall and f) F1-score.

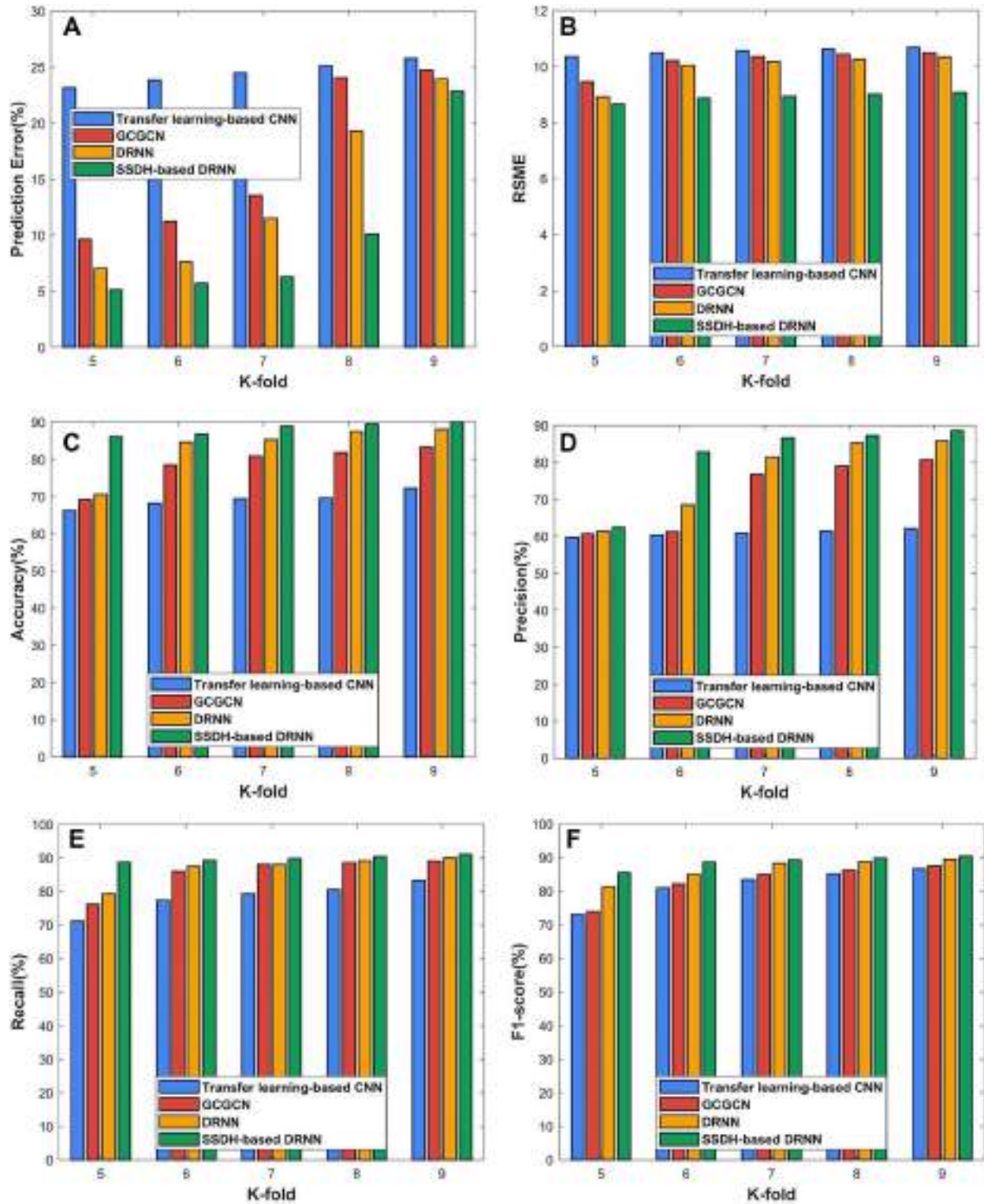


FIGURE 11. K-fold analysis using $c = 4$ considering a) prediction error b) RMSE c) accuracy, d) precision, e) recall and f) F1-score.

TABLE 2. Comparative analysis.

Classes		Metrics	Transfer-learning-based CNN	GCGCN	DRNN	Proposed SSDH-based DRNN		
$C = 2$	Training percentage	Prediction error	22.09	14.62	14.49	8.29		
		RMSE	9.01	8.57	8.10			
		Accuracy	83.00	87.49	87.75	90.26		
		Precision	69.35	82.02	84.52	90.80		
		Recall	87.69	89.05	90.01	90.97		
	K-fold	F1-Score	80.11	83.58	90.05	91.27		
		Prediction error	25.80	24.73	23.94	22.87		
		RMSE	10.61	10.47	10.06	9.89		
		Accuracy	82.02	86.50	86.77	89.27		
		Precision	68.37	81.03	83.53	89.81		
		Recall	86.71	88.07	89.03	89.99		
		F1-Score	79.13	82.59	89.06	90.29		
		$C = 3$	Training percentage	Prediction error	22.09	9.36	5.95	4.05
				RMSE	9.24	8.90	8.71	8.57
Accuracy	84.03			87.27	88.12	90.02		
Precision	64.35			82.10	88.10	89.96		
Recall	84.07			85.03	85.99	88.99		
K-Fold	F1-Score	86.35	87.06	88.07	89.08			
	Prediction error	25.80	19.94	18.79	16.80			
	RMSE	10.69	10.67	10.50	10.08			
	Accuracy	83.05	86.28	87.14	89.04			
	Precision	63.37	81.11	87.11	88.97			
	Recall	83.08	84.04	85.00	88.00			
	F1-Score	85.36	86.08	87.08	88.09			
	$C = 4$	Training percentage	Prediction error	22.09	8.56	5.95	4.05	
			RMSE	9.26	8.37	7.83	7.58	
Accuracy			73.22	84.22	89.08	90.98		
Precision			63.09	81.63	86.84	89.56		
Recall			84.30	90.11	91.07	92.03		
K-Fold		F1-Score	87.70	88.53	90.45	91.41		
		Prediction error	25.80	24.73	23.94	22.87		
		RMSE	10.69	10.50	10.33	9.07		
		Accuracy	72.23	83.23	88.09	89.99		
		Precision	62.11	80.64	85.86	88.58		
		Recall	83.32	89.13	90.09	91.05		
		F1-Score	86.71	87.54	89.46	90.42		

6. CONCLUSION

This paper presents a novel technique, namely SSDH-based DRNN, for predicting cancer survival rate using GE data. In this method, the gene expression data performs data transformation using the polynomial kernel method. Here, the transformed data are utilized for gene selection, wherein Bayesian fuzzy clustering with entropy is adapted. The Bayesian fuzzy clustering assists in grouping similar genes. From the similar genes, the best genes are selected for the prediction. Here, the

prediction of survival rate is made with the survival indicator, which is based on time series data features that involve SMA and the rate of change considering the selected gene. The prediction of survival rate is carried out using DRNN. The training of DRNN is carried out using the proposed SSDH algorithm. The proposed SSDH algorithm is devised by combining SSA and DHOA. The method reveals that small information is adequate for accomplishing precise sample classification. The proposed cancer survival prediction helps to refine the risk stratification and the proper guidance for diagnosis. Besides,

it is helpful for the clinical management of cancer patients, which improve the cancer prognosis. Future work can be done by analyzing the methods with other GE cancer datasets.

DATA AVAILABILITY STATEMENT

The data underlying this article are available in Pan-Cancer (PANCAN) dataset, at <https://xenabrowser.net/datapages/?dataset=GDC-PANCAN.survival.tsv&host=https%3A%2F%2Fgdc.xenahubs.net&removeHub=https%3A%2F%2Fxcna.treehouse.gi.ucsc.edu%3A443>

REFERENCES

- [1] Xiao, Y., Wu, J., Lin, Z. and Zhao, X. (2018) A deep learning-based multi-model ensemble method for cancer prediction. *Comput. Methods Prog. Biomed.*, 153, 1–9.
- [2] Gao, L., Ye, M., Lu, X. and Huang, D. (2017) Hybrid method based on information gain and support vector machine for gene selection in cancer classification. *Genomics Proteomics Bioinformatics*, 15, 389–395.
- [3] Alagukumar S and Lawrance R. (2016). Classification of microarray gene expression data using associative classification. In *Proceedings of International Conference on Computing Technologies and Intelligent Data Engineering (ICCTIDE'16)*, Kovilpatti, India, pp. 1–8. IEEE, Piscataway, New Jersey.
- [4] Ayyad, S.M., Saleh, A.I. and Labib, L.M. (2019) Gene expression cancer classification using modified K-nearest neighbors technique. *Biosystems*, 176, 41–51.
- [5] Halder, A. and Kumar, A. (2019) Active learning using rough fuzzy classifier for cancer prediction from microarray gene expression data. *J. Biomed. Inform.*, 92, 103136.
- [6] Torre, L.A., Bray, F., Siegel, R.L., Ferlay, J., Lortet-Tieulent, J. and Jemal, A. (2015) Global cancer statistics, 2012. *CA Cancer J. Clin.*, 65, 87–108.
- [7] Wang, C., Guo, J., Zhao, N., Liu, Y., Liu, X., Liu, G. and Guo, M. (2019) A cancer survival prediction method based on graph convolutional network. *IEEE Trans. Nanobioscience*, 19, 117–126.
- [8] Dettling, M. and Bühlmann, P. (2000) Boosting for tumor classification with gene expression data. *Bioinformatics*, 19, 1061–1069.
- [9] Mostavi, M., Chiu, Y.C., Huang, Y. and Chen, Y. (2020) Convolutional neural network models for cancer type prediction based on gene expression. *BMC Med. Genet.*, 13, 1–3.
- [10] López-García, G., Jerez, J.M., Franco, L. and Veredas, F.J. (2020) Transfer learning with convolutional neural networks for cancer survival prediction using gene-expression data. *PLoS One*, 5, e0230536.
- [11] Kumar, L. and Greiner, R. (2019) Gene expression based survival prediction for cancer patients—A topic modeling approach. *PLoS One*, 14, e0224446.
- [12] Pierfrancesco, F. et al. (2016) Unilateral paravertebral block compared with subarachnoid anesthesia for the management of postoperative pain syndrome after inguinal herniorrhaphy a randomized controlled clinical trial. *Pain*, 157, 1105–1113.
- [13] Maria, R.M., Antonio, B., Giuseppe, S., Gianluca, P., Riccardo, P., Paolo, M.B., Floriana, D.N, Giovanni, I., Vincenza, C., Ferdinando, D.O., Rocco, Z. (2010). The relationship between anger and heterosexual behavior. *An Investigation in a Nonclinical Sample of Urban Italian Undergraduates, The Journal of Sexual Medicine*, 7, 3899–3908.
- [14] Halder A and Misra S. (2014). Semi-supervised fuzzy K-NN for cancer classification from microarray gene expression data. In *Proceedings of First International Conference on Automation, Control, Energy and Systems (ACES)*, Adisaptagram, India, pp. 1–5. IEEE, Piscataway, New Jersey.
- [15] Zongzhen, H., Junying, Z., Xiguo, Y. and Yuanyuan, Z. (2021) Integrating somatic mutations for breast cancer survival prediction using machine learning methods. *Front. Genet.*, 11.
- [16] Hung, N.T. (2020). Deciphering the increased popularity of Vietnamese students' choice of Asian countries for overseas studies: The influence of motivation for studying abroad on career planning and decision-making process of Vietnamese students in Taiwan. In *The International Conference on Higher Education in Vietnam and Asia: Similarities and Possibilities of Cooperation*.
- [17] Hung, N.T. (2020). A Model of International Students' Choice: A Mixed-Methods Study. In *International Virtual Conference on Public Administration, Social Science & Humanities*.
- [18] Hung, N.T and Chang, J-C. (2019). Preliminary investigation of the current situation and influencing factors of international students in Taiwan under the background of new southbound policy. *Taiwan Educational Review*, 8.
- [19] Auslander, N., Wagner, A., Oberhardt, M. and Ruppim, E. (2016) Data-driven metabolic pathway compositions enhance cancer survival prediction. *PLoS Comput. Biol.*, 12, e1005125.
- [20] Maity, A.K., Bhattacharya, A., Mallick, B.K. and Baladandayuthapani, V. (2020) Bayesian data integration and variable selection for pan-cancer survival prediction using protein expression data. *Biometrics-J. Int. Biometric society*, 76, 316–325.
- [21] Dhillon, A. and Singh, A. (2020) eBreCaP: Extreme learning-based model for breast cancer survival prediction. *IET Syst. Biol.*, 14, 160–169.
- [22] Pan-Cancer (PANCAN) dataset taken from, "<https://xenabrowser.net/datapages/?dataset=GDC-PANCAN.survival.tsv&host=https%3A%2F%2Fgdc.xenahubs.net&removeHub=https%3A%2F%2Fxcna.treehouse.gi.ucsc.edu%3A443>", accessed on July 2020.
- [23] Breiman, L. (1996) Bagging predictors. *Mach. Learn.*, 24, 123–140.
- [24] Cho S.B and Won H.H. (2003). Machine learning in DNA microarray analysis for cancer classification. In *Proceedings of the First Asia-Pacific bioinformatics conference on Bioinformatics*, Adelaide, Australia, pp. 189–198. Australian Computer Society, Australia.
- [25] Mamoshina, P., Vieira, A., Putin, E. and Zhavoronkov, A. (2016) Applications of deep learning in biomedicine. *Mol. Pharm.*, 13, 1445–1454.
- [26] Bishop, C.M. (2006) *Pattern Recognition and Machine Learning*. Springer, New York.
- [27] Tan P L, Tan S C, Lim C P, Khor S E. (2011). A modified two-stage SVM-RFE model for cancer classification using microarray data. In *Proceedings of International Conference on*

- Neural Information Processing*, Shanghai, China, pp. 668–675. Springer, Berlin, Heidelberg.
- [28] Priscilla, R. and Swamynathan, S. (2013) A semi-supervised hierarchical approach: Two-dimensional clustering of microarray gene expression data. *Front. Comp. Sci.*, 7, 204–213.
- [29] Inoue, M., Inoue, S. and Nishida, T. (2018) Deep recurrent neural network for mobile human activity recognition with high throughput. *Artificial Life and Robotics*, 23, 173–185.
- [30] Jain, M., Singh, V. and Rani, A. (2019) A novel nature-inspired algorithm for optimization: Squirrel search algorithm. *Swarm and evolutionary computation*, 44, 148–175.
- [31] Brammya, G., Praveena, S., Preetha, N.S., Ramya, R., Rajakumar, B.R. and Binu, D. (2019) Deer hunting optimization algorithm: A new nature-inspired meta-heuristic paradigm. *Comput. J.*
- [32] Liu, J., Chung, F.L. and Wang, S. (2017) Black hole entropic fuzzy clustering. *IEEE Transactions On Systems, Man, And Cybernetics: Systems*, 48, 1622–1636.
- [33] Glenn, T.C., Zare, A. and Gader, P.D. (2014) Bayesian fuzzy clustering. *IEEE Trans. Fuzzy Syst.*, 23, 1545–1561.
- [34] Largeron, C., Moulin, C. and Géry, M. (2011). Entropy based feature selection for text categorization. In *Proceedings of the ACM symposium on applied computing*, TaiChung Taiwan, pp. 924–928. Association for Computing Machinery, New York, United States.

Plant Disease Classification Using Deep Bilinear CNN

D. Srinivasa Rao¹, Ramesh Babu Ch², V. Sravan Kiran¹, N. Rajasekhar^{3,*}, Kalyanapu Srinivas⁴,
P. Shilhora Akshay¹, G. Sai Mohan¹ and B. Lalith Bharadwaj¹

¹VNR VJIET, Hyderabad, 500090, India

²Geetanjali College of Engineering and Technology, Hyderabad, 501301, India

³Gokaraju Rangaraju Institute of Engineering and Technology, Hyderabad, 500090, India

⁴Kakatiya Institute of Technology and Science, Warangal, 506015, India

*Corresponding Author: N. Rajasekhar. Email: rajasekhar531@gmail.com

Received: 08 February 2021; Accepted: 24 April 2021

Abstract: Plant diseases have become a major threat in farming and provision of food. Various plant diseases have affected the natural growth of the plants and the infected plants are the leading factors for loss of crop production. The manual detection and identification of the plant diseases require a careful and observative examination through expertise. To overcome manual testing procedures an automated identification and detection can be implied which provides faster, scalable and precise solutions. In this research, the contributions of our work are three-fold. Firstly, a bi-linear convolution neural network (Bi-CNNs) for plant leaf disease identification and classification is proposed. Secondly, we fine-tune VGG and pruned ResNets and utilize them as feature extractors and connect them to fully connected dense networks. The hyperparameters are tuned to reach faster convergence and obtain better generalization during stochastic optimization of Bi-CNN(s). Finally, the proposed model is designed to leverage scalability by implying the Bi-CNN model into a real-world application and release it as an open-source. The model is designed on variant testing criteria ranging from 10% to 50%. These models are evaluated on gold-standard classification measures. To study the performance, testing samples were expanded by 5x (i.e., from 10% to 50%) and it is found that the deviation in the accuracy was quite low (0.27%) which resembles the consistent generalization ability. Finally, the larger model obtained an accuracy score of 94.98% for 38 distinct classes.

Keywords: Bilinear convolution neural networks (Bi-CNN's); plant disease classification; mobile API; deep learning; neural networks

1 Introduction

Agriculture is the only way for crop production and livelihood. One of the major risk factors of crop productions is dealing with plant diseases. Every single crop produced is linked with a plant disease, which is an obstacle for healthy crop production and this tops the list of reasons for the loss of crop production. If a crop has a plant disease then the symptoms can be noticed by keen observation of



This work is licensed under a Creative Commons Attribution 4.0 International License, which permits unrestricted use, distribution, and reproduction in any medium, provided the original work is properly cited.

different parts of the leaves. Plant diseases are categorized into pests, weeds and plant pathogens. The annually estimated average loss due to pathogens and pests are nearly 13%–22% on the world's major crop productions like Rice, Wheat, Maize, Potatoes etc. Over the past few decades, farmers used to identify these diseases by observing the leaves through naked-eye. However, this requires the farmer to be extremely skilled or would require the guidance of an agricultural scientist to notice the disease and this process consumes a lot of time.

One of the major reasons for the loss in production is due to diseases like bacterial spot, early blight, late blight, and leaf mould that occur frequently on the leaves of the tomato plant at different stages of its growth. Potatoes are one of the most dominant food crops where the yield of potatoes is reduced by diseases *Phytophthora infestans* (late blight) and *Alternaria solani* (early blight). The average yield loss at a global level due to pathogens and pesticides is around 17.2% in potatoes. Apple is been one of the most produced fruits because of its nutritional and medicinal importance where the severity caused by the diseases (Mosaic, Rust, Brown spot, and Alternaria leaf spot) on apple leaves led to huge production and economic loss which also affected the quality in production. Early detection of these types of conditions in the plants that are unhealthy allows us to take precautionary measures and alleviate the production of crops.

In this research, we mainly focus on developing automatic, accurate and less expensive Restful-API into a Mobile-App to detect and classify variant kinds of leaves using Bi-Linear Convolution Neural Networks (Bi-CNNs). The contributions to the body of the knowledge are mentioned as,

1. We propose a bi-linear convolution neural network (Bi-CNNs) for plant disease identification and classification with a leaf images as input.
2. Secondly, we fine-tune VGG and pruned ResNets and utilize them as feature extractors and they're connected to fully connected dense networks. The hyperparameters are tuned to reach faster convergence and obtain better generalization during stochastic optimization of Bi-CNN(s).
3. Lastly, the proposed model is designed to leverage scalability by implying the Bi-CNN model into a real-world application and release it as an open-source. The detailed explanations of the product are mentioned in the last section.

2 Motivation

The design paradigm of the proposed architecture is motivated by the two distinct cortical pathways of the human brain. These two cortical pathways oblige to understand the object vision and spatial vision separately. The occipitoparietal, the dorsal system, helps understand the visual location of the targeted object whereas, the occipitoparietal, the ventral stream, extracts the visual representations of objects i.e., identifying the objects [1]. These two critical pathways extract the information regarding an object from retrieval input to the striate cortex at a juncture. But, the occipitotemporal pathway interconnects the striate the pre-striate and activated to inferior temporal regions which eventually helps to identify the visual stimulus understanding the physical properties of the targeted object.

Further, the occipital parietal pathway the striate then pre-striate are activated to inferior parietal areas which help to localize the visual stimulus i.e., understanding the spatial location of the targeted object. Finally, the two cortical pathways are reintegrated by providing selective attention by adjoining the visual stimulus. These 2 selective attentions are provided to the external feature representation such as color, shape and spatial locations. These activations are seen in the exhaustive cortex. Thus, the neural architecture provides selective attention from the learned representations [2].

The main motive of this research is to provide an application-oriented deep bi-linear convolution neural network that provides selective attention in the neural network by adapting a neuroscience perspective for

classifying distinct plant leaves from their infection classes. The mathematical study is furnished in the methodology section.

3 Previous Research

Siddharth et al. [3] developed a model for the identification and classification of diseases in plant leaf images. The proposed model is based on Radial Basis Function Neural Network (BRBFNN) which uses bacterial foraging for optimization and increases the training speed of the network. The algorithm (Bacterial Foraging) searches for the common attribute by the grouping of seed points for identifying the features. Their classification results are based on validation evaluation partition coefficient (Vpc) and validation evaluation partition entropy (Vpe). They also compared their model with traditional machine learning methods such as K-means and SVM. The specificity of the proposed model for segmentation is 0.558 and for classification upon Vpc and Vpe is 0.8621 and 0.1118 respectively.

Aydin et al. [4] has experimented on various transfer learning models to analyze the classification performance. During experimentation, they have four models and analyzed this performance on publicly available datasets. Additionally, they have proposed a CNN model adjoined with LDA to classify the deep featured extracted from the pre-trained network (AlexNet & VGG16). To analyze the performance of the model five-fold cross-validation procedure was adapted and the input size of an image was considered as 100×100 . The proposed model obtained an accuracy score of 96.93% whereas the pre-trained VGG16 model outperformed with an accuracy of 99.80%. Karthik et al. [5] has researched tomato leaves diseases and proposed two variant CNN architectures. with the help of Residual Progressive Feature Extraction, the model has extracted spatial features with 0.6M parameters. By performing five-fold cross-validation the model obtained an accuracy of 98%.

Mohanty et al. [6] performed experimentation on plant village dataset by using AlexNet & GoogleNet. By contemplating variant types GoogleNet got an accuracy of 98% on grayscale, 99.34% on colour, and 99.25% on segmented images with 5 different splits on 20% test samples. Uday Pratap et al. [7] Multilayer Convolutional Neural Network (MCNN) for classification of mango leaves that are infected with anthracnose disease. The dataset consists of 1070 images of mango leaves which is a real-time dataset captured in a university. The proposed model was validated by 20% test samples and compared with various machine learning techniques. The MCNN model got an accuracy of 97.13%. Sandeep Kumar et al. [8] has implied a new optimization technique called Exponential Spider Monkey Optimization (ESMO) for plant disease identification. SPAM is applied for feature extraction to classify if a leaf is healthy or diseased. Distinct machine learning models are used to evaluate the performance, it was concluded that SVM outperformed other models with an accuracy of 92.1%.

Qiao Kang et al. [9] proposed a network that uses ResNet50 architectures as a backbone model to diagnose plant disease and severity estimation. The proposed network consists of shuffle units as an auxiliary structure which increases the performance of the model. The dataset was collected from the AI challenger Global AI contest which consists of 7 different plant species with an Image size of $256 \times 256 \times 3$. The proposed method got a classification accuracy of 98% and a recognition accuracy of 99%.

Ahmed et al. [10] introduced a model called CaffeNet, It was built on a Caffe framework to label paddy pest and paddy diseases. This work used a database that has 9 paddy pests and 4 paddy disease classes. The aforementioned model was fine-tuned over 30,000 iterations and obtained an accuracy score of 87%. Islam et al. [11] utilized machine learning algorithm and image preprocessing techniques to segment and identify potato disease from the plant village database. It was observed that SVM had an accuracy of 95% (over 300 images).

4 Methodology

4.1 Dataset Description

The complete data was collected from the open repository [12]. The dataset was publicly available for research and hence can be implied for classification and identification of distinct plant disease which can be achieved by designing a user-friendly mobile application. The experimentation is carried out in three folds. The First experimentation, which is named D_1 , was carried out in 18 classes. In which there are 9 variant fruit leaf images with healthy and unhealthy kinds. As a note, all the variants of unhealthy classes constructed in D_1 contains various types such as early blight, black rot, bacterial spot etc. This means all the infected kinds of plant leaves are considered as an unhealthy class of that particular leaf kind.

Next, the experimentation was carried out (D_2) where three variant plant leaf images are considered with their multiple infected classes. Lastly, the experimentation was carried out with (D_3) which contains the complete 38 classes. The description of the train and test for D_1 , D_2 , and D_3 is clearly illustrated below (refer to Tab. 1). The complete partitions of the dataset into D_1 , D_2 , and D_3 are mentioned in the repository¹.

Table 1: Variant models designed for different data sampling

Dataset Variants	Train-Test kinds	Classes	Train	Test	Total
D_1	G_1	18	20,006	20,004	40,010
	G_2	18	32,007	8003	40,010
	G_3	18	36,008	4002	40,010
D_2	Tomato (70–30)	10	12,712	5448	18,160
	Potato (70–30)	3	1506	646	2,152
	Maize (70–30)	4	4480	1920	6400
D_3	Whole data (70–30)	38	38,013	16,292	54,305

4.2 Feature Extraction Models

VGG Models were utilized while developing a Bi-CNN model where, the two models considered for extracting features are VGG16 and VGG19. The VGG16 and VGG19 contain consecutive convolution and pooling layers with a depth of 16 and 19 layers respectively. These models are pre-trained on the finest weights. The VGG16 and VGG19 models consume 138.3 and 143.6 Million parameters with an input shape of 224×224 with three coloring channels. While developing the Bi-CNN model it is assumed that one of the VGG models do capture spatial invariances and the other captures the location of an entity residing in the image [13].

ResNet Models ResNet models are also considered for feature extraction. Two flavors of ResNet’s are implied which are 50 layers deep and the other is 101 layers deep. These ResNet models can capture the invariances of the input by overcoming the problem of degradation. The deep residual connections help to rectify the vanishing gradients and regulate learning for deeper layers. These ResNets are not only computationally cheap but are much deeper and capable of capturing invariances with greater performance. Hence, the two flavors are implied by pruning the network appropriately [14].

The bottom layers with greater feature maps i.e., 2048 activations are excluded. The ResNet model is pruned by truncating the last four activations. During experimentation, it is observed that these activations (final activations) led to high computations. But the original model performance was higher than that of the pruned model. Hence, the ResNet model was pruned by truncating the last four layers

¹Source: <https://github.com/LalithBharadwaj/BiCNN-plant-leaf>.

with 512 as final activation maps (similar to that of VGG). Similarly, while developing the Bi-CNN model it is assumed that one of the ResNet models do capture spatial invariances and the other captures the location of an entity residing in the image.

Finally, these models (VGG and ResNet models) are fine-tuned with regulated training procedure to reach faster convergence with greater generalization.

4.3 Bi-Linear Convolution Neural Network (Bi-CNN's)

As mentioned, Bi-CNN's are motivated by the visual perception of the human brain through two cortical visual pathways. This motivation led to the design of a neural network that extracts spatial locations of the entity residing in an image and captures the structural invariances. So, to extract features bottleneck activations of the pre-trained network are utilized. A set of features for extracting spatial location and morphology of input are chosen as $Net - X$ and $Net - Y$ [15].

Whereas, in our methodology, we utilize not only pre-trained VGG models (as [15]) but also ResNet's intermediate activations by cautious architecture pruning. To classify D_1 only VGG models i.e., VGG16 and VGG19 are utilized. In the case of D_2 , Pruned ResNet and also VGG models are utilized. But for D_3 , only pruned ResNet is employed.

$$fv_x, fv_y \leftarrow Net - X(D), Net - Y(D); \quad (1)$$

$$fv_z \leftarrow \frac{1}{N} \left[\sum_{i=1} fv_x \cdot fv_y^T \right] + eI \quad (2)$$

Which can be simplifies as,

$$fv_z \leftarrow fv_x \odot fv_y \quad (3)$$

where \odot represents the element-wise product for given two feature vectors.

For a clear understanding, the bottleneck activations extracted from the feature extracting models i.e., fv_x and fv_y are pooled by implying second-order pooling i.e., outer-product is applied to pool those features to linearize to form fv_z as a feature vector. This feature vector contains the fine-grained features and the outer-product is appropriately described below. Next, to regularize the model normalization is adapted. This normalization is processed in three steps i.e., three normalization layers are sequentially attached. The first normalization layer is chosen as either natural logarithm of the square root of the individual features extracted from fv_z . So, after the first normalization, the features are followed up with a signed square-root as a normalization step. The mathematical formulation for the signed square-root is described below. Thirdly, the feature vectors are regularized through an l_2 -normalization constraint. When the non-linearities are not regulated properly the maximum probability mass function for each sample is assigned as logit i.e., activated via sigmoid. These assignments certainly cause fragile activations with a high chance for saddle points.

This scenario can be prevented by choosing l_2 -normalization as the final activation layer. Hence, these three normalization layers can produce effective outcomes by transforming features into a regulated latent space.

$$N_1 \leftarrow \sqrt{fv_z} \text{ or } \log(fv_z) \quad (4)$$

Both the normalizations i.e., square-root and logarithm are chosen. As a note, both the normalizations are not chosen at a time.

$$N_2 \leftarrow sgn(N_1) \cdot |N_1|^{\frac{1}{2}} \quad (5)$$

$$N_3 \leftarrow L_2 - Norm(N_2) \quad (6)$$

where,

$$L_2 - Norm \leftarrow \frac{x_i}{\sqrt{(\sum_{i=1} x_i^2)}} \quad (7)$$

Next, these latent representations which capture the information regarding the whole image are to be classified appropriately. Tsung Yu et al. [15] implied SVD and LYAP methods for computing the matrices. They are not end-to-end trained neural architectures. They do not have GPU computation end-to-end where; they only compute the extracted feature vectors by classifying them through CPU. For efficient end-to-end training, a fully connected neural network is chosen with successive dropout and batch normalization layers. The major differences from Tsung Ye et al. [15] is, they implied only VGG as pre-trained network and did not imply end-to-end training via backpropagation. But, in this research, a better feature extractor i.e., ResNet's are implied with end-to-end training.

As a note, the feature-extraction method is the same for all the models mentioned in Tab. 1. But the final layer activations are varied from 3 to 38 depending upon the model. In the given Fig. 1, it can be observed that N is mentioned at final softmax activation which is chosen based on the specific model to be fine-tuned. The feature extraction part is fine-tuned and the classification part is fully trained. In this complete procedure, the gradient flow in the network is appropriately analyzed.

4.4 Architecture Parameters

This section gives a complete illustration of the hyperparameter tuning and optimization of model during the course of training Bi-CNNs. The classification architecture is built by fully connected networks with 256-128-N as the pattern. Where N is number of classes for discriminating the input. Firstly, the feed is activated via ReLU as non-linearity. Further, the batch normalization layer is implied to reduce the problem of covariate shift [16]. Next, a dropout layer is added as a regularization method which eventually reduces overfitting [17]. The drop ratio of neurons for reducing overfitting using dropout is chosen as 30% (which is chosen while optimization). The weights for the initialization of the learning procedure are chosen to be glorot-normal [18].

There are variant models trained. The D1 models are trained using negative log-likelihood as cost function (Loss1). Whereas, for both of the D2, and D3 squared hinge (Loss2) is used as a cost function for stochastic optimization of neural network. The equations are formulated as mentioned as,

$$Loss_2 \leftarrow \sum_i \sum_k \max \left(0, \frac{1}{2} - y_k^{(i)} \widehat{y}_k^{(i)} \right) \quad (8)$$

$$Loss_1 \leftarrow - \sum_i \sum_k y_k^{(i)} \cdot \log \left(\widehat{y}_k^{(i)} \right) \quad (9)$$

where i is no. of instances (feature samples) and k is no. of class labels. $y^{(i)}$ is the ground truth class labels for the class k with an i^{th} instance. $\widehat{y}_k^{(i)}$ is the predicted class label. Further to optimize the model adam [19] is chosen as an optimizer with an initial learning rate of 0.0005. The training schedules are designed by motivating from the work by Samuel L et al. [20]. Where the noise during the training procedure is either reduced by increasing batch size or decaying learning rate (keeping the momentum variable to be constant). The noise during the training is mathematically understood as,

$$noise \propto D_{train} \left[\frac{rate}{batch. (1 - momentum)} \right] \quad (10)$$

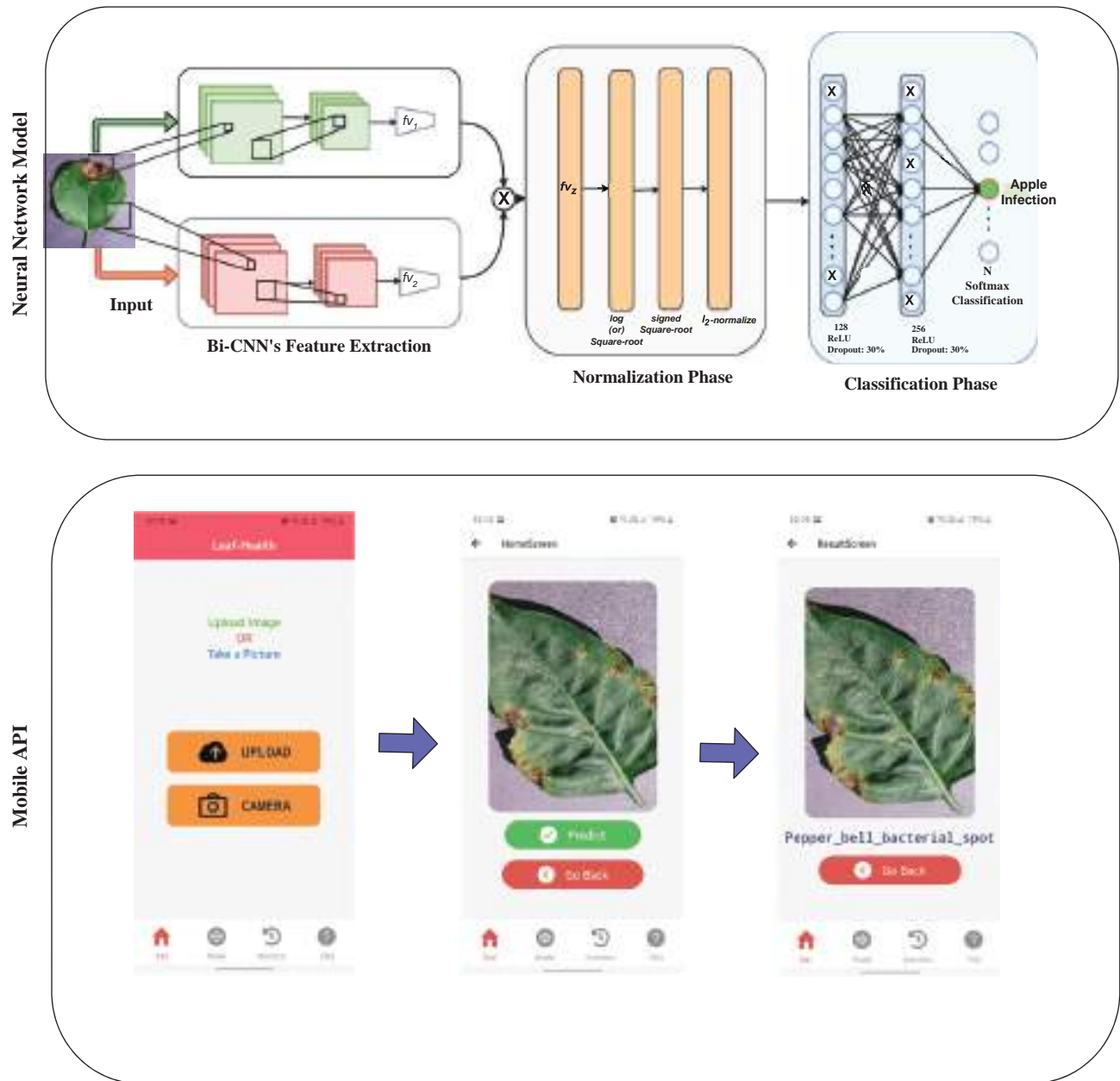


Figure 1: The proposed Bi-linear convolution neural network-integrated in a Mobile App

The aim is to decrease noise during training either tweaking the learning rate schedules or batch size. So, slowly increase the learning rate by increasing batch size to obtain faster convergence with greater generalization ability. As the training samples are large regularization provided by l2 would be useful and accordingly learning rates are scheduled [21]. To provide appropriate learning with faster convergence and proper generalization a definite training schedule is obtained, where for every single iteration (≈ 4 epochs) batch size and learning rate are updated cautiously.

At the first iteration, the batch size is initialized as 10 ($batch_0 \leftarrow 10$) and the learning rate is initialized as 0.5×10^{-3} ($rate_0 \leftarrow 0.5 \times 10^{-3}$). Next, in the second iteration learning is increased to 0.001 and batch size is increased twice of the previous batch i.e., 20. Finally in the third iteration learning is held constant to

0.001 and the batch is increased by 5 units per batch i.e., 25. This iterative computation for stochastic optimization of a neural network is chosen for D1, D2, and D3 respectively. This eventually aided to reach faster convergence with cautious hyperparameter tuning as mentioned² [22].

5 Results

To determine the performance of the Bi-CNN's, classification metrics are implied based on their significance. The metrics such as accuracy score, Receiver operating characteristics (ROC) area under the curve (AUC) [23] and mean-squared error (MSE) are utilized to determine the performance. Accuracy is chosen as the gold standard metric to evaluate classification performance as it aggregates the instances which are correctly classified and divide them with complete instances which are both classified as correct and incorrect.

Next, MSE is utilized as a metric to determine the performance of regression models which observes the deviation from the ground truth to that of predicted instances. So, the deviation can also help determine the performance of the model even when ground truth labels are provided. Finally, AUC is calculated by plotting the true positive rate on the y-axis and the false positive rate on the x-axis. The performance evaluation is carried out by developing variant models as per Tab. 1. The complete result section is divided into two different sections and is are explained below.

5.1 Evaluated on D_1

In D_1 one of the models is produced either by applying square-root as the first normalization layer and the other as a logarithm. Each of the models mentioned in Tab. 1 is evaluated with various metrics. During the evaluation, it is observed that the Bi-CNN model with square-root as the first normalization layer outperformed the logarithm in all of the generalization's splits.

But, to know whether the proposed model is providing visual attention to the required regions or not heat maps are generated. These heat maps are also known as class activation maps (CAM's). Heat maps visually describe the final layer activations of the model and impart color to the highly activated regions (i.e., coloring the region of interest). So, to understand these activations from the bottleneck layer f_{v_z} heat map is plotted for three different plant leaf kinds (apple, corn, peach) with infection classes and visually depicted in Figs. 2 and 3.

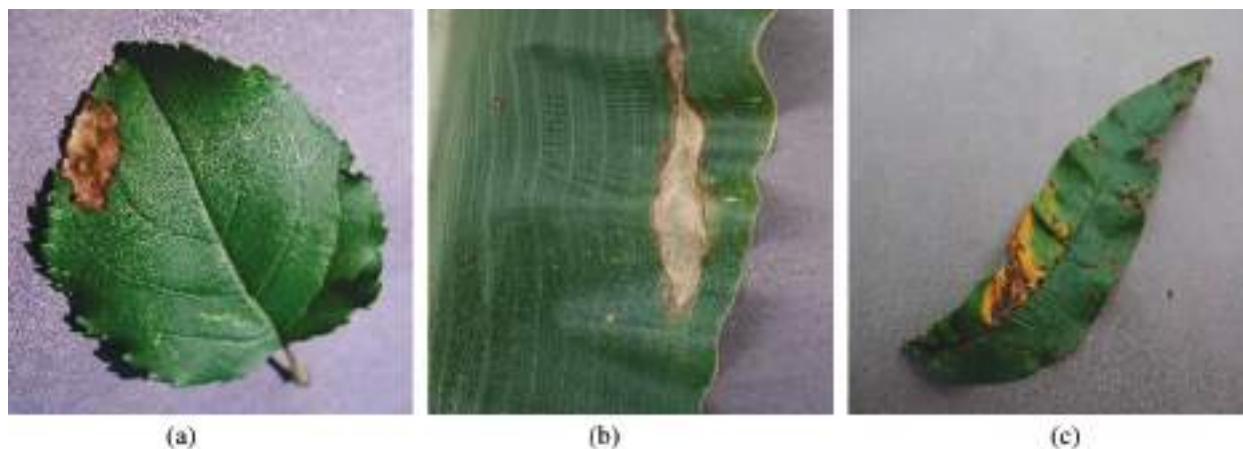


Figure 2: Infected leaves. (a) Unhealthy apple leaf (b) Unhealthy corn leaf (c) Unhealthy peach leaf

²To implement the proposed methodology Tensorflow is utilized in the backend [22].

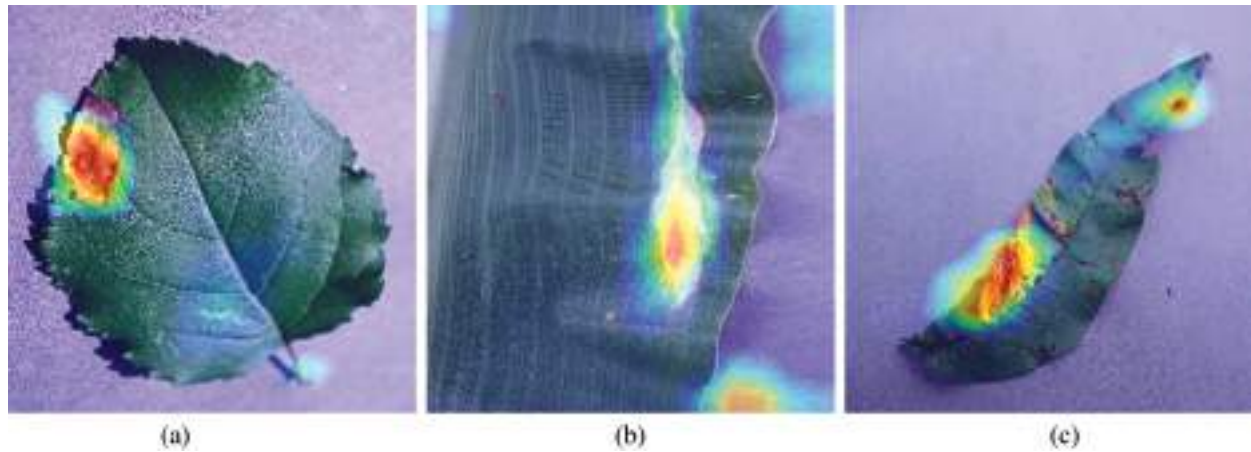


Figure 3: Class activation maps (CAM's) of Infected leaves. (a) CAM's of apple infected leaf (b) CAM's of corn infected leaf (c) CAM's of peach infected leaf

They have the unique property of being insensitive to alterations in the class distributions and can provide good relative instance scores. For handling multiple classes, ROC is calculated by considering one class (chosen) as positive and the remaining classes are considered to be negative ones. So, 18 different AUC-ROC curves are generated. These AUC-ROC curves are generated for the model Bi-CNN (sqrt), as its performance was optimal, for all the generalization splits and visualized in Fig. 4. Further, AUC-ROC curves [23] are generated for an individual class. AUC is used as a metric in Tab. 2 as they provide detailed characteristics of the classifier.

5.2 Evaluated on D_2 and D_3

In this section, D_2 , and D_3 models are evaluated with appropriate metrics. D_2 models are trained on highly imbalanced classes of plant leaves. The D_2 models consist of a single plant leaf with its healthy class and the remaining unhealthy classes.

To understand the model's performance, as mentioned, two variant feature extractors i.e., VGG and ResNet models are implied. When the model was fine-tuned as mentioned in Section 4.4, it is seen that ResNet models were able to extract invariant features and have good learning compared to that of VGG models. To see the convergence of the models D_2 set i.e., the plant leaves of tomato, potato, and maize (corn) are fine-tuned on both ResNet's and VGG models. It is observed that. For very few iterations (epochs = 25), the ResNet models were able to outperform VGG models in every scenario. The learning curves for the D_2 for both the feature extractors are plotted in Fig. 5. The performance of the individual D_2 model is illustrated in Tab. 3.

As observing the ability of ResNets, a set of 38 classes are end-to-end fine-tuned to compare the model's ability to generalize on unseen samples. This D_3 , consist of all the infected and healthy leaf images of variant plants. This model was trained as mentioned in Section 4.3, and further, the convergence appeared slow because the model utilized squared hinge as the objective function. The model attained an accuracy of 94.98% fine-tuned for ≈ 112 epochs. The performance of D_3 model is illustrated in Tab. 3.

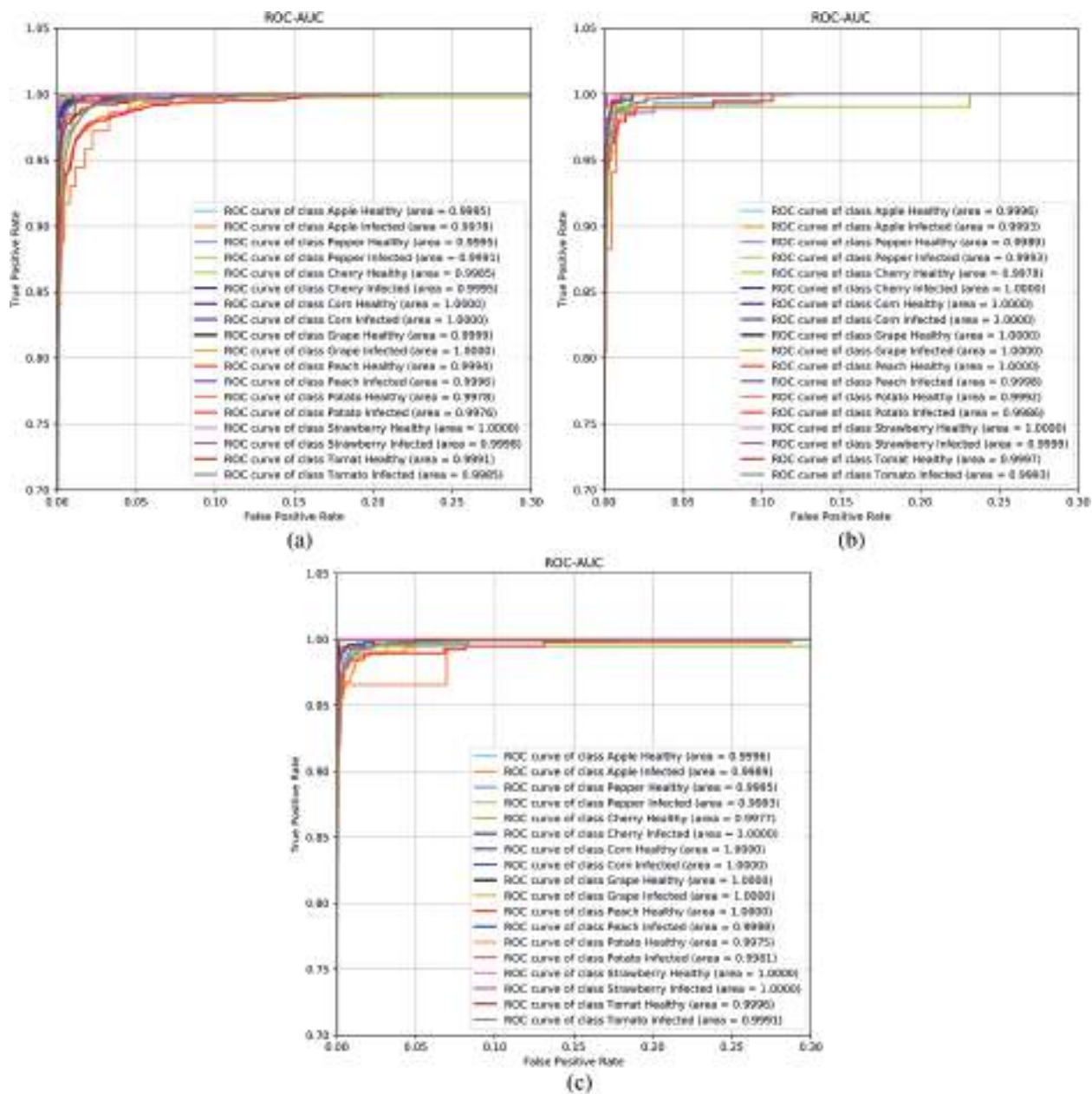


Figure 4: AUC-ROC curves of Bi-CNN's(sqrt) models. (a) AUC-ROC of Bi-CNN's(sqrt): G_1 (b) AUC-ROC of Bi-CNN's(sqrt): G_1 (c) AUC-ROC of Bi-CNN's(sqrt): G_1

Table 2: Performance of Bi-CNN models tested on D1

Models	Generalization	Accuracy (%)	AUC (%)	MSE
Bi-CNNs (log)	G-1	96.72	99.92	2.02
	G-2	97.36	99.94	1.66
	G-3	96.95	99.93	2.17
Bi-CNNs (sqrt)	G-1	97.26	99.94	1.91
	G-2	97.88	99.94	1.27
	G-3	97.53	99.95	1.58

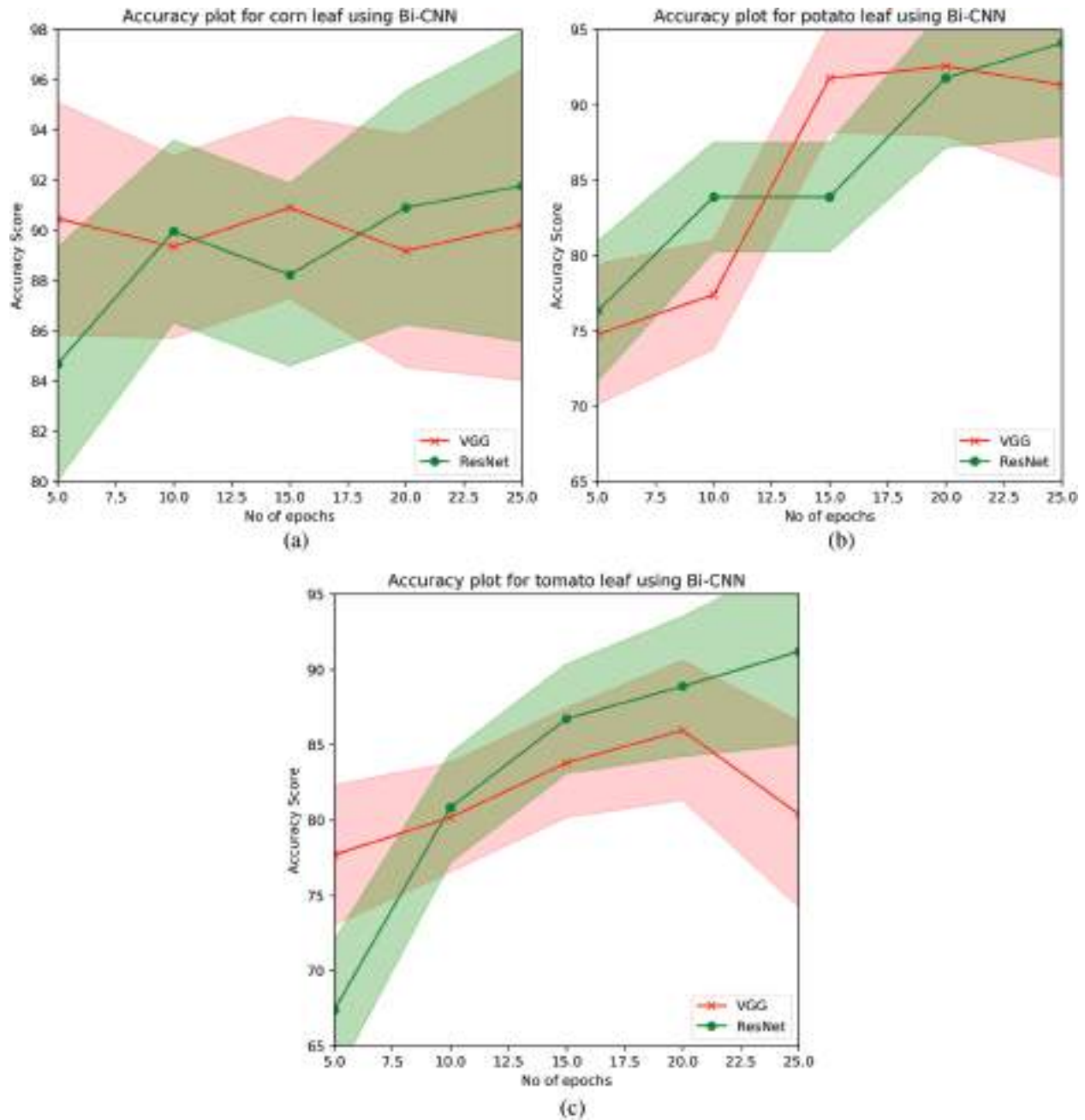


Figure 5: Learning curves of variant models for D_2 . (a) Accuracy curve of corn (b) Accuracy curve of potato (c) Accuracy curve of tomato

6 Discussion

Most of the previous research was held in extracting the features using machine learning methods that do not capture invariances for generic kinds i.e., these models are task-specific and required hand-engineered features. To overcome the problem of extracting features from hand-picked learning mechanisms deep-
 vision approaches are imparted. Most of the previous work was on developing a convolution neural

architecture for extracting features with precise optimization. But, after the evolution of transfer learning [24], many researchers tend to imply these pre-trained weights onto a similar task.

Table 3: Performance of D2, and D3 models

Models	Datasets	Classes	Accuracy (%)
VGG	D_2 -Potato	3	91.33
	D_2 -Corn	4	90.22
	D_2 -Tomato	10	80.41
ResNet	D_2-Potato	3	94.12
	D_2-Corn	4	90.92
	D_2-Tomato	10	91.20
ResNet	D_3	38	94.98

The advantage is, they do not require precise hyperparameter tuning and reduce the computational budget to a greater extent. Hence, these architectures provide pre-trained weights and many kinds of research apply these transfer learning techniques to extract innate bottleneck feature vectors from the given input to classify either using fully connected neural networks or utilizing machine learning classifiers such as SVM, decision trees etc. But, most of the research lack in providing appropriate visual attention to the models an important property of visual recognition task. Providing visual attention to the models can extract fine-grained features containing detailed and precise information regarding each entity. Further, training or fine-tuning mechanisms should be appropriate for the model to converge fast and generalize well. These problems are addressed by providing a resilient model for capturing detailed invariances and providing 3 level generalizations sets with faster convergence. Further, a Restful-API [25] and mobile application is created for capturing real-time images and classifying them by inserting the proposed model in the back-end. The details about the Restful-API and the application are described in the next section.

Table 4: Performance compared to previous literature

Authors	Methodology	Train-Test	Classes	Accuracy score
Siddharth et al. [3]	BRBFNN	–	6	–
Mohanty et al. [6]	CNN(GoogleNet)	80–20	38	99.35
U.P.Singh et al. [7]	MCNN	80–20	4	97.13
Q.Liang et al. [9]	PD^2 -SENet50	–	9,27,45	91,99,98
Cruz et al. [26]	CNN(Abstract-level Fusion)	75–35	3	98.6 ± 1.47
A.Marco et al. [27]	PDNet	70–30	42	93.67
J.Miaomiao et al. [28]	CNN(Inception+ResNet50)	80–20	4	98.57
K.Adithya et al. [29]	CNN+Auto encoders	60–30	6	97.50
E.C.Toor et al. [30]	CNN(DenseNet)	80–20	38	99.75
Dammalavalam et al. [31]	VGGNet(pre-trained)	80–20	2 (9)	97.48
Ramesh B et al. [32]	Bi-CNN (D_I)	90–10; 80–20;	18	97.26;97.88;97.53
		50–50		

Table 4 (continued).				
Authors	Methodology	Train-Test	Classes	Accuracy score
Proposed	Bi-CNN (Potato)	70–30	3	94.12
Proposed	Bi-CNN (Corn)	70–30	4	90.92
Proposed	Bi-CNN (Tomato)	70–30	10	91.20
Proposed	Bi-CNN (D_3)	70–30	38	94.98

The D_1 BiCNN's model performs outrageously even for large test samples providing minute deviation (0.27% for Bi-CNN (sqrt)) from test samples when increased by $5\times$. Bi-CNN (sqrt) model obtained the highest accuracy 97.88% for 20% test split and CAM activations [33] are visualized to illustrate visual attention.

Next, when tested on, D2, and D3 the model attained the highest accuracy score of 94.98 for 38 classes. When it is evaluated for individual leaf plants with high-class imbalance, ResNet models tend to outperform with an accuracy score of 94.12%, 90.92%, and 91.20% for potato, corn, and tomato plant leaf images respectively from Tab. 4.

7 Restful-API and Mobile Application

In this research, a deep learning model is created and deployed it as a Restful API and connected it to the mobile application for making predictions using an image as input. The REST architectural style is used because of its simplistic interface and modifiability of elements and its ability to adapt to changing needs (even when the application is running) portability of elements by moving data along the program code. It is also scalable for a large number of users. Fig. 6 shows the work-flow of the Restful API that is created. A deep learning model is deployed as REST API which is the most reliable and industrially practiced method for deployment of the deep learning model for making predictions remotely. As you can see in Fig. 6, API accepts base64 encoded image string as input and gives prediction result back in the JSON format. Flask is used for creating the API and also to act as a web server and gateway handler for the input request.

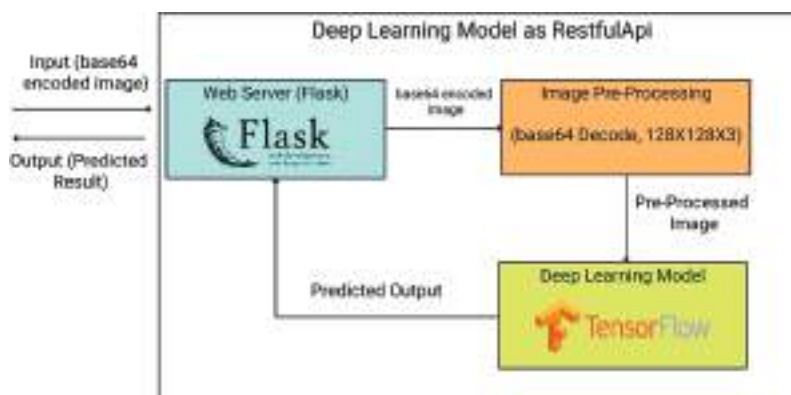


Figure 6: The complete mobile restful-API

In the next stage, the input base64 encoded image string is passed for pre-processing in this stage the base64 encoded image string is decoded and converted back into the image format and also resized the image to $128 \times 128 \times 3$ to be compatible with the model. After the fulfilment of the pre-processing stage,

the image is passed as input to the model to make the prediction. The predicted result is passed as output in JSON format. The whole process is wrapped in a single function in API which accepts the base64 encoded image string and outputs the predicted result. We connected this API to a mobile application. Where the user can download the app and predict by uploading or by capturing an image through the camera. Fig. 1 show and walk you through different stages and flow of the mobile app. When an image is uploaded or captured it is converted into a base64 encoded image string and passed to the API handler to handle with proper function then the function runs on the server by invoking the model and passing given base64 encoded image string as the input to the function. This working process is carried out by flask framework using gunicorn as a server in the backend. The restapi was deployed on the Heroku platform.³

The advancement in deep learning is leveraging the performance with the increase in size of data. This eventually led to designing an adaptable kernel [34] which would enhance the feature extraction process both for shallow and deep networks. It is observed that, smaller receptive field implied by VGG, a wavelet kernel [35] and Gaussian kernels [36] obliged in improving the quality of features acquired. The advancement in similarity metrics can acquire scalable features [37–42]. Transforming a sequence of redundant pixels using a specific similarity measure [43–46] is challenging and chosen as future scope for the present work.

8 Conclusion

This research provides unification with the extension of our conference work [32]. This study is motivated by the human visual cortex in designing an end-to-end trainable neural network named bilinear convolution neural network for plant leaf disease identification and classification. Bi-CNN models are developed for variant data divisions i.e., D_1 , D_2 , and D_3 . These models outperform the existing literature by extracting fine-grained features to provide visual attention through a second-order pooling mechanism. The model attained the highest accuracy score of 94.98% for D_3 , where 38 variant classes are considered. During this understudy, it is observed that ResNet when implied as a feature extractor outperform the VGG model and provide less computational expense with higher performance. Finally, the model is embedded in a mobile API and released as an opensource. Even with numerous advantages, the methodology didn't imply 10-fold cross-validation. The 10-fold cross-validation consumes high computational efforts. The proposed second-order pooling generally tend to provide attention only when bottleneck activations which of the same size. Whereas, a new pooling technique has to overcome this disadvantage. The present experiment was carried out on individual leaf images. In future, it is aimed to provide the solution by capturing aerial imaging techniques to extract a bunch of features from clustered plant leaf images with better precision and performance.

Acknowledgement: We are thankful to Jawaharlal Nehru Technological University Hyderabad for sponsoring the fund for publication from TEQIP III under the Collaborative Research Scheme.

Funding Statement: This work was partially supported by the TEQIP-III from Jawaharlal Nehru Technological University Hyderabad, under the Collaborative Research Scheme.

Conflicts of Interest: The authors declare no conflict of interest, financial or otherwise.

References

- [1] M. Mortimer, L. G. Ungerleider and K. A. Macko, "Object vision and spatial vision: Two cortical pathways," *Trends in Neurosciences*, vol. 6, pp. 414–417, 1983.
- [2] G. U. Leslie and J. V. Haxby, "'What' and 'where' in the human brain," *Current Opinion in Neurobiology*, vol. 4, no. 2, pp. 157–165, 1994.

³

The Implementation is deployed as an application. Source Code: [link](#)

- [3] S. S. Chouhan, A. Kaul, U. P. Singh and S. Jain, "Bacterial foraging optimization based radial basis function neural network (BRBFNN) for identification and classification of plant leaf diseases: An automatic approach towards plant pathology," *IEEE Access*, vol. 6, pp. 8852–8863, 2018.
- [4] K. Aydin, A. S. Keceli, C. Catal, H. Y. Yalic, H. Temucin *et al.*, "Analysis of transfer learning for deep neural network based plant classification models," *Computers and Electronics in Agriculture*, vol. 158, pp. 20–29, 2019.
- [5] R. Karthik, M. Hariharan, S. Anand, P. Mathikshara, A. Johnson *et al.*, "Attention embedded residual CNN for disease detection in tomato leaves," *Applied Soft Computing*, vol. 86, no. 105933, pp. 1–12, 2020.
- [6] M. P. Sharada, D. P. Hughes and M. Salathé, "Using deep learning for image-based plant disease detection," *Frontiers in plant science*, vol. 7, pp. 1–10, 2016.
- [7] U. S. Pratap, S. S. Chouhan, S. Jain and J. Sanjeev, "Multilayer convolution neural network for the classification of mango leaves infected by anthracnose disease," *IEEE Access*, vol. 7, pp. 43721–43729, 2019.
- [8] K. Sandeep, B. Sharma, V. K. Sharma, H. Sharma and J. C. Bansal, "Plant leaf disease identification using exponential spider monkey optimization," *Sustainable computing: Informatics and systems*, vol. 28, pp. 1–9, 2018.
- [9] L. Qiaokang, S. Xiang, Y. Hu, G. Coppola, D. Zhang *et al.*, "PD2SE-Net: Computer-assisted plant disease diagnosis and severity estimation network," *Computers and Electronics in Agriculture*, vol. 157, pp. 518–529, 2019.
- [10] A. A. Arib, Q. Chen and M. Guo, "Deep learning based classification for paddy pests & diseases recognition," in *Proc. of 2018 Int. Conf. on Mathematics and Artificial Intelligence*, 2018.
- [11] I. Monzurul, A. Dinh, K. Wahid and B. Pankaj, "Detection of potato diseases using image segmentation and multiclass support vector machine," in *2017 IEEE 30th canadian conf. on electrical and computer engineering (CCECE)*, IEEE, pp. 1–4, 2017.
- [12] H. David and M. Salathé, "An open access repository of images on plant health to enable the development of mobile disease diagnostics. *arXiv preprint arXiv:1511.08060*, 2015.
- [13] S. Karen and A. Zisserman, "Very deep convolutional networks for large-scale image recognition. *arXiv preprint arXiv:1409.1556*, 2014.
- [14] H. Kaiming, X. Zhang, S. Ren and J. Sun, "Deep residual learning for image recognition," in *Proc. of the IEEE conf. on computer vision and pattern recognition*, pp. 770–778, 2016.
- [15] L. T. Yu, A. R. Chowdhury and S. Maji, "Bilinear convolutional neural networks for fine-grained visual recognition," *IEEE transactions on pattern analysis and machine intelligence*, vol. 40, no. 6, pp. 1309–1322, 2017.
- [16] I. Sergey and C. Szegedy, "Batch normalization: Accelerating deep network training by reducing internal covariate shift," in *Int. conf. on machine learning*, PMLR, 2015.
- [17] S. Nitish, G. Hinton, A. Krizhevsky, I. Sutskever and R. Salakhutdinov, "Dropout: a simple way to prevent neural networks from overfitting," *Journal of Machine Learning Research*, vol. 15, no. 1, pp. 1929–1958, 2014.
- [18] G. Xavier and Y. Bengio, "Understanding the difficulty of training deep feedforward neural networks," in *Proc. of the thirteenth int. conf. on artificial intelligence and statistics*, JMLR Workshop and Conference Proceedings, 2010.
- [19] K. P. Diederik and J. Ba, "Adam: A method for stochastic optimization," *arXiv preprint arXiv:1412.6980*, 2014.
- [20] S. L. Samuel, P. J. Kindermans, C. Ying and Q. V. Le, "Don't decay the learning rate, increase the batch size," *arXiv preprint arXiv:1711.00489*, 2017.
- [21] B. Léon, "Stochastic gradient descent tricks," *Neural networks: Tricks of the trade*. Berlin, Heidelberg: Springer, pp. 421–436, 2012.
- [22] A. Martín, A. Agarwal, P. Barham, E. Brevdo, Z. Chen *et al.*, "Tensorflow: Large-scale machine learning on heterogeneous distributed systems," *arXiv preprint arXiv:1603.04467*, 2016.
- [23] F. Tom, "An introduction to ROC analysis," *Pattern Recognition Letters*, vol. 27, no. 8, pp. 861–874, 2006.
- [24] P. S. Jialin and Q. Yang, "A survey on transfer learning," *IEEE Transactions on Knowledge and Data Engineering*, vol. 22, no. 10, pp. 1345–1359, 2009.
- [25] R. T. Fielding, *Architectural styles and the design of network-based software architectures*, vol. 7. Irvine University of California, Irvine, 2000.

- [26] C. C. Albert, A. Luvisi, L. D. Bellis and Y. Ampatzidis, "X-FIDO: An effective application for detecting olive quick decline syndrome with deep learning and data fusion," *Frontiers in plant science*, vol. 8, no. 1741, pp. 1–12, 2017.
- [27] A. Marko, M. Karanovic, S. Sladojevic, A. Anderla and D. Stefanovic, "Solving current limitations of deep learning based approaches for plant disease detection," *Symmetry*, vol. 11, no. 7, pp. 1–21, 2019.
- [28] J. Miaomiao, L. Zhang and Q. Wu, "Automatic grape leaf diseases identification via United Model based on multiple convolutional neural networks," *Information Processing in Agriculture*, vol. 7, no. 3, pp. 418–426, 2020.
- [29] K. Aditya, G. Saini, D. Gupta, A. Khanna, S. Tiwari *et al.*, "Seasonal crops disease prediction and classification using deep convolutional encoder network," *Circuits, Systems, and Signal Processing*, vol. 39, no. 2, pp. 818–836, 2020.
- [30] T. E. Chebet, L. Yujian, S. Njuki and L. Yingchun, "A comparative study of fine-tuning deep learning models for plant disease identification," *Computers and Electronics in Agriculture*, vol. 161, pp. 272–279, 2019.
- [31] S. R. Dammavalam, C. R. Babu, V. S. Kiran, N. Rajasekhar, B. L. Bharadwaj *et al.*, *Leaf image classification with the aid of transfer learning: A deep learning approach*. Current Chinese Computer Science, 2020.
- [32] C. R. Babu, S. R. Dammavalam, V. S. Kiran, N. Rajasekhar, B. L. Bharadwaj *et al.*, "Deep bi-linear convolution neural network for plant disease identification and classification," in *Advanced Informatics for Computing Research, In press*. ICAICR, ISBN: 1393-1394, 2021.
- [33] Z. Bolei, A. Khosla, A. Lapedriza, A. Oliva and A. Torralba, "Learning deep features for discriminative localization," in *Proc. of the IEEE conf. on computer vision and pattern recognition*, pp. 2921–2929, 2016.
- [34] C. Youngmin and L. K. Saul, "Kernel methods for deep learning," in *Proc. of the 22nd Int. Conf. on Neural Information Processing Systems*, pp. 342–350, 2009.
- [35] H. Huaibo, R. He, Z. Sun and T. Tan, "Wavelet-srnet: A wavelet-based cnn for multi-scale face super resolution," in *Proc. of the IEEE Int. Conf. on Computer Vision*, pp. 1689–1697, 2017.
- [36] T. Meng, A. Djelouah, F. Perazzi, Y. Boykov and C. Schroers, "Normalized cut loss for weakly-supervised cnn segmentation," in *Proc. of the IEEE conf. on computer vision and pattern recognition*, pp. 1818–1827, 2018.
- [37] R. Vangipuram, R. K. Gunupudi, V. K. Puligadda and J. Vinjamuri, "A machine learning approach for imputation and anomaly detection in IoT environment," *Expert Systems*, vol. 37, no. 5, pp. 1–16, 2020.
- [38] S. Aljawarneh and R. Vangipuram, "GARUDA: Gaussian dissimilarity measure for feature representation and anomaly detection in Internet of things," *Journal of Super Computing, Springer*, vol. 76, pp. 4376–4413, 2020.
- [39] S. Aljawarneh, R. Vangipuram and A. Cheruvu, "Nimayam: fusion of iterative rule based decisions to build decision trees for efficient classification," in *Proc. of the 5th Int. Conf. on Engineering and MIS (ICEMIS '19), Association for Computing Machinery*, New York, NY, USA, pp. 1–7, 2019.
- [40] S. Aljawarneh, V. Radhakrishna and G. S. Reddy, "Mantra: A novel imputation measure for disease classification and prediction," in *Proc. of the First Int. Conf. on Data Science, E-learning and Information Systems (DATA '18), Association for Computing Machinery*, New York, NY, USA, pp. 1–5, 2018.
- [41] V. Radhakrishna, P. V. Kumar and V. Janaki, "SRIHASS - A similarity measure for discovery of hidden time profiled temporal associations," *Multimed Tools Applications, Elsevier*, vol. 77, pp. 17643–17692, 2018.
- [42] V. Radhakrishna, P. V. Kumar and V. Janaki, "Krishna Sudarsana: A z-space similarity measure," in *Proc. of the Fourth Int. Conf. on Engineering & MIS, 2018 (ICEMIS '18), Association for Computing Machinery*, New York, NY, USA, pp. 1–4, 2018.
- [43] V. Radhakrishna, S. A. Aljawarneh and P. V. Kumar, "ASTRA - A novel interest measure for unearthing latent temporal associations and trends through extending basic gaussian membership function," *Multimedia Tools and Applications*, vol. 78, pp. 4217–4265, 2019.
- [44] V. Radhakrishna, S. A. Aljawarneh, P. V. Kumar and V. Janaki, "A novel fuzzy similarity measure and prevalence estimation approach for similarity profiled temporal association pattern mining," *Future Generation Computer Systems*, vol. 83, pp. 582–595, 2018.
- [45] V. Radhakrishna, S. A. Aljawarneh, P. V. Kumar and K. R. Choo, "A novel fuzzy gaussian-based dissimilarity measure for discovering similarity temporal association patterns," *Soft Computing*, vol. 22, pp. 1903–1919, 2018.
- [46] R. Vangipuram, P. V. Kumar and V. Janaki, "Krishna Sudarsana-A z-space interest measure for mining similarity profiled temporal association patterns," *Foundations of Science, Springer*, vol. 25, pp. 1027–1048, 2020.

Research Article

Effect of Nano Ground Granulated Blast Furnace Slag (GGBS) Volume % on Mechanical Behaviour of High-Performance Sustainable Concrete

Seelam Srikanth ¹, Chunchu Bala Rama Krishna ¹, T. Srikanth,² K. J. N. Sai Nitesh,³ V. Swamy Nadh,⁴ Sanjeev Kumar,⁵ and Subash Thanappan ⁶

¹School of Civil Engineering, REVA University, Bangalore, India

²Department of Civil Engineering, Gokaraju Rangaraju Institute of Engineering and Technology, Hyderabad, India

³Department of Civil Engineering, Anurag University, Hyderabad, India

⁴Aditya College of Engineering, Affiliated to JNTUK, Surampalem, Andhra Pradesh, India

⁵Department of Civil Engineering, Graphic Era Deemed to be University, Bell Road, Clement Town, 248002 Dehradun, Uttarakhand, India

⁶Department of Civil Engineering, Ambo University, Ambo, Ethiopia

Correspondence should be addressed to Chunchu Bala Rama Krishna; chunchubalarama.krishna@reva.edu.in and Subash Thanappan; thanappansubash@gmail.com

Received 6 February 2022; Accepted 12 April 2022; Published 27 April 2022

Academic Editor: Lakshmiopathy R

Copyright © 2022 Seelam Srikanth et al. This is an open access article distributed under the Creative Commons Attribution License, which permits unrestricted use, distribution, and reproduction in any medium, provided the original work is properly cited.

Utilization of various mineral admixtures in producing mortar decreases the porosity and capillarity, hence improves the durability in opposition to water and competitive solutions. In this research work, Ground Granulated Blast Furnace Slag is used to replace 30 percent, 60 percent, and 70% of ordinary Portland cement (OPC) (GGBFS). Mechanical property (compressive strength) and durability properties (permeability, porosity, and sorptivity) of high-performance concrete (HPC) are tested. Water permeability of M85 is measured using three cell permeability apparatus. Compressive strength, porosity, and sorptivity of the same mixes are also found. According to the test results of HPC, 30% replacement level of GGBFS gives higher compressive strength than 60% and 70% replacement levels of GGBFS. An equation is developed for permeability of HPC based on mechanical strength and porosity. It is found that coefficient of permeability of water for HPC mixes ranges from 5.1×10^{-11} cm/sec to 7.8×10^{-11} cm/sec. It is concluded that 30% GGBFS used in HPC produces less porosity, less permeability, and less sorptivity than compared to other replacement levels.

1. Introduction

Excessive performance concrete (HPC) is a brand new magnificence of concrete that has evolved in latest decades. HPC has a low water content and can attain sufficient rheological properties by combining optimal granular packing with the addition of excessive-range water lowering admixtures. One primary high-quality best within the making of HPC is the virtual elimination of voids within the concrete matrix that generate deterioration. Therefore, HPC has a tendency to exhibit superior residences such as superior energy, dura-

bility, and lengthy-time period balance. In competitive contexts, the long-term durability of concrete systems is always a concern to consider. When it comes to structures that are continually in contact with water, such as offshore systems, parking decks, and dams, water penetration is the most important aspect that determines the structure's durability. As a result, the permeability of the concrete and its pore architecture are crucial to its long-term endurance. Supplementary cementitious materials in high-performance concrete showed excellent performance in durability [1]. Chakraborty et al. [2] reported concrete developed with

NANO GGBS produces a cohesive mix that reduces the permeability. Cheah and Chow [3] reported the replacement of cement by NANO GGBS improved the capillary penetration resistance of concrete significantly. Due to insufficient Ca (OH)₂ from cement hydration, NANO GGBS produces high amount of secondary C-S-H and C-A-S-H bonds that reduced both micro and macro pores in concrete. Therefore, an optimum performance was observed in tests of porosity, permeability, water absorption, and capillary absorption. It was reported concrete with NANO GGBS exhibited high resistance to ingress of chloride ions. Upon 80% or above replacement of NANO GGBS, compressive strength was greatly decreased [4]. Xie et al. [5] reported geo-polymer concrete developed with high amount of NANO GGBS exhibited decrease. Even after sulphate exposure during acid evaluations, there was less mass loss and a larger residual compressive electricity. As the amount of NANO GGBS in the diet grows, so does the sulphate resistance. Based on the findings of this literature review, it was discovered that there has been little research done on high-performance concrete made with large amounts of NANO GGBS. As a result, the primary goal of this project is to investigate the mechanical and durability properties of HPC for the desired concrete mixes developed with high volumes of NANO GGBS.

2. Experimental Studies

2.1. Ingredients of HPC. The cement used was Ordinary Portland Cement (OPC) 53 Grade having a specific gravity of 3.01. Effect of high volumes of NANO GGBS on strength and durability of high-performance concrete uses locally accessible river sand that conforms to grading zone II.

IS: 383–1970 [6] was used. The sand was screened at site to remove deleterious materials. Locally available coarse aggregate (12.5 mm) from quarry was used. Specific gravities of the coarse and fine aggregates have a density of 2.71 and 2.65, respectively. GGBFS (Ground Granulated Blast Furnace Slag) is a type of slag that comes from a blast furnace. Astrra chemicals, a local manufacturer company in India, was collected. Chemical properties were studied and compared to cement since being replaced as shown in Table 1. Super plasticizer GLENIUM B233, a modified polycarboxylic ether having pH ≥ 6 , was used.

2.2. Mix Design and Methodology. Methodology as shown in Figure 1 is followed in this research work. Concrete cubes of size 15 cm³ were kept in curing for 28 days to test permeability and sorption characteristics and also to determine strength as explained in methodology. Mix design procedure according to modified ACI method (Aitcin Method [7]) was followed and proportion is as shown in Table 2. In this mix, 30%, 60%, and 70% cement turned into changed by floor Granulated Blast Furnace Slag, retaining W/B ratio equal and the mix design named as GGBFS-30%, GGBFS-60%, and GGBFS-70% shown in Table 3. Formation of calcium silicate hydrate gel is the most important parameter in the concrete. The effect of maximum percentage of NANO GGBS may lead to less compressive strength in concrete.

TABLE 1: Chemical properties of mineral admixture.

Compound	Cement	GGBFS
SiO ₂	23.1	35.34
Al ₂ O ₃	4.51	11.59
Fe ₂ O ₃	2.5	0.35
CaO	63.3	41.99
MgO	1.0	8.04
Alkalies	0.88	0.94
SO ₃	1.3	1.3
Loss on ignition	2.41	0.45

2.3. Mixing and Specimen Testing Procedure. Mixing was performed in a concrete mixer gadget. Coarse aggregates, great aggregates, cement, and admixtures have been introduced to the mixer device and allowed to combine for 1 minute. Super-plasticizer was blended with the total water and then 50 percentage of water added to the mixture machine and allowed to mix for 2 minutes. Then, remaining 50 percentage of water poured in mixture machine and continued to mix for 2 minutes. Total mixing time was 5 minutes. Mixes were tried with varied mixing proportions and finally the proportion which gives the best results in terms of consistency and strength was selected. After demolding, the specimens had been saved for 28 days in curing water tank before testing. Dried specimens were examined for compressive electricity, porosity, permeability, and sorptivity. Compressive electricity takes a look at turned into carried out conforming to IS: 516 [8] on dice specimens of size one hundred mm \times a hundred mm \times a hundred mm. Permeability of 150 mm cube specimens and porosity of 100 mm cube specimens were calculated according to IS: 3085–1965 [9] and ASTM C642 [10], respectively. Sorptivity test of 100 mm cube specimens was carried out based on Taywood engineering (1993).

3. Results and Elobarations

3.1. Mechanical Strength. Compressive strength reduced with an addition of high volume of NANO GGBS as shown in Figure 2 and this reduction may be due to slower hydration rate and prolonged pozzolanic reaction [11]. Maximum compressive strength of 96.4 MPa at 28 days is found for the HPC specimens replaced with 30%. Table 4 shows the compressive strength of HPC concrete of GGBFS in Normal water curing. It is observed that performance of 30% replacement is almost similar to 0% replacement. This is due to the increase in the percentage of NANO GGBS in the mix design. Quantity of NANO GGBS decreases the quantity of gel formation.

3.2. Permeability. High volumes of NANO GGBS seriously affect durability. Permeability reduction is predominant at high NANO GGBS content [12]. As shown in Figure 3, permeability of HPC based on compressive power is expected. In comparison to GGBFS with a 30% substitution level, it has a low permeability value (3.2×10^{-11} cm/sec). It is

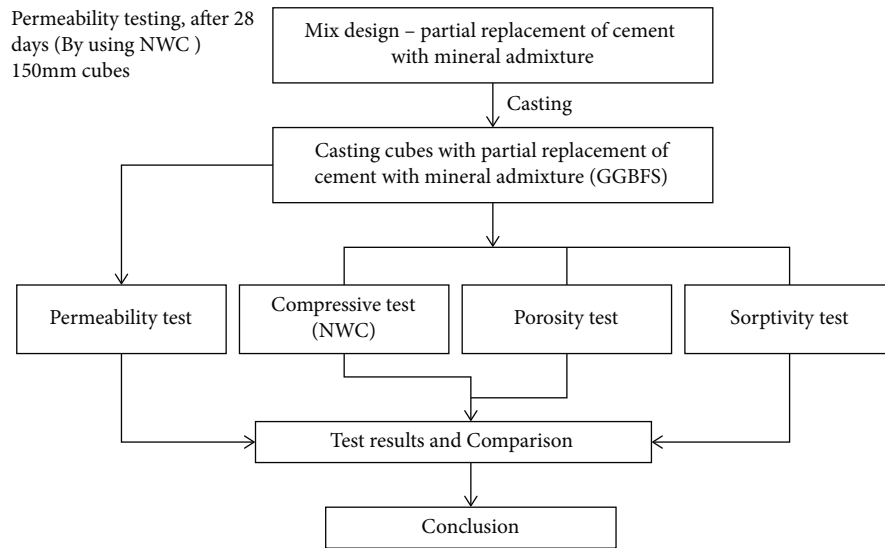


FIGURE 1: Methodology followed for testing HPC.

TABLE 2: Mix proportions for M80 grade concrete (Aitcin Method) were as mentioned.

W	C	FA	CA	SP
140	560	710.2	1075	5.7

TABLE 3: Mix design details of NANO GGBS.

Components	Replacement levels of NANO GGBS		
	GGBFS-30%	GGBFS-60%	GGBFS-70%
Water (lit.)	150.79	150.79	150.79
Cement (kg)	392	224	168
GGBFS (kg)	168	336	392
Coarse aggregate (kg)	1075	1075	1075
Fine aggregate (kg)	710.2	710.2	710.2
Super plasticizer (lit.)	5.503	5.503	5.503

TABLE 4: Compressive strength of HPC concrete at 28th day for various dosages of GGBFS.

Type of specimen	28th day compressive strength in N/mm ² (NWC)
0% GGBFS	97.375
30% GGBFS	96.4
60% GGBFS	82.34
70% GGBFS	73.5

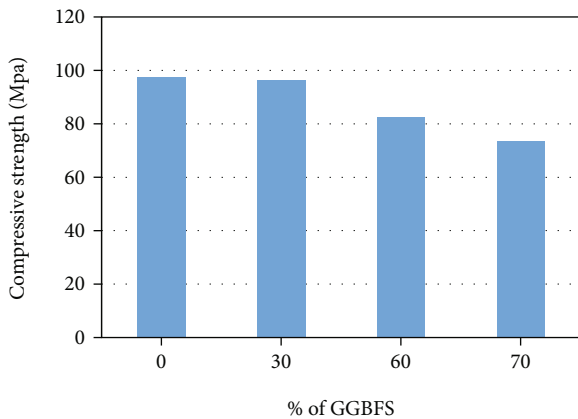


FIGURE 2: Variation of compressive strength at 28 days curing period.

observed 30% NANO GGBS exhibited promising performance amongst all concrete mixtures tested. NANO GGBS refines capillaries and hence dense structure of micro-pores is responsible for absorption.

$ok = A(fck)^2 + B(fck) + C$, where k and fck are the permeability (150 mm dice) and compressive energy (100 mm die) of concrete, respectively. The coefficients A , B , and C are obtained from the regression analysis [13].

The relationship between permeability and compressive power of concrete has been shown in parent four by way of employing NWC for GGBFS alternate levels [14]. From parent four, it was discovered that there was a significant association between permeability and concrete compressive strength, resulting in a regression coefficient (R^2) of zero. Permeability and compressive strength is shown in Figure 4.

3.3. *Porosity.* HPC was tested for porosity with various mineral admixtures (GGBFS). Table 5 shows the porosity results for the specimens that were tested [15]. GGBS gives more porous as this size is higher than the cement particles. That the reason we used NANO GGBS for better strength in the concrete. When compared to other replacements, GGBFS with 30% replacement level has a low porosity value (1.42 percent). To calculate the permeability of HPC using the porosity data provided in Figure 5 is sufficiently accurate [16].

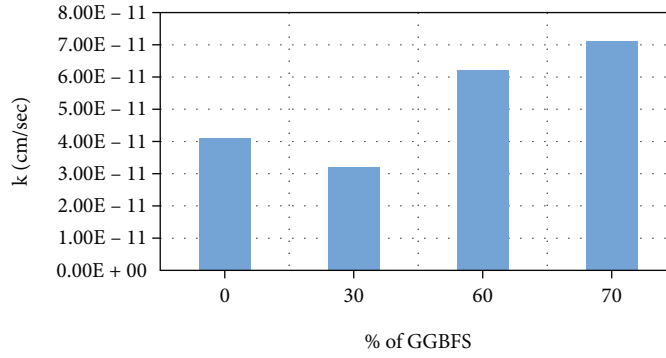


FIGURE 3: Variation of permeability at 28 days age.

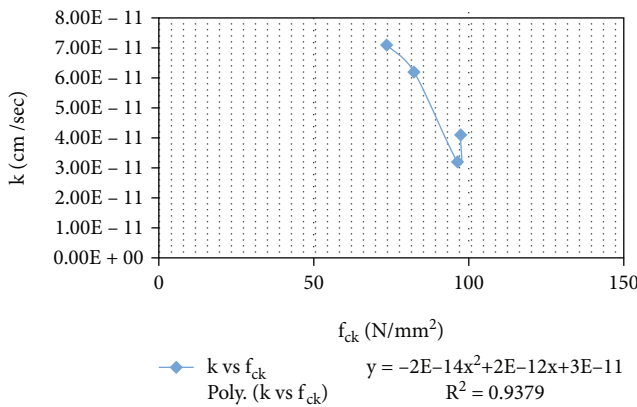


FIGURE 4: Permeability vs compressive strength.

TABLE 5: Porosity of HPC.

Mix	Porosity (%)
0% - GGBFS	1.65
30% - GGBFS	1.42
60% - GGBFS	2.08
70% - GGBFS	2.47

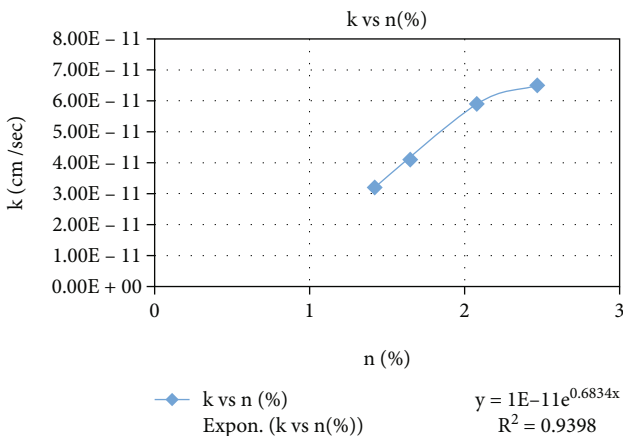


FIGURE 5: k vs n for GGBFS replacement levels.

TABLE 6: Sorptivity of HPC.

Mix	Sorptivity (m/√s) × 10 ⁻⁶	
	30 minutes	60 minutes
0% - GGBFS	1.68	1.95
30% - GGBFS	1.99	2.33
60% - GGBFS	2.13	2.6
70% - GGBFS	2.17	2.8

TABLE 7: Quality of concrete suggested by Taywood Engineering.

Concrete quality	Sorptivity (m/s ^{1/2}) × 10 ⁻⁴
Good	0.13
Acceptable	0.13 to 0.26
Poor	>0.26

Correlation between permeability and porosity

$k = A e^{Bn}$, where ' k ' represents the concrete's permeability (150 mm cubes) and ' n ' represents the concrete's porosity (100 mm cubes).

The coefficients A and B are the results of the regression analysis. For GGBFS replacements, a study of permeability vs porosity was conducted. Because of the significant association between permeability and porosity of the concrete shown in Figure 5, regression analysis yielded a correlation coefficient (R^2) of 0.939 [17].

3.4. Sorptivity. The test for sorptivity was conducted on 100 mm cubes [18]. Cubes were placed in a hot air oven at a temperature of 105°C up to which constant mass is obtained at an interval of time [19] and the weight was noted [20]. Then, the specimen is immersed in water for different interval of time (30 and 60 minutes), till the constant mass was obtained and it was noted. After 28 days of curing, all replacement levels of admixtures show less sorptivity as given in Table 6. 30-GGBFS replacement shows less value of sorptivity in 28 days curing. The obtained sorptivity values of HPC were in acceptable range according to Taywood engineering limits as given in Table 7.

4. Conclusions

NANO GGBS in high-performance concrete has exhibited promising performance in durability characteristics at 30% replacement compared to other concrete mixes. High volumes of NANO GGBS seriously affect durability. Permeability reduction is predominant at high NANO GGBS content. It is observed 0% NANO GGBS exhibited lower performance amongst all concrete mixtures tested. Compressive strength reduces with an increment in NANO GGBS content for cement replacement. However, 30% NANO GGBS concrete mix has mere performance to ordinary concrete. Both porosity and water absorption declined at 30% and increased at further replacements. Sorptivity values were in acceptable range and surface absorption increased due to NANO GGBS in concrete. It is necessary to evaluate the impact of twofold blending on HPC permeability and diffusivity.

Data Availability

The data used to support the findings of this study are included within the article. Should further data or information be required, these are available from the corresponding author upon request.

Conflicts of Interest

The authors declare that there are no conflicts of interest regarding the publication of this paper.

Acknowledgments

The authors thank REVA University and Aditya College of Engineering and Technology, Surampalem, for the technical assistance. The authors appreciate the support from Ambo University, Ethiopia.

References

- [1] S. Morino, "Recent developments on concrete-filled steel tube members in Japan," in *Composite Construction in Steel and Concrete*, vol. 4, pp. 644–655, Amsterdam, Netherlands, 2002.
- [2] S. Praburanganathan, N. Sudharsan, Y. B. S. Reddy, C. N. D. K. Reddy, L. Natrayan, and P. Paramasivam, "Force-deformation study on glass fiber reinforced concrete slab incorporating waste paper," *Advances in Civil Engineering*, vol. 2022, Article ID 5343128, 2022.
- [3] P. Sureshkumar, T. Jagadeesha, L. Natrayan, M. Ravichadran, D. Veeman, and S. M. Muthu, "Electrochemical corrosion and tribological behaviour of AA6063/Si₃N₄/Cu(NO₃)₂ composite processed using single-pass ECAP_A route with 120° die angle," *Journal of Materials Research and Technology*, vol. 16, pp. 715–733, 2022.
- [4] M. Udayakumar, S. Aravindan, and K. Rajkumar, "Experimental investigation of concrete-filled single-skin and double-skin steel oval hollow section stub columns," *Journal of Constructional Steel Research*, vol. 224, pp. 106–122, 2017.
- [5] K. Hemalatha, C. James, L. Natrayan, and V. Swamynadh, "Analysis of RCC T-beam and prestressed concrete box girder bridges super structure under different span conditions," *Materials Today: Proceedings*, vol. 37, no. 2, pp. 1507–1516, 2021.
- [6] F. X. Ding, D. R. Lu, Y. Bai et al., "Behaviour of CFRP-confined concrete-filled circular steel tube stub columns under axial loading," *Thin-Walled Structures*, vol. 125, pp. 107–118, 2018.
- [7] A. Merneedi, L. Natrayan, S. Kaliappan et al., "Experimental investigation on mechanical properties of carbon nanotube-reinforced epoxy composites for automobile application," *Journal of Nanomaterials*, vol. 2021, 7 pages, 2021.
- [8] J. Wang, Q. Shen, F. Wang, and W. Wang, "Experimental and analytical studies on CFRP strengthened circular thin-walled CFST stub columns under eccentric compression," *Thin-Walled Structures*, vol. 127, pp. 102–119, 2018.
- [9] S. Yogeshwaran, L. Natrayan, S. Rajaraman, S. Parthasarathi, and S. Nestro, "Experimental investigation on mechanical properties of epoxy/graphene/fish scale and fermented spinach hybrid bio composite by hand lay-up technique," *Materials Today: Proceedings*, vol. 37, no. 2, pp. 1578–1583, 2021.
- [10] R. S. Bhatia and K. Kudlipsingh, "The road to docker: a survey," *International Journal of Advanced Research in Computer Science*, vol. 8, no. 8, pp. 83–87, 2017.
- [11] F. Zhou and B. Young, "Tests of concrete-filled aluminum stub columns," *Thin-Walled Structures*, vol. 46, no. 6, pp. 573–583, 2008.
- [12] S. Yogeshwaran, L. Natrayan, G. Udhayakumar, G. Godwin, and L. Yuvaraj, "Effect of waste tyre particles reinforcement on mechanical properties of jute and abaca fiber-epoxy hybrid composites with pre-treatment," *Materials Today: Proceedings*, vol. 37, no. 2, pp. 1377–1380, 2021.
- [13] Q.-X. Ren, L.-H. Han, D. Lam, and C. Hou, "Experiments on special-shaped CFST stub columns under axial compression," *Journal of Constructional Steel Research*, vol. 98, pp. 123–133, 2014.
- [14] R. Suryanarayanan, V. G. Sridhar, L. Natrayan et al., "Improvement on mechanical properties of submerged friction stir joining of dissimilar tailor welded aluminum blanks," *Advances in Materials Science and Engineering*, vol. 2021, 6 pages, 2021.
- [15] Q. Wang, Q. Shi, E. M. Lui, and Z. Xu, "Axial compressive behavior of reactive powder concrete-filled circular steel tube stub columns," *Journal of Constructional Steel Research*, vol. 153, pp. 42–54, 2019.
- [16] L. Natrayan, A. Merneedi, G. Bharathiraja, S. Kaliappan, D. Veeman, and P. Murugan, "Processing and characterization of carbon nanofibre composites for automotive applications," *Journal of Nanomaterials*, vol. 2021, 7 pages, 2021.
- [17] Y. Geng, Y. Wang, and J. Chen, "Time-dependent behavior of recycled aggregate concrete-filled steel tubular columns," *Journal of Structural Engineering*, vol. 141, no. 10, article 04015011, 2015.
- [18] N. D. K. R. Chukka, L. Natrayan, and W. D. Mammo, "Seismic fragility and life cycle cost analysis of reinforced concrete structures with a hybrid damper," *Advances in Civil Engineering*, vol. 2021, 17 pages, 2021.
- [19] L. Natrayan and A. Merneedi, "Experimental investigation on wear behaviour of bio-waste reinforced fusion fiber composite laminate under various conditions," *Materials Today: Proceedings*, vol. 37, no. 2, pp. 1486–1490, 2021.
- [20] P. Manikandan, L. Natrayan, S. Duraimurugan, and V. Vasugi, "Influence of waste glass powder as an aluminosilicate precursor in synthesizing ternary blended alkali-activated binder," *Silicon*, vol. 15, pp. 1–10, 2022.

Cite this article

Lavanya C and Kumar ND (2022)
Effect of lime-stabilised copper slag cushion on swelling behaviour of highly plastic clay.
Geotechnical Research 9(1): 15–22,
<https://doi.org/10.1680/jgere.21.00006a>

Research Article

Paper 2100006a
Received 14/03/2021; Accepted 20/09/2021
Published online 29/10/2021
Published with permission by the ICE under the
CC-BY 4.0 license.
(<http://creativecommons.org/licenses/by/4.0/>)

Effect of lime-stabilised copper slag cushion on swelling behaviour of highly plastic clay

C. Lavanya PhD

Professor, Department of Civil Engineering, Gokaraju Rangaraju Institute of Engineering and Technology, Hyderabad, India

N. D. Kumar PhD

Assistant Professor and Head of the Department, Department of Civil Engineering, Jawaharlal Nehru Technological University Hyderabad College of Engineering Manthani, Peddapalli, India (corresponding author: ndkjntu@gmail.com)

Clay soil is prone to seasonal volume change due to variation in water content. The use of waste materials in civil engineering, especially in road construction, has been in vogue all over the world due to the development of road infrastructure. Copper slag is one such waste material available abundantly from the copper industry in India. This paper discusses the heave and swelling of copper slag-cushioned clayey subgrade prepared in a model test tank. The results revealed that the methodology adopted is effective in reducing the swelling of clay. The thickness ratios of the stabilised copper slag cushion and clayey subgrade bed adopted are 0.25, 0.5, 0.75 and 1.0. The copper slag cushion is stabilised with lime content varying from 2 to 10%. A reduction in heave of clayey soil subgrade bed is observed with an increase in the percentage of lime and the thickness of the copper slag cushion. For a cushion-clay soil subgrade thickness ratio $h_c/h_s = 1$, the reduction in the heave of a clayey subgrade bed is 84.4%. The swell potential observed from the present study follows well the trend obtained from the rectangular hyperbolic model.

Keywords: copper slag/cushion/expansive soil/heave/lime/stabilization/swelling potential

Notation

a, b	constants
h_c	thicknesses of lime-stabilised copper slag
h_s	thickness of expansive soil bed
S	amount of swell
T	time

1. Introduction

Swelling soils cause enormous damage to the buildings and pavements. Swelling soils are problematic because the clay mineral constituent which is present in them makes them exhibit shrink and swell behaviour. The shrink-swell behaviour makes the expansive soils unsuitable for construction directly in their natural form (Ikeagwuani and Nwonu, 2019). Expansive soils contain minerals such as clays that are capable of absorbing water. Since change in moisture content leads to swelling and shrinkage, it causes distress in structures; hence, it is mandatory to opt for suitable foundation/stabilisation techniques on these soils to avoid damages to buildings and road pavements due to distress.

Sharma *et al.* (2008) presented that the amounts of rice husk ash (RHA), lime and calcium chloride that were varied from 0 to 16%, 0 to 5%, and 0 to 2%, respectively, by the dry weight of soil, affected the unconfined compression strength (UCS) and California bearing ratio (CBR) of expansive clay. The stress-strain behaviour of expansive clay improved upon the addition of up to 5% lime or up to 1% calcium chloride. A maximum improvement in failure stress of 225 and 328% was observed at 4% lime and 1% calcium chloride, respectively. It was further concluded that the RHA content of 12% was found to be the optimum regarding both UCS and CBR in the presence of either lime or calcium chloride. The optimum dosages reported were 4% and 1% with respect to lime and calcium chloride even in clay-RHA mixes.

Kalkan (2011) studied the effects of wetting and drying cycles on the swelling behaviour of silica fume-modified expansive clayey soils and reported that the silica fume decreases the progressive deformation of modified expansive clayey soils.

The potential of copper slag as a replacement for fine aggregates in bituminous mixes can be a viable option. The mixture of copper slag, fly ash and soil has the potential for use in embankment, sub-base, base and wearing courses of road pavements (Havanagi *et al.*, 2007). The geotechnical properties of copper slag are like those obtained for medium sands; hence, copper slag can be used as a construction material in place of sand, as the backfill of retaining walls and as a fill material in embankment construction. Visser (2007) presented that sometimes, traditional laboratory tests are not able to predict the performance of these materials satisfactorily. Sometimes, conducting trial tests in the laboratory and field is important to identify a suitable stabiliser.

The favourable physico-mechanical characteristics of copper slag mean it can be utilised to make products like cement, fill, ballast, abrasive, aggregate, roofing granules, glass and tiles, apart from recovering the valuable metals by various extractive metallurgical routes (Bipra *et al.*, 2003). Copper slag is a non-plastic material, which has better compaction characteristics than sand, and its permeability is similar to that of sand. The material has a friction angle close to that of well-graded sand, and its use as backfill reduces the active lateral pressure on retaining walls (Dhir *et al.*, 2017). Deviator stress at failure and the elastic modulus of the slag/fly ash/dolime mixes are much greater than those of the wet mix macadam (WMM) (Patel and Shahu, 2017). A mix of 20% fly ash and 80% copper slag stabilised with 15% dolime gave optimum percentage for use in the base course of flexible pavements (Shahu *et al.*, 2013).

Copper slag specimens having 9% cement content and cured for a period of 28 days resulted in maximum compressive strength and tensile strength. Copper slag and fly ash when mixed in optimum proportions and stabilised with 6 and 9% cement can be effectively used as granular material in the sub-base and base layer of road pavement (Raj *et al.*, 2018). Copper slag can be used as a stabilising material for the improvement of problematic soils in embankments, pavement sub-grades and sub-bases. According to Katti (1979), an expansive soil, on saturation, helps arrest the heave below a depth of 1.0–1.2 m, due to the development of cementitious bonds in the soil. Copper slag when mixed with lime or cement can result in added advantage to stabilise expansive clay effectively (Lavanya *et al.*, 2014, 2017). Rao *et al.* (2008) reported that the fly ash cushion stabilised with 10% cement with thickness equal to that of the expansive soil bed had reduced heave by 75% in the first cycle, and with subsequent swell–shrink cycles, the performance further improved in arresting the heave. The experimental investigation and results are discussed in the following sections.

2. Experimental investigation

2.1 Tests conducted

The laboratory tests are conducted on the untreated and treated soil according to the standard test procedures presented in the Indian standard (IS) code of practices, and they are presented in Table 1.

2.2 Materials used

2.2.1 Expansive soil

Expansive clay soils are commonly found in the Telangana districts of India. Expansive clay used in the present study was collected from the Gundala Mandalam in the Telangana state of India. The soil collected was initially air-dried, and then the clay lumps were pulverised using a wooden mallet and sieved through a 20 mm sized sieve. Before using the clay soil sample for testing, it was kept in an oven for drying. Initially, the basic tests were conducted on a clay sample, and the basic properties of clay are presented in Table 2. The clay sample plasticity index is 40%, and its free swell index (FSI) value is 220%. The percentage of fine sand fraction present in the soil was 63.

Table 1. Tests conducted and their respective codes

Name of the test	IS code of practice
Grain size analysis	IS: 2720 (Part IV) (BIS, 1985a)
Liquid limit and plastic limit	IS: 2720 (Part V) (BIS, 1985b)
IS light compaction/standard compaction	IS: 2720 (Part VII) (BIS, 1980)
Free swell index	IS: 2720 (Part XXXX) (BIS, 1977)
California bearing ratio	IS: 2720 (Part XVI) (BIS, 1987)
Coefficient of permeability	IS: 2720 (Part XVII) (BIS, 1986)

IS, Indian standard

Table 2. Basic properties of soil

Property	Value
Grain size analysis	
Gravel: %	4
Sand: %	33
Silt and clay: %	63
Consistency limits	
Liquid limit: %	75
Plastic limit: %	35
Plasticity index	40
IS classification	CH
Free swell index: %	220
Degree of expansiveness	Very high
Maximum dry density: kN/m ³	14
Optimum moisture content: %	21
California bearing ratio: %	1
Coefficient of permeability, <i>k</i> : cm/s	0.53×10^{-7}

2.2.2 Copper slag

The copper slag used in the present study was collected from the Sterilite Industries, Tuticorin, Tamil Nadu state, India. The physical properties and chemical composition of the copper slag are presented in Table 3 and Table 4, respectively. Copper slag

Table 3. Physical properties of copper slag

Property	Value
Grain size analysis	
Gravel size: %	1.00
Sand size: %	98.9
Silt and clay sizes: %	0.05
Hardness on Moh's scale	6.5–7.0
Specific gravity	3.6
Plasticity index	Non-plastic
Swelling index	Non-swelling
Granule shape	Angular with sharp edges
Maximum dry density: kN/m ³	23.5
Optimum moisture content: %	6
Direct shear test	
Cohesion: kN/m ²	0
Angle of internal friction: °	40
Coefficient of permeability, <i>k</i>	1.54×10^{-2} cm/s
CBR: %	3.5

CBR, California bearing ratio

(Courtesy: Sterilite Industries Ltd, Tuticorin, Tamil Nadu, India)

Table 4. Chemical composition of copper slag

Compound	% by weight
Iron oxide	55–60
Silica	28–30
Aluminium oxide	1–3
Calcium oxide	3–5
Magnesium oxide	1.0–1.5

(Courtesy: Sterilite Industries Ltd, Tuticorin, Tamil Nadu, India)

has a 99% fine sand fraction. The specific gravity of copper slag is 3.6, and its hardness found on Moh's scale is in the range of 6.5 to 7. The maximum dry unit weight of copper slag is 23.5 kN/m³. The iron oxide and silica mineral compositions are predominant in the copper slag.

2.2.3 Lime

Lime is used as an admixture in the study and was obtained from the local market. The hydrated lime obtained has 95% of calcium hydroxide (CaO).

2.3 Sample preparation in model test tank

In this test set-up, galvanised iron cylindrical tanks of size 280 mm dia. and 400 mm height are used. The cylindrical test tank is initially filled with a 15 mm thick sand layer at the bottom and levelled. A 250 mm dia. and 350 mm high thin casing pipe is placed in the cylindrical test tank. Expansive clay soil which was mixed thoroughly at its optimum moisture content is taken and compacted inside the casing in three layers. Each layer of 50 mm thickness, the overall thickness of the clay bed being 150 mm, is compacted to the maximum dry unit weight in the cylindrical test tank within the casing pipe. The expansive clay bed thickness is referred to as h_s throughout the paper. Fine-to-medium sand is poured in the gap between the casing and the cylindrical tank up to the height of the proposed cushion. The 15 mm thick sand layer poured around the cylindrical test tank served as a drain to allow water into the soil bed. After clay bed is compacted, the casing is withdrawn slowly until it reached the desired height of 150 mm. A hollow polyvinyl chloride pipe is placed on the top of the expansive soil bed, and a heave stake is placed on the top of the expansive soil bed through the hollow pipe. On top of the heave stake, a dial gauge of 0.01 mm sensitivity is arranged to measure the corresponding soil heave. Copper slag and the desired quantity of lime are thoroughly mixed in dry condition, and then the water corresponding to optimum moisture content is added to it. The percentages of lime added to the copper slag are 2, 4, 6, 8 and 10%. Copper slag, stabilised with lime, is placed over the expansive soil bed and compacted in three layers to its maximum dry density. The copper slag stabilised at different dosages of lime is called the lime-treated copper slag cushion, and its thickness is referred to as h_c throughout the paper.

Specimens in the test tanks are prepared for different ratios of thicknesses of lime-stabilised copper slag (h_c) and the expansive soil bed (h_s). In this study, the thickness of the expansive soil bed (h_s) is kept constant as 150 mm. The h_c is varied such that the ratio of h_c to h_s is maintained at 0, 0.25, 0.50, 0.75 and 1.00. Before allowing the water through the sand drain into the expansive clay bed for saturation, the initial dial gauge reading is noted through the heave stake arrangement made in the test tank. Then, water is allowed into the test tank through sand drain for the saturation of the expansive soil. The heave readings are taken corresponding to the attainment of equilibrium. The attainment of equilibrium is considered when there is no change in the dial gauge reading. Corresponding to this equilibrium stage, the undrained cohesion and water contents of the

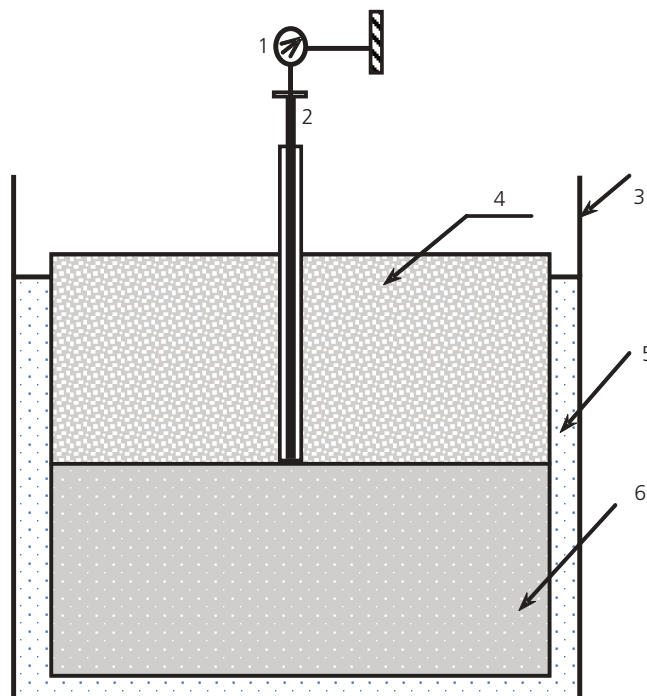


Figure 1. Schematic diagram of the experimental set-up: 1, dial gauge; 2, heave stake; 3, test tank (280 mm and 400 mm); 4, copper slag cushion with admixture thickness h_c ; 5, all around sand cushion 15 mm thick; 6, expansive clay bed thickness h_s

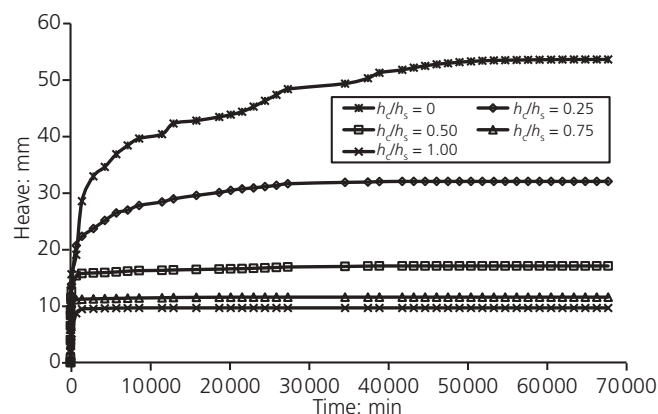


Figure 2. Time-heave plot of expansive soil bed with 6% lime added to the copper slag cushion

clay soil are measured, and these values are 26 kPa and 65%, respectively. A schematic diagram of the test tank set-up is shown in Figure 1.

2.4 Kondner's rectangular hyperbola

Some mathematical models are useful to simulate the non-linear swell-time curves of expansive soils to establish a relationship

between observed and predicted values. One such model, the Kondner's rectangular hyperbola (Kondner, 1963), is used to show the relationship between the time and heave for expansive soils and is presented in Equation 1:

$$1. \quad S = \frac{T}{(a + bT)}$$

where S = amount of swell corresponding to time T and 'a' and 'b' are constants.

The constants, a and b, can be obtained by linearising the non-linear curve. The maximum value of the swelling potential can be predicted by using the above equation.

3. Results and discussion

3.1 Influence of thickness ratio, h_c/h_s , on expansive clay bed

The heave of expansive clay bed laid under the lime-stabilised copper slag cushion of varied thicknesses is measured from the model test tank studies, and the respective results are discussed below. The clay bed of 150 mm thickness laid in the test tank without the lime-stabilised copper slag cushion – that is, $h_c/h_s = 0$ – showed a maximum heave of 53.64 mm. Figure 2 presents the variation of heave with passage of time for different cushion–soil thickness ratios, $h_c/h_s = 0, 0.25, 0.50, 0.75$ and 1.00 , for the copper slag cushion stabilised with 6% lime. From these curves, it is noticed that as the thickness ratio, h_c/h_s , increases from 0 to 1.00, the heave of the expansive clay bed is decreasing. Especially for thickness ratios $h_c/h_s = 0.50, 0.75$ and 1.00 , the increase in heave is

Table 5. Measured heave values in millimetres for various thickness ratios, h_c/h_s , and for lime proportions 2 and 4%

Time: min	Heave: mm for various thickness ratios, h_c/h_s , and 2% lime					Heave: mm for various thickness ratios, h_c/h_s , and 4% lime				
	0	0.25	0.50	0.75	1.00	0.25	0.50	0.75	1.00	
0	0.00	0.00	0.00	0.00	0.00	0.00	0.00	0.00	0.00	
1	0.09	0.22	0.59	0.78	0.27	0.50	0.20	0.31	0.06	
2	1.16	0.77	0.87	1.32	1.6	1.10	0.50	0.86	0.30	
5	2.93	2.08	3.3	3.31	2.51	3.00	4.12	2.91	1.19	
10	8.42	5.63	4.51	4.69	4.26	5.24	5.08	4.11	2.52	
20	9.99	7.99	6.52	5.43	4.26	7.40	6.85	5.05	3.43	
30	11.03	9.08	7.39	6.26	5.24	8.70	7.92	5.71	5.18	
60	12.68	12.29	8.67	7.87	7.92	11.72	9.76	6.74	5.18	
120	15.62	15.75	9.55	9.52	9.33	14.50	11.35	7.66	6.16	
720	19.08	20.44	10.09	11.29	10.72	17.50	12.55	9.85	7.65	
1440	28.56	22.92	12.2	11.62	11.31	21.55	14.15	11.49	8.88	
5760	36.87	27.05	13.9	12.16	12.13	25.47	15.23	11.72	10.09	
11 520	40.419	29.54	15.57	13.18	12.44	28.47	16.06	11.94	10.39	
37 440	50.32	33.39	19.08	13.85	—	31.99	17.55	12.14	—	
67 680	53.64	34.67	19.29	—	—	32.44	17.61	—	—	

Table 6. Measured heave values in millimetres for various thickness ratios, h_c/h_s , and for lime proportions 8 and 10%

Time: min	Heave: mm for various thickness ratios, h_c/h_s , and 8% lime					Heave: mm for various thickness ratios, h_c/h_s , and 10% lime				
	0	0.25	0.50	0.75	1.00	0.25	0.50	0.75	1.00	
0	0.00	0.00	0.00	0.00	0.00	0.00	0.00	0.00	0.00	
1	0.09	0.04	0.06	0.05	0.05	0.34	0.94	0.41	0.23	
2	1.16	0.31	0.63	0.13	0.15	0.96	1.54	0.82	0.32	
5	2.93	1.30	1.07	1.20	0.45	4.32	2.87	1.27	0.48	
10	8.42	2.23	2.00	2.26	0.94	6.92	3.85	1.73	0.61	
20	9.99	4.95	4.14	3.27	1.99	10.24	5.19	2.24	0.80	
30	11.03	9.11	5.70	4.52	2.87	11.58	6.37	2.61	0.94	
60	12.68	11.64	7.14	5.68	4.68	14.75	8.01	3.61	1.29	
120	15.62	14.43	10.29	8.48	7.14	17.86	9.69	4.91	1.81	
720	19.08	19.25	11.08	9.06	8.57	22.15	11.65	7.00	3.85	
1440	28.56	22.11	11.94	9.31	8.65	24.53	12.04	7.26	5.26	
5760	36.87	23.02	12.54	9.60	8.89	27.88	13.10	8.45	7.51	
11 520	40.419	24.77	13.28	10.33	9.15	29.46	13.69	8.91	8.37	
37 440	50.32	30.98	16.33	10.53	—	31.13	15.33	9.62	—	
67 680	53.64	31.49	16.36	—	—	31.24	15.35	—	—	

—, not applicable

Table 7. Percentage decrease in the heave of expansive soil bed with % lime added to the cushion

Thickness ratio (h_c/h_s)	% Lime				
	2	4	6	8	10
0.25	35.37	39.52	40.23	41.29	41.76
0.50	64.04	67.17	68.14	69.50	71.38
0.75	74.18	77.37	78.43	80.37	82.07
1.00	76.81	80.63	81.99	82.94	84.40

noticed within a short period of time, and thereafter, almost no change in heave is particularly noticed. The gradual increase in heave of expansive clay bed is noticed up to 28 days in the case of thickness ratio $h_c/h_s = 0.25$, and up to 40 days in the case of $h_c/h_s = 0$. The ultimate heave of the clay bed is achieved when the further passage of time does not cause any change or maintains a constant value. When compared to the ultimate heave of the clay bed for a thickness ratio of $h_c/h_s = 0$, the decrease in the ultimate heave for thickness ratios $h_c/h_s = 0.25, 0.50, 0.75$ and 1.00 is 40.2, 68.1, 78.4 and 82%, respectively. It means that at the

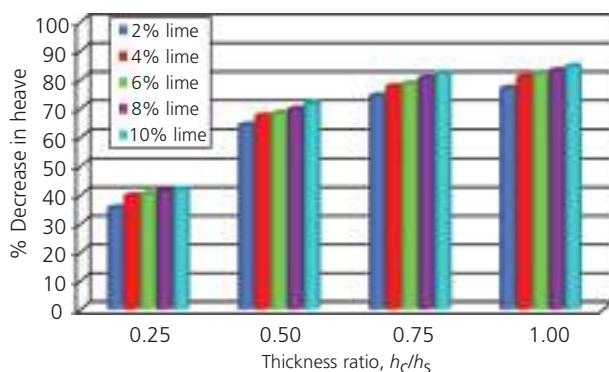


Figure 3. Percentage decrease in the heave of expansive soil with thickness ratio and % lime

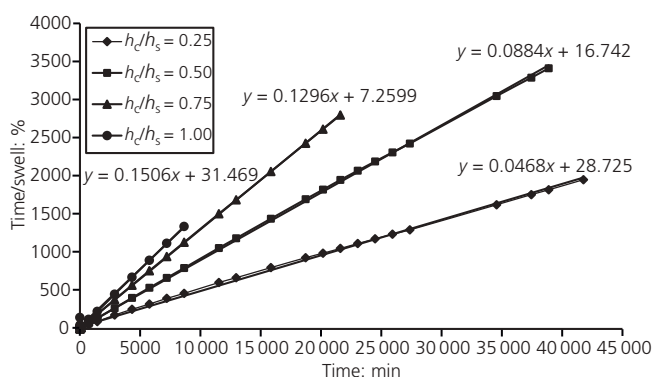


Figure 4. Time plotted against time/swell (%) of expansive soil bed with 6% lime added to the copper slag cushion

thickness ratios $h_c/h_s = 0.75$ and 1.00 , the copper slag cushion treated with 6% lime provides an optimal control of the heave of the expansive clay bed. It is further observed that it took very little time for almost the entire heave to occur when the expansive clay bed was overlain by the cushion. Such similar behaviour was noticed for the copper slag cushion treated with lime dosages of 2, 4, 8 and 10%. The heave-against-time data for copper slag cushions stabilised with lime dosages of 2, 4, 8 and 10% is presented in Tables 5 and 6.

It is further seen from Figure 2 that a large amount of the heave has occurred in the first two days following inundation, when the cushion was placed on the expansive soil bed. On the other hand, when a copper slag cushion was not provided over the expansive soil bed, the swelling was gradual, and it has taken a long time to attain equilibrium. This is one of the advantages of providing a cushion, as the time required to achieve equilibrium heave has significantly reduced. The percentage decrease in the heave of the expansive clay soil with various thicknesses of cushion when compared with no cushion placed on it is presented in Table 7. It is noticed that there is a significant reduction in the heave with the increase in the thickness of the cushion and with increase in the percentage of lime. The results presented in Table 7 are further depicted in the form of a histogram and presented in Figure 3. From this figure, it is clearly noticed that as the thickness ratio increases from 0.25 to 1.00, the reduction in heave is huge and it can be seen that it is almost the same level for the thickness ratios 0.75 and 1.00. It is also noticed that the influence of lime on the decrease in heave is nominal for any thickness ratio considered in the present study.

3.2 Swelling potential from rectangular hyperbola approach

Some mathematical models are useful to simulate the non-linear swell-time curves of expansive soils. Based on the rectangular hyperbola analysis, it is possible to establish a relationship between the observed values and the predicted values of the swelling potential of a lime-stabilised copper slag cushion-soil system. Kondner's rectangular hyperbola (1963) equation presented in Equation 1 is used to establish the relationship between the time and heave for expansive clay. A graph is plotted between time (as the abscissa) and time/swell (%) (as the ordinate). The legitimacy of the above equation can be demonstrated, if a transformed plot results in a straight line. The constants 'a' and 'b' are obtained from the slope of the straight line. The value 'b' gives the slope of the swelling path. The term 'b' is defined as the coefficient of the rate of swelling (Al-Rawas and Goosen, 2006; Hashim and Muntohar, 2006). A typical plot of time against time/swell (%) for different thickness ratios, $h_c/h_s = 0, 0.25, 0.50, 0.75$ and 1.00 , of expansive soil bed with 6% lime-stabilised copper slag cushion is shown in Figure 4.

Figures 5–9 show the typical graphs of the predicted and the observed swelling potential of the expansive clay for various thickness ratios and copper slag cushions which are stabilised with

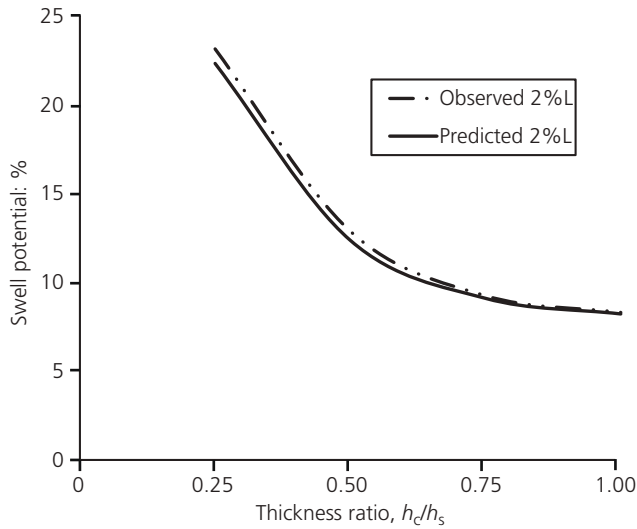


Figure 5. Predicted and observed values of swell potential of expansive soil bed with 2% lime added to the copper slag cushion for various thickness ratios

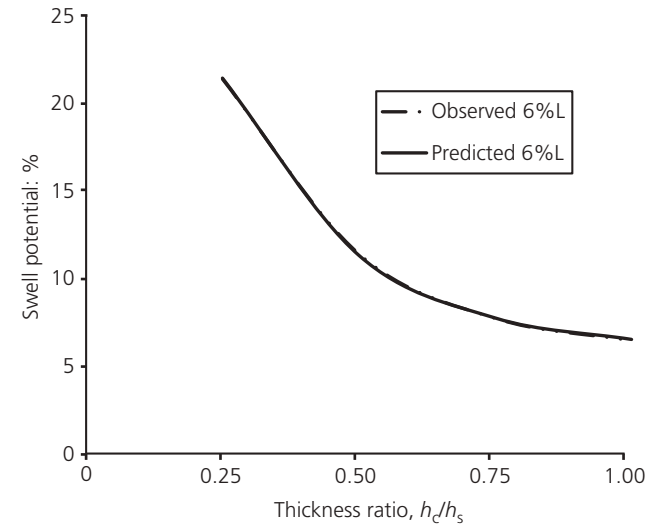


Figure 7. Predicted and observed values of swell potential of expansive soil bed with 6% lime added to the copper slag cushion for various thickness ratios

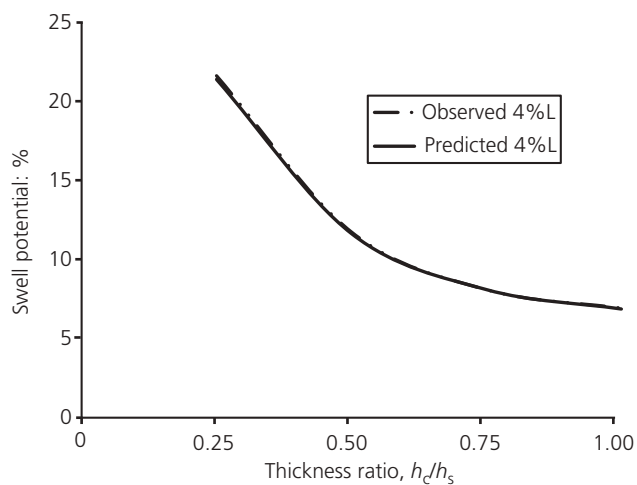


Figure 6. Predicted and observed values of swell potential of expansive soil bed with 4% lime added to the copper slag cushion for various thickness ratios

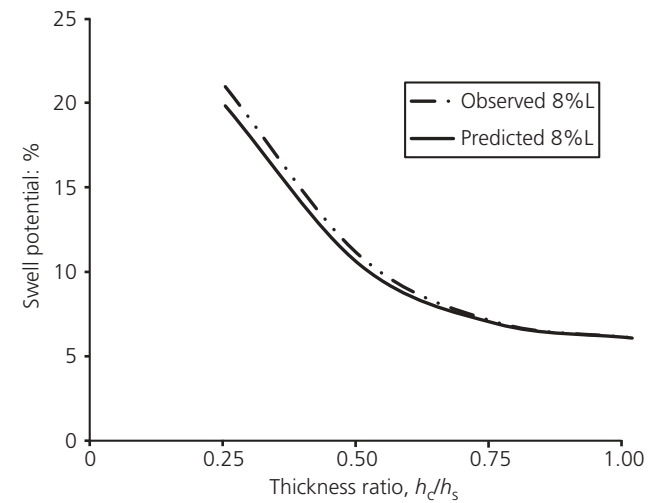


Figure 8. Predicted and observed values of swell potential of expansive soil bed with 8% lime added to the copper slag cushion for various thickness ratios

various percentages of lime. It can be seen that there is a close agreement between the predicted values of the swelling potential from the rectangular hyperbola and the observed values from the experimental work. The percentage decrease of observed and predicted values of the swelling potential of expansive clay soil with various thicknesses of the cushion when compared with no cushion placed on it is presented in Table 8. Earlier researchers have also observed that the hyperbolic relationship is accurate for predicting maximum swelling (Dakshnamurthy, 1978; Waddah *et al*, 1999). The percentage error is calculated for the predicted and observed values of the swelling potential. The percentage error of

the lime-stabilised cushions for various percentages of lime is 1.61, and the corresponding regression coefficient, R^2 , obtained is 0.998.

4. Conclusions

There is a considerable reduction in the heave of expansive soil subgrade bed when a lime-stabilised copper slag cushion is laid over it. With an increase in the percentage of lime, there is a reduction in heave, but it is marginal. However, the increased cushion thickness resulted in a significant reduction in heave. At all the thickness ratios, $h_c/h_s = 0.25, 0.50, 0.75$ and 1.00 , the decrease in the heave of the expansive soil subgrade overlain with

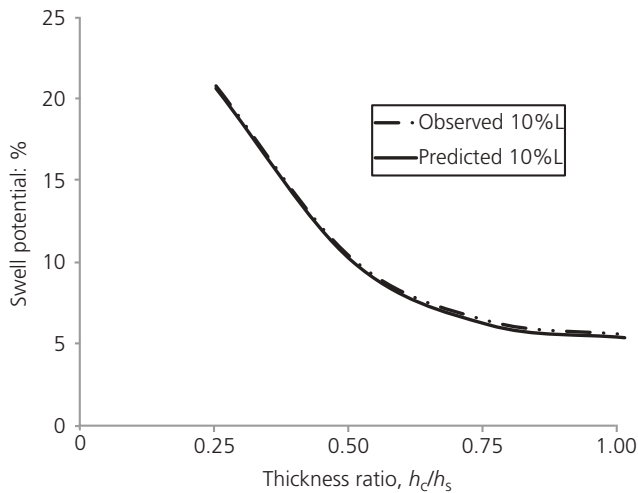


Figure 9. Predicted and observed values of swell potential of expansive soil bed with 10% lime added to the copper slag cushion for various thickness ratios

Table 8. Observed and predicted swell potential values (%) of expansive soil bed when lime is added to the cushion

% Lime	Values	Thickness ratio (h_c/h_s)			
		0.25	0.50	0.75	1.00
2	Observed value	23.11	12.86	9.23	8.29
	Predicted value	22.29	12.35	9.09	8.21
4	Observed value	21.63	11.74	8.09	6.93
	Predicted value	21.40	11.64	8.10	6.87
6	Observed value	21.37	11.39	7.71	6.44
	Predicted value	21.42	11.31	7.73	6.51
8	Observed value	20.99	10.91	7.02	6.10
	Predicted value	19.85	10.38	6.94	6.09
10	Observed value	20.83	10.23	6.41	5.58
	Predicted value	20.67	10.07	6.18	5.39

a lime-stabilised copper slag cushion when compared to the expansive soil subgrade bed without a cushion varies from 35.4 to 84.4%. The swelling potential of soil subgrade is predicted by using the rectangular hyperbola method of analysis. The predicted and observed values of swelling potential of expansive soil subgrade bed have been shown to vary by 1.61% for all the thickness ratios. It is concluded that the thickness ratio $h_c/h_s = 1$ is effective in controlling the heave.

REFERENCES

Al-Rawas AA and Goosen MFA (2006) *Expansive Soils – Recent Advances in Characterization and Treatment*. Taylor & Francis Group, London, UK.

Bipra Gorai B, Jana RK and Premchand (2003) Characteristics and utilisation of copper slag – a review. *Resources, Conservation and Recycling* **39**(4): 299–313, [https://doi.org/10.1016/S0921-3449\(02\)00171-4](https://doi.org/10.1016/S0921-3449(02)00171-4).

BIS (Bureau of Indian Standards) (1977) IS 2720, Part XXXX: Laboratory determination of free swell index. BIS, New Delhi, India.

BIS (1980) IS 2720, Part VII: Laboratory determination of standard proctor compaction (I.S. light compaction) (second revision). BIS, New Delhi, India.

BIS (1985a) IS 2720, Part IV: Laboratory determination of grain size analysis (second revision). BIS, New Delhi, India.

BIS (1985b) IS 2720, Part V: Laboratory determination of liquid limit and plastic limit (second revision). BIS, New Delhi, India.

BIS (1986) IS 2720, Part XVII: Laboratory determination of permeability (first revision). BIS, New Delhi, India.

BIS (1987) IS 2720, Part XVI: Laboratory determination of california bearing ratio (second revision). BIS, New Delhi, India.

Dakshanamuthy V (1978) A new method to predict swelling using a hyperbolic equation. *Geotechnical Engineering* **9**(1): 79–87.

Dhir RK, de Brito J, Mangabhai R and Lye CQ (2017) Use of copper slag in geotechnical applications. In *Sustainable Construction Materials: Copper Slag*. Woodhead, Duxford, UK, pp. 211–245.

Hashim R and Muntohar AS (2006) Swelling rate of expansive clay soils. In *Expansive Soils: Recent Advances in Characterization and Treatment* (Al-Rawas AA and Goosen MFA (eds)). Taylor & Francis Group, London, UK, pp. 139–148.

Havanagi VG, Mathur S, Prasad PS and Kamaraj C (2007) Feasibility of copper slag–fly ash–soil mix as a road construction material. *Transportation Research Record* **1989-2**: 13–20, <https://doi.org/10.3141/2F1989-43>.

Ikeagwuani CC and Nwonu DC (2019) Emerging trends in expansive soil stabilisation: a review. *Journal of Rock Mechanics and Geotechnical Engineering* **11**(2): 423–440, <https://doi.org/10.1016/j.jrmge.2018.08.013>.

Kalkan E (2011) Impact of wetting-drying cycles on swelling behavior of clayey soils modified by silica fume. *Journal of Applied Clay Science* **52**(4): 345–352, <http://doi.org/10.1016/j.clay.2011.03.014>.

Katti RK (1979) Search for solutions for problems in black cotton soils. *Indian Geotechnical Journal* **9**: 1–80.

Kondner RL (1963) Hyperbolic stress-strain response-cohesive soils. *Journal of Soil Mechanics and Foundation Division* **89**(1): 115–143, <https://doi.org/10.1016/0022-4898%2864%2990153-3>.

Lavanya C and Srirama Rao A (2017) Study of swelling potential of copper slag cushion laid over expansive soil bed. *Indian Geotechnical Journal* **47**(3): 280–285, <https://doi.org/10.1007/s40098-017-0227-9>.

Lavanya C, Srirama Rao A and Darga Kumar N (2014) Efficacy of copper slag cushion in arresting heave of an expansive soil. *International Conference on Recent Trends in Engineering & Technology, Pudukkottai, India*, pp. 658–662.

Patel S and Shahu JT (2017) Comparative study of slags stabilized with fly ash and dolime for utilization in base course. *Journal of Materials in Civil Engineering* **29**(10): 04017168, [http://doi.org/10.1061/\(ASCE\)MT.1943-5533.0002017](http://doi.org/10.1061/(ASCE)MT.1943-5533.0002017).

Raj S, Rai A and Havanagi V (2018) Suitability of stabilized copper slag and fly ash mix for road construction. *World Journal of Engineering* **15**(3): 336–344, <https://doi.org/10.1108/WJE-08-2017-0220>.

Rao MR, Rao AS and Babu RD (2008) Efficacy of cement-stabilized fly ash cushion in arresting heave of expansive soils. *Geotechnical and Geological Engineering* **26**(2): 189–197, <https://doi.org/10.1007/s10706-007-9156-1>.

Shahu JT, Patel S and Senapati A (2013) Engineering properties of copper slag-fly ash-dolime mix and its utilization in base course of flexible pavements. *Journal of Materials in Civil Engineering* **25**(12): 1871–1879, [https://doi.org/10.1061/\(ASCE\)MT.1943-5533.0000756](https://doi.org/10.1061/(ASCE)MT.1943-5533.0000756).

Sharma RS, Phani Kumar BR and Varaprasada Rao B (2008) Engineering behavior of a remolded expansive clay blended with lime, calcium chloride and rice husk ash. *Journal of Materials in Civil Engineering* **20**(8): 509–515, [https://doi.org/10.1061/\(ASCE\)0899-1561\(2008\)20:8\(509\)](https://doi.org/10.1061/(ASCE)0899-1561(2008)20:8(509)).

Visser AT (2007) Procedure for evaluating stabilization of road materials with non-traditional stabilizers. *Transportation Research Record* **1989-2**: 21–26, <https://doi.org/10.3141/1989-44>.

Waddah SA, Khalid AA and Al-Zou'bi SM (1999) Influence of pore water chemistry on the swelling behavior of compacted clays. *Applied Clay Science* **15(5-6)**: 447–462.

How can you contribute?

To discuss this paper, please submit up to 500 words to the editor at journals@ice.org.uk. Your contribution will be forwarded to the author(s) for a reply and, if considered appropriate by the editorial board, it will be published as a discussion in a future issue of the journal.

Analysis on effect of nanofluid on process parameters in machining of EN19 steel

Sateesh N , Ram Subbiah, BCh Nookaraju, A. Anitha Lakshmi &

Prashanth kumar P

Accepted 30 Jun 2021, Published online 22 Jul 2021

Download citation

<https://doi.org/10.1080/2374368X.2021.1953918>

Check for updates

Sample our
Physical Sciences
journals>> [Click here](#) to start your access
to the latest two volumes for 14 days

Full Article

Figures & data

References

Citations

Metrics

Reprints & Permissions

Get access

ABSTRACT

Machining is the most fundamental process in manufacturing industry. The heat generated on the working surface of the tool during machining is critical to determining the dimensional accuracy and surface quality of the workpiece. Conventional cutting fluids are hazardous to the health of workers and cause environmental pollution. This paper focuses on the effect of vegetable oil-based nanofluid on the machining performance in turning of EN19 steel through Minimum Quantity Lubrication (MQL). Canola oil is used as a base lubricant with various

inclusions of boric acid powder nanoparticles. Machining parameters such as tool temperature and cutting forces are measured during machining. After processing,

Article

Analysis of a Robot Selection Problem Using Two Newly Developed Hybrid MCDM Models of TOPSIS-ARAS and COPRAS-ARAS

Shankha Shubhra Goswami ^{1,†}, Dhiren Kumar Behera ^{1,†}, Asif Afzal ^{2,*}, Abdul Razak Kaladgi ^{3,†}, Sher Afghan Khan ³, Parvathy Rajendran ^{4,5,*}, Ram Subbiah ⁶ and Mohammad Asif ^{7,†}

¹ Department of Mechanical Engineering, Indira Gandhi Institute of Technology, Sarang 759146, Odisha, India; ssg.inch.official@gmail.com (S.S.G.), dkb_dgit@rediffmail.com (D.K.B.)

² Department of Mechanical Engineering, P. A. College of Engineering, Affiliated to Visveswaraaya Technological University, Belagavi, Mangaluru 574153, Karnataka, India; asifafzal@gmail.com

³ Department of Mechanical Engineering, Faculty of Engineering, International Islamic University, Kuala Lumpur 50100, Selangor, Malaysia; sakhani06@gmail.com

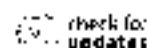
⁴ School of Aerospace Engineering, Universiti Sains Malaysia, Engineering Campus, Nibong Tebal 14300, Pulau Pinang, Malaysia

⁵ Faculty of Engineering & Computing, First City University College, Bandar Utama, Petaling Jaya 47800, Selangor, Malaysia

⁶ Gokaraju Rangaraju Institute of Engineering & Technology, Hyderabad 500078, Telangana, India; ramsubbiah@gmail.com

⁷ Department of Chemical Engineering, College of Engineering, King Saud University, P.O. Box 8001, Riyadh 11421, Saudi Arabia; masif@ksu.edu.sa

* Correspondence: asif.afzal@psg.nial.com (A.A.); separvathy@usm.my or parvathy.rajendran@firstcity.edu.my (P.R.)



Citation: Goswami, S.S.; Behera, D.K.; Afzal, A.; Razak Kaladgi, A.; Khan, S.A.; Rajendran, P.; Subbiah, R.; Asif, M. Analysis of a Robot Selection Problem Using Two Newly Developed Hybrid MCDM Models of TOPSIS-ARAS and COPRAS-ARAS. *Symmetry* **2021**, *13*, 1331. <https://doi.org/10.3390/sym13061331>

Academic Editors: Jan Awrejcewicz and Emil Bubek-Narancu

Received: 5 June 2021
Accepted: 20 July 2021
Published: 23 July 2021

Publisher's Note: MDPI stays neutral with regard to jurisdictional claims in published maps and institutional affiliations.



Copyright: © 2021 by the authors. Licensee MDPI, Basel, Switzerland. This article is an open access article distributed under the terms and conditions of the Creative Commons Attribution (CC BY) license (<http://creativecommons.org/licenses/by/4.0/>).

Abstract: Traditional Multi-Criteria Decision Making (MCDM) methods have now become outdated, therefore, most researchers are focusing on more robust hybrid MCDM models that combine two or more MCDM techniques to address decision-making problems. The authors attempted to create two novel hybrid MCDM systems in this paper by integrating Additive Ratio Assessment (ARAS) with Technique for Order of Preference by Similarity to Ideal Solution (TOPSIS) and Complex Proportional Assessment (COPRAS). To demonstrate the ability and effectiveness of these two hybrid models i.e., TOPSIS-ARAS and COPRAS-ARAS were applied to solve a real-time robot selection problem with 12 alternative robots and five selection criteria, while evaluating the parametric importance using the Criteria Importance Through Inter-criteria Correlation (CRITIC) objective weighting estimation tool. The rankings of the robot alternatives gained from these two hybrid models were also compared to the obtained results from eight other solo MCDM tools. Although the rankings by the applied methods slightly differ from each other, the final outcomes from all of the adopted techniques are consistent enough to suggest that robot 12 is the best choice followed by robot 11, and robot 4 is the worst one among these 12 alternatives. Spearman Correlation Coefficient (SCC) also reveals that the proposed rankings derived from various methods have a strong ranking relationship with one another. Finally, sensitivity analysis was performed to investigate the effects of weight variation and to validate the robustness of the implemented MCDM approaches.

Keywords: hybrid MCDM; ARAS; COPRAS; TOPSIS; robot selection

1. Introduction

In the last few decades, MCDM served as an efficient tool in the field of decision making. Researchers are working on this area, in order to upgrade the MCDM techniques and to fulfil the loop holes that exist in the previous methods. Moreover, researchers have developed new innovative MCDM models to make more precise and accurate decisions. Each day, MCDM methods are gaining importance, due to their inherent ability to judge



Development of high-performance aluminium 6061/SiC nanocomposites by ultrasonic aided rheo-squeeze casting method

Arunkumar^a, Pragnanathan^b, Lakshmi^c, R. S. J. Gokulakrishnan^d, Ram Subbiah^e, Karthikeyan Ramamurugan^f, Swasthika Manigandan^g

- ^a Department of Mechanical Engineering, CMR Institute of Technology, Bengaluru, India
- ^b Department of Aerospace Engineering, SRM Institute of Science and Technology, Kattankulathur, Chennai, India
- ^c Department of Mechanical Engineering, Gokaraju Rangaraju Institute of Engineering and Technology, Hyderabad, India
- ^d Department of Aerospace and Aircraft Engineering, Kingdon University, India, UK
- ^e Petroleum and Chemical Engineering, Faculty of Engineering, Umeedhi Tek. Jyoti, Brand, Bandar Sri Begawan BE1410, Ujung Darussalam

Received 11 May 2021, Revised 6 June 2021, Accepted 19 June 2021, Available online 13 June 2021, Version of Record 17 June 2021.

Check for updates

Show less

Outline | Share | Cite

<https://doi.org/10.1016/j.ultrasch.2021.105511>

Under a Creative Commons license

Get rights and content

Open access

Highlights

- Explored the ultrasonication aided novel fabrication process for Al/SiC cermet.
- This novel process enhanced the interfacial bonding between SiC & aluminium.
- SEM images confirm the nanoparticles homogeneous distribution & low-level porosity.

Abstract

In the modern era, the need for new products with novel processing and multi-purpose materials is increased. The current market requirements for engineering applications are lightweight, high strength and low-cost materials. This paper explores the novel development process of high-performance nano cermet material for aerospace applications. Herein, lightweight aluminium 6061 + 2% of SiC (40 nm) nano cermet was fabricated through the casting method. The effects of ultrasonication, double stir casting or rheocasting, and squeezing pressure on nano cermet fabrication were successfully investigated by comparing their physical, thermal and mechanical properties. Scanning electron microscopy was employed to analyse the morphology of the cermets, and the presence of reinforcements was verified through EDS. The reinforcement of SiC into Al 6061 improved density, hardness, and reduction in porosity and grain refinement. This study reveals a novel fabrication process of ultrasonic aided rheo-squeeze casting technique which enhanced the mechanical properties of the cermets compared to Al 6061 alloy due to nanoparticles homogeneous distribution, minimal agglomeration and porosity.

Previous

Next

Research Article

Mechanical Strength and Fatigue Fracture Analysis on Al-Zn-Mg Alloy with the Influence of Creep Aging Process

Muruganantham Ponnusamy ¹, Bhanu Pratap Polla,² T. Sathish ³,
Sivakumar Karthikeyan ⁴, S. Ravindran,⁵ Balachandra Pattanaik ⁶ and Ram Subbiah⁷

¹Deputy Registrar IIT, Kalyani, West Bengal, India

²Department of Mechanical Engineering, Addis Ababa Science and Technology University, Addis Ababa, Ethiopia

³Department of Mechanical Engineering, Sreevishva School of Engineering SSMATS, Chennai 602105, Tamil Nadu, India

⁴Department of Mechanical Engineering, SRM Valluvar Engineering College, Kattankulathur SRM Nagar 603203, Chennai, Tamil Nadu, India

⁵Department of Mechanical Engineering, Sri Sairam Engineering College, West Tambaram, Chennai 600044, Tamil Nadu, India

⁶Department of Electrical and Computer Engineering, Wailga University, Nakamta, Eritropia

⁷Department of Mechanical Engineering, Gokaraju Rangaraju Institute of Engineering and Technology, Nuzvid, Hyderabad, India

Correspondence should be addressed to Balachandra Pattanaik, balachandrapattanaik14251425@gmail.com

Received 25 June 2021; Revised 5 July 2021; Accepted 14 July 2021; Published 31 July 2021

Academic Editor: Samson Jerold Samuel Chelladurai

Copyright © 2021 Muruganantham Ponnusamy et al. This is an open access article distributed under the Creative Commons Attribution License, which permits unrestricted use, distribution, and reproduction in any medium, provided the original work is properly cited.

The Al-Zn-Mg alloy comes under the aluminium alloy; it possesses good capability of age hardening and superior strength in contrast to other alloys. The numbers of creep aging experiments are conducted with the support of different temperature levels such as 180, 200, and 200°C. The effects of tests are reflected on the tensile test and fatigue test, the temperature and stress directly affects the creep characteristics, mechanical strength, and fatigue performance of the Al-Zn-Mg alloy. The time period of the creep test is maintained as 15 hrs with constant load of 200 MPa and 220 MPa. The increasing temperature increases the tensile strength and fatigue life of the Al-Zn-Mg alloy under initial condition; furthermore, continuous movement reduces the strength and fatigue existence. In the fatigue test, the fatigue span of the Al-Zn-Mg is extremely enhanced by the application of creep aging at a particular temperature. The 3D profilometry image visibly shows the influence of temperature in forming a fracture in fatigue analysis through microstructure analysis.

1. Introduction

Creep aging is one class of forming process with merger of creep deformation and aging of material, both improve the material properties and life time of working. This creep aging process concentrated on fabrication of aircraft parts and more integral parts [1–3]. Creep aging is a precision forming, used to reduce the fracture while the material is processed. Most of the research conducted creep aging process to analyse and improve the microstructures and mechanical properties. Creep aging process is a method of heat treatment in the forming process with creep action; the material

for creep aging is loaded in elastic nature in a gripper. The loaded elastic material is kept in a temperature set for a predetermined time period [4, 5]. The constant load and under in thermal exposure of the material elements of the metal are undergone to impulsive and change of microstructure and the mechanical properties of the Al-Zn-Mg alloy. From the creep aging process, the change of the material properties and the spring back effects of the materials are easy to control [6]. The materials containing aluminium alloys and combination of elements such as copper, magnesium, and zinc are used in the industry. These alloys are developed by heat treatments; furthermore, these



Special Issue

Processing and Applications of Advanced Functional Materials

View this Special Issue

Research Article | Open AccessVolume 2021 | Article ID 9723699 | <https://doi.org/10.1155/2021/9723699>

Show Full Article

Parameters Optimization of Dissimilar Friction Stir Welding for AA7079 and AA8050 through RSM

M. Kavitha,¹ V. M. Manickavasagam,² T. Sathish ,² Bhiksha Gugulothu ,⁴ A. Sathish Kumar,⁵ Sivakumar Karthikeyan ,⁶ and Ram Subbali⁷

Show more

Academic Editor: Samson Jerold Samuel Chelladurai**Published:** 17 Jul 2021

Abstract

Aluminium alloy is widely used in engineering application, and it can be classified based on the constituent elements or alloying elements. Aluminium alloy is preferred for the nature of its tensile strength, ductility, and corrosion resistance in this research to make a dissimilar friction stir welding joint of aluminium alloys 7079 and 8050 materials. The tensile strength of the weld joint is estimated by the influence of the response surface methodology approach. The welding is carried out by preferred process parameters with a tool speed of 1000–2500 rpm, tool pin diameter of 2–6 mm, welding speed of 50–300 mm/min, and tool shoulder diameter of 10–20 mm. The ANOVA analysis and the prediction of tensile strength were conducted efficiently. From the RSM analysis, the tool pin diameter mostly modified the output of the result.

1. Introduction



Advances in Materials and Processing Technologies >

Latest Articles


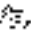
6 0

Views CrossRef citations to date Altmetric

0



Research Article

Analysis on effect of nanofluid on process parameters in machining of EN19 steel

Sateesh N , Ram Subbiah, BCh Nookaraju, A. Anitha Lakshmi  &

Prashanth kumar P

Accepted 30 Jun 2021, Published online 22 Jul 2021

 Download citation <https://doi.org/10.1080/2374068X.2021.1953918> Check for updates Full Article Figures & data References Citations Metrics Reprints & Permissions

Get access

ABSTRACT

Machining is the most fundamental process in manufacturing industry. The heat generated on the working surface of the tool during machining is critical to determining the dimensional accuracy and surface quality of the workpiece. Conventional cutting fluids are hazardous to the health of workers and cause environmental pollution. This paper focuses on the effect of vegetable oil-based nanofluid on the machining performance in turning of EN19 steel through Minimum Quantity Lubrication (MQL). Canola oil is used as a base lubricant with various inclusions of boric acid powder nanoparticles. Machining parameters such as tool temperature and cutting forces are measured during machining. After processing,



Advances in Materials and Processing Technologies >

Latest Articles

62 0


Views CrossRef citations to date Altmetric

Research Article

Wear and microstructure analysis on AISI420 stainless steel by annealing & tempering process under dry sliding conditions

Animesh Bain , Keerthi Reddy, Saranya Jagadeesan, A. Anitha Lakshmi , N Sateesh, Swadesh Kumar Singh & ...show all

Accepted 08 Jun 2021. Published online: 06 Jul 2021

 Download citation  <https://doi.org/10.1080/2374068X.2021.1945308> Check for updatesSample our
Physical Sciences
journalsClick here to start your access
to the latest two volumes for 14 days Full Article  Figures & data  References  Citations  Metrics Reprints & Permissions  Get access

ABSTRACT



AISI 420 martensitic stainless steel is accepted for its sensible corrosion resistance. Stainless steel is commercially available in the market at low cost. AISI 420 martensitic stainless steel has excellent hardness, strength, and wear resistance but it lacks in its ductility. Thus, to enhance the property of ductility, annealing and tempering processes were chosen to maintain a stable relationship with ductility and brittleness. The samples were chosen in the form of cylindrical shapes with

6 0

Views CrossRef citations to date Altmetric

Research Article

Analysis on effect of nanofluid on process parameters in machining of EN19 steel

Sateesh N  Ram Subbiah, BCh Nookaraju, A. Anitha Lakshmi  &

Prashanth kumar P

Accepted 30 Jun 2021, Published online: 22 Jul 2021

 Download citation  <https://doi.org/10.1080/2374068X.2021.1953918> Check for updates

Sample our
Physical Sciences
Journals

>>> [Click here](#) to start your access
to the latest two volumes for 14 days

ABSTRACT

Machining is the most fundamental process in manufacturing industry. The heat generated on the working surface of the tool during machining is critical to determining the dimensional accuracy and surface quality of the workpiece. Conventional cutting fluids are hazardous to the health of workers and cause environmental pollution. This paper focuses on the effect of vegetable oil-based nanofluid on the machining performance in turning of EN19 steel through Minimum Quantity Lubrication (MQL). Canola oil is used as a base lubricant with various inclusions of boric acid powder nanoparticles. Machining parameters such as tool temperature and cutting forces are measured during machining. After processing, the surface roughness of the part is measured. The change in the temperature of

Advances in Materials and Processing Technologies >

Latest Articles



62 0

0

Views CrossRef citations to date Altmetric

Research Article

Wear and microstructure analysis on AISI420 stainless steel by annealing & tempering process under dry sliding conditions

Animesh Bain , Keerthi Reddy, Saranya Jagadeesan, A. Anitha Lakshmi , N Sateesh, Swadesh Kumar Singh & ... [show all](#)

Accepted 08 Jun 2021, Published online: 06 Jul 2021

[Download citation](#) <https://doi.org/10.1080/2374068X.2021.1945308>[Check for updates](#)Sample our
Physical Sciences
journalsClick here to start your access
to the latest two volumes for 14 days

ABSTRACT

AISI 420 martensitic stainless steel is accepted for its sensible corrosion resistance. Stainless steel is commercially available in the market at low cost. AISI 420 martensitic stainless steel has excellent hardness, strength, and wear resistance but it lacks in its ductility. Thus, to enhance the property of ductility, annealing and tempering processes were chosen to maintain a stable relationship with ductility and brittleness. The samples were chosen in the form of cylindrical shapes with diameter 10 mm and length 40 mm, respectively. The samples were subjected to

RESEARCH ARTICLE



FINITE ELEMENT ANALYSIS OF CHROMIUM AND MOLYBDENUM ALLOYED STEEL BILLETS FORGED ON MULTI STEP PROCESS USING SIMUFACT FORMING

K. V. Durga Rajesh^a, Himanshu Mishra^b and Tanya Buddi^a

^aDepartment of Mechanical Engineering, Associate Professor, Koneru Lakshmaiah Education Foundation, Vaddeswaram, India; ^bDepartment of Mechanical Engineering, Asst. Prof. GRIET, Hyderabad, India

ABSTRACT

Simufact Forming covers the complete spectrum of working on forming technologies like rolling, forging, and sheet metal forming. In this paper, finite element comparative analysis was performed on two chromium- and molybdenum-alloyed steel billets, namely 42CrMo4 and 16CrMo4 alloyed steels, using multi-step forming process of hot closed die forging process using Simufact Forming software. 42CrMo4 alloy steel is most commonly used in making of automobile components, and 16CrMo4 alloyed steels are commonly utilised in the area of ship building, airplanes, etc. While working with these materials, with the help of forging process, lot of stresses, strains and temperatures will develop. In this paper, three state variables, namely effective plastic strain, equivalent stress and temperature, for two materials at the end of multi-step forming processes like chamfering, preforming and final forging stages are evaluated and compared. In cooling process, the initial temperature of billet is maintained at 1250°C for both materials. Finally, comparative analysis of two alloyed steel billets was done by considering three-state variables.

ARTICLE HISTORY



Accepted 25 May 2021

KEYWORDS

Simufact Forming; alloyed steel; effective plastic strain; equivalent stress; temperature

1. Introduction

Simufact Forming provides multiple application modules customised to the needs of different forming processes. Every application module has its own set of default settings for the solver, mesher and different process types including rolling, forging, extrusion, upsetting, etc., which allows the user to obtain good simulation results without having to dig into the more advanced settings. Simufact Forming completely supports result transitions from 2D to 3D simulations, and some application modules provide exclusive computer kinematics such as ring rolling, cold forming, hot forming, etc. One can set up the performing operations of a multi-stage process as 2D simulations and then turn to a 3D simulation when the shape of the workpiece requires it. This makes it possible to set up whole process chains quickly and easily. Simufact Forming is based around working with objects. Objects can be almost anything from geometries to materials, to physical properties or mesh information. Any object you used in your project is collected and

CONTACT K. V. Durga Rajesh  kanchurajesh@kief.ac.in  Department of Mechanical Engineering, Associate Professor, Koneru Lakshmaiah Education Foundation, Vaddeswaram, India

© 2021 Informa UK Limited, trading as Taylor & Francis Group

RESEARCH ARTICLE



Finite element analysis of chromium and nickel alloyed steel billets forged under warm forming process using Deform-3D

K. V. Durga Rajesh ^{1,2*} and Tanya Buddhi ^{1,2}

¹Department of Mechanical Engineering, Koneru Lakshmaiah Education Foundation, Vaddeswaram, Andhra Pradesh, India; ²Department of Mechanical Engineering, GRIET, Bachupally, Hyderabad, Telangana, India

ABSTRACT

Deform-3D is effective software for predicting flow of material in large deformation applications in absence of expense and time delays associated with shop trials. The Deform-3D software is used to build a 3D finite element open die forging model using warm forming process. Pre-processing, simulation, and post-processing are all phases that can be used to simulate. 17Cr-13Ni-2Mo and 17Cr-5Ni-5Mo-Ti alloyed steel billets were taken to perform analysis. Under warm forming allowable temperatures of 250°C, 500°C, and 750°C, simulation was performed using software. After 30 steps of simulation, results such as damage, strain effective, effective stress, total velocity, total displacement, and final Temperature are reported from the post-processing module. From results, comparative analysis will be carried out on performance characteristics at different billet temperatures. The Deform-3D software is used for finite element simulation during the forming process to accurately predict the deformation.

ARTICLE HISTORY

Accepted 08 June 2021



KEYWORDS

Deform-3d; warm forming; simulation; billet; temperature

1. Introduction

DEFORM is a process simulation system for metal forming and related industries that uses the finite element method (FEM) to analyse different heat treatment and forming processes. It is possible to undertake combined modelling of deformation and heat transfer in order to simulate cold, warm, or hot forging operations. The DEFORM device is a piece of engineering software that lets designers to model and simulate metal formation, machining, heat treatment, and mechanical joining processes on a machine rather than on the shop floor. For more than two decades, process simulation utilising DEFORM has helped top firms improve cost, quality, and delivery. Companies must use every instrument at their disposal in order to survive today's competitive environment. DEFORM has been shown to be extremely useful in a wide range of scientific, academic, and industrial applications. The DEFORM System is designed and maintained by Scientific Forming Technologies Corporation (SFTC).

Warm forming is a metal forming technique that occurs at temperatures above the cold working temperature range but below recrystallisation temperature of the metal.

CONTACT K. V. Durga Rajesh  kanchurajesh@koneru.ac.in  Department of Mechanical Engineering, Koneru Lakshmaiah Education Foundation, Vaddeswaram, Andhra Pradesh, India

© 2021 Informa UK Limited, trading as Taylor & Francis Group



Integrated Taguchi-GRA-RSM optimization and ANN modelling of thermal performance of zinc oxide nanofluids in an automobile radiator

Arun Kumar Kalogi^a, Avil Akshay^b, A. Muthu Manick^c, Deepak Thakur^d, Umithaga Lal^e, Saad Alshahrani^f, A. Umesh Babu^g, Ravi Subrah

- ^a Department of Mechanical Engineering, P. A. College of Engineering (Affiliated to VJSSV Group of Institutions, Bangalore), Mangaluru, 574153, India
- ^b Department of Mechanical Engineering, B. S. Abdur Rahman Crescent Institute of Science and Technology, Vandalur, Tamil Nadu, 600 048, India
- ^c Chitkara University Institute of Engineering and Technology, Chitkara University, Punjab 140401, India
- ^d Department of Mechanical Engineering, Faculty of Engineering, Erciyes University, 38020, Turkey
- ^e Department of Mechanical Engineering, College of Engineering, King Khalid University, PO Box 191, Abha, 51421, Saudi Arabia
- ^f Gokaraju Rangaraju Institute of Engineering & Technology, Hyderabad, India
- ^g Department of Mechanical Engineering, P. A. College of Engineering (Affiliated to VJSSV Group of Institutions, Bangalore), Mangaluru, 574153, India

Received 15 February 2021; Revised 3 May 2021; Accepted 5 May 2021; Available online 15 May 2021; Version of Record 24 May 2021.

Check for updates

Show less

Outline | Share | Cite

https://doi.org/10.1016/j.csite.2021.101068

Under a Creative Commons license

Get rights and content
Open access

Abstract

Impact of different input variables on the thermal performance features of an automobile radiator was investigated, statistically analyzed, and optimized using the powerful technique Taguchi's grey relational analysis (GRA) and Response surface methodology (RSM). Polyethylene glycol (PEG) nanofluids containing ZnO nanoparticles of various volume concentrations (0.2%–0.6%) were used. 1-Butyl-3-methylimidazolium bromide [C4mim][Br] ionic liquid was added to reduce particle accumulation and increase nanofluid dispersion. The main radiator used was an unmixed crossflow type. The analyses were carried out at various flow rates. Thermal performance parameters like Nusselt number (Nu), heat transfer coefficient (h_c), pressure drop, and pumping power were optimized by using weighted grey relational grade, depending on the experiments designed using Taguchi's Experiment Design. ANN modelling was used to get a better prediction of the non-linear form of critical data. Optimized Nu, h_c, pressure drop, and pumping power were obtained for different combination of Re, air velocity, and nanofluid concentration to maximize. The h_c estimated by ANN is found to be reasonably consistent with the experimental findings. From the research findings, it is also inferred that heat transfer enhancement does occur in radiators employing nanofluids but at the expense of the pressure drop and pumping power.

Previous

Next

Keywords

Automobile radiator; Forced flow; Nanofluids; Grey relational analysis; ANOVA; Zinc oxide

Nomenclature



Advances in Materials and Processing Technologies >

Latest Articles

57 0

0

Views CrossRef citations to date Altmetric


Research Article

Tribological behaviour of AA7168 hybrid composite sheets for aerospace structures fabricated through COMPO casting

Venkatesan S, Giridharan P. K., Sivakumar N S, Sharavanan S, Ram Subbiah & Senthamilselvi A

Accepted 14 Jul 2021, Published online 02 Aug 2021

 Download citation  <https://doi.org/10.1080/2374068X.2021.1959088>

 Check for updates

Sample our
Physical Sciences
journals
>> [Click here](#) to start your access
to the latest two volumes for 14 days

 Full Article  Figures & data  References  Citations  Metrics

 Reprints & Permissions [Get access](#)

ABSTRACT

In this research work, an attempt was made to reinforce AA7168 aluminium alloy with Boron Carbide (B_4C) and Silicon Carbide (SiC) through compos casting technique. Tribological test were performed by varying weight percentage (3, 6, 9, 12%), Load (10, 20, 30, 40 N), Sliding velocity (10, 20, 30, 40 m/s) and sliding distance (1000, 2000, 3000, 4000 m). The results revealed that the wear resistance increases with addition of reinforcing particles until a saddle point of 9 wt.% owing to the formation of mechanical mixed layer. At 12%, the wear resistance reduces because of the clustering of particles. Because of the hardness of the particles, the



Article

Development, Testing and Characterization of Al nanoTiC_p Composites through Powder Metallurgy Techniques

Gaurav Rajpat^{1,*}, Anuradha Tiwari², Rajesh Purohit^{1,3}, Vijay Panchore², Rashmi Dwivedi⁴ and Kusumaji Satyamurayana⁵¹ Department of Mechanical Engineering, Indian Institute of Technology, Kanpur, 209116, India² Department of Physics, Brahmamand Degree College Chhatrapati Shahu Maharaj University, Kanpur, 208024, India; tiwari.anuradha08@gmail.com³ Department of Mechanical Engineering, Maulana Azad National Institute of Technology, Bhopal, 462002, India; vijaypanchore36@gmail.com⁴ Department of Mechanical Engineering, Sagar Group of Institutions—SISTec, Bhopal, 462056, India; rashmidwivedi27@gmail.com⁵ Department of Mechanical Engineering, Gokaraju Rangaraju Institute of Engineering and Technology, Hyderabad 500090, India; satya.kesara@gmail.com* Correspondence: rajpat2180@gmail.com (G.R.); purohit.175@gmail.com (R.P.)

Citation: Rajpat, G.; Tiwari, A.; Anuradha, P.; Panchore, V.; Dwivedi, R.; Satyamurayana, K. Development, Testing and Characterization of Al nanoTiC_p Composites through Powder Metallurgy Techniques. *J. Compos. Sci.* **2021**, *3*, 221. <https://doi.org/10.3390/10310221>

Academic Editor: Francesco Tornabene

Received: 25 June 2021

Accepted: 15 August 2021

Published: 22 August 2021

Publisher's Note: MDPI stays neutral with regard to jurisdictional claims for published maps and institutional affiliations.



Copyright: © 2021 by the authors. Licensee MDPI, Basel, Switzerland. This article is an open access article distributed under the terms and conditions of the Creative Commons Attribution (CC BY) license (<http://creativecommons.org/licenses/by/4.0/>).

Abstract: In the present scenario, weight minimization and strength enhancement are the main requirements for escalating the application of a nano composite material in different sectors. Several industrial sectors, such as automobile, defense and aerospace, are making various components of nano composites with the help of powder metallurgy processing. In this study, Al nanoTiC_p composites (2, 4 and 6 wt %) were contrived through modified powder metallurgy (PM) techniques with the help of Cold Isostatic Compaction process (CIP). The mechanical properties such as density, porosity, micro-hardness, compressive strength and indirect tensile strength were increasing with the reinforcement of nanoTiC_p particles up to 4 wt % in Al metal matrix composites. Nevertheless, clustering of nanoTiC_p particles were found at 6 wt %, which was also observed in SEM images.

Keywords: powder metallurgy (PM); cold isostatic compaction process (CIP); Al nanoTiC_p composites; clustering; mechanical properties

1. Introduction

In the 21st Century, the application of nanotechnology has rapidly enhanced in all areas. There is a big scope in the field of nano composites in the area of material science because the function of nano composite materials enhances several properties such as chemical, mechanical, optical and/or physical properties in different aspects with light weight [1]. Nowadays, scientists have a big interest in aluminum matrix nano composites (AMNCs) due to their high stiffness, lightweight, high strength-to-weight ratio, lower-cost, ease of production and high dimensional tolerance [1]. It is widely used in automobile sectors and the aerospace industry [2]. Nevertheless, overall strength is found less in aluminum, therefore, to enhance this strength, nano particles are reinforced in aluminum matrix nano composites. It is observed that this overall strength is usually dependent of particle size, spacing, volume fraction and the nature of matrix and the reinforcement of the interface [3]. A lot of literature is available about several ceramic nano particles, such as SiC, B₄C, h-BN, TiC_p and MgO that are reinforced in the AMNCs to enhance the wear properties, mechanical properties and microstructure of the composites [4–12]. Nevertheless, TiC_p is a unique ceramic that shows high hardness, low wear, relatively high thermal stability and good wet ability due to its controlled three-dimensional structures [13]. Titanium Carbide (TiC) is a good ceramic that is used in wear resistant

Research Article

Investigation on Heat Transfer Enhancement in Microchannel Using Al₂O₃/Water Nanofluids

Arunkumar Munimathan¹, T. Sathish², V. Mohanavel³, Alagar Karthick⁴, R. Madavan,⁵ Ram Subbiah,⁶ Chaudran Masi,⁷ and S. Rajkumar^{1,8}

- ¹Department of Agriculture Engineering, Sri Shakti Institute of Engineering and Technology, Coimbatore, 641062 Tamilnadu, India
- ²Department of Mechanical Engineering, Sweetha School of Engineering, SIMATS, Chennai, 602105 Tamil Nadu, India
- ³Centre for Materials Engineering and Regenerative Medicine, Bharath Institute of Higher Education and Research, Chennai, 600073 Tamilnadu, India
- ⁴Department of Electrical and Electronics Engineering, KPR Institute of Engineering and Technology, Coimbatore, 641407 Tamilnadu, India
- ⁵Department of Electrical and Electronics Engineering, PSR Engineering College, Sivakasi, Tamilnadu, India
- ⁶Department of Mechanical Engineering, Gokulraj Ranganay Institute of Engineering and Technology, 500190, Nizampet, Hyderabad, India
- ⁷Department of Biotechnology, College of Biological and Chemical Engineering, Addis Ababa Science and Technology University, Addis Ababa, Ethiopia
- ⁸Department of Mechanical Engineering, Faculty of Manufacturing, Institute of Technology, Hawassa University, Ethiopia

Correspondence should be addressed to Arunkumar Munimathan; arzurunapdp@gmail.com and S. Rajkumar; rajkuma@hu.edu.et

Received 5 April 2021; Revised 25 July 2021; Accepted 16 August 2021; Published 14 September 2021

Academic Editor: Ahmad Utam

Copyright © 2021 Arunkumar Munimathan et al. This is an open access article distributed under the Creative Commons Attribution License, which permits unrestricted use, distribution, and reproduction in any medium, provided the original work is properly cited.

Nowadays, reducing heat generation in electronic devices while using microchannel cooling is used to solve this problem. Because the trend is globally marching toward the compact size, the component's dimensions get smaller, but the warmth involved within the component increases. Studies of heat transfer rate are conducted to determine the effect of a fully heated microchannel conductor's heat transfer performance. Experiments are performed using nanofluid Al₂O₃/water through a concentration percentage of 0.1% and 0.25% and deionized water through a microchannel conductor with 25 rectangular microchannel numbers with a dimension of (0.42 × 0.42 × 100) mm³. This present work deals with the effect of nanofluids and their concentration percentages. Finally, it concluded that better heat transfer performance was seen in nanofluids compared to deionized water. The reason is the high viscosity of nanofluid Al₂O₃/water due to these nanoparticles is deposited on the wall surface of the microchannel and outcomes timely improvement in the heat transfer. Finally, a high concentration percentage of nanofluids revealed a practical improvement in the transfer of microchannel. As a result, 0.25% of the concentration percentage achieved a satisfactory result compared to the remaining fluids and almost 52.5% and 26% of thermal resistance decrease.

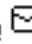
1. Introduction

The microchannel is one of the significant materials to reduce the channel's size to the small resolve reason rise in heat transfer rate. The microchannel is an essential material used to reduce the channel's size to a small resolution to

increase heat transfer [1]. Made of silicon based microchannels, the Pyrex cover plates are bonded to the anode and maintain constant heat flux. The maximum of 2100 is the Reynolds number, the heat transfer rate of 760 W/cm², and the 2 bar is the pressure drop [2]. It was found that the microchannel conductor will be prepared to dissipate over

Original Paper | Published: 19 October 2021

Time Dependent Behaviour of Amino Silane-treated Aramid Fibre and Waste Latex Rubber Powder Toughened Epoxy Composite

K. K. Arun, M. Bala Theja, L. Girisha, N. Arun Vignesh, N. S. Sivakumar, Ram Subbiah & S. Kaliappan 

Silicon **14**, 6837–6845 (2022)

69 Accesses | 6 Citations | [Metrics](#)

Abstract

The purpose of this research was to investigate the time-dependent behaviour of an epoxy composite prepared from silane-treated aramid fibre and waste latex rubber powder (LRP). To increase the adhesive behaviour of reinforcement with matrix, the aramid fibre and latex rubber powder were surface treated using amino silane. The composites were made using hand layup method and cured at room temperature. The fatigue strength of LRP in fibre-epoxy composite was improved up to 82.1 % when compared to fibre-epoxy composite. Similarly, incorporating LRP into the resin increased the energy storage up to 4.7GPa, which was equal to 34.04 % with neat epoxy. The addition of latex rubber powder to the resin enhanced the energy dissipation factor in dynamic mechanical analysis (DMA). These mechanically toughened

Research Article

Preparation of Polymeric Nanomaterials Using Emulsion Polymerization

Satyajeet Sahoo¹, Anitha Gopalan², S. Ramesh³, P. Nirmala⁴, G. Ramkumar²,
 S. Agnes Shifani⁵, Ram Subbiah⁶, and J. Isaac Joshua Ramesh Lalvani⁷

¹Department of Electronics and Communication Engineering, Vignana's Foundation for Science, Technology and Research (Deemed to be University), Vadlamudi, Guntur, Andhra Pradesh 522212, India

²Department of Electronics and Communication Engineering, Sreeatha School of Engineering, SMMAN, Chennai 602105, Tamil Nadu, India

³Department of Electronics and Communication Engineering, Sri Shakthi Institute of Engineering and Technology, Coimbatore 641052, Tamil Nadu, India

⁴Department of Electronics and Communication Engineering, Jeppiaar Manamella Engineering College, Chennai, Tamil Nadu, India

⁵Department of Mechanical Engineering, Goburaja Rangaraja Institute of Engineering and Technology, Vizampet, Hyderabad, India

⁶Department of Mechanical Engineering, Faculty of Mechanical and Production Engineering, AMIT, Anna Maria University, Arba Minch, Ethiopia

Correspondence should be addressed to Satyajeet Sahoo; satyajeetsahoo.edu@gmail.com and J. Isaac Joshua Ramesh Lalvani; isacjr@amu.edu.et

Received 29 August 2021; Accepted 23 September 2021; Published 8 October 2021

Academic Editor: P. Ganeshan

Copyright © 2021 Satyajeet Sahoo et al. This is an open access article distributed under the Creative Commons Attribution License, which permits unrestricted use, distribution, and reproduction in any medium, provided the original work is properly cited.

Nanoparticles are said to be active particles which are entrapped in the surface of the polymeric core. Since nanoparticles were used in medical and biotechnological fields, there is a great demand in the preparation of nanoparticles. Nanoparticles are prepared from different substances; mainly, polymer material is used in the field of preparing nanomaterials. There are different methods involved in the preparation of nanoparticles from the polymer. Various experiments and research studies were carried out on the basis of preparation of nanoparticles. Emulsion polymerization could be used to make polymeric nanoparticles with a high solid concentration without the need of surfactants. To make carboxylate polystyrene beads or amine polystyrene nanoparticles, polymeric nanocolloids containing surface functional groups were produced. In this research, the preparation of nanoparticles from emulsion polymerization is represented along with the size and distribution material.

1. Introduction

To achieve the challenges in drug delivery, polymer nanotechnology is considered as one of the promising systems. This involves drug targeting as well as delivering undelivered compounds such as oligonucleotides. The important challenges in nanotechnology are the preparation of nanoparticles, with suitable properties of

nanoparticles, and this concerns proper drug transporting and pointing [1]. Various grades of poly and copolymers are used to prepare the nanoparticles in a wide range. The ability to synthesize polymers with well controlled structures and conformation also paves the way for nanoparticles with precisely tuned characteristics, which are needed to meet drug targeting goals. This enthusiasm stems from the belief that nanoparticles with sizes ranging



Research Article

Influence of Fiber Volume and Fiber Length on Thermal and Flexural Properties of a Hybrid Natural Polymer Composite Prepared with Banana Stem, Pineapple Leaf, and S-Glass

K. B. Prakash,¹ Yahya Ali Fageehi,² Rajasekaran Saminathan,² P. Manoj Kumar iD,³ S. Saravanakumar,⁴ Ram Subbiah,⁵ B. Arulmurugan,³ and S Rajkumar ⁶

¹Department of Mechanical Engineering, Baereri Amman Institute of Technology, Sathyangalam 638401, Tamil Nadu, India
²Department of Mechanical Engineering, College of Engineering, Jazan University, Jazan, Saudi Arabia
³Department of Mechanical Engineering, KPR Institute of Engineering and Technology, Coimbatore 641467, Tamil Nadu, India
⁴Department of Mechanical Engineering, M. Kumarasamy College of Engineering, Karur 639113, Tamil Nadu, India
⁵Department of Mechanical Engineering, Gokaraju Rangaraju Institute of Engineering and Technology, Hyderabad 500096, Telangana, India
⁶Department of Mechanical Engineering, Faculty of Manufacturing, Institute of Technology, Hawassa University, Hawassa, Ethiopia

Correspondence should be addressed to S Rajkumar; rajkumar@ha.edu.et

Received 17 August 2021; Revised 17 September 2021; Accepted 18 September 2021; Published 2 October 2021

Academic Editor: Jinyang Xu

Copyright © 2021 K. B. Prakash et al. This is an open access article distributed under the Creative Commons Attribution License, which permits unrestricted use, distribution, and reproduction in any medium, provided the original work is properly cited.

There is more demand for natural fiber-reinforced composites in the energy sector, and their impact on the environment is almost zero. Natural fiber has plenty of advantages, such as easy recycling and degrading property, low density, and low price. Natural fiber's thermal properties and flexural properties are less than conventional fiber. This work deals with the changes in the thermal properties and mechanical properties of S-glass reinforced with a sodium hydroxide-treated pineapple leaf (PALF) and banana stem fibers. Banana stem and pineapple leaf fibers (PALF) were used at various volume fractions, i.e., 30%, 40%, and 50%, and various fiber lengths of 20 cm, 30 cm, and 40 cm with S-glass, and their effects on the thermal and mechanical properties were studied, and their optimum values were found. It was evidenced that increasing the fiber volume and fiber length enhanced the flexural and thermal properties up to 40% of the fiber volume, and started to decrease at 50% of the fiber volume. The fiber length provides an affirmative effect on the flexural properties and a pessimistic effect on the thermal properties. The PALF-S-glass combination of 40% fiber load and 40 cm fiber length provides maximum flexural strength, flexural modulus, storage modulus, and lowest loss modulus based on hybrid Taguchi grey relational optimization techniques. PALF-S-glass hybrid composite has been found to have 7.80%, 3.44%, 1.17% higher flexural strength, flexural modulus, and loss modulus, respectively, and 15.74% lower storage modulus compared to banana-S-glass hybrid composite.

1. Introduction

Due to the demand for lower dense material and green environment, fiber-reinforced composites (FRCs) have drawn more awareness towards the alternatives to metal-reinforced composites. Natural fibers are effectively utilized in polymer matrices as reinforcement [1]. Fillers such as particles or filaments are created with polymers to get items with the most needed mechanical, thermal, and electrical

properties. The characteristics of natural composites are primarily subject to their particular fiber characteristics [2]. There are different variables, which influence the properties of the microstructural boundaries, such as fiber radius, length of fiber, fiber spread, fiber direction, loading weight of the fiber, and production method [3]. Natural fibers have more limitations, such as hydrophilic behavior, which leads to decreased adhesive properties [4]. In addition, natural fibers have more attraction to water particles from moisture,



Research Article

Evaluating the Mechanical and Tribological Properties of DLC Nanocoated Aluminium 5051 Using RF Sputtering

L. Natrayan¹,^{*} Anjibabu Merneedi²,^{*} Dhinakaran Veeman³,^{*} S. Kaliappan⁴,
P. Sotyanarayana Raja,⁵ Ram Subbiah,⁶ and S. Venkatesh Kumar⁷

¹Department of Mechanical Engineering, Saveetha School of Engineering, SIMATS, Chennai, Tamil Nadu 602105, India
²Department of Mechanical Engineering, Aditya College of Engineering, Suvampaloo, 573437 Andhra Pradesh, India
³Centre for Additive Manufacturing, Chennai Institute of Technology, 605069, Chennai, India
⁴Department of Mechanical Engineering, Velammal Institute of Technology, Chennai, 601204 Tamil Nadu, India
⁵Department of Mechanical Engineering, Vardhman College of Engineering, Kothuram, Shamshabad, Hyderabad, 501218 Telangana, India
⁶Department of Mechanical Engineering, Gokaraju Rangaraju Institute of Engineering and Technology, Hyderabad, India
⁷Department of Mechanical Engineering, College of Engineering and Technology, Mettu University, Ethiopia P.O. Box: 118

Correspondence should be addressed to L. Natrayan; natrayanphd@gmail.com and S. Venkatesh Kumar; s.venkateshkumar@meu.edu.et

Received 3 September 2021; Revised 15 October 2021; Accepted 28 October 2021; Published 8 November 2021

Academic Editor: Lakshminaray R.

Copyright © 2021 L. Natrayan et al. This is an open access article distributed under the Creative Commons Attribution License, which permits unrestricted use, distribution, and reproduction in any medium, provided the original work is properly cited.

The diamond-like carbon (DLC) coating technique is used in the sliding parts of automotive engines, among other applications, to reduce friction and wear. In this work, DLC has been coated on the Aluminium 5051 sample to assess the mechanical and tribological properties. A sputtering deposition mechanism is used, and the DLC is coated using a graphite target. The developed DLC coatings are tested for adhesion strength, hardness, chemical composition using XRD, and wear behaviour. The developed DLC thin films have considerably increased the wear behaviour of the Aluminium 5051 sample and have fulfilled the objective of this study. The XRD data indicated the presence of amorphous carbon in the coating with a threefold increase in the hardness of the naked aluminium. This study provides insight into improving the aluminium wear resistance by developing a considerably hard coating.

1. Introduction

In today's machinery sector, surface engineering is critical. Hard coatings extend the service life of tools and moulds, yet hard coatings are difficult to apply to machine parts built of soft materials such as aluminium [1]. Thin films with high hardness can bear higher loads, but as the substrate is a soft material, the substrate fails the coating and the thin film too shall fail [2]. Surfaces take up a very little area in a matter when compared to the bulk. Still, they are extremely difficult to investigate [3] due to the very asymmetric nature of the forces acting on the surfaces. Pristine surfaces are highly susceptible to impurities and flaws. When two extremely pure surfaces come into contact, adhesive force is created, and

energy is used to separate those surfaces [4]. Adhesion energy is the energy exerted by atoms on the outer surfaces of nearby atoms when they come into contact with each other [5]. A simple van der Waal, covalent, ionic, or electrostatic force can be used as adhesive forces [6]. Cohesive forces hold atoms together in bulk materials. Atoms are held together by a cohesive force, and it takes a lot of force to rip a substance in half [7]. The breaking of cohesive links between atoms causes the metal to tear. The atoms with broken cohesive bonds on the new surfaces generated after breaking the parent material will be readily attracted to the new atoms [8]. Surface energy is the excess free energy per unit area on a crystal's surface. It is denoted by γ and plays a crucial role in thin-film adherence to the substrate. Surface tension,


Article Navigation

PROCEEDINGS PAPER

Effect of Die Velocity on Tube Deformation Mechanics During Low Pressure Tube Hydroforming Process Sequence Variation



Chetan P. Nikhane, Tarun Bujchi, Nitin Kokkonde, Swadesh Kumar Singh

 Check for updates

+ Author Information

Paper No: IMECE2021-70179, V02AT02A051; 10 pages

<https://doi.org/10.1115/IMECE2021-70179>

Published Online: January 25, 2022

Share > Cite Permissions

Abstract

Tube hydroforming is one of the successful manufacturing processes to create a variety of shapes using fluid pressure. The process fills the tube with fluid and pressurizes it to deform in various cross-sections. The method is categorized in three types: high pressure, pressure sequencing and low-pressure tube hydroforming. Tube hydroforming has gained popularity due to its many advantages such as part consolidation, uniform deformation, quality of the formed part and the possibility of unique shapes with indents or angles. Due to uniform thinning in the formed part, the parts can be lower weight and thus proven to be the technology to create light-weight parts for automotive and aerospace industries to increase the fuel economy. This paper focuses on low-pressure tube hydroforming. In low-pressure tube hydroforming, during the closing of the die the tube is marginally pressurized to a fixed volume. The previous study which was published in IMECE2019 and 2020 was focused on to investigate the effect of



Surface Modification of Strenx 900 Steel Using Electrical Discharge Alloying Process with Cu-10Ni- Cr Powder Metallurgy Sintered Electrode

S. Sridhar^{1*}, Srinivas Viswanath Valed², Vishwanath Koti³, S. Satish⁴, R. Raghun Chand⁵,

N.S. Sivakumar⁶, Mahesh. M⁷, Ram Subbiah⁸, G. Veerappan⁹

¹PSNA College of Engineering and Technology, Department of Mechanical Engineering, Dindigul.

²Aditya Engineering College, Department of Mechanical Engineering, Andhra Pradesh.

³Ramaiah Institute of Technology, Department of Mechanical Engineering, Bangalore.

⁴Ramakrishna Engineering College, Department of Mechanical Engineering, Coimbatore.

⁵Karavali Institute of Technology, Department of Mechanical Engineering, Mangalore.

⁶TISHK International University, Department of Mechatronics Engineering, Iraq.

⁷Centur Engineering College, Department of Mechanical Engineering, Andhra Pradesh.

⁸Gokaraju Rangaraju Institute of Engineering and Technology, Department of Mechanical Engineering, Hyderabad.

⁹Sri Krishna College of Engineering and Technology, Department of Mechatronics Engineering, Coimbatore.

Received: July 29, 2021; Revised: December 04, 2021; Accepted: December 28, 2021

The present investigation aims to coat the layer with Nickel (Ni) and Copper (Cu) over the surface of Strenx 900 steel using semi sintered Cu-10Ni-Cr₂ electrodes (x = 2, 4 & 6 wt. %). Three different proportions of semi sintered electrodes such as, Cu-10Ni-2 weight percentage of Chromium (Cr), Cu-10Ni-4 wt. % Cr, and Cu-10Ni-6 wt. % Cr were prepared by powder metallurgy route. Electric discharge alloying was completed based on L₉ orthogonal array and alloyed parameters were optimized using Taguchi method. The alloyed surfaces were characterized using scanning electron microscope and atomic force microscopy. The deposition of formation of intermetallic was studied using X-ray diffractometer. Higher Material Transfer Rate (MTR) was obtained at 9A, 350A and 6% chromium using Cu-10 Ni-Cu electrode. The chromium percentage was the foremost factor on Surface Roughness (SR) (73.71%) and MTR (96.56%). From Taguchi approach, the minimum SR was attained at percentage of chromium of 2%, compaction pressure of 250 Megapascal (MPa) and peak current of 9A. The maximum MTR was achieved at 6 percentage of Cr, compaction pressure of 350 MPa and peak current of 3A. Wear loss for Cu-10 Ni-Cr increases linearly with increase in sliding speed from 2m/s to 4m/s respectively.

Keyword: Electrical discharge alloying, Powder Metallurgy, Taguchi, Characterization, Atomic force microscopy.

1. Introduction

Electrical discharge machining is an unconventional machining process that involves eroding material from a work piece using a tool called electrode. The process occurs as a sequence of electrical discharges in the presence of dielectric fluid¹. In case of die sinking Electric Discharge Machining (EDM), the process should be carried out only with the dielectric fluids such as de-ionized water, kerosene and EDM oil². EDM process is a suitable technique manufacturing of micro holes. It is also an economic, quick and cost effective for producing holes in hard and soft materials³. The undesirable layer was formed after machining known as recast layer which is inevitable but could be controlled by varying EDM process parameters. The harder recast layers, on the other hand are helpful in improving the wear resistance, as demonstrated by deliberate surface alloying during EDM. The use of

partially sintered Powder Metallurgy (PM) electrodes, EDM in a metal powder suspended dielectric are the most popular methods for performing alloying during EDM that were been widely adopted in the past⁴. The common methods of surface modification using EDM is carried out by two means such as, use of semi sintered electrode and mixing powder in dielectric⁵. The surface texture effects were based on the level of control factors⁶. By using Powder metallurgy tool electrodes, EDM tooling costs can be reduced while tool electrodes can be produced in more quantity⁷.

The surface of moulds and tools has to be modified in order to increase their service life as well as withstand corrosion. Nevertheless, high machine price and complex processes makes to analyze novel surface modification processes⁸. During EDM of powder metallurgy of Cu-Zn, it was found that more contamination of dielectric medium was obtained due to the release of more copper powder from electrode. Poor surface

*Corresponding Author: sr_2855@psna.edu.in



Research Article

Comparative Study of Mechanical Properties and Thermal Stability on Banyan/Ramie Fiber-Reinforced Hybrid Polymer Composite

T. Raja¹, S. Ravi,² Alagar Karthick³, Asif Afzal,^{4,5} B. Saleh,⁶ M. Arunkumar⁷,
Ram Subbiah,⁸ P. Ganeshan⁹, and S. Prasath¹⁰

- ¹Department of Mechanical Engineering, Vel Tech Rangarajan Dr. Sagunthala R&D Institute of Science and Technology, Chennai 600062, India
- ²Centre for Materials Research, Chennai Institute of Technology, Chennai 600069, India
- ³Renewable Energy Lab, Department of Electrical and Electronics Engineering, KPR Institute of Engineering and Technology, Coimbatore 641047, Tamil Nadu, India
- ⁴Department of Mechanical Engineering, P.A. College of Engineering (Affiliated to Visvesvaraya Technological University, Anagavai), Marpalaya 574154, Tamil Nadu, India
- ⁵Department of Mechanical Engineering, School of Technology, Global University, Delhi Yamunawati Marg, III-57, Mirzapur Pule, Samanpur, Uttar Pradesh 247121, India
- ⁶Mechanical Engineering Department, College of Engineering, Taif University, P.O. Box 11099, Taf 21944, Saudi Arabia
- ⁷Department of Agriculture Engineering, Sri Shukthi Institute of Engineering and Technology, Coimbatore 642062, Tamil Nadu, India
- ⁸Department of Mechanical Engineering, Gokaraju Rangaraju Institute of Engineering and Technology, Nizampet, Hyderabad 500090, India
- ⁹Department of Mechanical Engineering, Satna Institute of Technology, Virudhunagar 626125, Tamil Nadu, India
- ¹⁰Department of Mechanical Engineering, College of Engineering and Technology, Mizan Topi University, Topi Campus, Topi 121, Ethiopia

Correspondence should be addressed to T. Raja; rajas28@gmail.com

Received 8 July 2021; Accepted 13 November 2021; Published 17 December 2021

Academic Editor: Pawel Klezwinski

Copyright © 2021 T. Raja et al. This is an open access article distributed under the Creative Commons Attribution License, which permits unrestricted use, distribution, and reproduction in any medium, provided the original work is properly cited.

The usage of natural fibers has increased recently. They are used to replace synthetic fiber products in aircraft and automobile industries. In this study, natural fibers of bidirectional banyan and ramie fibers are used for reinforcement, and the matrix is an epoxy resin to fabricate composite laminates by traditional hand layup technique at atmospheric temperature mode. Five different sequences of reinforcements are as follows to quantify the effect of thermal stability and mechanical behavior of silane-treated and untreated hybrid composites. The results revealed that silane-treated fabric composite laminates were given enhanced mechanical properties of 7% tensile, 11% flexural, and 9% impact strength compared with untreated fabric composite, and at the same time when the increasing of ramie fabric was given the positive influence of 41% improved tensile strength of 40.7 MPa, 49% improved in flexural strength of 38.9 MPa and negative influence in 57% lower impact strength at sample E and positive value in sample A. 21.12 J impact energy absorbed in the hybrid composite. Thermogravimetric analysis (TGA) revealed the thermal stability of the hybrid composite. In sample A, the thermal stability is more than in other samples, and 410°C is required to reduce the mass loss of 10%. The working mass condition of the hybrid composite is up to 3.25 g after it moves to degrade.



Depth Profiles of Residual Stresses in Inconel 718 Machined with Uncoated and Coated Tools

K. Satyanarayana^a, N. Ravi^b, T. Karthik Reddy^c, K. Rajkiran^a, & Kuldeep K. Saxena^a

^aDepartment of Mechanical Engineering, Gokaraju Rangaraju Institute of Engineering and Technology, Hyderabad 500 090, India

^bInternational Advanced Research Centre for Powder Metallurgy and New Materials, Hyderabad 500 005, India

^cDepartment of Mechanical Engineering, GLA University, Mathura 281 406, India

Received: 4 February 2021; Accepted: 1 September 2021

Inconel 718 is one of the super-alloy materials, belonging to nickel-chromium alloy family, which has major applications in aerospace sector such as engine parts and turbine components. Durability of these components during engineering performance is affected by residual stresses induced in them in the course of their manufacturing processes. The concept of the present paper is to provide an insight view of induced residual stresses in Inconel 718 work piece, when machined with coated (TiN) and uncoated tools at optimum conditions. For this purpose, turning experiments have been conducted on IN 718 material through statistical approach using L9 orthogonal array. Taguchi optimization method is exercised with the emphasis on minimizing the cutting forces resulted during machining. The residual stresses generated in the work piece at the optimum conditions employed for both the tools have been evaluated using XRD method. Conditions such as cutting speed of 50 m/min, feed of 0.068 mm/rev and depth-of-cut of 0.10 mm have been optimized for achieving minimum cutting forces during machining of IN 718 using both coated and uncoated tools. However, tensile stresses on the initial surface layer and compressive stresses in the sub-surface layers are found higher in the work piece material machined with uncoated tool. Surface roughness and temperature developed on the surface of the machined bar are higher in case of uncoated tool than those with coated tool.

Keywords: Residual stresses, surface roughness, temperature, Inconel 718, TiN coated tool

1 Introduction

Inconel 718 is a super alloy that belongs to nickel-chromium alloy family with 50-55% of nickel and 17-21 % of chromium. Due to high proportions of chromium, it is designated as anti-corrosive, non reactive and anti-oxidizing alloy¹. As Inconel 718 has some of the outstanding properties such as higher strength, greater corrosion resistance, low thermal conductivity and high temperature thermal stability, it is used as one of the major raw materials for manufacturing turbine blades, components of jet engine, aviation parts, cryogenic storage tanks, turbine casings etc.². Residual stresses are one of the key properties affecting the durability of such components during their real-time performance. For example, surface tensile residual stresses of turbine components adversely affect their fatigue properties. Residual stresses in materials are caused due to the inhomogeneous plastic deformations of grain structures when loads or forces are applied on them, especially, during machining. Quality of these

machined components is thus ensured by testing them for surface topology including presence of residual stresses as they have bearing on factor of safety in critical applications such as aero-engine parts³. Some of the oldest methods such as crack compliance technique proposed and developed by Cheng and Finnie⁴ has been successfully used to find out the residual stresses in materials. In this process, there is a narrow cut made into the material, making the test a destructive method. Later, measurements of the induced stresses have been carried out using hole-drilling technique⁵, which is considered a semi-destructive procedure. Currently, residual stresses are more conveniently measured by the non-destructive X-ray diffraction (XRD) method⁶.

Inconel 718 is a difficult-to-cut material⁷ and so, high amounts of forces are evolved during its machining. These forces tend to increase the stress concentrations in the material. Meng, Liu et al.⁸ in their experimentation, have concluded that hard to-cut materials need high thrust forces with outcomes of high tool wear and high induced stresses. Madariaga et al.⁹ have studied the effect of tool wear on

*Corresponding author (E-mail: satyanarayana.kosa@ijm@gmail.com)

Review Article

Processing of Aluminium-Silicon Alloy with Metal Carbide as Reinforcement through Powder-Based Additive Manufacturing: A Critical Study

R. Raj Mohan¹, R. Venkatraman¹, S. Raghuraman¹, P. Manoj Kumar²,
 Moti Lal Rinawa³, Ram Subbiah⁴, B. Arulmurugan², and S. Rajkumar⁵

¹School of Mechanical Engineering, SASIRA Deemed to be University, 614601, Thanjavur, Tamil Nadu, India

²Department of Mechanical Engineering, KPR Institute of Engineering and Technology, 641407, Coimbatore, Tamil Nadu, India

³Department of Mechanical Engineering, Government Engineering College, 326023, Jaipur, Rajasthan, India

⁴Department of Mechanical Engineering, Gokaraju Rangaraju Institute of Engineering and Technology, 500090, Hyderabad, Telangana, India

⁵Department of Mechanical Engineering, Faculty of Manufacturing, Institute of Technology, Hawassa University, Ethiopia

Correspondence should be addressed to S. Rajkumar; rajkumar@hu.edu.et

Received 13 September 2021; Revised 7 November 2021; Accepted 24 December 2021; Published 10 January 2022

Academic Editor: Heng Bo Jiang

Copyright © 2022 R. Raj Mohan et al. This is an open access article distributed under the Creative Commons Attribution License, which permits unrestricted use, distribution, and reproduction in any medium, provided the original work is properly cited.

Powder-based additive manufacturing (PAM) is a potential fabrication approach in advancing state-of-the-art research to produce intricate components with high precision and accuracy in near-net form. In PAM, the raw materials are used in powder form, deposited on the surface layer by layer, and fused to produce the final product. PAM composite fabrication for biomedical implants, aircraft structure panels, and automotive brake rotary components is gaining popularity. In PAM composite fabrication, the aluminium cast alloy is widely preferred as a metal matrix for its unique properties, and different reinforcements are employed in the form of oxides, carbides, and nitrides. However, for enhancing the mechanical properties, the carbide form is predominantly considered. This comprehensive study focuses on contemporary research and reveals the effect of metal carbide's (MCs) addition to the aluminium matrix processed through various PAM processes, challenges involved, and potential scopes to advance the research.

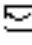
1. Introduction

Powder-based additive manufacturing (PAM), also known as additive fabrication, processes the metal powders in an enclosed purged chamber and follows the layer deposition approach [1]. The development of lightweight aluminium-based composite and desirable properties is possible through the PAM process [2]. Generally, PAM follows two process routes, namely, Direct Energy Deposition (DED) with a laser energy source and powder bed fusion (PBF) with laser and the electron beam as an element of source [3]. For routes mentioned above, the raw materials (aluminium alloy) are in powder form with a spherical shape due to powder flowability [4, 5], and specified particle size ranges from 20 to 63 microns in PBF and 20 to 200 microns in DED. The PBF has

the following advantages over DED: (i) excellent surface quality, (ii) high accuracy with precision, and (iii) a low dilution rate [6]. Laser source is chosen to melt/fuse the raw material in both routes due to its excellent optical characteristics such as coherence and high input energy transfer to the selective region [7]. The raw materials for PAM are manufactured by mechanical alloying and atomization process, namely, centrifugal, water, and gas atomization [8, 9]. The input parameters, such as layer or deposition height, energy density, scanning strategy, and hatch spacing, strongly influence the printed specimen's surface and mechanical properties [10, 11]. The most commonly used primary aluminium alloy with desirable properties in PAM is AlSi10Mg (hypoeutectic cast alloy), and its equilibrium diagram is shown in Figure 1 [12]. At optimum input parameters, the

Original Article | Published: 17 January 2022

Optimization of cardanol oil dielectric-activated EDM process parameters in machining of silicon steel

[N. Pragadish](#) , [S. Kaliappan](#), [M. Subramanian](#), [L. Natrayan](#), [K. Satish Prakash](#), [Ram Subbiah](#) & [T. Ch. Anil Kumar](#)

Biomass Conversion and Biorefinery (2022)

170 Accesses | 10 Citations | [Metrics](#)

Abstract

The current research uses Taguchi grey relational analysis to optimize the process parameters in micro electro discharge machining of silicon steel using nickel-coated brass (NCB) tool and waste cashew shell oil-activated water-based dielectric. The key goal of this study was to determine the most influencing process parameter, which had the greatest impact on material removal rate (MRR) and tool wear rate (TWR) while drilling silicon steel. Another goal was to optimize the micro EDM process parameters to achieve high MRR with reduced tool wear rate in coated tools. Using the electroless plating process, a 0.47 mm brass tool was coated with 0.5, 1.0, and 2 μm nickel; similarly, the dielectric medium was activated using 5, 10, and 15 wt.% of cardanol oil. The method parameters were optimized using an orthogonal

CNC Milling of Medical-Grade PMMA: Optimization of Material Removal Rate and Surface Roughness

Job Maveke Wambui, Decan Kinathi, University of Technology, Kenya*

<https://orcid.org/0000-0002-4097-2396>

Fredrick M. Mwangi, Dusan Kinathi, University of Technology, Kenya

<https://orcid.org/0000-0001-6116-5587>

Buddi Tanya, Dakraju Rangana, Institute of Engineering and Technology, India

<https://orcid.org/0000-0002-9108-2704>

Ties-Chen Jao, University of Johannesburg, South Africa

ABSTRACT

This study evaluates CNC milling parameters (spindle speed, depth of cut, and feed rate) on medical-grade PMMA. A single objective analysis conducted showed that the optimal material removal rate (MRR) occurs at a spindle speed of 1250 rpm, a depth of cut of 1.2 mm, and a feed rate of 350 mm/min. The ANOVA showed that feed rate is the most significant factor towards the MRR, and spindle speed (11.83%) is the least contributing. The optimal surface roughness (Ra) occurred at spindle speed of 500 rpm, depth of cut of 1.2 mm, and feed rate of 200 mm/min. The milling factors were insignificant. A regression analysis for prediction was also conducted. Further, a multi-objective optimization was conducted using the grey relational analysis. It showed that the best trade-off between the MRR and the Ra could be obtained from a combination of 1250 rpm (spindle speed), 1.2 mm (depth of cut), and 350 mm/min (feed rate). The depth of cut was the largest contributor towards the grey relational grade (54.43%), followed by the feed rate (10.36%), and finally, the spindle speed (4.28%).

KEYWORDS

ANOVA, Depth of Cut, Feed Rate, Grey Relational Analysis, Multi-Objective, Optimal, S/N Ratio, Spindle Speed

INTRODUCTION

Polymeric materials have attracted applications in various industries, especially the medical field, due to their desirable properties such as high strength and low weight and biocompatibility with human tissues. However, the manufacture of components from these materials has faced several challenges, including their poor machinability leading to the generation of poor surfaces and low production rates (Yao et al., 2021). These challenges necessitate the evaluation of the primary machining parameters

DOI: 10.4018/IJMMME.202325

*Corresponding Author

This article published as an Open Access article distributed under the terms of the Creative Commons Attribution License (<http://creativecommons.org/licenses/by/4.0/>) which permits unrestricted use, distribution, and reproduction in any medium, provided the author of the original work and original publisher source are properly credited.



Experimental studies and mathematical modelling of Inconel 600 with CVD coated TiN/TiCN/Al₂O₃/ZrCN inserts under dry machining Conditions

Krishna Mohan Buddaraju^{1,2*}, G. Ravi Kiran Sastry³, Satyanarayana Kousaraju¹, & Kuldeep Kr Saxena⁴

¹ Department of Mechanical Engineering, Gogoraju Rangaraju Institute of Engineering and Technology, Hyderabad 500 090, India

² Department of Mechanical Engineering, National Institute of Technology, Tadupalligudem, Andhra Pradesh 524 101, India

³ Department of Mechanical Engineering, GLA University, Mathura, Uttar Pradesh 281 406, India

Received: 25 January 2022 Accepted: 16 February 2022

Inconel 600 is a nickel-based super alloy with applications in the field of Aerospace, Nuclear energy, Heat treatment, and chemical processing industries, and is a difficult to cut material due to its high hot hardness and strength. Coated carbide inserts can improve the machinability of alloys like Inconel 600 and other super alloys. This work is about the machinability characteristics study on Inconel 600 alloy under dry turning environment with high speed machining using CVD coated TiN/TiCN/Al₂O₃/ZrCN cutting tool insert. Cutting speed (200, 250, and 300 m/min), feed rate (0.05, 0.1, 0.15 mm/rev), and back rake angle (+7, +5, -3°) are considered as machining process parameters. Full factorial design of experiments were performed to evaluate the performance of process parameters on surface roughness and material removal rate. It was found that surface roughness decreased with increase in cutting speed and increases with increase in feed rate. Surface roughness increases with increase in rake angle in negative direction. Material removal rate increases with increase in both cutting speed and the feed rate whereas rake angle had minimal influence. Mathematical modelling was done on the obtained results and found that R² value for surface roughness and material removal rate were 99.14% and 98.69% respectively. Analysis of Variance of surface roughness found that feed rate > feed rate is the most influencing parameter with maximum contribution of 34.16% whereas feed rate > cutting speed parameter has maximum influence on material removal rate with contribution of 83.03%.

Keywords: Analysis of Variance (ANOVA), CVD coated Inserts, Inconel 600, Material removal rate, Surface roughness

1 Introduction

Inconel 600 is a Nickel based superalloy which possesses excellent stability and strength at high temperature due to its austenitic structure. Nickel, Chromium and Iron are the major alloying elements of Inconel 600. Table 1 illustrates the chemical composition of the Inconel 600 alloy based on % weight of various elements. With high chromium content it exhibits resistance to oxidation at very high temperature making it suitable material for fabricating turbine parts in aerospace industry. High content of nickel provide Inconel 600 resistance against reduction, caustic, carburizing, and nitriding environments and also resistance to chloride-ion stress corrosion cracking (SCC)¹. With these characteristics Inconel 600 is suitable for heat treatment, chemical processing, food processing and nuclear reactor applications². Inconel 600 is the recommended material for fabrication of parts like trays, baskets, retorts, muffles, radiant tubes, mesh belts and fixtures which are used in heat treatment furnaces. Inconel 600 suitable for fabrication

of piping in nuclear steam generators because of its resistance against SCC in high purity water and corrosion resistance against mixtures of steam and air.³

Due to their high hot hardness, work hardening, inferior thermal conductivity, high strength at elevated temperatures, super alloys like Inconel 600 were considered as difficult to machine. With austenitic structure Inconel 600 possesses high strength and hardness even at elevated temperatures near to their melting point. During machining of these materials cutting zone temperature reaches up to 760-1010 °C. Since these materials have low thermal conductivity the amount of heat generated at the cutting zone will not be dissipated enough there by increasing the temperature of cutting zone. High temperatures at the cutting zone enhances condition

Table 1 — Chemical composition of work material based on % weight

Name of the Element	% weight
Nickel (Ni)	76.11
Chromium (Cr)	15.48
Iron (Fe)	7.49
Other elements	0.92

*Corresponding author (E-mail: mohan20khu@gmail.com)



Optimized power generation in solar using carbon substrate for reduced greenhouse gas effect

Suresh Kumar Tummala¹ · Satyanarayana Kosaraju² · Phaneendra Bahu Bobba¹

Received: 18 September 2021 / Accepted: 22 December 2021
 © King Abdulaziz City for Science and Technology 2022

Abstract

Traditionally, power is produced through non-renewable energy sources which has a major drawback of greenhouse gas emissions affecting the climatic conditions and ozone layer. In this paper, carbon substrate-deposited solar cell for improved power generation in reducing greenhouse gas effects are discussed with various analysis. Poly-crystalline solar cells are etched with carbon substrate for analysis. The same are compared with silicon carbide-etched solar cells. Scanning electron microscopy (SEM) analysis is carried out to show the variations in the cell structure. Electrical analysis is also carried out to show the performance difference in voltage and overall efficiency of the cell.

Keywords Carbon · Silicon carbide · Greenhouse gas · Solar cell · Etching

Introduction

Power generation through renewable energy sources has gained attention which reduces Greenhouse gases (GHG) as years pass on. In such renewable energy sources, solar energy is in front for producing electricity through sun radiation. Existing solar panel have been designed for power generation without any optimization (Saidi et al. 2020). Solar Module Glass does not absorb maximum radiation but acts a protective element for the panel from climatic conditions and there is no scope for storage of energy resulting in lower efficiency (app. 20%) (Tummala and Kosaraju 2020). Making solar or photovoltaic cells requires potentially toxic heavy metals such as lead, mercury, and cadmium (Basher et al. 2019). It even produces GHG, such as carbon dioxide, that contribute to global warming. Still, the researchers found that if people switched from conventional fossil fuel-burning power plants to solar cells, air pollution would be cut by roughly 95%.

A solar cell is an electronic gadget which straightforwardly changes over daylight into power. Light sparking

on the solar powered cell produces (Verayah and Tyadarai 2017; Tasoglu and Yildiz 2016) both a flow and a voltage to create electric force. This procedure requires light off the bat, a material wherein the retention of light causes an electron to a higher energy state, and further, note, the development of this higher energy electron from the solar cell into an outside circuit. The electron at that point discharges its energy in the outer circuit and comes back to the solar cell. An assortment of materials (Kaule et al. 2014) and procedures can conceivably fulfill the prerequisites for photovoltaic energy change, however, practically speaking about all photovoltaic energy transformation utilizes semiconductor materials as a p-n intersection.

The fundamental strides in the activity of a solar powered cell are:

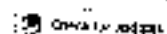
- the age of light-produced bearers,
- the assortment of the light-produced conveys to create a current,
- the age of an enormous voltage over the solar powered cell, and (Dohrzanski et al. 2013)
- the dispersal of intensity in the Leap and in parasitic protections.

Natural photovoltaic or solar cells are made of thin films (under 100 nm) of natural (Dohrzanski et al. 2013) semiconductor materials to change over sun-based energy into electrical energy. This innovation is increasingly pertinent per

[✉] Suresh Kumar Tummala
 suresh.kumar2514@gmail.com

¹ Electrical Engineering, Gokulraj Rangaraj Institute of Engineering and Technology, Hyderabad, India

² Mechanical Engineering, Kosaraju Rangaraju Institute of Engineering and Technology, Hyderabad, India



SEM & EDAX analysis of super capacitor

Suresh Kumar Tummala^a, Phaneendra Babu Bobba^a and Kosaraju Satyanarayana^a

^aElectrical Engineering, Gokaraju Rangaraju Institute of Engineering & Technology, Hyderabad, INDIA;

^bMechanical Engineering, Gokaraju Rangaraju Institute of Engineering & Technology, Hyderabad, INDIA

ABSTRACT

Super capacitors have the ability of high power densities for longer charging (or) discharging cycles. Material used in the super capacitors affects the performance of the device. It is obvious that the material used in super capacitors shall increase the energy density for smaller volumes while maintain the cycle stability. The right structure of super capacitors should exhibit best mechanical and electrical properties. The analysis of the above properties can be discussed by looking into the microstructure, elemental structure, etc. of the materials used. In this paper, scanning electron microscopy and energy dispersive X-ray analysis are performed on a super capacitor to study the microstructure and elemental parameters. This analysis will help in determining the electrical and mechanical properties of the super capacitors.

ARTICLE HISTORY

Accepted 6 February 2022

KEYWORDS

Super capacitors;
microstructure; elemental
analysis; SEM, EDAX

1. Introduction

Super capacitors possess the ability of storing energy (charge) in large amounts. Super capacitors are also referred as ultra capacitors or sometimes called as double layer capacitors (DLC) [1]. In ordinary capacitors, traditional dielectrics is used to store energy, whereas super capacitors use two methodologies to store energy, named as pseudo and double layer capacitance [2]. Pseudo uses electrochemical [3] and DLC uses electrostatic means to store energy. These two principles of energy storage when combined results in principle of energy storage of supercapacitors [4]. This principle of energy storage will result in capacitance up to 12,000 Farads with typical charge voltage in the range of 2.5 to 2.7 volts [5,6]. These super capacitors can replace batteries completely in future based on the electrical properties like fast charge and discharge time [7]. The best characteristic of a super capacitor lies on charge time, specific power, and cycle life and safety. Super capacitor can be fully charges in a time lesser than 2 minutes, whereas batteries consume several hours for full charge [8]. To have best characteristics of super capacitor, the material used for manufacturing plays a vital role. This is the main motto of the authors to pay attention on this work. When investigated about the size, super capacitors have 5 to 10 times more power than batteries in lesser size [9]. This can be understood by comparing a simple Li-ion battery with super capacitor. Li-ion battery has 1–3 kW of power per kg [10], whereas super capacitor has around 10 kW of power per kg [11].

CONTACT Suresh Kumar Tummala sureshkumar25@gmail.com Electrical Engineering, Gokaraju Rangaraju Institute of Engineering & Technology, Hyderabad, INDIA

© 2022 Informa UK Limited, trading as Taylor & Francis Group

Characterization of Bifacial Passivated Emitter and Rear Contact Solar Cell



Suresh Kumar Tummala, Plameendra Babu Bobba,
and Satyanarayana Kosaraju

Abstract A Passivated Emitter and Rear Contact Cell (PERC) defines a new architecture of solar cell which differs from standard cell architecture. PERC enhances light capture at the rear surface and to optimize electron capture. This leads to an increase (or) achieve better efficiency than when compared with standard cell which are reaching their physical limits. In this paper, the characterization of bifacial p-type PERC solar cell with various proportions of thickness and width, back Silicon Nitrate layer with various thickness are so combined. Most elevated back productivity of the bifacial solar cell (~22%) was obtained at AM 1.5 (air mass), 1000 W/m^2 , 26°C standard test condition.

Keywords PERC · Bifacial · Finger · Generation profile · Reflection · Absorption

Nomenclature

PERC	Passivated Emitter Rear Contact
LCDE	Levelized Cost of Energy
c-Si	Crystalline Silicon
UV	Photovoltaic
EQE	External Quantum Efficiency
P_{max}	Maximum Power
J_{sc}	Short Circuit Current
V_{oc}	Open Circuit Voltage
R_s	Series Resistance
R_{sh}	Shunt Resistance

S. K. Tummala (✉) · P. B. Bobba
Electrical and Electronics Engineering Department, Gokulraj Ranganuja Institute of Engineering and Technology, Hyderabad, India

S. Kosaraju
Mechanics Engineering Department, Gokulraj Ranganuja Institute of Engineering and Technology, Hyderabad, India

© The Author(s), under exclusive license to Springer Nature Singapore Pte Ltd. 2022
S. B. Subrah and P. Ray (eds.), *New Generation Smart Grids: Modeling, Control and Optimization*, Lecture Notes in Electrical Engineering, 824,
https://doi.org/10.1007/978-981-16-7794-5_14

Investigating Mechanical Properties of Hybrid Polymer Composite Reinforced with S-Glass and Luffa Fibres

N.Vigneshkumar¹, N.Harikannan², Selvakumar S³, P. Manoj Kumar⁴, Ram Subbiah⁴, P.T.Saravankumar⁵

¹Department of Mechanical Engineering, KPR Institute of Engineering and Technology, Coimbatore, 641407, Tamil Nadu, India.

²Department of Mechanical Engineering, PSNA College of Engineering and Technology, Dindigul, 624622, Tamil Nadu, India.

³Professor, Department of Aeronautical Engineering, Nehru Institute of Engineering and Technology, Coimbatore, 641105, Tamil Nadu, India.

⁴Department of Mechanical Engineering, Gokaraju Rangaraju Institute of Engineering and Technology, Hyderabad, 500090, Telangana, India.

⁵Department of Mechatronics Engineering, Hindusthan College of Engineering and Technology, Coimbatore, 641032, Tamil Nadu, India.

*Corresponding author: pasunathimanojkumar@gmail.com

Abstract. The mix of two different type of fibres, one is natural and another one is synthetic fibres were employed as reinforcing media in this study, and epoxy based polymer resin was employed as the matrix phase. S-glass and luffa fibres had been bonded with epoxy matrix to create a novel composite by compression moulding and to measure the effect of this hybridization in composite laminate utilizing five different sequencing. To determine the mechanical characteristics of this composite material using tensile, flexural, and compression strength, a specimen named 'SL4' had shown the highest mechanical strength, resulting in a tensile properties of 253 MPa, compression strength of 234 MPa, and flexural characteristics of 237 MPa. The increment in mechanical characteristics is found to exhibiting around 20% increase comparing to the specimen having next higher value in all the properties. The results evidenced that the presence of luffa fibre layers at the interior most portion of the composite displayed the progressive values in all the investigated mechanical characteristics.

Keywords: S-Glass; luffa; composite; mechanical properties; hybrid composite.

1. Introduction

In a prepared composite material, the mix of natural and synthetic fibres can result in distinct physical and chemical characteristics. These one-of-a-kind characteristics help to boost product efficiency while lowering environmental impact [1, 2]. Natural or synthetic composites can be made separately with the corresponding fibres. A typical composite is wood, which is made up of cellulose (wood fibres) and lignin. Lignin is an ordinary pasty material that would help in binding the fibres and further, it would strengthen wood [3, 4]. Engineers create several composites in different composition of fibre and matrix material. However, the use of natural fibres along with the artificially created fibres can enhance the mechanical characteristics of the polymer based composites, significantly [5, 6].

Outside factors would almost certainly affect the loading of designed structures, and this can be expected to happen during maintenance, assembly, and administration tasks [7, 8]. One of the major unknowns in matrix polymer composites is impact resistance. Composites are extremely sensitive to



Experimentally Investigating the Flat Plate Solar Water Heating System (FPSWHS) for South Indian Climate

T.S.Senthil^{1*}, M Porkodi², R. Rajith Kumar³, T Vijay Muni⁴, M. S. Karuna⁵,
Rani Subbiah⁶

¹Department of Mechanical Engineering, Panimalar Engineering College, Chennai, Tamil Nadu 600123, India.

²Department of Electrical and Electronics Engineering, Sona College of Technology, Salem, Tamil Nadu 636005, India.

³Department of Mechanical Engineering, St. Joseph's Institute of Technology, Chennai, Tamil Nadu 600119, India.

⁴Department of Electrical and Electronics Engineering, Koneru Lakshmaiah Education Foundation, Vaddeswaram, Andhra Pradesh 522502, India.

⁵Department of Chemical Engineering, M.J.P. Rohilkhand University, Bareilly, Uttar Pradesh 243006, India.

⁶Department Mechanical Engineering, Gokaraju Rangaraju Institute of Engineering and Technology, Ntzampet, Hyderabad, Telangana 500090, India.

*Corresponding author: reachts@gmail.com

Abstract. The heat transfer performance of a flat plate solar water heating system was investigated experimentally in this paper (FPSWHS). The main objective of this investigation is to analyze the behaviour of FPSWHS with a 1.5 m² receiver surface area in South Indian weather conditions and to calculate the heat energy created by the receiver for residential usages, which lessens electricity usage and assists the nation in conserving energy acquired from carbon fuels. Water was employed as the working medium in this investigation. The trials have been conducted in the first week of March 2021 at 13.0827° North, 80.2707° East. The findings confirmed that the solar thermal system's estimated average efficacy remained 44.3%, and the system's maximum output temperature of water was 67°C.

Keywords: FPC; SWH; energy efficiency; hot water; domestic solar water heater.

1. Introduction

Solar energy systems are devices which utilize the solar heat provided by the sunrays to boil water for residential and industrial usage. Solar water heating systems provide boiled water with a wide range of temperature [1, 2]. Additionally, they have the benefit of reducing reliance on electricity generated, minimize ecological degradation, producing higher power than solar cells, and achieving the requisite financial viability. Solar collectors are intended to transform solar energy striking the opening surface into thermal energy in the absorbing section and transport that energy to the coolants via the working medium [3, 4]. Solar heating systems are primarily composed of a collecting component, a heat exchange mechanism (which includes a circulating medium and circulating mechanism), and a water tank.

There are various varieties of solar heating system, but perhaps the most common seems to be the flat plate type collecting system, which is inexpensive, readily available locally, and simple to set up and manage [5, 6]. It is utilized in a variety of purposes, both residential as well as business, that need





115 0

0



Views CrossRef Citations to date Altmetric

Research Article

Analysis on behavior of Ti-6Al-4V & Ti-5553 by performing turning operation using deform-3d

Durga Bhavani Bathula, Tanya Buddi , Harrison Shagwira, F.M. Mwema  & K. V. Durga Rajesh 

Accepted 29 Jan 2022, Published online: 14 Mar 2022

 Download citation <https://doi.org/10.1080/2374068X.2022.2037064> Check for updates

Sample our
Physical Sciences
Journals
➤ Sign up now to start your access
to the latest two volumes for 14 days

ABSTRACT

This paper analyses the effect of turning parameters for Ti-6Al-4 V and Ti-5553, which are generally used in aerospace and industrial applications due to their superior strength to density ratio, corrosion resistance and ability to withstand elevated temperatures. The input variables used in this study are Cutting Speed (CS), Depth of Cut (DoC) and Feed Rate (FR). A three-dimensional machining model is designed in Deform-3D®, an FEM software, to predict results. The output parameters temperature, effective stress, effective strain, and effective strain rate obtained by turning Ti-6Al-4 V & Ti-5553 were analysed based on the input parameters. Taguchi technique and ANOVA were performed for statistical analysis



Study on machinability of Ti6Al4V with coated inserts—cutting force, surface finish and material removal rate prediction using ANN

Satyamarayana Kosaraju¹ · Devaraju Aruri² · Murahari Kolli³ · G. Sai Kumar⁴ · Phaneendra Babu Bobba⁵

Received: 14 January 2022 / Accepted: 15 March 2022

© The Author(s), under exclusive licence to Springer-Verlag France SAS, part of Springer Nature 2022

Abstract

Titanium alloys are known for their potentiality to withstand extreme environmental conditions. However, due to its higher fabrication and machinability cost of these alloys are limited their applications to defense, aerospace and marine sectors. To enhance their domestic applicability, either their fabrication or machining costs must be controlled. With an intention to reduce machinability cost, cutting force, surface roughness and material removal rate of Titanium alloy Ti6Al4V are predicted through artificial neural network computational technique was applied in this investigation. A full factorial design set of experiments are conducted on precision lathe machine to predict the influence of input parameters like cutting speed, feed, depth of cut and rake angle. The output responses emphasized are the cutting forces, surface roughness and material removal rate during machining with carbide tool inserts with coated TiAlN layer. Neural network models were developed using back propagation algorithms by training on this data to prediction output responses. The models are further validated by addition 8 different experimental data sets. Sufficient level of fitness was observed for the trained model. A comparison was made between experimental response values and the predicted values. The prediction accuracies were found to be sufficiently high which indicates the effectiveness of the model.

Keywords Machining · Ti6Al4V · Coated insert · Artificial neural network

1 Introduction

Usage of Titanium alloy has increased in the recent times in aerospace, marine, automobile industries and chemical processing industries because of their light weight, good fatigue strength and corrosion-resistance properties. The specific weight of titanium is about two thirds that of steel and

about 60 percent higher than that of aluminum. Whereas titanium's strength is far greater than that of many alloy steels, giving it the highest strength-to-weight ratio when compared to any of today's structural metals. Titanium alloys also have high melting points, which is usually a sign of excellent thermal stability [1]. Presently, Ti6Al4V is one of the most widely used titanium alloys, accounting for more than half of all titanium tonnage in the world, and no other titanium alloys threaten its dominant position [2, 3] because of its unique characteristics and applications. Ti6Al4V, $\alpha + \beta$ alloy constitutes nearly 20% of the wrought alloys produced. It features good machinability and excellent mechanical properties. The Ti6Al4V alloy offers the best all-round performance for a variety of weight reduction applications in aerospace, automotive and marine equipment. Despite increase of the usage and production of titanium alloys, they are expensive when compared to other metals because of the complexities of the extraction process, difficulties during melting, fabrication and machining [4–6]. In order to meet the demands, manufacturing process parameters have to be chosen in the best possible way. Different

✉ Satyamarayana Kosaraju
 satyamarayana.kosaraju@gnail.com

¹ Mechanical Engineering Department, Cokeraja Ranganaji Institute of Engineering and Technology, Hyderabad, Telangana, India

² Mechanical Engineering Department, Kakatiya Institute of Technology & Science, Warangal, Telangana, India

³ Department of Mechanical Engineering, Lakshmaiah Bahi Poddly College of Engineering, Mylavaram, Andhra Pradesh, India

⁴ Mechanical Engineering Department, Kakatiya Institute of Technology and Science, Warangal, Telangana, India

⁵ Electrical and Electronics Engineering Department, Cokeraja Ranganaji Institute of Engineering and Technology, Hyderabad, Telangana, India



Investigation on material removal rate and taper angle in abrasive aqua jet machining of Al 7075/SiC/Gr composites using RSM approach

Muralhari Kolli¹ · Bavi Prakash Babu Kocharla² · Dasari Sai Naresh³ · A. Devaraju⁴ · K. Satyanarayana⁵

Received: 15 January 2022 / Accepted: 13 April 2022

© The Author(s) under exclusive licence to Springer Verlag France SAS, part of Springer Nature 2022

Abstract

Machining the Hybrid Metal Matrix Composites possess significant challenges in maintaining sufficient accuracies due to the presence of hard reinforced particles in their matrix. Abrasive Aqua Jet Machining (AAJM) is one of the rapid, widely accepted, non-conventional tools for machining composites with a high degree of adaptability and it causes no changes to the physical and thermal properties of the work-piece material. In the present work, AAJM is used to perform machining of Al 7075/B₄C/Gr hybrid composite. Investigations are carried out to find Material Removal Rate and Taper Angle under the influence of Water Jet Pressure, Stand-off Distance and Traverse Speed. Response Surface Methodology–Central Composite Design approach is used to formulate the experimental runs and test strategies. The important input factors are found by conducting Analysis of Variance (ANOVA). Furthermore, an empirical relationship is established between input and output factors with RSM.

Keywords Material removal rate · Al7075/B₄C/Gr composite · AAJM · Response surface methodology · Central composite design approach

1 Introduction

Nowadays, manufacturing scenario changed from use of conventional materials to advanced materials. Metal Matrix Composites (MMCs) are prominent role in manufacturing sector due to their properties like high specific strength, light weight, specific stiffness, wear resistance, corrosion resistance and elastic modulus and are used in aerospace, automobile, marine, mining and mechanical structures. The

Al 7075 alloy is a strong material with high strength compared to steels has good fatigue strength with average machinability. The elements of Al 7075 alloys is iron, magnesium, zinc, copper, chromium, manganese, titanium, silicon and other metals [1]. The Al-MMCs regularly used reinforcements are Al₂O₃ and SiC, B₄C, etc. The present study, composite mixture of 12% of SiC and 4% of graphite is used. SiC is the hardest, high strength and low density reinforcement particle, added into Al matrix material to enhance the resistance to wear and abrasion of the metal. The graphite mixture exhibits great improvements in the production of fine surface finishes, good workability, and high thermal stability, electrical and thermal conductivity. These types of composite materials conventional machining is challenging task with influence the various factors like i.e. non-homogeneity, anisotropy, hardness, low ductility, toughness and intrinsic brittleness[2].

Weinert et al. studied the machinability characteristics of Aluminium MMCs. They reported that lower MRR, higher FWR, degraded surface finish and high manufacturing costs are associated with machining of Al MMCs [3]. Kishorap investigated the effect of drillity on Al 7075 alloy for finding the optimal cutting parameters and to construct the models

✉ Muralhari Kolli
 murhar_1915@gmail.com

¹ Department of Mechanical Engineering, Lakshmi Bala Reddy College of Engineering, Mylavaram, Krishna District, Andhra Pradesh, India

² Department of Mechanical Engineering, Ponnad V Pruthi Siddhanti Institute of Technology, Kazuru, Andhra Pradesh, India

³ R&D Metrologics, Design and Engineering, VEM Technologies Pvt Ltd, Hyderabad, Telangana, India

⁴ Department of Mechanical Engineering, Kakotya Institute of Technology and Science, Warangal, Telangana, India

⁵ Department of Mechanical Engineering, Gokaraju Rangaraju Institute of Engineering and Technology, Hyderabad, Telangana, India



RSM-TOPSIS multi optimization of EDM factors for rotary stir casting hybrid (Al7075/B₄C/Gr) composites

Devaraju Aruni¹ · Murahari Kolli² · Satyanarayana Kosaraju³ · G. Sai Kumar¹

Received: 15 January 2022 / Accepted: 7 April 2022

© The Author(s), under exclusive licence to Springer-Verlag France SAS, part of Springer Nature 2022

Abstract

Hybrid metal matrix composites are important materials used in marine, automobile, aerospace, structural, and entertainment fields because of their exceptional mechanical and physical properties such as lightweight, high strength, corrosion resistance, and elastic modulus. In this investigation, the die-sink electrical discharge machining (EDM) process is adopted for machining of hybrid Al 7075/B₄C/Gr composite. The effect of EDM input factors like current (I_p), pulse on time (T_{on}), pulse off time (T_{off}), and voltage (V) on the output factors such as material removal rate (MRR), surface roughness (R_a) and electrode wear rate (EWR) are studied. A response surface methodology (RSM) is employed for planning and the design of experimental layout and also to find output factors of EDM to acquire the maximum MRR, minimum SR, and TWR. Furthermore, the TOPSIS approach is applied to the final solutions for calculating the combined ideal solutions. The ANOVA result measures the most significant process parameters and their levels for performance factors. Mathematical equations are developed from the performance factors and by predicting the experimental results and observed a good agreement. The final results are noted that I_p and T_{on} are more significant factors and, T_{off} and V is less significant.

Keywords Al 7075/B₄C/Gr · Response surface methodology · TOPSIS · Multi optimization · ANOVA · Stir casting

1 Introduction

Nowadays, manufacturing industries are replacing the composite materials instead of monolithic materials for fabrication purposes due to their outstanding properties like lightweight, high strength, corrosion resistance, and elastic modulus. Aluminium metal matrix composites (MMCs) are

widely accepted and utilized in automobile and aerospace sectors due to good mechanical and physical properties; especially automobile field brake rotors, pistons, connecting rods, and integrally cast engine blocks [1–3]. The fabrication process plays a vital role in the improvement of mechanical and tribological properties of MMCs. Al 7075 hybrid MMC is used as a workpiece for experimentation. Al 7075 alloy, is a strong material with high strength compared to many steels as it has good fatigue strength and average machinability [3]. The important elements are zinc, iron, magnesium, copper, chromium, manganese, titanium, silicon, and other metals. Al-MMCs Al₂O₃ and SiC reinforcement particles are regularly used. In the present study, composite mixture of 12% of boron carbide (B₄C) and 3% of graphite (Gr) is used. B₄C is a second hardest, light weight and good strength material. The graphite mixture exhibits great improvements in the production of fine surface finishes, less electrode wear rate due to their properties like light-weight, good workability, high thermal stability, electrical and thermal conductivity. Consequently, hybrid composites are hindered by the effect of poor machinability techniques and high tool wear from traditional machining methods like milling, turning, drilling and grinding, etc., owing to their non-homogeneity, anisotropy,

✉ Devaraju Aruni
aruni_devaraj@yahoo.com

Murahari Kolli
kollihari1987@gmail.com

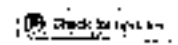
Satyanarayana Kosaraju
satyanarayana.kosaraju@gnit.ac.in

G. Sai Kumar
sai.gulakann@gmail.com

¹ Mechanical Engineering Department, Kakatiya Institute of Technology and Science, Warangal, Telangana, India

² Department of Mechanical Engineering, Lakshmaiah Bali Reddy College of Engineering, Mylavaram, Andhra Pradesh, India

³ Mechanical Engineering Department, Gokaraju Rangaraju Institute of Engineering and Technology, Hyderabad, Telangana, India



Real-time monitoring of battery state of charge using artificial neural networks

Sai Vasudeva Bhagavatula^a, Venkata Rupesh Bharadwar Yeflamraju^a, Karthik Chandana Eleruvu^a, P. N. Shashank^a,
Phaneendra Babu Bobba^a, Satyanarayana Kosaraju^b and Navcen Kumar Marati^c

^aDepartment of Electrical & Electronics Engineering, GRIT, Hyderabad, India; ^bDepartment of Mechanical Engineering, GRIT, Hyderabad, India; ^cArchitect, Electric Vehicle Co., Wipro Limited, Bangalore, India

ABSTRACT

The main highlight of this paper is to present the implementation of a battery health inquiry system using artificial neural networks (ANNs). We were able to predict the amount of charge in the battery only by taking preliminary parameters like voltage, current and ambient temperature of the battery in the growing field of portable energy storage (ES) technology. An optimal solution was demanded to increase the age of the battery. We were able to predict the state of the battery in terms of charge for its performance. A feed forward neural network (FFNN) and long short-term memory (LSTM) neural nets were used for the implementation whose prediction accuracy is acceptable for this application. An optimal data-driven model for FFNN and LSTM for the prediction which made sure that our neural network (NN) models can be used for the estimation of charge in the battery for any charging cycle based on the preliminary parameters. These results can also help us to extend the implementation by estimating the health condition of the battery and also to be used for real-time monitoring and prediction of the performance characteristics and to improvise various NN methods in these fields for perfect accuracy in predicting the performance.

ARTICLE HISTORY

Received 12 October 2021
Accepted 24 February 2022

KEYWORDS

BMS; battery management system; ESU; energy storage; SOC; state of charge; SoH; state of health; NN; real-time monitoring; artificial neural networks

1. Introduction

The recent growth in latest technologies like portable electronics, futuristic transportation, healthcare and areas of power & energy gave rise to the need of prodigious batteries or energy storage units (ESUs). The need for portability, durability, robustness and longevity in battery technology has become a challenge for battery engineers and researchers, different parameters for enhancement of these ESUs like supercapacitors, hybrid (battery-supercapacitors) or batteries alone were observed. Figure 1 shows the block diagram architecture of BMS.

A battery management system (BMS) in short BMS (He et al. 2012) is a device that manages, computes, protects, monitors and communicates with the battery (Lee, Kuo, and Wang 2004). A BMS is like a brain for a battery and can be used for any ESU as the parameters affecting the performance are the same. The SOC and SoH (Wang and Chen 2013) are the terms that give us an understanding on the performance of any ESU. SOC is the amount of charge in the ESU, and SoH (Yang et al. 2017) is the condition of ESU. Some factors that affect the SOC and SoH are as shown in Figure 2.

Formulating the performance using these parameters can be achieved in many ways also involving data-driven methods like machine learning (ML) and artificial neural network (ANN) being a branch of ML. Figure 3 is the graphical representation of various estimation techniques.

Neural network (NN) is a data-driven method (Zou et al. 2014) similar to ML that took its place in one of the fastest growing

technologies due to its ability to learn and model the relationships between inputs and outputs that are nonlinear and complex for any data. NN is widely used in many latest areas, inspired from multi-variable regression, and is being used for both regression and classification problems. Some of the mostly used NN architectures are mentioned in Figure 4.

Earlier, other methods like direct methods, battery based models (Reimlinger et al. 2011), filtering estimations involving methods like Coulomb counting, open circuit voltage (OCV) ECM-equivalent circuit model (ECM) and Kalman filtering methods (Chaikhegari and Farrokhi 2010; Wang and Chen 2020) and later due to increase in computational power of computer and many open-source frameworks, implementing NN has become easily available for all. The model-based methods discussed by Wei et al. (2021) and Bian et al. (2021b) clearly explain how the state of charge for lower order models can be clearly estimated and give comparatively better results than higher order models and estimating the state of charge in lithium-ion battery even in the absence of current sensor. Multiple parameters were taken into consideration for the performance estimation of the battery; these included vital attributes like voltage, current and temperature but battery researchers had to know the capacity of the battery which is also another vital parameter in order to understand the performance of the battery better. Capacity based estimation came out to be the best estimating techniques for battery performance as it elucidates how battery deteriorate over a period and how the instantaneous capacity of the battery, and its maximum

**DE GRUYTER**

Requires Authentication Published by De Gruyter May 23, 2022

Recent reviews on bio-waste materials for corrosion protection of metals

Lavanya Kandikonda, Saranya Jagadeesan, Ram Subbiah and Abdelkader Zarrouk

From the journal *Corrosion Reviews*

<https://doi.org/10.1515/corrrev-2021-0083>

You currently have no access to view or download this content. Please log in with your institutional or personal account if you should have access to this content through either of these. Showing a limited preview of this publication.

Abstract

The present paper is aimed to review the efficiency of eco-friendly, natural and cheap bio-waste materials as corrosion inhibitors on metal surfaces in different corrosive media. Various bio-waste materials are the best substitutes for the synthetic organic, inorganic and polymeric inhibitors. Most of the bio-waste material adsorbed on the metal surface in aqueous medium followed the Langmuir adsorption isotherm. The presence of organic constituents in bio-waste materials is responsible for the protection of metals in aggressive medium. The effectiveness of these bio-waste materials to inhibit metal corrosion is well studied by non-electrochemical methods like weight loss and atomic absorption spectroscopy techniques as well as electrochemical methods like polarization and impedance measurements. Surface studies were studied through SEM, EDS, XRD, AFM and XPS techniques. Computational studies using DFT and MDS were also reported.

Keywords: adsorption; AFM; bio-waste; impedance; polarization; SEM

Corresponding author: Saranya Jagadeesan, Department of Humanities and Sciences (Chemistry), Gokaraju Rangaraju Institute of Engineering and Technology,

<https://www.degruyter.com/document/doi/10.1515/corrrev-2021-0083/html?lang=en>

Influence of Nanofillers on the Mechanical characteristics of Natural Fiber Reinforced polymer composites

S.Suresh Kumar^{1*}, V.Mohanavel^{2*}, M.Ravichandran³, S.Rajkumar⁴, P.Velmurugan⁵, Ram Subbiah⁶

¹Department of Mechanical Engineering, Panimalar Polytechnic College, Chennai - 600029, Tamilnadu, India

²Centre for Materials Engineering and Regenerative Medicine, Bharath Institute of Higher Education and Research, Tambaram, Selaiyur, Chennai - 600073, Tamilnadu, India

³Department of Mechanical Engineering, K. Ramakrishnan College of Engineering, Trichy - 621 112, Tamil Nadu, India,

⁴Department of Mechanical Engineering, Faculty of Manufacturing, Institute of Technology, Hawassa University, Ethiopia.

⁵Centre for Materials Engineering and Regenerative Medicine, Bharath Institute of Higher Education and Research, Tambaram, Selaiyur, Chennai - 600073, Tamilnadu, India

⁶Department of Mechanical Engineering, Gokaraju Rangaraju Institute of Engineering and Technology, Hyderabad, Telangana 500090, India.

Email : sandysuresh@gmail.com, mohanavel.phd@gmail.com, m.ravichandran@hoimail.com, coetraj@gmail.com, palanivelvelmurugan@bharathuniv.ac.in, ram@msrmie@gmail.com

Abstract

For the first time, natural fibres are being considered as a viable alternative to traditional synthetic fibres. These bio-composites were created using epoxy resin, nano-sized fine nano-tamarind shell ash particles, and water hyacinth fibres in this experimental work. Nano tamarind shell ash particles (0, 1, 3, 5, 7, and 9 wt. percent) were mixed with epoxy resin and water hyacinth fibres to create six different composite mates by the compression moulding machine. The composite specimens are prepared from the mats using the water jet machining method, according to ASTM specifications. Mechanical properties of composite specimens have been determined using tensile, flexural, and impact tests under standard testing circumstances. According to the test results, the composites with nano tamarind shell ash particles in the weight percentage of five percent greatly improve their tensile and flexural capabilities. Increased incorporation of fine nano tamarind shell ash particles in composite specimens has reduced their impact energy and impact strength.

Keywords: epoxy resin, water hyacinth fiber, nano tamarind shell ash, bio-composites, Nano filler

1. Introduction

Development countries have a large supply of agricultural waste and fibres that can be turned into novel composite materials that can be better utilised and decrease deforestation in light of global warming concerns. India possesses the world's main tamarind potential [1]. Traditional materials are being displaced by lightweight composite buildings. Fibers like coconut and jute are often used as composite materials because of the strong strength of the materials when combined with resins, their low density, and their biodegradability [2]. With *Arundo Donax L.* leaves serving both as the matrix and reinforcement, the composite material is made up of prawn shell, tamarind, and dates seed powder. There are numerous various uses for epoxy, which is a form of resin.[3]. Reinforcement in the compression moulding machine was provided by tamarind seed fillers, which were tested for tensile,



Wear and microstructure analysis on AISI420 stainless steel by annealing & tempering process under dry sliding conditions

Animesh Bain, Keerthi Reddy, Saranya Jagadeesan, A. Anitha Lakshmi, N Sateesh, Swadesh Kumar Singh & Ram Subbiah

To cite this article: Animesh Bain, Keerthi Reddy, Saranya Jagadeesan, A. Anitha Lakshmi, N Sateesh, Swadesh Kumar Singh & Ram Subbiah (2021): Wear and microstructure analysis on AISI420 stainless steel by annealing & tempering process under dry sliding conditions, *Advances in Materials and Processing Technologies*. DOI: [10.1080/2374065X.2021.1945308](https://doi.org/10.1080/2374065X.2021.1945308)

To link to this article: <https://doi.org/10.1080/2374065X.2021.1945308>



Published online: 06 Jul 2021.



Submit your article to this journal [↗](#)



Article views: 10



View related articles [↗](#)



View Crossmark data [↗](#)



Evolution and Characterisation of ASS 316L at Elevated Temperature

Balaji Dharavath, Swadesh Kumar Singh, M.T. Naik & Satyanrayana Kosaraju

To cite this article: Balaji Dharavath, Swadesh Kumar Singh, M.T. Naik & Satyanrayana Kosaraju (2021), Evolution and Characterisation of ASS 316L at Elevated Temperature, Advances in Materials and Processing Technologies, DOI: 10.1080/2374068X.2021.1945294

To link to this article: <https://doi.org/10.1080/2374068X.2021.1945294>



Published online: 23 Jun 2021.



[Submit your article to this journal](#)



Article views: 4



[View related articles](#)



[View Crossmark data](#)



Effect of material discontinuity on springback in sheet metal bending

Chetan P Nikhare, Nitin Kulkunde & Swadesh Kumar Singh

To cite this article: Chetan P Nikhare, Nitin Kulkunde & Swadesh Kumar Singh (2021): Effect of material discontinuity on springback in sheet metal bending, *Advances in Materials and Processing Technologies*. DOI: [10.1080/2374068X.2021.1953925](https://doi.org/10.1080/2374068X.2021.1953925)

To link to this article: <https://doi.org/10.1080/2374068X.2021.1953925>



Published online: 13 July 2021



Submit your article to this journal [↗](#)



Article views: 11



View related articles [↗](#)



View Crossmark data [↗](#)



Comparative study of formability characteristics in deep drawing of DP 590 steel using analytical models

Sandeep Pandre, Nitin Kotkunde, Ayush Morchhale, Swadesh Kumar Singh & Ambuj Saxena

To cite this article: Sandeep Pandre, Nitin Kotkunde, Ayush Morchhale, Swadesh Kumar Singh & Ambuj Saxena (2021): Comparative study of formability characteristics in deep drawing of DP 590 steel using analytical models, Advances in Materials and Processing Technologies. DOI: [10.1080/2374068X.2021.1945273](https://doi.org/10.1080/2374068X.2021.1945273)

To link to this article: <https://doi.org/10.1080/2374068X.2021.1945273>



Published online: 22 July 2021



Submit your article to this journal [↗](#)



Article views: 31



View related articles [14](#)



View Crossmark data [↗](#)



Determination of Warm Deep Drawing Behavior of DP590 Steel Using Numerical Modeling and Experimental Process Window

Sandeep Pandre¹ · Ayush Morchhale¹ · Nishu Kotkunda¹ · Sivadesh Kumar Singh² · Navneet Khanna³ · Ambuj Saxena⁴

Received: 14 September 2020 / Accepted: 8 July 2021 / Published online: 3 August 2021
© King Fahd University of Petroleum & Minerals 2021

Abstract

The present work focuses upon the determination of deep drawing behavior of DP590 steel under different lubricating and warm forming conditions. The limiting drawing ratio (LDR) was observed to be 1.933 under 673K lubricated condition which is 3.53% more than other processing conditions. The modified Johnson–Cook (m-JC) and Johnson–Cook and Zerilli–Armstrong (JC–ZA) constitutive models have been used among which the JC–ZA model along with Hill 48 r-based displayed the best prediction ability of flow stress and yield locus, respectively. The stretch forming process has been performed to find the safe forming limits of the material and an effective improvement of 21% has been observed as the temperature increased from 300 to 673 K. Further, the adequate lubrication helped in increasing the strain ratio. Thus, helped in increasing the range of limiting strains. The strain-based FLD has been converted into stress based and triaxiality and equivalent plastic strain FLD in order to remove excessive dependency over limiting strains. The deep drawing deformation path has been found to be lying in the uniaxial stress region of FLD. The best numerically predicted results of thickness distribution and drawn height have been obtained using the combination of Hill 48 r-based yielding function and JC–ZA constitutive model. The coupled effect of high temperature and lubricating condition helped in increasing the LDR and the uniformity in thickness distribution along the walls of the deep drawn cup and further helped in reducing the maximum load needed for forming the cup.

Keywords DP590 steel · Deep drawing · Constitutive modeling · Warm forming · Process window · Stretch forming

1 Introduction

Steel is one of the most abundantly used metals by human-kind in day-to-day life [1]. They have a proper blend of properties such as low density and very high strength [2]. Dual-Phase (DP) steel is used in various applications of automotive industry because of high resistance toward easy fatigue, good ductility, and very high strength even at elevated temperatures [3, 4]. These favorable material

properties, in turn, helped by providing improvements in crash safety and vehicle fuel economy [5].

The formability of various metallic materials is characterized by using different forming processes such as deep drawing [6], stretch forming [2, 7, 8]. The deep drawing process is in greater demand for manufacturing various components with large depths and a complex profile. Several different approaches have been adopted for performing deep drawing operation on a commercial level. These approaches helped in increasing the forming ability of the material and also avoiding several defects such as thinning, spring-back, earing and wrinkling [9]. The desired formability of high strength material is difficult to achieve at room temperature, hence, deep drawing at elevated temperature can be adopted as a solution for this problem [10]. The indexes, namely, limiting drawing ratio (LDR), drawn height, and thickness distribution along the cup can be considered for analyzing the formability of metal and the quality of the drawn cup in the deep drawing process.

✉ Nishu Kotkunda
nink@hyderabad.bits-pi.ac.in

¹ Mechanical Engineering Department, BITS-Pilani, Hyderabad Campus, Hyderabad, India

² Mechanical Engineering Department, GRIET, Hyderabad, India

³ Mechanical Engineering Department, FITRAM, Ahmedabad, India

⁴ Mechanical Engineering Department, OJBIT, Greater Noida, India





High temperatures deformation and formability behavior of DP590 steel: mechanical characterization and modeling

K. Seshacharyulu¹ · Gauri Mahalle^{2,3} · Nitin Kotkunde² · Swadesh Kumar Singh^{3,4} · B. Balu Naik⁴

Received: 30 June 2021 / Accepted: 20 September 2021 / Published online: 30 September 2021
© The Brazilian Society of Mechanical Sciences and Engineering 2021

Abstract

In this study, the deformation and formability characteristics of DP 590 steel have been determined at high temperature. Firstly, theoretical uniaxial flow stress prediction has been studied by modified Arrhenius, Fields–Backofen, Khan–Huang–Liang and modified Fields–Backofen, type constitutive models in different test temperatures (773–1093 K) with strain rates (0.001–0.1 s⁻¹). The flow stress behavior of DP590 steel has been well predicted by the KHL model compared to other models. Furthermore, traditional yield functions such as, Hill 1948 and Barlat 1989, have been formulated. Barlat 1989 exhibits better prediction ability for all test temperatures. Additionally, Nakazima tests have been conducted for experimental determination of formability behavior by means of Forming limit Diagram (FLD), surface strain distribution, limit dome height and thickness distribution. Forming test temperature has significantly affected the formability behavior of the alloy. For theoretical prediction of FLD, Marciniak–Kuczynski (M–K) model has been implemented with different combination of uniaxial constitutive modeling and the yield function. The M–K model with a combination of KHL model with the Barlat 1989 yield function has given the best predictability with a 0.05 average error for all forming test temperatures. Furthermore, micrograph of the post stretched specimens has revealed a ductile fracture for test temperatures.

Keywords DP590 steel · Hot deformation · Constitutive modeling · Anisotropic yield criteria · MK model · FLD

1 Introduction

Advanced high strength (AHS) steels are extremely popular in the automotive industries for the collision-safe performance and the weight reduction, despite its reasonable combination of high strength and the ductility. This is mainly achieved by careful controlling the microstructure

of martensite, ferrite, and retained austenite components [1]. In this family, Dual phase (DP) steel is principal material in the fabrication of automotive chassis and structure. The microstructure of DP steel typically contains a soft ferrite phase with discrete martensite islands, where martensite phase is significantly stronger than ferrite phase. This martensite phase contributes to the tensile strength of steel material, whereas soft ferrite phase contributes for ductility of the steel material [2, 3]. Despite of high strength, some various limitations were noticed such as unexpected failures and large spring-back. During stretch forming operation, unexpected failure observed much earlier than the predicted failure either by forming limit diagrams or finite element simulations [4]. Also during the press forming operation, reasonable amount of spring-back observed. These are the main impediment for high efficiency production in automotive industries.

Advanced high strength steels exhibit relatively complex microstructures which lead to a typical plasticity [5]. For cost and time effective forming operation of automotive parts of DP steel, the research emphasis has been moved toward the deformation and failure aspects under room

Technical Editor: José Marciano Lourenço Reis.

✉ Swadesh Kumar Singh
swadesh@mlupm.com

¹ Mechanics Engineering Department, Sreevidya Engineering College, Hyderabad, Telangana 501510, India

² Mechanical Engineering Department, BITS Pilani-Hyderabad Campus, Hyderabad, Telangana 500078, India

³ Mechanical Engineering Department, GRIET Hyderabad, Telangana 500080, India

⁴ Mechanical Engineering Department, Jawaharal Nehru Technological University, Hyderabad, Telangana 500085, India



Analysis of Tensile Deformation Behaviour of Dual Phase -590 Steel at Different Temperatures and Strain Rates

K. Seshacharyulu, Gauri Mahalle, Nitin Kotkunde, Swadesh Kumar Singh & B. Balu Naik

To cite this article: K. Seshacharyulu, Gauri Mahalle, Nitin Kotkunde, Swadesh Kumar Singh & B. Balu Naik (2021). Analysis of Tensile Deformation Behaviour of Dual Phase -590 Steel at Different Temperatures and Strain Rates, *Advances in Materials and Processing Technologies*, DOI: [10.1080/2374068X.2021.1946339](https://doi.org/10.1080/2374068X.2021.1946339)

To link to this article: <https://doi.org/10.1080/2374068X.2021.1946339>



Published online: 02 Aug 2021



Submit your article to this journal [↗](#)



Article views: 5



View related articles [↗](#)



View Crossmark data [↗](#)



Investigation of fracture forming limits of dual phase steel under warm incremental forming process

Sandeep Pandre¹ · Nitin Korkunde¹ · Kurra Suresh¹ · Swadesh Kumar Singh^{2,3}

Received: 22 April 2021 / Accepted: 7 June 2022

© The Author(s), under exclusive licence to Springer-Verlag GmbH, part of Springer Nature 2022

Abstract

Dual phase (DP) steel is extensively used in automotive industries for making outer body structures due to its high strength-to-weight ratio. During forming operation, it exhibits low formability at room temperature (RT). To overcome this issue, the present work is mainly focused on warm incremental forming of DP steel at 400 °C. The fracture forming limits of DP steel have been investigated experimentally at 400 °C and validated it with various phenomenological-based damage models. Firstly, the varying wall angle conical (VWACH) and pyramidal (VWAPF) frustums are formed experimentally to evaluate the fracture forming limits. It is found that the height of the conical frustums has increased by 15.06% whereas the pyramidal frustum has shown a 7.5% improvement compared to forming at RT. Also, the fracture limits of the material have improved by 14.06%. The triaxiality ratio of VWAPF is considerably more than VWACH which indicates the early failure of the VWAPF. Furthermore, the various phenomenological-based damage models namely: Oyane (Oy), Cockcroft–Latham (C–L), Mc-CI neck (Mc-CI), Broz (Br), and Kojima (Koj) have been formulated for the theoretical prediction of fracture limiting strains. The prediction capability of these models is assessed based on the correlation coefficient (*R*), Squared Euclidean Distance (SED), and Average Absolute Error (AAE). The prediction capability of Oy's model shows best agreement with the highest value of *R* as 0.9959, the least SED, and AAE as 0.0275, 7.779, respectively. Additionally, the experimental findings are supported by microstructural examination using the EBSD technique.

Keywords DP steel · Warm incremental forming · Fracture limits · Damage models · Textural evolution

1 Introduction

Dual phase (DP) steel alloy exhibits superior mechanical properties like strength to weight ratio compared to conventional steels [1]. However, the limited ductility of DP steel at Room Temperature (RT) makes it difficult to form which requires high forming loads. To overcome these difficulties of forming high-strength materials, an alternative approach such as warm/hot forming of conventional stamping processes has been implemented earlier by many researchers [2]. Recently, the implementation of novel forming techniques

has also proved to be a better solution for complex shapes with ease. Among the available novel forming processes, incremental sheet forming (ISF) has established itself in the manufacturing area as a rapid prototyping process, and an emerging cost-effective solution for customized components [3]. The ISF process was implemented by many automotive manufacturers for the manufacturing of different parts like fenders, hoods, light casings, etc. [4]. Recently the ISF has also been used in the bio-medical field for the fabrication of knee, jaw, and cranial implants [5].

In recent years, sufficient research has been reported on the establishment of the ISF process for different materials [6]. However, it is a well-known fact that the forming limits attained through the ISF process are significantly higher relative to the conventional stamping processes [7]. The extent of formability of sheet material is generally evaluated based on Forming Limit Diagram (FLD) [8, 9]. The limiting strain values are generally measured based on diffuse/ localized necking. During the ISF process, the material fails without


Nitin Korkunde
nitink@hccentral.hyderabad.ac.in

¹ Mechanical Engineering Department, BITS Pilani, Hyderabad Campus, India

² Mechanical Engineering Department, GRIFP, Hyderabad, India

³ Adjunct Professor at Institute for Sustainable Industries & Livable Cities, Victoria University, Melbourne, Australia

Stretch flanging behaviour and microstructural analysis of DP steel using punch stretching and incremental forming processes

Sandeep Pandey, Ayush Mankhale, Nitin Korkkane , Sujra Suresh & Praveesh Kumar Singh

Archives of Civil and Mechanical Engineering 22, Article number: 153 (2022) | [Cite this article](#)

134 Accesses | [Metrics](#)

Abstract

The main aim of the present study is to analyse the stretch flanging behaviour of the DP steel sheet using the punch stretching (PS) and incremental sheet forming (ISF) at different temperatures. Firstly, the material properties and Lankford coefficients have been determined using uniaxial tension tests. Subsequently, the stretch flanging process has been carried out experimentally on the specimens with different flange widths and lengths using PS and ISF processes. Different critical formability and quality parameters, namely, strain path, thickness distribution, forming forces, and geometrical accuracy, have been analysed experimentally and numerically. The minimum flange thickness has been found near the edge of the bend region, which forms during the punch stretching process. The thickness of the flange is found to be

Your Privacy

We use cookies to make sure that our website works properly, as well as some optional cookies to personalise content how people use our site. By accepting some or all optional cookies you give consent to the processing of your personal data outside of the European Economic Area that do not offer the same data protection standards as the country where you are located. You can manage these preferences at any time by clicking on 'Manage Settings', where you can also find more information about how your personal data is processed. You can also find more information about our privacy practices here.

[Accept all cookies](#)

[Manage preferences](#)

Original Paper | Published: 18 July 2022

Investigation of fracture forming limits of dual phase steel under warm incremental forming process

Sandeep Pandre, Niran Ketkande[✉], Kunal Jureish & Swarnesh Kumar Singh

International Journal on Interactive Design and Manufacturing (IJDes), (2022) | [Cite this article](#)






102 Accesses | [Metrics](#)


Abstract









Dual phase (DP) steel is extensively used in automotive industries for making outer body structures due to its high strength to-weight ratio. During forming operation, it exhibits low formability at room temperature (RT). To overcome this issue, the present work is mainly focused on warm incremental forming of DP steel at 400 °C. The fracture forming limits of DP steel have been investigated experimentally at 400 °C and validated it with various phenomenological-based damage models. Firstly, the varying wall angle conical (VWACF) and pyramidal (VWAPF) frustums are formed experimentally to evaluate the fracture forming limits. It is found that the height of the conical frustums has increased by 15.06%, whereas the pyramidal frustum has shown a 7.5% improvement (compared to forming at RT). Also, the fracture limits of the material have improved by 1.06%. The proximity ratio of VMADE is

Registered address Research article First published online June 11, 2024

A study on tensile flow and strain hardening behaviour of β -Titanium at elevated temperatures

Indrani Banerjee, Smita Suresh  Swadesh Kumar Ghosh  Anand Kumar  Debjit Ghosh  Subrata Ghosh 

Subrata Ghosh  [https://orcid.org/10.1038/s41598-024-57507-7](#)

 Learning  Get access  Check for updates  Information on this journal  Check for updates  Information on this journal  Check for updates  Check for updates

Abstract

In this paper, the tensile flow and work hardening behaviour of β -Titanium alloy was examined over a wide temperature range of 28 to 500°C. The work hardening of the material was modelled using different empirical relations such as Swift, Voce and Ludwik, and the prediction of the flow of these models were compared with different statistical parameters. The hardening rate of the material was analysed with K-M analysis. The fracture behaviour of the tensile samples was studied using SEM results. The yield strength and ultimate tensile strength of the material was found to be decreased from room temperature to 200°C followed by a gradual increase with increase in temperature. Uniformly distributed serrations were observed in the entire plastic region of the flow curve in the temperature range of 300–400°C. This serrated behaviour could be due to the manifestation of dynamic strain ageing in this temperature range. The work hardening model was identified as a best hardening model for β -Titanium alloy. SEM results revealed the ductile mode of fracture at all temperature with large number of dimples in fractography.

Get full access to this article

View all access and purchase options for this article.



Check for updates



Open Access | Research article | Published online: 2023-09-15

Flow stress and work hardening behaviour of Mg-3Al-12In alloy

[Badr Al-Husseini](#), [Saeed Kadhim](#) | [Saeed Al-Husseini](#) | [saeed.alhusseini@uq.edu.iq](#)

[b.alhusseini@uq.edu.iq](#) | [saeed.alhusseini@uq.edu.iq](#)

[Contents](#) | **Open Access** | [Abstract](#) | [Introduction](#) | [Materials and Methods](#) | [Results and Discussion](#) | [Conclusion](#) | [References](#) | [Cite this article](#) | [Share this article](#) | [Download PDF](#) | [View Full Text](#) | [Metrics](#)

Abstract

In the present study, the uniaxial tensile flow stress behaviour and work hardening behaviour of AZ31B alloy has been investigated across a wide range of temperatures (25°C–250°C) at various strain rates (10⁻³ s⁻¹–10² s⁻¹). The flow stress behaviour of the AZ31B sheet has been analysed at different temperatures, quasi-static strain rates and sheet orientations. It has been found that flow stress behaviour is highly influenced by the variation of temperatures, strain rates, and sheet orientations. The various important mechanical properties such as yield strength, ultimate tensile strength, percentage elongation, strain hardening exponent, and strain rate sensitivity have been determined. There has been a significant improvement in ductility (201.71%) of AZ31B alloy at 250°C compared to 25°C. The decrement in yield strength and ultimate strength has been found to be 47.5% and 53.0%, respectively. It has been observed that the AZ31B alloy is found to be more strain rate sensitive at elevated temperatures ($m = 0.11$) at 250°C than



Restricted access | Research article | Published: 22 September 2022

Analysis of forming characteristics for dual phase steel under warm incremental forming process

Seokseon Park¹, Seungja Park² and Seungja Park³ | [Seungja Park](#) | [Seungja Park](#) | [Seungja Park](#)

Citation: Processes 2022, 10, 1404; doi:10.3390/Processes10091404

[View Full Article](#) | [Full Access](#) | [Article Metrics](#) | [Article History](#) | [Reprints and Permissions](#) | [View Article](#)

Abstract

The demand for rapid prototyping technologies has been increasing, in the field of automotive for the manufacturing of various parts with complex shapes. The present work, experimental and numerical investigations have been performed on an automotive grade DP steel using an incremental sheet forming process at Room Temperature (RT) and 400°C. Various formability parameters such as fracture forming limits, limiting wall angle, forming forces, wrinkling formation, and geometrical accuracy have been analysed. The fracture limits of the material are evaluated by forming varying wall angled conical (VWAC) and pyramidal (VWAP) frustums. The fracture limits of the material formed at 400°C have been found to be 14.55% higher compared to room temperature fracture limits. The limiting wall angle for VWAC and VWAP are found to be $70.77^\circ \pm 1.41^\circ$ and $67.97^\circ \pm 1.48^\circ$ which are also higher than the formed conical wall angled frustum. The forming forces measured from experimental and FEM simulations are in good



256

2022

0

0 (0%)

0 (0%)

0

0 (0%)

Keywords

Heat treatment and temperature effects on formability of AA2014-T6 in incremental forming

Rakhy Alkhatib¹ [✉] alkhatib@mech.ktu.edu.tr · alkhatib@mech.ktu.edu.tr · alkhatib@mech.ktu.edu.tr**Received:** alkhatib@mech.ktu.edu.tr · **Accepted:** alkhatib@mech.ktu.edu.tr

Full Article Favorite (0) Reference Cite (0) Share Page 6/10 Page 6/10 Page 6/10

ABSTRACT

At this point, the effect of heat treatment on the formability of the plate and sheet materials, reduction of the force weight, strength, and thickness of the plate is being investigated. In this study, the formability of AA2014-T6 is investigated for its formability to form a cylindrical shape in the incremental forming at room and elevated temperature of 150 °C. The mechanical properties and formability of the material are evaluated using uniaxial tensile test and energy (Nal Analytical Software (PAM-FEM)) respectively. A novel experimental setup is designed with an insulation shield to maintain constant elevated temperatures for incremental forming. As received sheets cannot form in the incremental forming process at elevated temperatures. As a result, the formability of the sheets is improved for elevated temperatures. The increased formability was attributed to formability due to the annealing of the sheets at 150 °C for 3 hours.